

**THE VARIABLE LIGHT ENVIRONMENT WITHIN
COMPLEX 3D CANOPIES**

ALEXANDRA JACQUELYN BURGESS

BA (Hons) Oxon

Thesis submitted to the University of Nottingham for the degree of Doctor of
Philosophy

September 2016

Abstract

With an expanding population and uncertain consequences of climate change, the need to both stabilise and increase crop yields is important. The relationship between biomass production and radiation interception suggests one target for improvement. Under optimal growing conditions, biomass production is determined by the amount of light intercepted and the efficiency with which this is converted into dry matter. The amount of light at a given photosynthetic surface is dependent upon solar movement, weather patterns and the structure of the plant, amongst others. Optimising canopy structure provides a method by which we can improve and optimise both radiation interception and also the distribution of light among canopy layers that contribute to net photosynthesis. This requires knowledge of how canopy structure determines light distribution and therefore photosynthetic capacity of a given crop species.

The aim of this thesis was to assess the relationships between canopy architecture, the light environment and photosynthesis. This focused on two core areas: the effect of varietal selection and management practices on canopy structure and the light environment and; the effect of variable light on select photosynthetic processes (photoinhibition and acclimation). An image-based reconstruction method based on stereocameras was employed with a forward ray tracing algorithm in order to model canopy structure and light distributions in high-resolution. Empirical models were then applied using parameterisation from manually measured data to predict the effects of variable light on photosynthesis.

The plasticity of plants means that the physical structure of the canopy is dependent upon many different factors. Detailed descriptions of canopy architecture are integral to predicting whole canopy photosynthesis due to the spatial and temporal differences in light profiles between canopies. This inherent complexity of the canopy means that previous methods for calculating

light interception are often not suitable. 3-dimensional modelling can provide a quick and easy method to retain this complexity by preserving small variations. This provides a means to more accurately quantify light interception and enable the scaling of cellular level processes up to the whole canopy.

Results indicate that a canopy with more upright leaves enables greater light penetration to lower canopy layers, and thus higher photosynthetic productivity. This structural characteristic can also limit radiation-induced damage by preventing exposure to high light, particularly around midday. Whilst these features may lead to higher photosynthetic rates per unit leaf area, per unit ground area, photosynthesis is usually determined by total leaf area of the canopies, and within this study, the erect canopies tended to have lower total leaf areas than the more horizontal canopies. The structural arrangement of plant material often led to low levels of light within the lower canopy layers which were punctuated by infrequent, high light events. However, the slow response of photosynthesis to a change in light levels meant that these sun flecks cannot be used by the plant and thus the optimal strategy should be geared towards light harvesting and efficient photosynthesis under low light conditions.

The results of this study contribute to our understanding of photosynthetic processes within the whole canopy and provide a foundation for future work in this area.

Publications

In Peer-reviewed Journals

Burgess AJ, Retkute R, Preston SP, Jensen OE, Pound MP, Pridmore TP, and Murchie EH. The 4-dimensional plant: biological implications of wind-induced movement. *Frontiers in Plant Science* 7: 1392

Burgess AJ*, Retkute R*, Pound MP, Preston SP, Pridmore TP, Foulkes MJ, Jensen OE, and Murchie EH (2015) High-resolution 3D structural data quantifies the impact of photoinhibition on long term carbon gain in wheat canopies in the field. *Plant Physiology*, **169(2)**: 1192-1204

Retkute R, Smith-Unna SE, Smith RW, **Burgess AJ**, Jensen OE, Johnson GN, Preston SP, and Murchie EH (2015) Exploiting heterogeneous environments: does photosynthetic acclimation optimize carbon gain in fluctuating light? *Journal of Experimental Botany* **66**: 2437-2447

Burgess AJ, Retkute R, Pound MP, Mayes S, and Murchie EH. Applications of image-based 3D reconstruction and modelling in assessing light interception and productivity in multi-species intercrop systems. *Annals of Botany*, *in press*

Pre-published or under review

Pound MP, **Burgess AJ**, Wilson MH, Atkinson JA, Griffiths M, Jackson AS, Bulat A, Tzimiropoulos G, Wells DM, Murchie EH, Pridmore TP and French AP (2016) Deep Machine Learning provides state-of-the-art performance in image-based plant Phenotyping. Pre-published at bioRxiv doi: <http://dx.doi.org/10.1101/053033>

Burgess AJ, Retkute R, Chinnathambi K, Randall JWP, Smillie IRA, Carmo-Silva E, and Murchie EH. Sub-optimal photosynthetic acclimation in wheat is revealed by high resolution 3D canopy reconstruction. *New Phytologist*

Burgess AJ, Herman T, Retkute R and Murchie EH. Is there a consistent relationship between canopy architecture, light distribution and photosynthesis across diverse rice germplasm? *Frontiers in Plant Science*

Manuscripts

Burgess AJ, Herman T, and Murchie EH. The effect of nitrogen on rice canopy architecture and photosynthesis; assessed using high-resolution reconstruction and modelling.

Burgess AJ, Retkute R, Simpson C and Murchie EH. The effect of fluctuating light on dynamic acclimation of *Arabidopsis thaliana*.

Book Chapters

Lin BB, **Burgess AJ** and Murchie EH (2015) Adaptation for climate sensitive crops using agroforestry: case studies for coffee and rice. Chapter 11 in Ong C, Black C and Wilson J. 2nd Eds *Tree-Crop Interactions: Agroforestry in a Changing Climate*, CABI

Contributing author to Karunaratne, A.S. (2015) (eds) *Proso Millet (Panicum miliaceum L.)-Agronomy, Botany, Ecophysiology and Nutrition*. Faculty of Agricultural Sciences, Sabaragamuwa University of Sri Lanka, 70140, Belihuloya, Sri Lanka.

Acknowledgements

Firstly, I would like to thank my supervisors, Erik Murchie, Sean Mayes, Debbie Sparkes and Festo Massawe, for tuition, support and guidance throughout the course of my PhD.

I would also like to thank: Renata Retkute for helping me with the modelling aspects of my project and assistance with figures; Michael Pound for help with reconstructions and image analysis; John Alcock and Matt Tovey for running the field trials; Jools Marquez for organising the laboratory; Tiara Herman, Hayley Smith, Kannan Chinnathambi, Jamie Randall, CC Foo, Conor Simpson and Lorna Mcausland for assistance with the laboratory and field work and; my internal examiner, Kevin Pyke, for his invaluable advice.

My grateful thanks to my funders, Crops For the Future and the University of Nottingham.

Finally, I would like to thank my family and my fiancé, Toby Townsend, for supporting me throughout my studies and providing inspiration whilst I was writing my thesis.

Abbreviations

<i>2D</i>	2 Dimensional
<i>3D</i>	3 Dimensional
<i>4D</i>	4 Dimensional
<i>AGDM</i>	Above ground dry matter
<i>ANOVA</i>	Analysis of Variance
<i>C</i>	Carbon
<i>chl</i>	Chlorophyll
<i>CL</i>	Constant Light
<i>cLAI</i>	Cumulative leaf area index
<i>CO₂</i>	Carbon dioxide
<i>Col</i>	Columbia (<i>Arabidopsis thaliana</i> accession)
<i>DAS</i>	Days after sowing
<i>DAT</i>	Days after transplanting
<i>F/ FI</i>	Fractional Interception
<i>FL</i>	Flag leaf
<i>FL</i>	Fluctuating Light
<i>GM</i>	Gross margins
<i>GS</i>	Growth stage
<i>H₂O</i>	Water
<i>HI</i>	Harvest Index
<i>J_{max}</i>	Maximum rate of electron transport
<i>K</i>	Potassium
<i>LAD</i>	Leaf area duration
<i>LAI</i>	Leaf area index
<i>LCP</i>	Light compensation point
<i>LEC</i>	Land equivalence coefficient
<i>LED</i>	Light emitting diode
<i>LER</i>	Land equivalence ratio
<i>Ler</i>	Landsberg erecta (<i>Arabidopsis thaliana</i> accession)
<i>LHC</i>	Light harvesting complex
<i>LRC</i>	Light response curves
<i>MAGIC</i>	Multi-parent advanced generation intercross
<i>N</i>	Nitrogen
<i>NUE</i>	Nutrient use efficiency

O_2	Oxygen
P	Phosphorous
PAR	Photosynthetically active radiation
P_{max}	Maximum photosynthetic capacity
\bar{P}_{max}	Maximum photosynthetic capacity if the [fluctuating] light pattern was replaced by the average irradiance
P_{max}^{opt}	Optimal maximum photosynthetic capacity
$PNUE$	Photosynthetic nitrogen use efficiency
$PPFD$	Photosynthetic photon flux density
PSI	Photosystem I
$PSII$	Photosystem II
R_d	Dark respiration
RGB	Red green blue
RH	Relative humidity
ROS	Reactive oxygen species
RUE	Radiation use efficiency
SF	Scaling factor
SF_{12}	Scaling factor at 12:00 h
TPU	Triose phosphate utilisation
TSP	Total soluble protein
TVC	Total variable costs
V_{cmax}	Maximum rate of carboxylation
Ws	Wassilewskija-4 (<i>Arabidopsis thaliana</i> accession)
WT	Wild type
WUE	Water use efficiency
θ	Convexity
ϕ (QUE)	Quantum use efficiency/ quantum yield

Table of Contents

Abstract	i
Publications	iii
Acknowledgments	v
Abbreviations	vi
List of Figures	xv
List of Tables	xx
Chapter 1: Introduction	1
1.1 Research Context.....	1
1.2 Photosynthesis and Biomass Production.....	3
1.3 The Canopy Light Environment and Architectural Characteristics...	13
1.3.1 Canopy Architecture.....	15
1.3.1.1 Architectural Features.....	16
Leaf Area.....	16
Clumping.....	17
Leaf Shape and Size.....	19
Leaf Inclination and Orientation.....	20
Leaf Movement.....	22
1.3.2 Direct versus Diffused Light.....	23
1.4 Linking Architecture, Photosynthesis and Biomass Production.....	24
1.5 Modelling.....	26
1.5.1 Plant Structural Modelling.....	26
1.5.2 Light Modelling.....	29
1.5.3 Plant Process Modelling: empirical versus mechanistic....	31
1.6 Knowledge Gaps.....	33
Aims and Objectives.....	34
Hypotheses.....	34
Thesis Layout.....	35
Chapter 2: Core Methods and Method Development	36
2.1 The Reconstruction Process.....	36
2.1.1 Imaging.....	38
Canopy Imaging: Imaging <i>in situ</i>	38
Single Plant Imaging.....	38
2.1.2 Reconstructions.....	39
2.1.2.1 Point Cloud Reconstruction.....	40

2.1.2.2 Surface Estimation.....	41
2.1.2.3 Canopy Formation.....	47
2.2 Reconstruction Method Development.....	49
2.2.1 Reconstruction Optimisation.....	49
2.2.2 Optimisation on the Artificial Dataset.....	50
2.3 The Canopy Light Environment: Ray Tracing.....	57
PART I: THE EFFECT OF CROP CHOICE AND AGRONOMIC PRACTICES ON CANOPY PHOTOSYNTHESIS.....	59
Chapter 3: Methods for exploring the light environment within multi-species cropping systems (intercropping).....	61
Paper Details.....	61
Abstract.....	62
Introduction.....	63
Materials and Methods.....	69
Plant Material.....	69
Imaging and Ray Tracing.....	69
Gas Exchange.....	71
Ceptometer.....	72
Statistics.....	72
Modelling.....	72
Results.....	75
Validation of imaging and modelling.....	75
The Light Environment.....	76
Assessing Productivity.....	80
Discussion.....	84
High-resolution digital reconstruction as a method to explore the intercrop light environment.....	84
Studying light interception in heterogeneous canopies.....	90
Designing the optimal intercropping system.....	92
Concluding remarks.....	94
Supplementary Material.....	96
Chapter 4: The relationship between canopy architecture and photosynthesis.....	102
Paper Details.....	102
Abstract.....	103
Introduction.....	104

Materials and Methods.....	107
Plant Material and Growth.....	107
Physiological Measurements.....	108
Imaging and Ray Tracing.....	108
Gas Exchange.....	109
Statistical Analysis.....	110
Modelling.....	110
Results.....	114
Architectural Features.....	114
Light Environment	118
Photosynthesis.....	120
Discussion.....	126
The relationship between canopy architecture and photosynthesis.....	127
Supplementary Material.....	133
Chapter 5: The effect of wind-induced movement on light patterning and photosynthesis.....	138
Paper Details.....	139
Abstract.....	139
Introduction.....	140
Materials and Methods.....	144
Growth of rice plants.....	144
3D Reconstruction and Modelling.....	144
Results.....	148
Constant Displacement.....	148
Dynamic Displacement.....	152
Discussion.....	156
Mechanical canopy excitation: a means to manipulate photosynthesis?	157
The technology required for simulating the 4-dimensional canopy.....	160
Supplementary Material.....	165
Chapter 6: The effect of nitrogen on rice growth, development and photosynthesis.....	166
Paper Details.....	167
Abstract.....	167

Introduction.....	168
Nitrogen, canopy architecture and photosynthesis.....	169
Materials and Methods.....	173
Plant Material and Experimental Design.....	173
Physiological Measurements.....	173
Reconstruction and Ray Tracing.....	174
Gas Exchange.....	175
Statistical Analysis.....	176
Modelling.....	176
Results.....	179
Physiological Measurements.....	179
Photosynthesis.....	187
Discussion.....	191
Use of modelling approaches within nutrient or stress studies...	191
The effect of N availability on crop physiology.....	193
Concluding Remarks.....	196
Supplementary Material.....	197
PART II: THE EFFECT OF VARIABLE LIGHT ON	
PHOTOSYNTHETIC PROCESSES	202
Chapter 7: Modelling the effect of photoinhibition in a wheat canopy.....	204
Paper Details.....	205
Abstract.....	205
Introduction.....	206
Materials and Methods.....	210
Plant Material.....	210
Imaging and Ray Tracing.....	211
Leaf angle, dry weight and leaf area measurements.....	212
Field Data: Gas Exchange and Fluorescence.....	212
cLAI and the light extinction coefficient.....	213
Model Set Up.....	214
Results.....	219
The light environment in a leaf canopy.....	219
Incorporating physiological measurements into the	
Photoinhibition Model.....	225
Effect of photoinhibition on carbon gain: model output.....	228
Discussion.....	233

High-Resolution digital reconstruction of field-grown plants as a unique tool.....	233
Accounting for carbon loss at the whole-canopy level.....	235
Managing and mitigating photoinhibition.....	237
Conclusion.....	239
Supplementary Material.....	240
Chapter 8: Modelling the effect dynamic acclimation on photosynthesis.....	248
Paper Details.....	248
Abstract.....	249
Introduction.....	250
Materials and Methods.....	255
Theoretical Framework.....	255
Experimental Data.....	256
Model Parameterisation.....	257
Results.....	259
Quasi-steady net photosynthetic rate.....	259
Light pattern: alternation between two light levels.....	261
Influence of the light intensity switching period.....	263
Fluctuating light.....	264
Comparison with experimental data.....	265
Discussion.....	267
Conclusion.....	271
Supplementary Material.....	272
Chapter 9: The effect of fluctuating light on acclimation in <i>Arabidopsis</i> <i>thaliana</i>.....	274
Paper Details.....	274
Abstract.....	275
Introduction.....	276
Materials and Methods.....	280
Plant Growth.....	280
Physiological Measurements.....	281
Gas Exchange.....	282
Statistical Analysis.....	283
Curve fitting and Modelling.....	284
Results.....	286
Growth.....	286

Light response curves.....	286
Chlorophyll Assays.....	288
Response of Photosynthesis to a change in irradiance.....	290
Acclimation Model.....	292
Discussion.....	295
Supplementary Material.....	300
Chapter 10: Whole Canopy Acclimation.....	304
Paper Details.....	304
Abstract.....	305
Introduction.....	306
Materials and Methods.....	310
Experimental and Modelling Strategy.....	310
Plant Material.....	310
Plant Physical Measurements.....	310
Imaging and Ray Tracing.....	311
Gas Exchange and Fluorescence.....	312
Rubisco Quantification.....	313
Modelling.....	314
Results.....	317
The Canopy Light Environment.....	317
Effect of Light Levels on Acclimation: Model Output.....	323
Discussion.....	332
Influence of canopy architecture on acclimation.....	332
Implications in terms of nutrient budgeting.....	335
Concluding Remarks.....	337
Supplementary Material.....	338
Chapter 11: Discussion.....	342
Limitations to work presented in this thesis.....	344
11.1 Improving Agricultural Productivity.....	345
The Yield Gap.....	345
11.1.1 Targets for Improvement arising from this thesis.....	347
Creation of site and situation specific cultivars.....	347
11.1.2 Genetic Improvement of Crop Plants.....	349
11.1.2.1 Genetic manipulation of canopy architecture...	349
11.1.2.2 Genetic manipulation of plant processes.....	351

11.1.3 Underutilised Crops.....	356
11.1.4 Cropping Systems and Management Practices.....	356
Sustainability.....	357
Resilience.....	358
11.2 The use of plant reconstruction and modelling techniques in studies of crop processes and productivity.....	359
Applicability of techniques for other situations.....	360
Applicability of techniques for use in developing countries.....	361
11.2.1 Problems with modelling methods.....	362
11.2.2 Improvements to the reconstruction and modelling techniques.....	364
Improvements to the reconstruction technique.....	364
Improvements to the modelling technique.....	365
11.3 The Future of Canopy Research.....	367
11.4 Concluding Remarks.....	368
REFERENCES.....	369
APPENDICES.....	424
Appendix I.....	425
Ray Tracing Details and Command Line.....	425

List of Figures

Figure	Legend	Page No.
Chapter 1		
1.1	<i>Example light response curves as denoted by the non-rectangular hyperbola indicating the shaping parameters.</i>	4
1.2	<i>Example light response curves from a C₃ versus C₄ leaf.</i>	6
1.3	<i>Example light response curves from a sunlit versus shaded leaf.</i>	9
1.4	<i>Example light response curves from uninhibited versus a photoinhibited leaf.</i>	11
1.5	<i>Example light response curves of a population of photosynthetic cells (i.e. a leaf or a whole canopy).</i>	13
1.6	<i>Fractional interception for a horizontal versus an erect canopy and their optimal LAI.</i>	17
1.7	<i>The effect of leaf dispersion and leaf area index on light transmission.</i>	19
1.8	<i>Exponential decay of light through a horizontal versus an erect canopy.</i>	21
1.9	<i>The determinants of canopy productivity.</i>	24
1.10	<i>The effect of leaf angle and canopy structure on photosynthesis with relation to the light response curve.</i>	25
1.11	<i>Overview of plant modelling approaches.</i>	28
1.12	<i>Hierarchical classification scheme of different modelling techniques based on the system being modelled, timeframe, modelling method data source and resolution.</i>	32
1.13	<i>Types of models, data requirements and their approximate running times.</i>	32
Chapter 2		
2.1	<i>Flow diagram showing the general overview of the stages of plant modelling used within this thesis</i>	37
2.2	<i>Set up of the imaging studio for single plant imaging.</i>	39
2.3	<i>Output of VisualSFM indicating the automatically calculated camera positions and corresponding photographs surrounding the target plant</i>	40
2.4	<i>The effect of altered threshold settings (parameters in VisualSFM) on the output point clouds of the same rice plant</i>	41

2.5	<i>Segmentation of a point cloud into clusters.</i>	42
2.6	<i>The effect of altered parameters (given in Table 2.1) on the resulting output mesh of a given section of leaf.</i>	45
2.7	<i>Overview of the imaging process for different crops (A) Wheat, (B) Proso Millet, (C, D) Bambara Groundnut (50 DAS, 80 DAS respectively).</i>	46
2.8	<i>Example of a fully reconstructed intercrop canopy of Proso millet and Bambara groundnut with a 3:1 orientation.</i>	48
2.9	<i>Effect of altered boundary sample rate on the output mesh.</i>	49
2.10	<i>Source of light rays in fastTracer3.</i>	57
2.11	<i>Simulated light components (from fastTracer3) over the course of the day for a single point within a canopy.</i>	58
<hr/>		
Chapter 3		
3.1	<i>Theoretical example of light transmission through a monocropped canopy versus an intercrop canopy.</i>	65
3.2	<i>Validation of light interception in a sole Bambara Groundnut canopy.</i>	75
3.3	<i>Representative reconstructed canopies with the maximum PPFD ranges colour coded for 12:00 h.</i>	77
3.4	<i>Frequency of PPFD values according to the fraction of surface area received at the top layer within each canopy.</i>	78
3.5	<i>Modelled total canopy light interception over the course of the day for different intercrop treatments and respected sole crops.</i>	79
3.6	<i>Example light response curves.</i>	81
3.7	<i>Modelled predicted carbon gain over the course of the day for different intercrop treatments and respected sole crops.</i>	83
3.8	<i>Reconstruction time course of a 3:1 (Bambara groundnut: Proso millet) intercrop canopy development.</i>	89
<hr/>		
S3.1	<i>Photograph of the 2:2 (Bambara groundnut: Proso millet) intercrop treatment in the FutureCrop Glasshouse facilities, University of Nottingham, Sutton Bonington Campus, UK.</i>	96
S3.2	<i>Example overview of the Reconstruction Process.</i>	97
S3.3	<i>Example of a full Intercrop Canopy Reconstruction; 3:1 Row layout.</i>	98
S3.4	<i>The relationship between LAI and total PPFD per unit leaf surface area along a row.</i>	99

S3.5	<i>Component contribution to leaf area index (LAI) and total intercepted photosynthetic photon flux density (PPFD).</i>	100
S3.6	<i>Frequency of light levels as a function of the fraction of the total surface area of the canopy received at 1200 h by the different treatments.</i>	101
<hr/>		
Chapter 4		
<hr/>		
4.1	<i>Plant height over the course of the experiment, calculated as the average of 5 measurements per plot.</i>	116
4.2	<i>Modelled cLAI, the area of leaf material (or mesh area) per unit ground as a function of depth through the canopy.</i>	117
4.3	<i>Modelled leaf inclination angles throughout depth in the canopy.</i>	118
4.4	<i>Modelled fractional interception as a function of depth in the canopy at 12:00 h.</i>	119
4.5	<i>Whole canopy acclimation model output.</i>	124
<hr/>		
S4.1	<i>Example of a time-weighted light pattern at $\tau=0.2$ relative to a non-weighted line.</i>	137
<hr/>		
Chapter 5		
<hr/>		
5.1	<i>Overview of solid body rotation distortion method.</i>	145
5.2	<i>Changing light patterns due to simulated Easterly wind.</i>	148
5.3	<i>Frequency of PPFD values according to the fraction of surface area received at by the central plant in the canopy.</i>	151
5.4	<i>Angle distribution relative to vertical.</i>	152
5.5	<i>Changes as a result of dynamic movement at three time points throughout the day.</i>	155
<hr/>		
S5.1	<i>Movie: Change in overall canopy light distribution due to an Easterly wind at 12:00 h between 0-10° distortion.</i>	165
S5.2	<i>Light response curves used to calculate canopy carbon gain.</i>	165
<hr/>		
Chapter 6		
<hr/>		
6.1	<i>Whole canopy reconstruction developmental timecourse.</i>	180
6.2	<i>Physiological Measurements of individual lines.</i>	181
6.3	<i>Depth distributions of leaf material and light interception.</i>	185
6.4	<i>Averaged light as a fraction of surface area in the top third of each canopy at 12:00 h.</i>	186
6.5	<i>(A) Change in SPAD over time. (B) Chlorophyll content analysis</i>	187
6.6	<i>Modelled predicted carbon gain per unit leaf and ground area for each growth stage.</i>	189
<hr/>		

S6.1	<i>Change in rice production in South East Asia versus Malaysia.</i>	199
S6.2	<i>Trends in Nitrogen fertiliser production, import, export and consumption dynamics in Malaysia.</i>	199
S6.3	<i>Distance between major veins in each of the treatments.</i>	200
S6.4	<i>Depth distributions of leaf material and light interception for all growth stages.</i>	201
<hr/>		
Chapter 7		
7.1	<i>Stages of the reconstruction of a single plant from multiple color images.</i>	220
7.2	<i>Wheat canopy reconstructions.</i>	221
7.3	<i>Properties of each canopy.</i>	222
7.4	<i>Diagrams depicting the heterogeneity of light environment of the three contrasting wheat canopies.</i>	223
7.5	<i>Experimental validation of the predicted light levels.</i>	224
7.6	<i>Simplified overview of the modeling method.</i>	225
7.7	<i>Data used for the parameterisation of the photoinhibition model.</i>	226
7.8	<i>Results of the model: the predicted effect of photoinhibition on carbon gain</i>	229
7.9	<i>Graph indicating the frequency of light levels received at midday</i>	232
<hr/>		
S7.1	<i>Angle distributions within the canopy</i>	240
S7.2	<i>Values of the maximum photosynthetic capacity for each layer were obtained from fitted Light Response Curves.</i>	241
S7.3	<i>Changes in scaling factor over the course of the day for the top and middle layers.</i>	242
S7.4	<i>Fractional interception as a function of cumulative LAI.</i>	243
S7.5	<i>Frequency of PPFD values according to the fraction of surface area received at the top layer at different times during day.</i>	233
<hr/>		
Chapter 8		
8.1	<i>Net photosynthetic rate as a function of PPFD (light intensity L) and P_{max}.</i>	260
8.2	<i>Photosynthetic acclimation under alternation between two light levels.</i>	262
8.3	<i>Influence of the light switching period, S, and time-weighted average timescale, τ, on P_{max}^{opt}</i>	263
8.4	<i>Predicted P_{max} as a function of τ for a typical diurnal variation in PPFD.</i>	265

8.5	<i>Comparing model predictions with experimental data.</i>	266
S8.1	<i>(A) Quasi-steady net photosynthetic rate model. (B) Analysis of light intensity regime under alternation between two light levels. (C) Small amplitude light fluctuations.</i>	272
Chapter 9		
9.1	<i>Light patterns used for the analysis of dynamic acclimation in Arabidopsis thaliana.</i>	281
9.2	<i>Rosette area timecourse.</i>	287
9.3	<i>Light response curves for plants grown under constant light versus fluctuating light.</i>	288
9.4	<i>Chlorophyll analysis of plants.</i>	289
9.5	<i>Response of Photosynthesis to light level in the days following a change in the light pattern.</i>	291
9.6	<i>Acclimation Model output.</i>	294
S9.1	<i>Normalised response photosynthesis to a change in irradiance in the days following a change in the light pattern.</i>	300
S9.2	<i>Light motif taken from the fluctuating light pattern.</i>	301
S9.3	<i>Example of a time-weighted light pattern at $\tau=0.3$ relative to a non-weighted line (i.e. $\tau=0$).</i>	301
Chapter 10		
10.1	<i>Overview of the Reconstruction Process.</i>	317
10.2	<i>Example Canopy Reconstructions from front and top down views.</i>	318
10.3	<i>Progressive lowering of the canopy position in a canopy.</i>	321
10.4	<i>Experimental validation of the predicted light levels.</i>	322
10.5	<i>Fitted Light response curves.</i>	323
10.6	<i>Whole canopy acclimation model output versus gas exchange measurements.</i>	325
10.7	<i>Relationships between photosynthesis and Rubisco properties.</i>	331
S10.1	<i>Diurnal Dynamics of Fv/Fm over the whole day.</i>	338
S10.2	<i>Example of a time-weighted light pattern at $\tau=0.3$ relative to a non-weighted line (i.e. $\tau=0$).</i>	339
S10.3	<i>Model output versus gas exchange measurements.</i>	340
S10.4	<i>Whole canopy acclimation model output versus gas exchange measurements.</i>	341

List of Tables

Table	Legend	Page No.
Chapter 2		
2.1	<i>Details and default values of parameters in the Reconstructor software.</i>	43
2.2	<i>Simulated reconstruction features in terms of the parameters used with outputs of the total number of triangles, mesh area and difference relative to the ground truth model.</i>	52
2.3	<i>Simulated reconstruction features in terms of the parameters used with outputs of the Hausdorff distance between each mesh, true Hausdorff distance and the resulting percentage difference relative to the ground truth model.</i>	55
Chapter 3		
3.1	<i>Total leaf area index (LAI) for each of the treatments.</i>	80
Chapter 4		
4.1	<i>Canopy reconstructions and description.</i>	115
4.2	<i>Parameters taken from ACi curve fitting.</i>	120
4.3	<i>Chlorophyll content and ratio at GS2 (85 DAT).</i>	121
4.4	<i>Maximum quantum yield of PSII (Fv/Fm) measured after 20 minutes dark adaptation.</i>	121
4.5	<i>Gas exchange and modelling results at each growth stage.</i>	123
4.6	<i>The relationship between canopy architectural traits and photosynthesis.</i>	127
S4.1	<i>Agronomic details on the 16 Parental Lines used to develop the indica and japonica MAGIC Populations.</i>	133
S4.2	<i>Physiological characteristics of the 15 parental MAGIC lines + IR64 used in the initial screening.</i>	135
Chapter 5		
5.1	<i>Daily carbon gain per unit leaf area and total canopy light interception for each of the simulated wind directions.</i>	150
Chapter 6		

6.1	<i>Plant Height at each of the studied growth stages.</i>	182
6.2	<i>Dry weight measurements.</i>	183
6.3	<i>Pmax values taken from fitted LRCs at GS5.</i>	188
6.4	<i>Parameters taken from ACi curve fitting.</i>	190
<hr/>		
S6.1	<i>Stomatal Physiology.</i>	197
S6.2	<i>Pmax values taken from fitted LRCs, used to calculate canopy carbon gain.</i>	197
S6.3	<i>Canopy K Values</i>	198
<hr/>		
Chapter 7		
<hr/>		
S7.1	<i>Leaf angle for measured versus reconstructed canopies.</i>	245
S7.2	<i>Reconstruction and Canopy Details.</i>	245
S7.3	<i>Leaf versus stem area for measured and reconstructed canopies.</i>	245
S7.4	<i>Symbol Definitions</i>	246
<hr/>		
Chapter 8		
<hr/>		
8.1	<i>Symbol definitions</i>	258
<hr/>		
Chapter 9		
<hr/>		
S9.1	<i>Normalised photosynthesis at stages 1-4 and 6 and the time taken to achieve a normalised photosynthesis.</i>	302
<hr/>		
Chapter 10		
<hr/>		
10.1	<i>Physical canopy measurements of each Line.</i>	319
10.2	<i>Plant and canopy area properties.</i>	320
10.3	<i>Parameters taken from curve fitting.</i>	327
10.4	<i>Rubisco, total soluble protein and chlorophyll content plus chlorophyll a:b and Rubisco: chlorophyll ratios with each layer through the canopy at the postanthesis stage.</i>	330
<hr/>		

Chapter 1: Introduction

1.1 Research Context

With an expanding population, conflicting demands for land use and uncertain consequences of future climate change, pressure is placed upon both stabilising and improving crop yield. This is confounded by the need to also find alternative sources of energy, particularly if these new sources compete with food production (i.e. growth of crops solely for biofuels as opposed to consumption/multi-use). With few opportunities to increase the amount of cropland available for cultivation worldwide, any such improvements will hinge upon increasing the productivity of our existing cropping systems (Pinstrup-Andersen & Pandya-Lorch, 1994; Moore, 2007; Zhu *et al.*, 2008). However, studies indicate that both management- and genetic-based improvements are not increasing yields sufficiently to keep up with demand in several different regions of the globe (Peltonen-Sainio *et al.*, 2009; Finger, 2010; Gouache *et al.*, 2010; Ray *et al.*, 2012; 2013). By 2050, global agricultural production requires an increase of 60-110% (FAO, 2009; Tilman *et al.*, 2011); a target exacerbated by the need to provide food security for the approximately 795 million people thought to be chronically undernourished (FAO, 2015). Therefore any future improvements will require a concerted effort (both political and scientific) in order to meet demand.

The ability to generate high levels of biomass in a diverse range of agroecological environments will be an important feature and will be necessary to underpin the required yield increases of both food and energy crops. There are a number of lines of evidence to suggest that biomass production is below the theoretical optimum in crop systems (e.g. Ainsworth & Long, 2005; Lobell *et al.*, 2009; Godfray *et al.*, 2010; Wang *et al.*, 2012), which may be both due to lack of adaptation (i.e. genetic) and environmental constraints. The harvest index (HI: the ratio of grain to above ground dry matter) of our staple crop species is reaching an upper limit (e.g. Shearman *et al.*, 2005; Lorenz *et al.*,

2010) thus future increases in biomass and grain yield will come from an increased in total above ground dry matter (AGDM). This will require improved cropping practices, improved crop species and varietal selection (including emphasis on new, so called “underutilised” crops), matching crops to their growing conditions, and optimisation of agronomic practices.

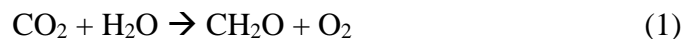
The relationship between biomass production and radiation interception suggests one method through which we are able to improve crop yield. Under optimal growing conditions, biomass production is determined by the amount of light intercepted and the efficiency with which this is converted into dry matter. For most crops, in the absence of biotic and abiotic stress, the amount of dry matter accumulated is linearly related to the amount of photosynthetically active radiation (PAR) intercepted by green leaf area (Cooper, 1970; Monteith & Moss, 1977). Furthermore, due to the non-linear response of leaf photosynthesis to light, near maximum photosynthetic rates can be achieved at less than 100% maximal sunlight intensity (Hesketh & Musgrave, 1962; Mock & Pearce, 1975). For example, exposing maize leaves to 50% of maximal sunlight available is sufficient to achieve 80% of the maximal photosynthetic rate and even greater values can be seen in C₃ plants (e.g. soybean, cotton, alfalfa and tree species; see Fig. 1 in Mock & Pearce, 1975). Thus two different routes for improvement are possible: maximising the amount of light intercepted or maximising the efficiency with which light energy can be converted into biomass.

Optimising canopy structure provides a method by which we can improve and optimise both radiation interception and also the distribution of light among canopy layers that contribute to net photosynthesis. This requires knowledge of how canopy structure determines light distribution and therefore photosynthetic capacity of a given crop species. Canopy structure refers to the amount and organization of above ground plant organs; including size, shape and orientation (Norman & Campbell, 1989). There is a great diversity in canopy structure across species (Duncan, 1971; Norman, 1980), with each plant community containing a unique spatial pattern of photosynthetic surfaces,

partly as a result of plasticity (Nobel *et al.*, 1993). Plant architecture is the key determinant of the microenvironment surrounding the leaves. This includes factors such as radiant flux density, air, soil and leaf temperature, air vapour pressure, soil heat storage, wind speed and interception of precipitation (Ross, 1981; Norman & Campbell, 1989; Nobel, 1991). Therefore knowledge of how canopy structure influences resource capture and plant metabolism is key to understanding energy flux between plants and their environment.

1.2 Photosynthesis and Biomass production

To reach our goal of doubling productivity of agricultural systems we must establish the maximum efficiency of photosynthesis (Zhu *et al.*, 2008). Photosynthesis is the process by which plants use solar energy in order to create dry matter. Green plants use external resources, predominantly light, water, CO₂ and nutrients, to drive the production of biomass. The chemical pathway involves the conversion of water and atmospheric CO₂ into carbohydrates and water in the presence of sunlight (Eq 1).



The efficiency of photosynthesis under a certain set of conditions will depend upon the absorption of photons by the plant, the transfer of this energy to reaction centres and its final use in carbon assimilation (Eq 1). Four aspects of light are important for driving photosynthesis and controlling plant growth and development: irradiance, duration, quality and timing (Geiger, 1994). Irradiance determines the rate at which energy is delivered to the reaction centres; duration influences the total energy received during a given period; spectral quality influences the ability to drive carbon sequestration due to the probabilities of absorbing different wavelengths; and timing determines the effectiveness of light in the regulation of various plant processes according to plant development, for example; source – sink effects. PAR refers to the spectral range of solar radiation that can be used by plants; between 400 and 700 nm. This is usually quantified as $\mu\text{mol photons m}^{-2} \text{ s}^{-1}$ and often referred to as the photosynthetic photon flux density; or PPFD, with a quantum of light

called a photon. Photons are absorbed by pigment molecules (such as chlorophyll) and the light energy is converted into chemical energy in the form of carbohydrates. The PPFD at each section of leaf, and the total amount of PPFD intercepted, are the key determinants of the rate of CO₂ assimilation; and thus of whole plant photosynthesis (Duncan, 1971; Norman, 1980).

Leaf photosynthesis responds non-linearly to light intensity. Under highly heterogeneous light environments, light intensities will vary from limited to excessive depending on the shape of light response curve. The light response curve may be described by a non-rectangular hyperbola (Eq 2).

$$P(L, \phi, \theta, P_{max}, \alpha) = \frac{\phi L + (1 + \alpha)P_{max} - \sqrt{(\phi L + (1 + \alpha)P_{max})^2 - 4\theta\phi L(1 + \alpha)P_{max}}}{2\theta} - \alpha P_{max} \quad (2)$$

The curve relates net photosynthetic rate, P , to PPFD, L . In the absence of light, net photosynthesis will be negative and relate to a dark respiration rate, R_D . It is assumed that the rate of dark respiration is proportional to the maximum photosynthetic according to the relationship $R_D = \alpha P_{max}$. The light response curve can be characterised by three shaping parameters: quantum yield (ϕ), convexity (θ) and maximum photosynthetic capacity (P_{max}). The quantum yield refers to the initial linear portion of the curve and describes the maximum efficiency with which light can be used to fix carbon whilst the convexity, or bending factor, describes the curvature. The net photosynthesis rate (P) rises until it reaches a maximum: the maximum photosynthetic capacity (P_{max}). The value at which photosynthesis matches respiration (where net carbon assimilation is equal to zero) is known as the light compensation point. An example light response curve indicating each of the parameters is given in Figure 1.1.

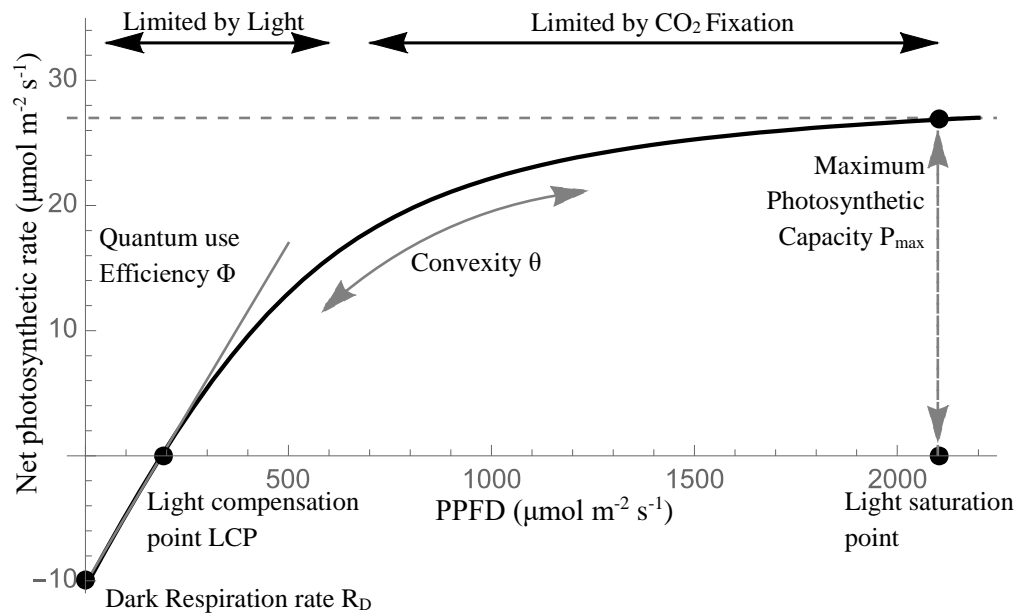


Figure 1.1: Example light response curves as denoted by the non-rectangular hyperbola indicating the shaping parameters.

The shape of the light response curve, and thus the values of the shaping parameters, will depend upon the biochemical pathway employed (i.e. C_3/C_4) the light absorption properties of the leaf, the relative concentration of the structures involved in light harvesting and the current status of the leaf (Adamson *et al.*, 1991; Chow *et al.*, 1991; Murchie & Horton, 1997; Retkute *et al.*, 2015). There are a number of different processes and pathways that can influence this shape.

The underlying biochemical pathway used to assimilate CO_2 can also determine the productivity of the plant and thus the shape of the light response curve. CO_2 can be reduced to carbohydrates via two different carboxylation pathways. In C_3 plants, the Calvin cycle reduces CO_2 initially into a 3-carbon compound whereas in C_4 plants a 4-carbon compound is first produced before entering the Calvin cycle. Differences between the two modes of photosynthesis extend from the biochemical to higher levels of organisation including structural differences such as the cellular organisation in C_4 plants known as “Kranz anatomy”, used to compartmentalise the pathway and concentrate CO_2 (Sage & Monson, 1999). These different mechanisms of

carboxylation can lead to different photosynthetic productivities. Because C_4 plants contain this mechanism for concentrating CO_2 within leaves, photorespiration (the alternative reaction catalysed by Rubisco using O_2) is effectively eliminated, as oxygen is unable to compete with CO_2 for the active binding site of Rubisco. This enables C_4 plants to have a higher efficiency than C_3 plants (Gowik & Westhoff, 2011). As well as the biochemical and structural differences between C_3 and C_4 plants, they also differ in their response to external stimuli including rising CO_2 levels, temperature and light (Still *et al.*, 2003). Example light response curves from a C_3 versus a C_4 plant is given in Figure 1.2.

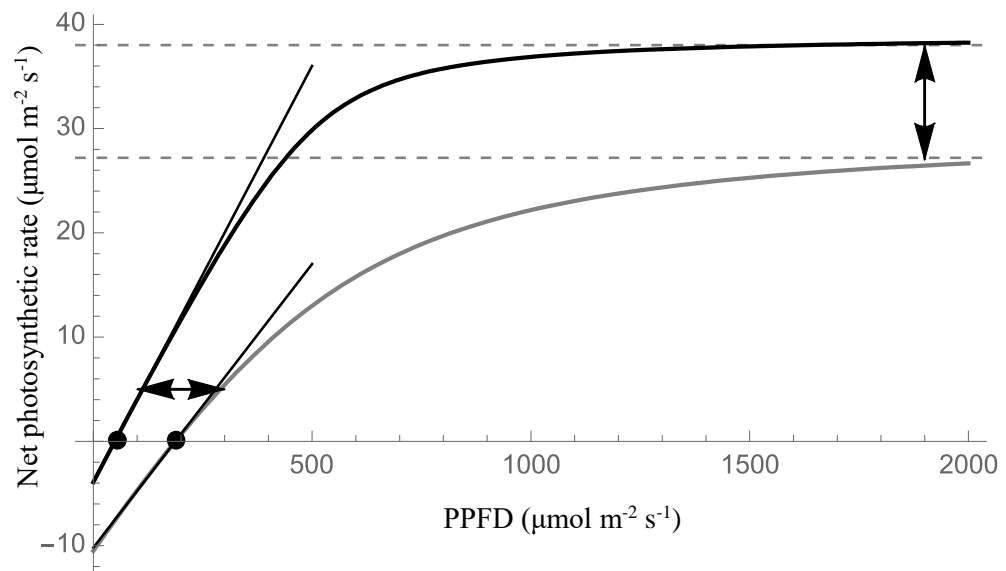


Figure 1.2: Example light response curves from a C_3 (grey line) versus C_4 (black line) leaf. Arrows denote the differences in the light compensation point and P_{max} .

Due to the inherent differences in their photosynthesis and associated water- and nutrient-use efficiencies (WUE and NUE), the advantages of C_4 photosynthesis over C_3 are maximal under high temperatures, high light intensities and limited water (Ehleringer & Bjorkman, 1977). As such, C_3 crops are located in most temperate regions whilst C_4 plants are typically found in tropical or semi-tropical habitats, often with high light and temperature conditions and often drought. C_3 species include temperate crops, root crops,

tropical legumes and trees whereas C₄ crops include most tropical cereals and grasses (Azam-Ali & Squire, 2002).

The shape of the light response curve is not fixed, but rather can change as a result of the environmental conditions to which the plant is exposed. The sessile lifestyle of plants necessitates a sophisticated acclimation mechanism to optimise resource capture in a changing environment (Dietzel & Pfannschmidt, 2008). Such mechanisms occur over different time scales to enable plants to adapt to and cope with the variations of light experienced in the natural world; both in terms of light intensity and of spectral quality (Niinemets & Anten, 2009). As the most variable environmental driver light imposes a two-fold challenge; the need to efficiently utilise as many photons as possible whilst simultaneously preventing harm caused by excess radiation. Achieving the optimal balance between these two states is critical to maximise both productivity and mitigate radiation-induced damage (Demmig-Adams *et al.*, 2012).

Two such mechanisms that enable plants to respond to changes in light are acclimation and photoprotection. Acclimation refers to a long term (days) change in the composition and organization of photosynthetic apparatus and leaf morphology (Walters, 2005). Acclimation can be broadly split into two different mechanisms: developmental acclimation and dynamic acclimation. Developmental acclimation refers to changes occurring during leaf development which are largely irreversible whereas dynamic acclimation is the ability for fully developed leaves to change their photosynthetic capacity (Minorsky, 2010). Dynamic acclimation is plastic, fluctuating over timescales of hours to days (Murchie & Horton, 1997). Photoprotection is usually a short-lived process describing the pathways and mechanisms that regulate the absorption and dissipation of light energy which is especially important when chlorophyll absorbs more energy than can be used in photosynthesis (Murchie & Niyogi, 2011). These mechanisms are an integral part of photosynthetic regulation and there is emerging evidence that any alterations to these processes may impact upon the ability of a plant to assimilate carbon over long

periods of time; thus affecting biomass production (Külheim *et al.*, 2002; Athanasiou *et al.*, 2010; Murchie & Niyogi, 2011). Such differences in leaf properties are part of a set of integrated mechanisms including biomass partitioning and night-time respiration (Sims & Pearcy, 1994) and their impact can be seen through changes to the light response curve.

Any given acclimation state of a leaf is defined by the maximum photosynthetic capacity (P_{max}) value as well as dark respiration (R_D) (see Fig. 1.1). There is substantial variation between species in their ability to acclimate, with plants from semi-shaded environments exhibiting the greatest plasticity in acclimation capacity (Murchie & Horton, 1997). This suggests that there are both benefits and costs associated with acclimation. At the whole canopy level, the ability for individual plant leaves to acclimate is also dependent upon leaf age and availability of nutrients (Field, 1981; Pons *et al.*, 2001; Murchie *et al.*, 2002; 2005; Hikosaka, 2005). This inherent plasticity enables foliage photosynthetic potentials to increase with an increasing light availability (e.g. Hirose & Werger, 1987; Thornley, 2004; Johnson *et al.*, 2010). Depending upon the species, photosynthetic capacity can vary between two- and 20-fold from the canopy top to bottom.

One of the simplest examples of acclimation within a spatial scale can be seen in the anatomical and physiological differences between sun and shade leaves, and is a key example of developmental acclimation. Sun leaves differ from shade leaves primarily in their higher light-saturated rates of photosynthesis (P_{max}) (Lambers *et al.*, 2008) and higher dark respiration (R_D) rates (Figure 1.3). Differences in anatomy, which are determined early in development and are largely irreversible, can constrain the potential of leaves to acclimate further (dynamically acclimate) (Murchie *et al.*, 2005). Sun leaves are generally thicker, with differing cellular structure, providing more space for photosynthetic components per unit leaf area, and have thicker palisade parenchyma. Contrary to this, shade leaves are often thinner with a greater surface area, requiring less investment in terms of nitrogen and carbon. Further differences can be seen in the biochemical properties of the two types of

leaves; sun leaves contain a greater chlorophyll a: chlorophyll b ratio, larger amounts of Calvin-cycle enzymes, and more components of the electron transport chain (including b₆f cytochromes and ATPase). For some plants, the change in P_{max} between different acclimation states shows an almost linear relationship to an increase in the amount of photosynthetic compounds (Evans & Seemann, 1989), thus investment in compounds that determine photosynthetic capacity translates to higher photosynthetic rate at increased irradiance levels (e.g Anderson., 1995; Evans & Poorter, 2001; Murchie *et al.*, 2002; Walters, 2005). These differences help sun leaves to exploit high irradiances more efficiently. Their ability to regenerate more ATP and NADPH to alleviate the over-reduction of PSII reaction centres at high PPFD helps to minimise their risk of photoinhibition (Chow, 1994; Baker & Oxborough, 2004).

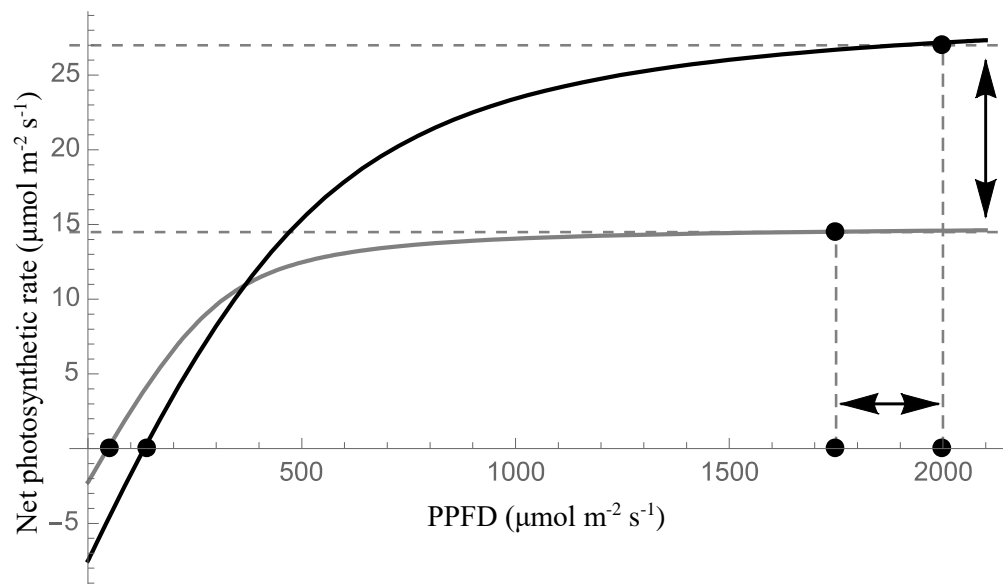


Figure 1.3: Example light response curves from a sunlit (high-light acclimated; black line) versus shaded (low-light acclimated; grey line) leaf.

The ability of preexisting foliage to dynamically acclimate requires a transition from high photosynthetic capacity under high irradiances to high light efficiency under low irradiances and vice versa (Hikosaka & Terashima, 1995). Such a transformation will alter both the total carbon assimilation and the susceptibility to photoinhibition (Baker & Oxborough, 2004). Acclimation to an increased irradiance can include adjustments in both physiological and morphological traits to achieve an increase in amounts of photosynthetic

components per unit area. The extent of these changes will depend on whether the increase in irradiance occurs before or after leaf development becomes fixed (i.e. before or after leaf expansion) (Turnball *et al.*, 1993; Murchie *et al.*, 2005). Contrary to biochemical changes, morphological features are largely irreversible (Eschrich *et al.*, 1989; Sims & Pearcy, 1992). This may limit complete acclimation to the light environment in some cases (Oguchi *et al.*, 2005; 2003; Tognetti *et al.*, 1998). This is of relevance because the ability of mature leaves to acclimate to changes in irradiances is generally limited to existing chloroplasts and cells and, coupled with gene expression data, requires modification of an existing protein profile.

The resulting effect of acclimation is highly dependent upon the light environment in which the plant is grown. Whilst it is relatively well understood how a plant responds to a change from low to high growth irradiance, or vice versa, response to fluctuating light is less well understood. Furthermore, understanding the response of a collection of photosynthetic cells (i.e. a whole leaf or the whole canopy), is even more complex. The final response will also be dependent upon species or varietal selection, with evidence for species-specific differences in the relative durations of cellular division and expansion during leaf development (Van Volkenburgh, 1999; Stiles & Van Volkenburgh, 2002) and biochemical differences i.e. in chlorophyll contents and ratios, Rubisco amounts, electron transport capacity or enzyme activity (Evans, 1989; Murchie & Horton, 1997; Carmo-Silva & Salvucci, 2013; Carmo-Silva *et al.*, 2015; Orr *et al.*, 2016).

As growth irradiance increases, absorbed photons may become in excess if they are produced quicker than they can be used in photosynthesis (Murchie & Niyogi, 2011). Due to the sensitivity of PSII, high light levels may lead to damage to the photosynthetic apparatus, for example through the production of reactive oxygen species, resulting in a sustained decrease in quantum yield. Plants have an ability to regulate the amount of light they intercept through changes in leaf area, leaf angle (see section 1.3.1) or chloroplast movement, or on a molecular level, through acclimatory adjustments in LHC antenna size

(state transitions). However, if excess energy has been absorbed, it can be dissipated via a number of different routes, broadly termed photoprotection. The effect of photoinhibition on shaping parameters of the photosynthesis light response curve is already well characterised (Figure 1.4). The primary effect of photoinhibition is the reduction in Φ , which is important under low light conditions (Powles, 1984; Björkman and Demmig, 1987; Krause and Weis, 1991). However under conditions causing photoinhibition, a reduction in Φ is often accompanied by a similar reduction in θ (Ögren and Sjöström, 1990; Leverenz, 1994).

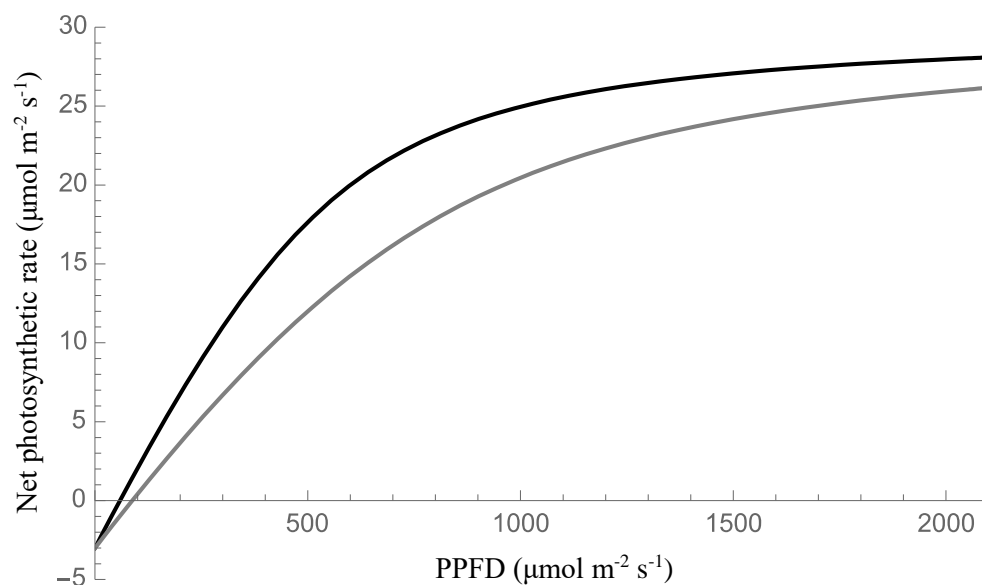


Figure 1.4: Example light response curves from uninhibited (black line) versus a photoinhibited (grey line) leaf.

Both acclimation and photoprotection represent a subset of regulatory mechanisms used in order to accommodate for variations in light availability, and can be effective in reducing damage due to excess excitation energy. However the different processes will interact together and thus the actual productivity of the plant will depend upon the balance between different states. For example, exposure to excess light levels may lead to the enhancement of photoprotective mechanisms and in turn photoprotection may place an upper limit on the capacity to acclimate (e.g. Sheehy *et al.*, 2000, Demmig-Adams *et al.*, 2012). Optimal plant metabolism would track current environmental

changes and alter photosynthesis instantaneously (Retkute *et al.*, 2015). However, this does not happen and there is a time lag before the leaf can fully respond to changes (Walters & Horton, 1994; Athanasiou *et al.*, 2010). The length of the time lag will depend upon the process being evoked. For acclimation to a change in light intensity, the time lag for increasing light intensity is longer than that for a decreasing light intensity. This is thought to be due to the protein synthesis, maintenance and investment requirements (in terms of carbon, nitrogen and other resources) for an increased P_{\max} (Athanasiou *et al.*, 2010; Retkute *et al.*, 2015).

The relationship between light and photosynthesis can also be extended to a population of photosynthesising cells; for example a leaf or a whole canopy. Each section of photosynthetic material on a plant will place somewhere along the light response curve, this can be summed up over the organ or plant and thus build a curve that represents the whole structure. The shape of the resultant curve will depend upon a number of factors including those mentioned above as well as structural characteristics. The variability of light within a whole plant stand and the features of plants that determine these differences are discussed in more detail in the next section (1.3). An example light response curves is given in Figure 1.5. In the case of a canopy, a dense structure that absorbs the majority of light within the top portion of leaf material will have a whole canopy light response curve that rises sharply and then saturates (solid line in Fig. 1.5). However, if light is able to penetrate into deeper canopy layers the shape of the curve will not saturate until higher levels and may not saturate at all. Similarly, at the organ level, thicker leaves lead to a more asymptotic response.

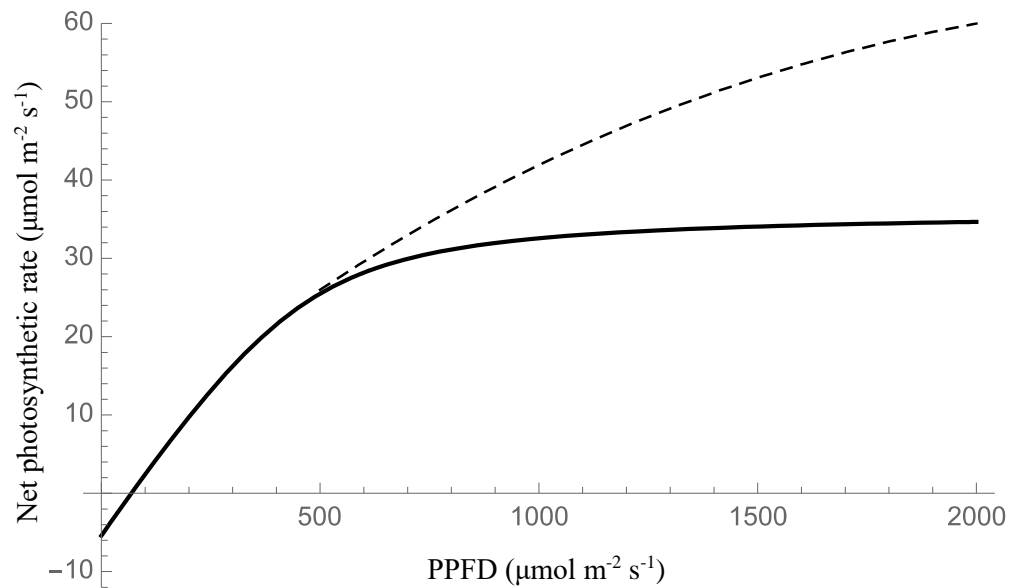


Figure 1.5: Example light response curves of a population of photosynthetic cells (i.e. a leaf or a whole canopy). The thicker the population, the more light is absorbed in the upper layers (solid line) whereas a less dense/ thick population absorbs radiation over a greater surface area (dashed line) thus leading to saturation at a higher incident radiation.

1.3 The Canopy Light Environment and Architectural Characteristics

Light availabilities can differ between 20- and 50-fold between the top and bottom within a closed plant canopy (Stadt *et al.*, 1999). Interception depends on a number of different factors including leaf orientation and shape, the spatial arrangement of photosynthetic surfaces (i.e. uniform versus clumping), sun elevation, the finite width of the sun's disc and changes in spectral distribution of PPFD within the canopy (Nobel *et al.*, 1993). It was discovered that absorption of light by a canopy approximates the absorption of light through a liquid, as described by Beer's law, particularly when there is a random distribution of leaves (Duncan, 1971; Monsi *et al.*, 1973; Norman, 1980).

When applied to canopies, Beer's law of exponential decay states that:

$$\frac{I}{I_o} = e^{-KL} \quad (\text{Eq. 3})$$

where I refers to radiation at a specific point in the canopy, I_o refers to radiance at the top of the canopy, L refers to leaf area index (LAI; the area of leaves per unit area of ground; calculated as the number of plants per unit area multiplied by the number of leaves per plant and the mean area of plant leaf; section 1.3.1) and K is the extinction coefficient for radiation. The extinction coefficient, K , is determined by the angle and orientation of foliage plus its transparency, and is often species or variety specific. Beer's law shows that as we move vertically down through a canopy, radiation decreases exponentially with the amount of leaf material encountered (Monsi & Saeki, 1953; Monsi *et al.*, 1973) as a function of distribution of leaf area along canopy height and of spatial aggregation and foliage inclination angle (Cescatti & Niinemets, 2004). The radiation is intercepted with depth in the canopy and either reflected or absorbed. This law formed the basis for the first mathematical description of canopy photosynthesis. As canopy characteristics determine the K and L values, it is important to quantify the architecture of plants.

Variations in light intensity can occur over different spatial or temporal scales. Spatial scales include variation that can be attributed to shading effects within a plant stand, or a single plant canopy, whereas temporal scales may refer to long-term solar radiation changes (for example, as a result of seasonal change) or short-term response such as fluctuating light enforced by sun position, cloud or leaf movement. Therefore the interception of light will depend on a number of different factors including leaf orientation and shape, the spatial arrangement of photosynthetic surfaces (i.e. uniform versus clumping), sun elevation, the finite width of the sun's disc and changes in spectral distribution of PPFD within the canopy (Nobel *et al.*, 1993). Such variable patterns will lead to periods of time where photosynthesis is fully saturated, and others where photosynthesis may be below or approaching the light compensation point.

1.3.1 Canopy Architecture

Plant architecture refers to the spatial organisation of plant organs (Barthelemy & Caraglio, 2007). The resultant structure impacts many processes within the plant including mechanical stability (Mouliia *et al.*, 2006; Niklas, 1994), productivity and yield (Khush, 1996; Sakamoto & Matsuoka, 2004), disease and stress resistance (Coyne, 1980; Wolfe, 1985; Jung *et al.*, 1996; Ando *et al.*, 2007; Grumet *et al.*, 2013) and photosynthesis (Song *et al.*, 2013).

Canopy architecture varies greatly both within and between species. The arrangement of plant material, both spatially and temporally, leads to a highly heterogeneous light environment. Canopy photosynthesis depends upon two factors: the distribution of light within the canopy, and the biochemical capacities of the canopy elements (Horton, 2000; Sinoquet *et al.*, 2001; Valladares & Niinemets, 2007; Zhu *et al.*, 2010; Matloobi, 2012). In terms of canopy photosynthesis, the most efficient canopy architecture is that in which all the leaves are evenly illuminated at quantum flux densities which saturate photosynthesis (Valladares & Niinemets, 2007). In other words, optimal utilization of light generally occurs when incident radiation is distributed uniformly across all leaf layers due to the non-linear hyperbolic relationship between photosynthesis and light. The number of leaves that are exposed to radiation levels above that required for positive net photosynthesis (above photosynthetic light compensation but below light saturation) is maximised under these conditions (Clendon & Millen, 1979; Hodanova, 1979; Turitzin & Drake, 1981). Such strategies help to increase the amount of intercepted PAR thus unifying the photosynthetic rates within the canopy by reducing the foliar absorption coefficient of upper leaves and optimizing photosynthetic performance and productivity (Stewart *et al.*, 2003; Cescatti & Niinemets, 2004; Sarlikioti *et al.*, 2011). This may, in part, be due to leaf acclimation to lower light intensities and increased physiological age of leaves in lower canopy layers (Niinemets, 2007). However, this canopy structure is rarely found in nature. More commonly, leaves positioned at the top of the canopy are

exposed to irradiances that are in excess of those required for photosynthesis whereas leaves at the bottom of the canopy receive very low levels of light.

Light is the most heterogeneous environmental factor influencing plant growth and survival. A number of different canopy properties can alter the light environment in a given canopy, thus altering photosynthesis: these are detailed in the following section.

1.3.1.1 Architectural Features

The distribution and arrangement of plant elements within a canopy or tree crown are critical in determining the light harvesting efficiency per unit foliage area (Baldocchi & Collineau, 1994; Chen *et al.*, 1997; Kull *et al.*, 1999; Valladares & Niinemets, 2007; Matloobi, 2012). Features such as leaf size and shape, leaf inclination angle, leaf area, clumping and movement are fundamental in determining the probability that a light beam will penetrate through to lower canopy levels and be intercepted.

- *Leaf Area*

One of the most basic structural properties of a canopy that influences light interception is the total leaf area, i.e. LAI. The persistence of LAI with time is called the leaf area duration (LAD). If LAI and LAD are maximised, in theory interception will be optimised (Beadle & Long, 1985). As LAI increases, and thus the canopy become denser, more solar radiation will be absorbed or reflected and less will be transmitted to lower canopy layers (Bonan, 2002).

The relationship between LAI and light interception is given in Beer's Law (above). As light passes through the canopy, it is absorbed as exponential decay, with more light absorbed in the upper canopy layers and less in lower layers. Different architectures can have the same LAI due to the arrangement or stacking of the foliage yet intercept light very differently. This is particularly relevant in situations whereby LAI is not distributed equally along the vertical

axis; i.e. the cumulative LAI does not have a linear relationship with depth through the canopy. Due to the differences in light absorption between different canopy structures, fractional interception (F) will also differ. At maturity, crops should obtain a fractional interception as close to 1 as possible (meaning they are absorbing all light available). It is advantageous for crops to achieve this with as low an LAI as possible, as it will conserve resources, however, depending upon the architectural features, there will be an optimal LAI for the given crop (Figure 1.6), the value of which will be larger for an erect canopy than for a flatter canopy.

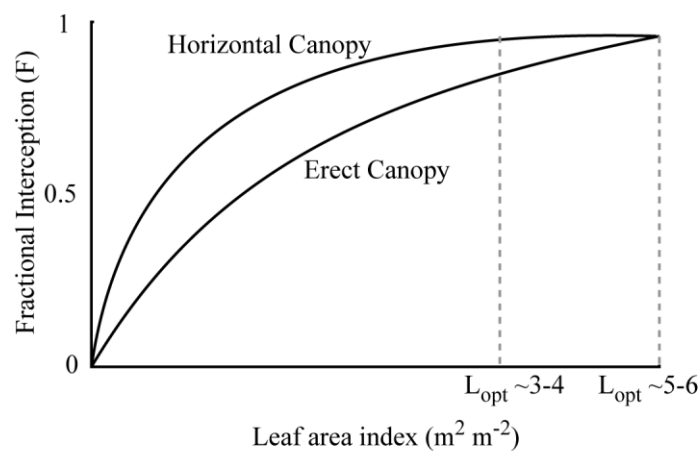


Figure 1.6: Fractional interception for horizontal versus erect canopies and their optimal LAI (L_{opt} : the value where fractional interception is equal to 1).

The relationship between LAI and other architectural traits will be discussed further below.

- *Clumping*

Canopies with the same leaf area index can have very different efficiencies in light capture due to the arrangement of plant matter (Baldochi & Collineau, 1994; Valladares & Niinemets, 2007). Foliage is often clumped, for example in branches or shoots, leading to a greater fraction of canopy gaps and light transmission relative to a canopy with randomly arranged leaves (Baldochi & Collineau, 1994; Cescatti, 1998; Godin & Sinoquet, 2005; Law *et al.*, 2001; Zhao *et al.*, 2012). All else being equal, canopies exhibiting regular dispersion

intercept more light, and those with aggregated dispersion less light, than canopies with random dispersion (Niinemets & Anten, 2009). Whilst clumping results in less efficient light interception, it enables canopies to reach greater LAI. For example canopies with random dispersion can intercept all light at an LAI of 5 whereas for canopies with highly aggregated foliage (e.g. conifers) LAI values can reach 15 (Cescatti, 1998; Van Pelt & Franklin, 2000; Asner *et al.*, 2003). Such clumping in conifers is predicted to result in an efficiency of light harvesting only 10-40% of that of the equivalent foliage area on a horizontal plane (Stenberg *et al.*, 2001; Niinemets *et al.*, 2002; 2006; Cescatti & Zorer, 2003). However, in the case of conifers, clumping structure may provide other benefits relating to the environments in which they grow such as the prevention of damage by heavy snow. For shoots that are found under radiation conditions that exceed saturation point for photosynthesis, clumping should not necessarily reduce daily photosynthesis, but allows the concentration of photosynthetic biomass under conditions where photosynthetic gains are largest (Niinemets & Anten, 2009).

An alternative strategy is to have regular arrangement of foliage, reducing canopy gaps. Such canopies achieve a greater light harvesting for a given LAI and is often favoured under low light environments and late-successional mono-layer species (Horn, 1971; Kempf & Pickett, 1981; Valladares & Niinemets, 2007; Pan *et al.*, 2013). Reduced aggregation in low light leads to greater light harvesting efficiency and increased productivity under limited light conditions. Therefore, the degree of aggregation provides another structural response to unify radiation levels within a canopy (Cescatti, 1998; Cescatti & Niinemets, 2004). The effect of leaf dispersion on light interception is given in Figure 1.7 whereby clumped canopies have the greatest amount of canopy gaps and regular the least.

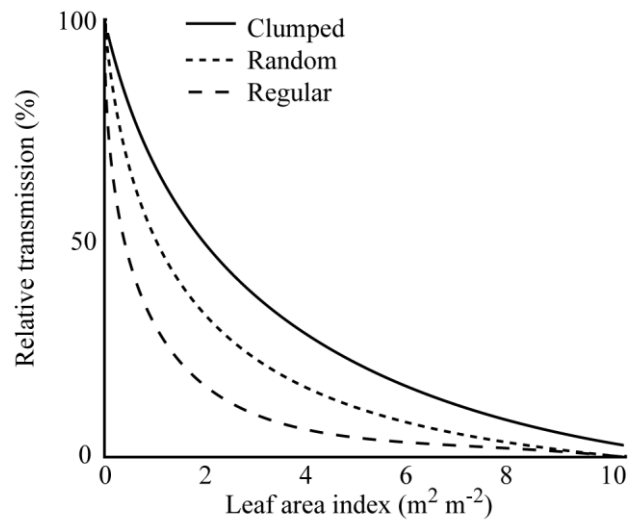


Figure 1.7: The effect of leaf dispersion and leaf area index on light transmission. Modified from Valladares & Niinemets (2007).

- *Leaf Shape and Size*

The geometry of leaves, particularly their shape and size, is result of a trade-off between light harvesting and temperature regulation plus more efficient use of resources (Bonan, 2002). The leaf properties are a result of the local environmental conditions. As such, studies are able to combine photosynthetic properties and the energy budget of a leaf to predict the optimal leaf size for a given environment (Parkhurst & Loucks, 1972; Givnish & Vermeij, 1976; Woodward, 1993). It is assumed that leaf size should be optimised in order to maximise water-use efficiency. Leaves experiencing high light intensities, hot arid environments or cold arctic or alpine conditions are often smaller and more deeply lobed than those under low light conditions. This is, in part, due to the effect of geometry on leaf boundary layer resistance, thus enabling greater heat and moisture transfer. Contrary to this, leaves in more shaded environments are often larger to enable more efficient light harvesting (Parkhurst & Loucks, 1972). Due to transpiration, larger leaves will only be favoured in mesic environments (Bonan, 2002). The relationship between environmental conditions and leaf form is so distinct that the geometry (particularly leaf area plus the number and depth of serrations) of fossil leaves

can be used as an indicator of past climatic conditions (Bonan, 2002; Peppe *et al.*, 2011; Chitwood *et al.*, 2012; Royer, 2012).

- *Leaf Inclination and Orientation*

Differences in foliage relative to vertical and the azimuthal orientation of leaves can generate varying patterns in light interception in canopies with similar levels of clumping or LAI. When the sun is located overhead, vertical leaves absorb less PPFD than horizontal leaves, thus reducing interception of excessive solar irradiance at midday (Valladares & Niinemets, 2007). This is often seen within grass species that contain erect leaf angles. This architecture is known as erectophile and is characterised by a low K value. Alternatively, those plants with more horizontal leaf angles (e.g. potato, bean, clovers etc.) are known as planophiles and have a correspondingly high K value. The differences between erectophile versus planophile canopies can be seen in Figure 1.8 for an LAI of 3. Horizontal leaf angles are beneficial in an understory environment where most light enters from low zenith angles (Muraoka *et al.*, 1998). Therefore leaf dimension and angle are key factors in assessing plant strategies for optimising light acquisition. For example, it was shown that 30% of the difference in light capture by upper and lower canopy species within a tall-grass meadow can be explained by differences in leaf orientation (Anten, 1999).

The effects of leaf angle distribution are greater for canopies with larger LAI (Duncan, 1971; Gutschick and Wiegel, 1988; Norman, 2012). As solar position varies over the course of the day, leaf angle has minor effects at LAIs of less than approximately 3 (Duncan, 1971; Gutschick & Wiegel, 1988). Horizontal leaves at the top of the canopy exhibit maximum light interception efficiency when irradiance is above the light saturated rate of photosynthesis. Thus at higher LAIs and higher solar elevations, erectophile crops show a marked yield advantage over planophiles (Monteith, 1965; Wang *et al.*, 1995; Struik, 2001; Valladares & Niinemets, 2007).

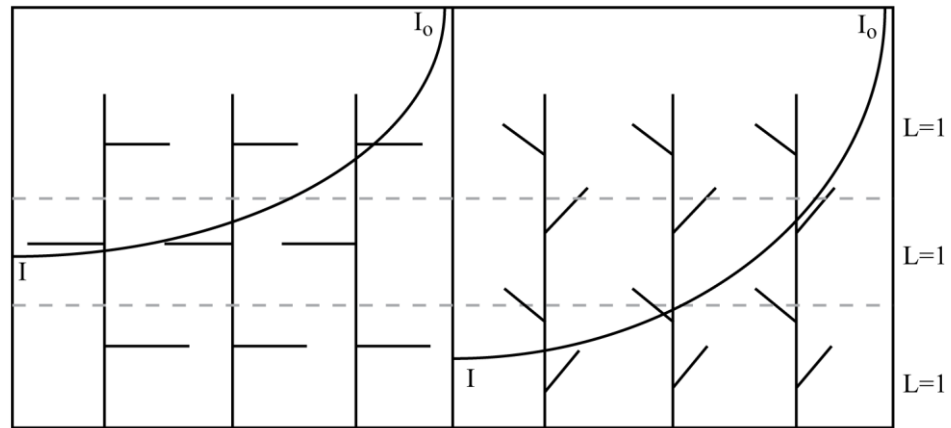


Figure 1.8: Exponential decay of light through a horizontal (left) versus an erect (right) canopy. Each canopy is divided into three layers of equal LAI. The radiation, I , received at any point in the canopy can be described by Beer's law (Eq. 3). Modified from Azam-Ali & Squire (2002).

Not only does leaf inclination angle effect light distribution within the canopy as a whole, but it also effects the distribution of light between the upper and lower leaf surfaces (DeLucia *et al.*, 1991; Valladares & Pearcy, 1999; Valladares & Niinemets, 2007). Depending upon the differing photosynthetic characteristics within the leaf and the ability for the two sides to acclimate to long-term light levels, any changes in the light may have profound consequences for leaf photosynthesis or may have little effect (Poulson & DeLucia, 1993; Valladares & Pearcy, 1999). More vertically orientated leaves project smaller fractions of their area during central hours of the day, thus leading to a greater penetration of light through the canopy. Although vertical leaves may reduce light interception at the individual leaf level, the reduction can vary from strongly limiting to negligible or even improving photosynthetic carbon fixation of the plant or whole canopy (Valladares & Pearcy, 1999; Valladares & Niinemets, 2007).

Observations indicate a range of leaf inclination angles within a canopy with many canopies exhibiting more vertical leaves at the top of the canopy and more horizontal leaves at the bottom (Thomas & Winner, 2000; Niinemets *et*

al., 2004; 2005; Kim *et al.*, 2011; Vince & Zoltán, 2011). This is related to LAI of the canopy, with erect leaves near the top and horizontal leaves near the base of a canopy tending to have higher productivity than an equivalent canopy with random or uniform leaf orientations for an LAI exceeding ~ 3 (Nobel *et al.*, 1993). Such distribution results in a greater penetration of light through the canopy to enable more uniform light levels (Herbert, 1991; Falster & Westoby, 2003). Greater penetration of light means that fewer leaves at the top of the canopy at light saturated and more leaves at the bottom of the canopy receive light above the compensation point. This maximises overall plant productivity. This is verified by simulation studies, such as that carried out on maize (McLean *et al.*, 2009), indicated that vertically oriented leaves in the upper portion of the canopy leads to a reduction in the light extinction coefficient thus permitting greater light penetration to lower canopy layers. This architecture is present in many crop plants including sugar beet, agaves and pineapple. Canopies with varying inclination angles can sustain greater foliage areas than canopies with constant angles (Russell *et al.*, 1989; Valladares & Niinemets, 2007).

- *Leaf Movement*

The level of photon irradiance incident upon a leaf can be regulated and modified by diurnal movements of foliage. A number of species move their leaves so as to keep the blade either parallel (paraheliotropic) or perpendicular (diaheliotropic) to the direct rays of the sun. Leaf movements are capable of enhancing light interception by as much as 35% compared to leaves in fixed positions (Ehleringer & Forseth, 1980, 1990; Ehleringer & Werk, 1986), or help maintain a constant PPFD incident on a leaf over the course of the day (Vince & Zoltán, 2011). Leaf solar tracking is most common in annuals and herbaceous species (Ehleringer & Werk, 1986; Pugnaire & Valladares, 1999). The effect of leaf movements on canopy photosynthesis is most prominent at low LAIs where photons can be absorbed that would otherwise pass through the canopy. However, at LAIs greater than 4, leaf movement can reduce canopy productivity as it restricts photosynthesis to the upper canopy layers (Ehleringer & Forseth, 1990).

1.3.2 Direct versus Diffused Light

Both direct and diffused light are important components of incident radiation (Gutschick & Wiegel, 1988; Herbert, 1991; Cavazzoni *et al.*, 2002; Brodersen *et al.*, 2008; Sarlikioti *et al.*, 2011; Matloobi, 2012). Whilst all canopy characteristics effect the distribution of direct light within the canopy, diffused light distribution is mainly affected by foliage arrangement and by leaf angle to only a minor degree (Cavazzoni *et al.*, 2002; Cescatti & Zorer, 2003). The shape, size and arrangement (including proximity) of the leaves affect the transmission of diffused light into lower canopy layers thus can influence canopy photosynthesis under both low- and high-light conditions (Valladares & Pearcy, 1999; Valladares & Niinemets, 2007). This is clearly seen within forests where the orientation of leaves in tree crowns in the vicinities of forest gaps frequently respond to diffuse rather than direct light (Valladares & Niinemets, 2007; as seen in Ackerly & Bazzaz, 1995; Clearwater & Gould, 1995; King, 1998). Alterations in the transmission of diffused light caused by differing architectures or global climate change (i.e. amount of cloud cover) could maximise canopy photosynthesis through a more even distribution of light (Brodersen *et al.*, 2008).

Leaf clumping is another trait that influences the transmission of direct and diffused light through the canopy and is able to alter the transmission of each component differently. For example, leaf clumping in tree crowns in Norway Spruce is able to increase the average transmittance at the base of the canopy by 4.9% for direct radiation and up to 10.9% for diffused radiation (Cescatti, 1998).

1.4 Linking Architecture, Photosynthesis and Biomass Production

Photosynthesis sets the potential upper limit to the efficiency that solar radiation may be converted into biomass (Beadle & Long, 1985; Zhu *et al.*, 2008). The strong correlation between biomass production and light interception means that canopy architecture is critical in determining the overall biomass. The link between light interception and biomass for different crops is given in Figure 1.9.

A. Per hectare for given time:

Amount of incident radiation	X	Canopy interception efficiency	X	Radiation use efficiency	=	Biomass ha ⁻¹
------------------------------------	---	--------------------------------------	---	--------------------------------	---	--------------------------

B.

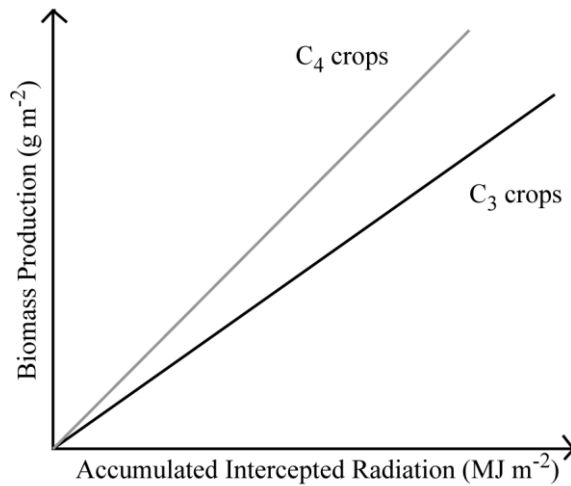


Figure 1.9: The determinants of canopy productivity. (A) Biomass production depends upon incident radiation, canopy interception and the efficiency with which it can be used. (B) Dry matter accumulation for C₃ versus C₄ crops (crop radiation use efficiency).

One example of how canopy architecture influences photosynthesis and therefore biomass production can be seen in the difference between vertical

versus horizontal leaf angular distributions. The effect of different canopy architectures on biomass will depend upon the environment in which they are grown. For example, crops with more upright leaves are considered more productive at low latitudes, or where LAI >4 and sun angles are high (Trenbath & Angus, 1975; Oker-Blom & Kellomäki, 1982). The effect of different leaf inclination angles on photosynthesis can be seen in Figure 1.10.

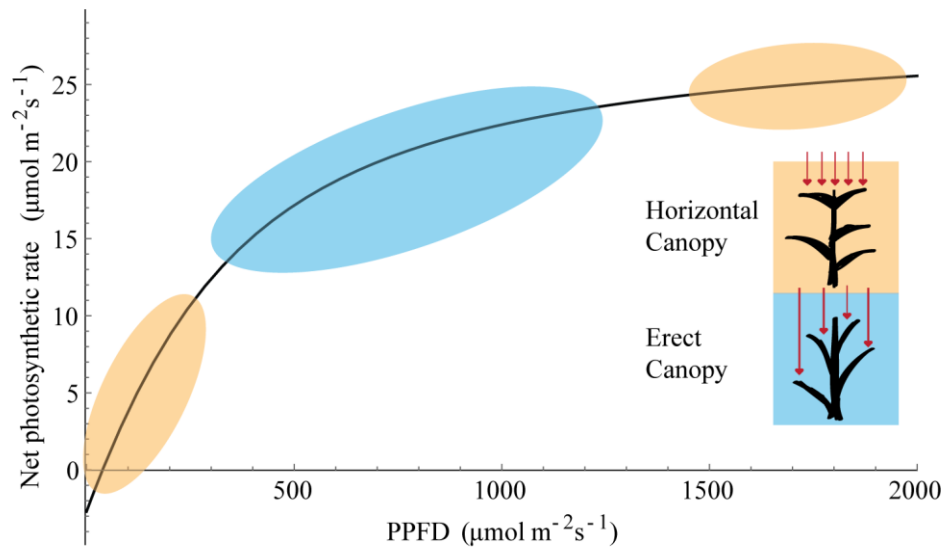


Figure 1.10: The effect of leaf angle and canopy structure on photosynthesis with relation to the light response curve. The leaves at the top of the horizontal canopy receive high levels of light and thus photosynthesis is saturated. However, leaves lower down in the canopy receive low levels of light therefore have low photosynthetic capacities. Contrary to this, in the more upright canopy, light is able to penetrate through thus is absorbed over a greater area, leading to higher photosynthetic rates. In this example, the upright canopy is the most productive.

In the natural world, canopies vary greatly and it is not a simple dichotomy of upright versus horizontal canopies. To quantify canopy architecture therefore requires complex methods.

1.5 Modelling

1.5.1 Plant Structural Modelling

In order to assess the impact of plant architecture on processes and, ultimately, plant productivity and yield, detailed quantification of such structures is necessary. This desire for the creation of complex, geometrically accurate three-dimensional models of plants has led to the development of a number of different techniques in order to capture plant structure (e.g. Watanabe *et al.*, 2005; Quan *et al.*, 2006; Song *et al.*, 2013; Pound *et al.*, 2014). Applications of such models are diverse, including the study of photosynthesis for both single plants and whole canopy structures (e.g. Song *et al.*, 2013).

Canopy architecture must first be quantified before it can be modelled. There are many different methods by which we can quantify canopy structure; this includes both destructive and non-destructive methods (Wilson, 1963; Anderson, 1971; Ross, 1981; Campbell & Norman, 1989; Chen *et al.*, 1997; Bréda, 2003; Jonckheere *et al.*, 2004; Weiss *et al.*, 2004). Destructive methods require identification of the key architectural features of the plant, defined by a number of different parameters such as leaf length, angle and number etc., taking averages across a number of plants, then reconstructing a representative canopy (Watanabe *et al.*, 2005; Alarcon & Sassenrath, 2011; Song *et al.*, 2013). Reconstructing the plant structure from data, *in silico*, are often time-consuming and tedious due to the rigorous measurements required (Fourcaud *et al.*, 2008; Vos *et al.*, 2010).

Non-destructive methods can be broadly split into two categories with differing levels of accuracy. Low accuracy methods use approximations of plant 3D structure can be used in which leaf angle can be assumed to be constant (e.g. Pagès *et al.*, 2009) or follow an ellipsoidal or spherical distribution (Rakocevic *et al.*, 2000; Farque *et al.*, 2001). These assumptions are particularly relevant in crops that exhibit regular and coordinated development, such as rice and wheat (Evers *et al.*, 2005; Pagès & Drouet, 2007; Zheng *et al.*,

2008). This method plus the destructive method is known as a rule-based approach to modelling. However, for those crops which exhibit highly heterogeneous canopies, use of standard leaf angle distributions can lead to a 4-15% difference (depending on light conditions and number of photosynthetic parameters used) in calculated photosynthesis values compared to 3-D models with explicitly described leaf angles (Sarlikioti *et al.*, 2011). Alternatively, highly accurate methods rely on digitising a pre-existing structure, but using a set of images as a basis. This is known as the image-based approach. See Figure 1.11 for an overview of different approaches.

The image-based models are highly desirable as a method of plant phenotyping (Houle *et al.*, 2010; Santos & Oliveira, 2012; White *et al.*, 2012), with the information needed to calculate a number of plant traits including leaf areas and angles, plant height, etc. However, the complexity of plant architecture means that image-based approaches are often challenging. In particular, similarities between multiple small leaf segments, lack of texture for feature matching and the high amount of self-occlusion lead to difficulties during reconstruction (Pound *et al.*, 2014). The models produced may also be of limited application. For example, the silhouette-based method produces a static model which cannot be used for modelling aspects such as plant or leaf movement and the point cloud data cannot be used for modelling photosynthesis; for this surface detail is required (see Pound *et al.*, 2014). Therefore, when designing an imaging platform, a number of different considerations must be taken into account including quantity of imaging required, accessibility to technology, including money availability, and the type of model required; i.e. whether for basic phenotyping measurements or for further modelling such as photosynthesis and leaf movement.

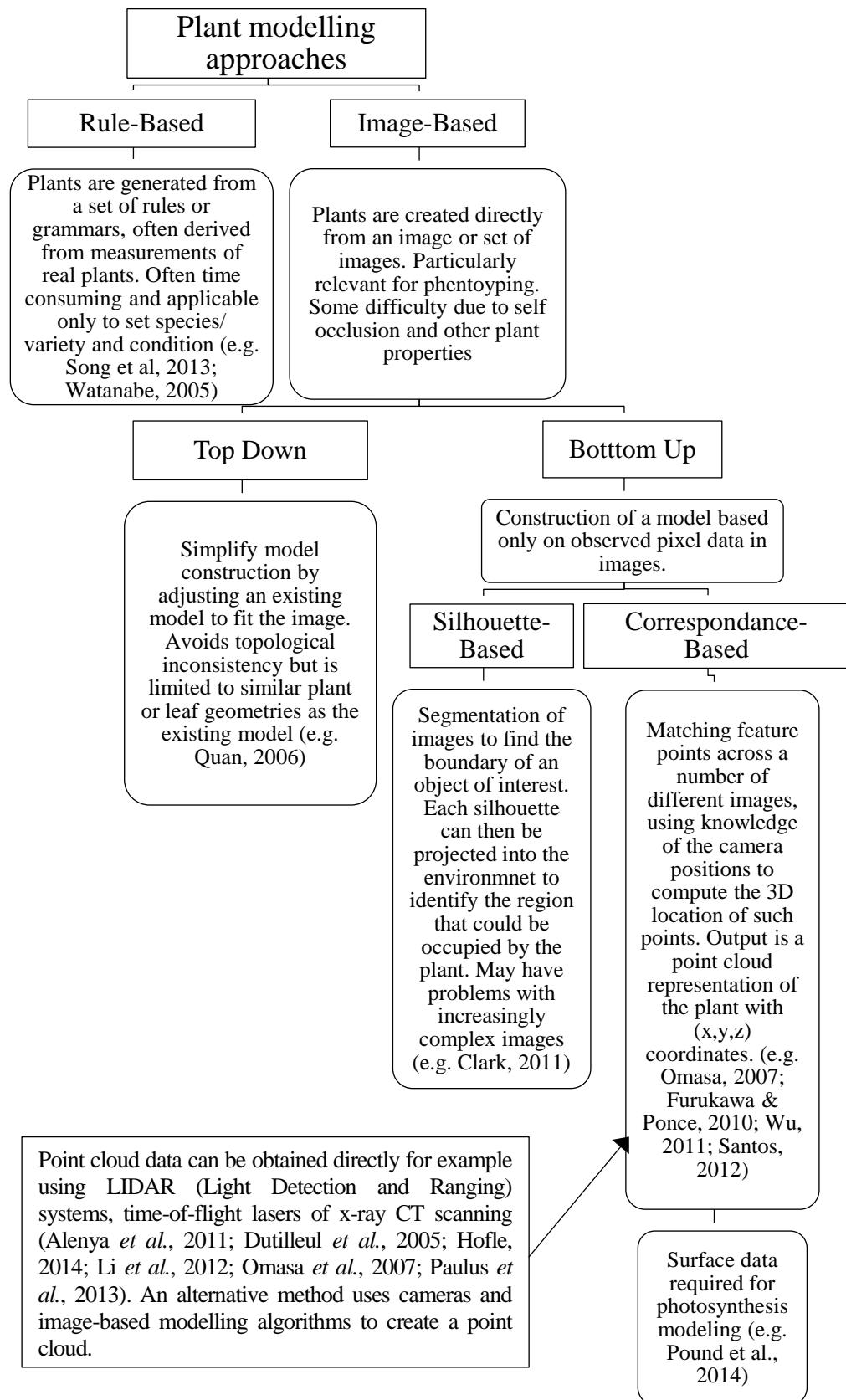


Figure 1.11: Overview of plant modelling approaches

1.5.2 Light Modelling

Based on the position of a section of leaf within the canopy, the light environment will be highly variable throughout the day. This can be extremely difficult, if not impossible, to measure. Once detailed structure is known, the next stage of scaling up canopy processes requires modelling the light environment experienced by individual leaf elements. By modelling the radiative exchanges between plant organs, light models are able to estimate the radiative fluxes received by each organ (Chelle and Andrieu, 2007). Such models take into account the fate of a light ray incident upon a leaf surface; whether it is reflected, absorbed or transmitted, and integrate these local processes over the whole structure. The complexity of the integration will depend upon the accuracy of the structural description of the canopy. The 3D plant model obtained in processes described above can be used so that light interception can be calculated using spatial representation of vegetation components (Borel *et al.*, 1991; Goel *et al.*, 1991; Chelle *et al.*, 1998; Evers *et al.*, 2015). Advantages of this approach include fluxes for individual geometric elements and consideration of their size, position and orientation (Chelle and Andrieu, 2007). Thus these are able to provide more information on the interception of light at the organ scale (Chelle, 2005) at the cost of increased numerical complexity. Both ray tracing and projection represent mechanisms of calculating primary lighting on a surface.

Due to the differential fate of light rays, radiation absorbed by each plant organ may come either directly from the sky hemisphere, or indirectly after scattering (direct or diffuse light). The proportion of the light that is reflected or transmitted varies with wavelength and depends upon leaf type, state and age. Calculating primary lighting of a set of surfaces can be achieved through either a source- or recipient-based approach (Wang *et al.*, 2008). In the source-based approach, sampling occurs by following the propagation of light from selected directions in the sky hemisphere, and determining the surface element hit by each ray. Whereas the recipient-based approach uses the inverse sense of light propagation is followed from specific surface elements, into the sky hemisphere (Liu and Chen 2003; Zhang and Zhao, 2007). Primary light is

effectively described when the irradiance of a surface reflects the sum of the contribution of each individual source.

Both ray tracing and projection represent mechanisms of calculating primary lighting on a surface (Chelle and Andrieu, 2007). Projection enables the surface element to be superimposed onto discretised screen located above the canopy, normal to the direction of light. Whilst this method is efficient in terms of speed and accuracy, there is risk of low resolution, particularly for small structural elements. Ray tracing is a stochastic method that relies upon the Monte Carlo method (Kalos and Whitlock, 1986) to account for the fate of light rays. It consists of casting light rays from a given light source, and following their paths through a canopy (Vos *et al.*, 2010). When a ray encounters an object, the subsequent path depends on the optical properties of the material (Sinoquet *et al.*, 1998). The Monte Carlo method is general and requires few assumptions. It enables simulations for large sets of variables; simulations of almost any type of light source, canopy structure and optical properties and separates the contribution of the different orders of scattering to the radiative variables (Chelle and Andrieu, 2007). Variants on the method have also been implemented to achieve higher efficiency, such as Quasi-Monte Carlo ray tracing (Cieslak *et al.*, 2008).

Radiative models have been used in two main types of study: (i) investigating how a given canopy intercepts light; and (ii) simulating plant-light interactions dynamically, through the use of virtual plant models accompanied with specific organ irradiances. Knowledge of how the canopy intercepts light enables scaling from leaf/organ photosynthesis to whole canopy photosynthesis. This requires an understanding of the distribution of photosynthetic capacity (Kull, 2002). The changes in light profile resulting from sun flecks and sun angle cause the proportion of canopy light absorbed by individual leaves to change on a time scale too rapid for acclimation of leaf photosynthetic capacities (de Pury and Farquhar, 1999). This requires further consideration for models of whole canopy photosynthesis.

1.5.3 Plant Process Modelling: empirical versus mechanistic

Models of plant processes can be either empirical or mechanistic, or a combination of both. Mechanistic models are based on known relationships between components within a system whereas empirical models are based on observations without knowledge of underlying mechanisms or kinetics. Mechanistic models may offer insight into the complex relationship between biochemical processes and links to environmental variables and thus may allow a deeper understanding of the system. However, they can have limitations such as extensive data requirements for model parameterisation, which is often not available, computational requirements and inapplicability to a wide range of situations (Estes *et al.*, 2013). Alternatively, empirical models may be used to analyse its impact as they favour simple relations between observed state variables. However, whilst empirical models often have some basis in a species' physiology, the relationship between variables may be based upon empirical best fit without causal links therefore they have been criticised due to their lack of mechanistic representation of biotic or abiotic interactions (Dormann, 2007). An overview of the hierarchy classification of model types, the system level they apply to, the timescales they cover and the predominant data source are given in Figure 1.12.

Within this hierarchical classification, general broad themes can be seen (Reynolds & Acock, 1985). As empirical models often describe the relationship between variables without a specific reference to the underlying process, they are generally more prevalent with a decrease in resolution, whereas mechanistic models intend to represent causality between variables, and thus can be used at increasing levels of resolution (Reynolds & Acock, 1985). Models can be separated into two broad groups: general models and process-based models. More detailed process-based models tend to be mechanistic; use data from predominantly controlled experiments and; tend to be based on short-scale sub-organ level processes. However process-based models may also be empirical and aim at the higher system level (as presented in Part II of this thesis). In contrast, general models usually make predictions over long time periods and at the larger scale. These can either be full

empirical models or contain a mixture of empirical modelling with subsystem mechanistic modelling (Figure 1.13).

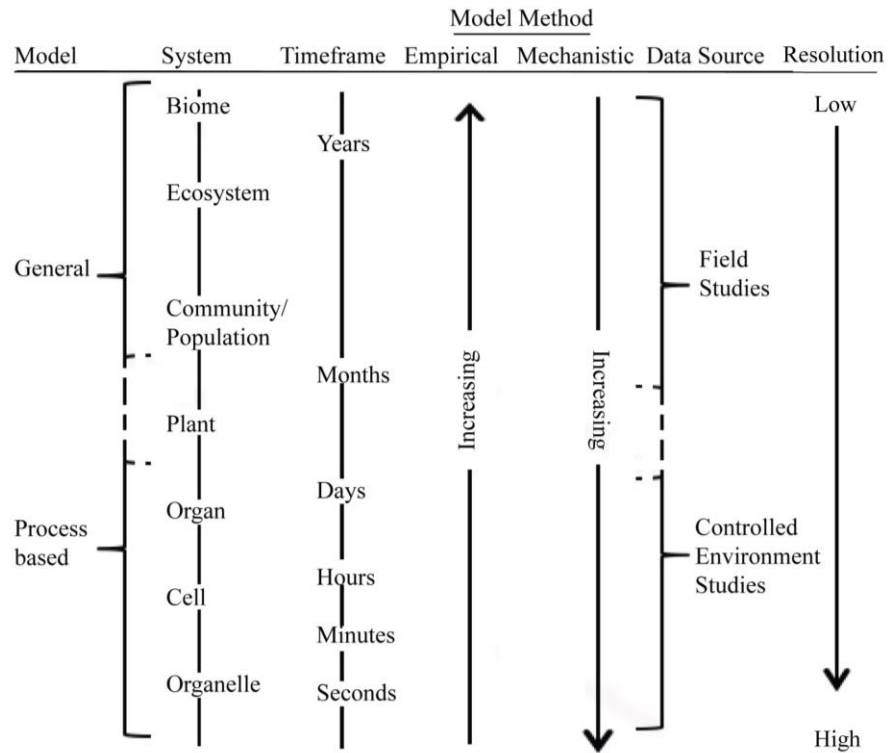


Figure 1.12: Hierarchical classification scheme of different modelling techniques based on the system being modelled, timeframe, modelling method, data source and resolution. Figure adapted from (Reynolds & Acock, 1985).

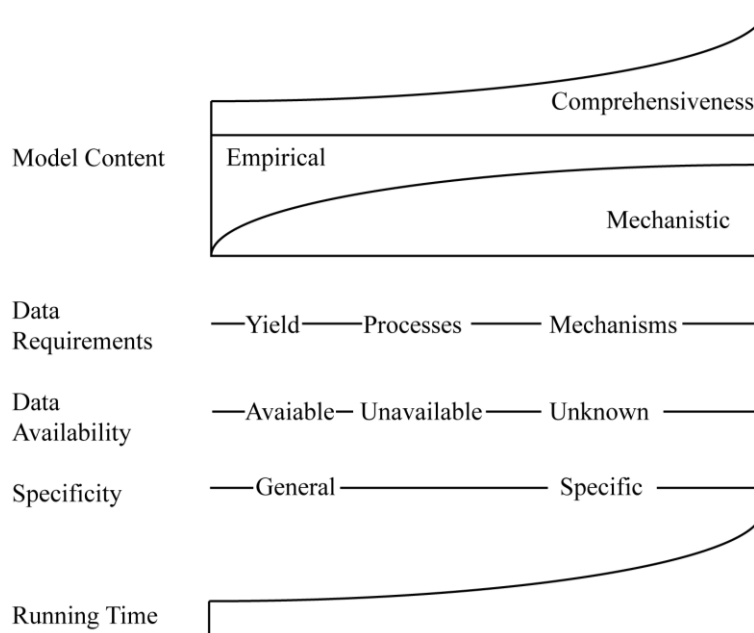


Figure 1.13: Types of models, data requirements and their approximate running times. Adapted from (Reynolds & Acock, 1985).

Whilst distinguishing between empirical and mechanistic models can be useful, many models used to study plant growth and development processes use a mixture of both forms of model. Empirical models have traditionally been a highly useful tool in scientific studies. However, their predictive ability is restricted, and predictions outside the range of their resolution are not recommended. In contrast, whilst mechanistic models can lead to more accurate predictions of processes, their use is restricted to the system under study, the amount of data available for parameterisation and the underlying knowledge of the mechanism under investigation and its relationship to other processes. The type of model required or possible will depend on a number of different factors (including resolution and data availability).

1.6 Knowledge Gaps

Understanding the response of photosynthesis to a change in irradiance will be critical in determining productivity of plants and crop species, and how this relates to yield. This will require knowledge of how photosynthesis responds to both rapid and realistic fluctuations in light; how the arrangement of plant material, in time and in space, determines the levels of light received by a given photosynthesising cell and; how populations of photosynthesising cells determine overall productivity of a system, in this case the whole canopy structure.

Aims and Objectives

- To assess the productivity of existing canopy architectures with relation to the light environment, photosynthesis and biomass production
- To propose alternative approaches for exploring the light environment within different crop treatments, and compare these new methods to existing methods
- To assess the light environment inside a crop canopy consisting either of a single crop, or multiple crops (intercropping)
- To assess how different photosynthetic processes are affected by the level of light they receive, as a result of the canopy structure or the environment
- To help create a model/models that combines detailed canopy structure and light information with photosynthetic processes

Hypotheses

- A combination of 3-dimensional reconstruction and modelling can be used to explore the light environment within complex canopy structures in high resolution and provide a means to scale leaf level responses up to the whole canopy
- Modelling approaches can provide new architectural and functional information that cannot be measured manually
- A canopy structure which permits higher light levels over a greater surface area will lead to greater photosynthesis; however, this may not necessarily translate into greater productivity of the whole system if the total leaf area is lower
- The architectural traits and resulting canopy structure will determine the levels of light at each point in a canopy
- Leaf movement, such as that caused by wind, will alter the light environment and thus the productivity of the canopy

- Availability of growth resources, such as water or nitrogen, will alter canopy structure
- If light levels are too high, productivity may be reduced due to photoinhibitory effects
- The response of photosynthesis to a change in irradiance will depend upon the magnitude of response, the amount of time spent under different conditions and the previous light history
- Sub-optimal acclimation will affect the productivity of the canopy

Thesis Layout

The thesis is split into two broad sections; Part I assesses the light environment within canopies and assesses their productivity in terms of biomass production. This includes the effect of cropping system and layouts on light interception (Chapter 3); varietal selection and the links between architecture and photosynthesis (Chapter 4); wind-induced movement (Chapter 5); and nitrogen fertilisation (Chapter 6). Part II looks at scaling up individual photosynthetic processes to the whole canopy level including photoinhibition (Chapter 7) and photoacclimation (Chapters 8, 9 and 10). A core methods and method development chapter (Chapter 2) covers the main methods used throughout the whole thesis, with more in depth materials and methods given within each of the chapters for the select work carried out. There is a final discussion chapter to tie both parts together. The thesis is written in a “thesis by publication” format, with chapters replaced by published papers or manuscripts where relevant.

Chapter 2: Core Methods and Method Development

The work is split into two core approaches; a practical approach and modelling approach. However, these are not mutually exclusive and the modelling work relies upon data that comes from the practical work.

As this thesis is written in a “by publication” format, materials and methods for each set of work will be present in the papers and manuscripts although a brief overview and details not given elsewhere will be given here. The chapter will begin with a brief literature review covering different modelling techniques before describing the reconstruction method and development (including optimisation tests) plus ray tracing.

2.1 The Reconstruction Process

An overview of the process from imaging to modelling is given in Figure 2.1.

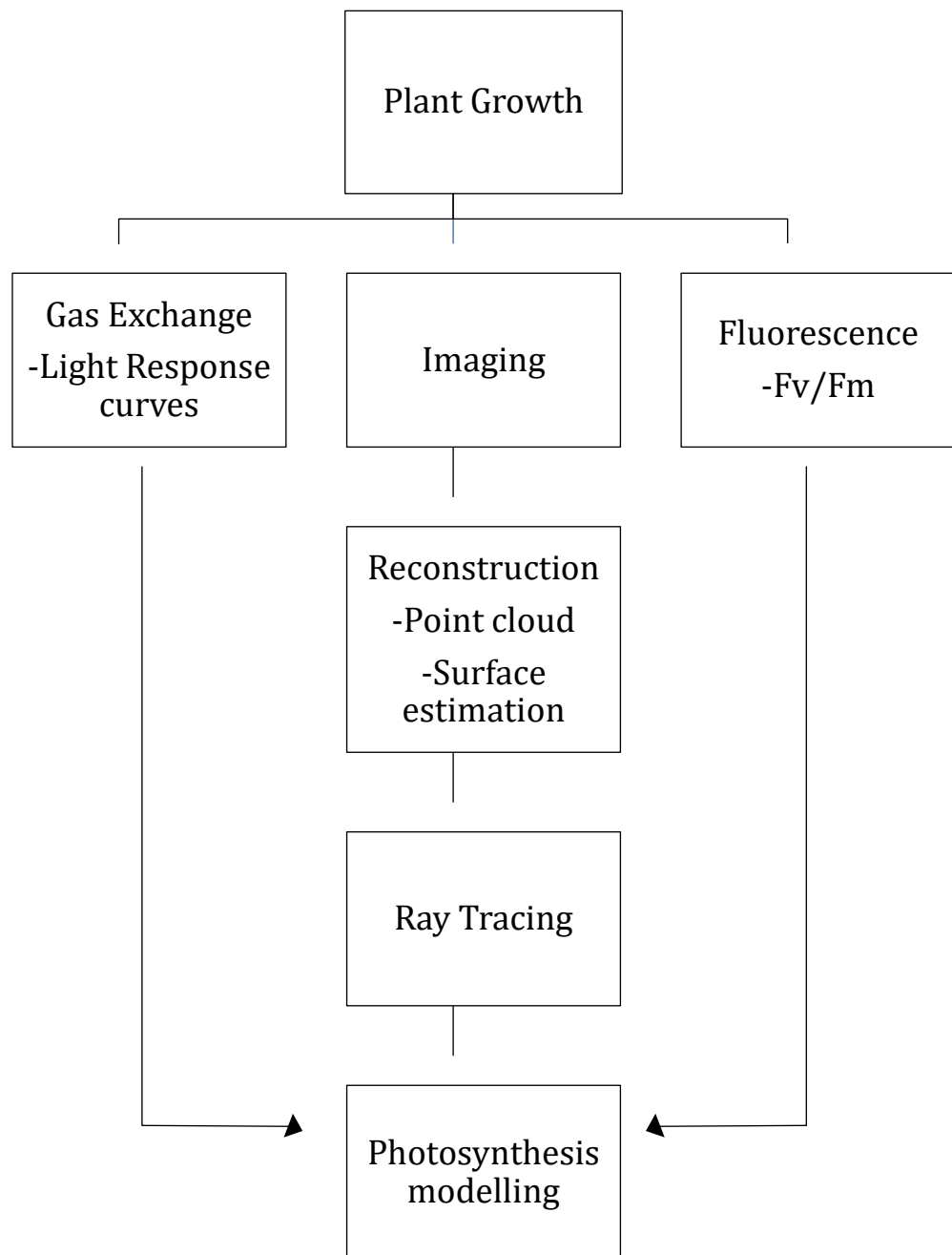


Figure 2.1: Flow diagram showing the general overview of the stages of plant modelling used within this thesis

2.1.1 Imaging

Plants can be imaged either *in situ* or in a dedicated imaging studio (single plant imaging). All following stages of the reconstruction method are the same, regardless of where the images were taken.

- **Canopy Imaging: Imaging *in situ***

Plants can be imaged *in situ* by taking multiple images around the plant growing in a stand. This can work reasonably well, but is dependent on the architecture of the plant and how it is growing. For example, Bambara Groundnut is very short with the canopy low to the ground so images across the top are able to reproduce the canopy structure quite well. In contrast to this, denser and taller plants (such as the cereals) will not reproduce so well and images will only be able to capture the outer edge plants. This method has limited application for the modelling that is required for addressing the aims of this project.

- **Single Plant Imaging**

An alternative method of imaging the plants is using a dedicated imaging studio (see Figure 2.2). Multiple plants are grown together to represent field conditions; this is important as plant architecture varies based on the adjacent plants and therefore plants cannot be grown separately in pots. An individual plant is removed from the soil (maintaining the roots if the plant is to be returned) and placed in pots. These are then taken to the studio which, depending on the equipment being used, can be set up next to the where the plants are grown.



Figure 2.2: Set up of the imaging studio for single plant imaging. Plants are imaged using 3 fixed Canon 650D cameras on tripods. A turntable enables the plant to easily be rotated whilst a calibration target (coloured cardboard) aids the process and is of a fixed size, to allow the reconstructions to be scaled back to the original units. Supplementary lighting is provided if necessary.

The studio consists of backing paper (to exclude any background and to facilitate the next stage), a turntable, supplementary lighting (if required), three cameras set at varying heights, and a calibration target. The calibration target serves two purposes; firstly it aids the next stage of the reconstruction process (point cloud reconstruction), and secondly, it is of a known size so can be used to scale the final reconstruction back to the original units (see section 2.1.2.2). To provide sufficient detail in the model, over 40 images per plant are required.

2.1.2 Reconstructions

All reconstructions are carried out using the protocol of Pound *et al.* (2014). Such reconstructions require a two-stage process.

2.1.2.1 Point Cloud Reconstruction

The first stage of the process entails production of an initial point cloud estimate using the software-based technique: patch-based multi-view stereo (PMVS; Furukawa & Ponce, 2010). This software uses the two-dimensional images (section 2.1.1) to reconstruct a three-dimensional point cloud model of the plant or canopy. The algorithm requires that the intrinsic (focal length) and extrinsic (3D position and orientation) camera parameters are known. VisualSFM (Wu, 2011) is used to carry out automatic camera calibration (see Figure 2.3). Feature matching by SIFT features (Lowe, 1999) is carried out to find similarities between the input images which can be used to calculate the relative position of each camera to every other. The software enables the parameters to be changed in order to achieve an optimal output. The only parameter that will be altered during this project is PMVS threshold, which determines the level of similarity required between two images to produce a point in the final cloud. Figure 2.4 represents the difference between two different PMVS threshold settings.

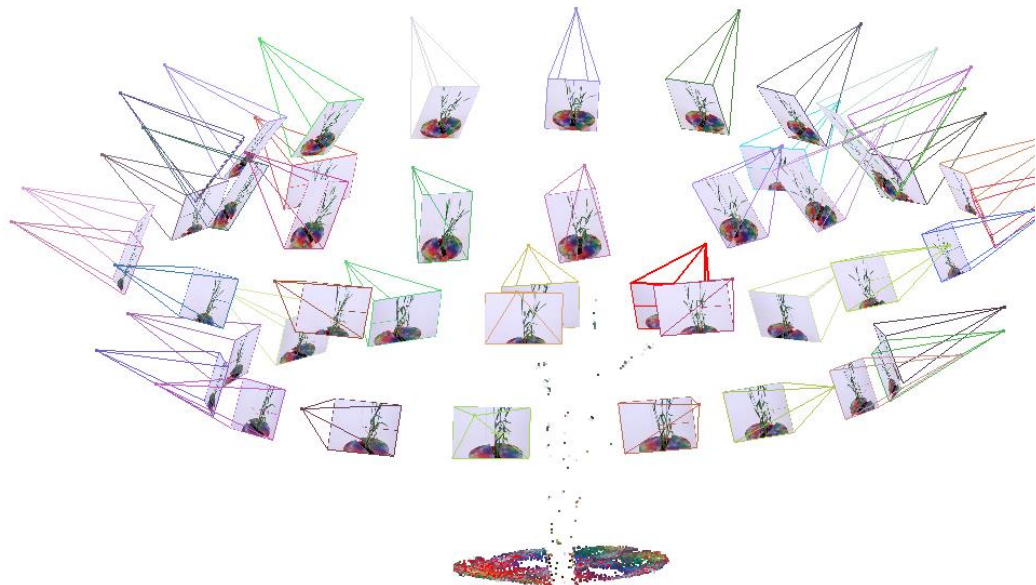


Figure 2.3: Output of VisualSFM indicating the automatically calculated camera positions and corresponding photographs surrounding the target plant. This enables the creation of a 3-dimensional point cloud.



0.45

0.7

Figure 2.4: The effect of altered PMVS threshold settings on the output point clouds of the same rice plant. The PMVS threshold is a setting in VisualSFM which determines the level of similarity required between images in order to produce a point in the final cloud

The output of the method is a 3D point cloud representation of the model. Whilst this technique has already been recognised as a platform for phenotyping, the point cloud is insufficient to carry out photosynthesis modelling, particularly for use in forward ray tracing (Song *et al.*, 2013), as a surface estimation is first required.

2.1.2.2 Surface Estimation

Surface estimation is carried out using the method of Pound *et al.* (2014). This uses the point cloud data obtained by PMVS to fit leaf surface patches as an overall representation of the plant material. This is achieved by first separating the point cloud into a number of different clusters; containing a set number of points within set bounds (see Figure 2.5 where each colour represents a different cluster). To reduce image noise, these points are then flattened onto a plane and a surface patch is assigned to each cluster. The initial surface patches are then re-sized and re-shaped according to the input images

plus information from any neighbouring patches (to prevent overlap). The resulting surface patches are then triangulated to produce a smooth mesh, representative of the original plant.

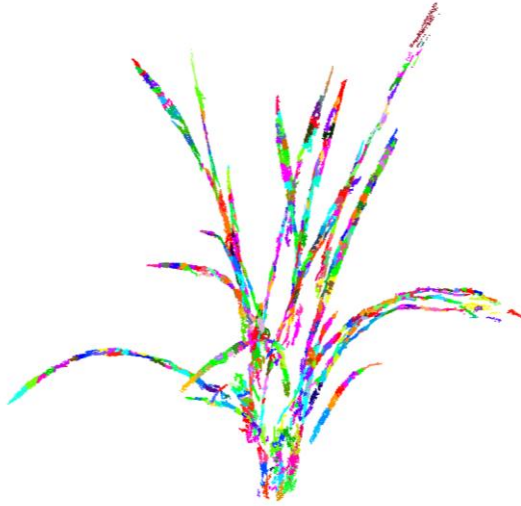


Figure 2.5: Segmentation of a point cloud into clusters. This is carried out in the Reconstructor software to enable the plant to be reconstructed as a series of 2-dimensional leaf surface patches, which, together, represent the 3-dimensional plant.

The method is user guided; therefore, depending upon the quality of the images and resulting mesh created by PMVS, a number of different settings can be altered in order to achieve the optimal mesh. A description of these parameters is given in Table 2.1. and examples of output meshes for different parameter settings are given in Figure 2.6.

Table 2.1: Details and default values of parameters in the Reconstructor software.

Parameter	Expected Value	Default	Details
Segmentation radius	Positive real number	0.01	The maximum distance between points where points are considered to be part of the same cluster. The value will depend upon the scale of the point cloud.
Alpha radius	Positive real number	0.01	The alpha value used when creating the alpha shape surface estimate. This value should be similar to segmentation radius as they both represent the expected distance between points on the same surface.
Minimum cluster size	Any integer above 0	10	The minimum number of points allowed to segregate within the same cluster. Any clusters with fewer points than this will be discarded.
Maximum cluster size	Any integer greater than minimum cluster size	60 (although standard setting is 120)	The maximum number of points allowed to segregate within a single cluster. Any extra points will be split into a separate cluster.
Level set iterations	Any positive integer	200	The number of level set iterations to run.

Boundary sample rate	Any positive integer	3	How often the boundary is sampled to calculate the final triangulation. Lower values increase boundary resolution but significantly increase the size of the output mesh (total number of triangles).
Plane filter	-	-	Indicates whether to apply a planar clipping line to the point cloud before processing. The position and orientation must be supplied in a clip.txt folder. Particularly important when imaging on a base or with the calibration target.
Colour filter	-	-	Indicates whether to apply a green-based colour filter prior to reconstruction to remove non-plant structures.

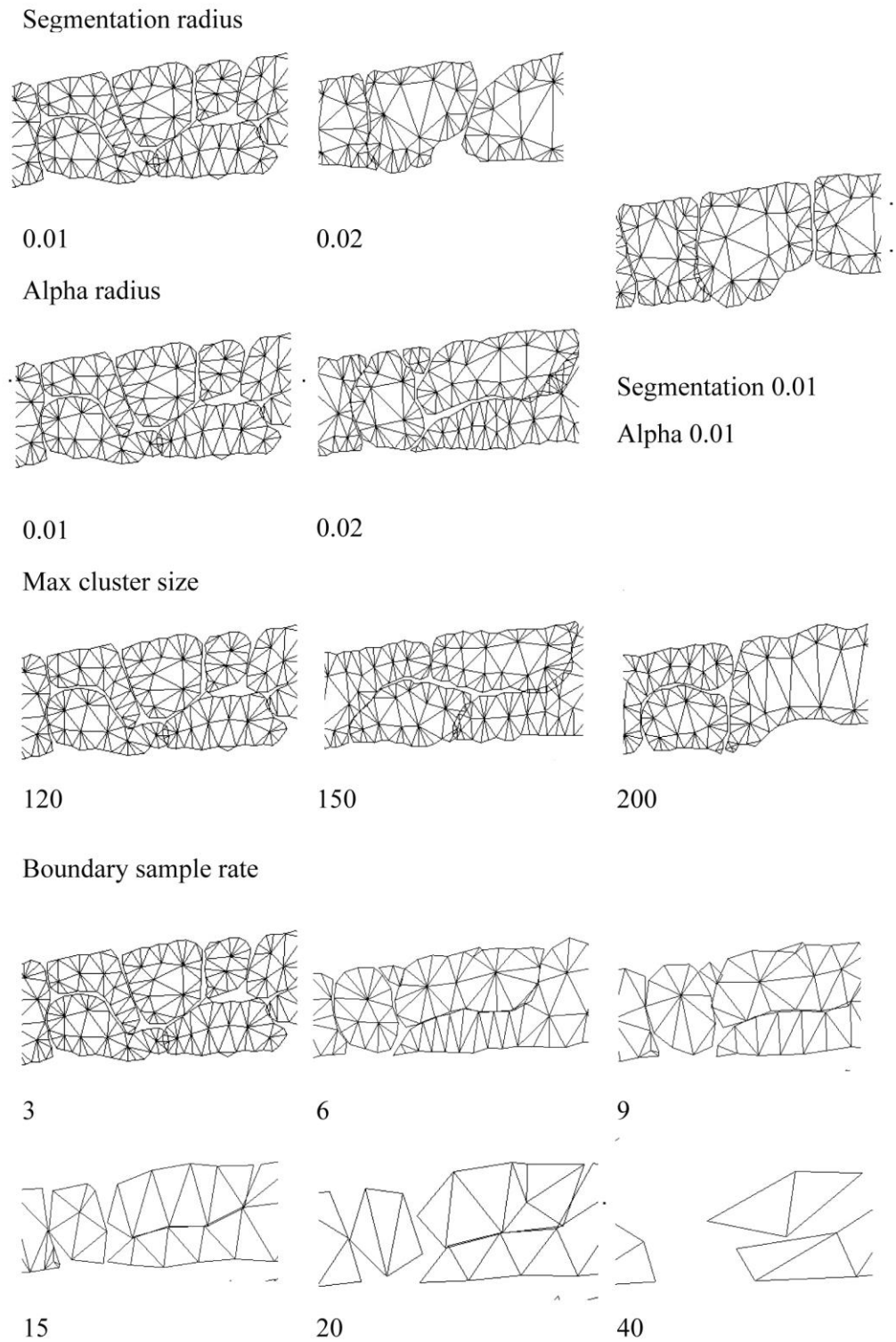


Figure 2.6: The effect of altered parameters (given in Table 2.1) on the resulting output mesh of a given section of leaf.

- *Single Plant Scaling*

The calibration target (Section 2.1.1) serves two purposes; as a tool for more accurate point cloud reconstruction, and as a means to scale the output mesh. Both PMVS and the Reconstructor software produces a model using the same ‘World coordinate’ system. When creating field plots from images of single plants, the world coordinates must be scaled back to real coordinates, in order to set accurate distances between plants. This uses the ‘Transform: Scale’ tool under the ‘Filters> Normals, Curvatures and Orientation’ menu of MeshLab, using a scaling factor calculated in Equation 2.1.

$$\text{Scaling factor} = \frac{\text{Real length of c.target}}{\text{World coordinate length of c.target in PMVS}} \quad (2.1)$$

N.B. the equivalent world coordinate length of the calibration target was calculated using the measuring tool in MeshLab. The scaled mesh was then rotated, to approximate an upright position if leaning, and translated up the Y-axis (from the origin) to account for any stem material between the soil surface and top of the calibration target, using tools in same Render menu of MeshLab.

An overview of images from each stage of the reconstruction process can be seen in Figure 2.7.

A.



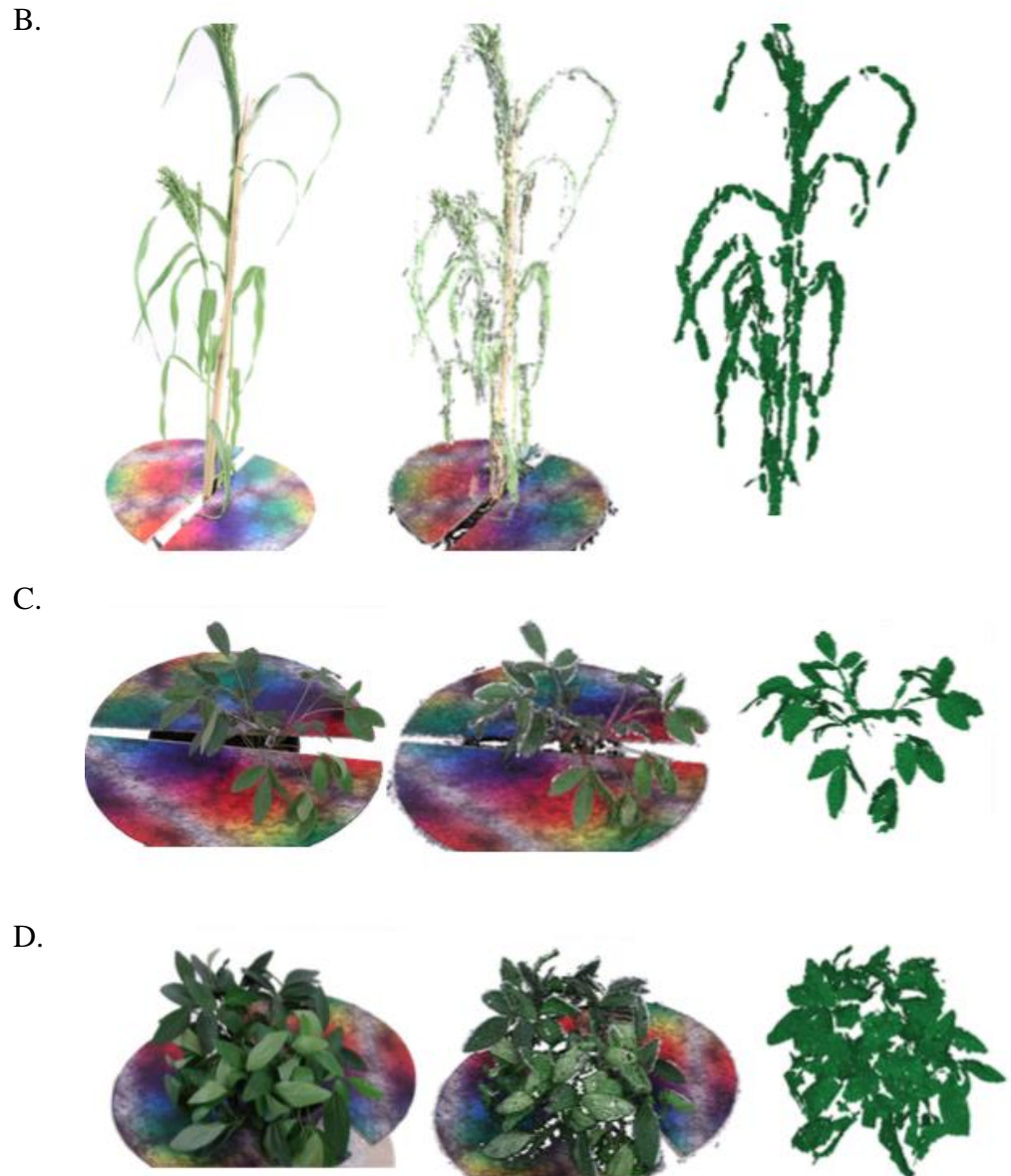


Figure 2.7: Overview of the imaging process for different crops (A) Wheat, (B) Proso millet, (C, D) Bambara groundnut (50 DAS, 80 DAS respectively), where the left image is one of the original photographs, middle is the point cloud reconstruction and right is the final output mesh

2.1.2.3 Canopy Formation

The final stage of the reconstruction process is canopy formation, where each of the single plant reconstructions is used to repopulate a canopy. The images can be rotated and spaced such that they create a heterogeneous canopy with

set crop spacing. Figure 2.8 shows an example of an intercrop canopy consisting of Proso Millet and Bambara Groundnut.

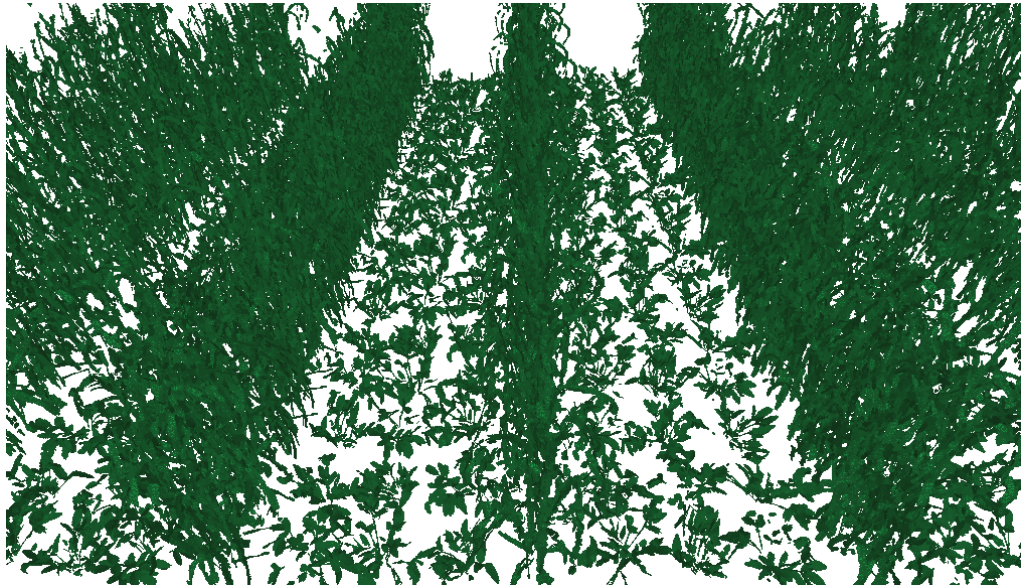


Figure 2.8: Example fully reconstructed intercrop canopy of Proso millet and Bambara groundnut with a 3:1 orientation.

2.2 Reconstruction Method Development

Because the reconstruction software was a new tool with little developmental work carried out, optimisation was required in order to achieve the best outputs for the work that was required. Achieving the optimal reconstruction output imposes a two-fold challenge: the need to represent the canopy structure as accurately as possible whilst minimising the number of triangles within the output due to time constraints of the following modelling steps (e.g. the ray tracing software: see section 2.3).

2.2.1 Reconstruction Optimisation

The 3D reconstruction method used (see Pound *et al.*, 2014), requires user-interaction to guide the process, and alter the process in order to optimise the final output mesh. In theory, it can be expected that the most accurate reconstruction mesh will have the maximal number of triangles in order to accurately represent alpha shapes, and boundaries (see methods 2.1.2.2). However, in some instances, this may not always be the case. For example, where neighbouring alpha shapes do not meet, a boundary sample rate that straightens out the resulting shape, as opposed to producing concave or convex regions, may produce a better leaf surface estimate (see Figure 2.9).

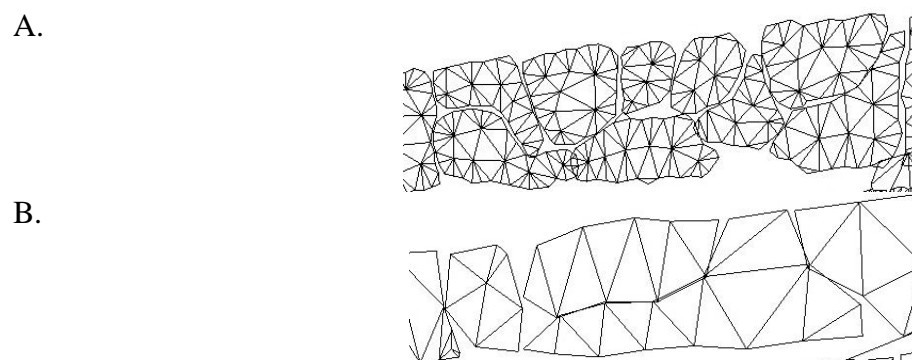


Figure 2.9: Effect of altered boundary sample rate on the output mesh. (A) Boundary sample rate set at 3. (B) Boundary sample rate set at 15. N.B. The grouping of alpha shapes in (B) may suggest a better leaf surface estimate in this region.

In instances where the maximal number of triangles optimises the reconstruction, a time constraint will be introduced due to the ray tracing step of the process (see methods 2.3). This introduces a trade-off between the need to accurately represent the model plant or canopy, but also reduce the total time taken for modelling the whole system (including imaging, reconstruction, ray tracing and photosynthesis modelling). With these trade-offs in mind, optimisation was carried out in order to indicate the optimal settings for reconstruction. As ray tracing is carried out on a sample ‘field plot’ containing multiple plants, the optimal number of triangles for a single plant reconstruction is predicted to be around 5,000 in order to minimise time taken for ray tracing.

2.2.2 Optimisation on the Artificial Dataset

To verify the accuracy of the whole reconstruction approach, Pound *et al.* (2014) created an additional artificial dataset based on a rice plant. The rice plant was initially manually modelled using the point cloud created from PMVS and 3D graphics software (Topogun, Blender). The virtual plant was coloured and textured in order to represent rice leaves before simulated image capture was carried out to render the model from 40 distinct camera angles. This created a quantifiable ground truth model, which can be used as a basis for comparing the reconstructions. Optimisation of the artificial dataset focused on altering the parameters of Reconstructor process; namely the maximum cluster size, segmentation radius, alpha radius and the boundary sample rate (see Section 2.1.2.2 for details on each of the parameters).

The accuracy of the reconstruction was assessed by comparing the percentage difference of the total mesh area of the reconstruction relative to the ground truth model (see Table 2.2.B). Mesh area was calculated using the ‘Compute Geometric Measures’ tool under the ‘Filters> Quality Measure and Computation’ menu of MeshLab. The percentage difference between the area of the ground truth model and that of the reconstruction are given. A negative value indicates the reconstructed mesh is smaller than the ground truth model, and therefore underestimates total surface area, and conversely a positive value

indicates the reconstructed mesh is larger, thus overestimates total surface area. The reconstructions model numbered 1-12 (Table 2.2) look at different combinations of maximum cluster size, segmentation plus alpha radius. As these parameters show little effect in terms of the total number of triangles produced in the mesh (bar the difference between model 1 and 2) these parameters were left at max cluster size of 120 and default settings for segmentation and alpha radius when looking for changes in boundary sample rate (models 1 plus 13-23).

Table 2.2: Simulated reconstruction features in terms of the parameters used with outputs of the total number of triangles, mesh area and difference relative to the ground truth model. N.B. Negative values for % difference indicate the reconstructed mesh is smaller, whereas positive values indicate a larger mesh, relative to the ground truth.

Model Number	Max Cluster Size	Segmentation Radius	Alpha Radius	Boundary Sample Rate	Number of Triangles	Total Mesh Area	% Difference to model
Model	-	-	-	-	-	0.250	-
1	120	0.01	0.01	3	42,289	0.249	-0.375
2	150	0.01	0.01	3	35,652	0.272	8.973
3	200	0.01	0.01	3	33,695	0.274	9.969
4	120	0.02	0.01	3	33,271	0.265	6.050
5	150	0.02	0.01	3	32,721	0.267	6.841
6	200	0.02	0.01	3	31,345	0.272	9.102
7	120	0.01	0.02	3	37,396	0.276	10.718
8	150	0.01	0.02	3	35,535	0.276	10.738
9	200	0.01	0.02	3	33,722	0.277	11.144
10	120	0.02	0.02	3	33,341	0.265	6.300
11	150	0.02	0.02	3	32,354	0.265	6.179

12	200	0.02	0.02	3	31,149	0.271	8.673
13	120	0.01	0.01	6	16,951	0.267	6.850
14	120	0.01	0.01	9	10,970	0.267	5.233
15	120	0.01	0.01	12	8,345	0.257	2.904
16	120	0.01	0.01	15	6,734	0.250	0.208
17	120	0.01	0.01	18	5,778	0.243	-2.573
18	120	0.01	0.01	20	5,215	0.237	-4.998
19	120	0.01	0.01	25	4,265	0.219	-12.186
20	120	0.01	0.01	30	3,464	0.198	-20.534
21	120	0.01	0.01	35	2,835	0.176	-29.391
22	120	0.01	0.01	40	2,438	0.153	-38.695
23	120	0.01	0.01	50	1,396	0.095	-61.929

Comparison of reconstructions in terms of total mesh area using this artificial dataset suggests that the optimal settings are with maximal cluster size of 120, alpha and segmentation radius at 0.1 and boundary sample rate set at 15 (model 16). The resulting mesh under these settings contains 6,734 triangles; not too much more than the suggested optimal of 5,000 for ray tracing.

Optimising in terms of total mesh area is justified as this method will theoretically represent the same area for photosynthesis modelling as is present in the model plant. However, the reconstruction method of Pound *et al.* (2014) has a tendency to overpredict area due to the segmentation method. Thus the optimal reconstruction in terms of area may not accurately represent the plant structure. Therefore a more accurate method of optimisation could be through use of a distance measurement to indicate the “closeness” of the reconstruction relative to the ground truth model. This uses the ‘Hausdorff Distance’ tool under the ‘Filters>Sampling’ of MeshLab. Hausdorff Distance is a measure of how far two subsets of metric space are from each other, or in this instance, how different two meshes are from each other (i.e. the ground truth model mesh and the reconstructed mesh).

Hausdorff Distance is calculated as the maximum between the two so-called one-sided Hausdorff Distances of the meshes given as:

$$d_H(X, Y) = \max\{\sup_{x \in X} \inf_{y \in Y} d(x, y), \sup_{y \in Y} \inf_{x \in X} d(x, y)\} \quad (2.2)$$

The value obtained in MeshLab will depend upon which mesh you set as X and which is set as Y; in other words, they are not symmetric. Thus both must be calculated and the largest is given as the true Hausdorff Distance. The percentage difference between the reconstructed mesh and the ground truth mesh is given in Table 2.3. The Hausdorff distance measurement suggests that the reconstruction obtained using the same settings as that for optimal mesh area (max cluster of 120, segmentation and alpha radius of 0.1 and boundary sample rate of 15; model 16) is a good representation, with only 1.5% deviation between the two meshes.

Table 2.3: Simulated reconstruction features in terms of the parameters used with outputs of the Hausdorff distance between each mesh, true Hausdorff distance and the resulting percentage difference relative to the ground truth model. Model uses the same parameters as equivalent in Table 2.2.

Model Number	X= Ground truth Y= Reconstruction	Mean	X= Reconstruction Y= Ground Truth	Mean	True Hausdorff Distance	% Difference
1	0.0135	0.00085	0.0087	0.0011	0.0135	1.347
2	0.0149	0.00086	0.0118	0.0013	0.0149	1.489
3	0.0134	0.00094	0.0115	0.0014	0.0134	1.344
4	0.0228	0.00087	0.0139	0.0013	0.0227	2.277
5	0.0211	0.00092	0.0124	0.0013	0.0211	2.114
6	0.0227	0.00096	0.0113	0.0014	0.0227	2.267
7	0.0123	0.00082	0.0094	0.0012	0.0123	1.229
8	0.0094	0.00085	0.0123	0.0013	0.0123	1.228
9	0.0117	0.00093	0.0114	0.0014	0.0117	1.172
10	0.0178	0.00086	0.0115	0.0013	0.0178	1.784
11	0.02016	0.00093	0.0110	0.0013	0.0202	2.016
12	0.0191	0.00097	0.0136	0.0015	0.0191	1.905
13	0.0136	0.00082	0.0088	0.0012	0.0136	1.358

14	0.0136	0.00083	0.0090	0.0013	0.0136	1.358
15	0.0143	0.00085	0.0075	0.0013	0.0143	1.431
16	0.0148	0.00087	0.0087	0.0013	0.0148	1.482
17	0.0156	0.00089	0.0075	0.0013	0.0156	1.558
18	0.0143	0.00092	0.0078	0.0013	0.0143	1.432
19	0.0267	0.00105	0.0078	0.0013	0.0267	2.665
20	0.0304	0.00142	0.0087	0.0013	0.0304	3.042
21	0.0317	0.00203	0.0070	0.0013	0.0317	3.173
22	0.0505	0.00337	0.0078	0.0014	0.0505	5.0523
23	0.1023	0.12191	0.0078	0.0014	0.1022	10.227

2.3 The Canopy Light Environment: Ray Tracing

The canopy reconstructions can be combined with ray tracing to calculate the incident PPFD at each triangle over the course of the day/at set time points.

Ray tracing is carried out using *fastTracer* (Song *et al.*, 2013). *fastTracer* is a C++ program that uses a forward ray tracing algorithm to simulate light (specifically photon flux density) distribution within a plant canopy. The program simulates the emission of rays of light from a source and follows their path through the canopy considering reflection and transmission from vegetative surfaces. *fastTracer* version 3 is used in this project provides output values for direct, diffused and scattered light (Figure 2.10). An output of ray tracing for a single triangle in a rice canopy can be seen in figure 2.11.

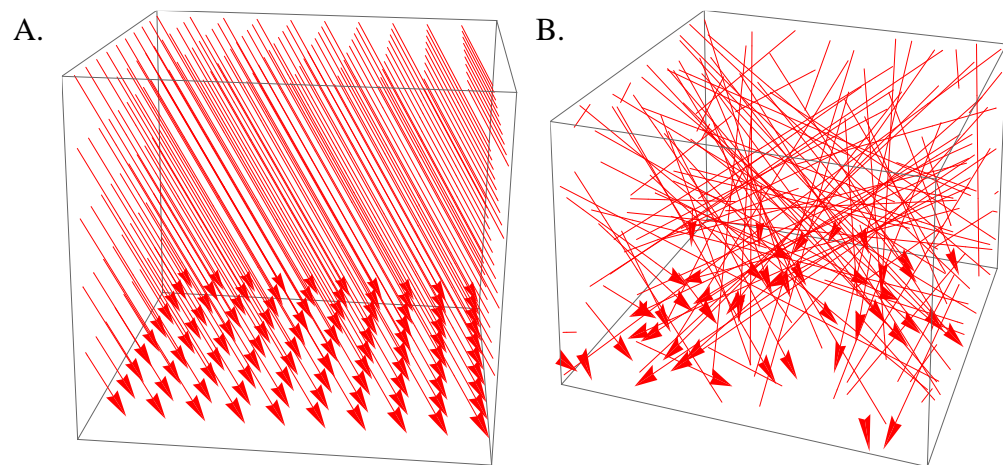


Figure 2.10: Source of light rays in *fastTracer3* for (A) direct and (B) diffused light

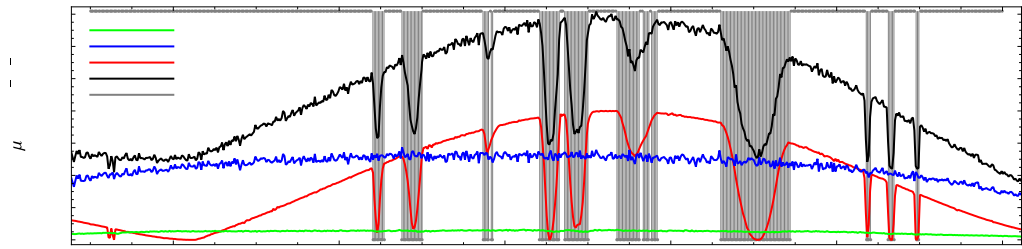


Figure 2.11: Simulated light components (from *fastTracer3*) over the course of the day for a single point within a canopy. NB. Grey shaded out areas indicate points in time where the patch of leaf (triangle) was shaded by overlapping foliage.

The full details of *fastTracer* including the command line are given in Appendix I.

Part I:
The Effect of Crop Choice and
Agronomic Practices on
Canopy Photosynthesis

Overview

This section will look at how crop choice and agronomic factors affect the canopy structure, light environment and ultimately the productivity of our cropping systems. The focus is on 4 core areas: cropping practices (monocropping versus intercropping); crop selection in relation to contrasting architectural types and the resulting light environment; wind-induced movement and; fertiliser application.

Chapter 3: Methods for exploring the light environment within multi-species cropping systems

Paper as accepted by *Annals of Botany*

Chapter 3 offers an application for the reconstruction method, ray tracing and modelling as a means to explore the light environment within an intercrop canopy. Examples from Proso millet (*Panicum miliaceum*) and Bambara groundnut (*Vigna subterranea* (L.) Verdc.) are used. This has been accepted and is in press by the *Annals of Botany*, so is presented in “paper format”.

Author contribution:

Experiment conceived by AJ Burgess

Project supervision performed by EH Murchie

Reconstruction process overviewed and aided by MP Pound

General advice and modeling section aided by R Retkute

General advice and draft editing performed by S Mayes

Glasshouse work including plant growth and measurements (gas exchange, physiology and yield etc), plant reconstruction, modelling and paper construction performed by AJ Burgess

Image-based 3D canopy reconstruction to determine potential productivity in complex multi-species crop systems

Alexandra J. Burgess, Renata Retkute, Michael P. Pound, Sean Mayes and Erik H. Murchie

Abstract

- **Background and Aims.** Intercropping systems contain two or more species simultaneously in close proximity. Due to contrasting features of the component crops, quantification of the light environment and photosynthetic productivity is extremely difficult. However it is an essential component of productivity. We present a low-tech but high-resolution method that can be applied to single and multi-species cropping systems, to facilitate characterisation of the light environment. We use different row layouts of an intercrop consisting of Bambara groundnut (*Vigna subterranea* (L.) Verdc.) and Proso millet (*Panicum miliaceum*) and analyse the new opportunities presented by this approach.
- **Methods.** Three-dimensional plant reconstruction, based on stereocameras, combined with ray-tracing was implemented to explore the light environment within the Bambara groundnut-Proso millet intercropping system and associated monocrops. Gas exchange data was used to predict the total carbon gain of each component crop.
- **Key Results.** The shading influence of the tall Proso millet on the shorter Bambara groundnut results in a reduction in total canopy light interception and carbon gain. However, the increased leaf area index (LAI) of Proso millet, higher photosynthetic potential due to the C₄ pathway and sub-optimal photosynthetic acclimation of Bambara groundnut to shade means that increasing the number of rows of millet will lead to greater light interception and carbon gain per unit ground area, despite Bambara groundnut intercepting more light per unit leaf area.

- **Conclusions.** Three-dimensional reconstruction combined with ray tracing provides a novel, accurate method of exploring the light environment within an intercrop that does not require difficult measurements of light interception and data-intensive manual reconstruction, especially for such systems with inherently high spatial possibilities. It provides new opportunities for calculating potential productivity within multispecies cropping systems; enables the quantification of dynamic physiological differences between crops grown as monoculture and those within intercrops or; enables the prediction of new productive combinations of previously untested crops.

Introduction

Intercropping systems contain two or more species simultaneously and in close proximity for at least part of their growth season. The practice of intercropping is widespread in many areas of world including regions such as the tropics where it can be the dominant form of agriculture (Kass, 1978; Beets, 1982; Francis, 1986; Vandermeer, 1989). Globally, most intercropping occurs on a small-scale in resource-poor environments (Lithourgidis *et al.*, 2011), although adoption is increasing in developed countries such as USA and areas of Europe (Jensen *et al.*, 2005; Blackshaw *et al.*, 2007; Hauggaard-Nielsen *et al.*, 2009). The production of a greater yield on a given piece of land (per equivalent component crop area) is the most commonly perceived advantage of intercropping systems (e.g. Willey, 1979; 1990; Vandermeer, 1989; Keating & Carberry, 1993; Dhima *et al.*, 2007; Mucheru-Muna *et al.*, 2010; Lithourgidis *et al.*, 2011). Often, growth resources such as light, water and nutrients can be more efficiently exploited within the intercrop system as a result of differences in the growth and competitive ability of the component crops (Midmore, 1993; Tsubo *et al.*, 2001). The benefits achieved will depend upon the crop combination used (for reviews on the benefits of intercropping see Malézieux *et al.*, 2009; Lithourgidis *et al.*, 2011; Brooker *et al.*, 2015), although cereal-legume intercropping systems are commonly adopted as a synergistic system due to the nitrogen-fixing ability of the legume component

and provide increased yield under adverse conditions (Ofori & Stern, 1987; Dhima *et al.*, 2007).

Understanding and maximising the productivity of intercropping systems is limited by the ability to accurately predict the resources captured and used by each of the components (Azam-Ali and Squire, 2002). One of the key features of an intercropping system is the complex canopy structure achieved within a multiple species assemblage. Differences between the component crops in terms of developmental pattern and response to the competitive presence of other plants, planting density, row orientation and the local environment leads to differences in architectural features such as plant height, leaf size, shape and orientation plus the degree of foliage overlap (Keating & Carberry, 1993; Jaya *et al.*, 2001). Furthermore, canopy characteristics are not fixed, but will alter in response to the competitive presence of the other species (Keating & Carberry, 1993; Zhu *et al.*, 2016). This can be seen within a wheat-maize intercropping system, where key architectural features (including tiller production, tiller survival rate and leaf size) differed between sole cropped wheat plants; wheat plants bordering maize plants (i.e. with maize one side and wheat the other) and wheat plants in the inner row (i.e. with wheat either side; Zhu *et al.*, 2016). This necessitates the need to develop methodologies that can incorporate this level of complexity and separate out responses of different component crops, or even different row responses.

The unique changes in architectural traits of intercropping systems also have consequences in terms of light transmission and absorption. Two or more species growing together in close proximity will intercept light both quantitatively and qualitatively differently than the equivalent monocrops (Vandermeer, 1989). As solar radiation provides the energy for photosynthetic processes, this will determine the potential for system productivity. Therefore both light interception and radiation use efficiency (biomass generated per unit radiation intercepted) provide two routes (either singularly or in combination) of improving intercropping systems (Willey, 1990). Light interception can be improved both temporally and spatially; by lengthening the period of soil

coverage (i.e. extending the growing season; temporal complementarity) by one or more crop species or by optimising the distribution of leaf material within the canopy to maximise interception (spatial complementarity; Fig. 3.1) (Keating and Carberry, 1993; Brooker *et al.*, 2015). Separating spatial and temporal complementarity provides two benefits when considering and optimising intercropping systems. Firstly, it highlights the importance of crop features which can lead to better resource use (e.g. plasticity; Zhu *et al.*, 2015; 2016). Secondly, it indicates two means through which resource use can be improved: through greater resource ‘capture’ or through greater resource conversion efficiency (e.g. photosynthesis and transpiration). As well as increased light interception, rapidly growing crops that show early canopy closure could contribute to weed suppression (Midmore, 1993), a common problem in many cropping systems (e.g. Asiwe & Kutu, 2007). Earlier work on drought tolerance in Bambara groundnut cropping systems indicates that early in the season, canopy cover is the major limitation to productivity, with reductions in leaf production and expansion negatively affecting dry matter production (Collinson *et al.*, 1999).

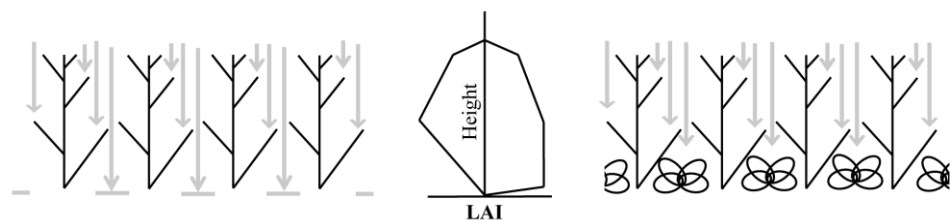


Figure 3.1: Theoretical example of light transmission through a monocropped canopy (left) versus an intercrop canopy (right). The estimated leaf area index (LAI) as a function of depth is given for each canopy.

Within the rest of this paper, we will focus on methods to optimise resource capture; namely light interception. However, in order to optimise systems further, accurate predictions of light interception within the system is first required. In theory, light capture by intercrops could be measured by similar methods to that seen for sole crops (Azam-Ali & Squire, 2002). This could be

through the use of PAR sensors, tube solarimeters, ceptometers and line sensors, placed such that they capture a representative sample of the crop system (Francis, 1986; Azam-Ali and Squire, 2002). Such methods could provide good estimates where the component crops are distinctly separate (i.e. the component occupy separate canopy volumes) and are relatively uniform, for example; early in the growth stage or with sufficient distance between rows or in strip intercropping (Marshall & Willey, 1983; McMurtrie & Wolf, 1983; Zhang *et al.*, 2014). However they will be less accurate in more heterogeneous systems and will not be able to capture small scale features needed for high resolution modelling. Traditional sensors can also be used for morphologically similar component crops (e.g. Clover swards; Black, 1960; 1961) where it can be assumed that light interception can be attributed to the proportion of total leaf area of each component. Horizontal uniformity within canopies can be assumed in these instances (Duncan *et al.*, 1967) but due to leaf clumping and row arrangement of crops, light penetration through the canopy is often underestimated. Where the different crops are structurally different, details of light interception by each component would be difficult to obtain and would require an extensive amount of sensors and architectural differences between the component crops will lead to inaccurate predictions, as interception dependencies based on surface area will diverge for each component. Estimations in these cases will often result in large errors as a result of the spatial variation within intercrop canopies, particularly the row arrangements, orientations and distribution of foliage (Azam-Ali and Squire, 2002). Furthermore, heterogeneity is more common in low resource agricultural systems where intercropping is common. For these reasons, direct measurements of light interception by each component within a multi species system are not economically or experimentally feasible (Sonohat *et al.*, 2002).

Contrary to direct measurement techniques, modelling approaches for estimating light within multispecies systems are advancing rapidly. To explore the relationships between intercrop design, canopy architecture and the resulting light environment and productivity, experimental results need to be combined with high-resolution methods of plant modelling (Zhu *et al.*, 2016).

For morphologically distinct component crops, detailed measurements of individual species canopy structure can be combined with mathematical models of light patterning in order to model interception within intercrop canopies. Models in the literature range from low- to high- resolution, with low-resolution methods often assuming uniformity as discussed above. More accurate estimations of the light environment within an intercrop canopy require detailed, geometrically accurate three-dimensional models of component plants. Advances in computing power combined with affordability of both software and hardware has led to the development of a number of different techniques in order to capture plant structure (Watanabe *et al.*, 2005; Quan *et al.*, 2006; Song *et al.*, 2013; Pound *et al.*, 2014; Zhu *et al.*, 2015). One example of this is 3D reconstruction based on stereocameras, which relies on digitising a pre-existing structure, using a set of images as a basis (image-based reconstruction). Applications of image-based methods are diverse including the estimation of canopy height, diameter and crown volume in isolated trees (e.g. Brown *et al.*, 2000; Phattaralerphong and Sinoquet, 2005; Patterson *et al.*, 2011); for the study of structural properties in sole cropping canopies (e.g. Ivanov *et al.*, 1995; Burgess *et al.*, 2015) or root systems (e.g. Lobet *et al.*, 2011) and for predictions on light interception or photosynthetic modelling (e.g. Andrieu *et al.*, 1995; Pound *et al.*, 2014; Burgess *et al.*, 2015). Accessible but high resolution methods are increasingly needed to explore the complex temporal and spatial dynamics of light environment within canopies and have distinct advantages for multispecies intercrops where spatial possibilities are greater.

In this paper we put modern methods for canopy reconstruction in the context of multispecies cropping systems and aim to test (1) whether image-based reconstruction can be used as a means to explore the light environment at high spatial resolution within a multi-species assemblage (2) if such methods provide new architectural and functional information (not achievable with previous manual measurements) when combined with ray tracing and (3) whether suboptimal photosynthetic acclimation affects productivity of the systems. We have employed the reconstruction method of Pound *et al.* (2014),

in which a 3D point cloud can be obtained with inexpensive SLR cameras and then automatically converted to a 2D leaf surface, for use in ray tracing (Song *et al.*, 2013). This method reconstructs the full canopy structure (not just the canopy surface) and ‘maps’ the complex patterns of light within the canopy over a whole day. We use examples from an intercropping system consisting of Bambara groundnut (*Vigna subterranea* (L.) Verdc) and Proso millet (*Panicum miliaceum*) and their monocultures in order to assess light interception and potential productivity. The component crops were selected due to their compatibility as intercrops in terms of climate and soil requirements, differing growth durations and previous work carried out on legume-cereal systems, including Pearl millet and Groundnut (Willey, 1990). The tall (>1.2m) Proso millet combined with the much shorter (<50cm), broad leaved Bambara groundnut crop provides an interesting combination for exploring the light environment due to shading effects, yet the shorter growth duration of Proso millet (60-90 days, compared to up to 150 days for Bambara groundnut) means that this shading would not be present for the whole growth season. This system therefore provides a means to explore the potential for both spatial and temporal complementarity. A modelling approach explores how different row layouts of the intercrop may influence the light environment and productivity in terms of total light interception and canopy carbon gain. This is the first such method to date that combines high-resolution modelling of ‘real’ intercrop canopy architecture (i.e. not simulated architecture) with a simulation of light to predict photosynthetic responses within the whole intercrop system.

Materials and Methods

Plant Material

Bambara groundnut X Dip C (*Vigna subterranea* (L.) verdc.) and Proso millet (*Panicum miliaceum*; landrace from Sri Lanka) were sown directly into beds in the FutureCrop Glasshouse facilities, University of Nottingham Sutton Bonington Campus, UK on the 20th May 2014. This is an agronomy style glasshouse designed and built by CambridgeHOK (Brough, UK) for the analysis of whole crop canopies under controlled conditions. It consisted of a concrete tank 5 m x 5 m x 1.25 m positioned at ground level. The tank was filled entirely with a sandy loam soil, extracted from local fields and sieved through a fine mesh. Plants were sown as four treatments: sole Bambara groundnut, Sole Proso millet, 3 rows of Bambara groundnut: 1 row of Proso millet (3:1) and 2:2, with 25cm between rows, 25cm between plants within rows of Bambara groundnut and 10cm between plants within rows of Proso millet. Irrigation was supplied using drip irrigation for 5 minutes, twice daily. Metal halide lamps provided additional lighting whenever the photosynthetically active radiation (PAR) fell below 200 $\mu\text{mol m}^{-2} \text{s}^{-1}$ and a 12-h photoperiod (0700 h to 1900 h) was maintained using blackout blinds. A constant temperature of $28\pm 3^\circ\text{C}$ and relative humidity (RH) of 50–60% was maintained throughout. As intercroops are generally grown under low input agriculture, no additional fertiliser was supplied during the trial to both the intercrop treatments or the sole plots. The previous crop was rice. An image of the 2:2 intercrop treatment is given in Supplementary Figure S3.1.

Imaging and Ray Tracing

3D analysis and reconstruction of plants was made according to the protocol of Pound *et al.* (2014). Following photosynthesis measurements, the Bambara groundnut and Proso millet plants (roots and shoots) were carefully removed from the glasshouse, placed into pots and taken to the imaging studio located nearby to prevent excessive movement and damage to leaves. For the light

analysis, plants were removed 53 days-after-sowing (DAS) for imaging. Roots were supplied with water to prevent wilting. It was found that this process did not alter the key architectural or structural features of the plants. They were imaged within 1 hour according to the protocol of Pound *et al.* (2014) and Burgess *et al.* (2015). An overview of the reconstruction process for an example Bambara groundnut and Proso millet plant can be seen in Supplementary Figure S3.2.

Three replicate plants representative of the morphology of Bambara groundnut and Proso millet were taken and reconstructed to form the final canopies. The Proso millet panicles were manually removed from the resultant mesh, as the reconstructing method is unable to accurately represent their form. Duplicating and randomly rotating the millet reconstructions in a 5x3 grid pattern, with 25 cm between rows and 10 cm between plants within rows, created the Sole Proso millet canopy. Sole Bambara groundnut canopies similarly but in a 3x3 grid pattern with 25 cm within and between rows. Intercropping canopies with different orientations (1:1, 2:1, 3:1, 4:1) were created similarly, with 25 cm between rows, 25 cm between plants within rows of Bambara groundnut and 10 cm between plants within rows of Proso millet. An example of a full intercrop canopy reconstruction (3:1 row layout) is given in Supplementary Figure S3.3. Reconstructed canopies consist of n triangles with coordinates of i th triangle given by a vector $\{x_i^1, y_i^1, z_i^1, x_i^2, y_i^2, z_i^2, x_i^3, y_i^3, z_i^3\}$, where coordinates x and y correspond to the coordinates on the ground, and coordinate z corresponds to height above the ground.

Total light per unit leaf area for the i th triangle at time t , $L_{-i}(t)$, was predicted using a forward ray-tracing algorithm implemented in fastTracer (fastTracer version 3; PICB, Shanghai, China; (Song *et al.*, 2013)). Latitude was set at 4.2, atmospheric transmittance at 0.5, light reflectance at 7.5% and light transmittance at 7.5%. The diurnal course of light intensities over a whole canopy was recorded at 6 minute intervals. The ray tracing boundaries were positioned so as to achieve further intercropping treatments (1:1, 2:1, 2:2, 3:1,

3:2, 4:1, 4:2). The software fires rays through a box with defined boundaries: when they exit one boundary (i.e. the side) they enter again from the opposite side; effectively replicating anything within the designated boundaries.

For a proof of concept canopy development time course, Bambara groundnut plants were grown in 5 L pots and Proso millet in 3 L pots, which were sunk into the experimental plots, these were removed every 9 days (from 21 DAS) for imaging then replaced. This was due to space constraints in the glasshouse meaning that multiple plants could not be removed every 9 days. The same reconstruction process was carried out on these plants but they were not analysed for light interception (ray tracing).

Physical and physiological measurements

Gas Exchange

Measurements were made on glasshouse-grown Proso millet and Bambara groundnut in plots in the same week in which the plants were imaged (early July 2014). Leaf gas exchange measurements were taken with a Licor 6400XT infra-red gas-exchange analyser (LI-COR, Nebraska). The block temperature was maintained at 30°C using a flow rate of 500 ml min⁻¹. Light was provided by a combination of in-built red and blue LEDs. Light-response curves were taken on leaves that had not been dark-adapted. Illumination occurred over a series of 9 photosynthetically active radiation values between 0 and 2000 $\mu\text{mol m}^{-2} \text{s}^{-1}$, with a minimum of 2 minutes and maximum of 3 minutes at each light level, starting at high intensities before reducing to zero. Light-response curves were taken at 3 different canopy heights; labelled top, middle and bottom for Proso millet, and 2 different canopy heights; labelled top and bottom for Bambara groundnut, approximately equidistant throughout canopy depth, with height above ground being noted. Three replicates were taken per treatment per crop (sole Proso millet, Sole Bambara groundnut, 2:2 and 3:1) for each canopy layer.

Ceptometer

To validate the light interception predicted by ray tracing, fractional interception was calculated at varying distance from the centre of a plant (i.e. along a row) using a ceptometer (AccuPAR) in a sole Bambara groundnut canopy. Light levels at the top and bottom of the plant canopies at 0, 2.5, 5, 7.5, 10 and 12.5 cm from the centre of a Bambara groundnut plant were measured. 10 replicates were taken per location. This was compared to fractional interception calculated from ray tracing (Fig. 3.2).

Statistics

Analysis of variance (ANOVA) was carried out on the fitted P_{\max} parameter from light response curves using GenStat for Windows, 16th Edition (VSN International Ltd.). Data was checked to see if it met the assumption of constant variance and normal distribution of residuals.

Modelling

All modelling was carried out using Mathematica (Wolfram).

All triangles in each canopy reconstruction were assigned an identification code depending upon whether they were part of a Proso millet Reconstruction or Bambara groundnut. The ray tracing files were then separated according to this identification code so the different component crops could be treated separately. A filter was applied to remove any data with PPF_D values below 0 (i.e. those outside of the ray tracing boundaries or in the simulated “night time”) and direct, diffused and scattered light were combined per triangle and time point to give a single PPF_D value.

Total canopy light interception per unit leaf area was calculated according to Eq 1.

$$TL_{LA} = \frac{\sum_{i=1}^n S_i \int_5^{22} L_i(t) dt}{\sum_{i=1}^n S_i} \quad (1)$$

where S_i is the area of triangle i .

Total canopy light interception per unit ground area was calculated as light interception divided by the area of the ground each row of the component in the treatment took up (Eq. 2).

$$TL_{LA} = \frac{\sum_{i=1}^n S_i \int_5^{22} L_i(t) dt}{N_{rows} (\text{row.max } x_i - \text{row.min } x_i) (\text{row.max } y_i - \text{row.min } y_i)} \quad (2)$$

To predict the productivity of each of the intercrop treatments, as they would occur in the field, total canopy light interception per unit ground area for both components together was calculated as a ratio of the number of rows of each component together (Eq. 3).

$$TLI = \frac{N_{rows}^{BG} * TL_{LA}^{BG} + N_{rows}^{PM} * TL_{LA}^{PM}}{N_{rows}^{BG} + N_{rows}^{PM}} \quad (3)$$

For each depth (d ; distance from the highest point of the canopy), we found all triangles with centres lying above d (Eq. 4).

$$d_i = \max_{j=1,2,3; 1 \leq i \leq n} z_i^j - (z_i^1 + z_i^2 + z_i^3)/3 \quad (4)$$

The response of photosynthesis to light irradiance, L , was calculated using a nonrectangular hyperbola given by Eq. 5:

$$F_{NRH}(L, \phi, \theta, P_{max}, \alpha) = \frac{\phi L + (1 + \alpha) P_{max} - \sqrt{(\phi L + (1 + \alpha) P_{max})^2 - 4\theta \phi L (1 + \alpha) P_{max}}}{2\theta} - \alpha P_{max} \quad (5)$$

The nonrectangular hyperbola is defined by four parameters: the quantum use efficiency, ϕ ; the convexity, θ ; the maximum photosynthetic capacity, P_{max} and; the rate of dark respiration, R_d . We assumed that the rate of dark respiration is proportional to the maximum photosynthetic capacity, according to the relationship $R_d = \alpha P_{max}$ (Givnish, 1988; Niinemets and Tenhunen, 1997;

Retkute *et al.*, 2015). Curve fitting was carried out using the Mathematica command **FindFit** with a minimum constraint on α at 0.05 and θ at 0.6.

The carbon assimilation at triangle i was calculated by combining Eq. 5 with the predicted PPFD at triangle i for each hour. Daily carbon assimilation, P_i (Eq. 6), was then calculated by integrating the rate of photosynthetic carbon uptake over the day and multiplying by the area of the triangle, S_i .

$$P_i = S_i \int_5^{22} F_{NRH}(L_i(t), \phi, \theta, P_{max}, \alpha) dt \quad (6)$$

As each canopy was divided into 3 layers for Proso millet and 2 layers for Bambara groundnut, each triangle from the digital plant reconstruction was assigned to a particular layer, m , according to the triangle centre (i.e. with triangle centre between upper and lower limit of a layer depth). Carbon gain per unit leaf area, C_l , was calculated as daily carbon assimilation over a whole canopy divided by the total surface area of the canopy according to Eq. 7.

$$C_l = \frac{\sum_{i=1}^n P_i}{\sum_{i=1}^n S_i}. \quad (7)$$

Carbon gain per unit ground area, C_g , was calculated as daily carbon assimilation over a whole canopy divided by the area of the ground each row of the component in the treatment took up according to Eq. 8.

$$C_g = \frac{\sum_{i=1}^n P_i}{N_{rows}(\text{row}_i \max x_i - \text{row}_i \min x_i)(\text{row}_i \max y_i - \text{row}_i \min y_i)} \quad (8)$$

Results

Validation of imaging and modelling

Previous studies validated the imaging and ray tracing techniques, showing that they are able to accurately and quantitatively predict physical properties within sole cropped cereal canopies. The difference in leaf area using manual measurements and reconstructed plants has been shown to be low (4% in Pound *et al.*, 2014, and 1% in Burgess *et al.*, 2015) and similar percentages of leaf and stem material plus accurate leaf angles can be reproduced (Supp. Tables S1 and S2 in Burgess *et al.*, 2015). Light interception throughout canopy depth has also been shown to be accurate (see Fig. 5 in Burgess *et al.*, 2015). In this study we strengthen this: physical measurements were made to validate spatial differences in light interception. Fractional interception along a row in sole cropped Bambara groundnut was calculated from ceptometer data and from modelled data; the results are given in Fig. 3.2. Good correspondence between measured and predicted values was seen. Despite this being a sole canopy it has the same bimodal properties as seen in intercrops.

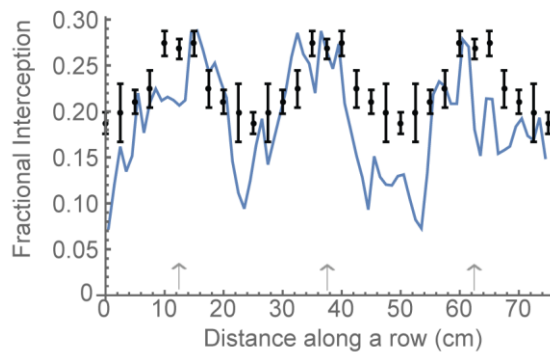


Figure 3.2: Validation of light interception in a sole Bambara Groundnut canopy. Fractional interception was measured with a ceptometer (dots: mean \pm SEM) and calculated from ray tracing (line) with distance along a row. Arrows indicate the location of the centre of the plants in a row.

The Light Environment

The light environment within the intercropping treatments is most easily visualised by colouring the leaf material in the reconstructions according to the light levels they experience (see Fig. 3.3 for values at 1200 h). As the reconstructed canopies are represented as a series of triangles, they may each be coloured according to the PPFD value from the ray tracing output for any time of day. More red indicates high levels of light whereas more grey indicates low levels of light. This is a useful way of instantly visualising light distribution in different canopy arrangements across small spatial scales that was not before possible with techniques that integrate light over greater spatial scales. A quantitative method of visualising the light dynamics between different treatments can be seen in Fig. 3.4. By plotting the average PPFD received as a function of the fraction of the surface area of each component canopy, we can see peaks in distribution indicating that large proportions of the canopy leaf area are receiving similar levels of light. There is a shift in distribution towards a greater fraction of surface area under higher PPFD levels as the proportion of Bambara groundnut increases. This is due to the shading effects imposed by Proso millet in the intercrop treatments. Contrary to this, there is a progressive shift in the opposite direction towards lower PPFD values for the sole Proso millet relative to any of the intercropping canopies as less light is able to penetrate within and between the rows. This shows that increasing the ratio of Bambara to millet increases the amount of light received per plant for both species. The relationship between LAI and total PPFD per unit leaf area along a row for the sole cropping and a 2:1 intercropping treatment is given in Supp Fig. S3.4; the position of the centre of plants in each row is given by arrows.

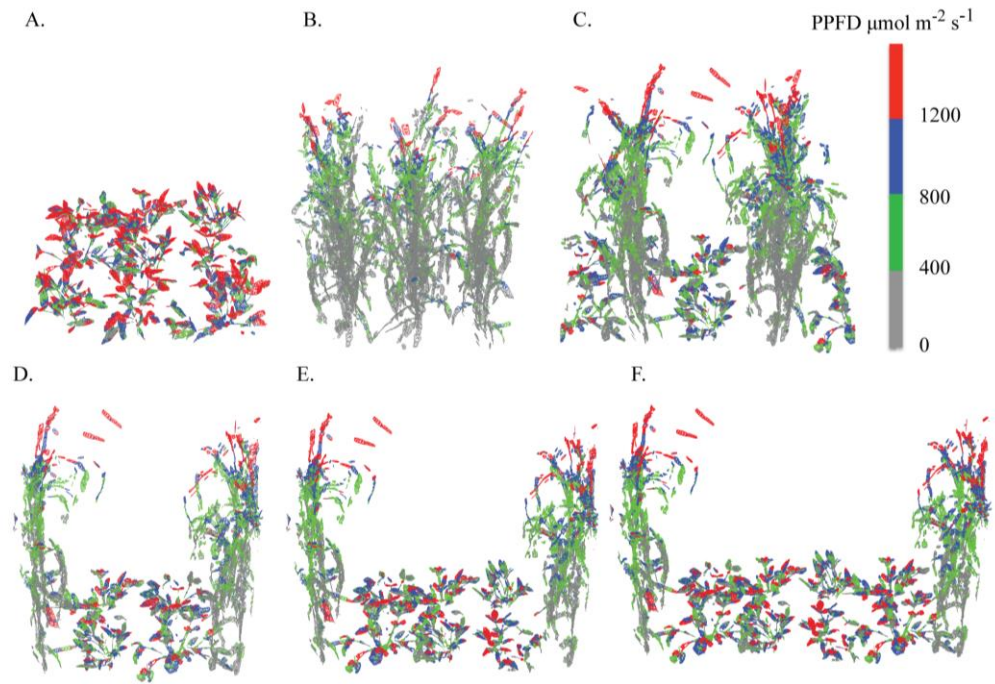


Figure 3.3: Representative reconstructed canopies with the maximum PPFD ranges colour coded for 1200 h. (A) Sole Bambara groundnut, (B) Sole Proso millet, (C) 1:1, (D) 2:1, (E) 3:1 and (F) 4:1 (Rows of Bambara groundnut: Proso millet).

To quantify how much light each of the components and treatments are receiving, total light interception was calculated (Fig. 3.5; Eqs. 1-2; Materials and Methods). On a unit leaf area basis, sole Bambara groundnut intercepts more light than sole Proso millet however, the opposite is seen on a per unit ground area basis, due to the much higher LAI of Proso millet (LAI values given in Table 3.1). Similar patterns can be seen when looking at each separate component on a per unit leaf area and ground area basis (Fig. 3.5A-D). For example, of the intercrop treatments tested within this study, both Bambara groundnut and Proso millet exhibit a greater light interception (leaf area⁻¹ and ground area⁻¹) in the 4:1 row orientation. As the number of rows of Bambara groundnut decreases, the total light interception also decreases. The greater number of rows of millet *also* reduces total light interception. However, to fully assess light interception by an intercrop, both components must be studied together (Eq. 3; Materials and Methods; Fig. 3.5E). The average interception per unit ground area indicates that a sole Proso millet canopy

intercepts the most amount of light and the sole Bambara groundnut canopy the least amount of light of all treatments tested (monocrop and intercrop). Of the intercrop treatments, 1:1 gives the greatest light interception, with reducing interception with increased rows of Bambara groundnut. These results are consistent with the LAI values for each of the treatments (Table 3.1), with the greatest LAI leading to the greatest total light interception value. Similarly to Barillot *et al.* (2011), we found a strong relationship between the component contribution to LAI and the PPFD intercepted (Supp Fig. S3.5). There was a tendency for a higher PPFD interception by Proso millet relative to contribution LAI for all intercrop treatments.

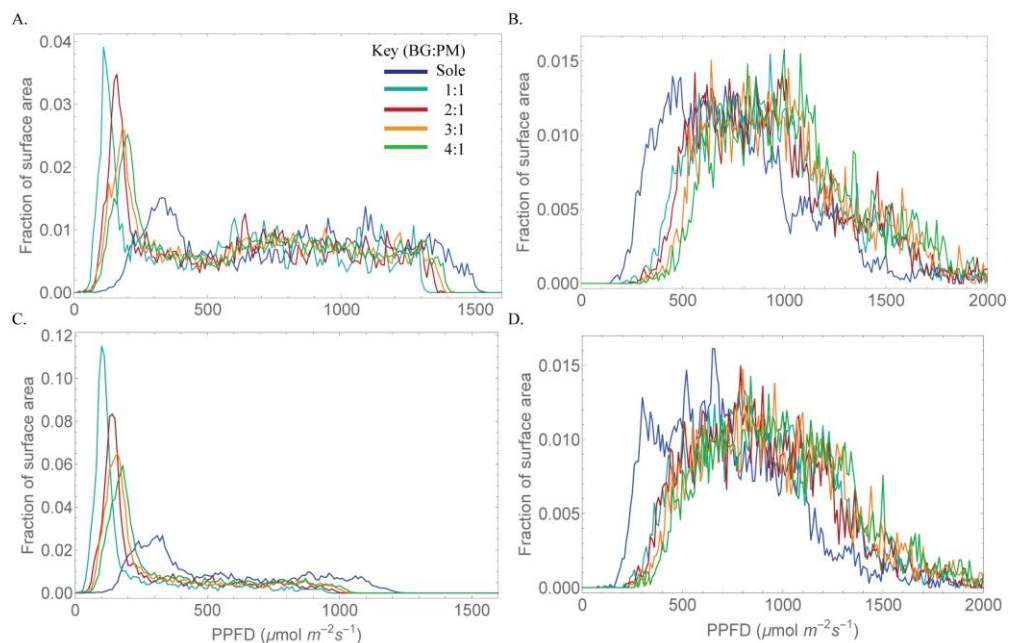


Figure 3.4: Frequency of PPFD values according to the fraction of surface area received at the top layer within each canopy. (A,C) Bambara groundnut and (B,D) Proso millet where (A,B) 1200 h (direct light from above) and (C,D) 1500 h (direct light from the side).

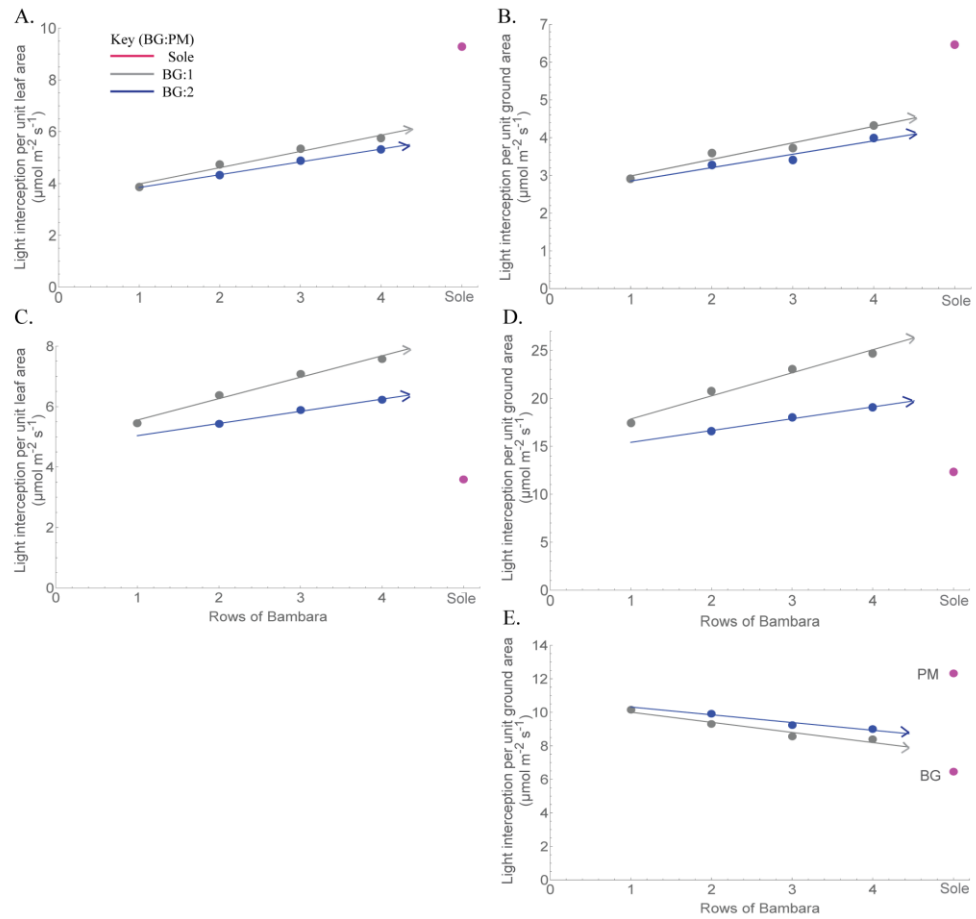


Figure 3.5: Modelled total canopy light interception over the course of the day for different intercrop treatments and respected sole crops. (A,C) per unit leaf area and (B,D,E) per unit ground area. (A,B) Bambara groundnut, (C,D) Proso millet and (E) both component crops.

Treatment (BG:PM)	LAI
Sole BG	0.701258
Sole PM	3.42008
1:1	1.97273
2:1	1.59127
2:2	1.90878
3:1	1.338
3:2	1.64266
4:1	1.25194
4:2	1.52017

Table 3.1: Total leaf area index (LAI) for each of the treatments. LAI was calculated as the area of all triangles (from both Bambara groundnut and Proso millet reconstructions) within the ray tracing boundaries divided by the ground area within the boundaries.

Assessing Productivity

Intercepted light must be used efficiently i.e. the proportion of light in excess of photosynthetic requirements should be as low as possible. The method described here is able to distinguish light distribution with high spatial resolution and therefore photosynthesis modelling becomes highly accurate and presents more opportunities for calculating the proportion of excess light in different systems. Here we use an empirical model with light response curves; measured at 3 different canopy layers for Proso millet and 2 layers for Bambara groundnut. A nonrectangular hyperbola (Eq. 5; Materials and Methods) was fitted to the experimental data in order to determine the quantum use efficiency (ϕ), convexity (θ) and maximum photosynthetic capacity (P_{\max}). Fitted curves are given in Fig. 3.6. These results are in broad agreement with previous studies on Bambara groundnut and C_4 species (e.g. Dias-Filho, 2002; Cornelissen, 2005). The maximum photosynthetic capacity decreased with depth in the canopy for each of the component crops. Such responses are typical of canopy depth-dependent changes caused by light acclimation and

leaf ageing (Murchie *et al.*, 2002). There was no significant difference in P_{\max} for any layer between the intercrop treatments of sole cropping for either component crop.

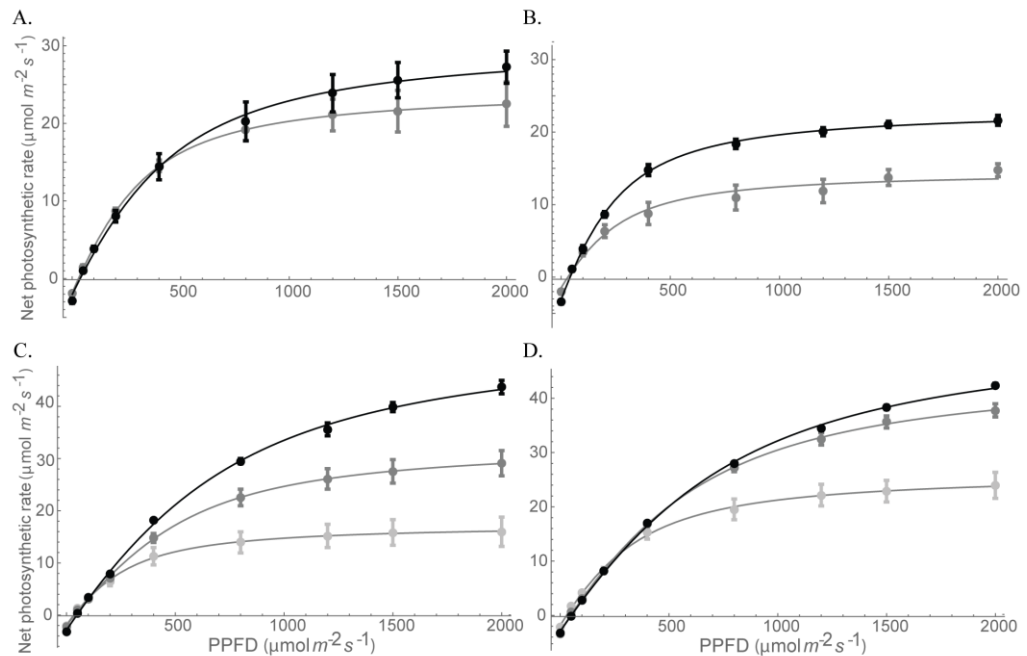


Figure 3.6: Example light response curves. (A,B) Bambara groundnut layers top (black) and bottom (grey); sole plot and intercrop (3:1) treatment, respectively. (C,D) Proso millet layers top (black), middle (dark grey) and bottom (light grey); sole plot and intercrop (3:1) treatment, respectively.

The analyses in Fig. 3.4 and 3.6 can be compared to see how the levels of photosynthesis match light availability (see Supp. Fig. S3.6 for overlaid graph). Generally speaking large peaks at low light levels in Fig. 3.6 will reduce canopy productivity since they match lower photosynthesis rates. The optimal position is at the point of light saturation of photosynthesis, which broadly for Bambara groundnut is between 600 and 800 $\mu\text{mol m}^{-2} \text{s}^{-1}$ regardless of canopy position or cropping arrangement. However Fig. S3.6 also shows the average canopy light level superimposed with light response curves for midday. Photosynthesis in most leaves was near- saturated at mid-day in Bambara and position ranked according to cropping pattern. The higher the proportion of

Bambara in the system the more saturated was photosynthesis and the greater the potential proportion of excess absorbed light energy. In contrast the Proso millet crop was only part saturated even at $1000 \mu\text{mol m}^{-2} \text{s}^{-1}$, consistent with C_4 physiology. The point at which saturation was reached was around the same value for all canopy positions. Greater spacing and light penetration (Fig. 3.4) resulted in a higher rate of light saturated photosynthesis in lower canopy layers due to acclimation of photosynthesis (Fig. 3.6) (Murchie and Horton 1997; Murchie *et al.*, 2002; Anderson 1995). For Bambara groundnut the opposite is the case with acclimation to low light reducing light saturated photosynthesis in both cases. Therefore, Bambara intercrop component would not be able to make use of higher direct light at midday. Additionally comparison with Fig. 3.4 and the measured differences in light compensation point and dark respiration rates, which were small, suggests that they would not substantially better at exploiting the lower light levels than the sole crop. Therefore such suboptimal acclimation of photosynthesis in Bambara should play an important role in restricting productivity in intercrops.

To predict canopy productivity, daily net photosynthesis per unit leaf area and per unit ground area was also calculated for each component per treatment (see Eqs. 6-7; Materials and Methods); results are given in Fig. 3.7. A line of best fit indicates the relationship between the number of rows of Bambara groundnut between each row of Proso millet and the total canopy carbon gain for each component crop. The total canopy carbon gain per unit ground area (both components combined) was also calculated (Eq. 8) and results given in Fig. 3.7E. The sole Proso millet represents the maximal whole canopy carbon gain per unit ground area available of all treatments, whilst sole Bambara groundnut represents the least productive, with intercropping values approaching this lower limit with increasing rows of Bambara groundnut. The declining carbon gain with increasing Bambara component showed a much steeper slope than that of intercepted light (compare Fig. 3.5E and 3.7E) indicating that the Bambara component was not able to compensate the reduced Millet component despite the increased photosynthetic productivity of the latter on a leaf area basis (Fig. 3.6). This is due to (1) the C_3 pathway being

relatively less productive than C₄; (2) acclimation to low light in the Bambara component when grown as an intercrop such that it cannot exploit periods of high light.

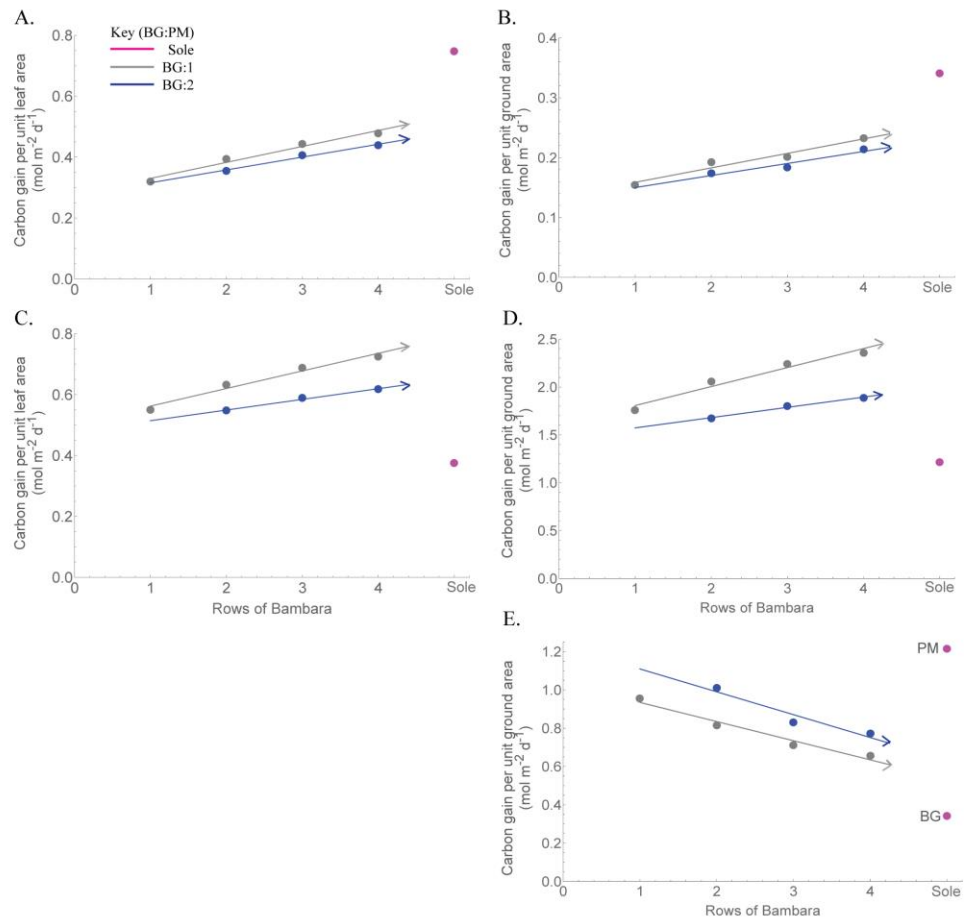


Figure 3.7: Modelled predicted carbon gain over the course of the day for different intercrop treatments and respected sole crops. (A,C) per unit leaf area and (B,D,E) per unit ground area. (A,B) Bambara groundnut, (C,D) Proso millet and (E) both component crops.

Discussion

The structural complexity of intercropping systems containing contrasting plant types of different dimensions often results in a canopy with much greater spatial variation, which means that predicting system-level productivity is more difficult than that for monocrop systems. This necessitates the need for new approaches to study intercropping systems that can capture this level of complexity and separate out responses of each component.

High-resolution digital reconstruction as a method to explore the intercrop light environment

Here we describe a high-resolution method of capturing canopy geometry and exploring the light environment within an intercropping system. Without difficult and inaccurate manual measurements, we are able to (1) define structural and photosynthetic features throughout the vertical profile of the canopies, (2) separate each component of the intercrop by assigning identification codes to the reconstructions and then combine them when required (3) use different methods to visualise the shading influence of a tall component crop on a shorter crop (4) accurately predict total light interception and include gas exchange data as a means to predict productivity within each of the systems (5) acquire light data with high spatial and temporal resolution that can be used for dynamic photosynthesis measurements rather than integrated averages and (6) make predictions for multiple different locations and treatments via modelling. This paper represents how simulations of different row patterning within an intercrop of Proso millet and Bambara groundnut influence the light environment reaching each component crop and the resulting productivity.

Image analysis and reconstruction methods have previously been shown to accurately represent key physiological measurements and distinguish between different phenotypic traits such as leaf curling, shape and area (e.g. Burgess *et al.*, 2015) and root morphology, geometry and topology (e.g. Lobet *et al.*,

2011). Image-based systems have practical and economic advantages due to the use of low cost equipment; this means that digitising canopies for 3-dimensional modelling *in silico* will become increasingly accessible. Furthermore, compared to other systems required for capturing plant structure (e.g. laser systems or Phenotyping platforms), cameras are easily portable and can be used within the field. As image-based reconstruction works by digitising existing plants, any structural differences found within the field grown plants will be preserved into the final 3-dimensional model. The method could therefore be applied to study any structural differences and quantify differences in growth rate or development within the component crops as a result of intercropping. Within this study, 53 DAS corresponds to an early vegetative stage of Bambara groundnut, and we did not witness any differences in structure between the intercrop or sole treatment plants.

De novo construction of 3D plants *in silico* would require knowledge of plant topology and multiple, intensive measurements of architectural features (i.e. leaf and stem length, leaf angle distributions etc). Whilst few models are available for a select number of sole crops (e.g. Fournier *et al.*, 2003; Evers *et al.*, 2005; Valladares *et al.*, 2005; Song *et al.*, 2013), we are unaware of any such models specifically parameterised from intercropping data, although sole cropping models have been extrapolated towards use in intercropping scenarios (e.g. Corre-Hellou, 2009; Barillot *et al.*, 2014). Furthermore, these rule-based methods can be time and parameter-intensive (Fourcaud *et al.*, 2008; Vos *et al.*, 2010) and the averaged measurements can lead to large disparities from models containing explicitly described leaf angles (Sarlikioti *et al.*, 2011; for a review of functional structural plant modelling see Fourcaud *et al.*, 2008; Vos *et al.*, 2010; DeJong *et al.*, 2011). Rule-based reconstruction of 3D plants could also miss unique features of the canopy structure, which could determine light interception properties of the stand (Sonohat *et al.*, 2002). As canopy architecture is influenced a number of different factors including the competitive presence of other vegetation, features of a select crop grown within an intercrop setting are likely to differ from those grown in monoculture, thus existing models are unlikely to be suitable for application in

such scenarios. It would be necessary to grow the plants in the intercrop setting to generate the correct morphology. This can be seen through differences in traits that confer plasticity to the plants and enable them to adapt to the situation in which they are grown (e.g. Reddy and Willey, 1981; Barillot *et al.*, 2011; Zhu *et al.*, 2015; 2016). Within a wheat-maize intercropping system, the yield advantage and increased land use efficiency (measured as the Land Equivalence Ratio; LER) of the intercropped system relative to sole wheat was attributed to the over-yielding of the border-row wheat (Zhu *et al.*, 2016). This over-yielding was a result of the plastic responses of the wheat to the intercropped environment; the plants exhibited higher tiller survival rate, a higher number of kernels per ear, higher N yield and larger sizes of leaves at the top of the canopy. This is consistent with the photosynthetic responses of millet seen in this study. An image-based approach would be able to capture the heterogeneity of component intercrops as it digitises existing structures, and can achieve representative canopies over a much shorter time scale. This also means that plasticity present within the system adopted will also be reproduced in the final reconstruction.

We used an image-based reconstruction technique to study the partitioning of intercepted light between crop components in different planting arrangements in high spatial and temporal resolution. The proportion of light intercepted by each component varies according to LAI, its height and architecture. We show that any intercropping treatment that favours more rows of Proso millet, or a taller component crop/ component with higher leaf area, will have a greater total light interception, despite the shading influence and reduced interception by the Bambara groundnut component. The predicted light distribution given by ray tracing shows both spatial and temporal differences between each of our treatments. Achieving such high-resolution, particularly with the ability to separate out responses of the intercrop components, would not be possible using manual measurements within the field/ glasshouse and any attempts would require a large amount of sensors and data processing. For this reason, we were unable to validate the light simulation measurements for the intercropping scenario but previous work has shown that the ray tracing

technique is able to accurately predict light interception within sole cropped cereal canopies (see Fig. 5 in Burgess *et al.*, 2015) and here we extend that to look at spatial differences along a row (Fig. 3.2).

Further we can make some novel predictions using photosynthesis measurements. A comparison between Figures 3.4 and 3.6 enables us to visualise how much light is in excess of photosynthesis requirements. Proso millet being taller becomes more productive due to absorption of light from all sides and exploitation of low solar elevations while Bambara suffers from being shaded. Photosynthesis measurements reveal opposing patterns of photosynthetic acclimation in the two species. Acclimation is the process by which leaves adjust the composition and function of the photosynthetic apparatus (over a period of days) to enhance photosynthetic efficiency and productivity according to the prevailing light environment. Typically, low light leaves have a lower light compensation point, lower photosynthetic capacity P_{max} and lower dark respiration rate (Anderson, 1995; Murchie and Horton, 1997). Millet acclimates to the higher light intensities in the lower canopy positions (raises P_{max}) and Bambara acclimates to the lower light in the intercrop (lower P_{max}). This is likely to enable millet to be relatively more productive because Bambara will not be able to exploit high light periods (1200 h) and does not demonstrate substantial changes in dark respiration or light compensation point hence the advantage under low light is reduced. These photosynthetic data help to explain why the increased Bambara component were not able to compensate the loss of Proso millet despite the greatly increased photosynthetic capacity of the other per unit leaf area. It raises the intriguing possibility that superior ability to acclimate to shade is essential in a component intercrop and that we may need to select for varieties with such characteristics.

It is not sufficient to examine long term changes such as acclimation alone, we need to understand photosynthesis as a dynamic process that responds locally and extremely rapidly to environmental fluctuations. Suboptimal responses on a timescale of seconds can affect canopy photosynthesis for

example via delayed relaxation of quantum yield of CO₂ fixation (Zhu *et al.*, 2004). Traditional methods that integrate measurements of light and photosynthesis over spatial scales and long time periods renders such physiological processes into an intractable black box. By studying 3D architecture in combination with ray tracing we are able to accurately define the experimental framework within which photosynthetic dynamics operates, and this can include Rubisco activation, stomatal responses and photoprotection (Lawson and Blatt, 2014; Burgess *et al.*, 2015). A future system that measures 3D architecture and physiological status, simultaneously, would be paradigm shifting.

We have thus far considered a ‘snapshot’ of a canopy in time. By capturing images at multiple times throughout the growth season, it is also possible to explore how development and differential growth of each component may alter the light patterning and productivity. Fig. 3.8 shows the reconstructed canopy of a 3:1 intercrop every 9 days from 21 DAS. Time courses could be used in order to assess altered growth patterning as a result of the planting layout. This form of analysis could also be invaluable if it is known that one of the intercrop components (particularly the shorter component) has a specific light requirement at set stages during development, and thus planting date could be altered to fulfil these requirements. Alternatively, the plastic responses of a component crop to the competitive presence of another that differs in planting date could be explored.

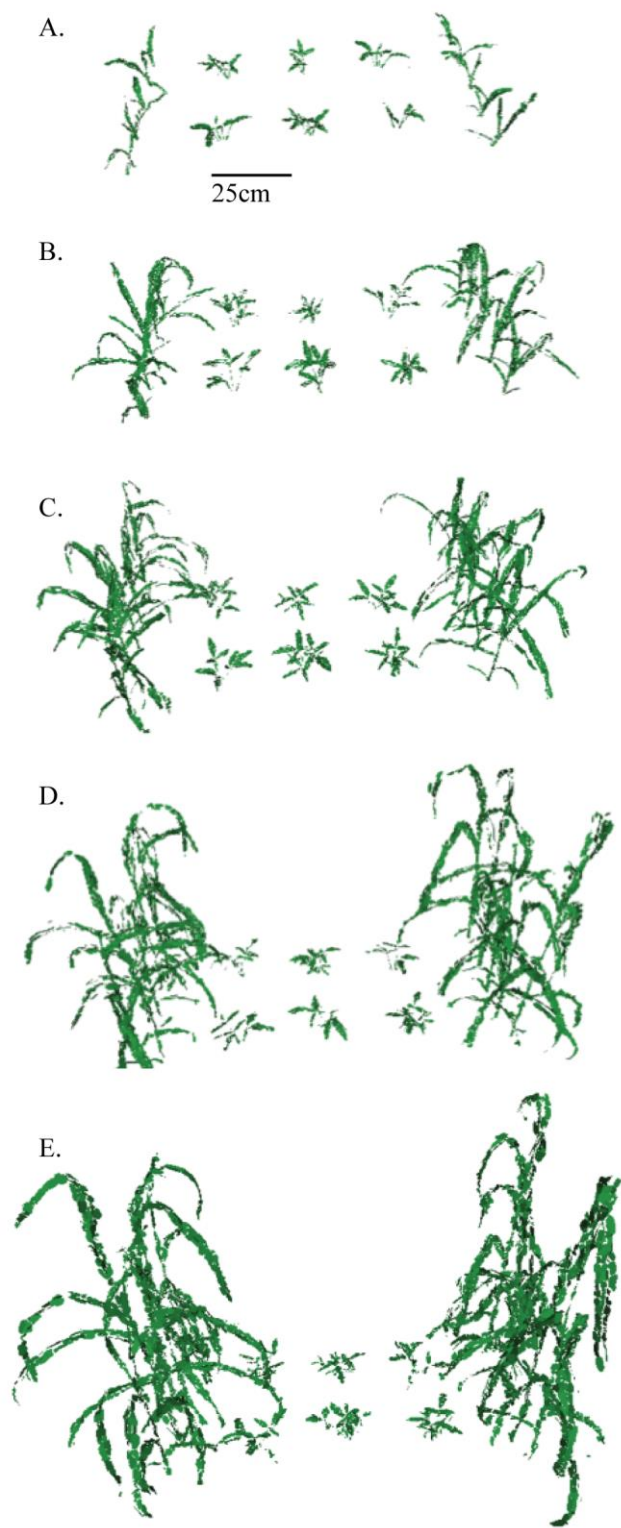


Figure 3.8: Reconstruction time course of a 3:1 (Bambara groundnut: Proso millet) intercrop canopy development. (A) 21 DAS, (B) 30 DAS, (C) 39 DAS, (D) 48 DAS and (E) 57 DAS.

Studying light interception in heterogeneous canopies

The turbid medium approach to study light attenuation through a canopy relies on two main assumptions; leaves are small and they are evenly dispersed throughout canopy structure (Ross, 1981). However, homogeneity is rarely attainable in the field both in sole cropping and multiple cropping systems and departure from random leaf dispersion (i.e. through clumping) is common (for reviews see Myneni *et al.*, 1989; Baldocchi & Collineau, 1994; Valladares & Niinemets, 2007). Previous work on droughted Bambara groundnut (in a sole cropped system), indicates how the non-uniformity of a canopy results in an inappropriate use of Beer's law (Collinson *et al.*, 1999). The sparse canopy resulting from water stress, combined with changes in leaf orientation of individual plants, led to a non-random arrangement of leaves. This altered the light transmission towards a linear decay of light as opposed to exponential decay (Kasanga & Monsi, 1954). A study on the application of the turbid medium based approach for the study of grass-legume intercropping systems indicated that the approach was suitable for certain situations however where there was considerable vertical heterogeneity in the canopy, more detailed canopy descriptions are required (Barillot *et al.*, 2011). Variability throughout depth in the canopy results in differences in the vertical distribution of leaf area: with triangular distributions common in both sole and multiple cropping systems (Ross, 1981; Lantinga *et al.*, 1999; Sonohat *et al.*, 2002; Barillot *et al.*, 2011), although regular profiles can be seen for certain crops (e.g. Barillot *et al.*, 2011).

Studies on architectural characteristics within intercropping systems indicate how the assumption of homogeneity may not apply to a multiple cropping system even if the component crops are thought to be distinctly separate and the sole cropped systems do exhibit regular dispersion (e.g. Sinoquet, 1993; Zhu *et al.*, 2016). Architectural traits such as leaf development and size, leaf angle distribution and tillering dynamics have been shown to be altered as a result of intercropping with maize (in a system containing 6 rows of wheat and 2 rows of maize) relative to sole cropping (Zhu *et al.*, 2016). Furthermore, differences were also seen within wheat that occupied the border rows of the

intercrop (i.e. those immediately next to maize) relative to those that occupied the rows inside the wheat strip (i.e. those with wheat either side). The authors did not find any significant differences in the fraction of PAR penetrating to ground level at solar noon in the different canopy positions tested (apart from the position in the boundary between wheat and maize), however it can be argued that the sampling approach adopted may not have been sensitive enough to locate any differences present. The authors did find significant differences in the PAR at ground level in the intercrop treatment relative to sole cropping. Furthermore, the pattern of change between the fraction of PAR at ground level over time differed between the intercrop and sole cropping treatment (Fig. 8 in Zhu *et al.*, 2016). Thus within this strip cropping system, assuming independence would be inappropriate.

Because Beer's law primarily describes the transmission of light through a canopy, in itself it is not enough to predict the light interception by individual components unless they are distinctly separate. For example, light sensor data will be unable to infer the proportional interception by each crop component where they are overlapping in the same volume (Sonohat *et al.*, 2002). This can be manually overcome using the cumbersome visual point quadrat method (e.g. as applied to rye grass- clover mixtures in Lantinga *et al.*, 1999), but requires a large amount of data and processing. Alternatively, 3D models can be used to assess the light interception in a canopy setting. In particular, it is able to overcome the assumptions of random dispersion and requirement of small leaf size relative to plot size (Ross, 1981). Beer's law and the visual point quadrat methods account for the light attenuation through a canopy from a specific direction: directly above. However, within nature, the solar angle means that light predominantly enters from the side, and thus homogeneity is unlikely to apply in such situations. To accurately manually measure light transmission from all solar angles would require extensive data collection, and would only apply to the situation in which the data was collected.

Within this study, distinct variations in leaf material distribution throughout both the horizontal and vertical plane are present and their structural

differences indicate patterns of light partitioning that cannot be validated using manual measurements. These findings indicate the problems in assessing total light interception by a multi-species assemblage, or even within a highly heterogeneous monocropped canopy, and how existing techniques or ideas, such as Beer's Law may not be appropriate.

Designing the optimal intercropping system

Understanding the plant response to the environment in which it is grown, including the cropping system or practices adopted, will be critical in optimising our agricultural systems. Traits that may confer optimal performance within one setting, for example in a monocrop, may be different to those that benefit another system; in this case an intercrop (Zhu *et al.*, 2015; 2016). One example can be seen with respect to leaf arrangements and traits that enable maximal light interception. Within monocropping systems, smaller more erect leaves towards the top of the canopy and more horizontal leaves towards the bottom enables a greater distribution of light throughout all depths within the canopy (e.g. Duncan, 1971; Nobel *et al.*, 1993; Loss & Siddique, 1994; Peng *et al.*, 2008). This can be achieved in an intercrop by combining a tall erect canopy with a shorter horizontal canopy (Fig. 3.1) (Malézieux *et al.*, 2009). However, within an intercrop setting, direct light predominantly enters the canopy and reaches the shorter component from the side, as opposed to the top, thus negating the requirement for improved light transmission straight down. Within intercrop systems containing component crops of different heights, light transmission and interception must be balanced so as to enable transmission to the smaller component crop but still enable absorption by the taller component. The taller component will also be subject to higher light levels than within its monocropped counterpart; thus requiring other considerations such as the prevention of damage caused by excess light (e.g. Burgess *et al.*, 2015). Within Bambara groundnut, changes in leaf reflectivity and orientation to reduce incident radiation reaching the leaf surface is associated with drought tolerance, resulting in reduced transpiration and photoinhibition (Collinson *et al.*, 1999). However, if plants are less likely to incur damage from direct radiation as a result of their cropping system, these

traits may not be required. This means that future breeding programs may be required to take a more targeted approach to creating plant varieties for use within an intercrop system, and it is likely that these will diverge in traits required for monocropping systems (Zhu *et al.*, 2016).

Previous work on a Bambara groundnut- Maize intercropping system at different planting densities highlights the importance of evaluating crop varieties for use within the intercropping system (Adu-Alhassan & Onyilo-Egbe, 2014). Whilst intercrop advantage (measured as land equivalence ratio (LER), land equivalence coefficient (LEC) and economic parameters; total variable costs (TVC), gross margins (GM) and net benefits) was found under all combinations tested, low yields of each component indicate the potential for further improvement of the system. The work shown here in terms of sub-optimal photosynthesis acclimation demonstrates this point. This improvement could be achieved through more optimal planting densities or through altered canopy architecture of the wheat component to reduce the dominance of the cereal. Thus the ability to manipulate the light environment within a system will be critical in determining both the productivity of the final system and the balance between the component crops (Ofori & Stern, 1987; Keating & Carberry, 1993; Sinoquet & Caldwell, 1995; Malézieux *et al.*, 2009).

Following accurate quantification of canopy architecture and the resultant light environment within a multi-species assemblage, a number of applications open up. Combining simulation data with small-scale trials (necessary to account for morphological adjustment of individual plants) aimed at collecting select measurements may provide the first stage in a process to help predict the optimal row layout of previously untested crop combinations. Whilst the simulations themselves would not be sufficient in accurately predicting the behaviour of the crops in the field, they may give an early indication as to which layout could prove the most productive in terms of light acquisition and potential carbon gain of the system. Using modelling approaches as a means to predict productivity enables both the assessment of extreme combinations of crops, but also enables different locations to be tested if climatic or weather

data can be inputted. Such methods could provide an initial screening process for assessing intercrop combinations before more time-, labour- and space-incentives methods are used. Modelling of the same crops, but under different abiotic limitations to their yield potential would also permit the synergistic effects of particular combinations to be identified and further investigated. Alternatively, coupling physical modelling with dynamic growth models could provide a means to link causative genomics with yield models, particularly where yield models are aimed primarily at optimising sustainable yields in complex systems, such as intercrops.

There are other considerations when selecting an intercrop that may influence the crop combination chosen and the row layout, which may not coincide with the system that could achieve maximal light interception and productivity. Multiple cropping systems may provide a means to improve the outputs of an agricultural system that is limited by climate or environment as is almost always the case for low-input agricultural systems where intercropping tends to be practiced. For example, relay intercropping (seeding a second crop into an existing crop before the harvest of the first crop) is able to extend the growing season and enable production of two crops in the same field allowing producers to spread the production costs and fixed costs of equipment and land over two or more crops (Palmer *et al.*, 1993). The choice of component crops and their layouts may also be tailored depending on any environmental constraints of the land in which they are to be grown or consumer habits and dietary information may influence the quantities of crops required. Combining these other considerations into prediction models could achieve the best layout for both physiological and economic incentives of a set location.

Concluding remarks

3D reconstruction combined with ray tracing provides a novel, high-resolution method of exploring the light environment within an intercrop canopy and provides a platform for trying untested combinations and row layouts of multiple cropping systems. The contrasting component crops, in terms of both architecture and photosynthetic properties, would usually result

in difficulties in predicting the productivity and light partitioning within such systems at high spatial and temporal resolution. However, using an image-based approach to plant reconstruction and the ability to separate out the different crop components when modelling means that quick, detailed assessments of the canopy light environment can be made. Hence dynamic aspects of physiology can also be incorporated. This method, either alone or in combination with other data provides an early platform for the assessment of new cropping systems.

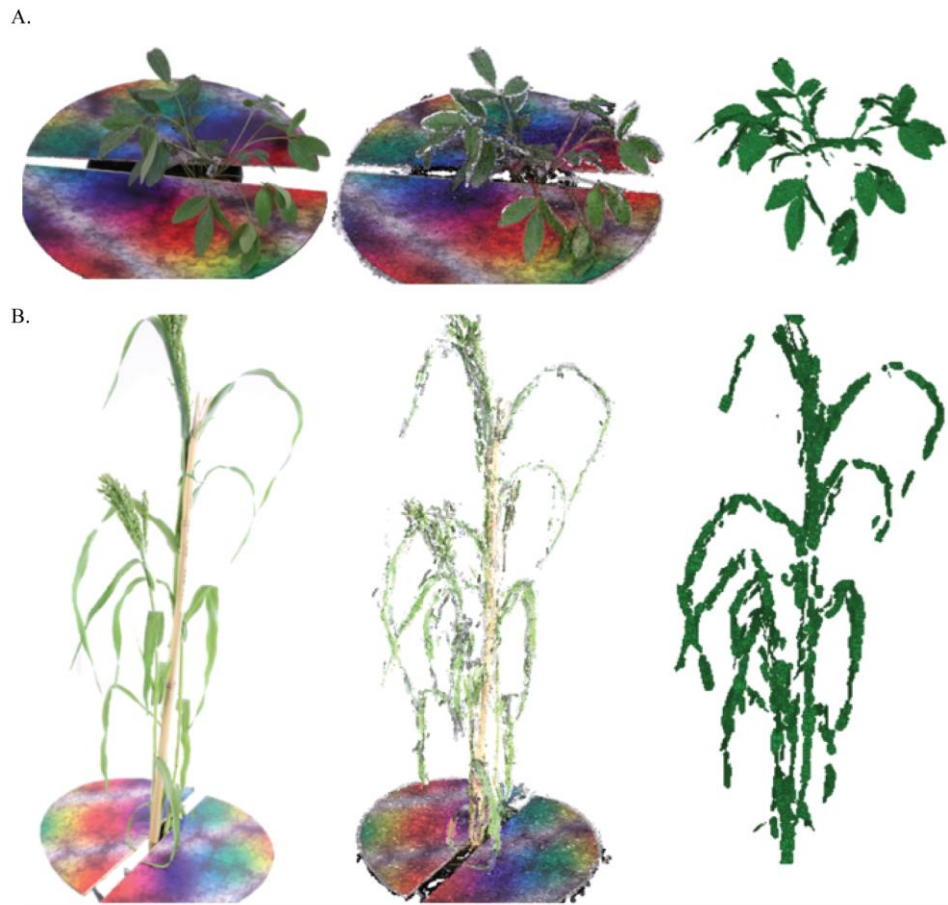
Supplementary Material

Supplementary Figure S3.1



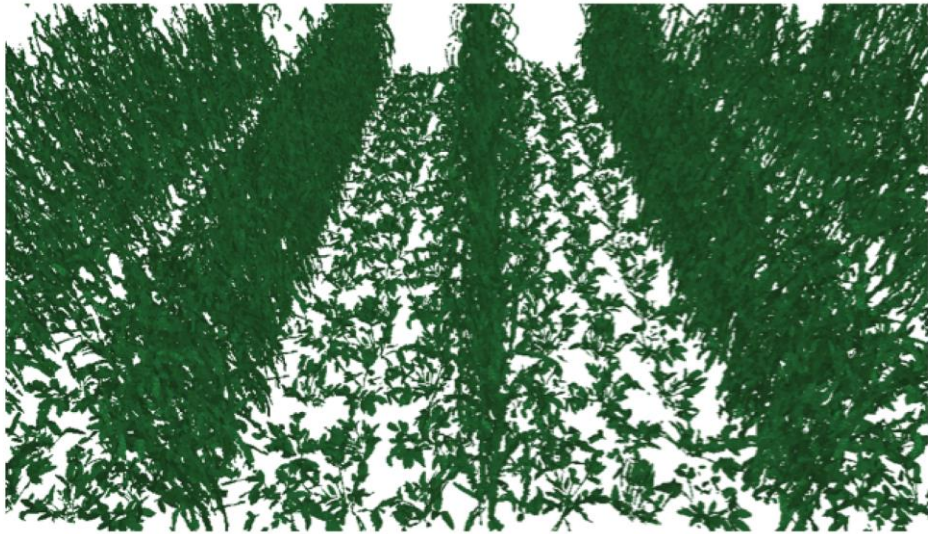
Supplementary Figure S3.1: Photograph of the 2:2 (Bambara groundnut: Proso millet) intercrop treatment in the FutureCrop Glasshouse facilities, University of Nottingham, Sutton Bonington Campus, UK, prior to plant removal from imaging and reconstruction.

Supplementary Figure S3.2



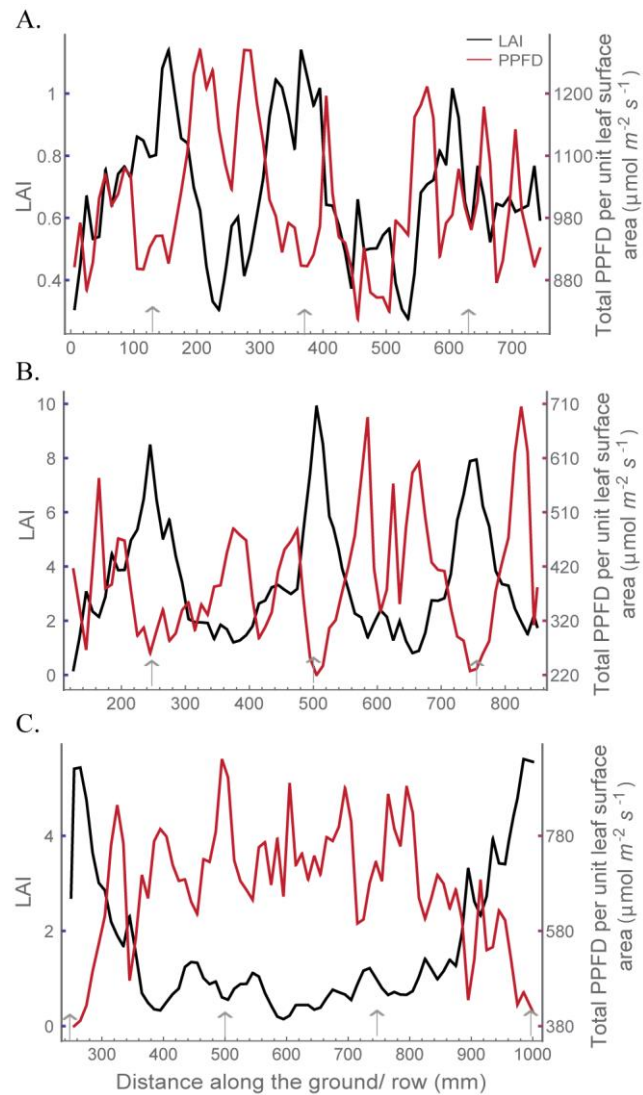
Supplementary Figure S3.2: Example overview of the Reconstruction Process for (A) Bambara groundnut and (B) Proso millet. Left hand panel shows one of the original photographs of the plant (40+ used per plant), the middle panel shows the point cloud reconstruction derived from VisualSFM software (Furukawa & Ponce, 2010; Wu, 2011) and the right hand panel shows the final reconstructed mesh derived from (Pound et al., 2014). N.B. The colourful circle in the two left panels is a calibration target used to optimise the reconstruction method and scale the final reconstructions back to the correct units.

Supplementary Figure S3.3



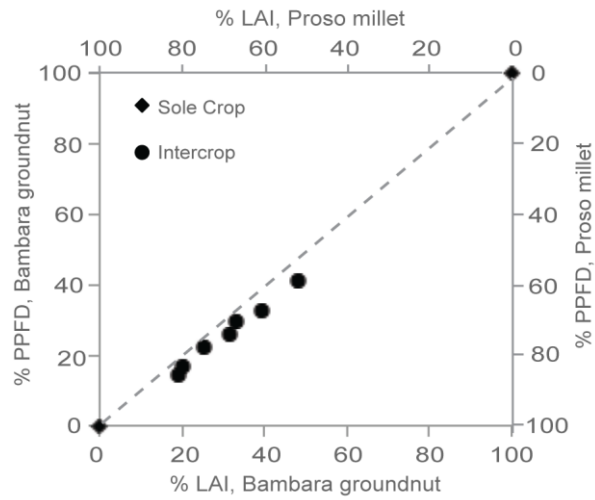
Supplementary Figure S3.3: Example of a full Intercrop Canopy Reconstruction; 3:1 Row layout. 3 representative Bambara groundnut reconstructions and 3 representative Proso millet reconstructions were duplicated and randomly rotated. These were then arranged within the canopy with 25 cm between rows, 25 cm within the rows for Bambara groundnut and 10 cm within the rows for Proso millet.

Supplementary Figure S3.4



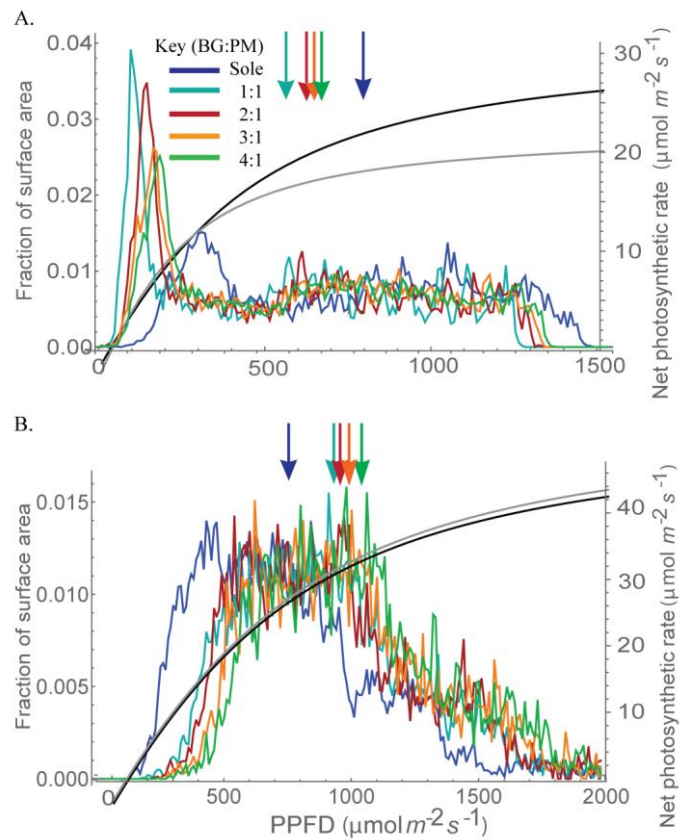
Supplementary Figure S3.4: The relationship between LAI and total PPFD per unit leaf surface area along a row for (A) sole Bambara groundnut, (B) sole Proso millet and (C) 2:1 (BG:PM) intercropping treatment. Arrows indicate the location the centre of the plants in the row.

Supplementary Figure S3.5



Supplementary Figure S3.5: Component contribution to leaf area index (LAI) and total intercepted photosynthetic photon flux density (PPFD). The relationship that represents an equal contribution by each component is given in the dashed line.

Supplementary Figure S3.6



Supplementary Figure S3.6: Frequency of light levels as a function of the fraction of the total surface area of the canopy received at 1200 h by the different treatments of (A) Bambara groundnut (B) Proso millet and the average irradiance, indicated by arrows, overlaid on the light response curves of the sole (black) versus intercropped (grey) plants. This graph combines data presented in Fig. 3.4 and Fig. 3.6.

Chapter 4: The relationship between canopy architecture and photosynthesis

Paper as submitted to *Frontiers in Plant Science*

Chapter 4 uses a combination of physiological and gas exchange measurements combined with 3D plant reconstruction and modelling to investigate the effects of canopy architecture on the resulting light environment and photosynthesis from a phenotyping perspective. This has been submitted to *Frontiers in Plant Science*, so is presented in “paper format”.

Author contribution:

Experiment conceived by AJ Burgess and EH Murchie

Project supervision performed by EH Murchie

Physiological measurements (SPAD, plant heights, chlorophyll assays) in initial screening of 16 lines plus paper construction performed by T Herman

Model development and implementation performed by R Retkute

Experimental work (both experiments), gas exchange and physiological measurements, plant reconstructions, modelling and paper construction performed by AJ Burgess

Is there a consistent relationship between canopy architecture, light distribution and photosynthesis across diverse rice germplasm?

Alexandra J. Burgess, Renata Retkute, Tiara Herman and Erik H. Murchie

Abstract

The arrangement of leaf material is critical in determining the light environment, and subsequently the photosynthetic productivity of complex crop canopies. However, causal links between specific canopy architectural traits and photosynthetic productivity across a wide genetic background are poorly understood for field grown crops. The architecture of five genetically diverse rice varieties - four parental founders of a multi-parent advanced generation intercross (MAGIC) population plus a high yielding Philippine variety (IR64) - was captured at two different growth stages using a method for digital plant reconstruction based on stereocameras. Ray tracing was employed to explore the effects of canopy architecture on the resulting light environment in high-resolution, whilst gas exchange measurements were combined with an empirical model of photosynthesis to calculate carbon gain and total light interception. To further test the impact of different dynamic light patterns on photosynthetic properties, an empirical model of photosynthetic acclimation was employed to predict the optimal P_{\max} throughout canopy depth, hypothesising that light is the sole determinant of productivity. First we show that a plant type with steeper leaf angles allows greater penetration of light into lower canopy layers and this, in turn, leads to a greater photosynthetic potential. Second the predicted optimal P_{\max} is consistently linked to fractional interception, leaf angle and leaf area index across this diverse germplasm. Lastly, varieties with more upright architecture exhibit higher maximum quantum yield and originate from areas closer to the equator; this suggests a

potential latitude dependent relationship with architectural traits or the influence of the japonica background.

Introduction

The rate of photosynthesis of a given stand of crops is dependent on a multitude of environmental factors including weather, season, temperature, leaf age and plant development. Photosynthesis, in turn, is closely linked to potential yield (Zhu *et al.*, 2010; Murchie *et al.*, 2009). However, the complex arrangement of overlapping leaves of different ages and in different states of photosynthesis means that assessing canopy level photosynthesis from individual leaf activity is difficult and time consuming. For an accurate prediction of canopy photosynthesis from leaf measurements, it is necessary to have data on multiple leaf characteristics including physical orientation, positioning and physiological characteristics, including photosynthesis (Burgess *et al.*, 2015; 2016). However, predicted productivity tends to be higher than that measured in the field (Zhu *et al.*, 2010). The cause of this disparity is unclear, but it seems likely that losses are partly caused by suboptimal interactions between photosynthesis and architectural traits (Zhu *et al.*, 2010, Burgess *et al.*, 2015).

In the absence of methods for whole canopy measurements, such as in Song *et al.* (2016), predictions require knowledge of the architectural characteristics and its effect on canopy light distribution. Photosynthetic rate is highly sensitive to light intensity, and, in turn, the light intensity within crop canopies has high spatio-temporal variability, and is dependent upon features such as leaf angle, size and shape, leaf number and the arrangement of this material in three-dimensional space. These findings have led to the concept of an “idealised plant type” or “ideotype”. For example, the International Rice Research Institute (IRRI) proposed that upright leaves, large panicles and fewer tillers would represent the ideal structure for rice (Dingkuhn *et al.*, 1991; Virk *et al.*, 2004). Erect leaf morphology is a characteristic that repeatedly arises within the concept of an ideotype. This is due to the increased light penetration to deeper canopy layers leading to uniformity of light within the

canopy setting and maximal net photosynthesis (Clendon and Millen, 1979; Hodanova, 1979; Normile, 1999; Setter *et al.*, 1995; Turitzin and Drake, 1981). Also the potential that steeper leaf angles leads to an improvement in whole day carbon gain by enhancing light absorption at low solar angles (Falster and Westoby, 2003). Erect leaf stature is also associated with reduced susceptibility to photoinhibition and reduced risk of overheating (King, 1997; Murchie *et al.*, 1999; Werner *et al.*, 2001; Falster and Westoby, 2003; Burgess *et al.*, 2015). As such, the erect ideotype is predicted to be most effective in low latitudes but it has also been found to be productive in high latitudes (Reynolds and Pfeiffer, 2000; Peng *et al.*, 2008; Govindjee, 2012 and references within). However, despite this, there is still variation in crop morphology and the erect ideotype is not widespread in many species. As such, altering canopy architectural characteristics has become one of the primary breeding strategies for improving yield-potential (Reynolds *et al.*, 2000; Khush, 2005; Khan *et al.*, 2015; Rötter *et al.*, 2015).

There is currently no method for high-resolution reconstruction of entire field grown crop canopies due to problems of occlusion at high leaf densities. Such techniques would be highly advantageous for testing hypothesis within fundamental or applied research. However, advances in hardware and technology have led to new methods for capturing and evaluating plant architecture. These methods have been used for numerous purposes including both plants grown in pots and those grown under field conditions (e.g. Falster and Westoby, 2003; Godin and Sinoquet, 2005; Watanabe *et al.*, 2005; Quan *et al.*, 2006; Sinoquet *et al.*, 2007; Zheng *et al.*, 2008; Burgess *et al.*, 2015). Whilst previous studies have attempted to look at the relationship between canopy architecture and the light environment (e.g. Zheng *et al.*, 2008; Song *et al.*, 2013; Burgess *et al.*, 2015), assessments have been restricted due to the inaccurate reconstruction and modelling techniques used and the limited genetic variation and architectural types studied. As architectural traits are so inherently linked to the resulting light environment, which in turn determines photosynthesis, it therefore follows that photosynthetic traits will be dependent upon architecture. It can also be predicted that, due to dilution effects, there will be a negative relationship between leaf area and photosynthesis

(commonly measured as photosynthetic capacity, P_{\max}) on a unit leaf area basis.

This study uses a new approach for high resolution 3D reconstruction of crop plants (Pound *et al.*, 2014; Burgess *et al.*, 2015) to investigate fundamental structure-function canopy properties. The parental lines used for the creation of multi-parent advanced generation inter-cross (MAGIC) populations in rice (Bandillo *et al.*, 2013) were selected for analysis within this study. These lines have a well-researched genetic background and contain desirable traits for yield, grain quality and biotic and abiotic stress resistance (more details on each line are given in Supplementary Table S1). Furthermore, the contrasting origin of each line means that they are cultivated in diverse habitats with different stressors and constraints. The initial phase of this study involved a small-scale screening experiment to preliminary assess differences in terms of architectural and physiological features for fifteen of the lines (referred to here as M1-M15 in Supplementary Table S4.1). Four of these lines, Shan-Huang Zhan-2 (SHZ-2), IR4630-22-2-5-1-3, WAB 56-125 and Inia Tacuari (referred to here as M2, M4, M11 and M13, respectively), plus the Philippine high-yielding variety IR64 were chosen for an in depth physiological study. These lines were chosen due to their differences in a number of features including leaf area index (LAI; leaf area per unit ground area), chlorophyll a:b ratios and content plus physical appearance. The aims are to: 1) assess the method for image based reconstruction on genetically variable ‘field’ grown rice plants; 2) test the hypothesis that there are common links between canopy architecture and photosynthetic traits across genetically diverse rice cultivars (such as leaf angle, light distribution and photosynthetic capacity) and; 3) test the hypothesis that canopy-induced dynamic light properties determine the acclimation status of leaves in diverse structures. The latter uses a new empirical acclimation model which predicts the optimal P_{\max} (if light were the sole determinant) (Retkute *et al.*, 2015). Acclimation is a process whereby leaves adjust their photosynthetic capacity, dark respiration and light compensation point according to long term changes in the light environment. However, the ability to acclimate optimally in fluctuating conditions has not been fully tested

(Murchie and Horton, 1997; 1998; Yano and Terashima, 2001; Walters, 2004; Anderson *et al.*, 1995; Athanasiou *et al.*, 2012; Retkute *et al.*, 2015).

Materials and Methods

Plant Material and Growth

The preliminary screening used 15 of the possible 16 parental lines from a MAGIC rice population (Bandillo *et al.*, 2013) (details given in Supplementary Table S1 with results of the screening in Supplementary Table S2). Seeds were sown into module trays containing Levington Module compost (plus sand) in the FutureCrop Glasshouse facilities, University of Nottingham Sutton Bonington Campus (52°49'59" N, 1°14'50" W), UK on the 7th May 2015. The FutureCrop Glasshouse is a south – facing glasshouse designed and built by CambridgeHOK (Brough, UK) for the growth of crop stands within a controlled environment. It consists of a concrete tank 5 m x 5 m x 1.25 m positioned at ground level. The tank is filled entirely with a sandy loam soil, extracted from local fields and sieved through a fine mesh. The seedlings were transplanted into microplots (containing 5 x 5 plants with 10 x 10 cm spacing between adjacent plants; 100 plants m⁻²) within soil beds 7 days after root establishment. For the preliminary screen, key measurements were made 55-60 days after transplanting (DAT), corresponding to a vegetative growth phase (Supplementary Table S2). Following the preliminary screening, 4 lines; Shan-Huang Zhan-2 (SHZ-2), IR4630-22-2-5-1- 3, WAB 56-125 and Inia Tacuari (referred to here as M2, M4, M11 and M13, respectively), were selected for the in depth study as well as the popular Philippine variety IR64, from IRRI. Selection was made largely on the basis of contrasting architecture including leaf area index (LAI; leaf area per unit ground area), chlorophyll a:b ratios and content plus physical appearance. This selection also represents rice from diverse origins (Supplementary Table S1) and genetic backgrounds (M2, M4 and IR64 of indica and M11 plus M13 of japonica). The seeds were sown into module trays on the 15th October 2015 and transplanted into replicate microplots of 6 x 6 plants using a completely randomised design. The glasshouse conditions were kept consistent for both the screening and the in depth study. Irrigation was supplied using drip irrigation for 15 minutes, twice

daily. Sodium (Son T- Agro, Philips) lamps provided additional lighting whenever the photosynthetically active radiation (PAR) fell below $300 \mu\text{mol m}^{-2} \text{s}^{-1}$ and a 12 h photoperiod (07:00 to 19:00) was maintained using blackout blinds. A temperature of $28 \pm 3^\circ\text{C}$ and relative humidity (RH) of 50–60% was maintained throughout. Yara Milla complex fertiliser (containing 50 kg ha^{-1} of N plus micronutrients) was applied to the plots, 80 days after transplanting (DAT).

Physiological Measurements: in depth study

In depth measurements were made at two different growth stages: 45 and 85 DAT, which correspond to an early (prior to full canopy development) and late (full canopy development prior to flowering) vegetative phase. Here, we refer to these stages as growth stage 1 (GS1) and growth stage 2 (GS2), terms used in this study only. Five replicate measurements of plant height per plot were taken weekly, from 4 DAT. Five replicate measurements per plot were taken for tiller numbers at each of the growth stages. Three replicate plants per line were taken for leaf width, leaf area, fresh and dry weight measurements at each growth stage. Individual plant dry weight and area was analysed by passing material through a leaf area meter (LI3000C, Licor, Nebraska) and drying in an oven at 80°C for 48 hours or until no more weight loss was noted. Measured LAI (leaf area per unit ground area: m^2) was calculated as the total area (leaf + stem) divided by the area of ground each plant covered (distance between rows x distance within rows) and averaged across the replicate plants. Chlorophyll a and b content and ratios were determined through chlorophyll assays corresponding to GS2. Frozen leaf samples of known area were ground in 80% acetone, centrifuged for 5 minutes at 3000 rpm, 1600 g, and the absorbance (at 663.6 and 646.6 nm) of the supernatant was measured using a spectrophotometer according to the method of Porra *et al.* (1989).

Imaging and Ray Tracing

3D analysis of a plant from each plot (i.e. three replicate plants per line) was made according to the protocol of Pound *et al.* (2014) in the in-depth analysis (GS1 and GS2). The reconstructions were duplicated and rotated to form a 3 x

3 canopy grid (with set 10 cm spacing between plants), with the same leaf area index (LAI) as the measured plants (see Table 1). The LAI of each reconstructed canopy was calculated as the area of mesh inside the ray tracing boundaries divided by the ground area. A forward ray-tracing algorithm, fastTracer (fastTracer version 3; PICB, Shanghai, China from Song *et al.*, 2013), was used to calculate total light per unit leaf area throughout the canopies. Latitude was set at 14.2 (for the Philippines), atmospheric transmittance 0.5, light scattering 7.5%, light transmittance 7.5%, days 344 (GS1 10th December) and 21 (GS2 21st January). The diurnal course of light intensities over a whole canopy was recorded at 1 min intervals. The aim was to study the effect of canopy architecture on the resultant light environment and the impact on whole canopy photosynthesis thus the same parameters for ray tracing were used for each of the canopies, despite the diverse origin of each of the lines (see Supplementary Table S4.1).

Gas Exchange

For light response and A_{Ci} response curves, leaves were not dark-adapted prior to measurements. LRCs were taken at GS1 and 2 whereas A_{Ci} curves were taken at GS1 only. Leaf gas exchange measurements (LRC and A_{Ci}) were taken with a LI-COR 6400XT infra-red gas-exchange analyser (LI-COR, Nebraska). The block temperature was maintained at 30°C using a flow rate of 500 ml min⁻¹ and ambient humidity. For light response curves, light was provided by a combination of in-built red and blue LEDs. Illumination occurred over a series of 12 photosynthetically active radiation values (low to high), between 0 and 2000 μmol m⁻² s⁻¹, with a minimum of 2 minutes and maximum of 3 minutes at each light level at two different canopy heights; labelled top and bottom. For the A-C_i curves; leaves were exposed to 1500 μmol m⁻² sec⁻¹ throughout. They were placed in the chamber at 400 p.p.m. CO₂ for a maximum of 2 min and then CO₂ was reduced stepwise to 50 p.p.m. CO₂ was then increased to 1500 p.p.m. again in a stepwise manner. Two replicates were taken per layer per treatment plot for both sets of measurements apart from LRCs for GS2, which has five replicates overall for each of the 5 varieties.

Statistical Analysis

Analysis of variance (ANOVA) was carried out using GenStat for Windows, 17th Edition (VSN International Ltd.). Data was checked to see if it met the assumption of constant variance and normal distribution of residuals. A correlation matrix was used to investigate the relationships between different physiological traits.

Modelling

All modelling was carried out using Mathematica (Wolfram).

Cumulative leaf area index (cLAI; leaf area per unit ground area as a function of depth) was calculated from each of the canopy reconstructions. For each depth (d ; distance from the highest point of the canopy), all triangles with centres lying above d were found (Eq. 1).

$$d_i = \max_{j=1,2,3; 1 \leq i \leq n} z_i^j - (z_i^1 + z_i^2 + z_i^3)/3 \quad (1)$$

The sum of the areas of these triangles was calculated and divided by the ground area. The cumulative LAI as a function of depth through the canopy was calculated using Eq. 2.

$$cLAI(d) = \frac{\sum_{i=1}^n I(d_i \leq d) S_i}{\left(\max_{1 \leq i \leq n} x_i - \min_{1 \leq i \leq n} x_i \right) \left(\max_{1 \leq i \leq n} y_i - \min_{1 \leq i \leq n} y_i \right)}, \quad (2)$$

where $I(A)=1$ if condition A is satisfied and S_i is the area of a triangle i .

The light extinction coefficient of the canopy was calculated using the 3D structural data and the light distribution obtained from ray tracing. In order to calculate fractional interception within a canopy as a function of depth at time t , all triangles lying above depth, d , were identified (Eq. 1). Their contribution to intercepted light was then calculated by multiplying PPFD received per unit surface area (ray tracing output) by the area of triangle. The light intercepted was summed for all triangles above the set d , and divided by light intercepted by ground area according to Eq. 3.

$$F(d, t) = \frac{\sum_{i=1}^n I(d_i \leq d) S_i L_i(t)}{L_0(t) * \text{ground area}}, \quad (3)$$

where $L_0(t)$ is light received on a horizontal surface with a ground area $\left(\max_{1 \leq i \leq n} x_i - \min_{1 \leq i \leq n} x_i\right) \left(\max_{1 \leq i \leq n} y_i - \min_{1 \leq i \leq n} y_i\right)$, and $L_i(t)$ is light intercepted by a triangle i .

The light extinction coefficient, k , was calculated by fitting (by least squares) the function

$$f(x) = a(1 - e^{-kx}) \quad (4)$$

to the set of points $\{cLAI(d), F(d, t)\}$ calculated by varying depth from 0 to the height at total $cLAI$ with step $\Delta d = 1$ mm, a in Eq.(4) is a fitted parameter.

The response of photosynthesis to light irradiance, L , was calculated using a nonrectangular hyperbola given by Eq. 5:

$$F_{NRH}(L, \phi, \theta, P_{max}, \alpha) = \frac{\phi L + (1 + \alpha)P_{max} - \sqrt{(\phi L + (1 + \alpha)P_{max})^2 - 4\theta\phi L(1 + \alpha)P_{max}}}{2\theta} - \alpha P_{max} \quad (5)$$

Values for P_{max} were determined from leaf gas exchange measurements (see section “Gas Exchange”). The value of α was obtained by fitting a line of best fit between all measured P_{max} and Rd values. All other parameters (e.g. P_{max} , ϕ and θ) were estimated from the light response curves for three canopy layers using the Mathematica command **FindFit**.

As each canopy was divided into 2 layers, and each triangle from the digital plant reconstruction was assigned to a particular layer, m , according to the triangle centre (i.e. with triangle centre between upper and lower limit of a layer depth). Carbon gain per unit canopy area was calculated as daily carbon assimilation over a whole canopy divided by the total surface area of the canopy according to Eq. 6.

$$C = \frac{\sum_{i=1}^n P_i}{\sum_{i=1}^n S_i} \quad (6)$$

Total canopy light interception per unit leaf area was calculated according to Eq 7.

$$TL_{LA} = \frac{\sum_{i=1}^n S_i \int_6^{18} L_i(t) dt}{\sum_{i=1}^n S_i} \quad (7)$$

where S_i is the area of triangle i .

An empirical model of acclimation was employed to predict the distribution of optimal P_{max} values throughout each of the canopies. Details of the model can be found in Retkute *et al.* (2015). The model can be used to predict the maximum photosynthetic capacity, P_{max}^{opt} , as the P_{max} that represents maximal carbon gain at a single point within the canopy, based on the light pattern that point has experienced (i.e. using the light pattern output from ray tracing). This was predicted across 250 canopy points, thus leading to distribution of P_{max}^{opt} values throughout each of the canopies. The canopy locations were chosen as a subset of triangles that were of similar size (i.e. area) and constitute a representative sample distribution throughout canopy depth.

Carbon gain, C (mol m⁻²) was calculated over the time period $t \in [0, T]$ (Eq. 8).

$$C(L(t), P_{max}) = \int_0^T P(L(t), P_{max}) dt \quad (8)$$

Experimental data indicates that the response of photosynthesis to a change in irradiance is not instantaneous and thus to incorporate this into the model Retkute *et al.* (2015) introduced a time-weighted average for light (Eq. 9).

$$L_{\tau}(t) = \frac{1}{\tau} \int_{-\infty}^T L(t') e^{-\frac{t-t'}{\tau}} dt' \quad (9)$$

This effectively accounts for photosynthetic induction state, which is hard to quantify *in situ* as it varies according to the light history of the leaf. The more time recently spent in high light, the faster the induction response, thus the time-weighted average effectively acts as a “fading memory” of the recent light pattern using an exponentially decaying weight. If $\tau = 0$ then a plant will be able to

instantaneously respond to a change in irradiance, whereas if $\tau > 0$ the time-weighted average light pattern will relax over the timescale τ . Within this study, τ was fixed at 0.2 (unless otherwise stated) in agreement with previous studies and fit with past experimental data (Pearcy and Seemann 1990, Retkute *et al.*, 2015) and measurements of induction state in rice leaves. The time-weighted average only applies to the transition from low to high light; from high to low, response is instantaneous and does not use the weighted average (see Supp. Fig. S4.1). The model was parameterised using the convexity and dark respiration values taken from the fitted LRCs. A moving average of the P_{max} throughout canopy height was fitted using the Mathematica command **MovingAverage** to give an approximate relationship between canopy height and optimal P_{max} based on the light environment.

Results

Architectural Features

- *Measured Data*

A summary of the key architectural features is given in Table 4.1 (see Supplementary Table S4.2 for the initial screening experiment). Similarities can be seen between the key architectural features between the initial screening experiment and the in-depth study (Table 4.1 and Supplementary Table S4.2) however the variation seen between the lines was reduced in the second, in depth experiment. For the rest of the paper, only data from the in-depth study will be considered. Plant height varied between lines in both growth stages ($P=0.001$ for GS1 and $P=0.005$ for GS2), with M2 the shortest and M13 the tallest of the five lines. The change in plant height over the course of the experiment is given in Figure 4.1. Leaf blade width differed between the lines at each growth stage ($P<0.001$ GS1 and 2) with M11 and M13 exhibiting the widest leaf blades (Table 1). Leaf number and tiller number also differed significantly between the lines ($P<0.001$ both growth stages) with M13 containing the fewest number of leaves and IR64 the greatest, however there was no significant difference in leaf area index (LAI) at either growth stage (Table 4.1).

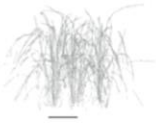









	Line					Mean	P	SED
	M2	M4	M11	M13	IR64			
GS1								
Plant Height (cm)	36.60±3.12	47.07±0.47	52.20±3.14	59.53±1.40	49.4±1.06	54.30	0.001	3.250
No. of Tillers	4.47±0.18	4.47±0.18	3.07±0.18	2.67±0.07	4.93±0.24	3.92	<0.001	0.249
No. of Leaves	22.33±1.20	18.67±1.20	15.67±2.4	10.33±0.67	25.67±0.67	18.53	<0.001	1.955
Leaf Width (cm)	0.90±0.03	0.92±0.02	1.05±0.00	1.08±0.03	0.87±0.02	0.963	<0.001	0.032
Dry Weight (g)	1.22±0.13	1.31±0.07	1.69±0.07	1.20±0.07	1.52±0.30	1.39	0.207	0.223
Measured LAI	2.19±0.18	2.22±0.26	2.45±0.13	1.86±0.48	2.82±0.09	2.31	0.206	0.378
Reconstruction LAI	2.21	2.22	2.47	1.86	2.83			
GS2								
Plant Height (cm)	54.87±3.89	65.00±0.92	69.27±1.85	70.13±1.70	67.07±1.88	65.30	0.005	3.210
No. of Tillers	5.40±0.31	4.87±0.52	4.13±0.47	2.53±0.18	5.67±0.29	4.52	<0.001	0.528
No. of Leaves	28.67±2.19	27.33±2.6	21.33±3.33	14.00±2.52	51.00±3.06	28.50	<0.001	3.920
Leaf Width (cm)	0.97±0.03	1.05±0.03	1.18±0.04	1.38±0.02	1.02±0.04	1.12	<0.001	0.049
Dry Weight (g)	3.13±0.56	4.70±0.46	3.47±0.80	5.2±0.59	6.60±0.40	4.62	0.011	0.817
Measured LAI	4.72±0.83	5.46±0.68	4.12±0.59	3.67±0.34	8.75±3.11	5.35	0.206	2.125
Reconstruction LAI	4.75	5.44	4.18	3.68	8.69			

Table 4.1: Canopy Reconstructions and Description

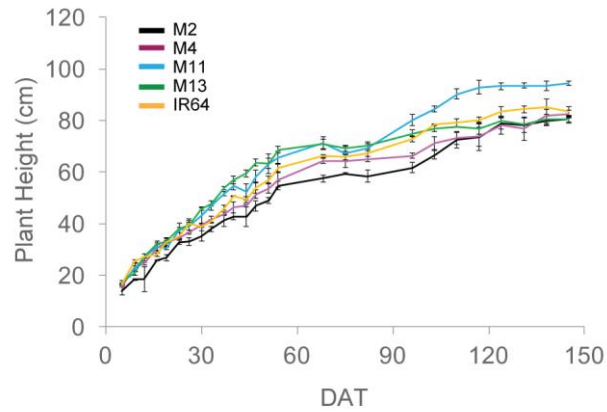


Figure 4.1: Plant height over the course of the experiment, calculated as the average of 5 measurements per plot. The means of three plots are shown with standard errors of the mean.

- **Modelled Data**

Each plant within the *in silico* canopy was rotated around the vertical axis such that the LAI inside the ray tracing boundaries was consistent with measured data (Table 4.1; see Materials and Methods). Previous papers have validated the modelling using measured data of LAI and extinction coefficients (Burgess *et al.*, 2015). Cumulative leaf area index (cLAI) was calculated through canopy depth (i.e. from top-down; see Materials and Methods: Modelling) for each of the canopies at each growth stage (see Figure 4.2A and B). A curve was deliberately not fitted because the reconstruction and modelling approach used within this study permits the actual relationship between LAI and depth in the canopy to be depicted, without the need for curve fitting. Generally, a sigmoidal response was seen for most genotypes with a more rapid accumulation of leaf area toward the centre of the canopy. At GS1, M2 and M13 contrast in terms of the position of accumulation of LAI according to depth (distance from the top of the canopy) with the latter accumulating more in the bottom half of the canopy (Figure 4.2A). At GS2 (Figure 4.2B) this pattern is not pronounced with other lines showing a similar increase in cLAI up to approximately 20 cm depth. From here on, differences are shown with M11 and M13 exhibiting least accumulation of leaf material and IR64 exhibiting the greatest. This variation is consistent with total measured LAI values, with IR64 exhibiting a much higher overall LAI

compared to the other lines (Table 4.1), although according to ANOVA on the measured leaf area, this is not significant.

These distinctive patterns are partly as a result of architecture and arrangement, specifically angles of the leaves, within each canopy. This technique allows automatic and rapid calculation of leaf angle of every triangle in the reconstruction. Leaf angle distributions were calculated for each canopy and averaged at each canopy depth (see Materials and Methods: Modelling; Figure 4.3A and B), where a leaf inclination angle towards 0 indicates a more horizontal leaf and an inclination angle of 90 indicates a more vertical leaf. M2, M4 and IR64 lines exhibited a trend toward more horizontal leaves at base of canopy at both growth stages 1 and 2, with M11 and M13 more vertical stature.

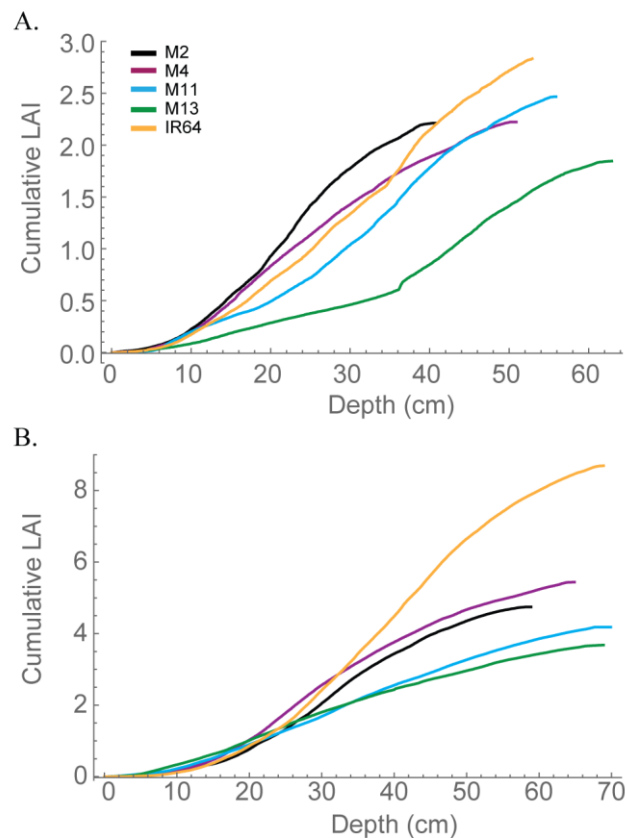


Figure 4.2: Modelled cLAI, the area of leaf material (or mesh area) per unit ground as a function of depth through the canopy (i.e. distance from the top) at 12:00 h for (A) GS1 and (B) GS2.

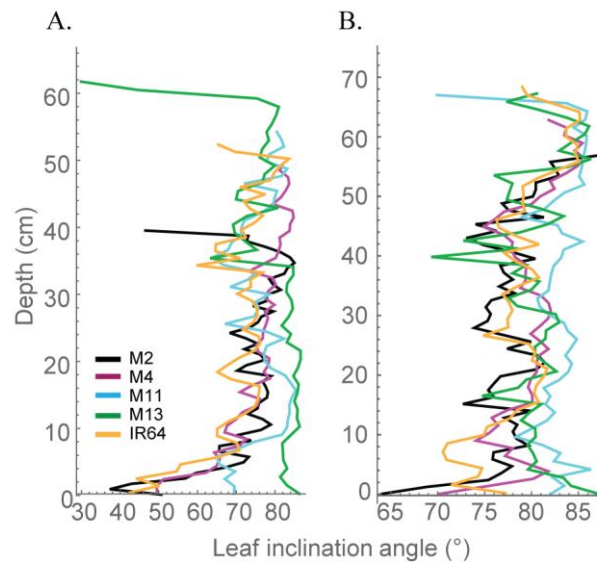


Figure 4.3: Modelled leaf inclination angles throughout depth (i.e. distance from the top) in the canopy. (A) GS1 and (B) GS2. The average triangle inclination angle throughout the horizontal subsection was calculated with respect to vertical, where a leaf inclination angle towards 0 indicates a more horizontal leaf and an inclination angle of 90 indicates a more vertical leaf.

Light Environment

- **Modelled Data**

To explore interactions between depth and light interception, modelled fractional interception was calculated as a function of depth (Figure 4.4A and B). This enables the interception to be calculated at 1 mm sections throughout the canopy. Generally, the pattern was similar to that of modelled LAI. At GS1 (Figure 4.4A), M2 and M4 are achieving approximately 60% of interception within the top 25 cm of the canopy. This can be compared to M13, which exhibits a near linear relationship between fractional interception and canopy depth. By GS2 (Figure 4.4B), the lines exhibit a more similar interception within the top 20 cm of the canopy but a greater variation in the bottom layers in the canopy. M2, M4 and IR64 achieve the greatest fractional interception and M11 and M13 the lowest.

We hypothesise that leaf angle will be related to vertical F and LAI distribution: we note that towards the top of the canopy, leaves tend to be more horizontal (i.e angles approaching 0) for those lines with a higher LAI (Fig. 4.2 and 4.3), and this contributes to a higher interception of light (Fig. 4.4). In the lines studied here, erectness does not seem to be associated with a higher LAI.

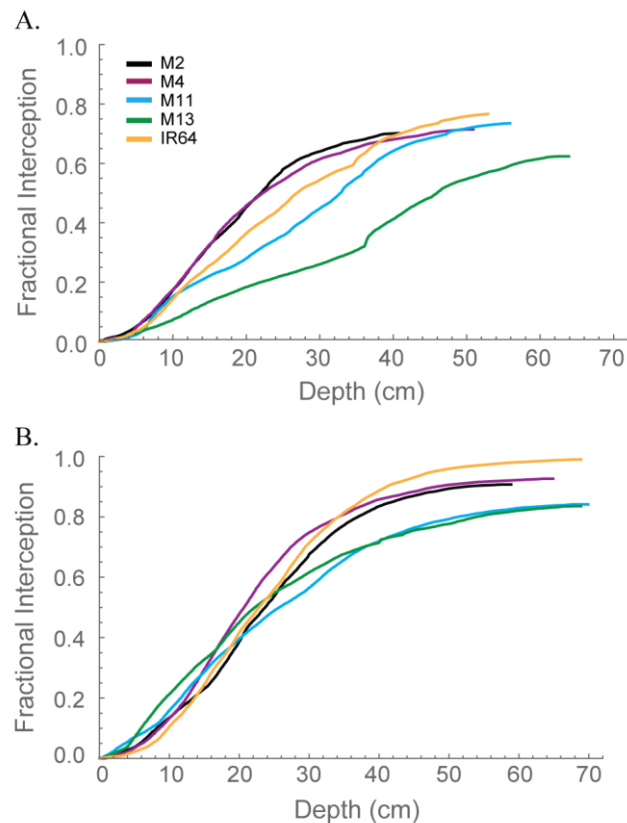


Figure 4.4: Modelled fractional interception as a function of depth in the canopy at 12:00 h for (A) GSI and (B) GS2, using ray tracing data. Curves were calculated with step $\Delta d = 1$ mm.

Photosynthesis

- **Measured Data**

There were no significant differences between any of the ACi curve parameters (V_{cmax} , J and TPU) at either growth stage (see Table 4.2). There was a significant difference in Chlorophyll a content ($P=0.034$) and total chlorophyll content ($P=0.041$) between the lines with M11 and M13 containing the highest levels (Table 4.3). The dark-adapted Fv/Fm measurement measured

at the top of the canopy also shows significant differences between the lines at both growth stages under two different weather conditions, full sun and cloudy with supplementary lights, ($P < 0.002$ for all) with the lowest Fv/Fm value found in M2 (Table 4.4). This is in agreement with previous work on canopy architecture and susceptibility of plants to photoinhibition, whereby erect architectures are less susceptible to high light and have a higher Fv/Fm in accordance (Burgess *et al.*, 2015).

Line	Layer	V_{cmax}	J	TPU
M2		140.5±13.4	187.6±11.1	13.1±0.7
M4		145.9±18.0	202.7±9.0	13.7±0.6
M11	Top	135.6±12.0	195.8±16.3	12.9±1.0
M13		143.4±12.3	186.9±12.3	12.4±0.5
IR64		134.8±12.7	181.3±9.2	12.0±0.6
Mean		140	190.9	12.82
	P	0.982	0.847	0.695
	SED	22.23	20.45	1.21
M2		120.4±8.0	173.1±9.1	11.5±0.8
M4		131.4±19.9	180.2±11.8	11.8±0.5
M11	Bottom	127.3±10.8	201.6±24.9	13.0±0.8
M13		141.2±17.0	182.0±6.9	11.6±0.5
IR64		126.1±15.7	166.3±11.0	11.4±0.9
Mean		129.3	180.6	11.83
	P	0.905	0.606	0.551
	SED	22.05	22.07	1.05

Table 4.2: Parameters taken from ACi curve fitting at GS1 (45 DAT) using Sharkey *et al.* (2007; fitting at 30°C). The means of six independent curves are shown with standard errors of the mean. P value corresponds to ANOVA.

We assessed photosynthesis at different canopy layers and compared it to patterns of LAI accumulation above. P_{\max} for the top layer varied between species for GS1 ($P < 0.001$), with M13 having a higher P_{\max} than M4, but not GS2 ($P = 0.053$; Table 4.5). There was no significant difference in P_{\max} for the bottom layer at either growth stage ($P = 0.062$ for GS1 and $P = 0.321$ for GS2). There were no apparent consistencies between canopy structure and

distribution of P_{\max} except that the highest P_{\max} , and the largest decline in P_{\max} for the top layer between GS1 and 2 is shown by M13; the line with the lowest cumulative LAI (Fig 4.2).

Line	Chl a ($\mu\text{g}/\text{cm}^2$)	Chl b ($\mu\text{g}/\text{cm}^2$)	Chl a+b ($\mu\text{g}/\text{cm}^2$)	Chl a:b
M2	36.10 \pm 2.40	8.46 \pm 0.55	44.56 \pm 2.92	4.27 \pm 0.08
M4	36.53 \pm 2.71	8.93 \pm 0.85	45.46 \pm 3.43	4.19 \pm 0.19
M11	45.67 \pm 3.78	10.30 \pm 0.80	55.98 \pm 4.57	4.42 \pm 0.07
M13	53.69 \pm 2.61	11.70 \pm 0.50	65.40 \pm 3.08	4.58 \pm 0.08
IR64	39.01 \pm 1.71	9.19 \pm 0.39	48.20 \pm 2.06	4.25 \pm 0.09
Mean	42.2	9.72	51.9	4.344
P	0.034	0.126	0.041	0.356
SED	5.28	1.20	6.41	0.20

Table 4.3: Chlorophyll content and ratio at GS2 (85 DAT). The means of three plots are shown with standard errors of the mean. P value corresponds to ANOVA.

Line	GS1		GS2	
	Full Sun	Clouds + Sup lights	Full Sun	Clouds + Sup lights
M2	0.748 \pm 0.009	0.780 \pm 0.010	0.788 \pm 0.005	0.801 \pm 0.004
M4	0.785 \pm 0.004	0.805 \pm 0.003	0.803 \pm 0.007	0.830 \pm 0.006
M11	0.813 \pm 0.001	0.828 \pm 0.004	0.810 \pm 0.007	0.838 \pm 0.006
M13	0.814 \pm 0.013	0.848 \pm 0.009	0.841 \pm 0.007	0.846 \pm 0.004
IR64	0.792 \pm 0.007	0.816 \pm 0.003	0.816 \pm 0.003	0.826 \pm 0.003
Mean	0.791	0.819	0.812	0.828
P	0.001	0.002	0.001	<0.001
SED	0.0115	0.0090	0.0084	0.0067

Table 4.4: Maximum quantum yield of PSII (F_v/F_m) measured after 20 minutes dark adaptation. Five measurements were taken per plot. The means of three plots are shown with standard errors of the mean. Growth stage 1 corresponds to 45 DAT and 2 at 85 DAT.

- ***Modelled Data***

An empirical model of photosynthesis was employed to calculate the total canopy carbon gain per unit leaf area and per unit ground area (see Materials and Methods); results are presented in Table 4.5. For GS1, M13 exhibits the highest carbon gain per unit leaf area followed by M2 and M4, respectively, with IR64 showing the lowest value. For carbon gain per unit ground area, M13 remains the highest, followed by M2 and M11. This can be attributed to the higher P_{\max} for that line, despite the reduced LAI. At GS2, all canopies show a reduced carbon gain per unit leaf area and increased carbon gain per unit ground area. This is presumably due to an increase in LAI of all canopies and a concurrent increase in proportion of shaded leaves. Per unit leaf area M11 and M13 show the highest values of carbon gain and per unit ground area M11 is the highest, followed by M2 and M13. However, we saw only weak correlations between P_{\max} and carbon gain per unit leaf area and ground area (data not shown).

Canopy structures result in dynamic fluctuations in light from solar movement. The different architectures studied here are likely to generate different characteristics of fluctuations, in addition to the light interception shown above (Burgess *et al.*, 2015). The most appropriate approach is a functional analysis of this variation in dynamic light via the impact that it has on the predicted distribution of a modelled optimal P_{\max} . This was calculated using an empirical model of acclimation (see Materials and Methods: Modelling; Retkute *et al.*, 2015). The model takes into account the fluctuating light over a full day within the canopy and provides an optimal P_{\max} ; the value of P_{\max} that is optimised in terms of carbon gain for that particular light environment, if light were the sole determinant, using the frequency and duration of high light periods. This differs from previous models that use integrated light over the whole day (Stegemann, 1999). Thus the optimal P_{\max} provides a means of analysing both the frequency and duration of high light events in the canopy.

Growth Stage	Line	P_{\max} Top Layer ($\mu\text{mol m}^{-2} \text{s}^{-1}$)	P_{\max} Bottom Layer ($\mu\text{mol m}^{-2} \text{s}^{-1}$)	Carbon Gain per Unit Leaf Area ($\text{mol m}^{-2} \text{d}^{-1}$)	Carbon Gain per Unit Ground Area ($\text{mol m}^{-2} \text{d}^{-1}$)	Total Light Interception ($\text{mol m}^{-2} \text{d}^{-1}$)
1	M2	24.29±1.61	20.23±1.69	0.241	0.532	11.98
	M4	22.67±1.76	17.91±1.82	0.220	0.489	12.25
	M11	29.99±2.37	24.52±2.53	0.204	0.504	11.16
	M13	38.65±2.82	27.34±3.54	0.432	0.798	13.34
	IR64	25.96±1.63	20.24±1.70	0.169	0.480	10.18
	Mean	28.31	22.1			
	P	<0.001	0.062			
SED	2.96	3.34				
2	M2	20.15±0.77	14.14±1.82	0.174	0.827	7.08
	M4	22.67±1.78	14.78±1.87	0.121	0.661	6.28
	M11	26.83±2.72	17.69±1.63	0.232	0.968	7.72
	M13	23.53±1.11	18.83±1.34	0.236	0.828	8.57
	IR64	26.35±1.02	15.90±1.715	0.082	0.714	4.08
	Mean	23.91	16.33			
	P	0.053	0.321			
SED	2.32	2.39				

Table 4.5: Gas exchange and modelling results at each growth stage. Measured P_{\max} for the top and bottom layer was calculated from light response curve fitting; mean \pm SEM is presented, $n=6$ (GS1) or 5 (GS2). P value corresponds to ANOVA. An empirical model of photosynthesis was employed to calculate carbon gain per unit leaf area and ground area using light levels predicted by ray tracing. Total light interception over the course of the day was also calculated. Growth stage 1 corresponds to 45 DAT and 2 at 85 DAT.

The moving average of the distribution in optimal P_{\max} for each of the canopies is given in Figure 4.5. This shows distinctive differences between the lines. At GS1, M4, M11 and IR64 show similar patterns for distribution of photosynthetic capacity. M13 shows a similar pattern for reduction in optimal P_{\max} throughout but a greater value achieved at all canopy layers (depths) and a plateau in optimal P_{\max} towards the top of the canopy. By GS2, differences between each of the canopies are less obvious. All canopies exhibit similar steep gradients in reduction of potential within the top section of the canopy followed by a shallower gradient at the bottom of the canopy. IR64 has the lowest predicted optimal P_{\max} values of all canopies with the bottom ~40 cm under $5 \mu\text{mol m}^{-2} \text{s}^{-1}$.

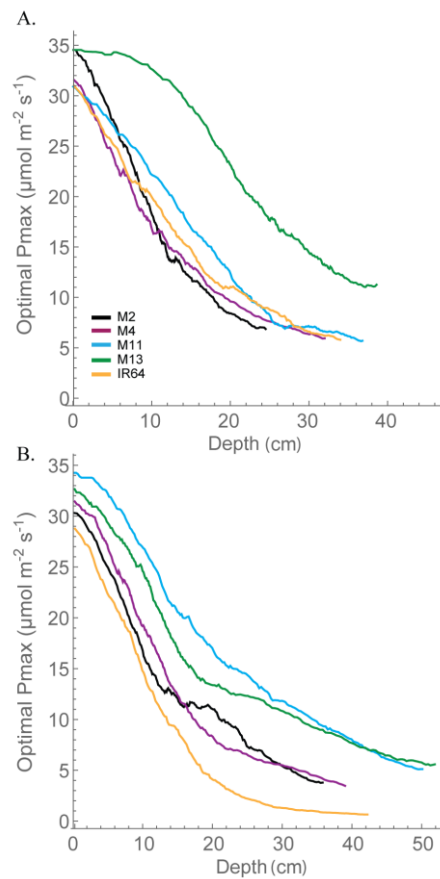


Figure 4.5: Whole canopy acclimation model output. The acclimation model was run at 250 locations throughout canopy depth to predict the optimal P_{\max} at each location throughout canopy depth (i.e. from the top of the canopy) dependent upon the light environment that it experienced, calculated via ray tracing. A moving average has been fitted to the data. (A) GS1 and (B) GS2.

Discussion

Canopy reconstructions

Plant canopies often consist of an assemblage of structurally diverse plants with particular spatial distributions of photosynthetic material. The way in which these photosynthetic surfaces intercept light energy and assimilate CO₂ is the basis for whole canopy photosynthesis, and thus the arrangement of plant material that optimises light interception will inherently lead to increased productivity. If all incident light is absorbed ($F=1$) then whole canopy photosynthesis is a result of the efficiency of distribution of light across a particular LAI. The architectures of five diverse rice cultivars at two different growth stages were captured using a low-tech method for high-resolution canopy reconstruction. This reconstruction method has previously been shown to provide an accurate representation of the plants with replication of leaf area between 1-4 % of that of measured data and accurate capture of leaf angles (Pound *et al.*, 2014; Burgess *et al.*, 2015). In combination with ray tracing using fastTracer3, the reconstruction method provides an accurate depiction of the light gradients found within real life canopies in field settings (Burgess *et al.*, 2015). The structural differences (i.e. cLAI and leaf angle distributions) between diverse rice lines and their relationship to whole canopy photosynthesis can be explored in more depth using this modelling approach than would be possible using manual methods under field conditions.

The relationship between canopy architecture and photosynthesis

To investigate the relationships between architectural features and photosynthetic traits, a correlation matrix was produced for manually measured data. Significant correlations (both positive and negative, given in bold) relating to canopy architectural features are given in Table 4.6. Among the factors that influence photosynthesis (here associated with P_{\max} for the top (T) and bottom (B) canopy layers) are: tiller number, plant height, leaf number and leaf width. However, these relationships are only significant at the first growth stage, not the second, indicating either (i) the architecture at certain developmental stages are more critical in determining photosynthesis characteristics, (ii) past a certain developmental stage, or a certain amount of

leaf area, the levels of light inside the canopy are below a certain threshold so as to not significantly influence photosynthetic characteristics or (iii) photosynthetic performance is determined by factors other than architectural traits. There is a positive correlation, although weak, between plant height and photosynthesis during GS1, which may be initially contrary to what would be expected. Whilst extra height may provide an advantage during competition with shorter neighbours, it is also possible that height may increase shading over a greater surface area of the canopy, thus could intuitively reduce canopy productivity (diffuse light notwithstanding). Alternatively, plant height could be linked closely with leaf angles, with taller plants containing more elongated and erect leaves (as seen within our two tallest study lines: M11 and M13), which can lead to greater penetration of light throughout the canopy especially at mid-day, despite the greater height. Conversely, increased photosynthetic potential could provide plants with the means to achieve greater height. There is increasing evidence that tall plants provide greater sinks for photosynthate (i.e. within the stems) that can reduce limitations based on source-sink processes. This can lead to higher photosynthetic rates, at the leaf level, within taller crops. Therefore, the positive correlation between plant height and photosynthesis at GS1 could be a result stem sink development during this stage.

To explore how canopy architecture influences photosynthesis and light interception at the whole canopy level, a line of best fit between measured LAI and modelled data were made. Total canopy light interception is negatively correlated to measured LAI at both growth stages ($R^2= 0.981$ and 0.967 for GS1 and GS2 respectively). Similarly, there is also a negative correlation between measured LAI and carbon gain per unit leaf area ($R^2= 0.775$ and 0.914 for GS1 and GS2 respectively). Thus across the five rice lines, an increase in leaf area leads to a decrease in total light intercepted and in carbon gain per unit leaf area, possibly representing the 'dilution effect' (Field and Mooney, 1983), although this does not translate to a significant decrease in measured P_{max} (Table 4.5), nor does it translate into an effect on carbon gain per unit ground area, with no clear relationship at either growth stage ($R^2= 0.311$ and 0.091 for GS1 and GS2 respectively).

Growth Stage		Tiller Number	Plant Height	Leaf Area	Leaf Number	Leaf Width (B)	Leaf Width (T)
1	Plant Height	-0.638*	-				
	Leaf Area	0.412	-0.221	-			
	Leaf Number	0.890*	-0.629*	0.521*	-		
	Leaf Width (B)	-0.240	0.601*	-0.045	-0.420	-	
	Leaf Width (T)	-0.907*	0.635*	-0.358	-0.813*	0.445	-
	Pmax (B)	-0.574*	0.601*	0.112	-0.425	0.513	0.519*
	Pmax (T)	-0.721*	0.730*	-0.189	-0.624*	0.626*	0.737*
	Fv/Fm Sun	-0.561*	0.830*	0.066	-0.585*	0.480	0.555*
	Fv/Fm Cloudy	-0.755*	0.881*	-0.150	-0.692*	0.589*	0.675*
	FI/Height	0.101	-0.713*	-0.012	0.158	-0.578*	-0.2145
2	Leaf Area	0.389	-0.053	-			
	Leaf Number	0.689*	-0.166	0.663*	-		
	Leaf Width (B)	-0.615*	0.408	-0.307	-0.627*	-	
	Leaf Width (T)	-0.819*	0.673*	-0.413	-0.652*	0.683*	-
	Pmax (B)	-0.524*	0.587*	-0.357	-0.645	0.706*	0.825*
	Pmax (T)	-0.311	0.453	-0.088	0.165	-0.065	0.176
	Fv/Fm Sun	-0.736*	0.486	-0.040	-0.195	0.294	0.694*
	Fv/Fm Cloudy	-0.709*	0.661*	-0.236	-0.382	0.441	0.734*
	Chl a	-0.752*	0.5645*	-0.251	-0.470	0.401	0.689*
	Chl b	-0.692*	0.619*	-0.290	-0.453	0.329	0.643*
FI/height	-0.2241	-0.5415*	-0.1975	-0.3912	0.2445	-0.0507	

Table 4.6: The relationship between measured canopy architectural traits and photosynthesis: the sample correlation coefficient value taken from the correlation matrix output for select canopy architectural and physiological traits. Growth stage 1 corresponds to 45 DAT and 2 at 85 DAT. Significant correlations are given in bold, * indicates $P < 0.05$.

It might be expected that leaf angle, canopy light interception and LAI distribution are closely related: indeed this was shown in Figures 4.2, 4.3 and 4.4 at depths between 10 – 30 cm. The conclusion is that a more upright leaf angle permits a greater light penetration but a greater LAI accumulation at GS2 lessens this effect. This is consistent with previous work e.g. Song *et al.* (2013).

The dynamic light pattern cast by canopies presents a complex problem: how do leaves determine the optimal properties of a light response curve for a given time period? We used a model that predicts the optimal P_{\max} following ray tracing throughout the canopy depth. The optimal P_{\max} distribution (Fig 4.5) follows a similar pattern (in terms of ranking responses among lines) to LAI and F. The differences between each of the lines, particularly at the first growth stage, indicate that whilst the quantity of leaf material (i.e. the LAI) may be similar, the arrangement of this material in 3-dimensional space can lead to dramatic changes in carbon assimilation in different canopy layers. The greater potential optimal P_{\max} at the bottom of the canopy in M13 at GS1 relative to the other varieties can be linked to the low accumulation of leaf material with canopy depth (as seen with cLAI; Figure 4.2A and 4.B) and the reduced fractional interception of light (Fig. 4.4) but an increased total light intercepted over the whole canopy (Table 4.5). This suggests that architecture which enables greater light penetration to lower canopy layers leads to a greater assimilation of carbon at lower canopy layers, which contributes to overall canopy photosynthesis. This is seen as an increased carbon gain per unit leaf area relative to the other lines (Table 4.5). However, when assessing the carbon assimilation per unit ground area, M13 ranks in the middle of the five varieties, indicating that despite the open canopy and greater light penetration, the reduced LAI of the variety leads to reduced productivity on a per land area basis. This is highly significant because it indicates a level of consistency between diverse canopy architectural traits and the long-term responses of photosynthesis to the light environment. Moreover, it shows that the architectural traits measured and modelled in this study are having a consistent impact on the light dynamics within the canopy. However, it is not possible to conclude whether it is possible to predict acclimation state from the

distribution of F and LAI within the canopy without detailed direct photosynthetic analysis of a wider range of genotypes.

The leaf inclination angle is critical in determining the flux of solar radiation per unit leaf area (Ehleringer and Werk, 1986; Ezcurra *et al.*, 1991; Falster and Westoby, 2003). Plants containing steep leaf inclination angles tend to have a decreased light capture when the sun is directly overhead (i.e. during midday hours or during summer) but increases light capture at lower solar angles (i.e. start/ end of the day or during seasonal changes in the higher latitude regions). This feature has a number of practical applications including the decrease in susceptibility to photoinhibition (Burgess *et al.*, 2015; Ryel *et al.*, 1993; Valladares and Pugnaire, 1999; Werner *et al.*, 2001); reduced risk of overheating due to reduction in mid-day heat loads (King, 1997); and minimised water-use relative to carbon gain (Cowan *et al.*, 1982). This architecture feature, combined with a relatively open canopy, has been adopted within our studied line; M13, and contributes to its inherent heat tolerance and higher Fv/Fm values (Fig 4.3, Table 4.4). The erect leaf stature and higher Fv/Fm is also present in our studied line M11 (Fig 4.3, Table 4.4). This may suggest a relationship between erectness, maximum quantum yield and latitude of origin of the lines with M11 and M13 originating in locations closer to the equator (Latin America including equatorial regions and WARDA (now AfricaRice), Western Africa, respectively) relative to the other lines. Such characteristics are in line with previous work to predict the optimal leaf angle according to latitude (Baldocchi *et al.*, 1985; Ehleringer, 1988; Herbert, 2003) and work in *Arabidopsis thaliana* (Hopkins *et al.*, 2008). Correlations between architectural traits and latitude have also been seen within tree species, with a linear decrease in petiole length with an increase in latitude and change in leaf arrangement (King and Maindonald, 1999). The differences in Fv/Fm between the varieties may also be linked to the genetic background of the lines M11 and M13 with the *japonica* background and M2, M4 and IR64 with the *indica* background. This is in agreement with previous work on rice with higher Fv/Fm values found in *japonica* cultivars relative to *indica* (Kasajima *et al.*, 2011). Differences in Fv/Fm between the two groups are also mirrored in the

capacity for nonphotochemical quenching (NPQ) for energy dissipation, with much higher NPQ values found in *japonica* lines (Kasajima *et al.*, 2011).

Rice cultivation areas are highly diverse and are affected in differing ways by fluctuations in environmental conditions. Thus the origin of each of the parental founders may also indicate why these specific architectural traits are present and how they interact with leaf photosynthetic properties. The five lines selected for this study have diverse origins including China (M2), South East Asia (International Rice Research Institute; M4 and IR64), Africa (M13) and Latin America (M11). The rapid maturation and early flowering of M13 relates to the short-growing seasons of upland rice production in Western Africa whilst stable yields under low nitrogen inputs enables relatively high yields under low-input upland systems (Gridley *et al.*, 2002). Whilst there is little data relating to canopy architecture in divergent rice lines grown across the world, there has been some work done studying architectural differences between key African and Australian savannah tree taxa (Moncrieff *et al.*, 2014). They found distinct differences between the two sets of taxa in key architectural traits including plant height and canopy area, and attributed the differences not to disparities in the environmental conditions in which the trees grew, but rather in the differing evolutionary history of African versus Australian savannas. This may indicate that when assessing regional differences in rice architecture, we must take into account not only the biotic and abiotic differences between areas but also the biogeography, interactions with other species and historic cultivation practices.

This is the first high-resolution study that has been used to attempt to assess the link between canopy architecture and photosynthesis characteristics. One of the drawbacks of this study was the inability to grow the lines in the location they originated, or under a range of different environments. This poses a challenge as canopy architecture is determined by a combination of the genetics of plant but also the conditions in which the plant was grown, including climate, weather patterns, soil type and the competitive presence of neighbouring plants. Thus the architecture taken on by the crops in this study may not be totally representative to that when grown elsewhere due to

differences in growing conditions. In this study, we used the latitude of the Philippines as a fastTracer3 parameter as a standard to compare the different lines, which will be a different light environment to those in which the plants were grown or in which the lines traditionally grow or have originated. However, the conditions we used were enough to expose significant differences in architecture between lines which are genetically different in origin.

Other factors relating to whole canopy photosynthesis must also be taken into account such as: the angular relationship between the photosynthetic leaf surfaces and the sun; environmental conditions (i.e. wind speed, temperature, CO₂ concentration); soil properties; the photosynthetic pathway used and; the presence of other biotic or abiotic stressors (Baldocchi and Amthor, 2001). This highlights the need for more in depth studies of canopy photosynthesis and architecture within the range of different environmental conditions in which a plant is likely to be exposed to. Also for more realistic modelling; i.e. modelling mimicking the weather conditions or more realistic representations of the plant stands in general (such as incorporating canopy movement due to wind: Burgess *et al.* (2016)). These high-resolution studies will be critical in determining the exact relationships between canopy architectural features, photosynthesis, the light environment and productivity of our cropping systems and will provide the framework necessary for any future improvements.

Use of the parental founders of an elite MAGIC population of rice leads to a number of possibilities for future studies into the genetic control of specific architectural features or breeding attempts to produce an 'optimal plant type'. Whilst the genetic control of certain architectural traits is relatively understood (e.g. Wang and Li, 2006; Busov *et al.*, 2008; Neeraja *et al.*, 2009; Pearce *et al.*, 2011), the interactions between genotype, phenotype, management and the environment are less well known. These relationships are confounded further by the variability in weather patterns and the relatively unknown effects of climate change on our agricultural systems. However, combining high-resolution studies and crop simulations with new breeding methods and genetic modelling provides a promising future for accelerating the discovery and

creation of new idealised plant types. Multi-parent populations provide an attractive background for study when combined with high-throughput SNP genotyping (Bandillo *et al.*, 2013).

Supplementary Material

ID	Name	Varietal Type	Origin	Relevance
M1	Fedearroz 50	<i>indica</i>	Columbia	Popular and widespread. Stay green/ delayed senescence, disease tolerance, progenitor to many breeding lines
M2	Shan-Huang Zhan-2 (SHZ-2)	<i>indica</i>	China	Blast resistant, high yielding; in the pedigrees of many varieties in south China
M3	IR64633-87-2-2-3-3 (PSBRc82)	<i>indica</i>	IRRI	High yielding and most popular variety of the Philippines
M4	IR77186-122-2-2-3 (PSBRc 158)	<i>indica</i> / <i>japonica</i>	Tropical IRRI	High yielding variety in New Plant Type II background
M5	IR77298-14-1-2-10	<i>indica</i>	IRRI	Drought tolerant in lowlands with IR64 background and tungro resistance
M6	IR4630-22-2-5-1-3	<i>indica</i>	IRRI	Good plant type, salt tolerant at seedling and reproductive stages
M7	IR45427-2B-2-2B-1-1	<i>indica</i>	IRRI	Fe toxicity tolerant
M8	Sambha Mahsuri + Sub1	<i>indica</i>	IRRI	Mega variety with wide compatibility, good grain quality and submergence tolerance
M9	CSR 30	Basmati group	India	Sodicity tolerance, Basmati type long aromatic grain
M10	Cypress	Tropical <i>japonica</i>	USA	High yielding, good grain quality and cold tolerant

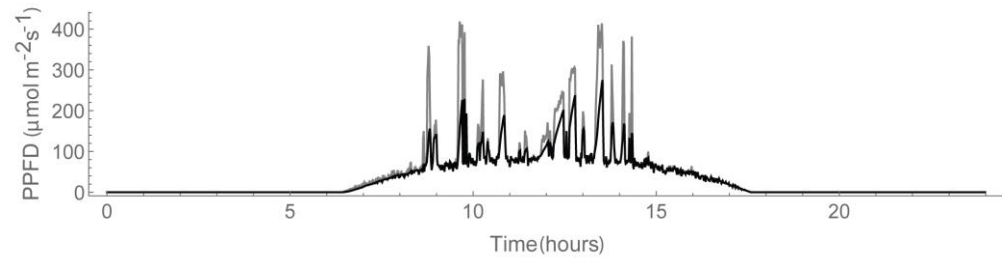
M11	IAC 165	Tropical japonica	Latin America	Aerobic rice adaptation
M12	Jinbubyeo	Temperate japonica	Korea	High yielding and cold tolerant
M13	WAB 56-125	<i>O. glaberrima</i> in indica background	WARDA	NERICA background (<i>O. glaberrima</i>); heat tolerant and early flowering
M14	IR73571-3B-11-3-K2	Tropical japonica x indica	IRRI-Korea Project	Tongil type, salinity tolerant
M15	Inia Tacuari	Tropical japonica	Uruguay	Earliness, wide adaptation and good grain quality
M16	Colombia XXI	Tropical japonica	Colombia	High yielding and delayed senescence

Supplementary Table S4.1: Agronomic details on the 16 Parental Lines used to develop the indica and japonica MAGIC Populations. Taken from (Bandillo et al., 2013). The four lines selected for in depth study are given in bold.

Line	SPAD GS1	Chlorophyll a:b	Chlorophyll content (a+b: $\mu\text{g cm}^{-2}$)	Plant Height GS1 (cm)	LAI	GS1 Fresh Weight (g plant ⁻¹)	GS1 Dry Weight (g plant ⁻¹)	Harvest Dry Weight (g plant ⁻¹)	Seed Dry Weight (g plant ⁻¹)
M1	43.4±1.6	4.3±0.2	8.3±0.8	79.5±1.7	11.7±2.2	48.8±11.6	11.2±3.0	32.8±7.0	26.4±7.7
M2	38.4±0.8	3.6±0.1	7.4±0.1	71.8±1.3	7.7±2.2	38.5±10.2	8.8±2.1	37.9±6.3	22.2±5.0
M3	41.6±1.0	4.2±0.1	10.0±0.9	88.9±2.6	8.9±3.5	37.8±13.1	9.3±3.1	34.0±6.3	26.5±5.1
M4	41.4±0.8	3.9±0.1	10.7±1.2	74.4±2.5	6.0±1.3	28.2±6.4	6.4±1.4	28.2±6.4	8.0±3.1
M5	41.0±0.8	3.8±0.1	9.4±0.5	73.0±1.5	7.2±1.6	31.2±6.9	6.8±1.5	10.2±1.0	15.1±1.7
M6	39.5±1.4	4.1±0.0	9.5±0.6	71.4±2.9	7.3±2.1	33.8±8.9	7.9±1.9	22.8±3.2	14.6±2.3
M7	44.2±2.1	4.1±1.0	7.1±1.4	83.5±1.9	7.4±3.1	35.8±15.7	9.1±3.7	30.9±6.5	
M8	42.1±1.8	4.0±0.2	7.4±1.0	85.5±1.3	8.1±1.7	40.1±7.4	9.1±1.7	18.0±2.6	7.9±0.7
M9	39.5±0.6	4.4±0.1	9.0±0.4	105.4±3.8	8.5±3.2	47.8±15.6	11.2±3.7	34.3±4.1	23.7±3.1
M10	48.2±0.6	3.8±0.4	7.2±0.7	95.5±1.6	5.4±2.3	30.1±9.2	8.2±2.6		
M11	41.8±1.7	3.9±0.4	7.1±1.9	91.8±1.9	3.6±0.7	23.9±4.9	4.9±0.9	26.3±3.5	15.0±2.8
M12	39.1±1.7	4.1±0.1	7.9±1.0	78.5±2.2	5.7±0.3	26.1±0.4	6.4±0.3	20.5±2.0	14.1±1.1
M13	47.3±0.9	4.1±0.1	11.6±1.2	90.6±3.0	4.7±0.4	37.0±0.4	7.3±0.2	22.6±3.2	18.6±2.4
M14	41.5±2.4	3.8±0.1	7.8±0.9	87.5±2.1	4.1±0.2	26.7±2.6	5.7±0.7	15.8±2.6	16.1±3.7
M15	39.3±1.8	4.4±0.3	7.8±0.9	77.3±2.2	8.1±0.0	38.5±3.1	8.1±0.4	15.8±3.6	5.0±1.2
IR64	42.4±0.8	4.0±0.1	9.7±1.1	81.2±1.7	12.3±0.0	47.5±5.0	10.6±1.2	19.4±1.9	14.4±1.4

Supplementary Table S4.2: Physiological characteristics of the 15 parental MAGIC lines + IR64 used in the initial screening. Mean \pm SEM presented, n=3. The bold lines are those selected for use in the in depth study due to their contrasting physiological features.

Supplementary Figure S4.1



Supplementary Figure S4.1: Example of a time-weighted light pattern at $\tau=0.2$ (black line) relative to a non-weighted line (i.e. $\tau=0$). The time weighted average (Eq. 9) is an exponentially decaying weight used to represent the fact that photosynthesis is not able to respond instantaneously to a change in irradiance levels. If $\tau=0$ then a plant will be able to instantaneously respond to a change in irradiance, whereas if $\tau>0$ the time-weighted average light pattern will relax over the timescale τ . Within this study, τ was fixed at 0.2.

Chapter 5: The effect of wind-induced movement on light patterning and photosynthesis

Paper as published in *Frontiers in Plant Science*

Chapter 5 uses a simple modelling approach based on solid body rotation to investigate the effects of wind-induced canopy movement (here termed mechanical canopy excitation) on the resulting light environment and photosynthesis of a rice canopy. This has been published in *Frontiers in Plant Science* (Burgess *et al.* 2016. 7: 1392), so is presented in “paper format”.

Author contribution:

Experiment and approach conceived by AJ Burgess

Project supervision performed by EH Murchie

AJ Burgess performed most of the modelling work with the assistance of R Retkute.

OE Jensen and SP Preston provided information and knowledge on mechanical mathematical modelling.

MP Pound and TP Pridmore provided information and knowledge on the hardware and technologies required for capturing plant movement and image analysis

AJ Burgess and EH Murchie wrote the article with the contributions of the other authors.

Hypothesis and Theory

The 4-dimensional plant: effects of wind-induced canopy movement on light fluctuations and photosynthesis

Alexandra J. Burgess, Renata Retkute, Simon P. Preston, Oliver E. Jensen, Michael P. Pound, Tony P. Pridmore, and Erik H. Murchie

Abstract

Physical perturbation of a plant canopy brought about by wind is a ubiquitous phenomenon and yet its biological importance has often been overlooked. This is partly due to the complexity of the issue at hand: wind-induced movement (or mechanical excitation) is a stochastic process which is difficult to measure and quantify; plant motion is dependent upon canopy architectural features which, until recently, were difficult to accurately represent and model in 3-dimensions; light patterning throughout a canopy is difficult to compute at high-resolutions, especially when confounded by other environmental variables. Recent studies have reinforced the expectation that canopy architecture is a strong determinant of productivity and yield; however, links between the architectural properties of the plant and its mechanical properties, particularly its response to wind, are relatively unknown. As a result, biologically relevant data relating canopy architecture, light dynamics and short-scale photosynthetic responses in the canopy setting are scarce. Here, we hypothesise that wind-induced movement will have large consequences for the photosynthetic productivity of our crops due to its influence on light patterning. To address this issue, in this study we combined high resolution 3D

reconstructions of a plant canopy with a simple representation of canopy perturbation as a result of wind using solid body rotation in order to explore the potential effects on light patterning, interception and photosynthetic productivity. We looked at two different scenarios: firstly a constant distortion where a rice canopy was subject to a permanent distortion throughout the whole day; and secondly, a dynamic distortion, where the canopy was distorted in incremental steps between two extremes at set time points in the day. We find that mechanical canopy excitation substantially alters light dynamics; light distribution and modelled canopy carbon gain. We then discuss methods required for accurate modelling of mechanical canopy excitation (here coined the 4-dimensional plant) and some associated biological and applied implications of such techniques. We hypothesise that biomechanical plant properties are a specific adaptation to achieve wind-induced photosynthetic enhancement and we outline how traits facilitating canopy excitation could be used as a route for improving crop yield.

Introduction

Plant movement can be classed as autonomic (spontaneous) or occur as a biological response to stimuli. Here, movement most commonly refers to tropic, tactic or nastic effects, which involve part of the plant, either an organ or organelle, responding to an external stimulus through processes of development. Such movements have been a popular focus for scientists because they involve key survival or adaptive mechanisms, including motion according to light, gravity, chemistry or water. Charles Darwin was one of the first to document systematic experiments in this area in order to reveal underlying mechanisms (Darwin, 1880). Many years later and after enormous research effort we now understand this type of movement involves a highly sophisticated sensing and signalling system which allows the plant, over time, to grow and position itself to optimise resource capture and competitive ability (Bhattacharya, 2010; Sussex and Kerk, 2001; Davies, 2013). However, the type of plant movement most immediately obvious to us is very different, and is that produced by physically perturbing the canopy, usually as a result of wind, here referred to as mechanical canopy excitation (Grace, 1977; de Langre, 2008).

Despite its wide occurrence and a broad inter-disciplinary literature, there are many fundamental questions remaining concerning its effects on plant biology and especially photosynthesis. This class of movement can also occur in response to touch and a certain amount is known at the molecular level about signalling events involved (Knight *et al.*, 1992; Chehab *et al.*, 2005). Being a stochastic process, mechanical canopy excitation is difficult to quantify and measure and hard to link to fundamental plant processes.

The impact of wind on plants largely depends on speed, duration and the extent to which wind can penetrate canopy layers. Sufficient wind speeds can affect plant development, form and function, resulting in reductions in leaf size, plant size (dwarfing) and damage to plant surfaces (Grace, 1977; 1988; Ennos, 1997; Smith and Ennos, 2003; de Langre 2008; Onoda and Anten, 2011). High winds can also cause stem breakage and lodging (Berry *et al.*, 2004), affect insect activity and population growth and the development and dispersal of pests and diseases within cropping systems (Aylor, 1990; Moser *et al.*, 2009; Shaw, 2012). Wind alters heat and mass transfer, for example, by increasing leaf transpiration rate through reduction of boundary layer resistance, and the airflow regulates the microclimate of the vegetation (Grace, 1977; 1988; de Langre, 2008). Moderate wind speeds can alter transpiration rates, indirectly affecting photosynthesis via changes in stomatal conductance and leaf temperature (Smith and Ennos, 2003) but this would be dependent upon the local environmental conditions. For example, in a hot environment, increases in transpiration and concurrent decreases in leaf temperature could be beneficial, assuming water is not limiting. However, under other less favourable conditions, the impact of moderate wind speeds on boundary layers alone may not affect leaf photosynthesis rates significantly or could negatively affect them (Grace, 1988).

A substantial impact of wind should arise through the altered light dynamics caused by movement of leaves (Roden, 2003; de Langre, 2008). Plant canopies are highly variable in terms of their light transmission characteristics, with leaf angle, clumping, density and leaf area index all playing a role in determining

patterns of light extinction (Hirose, 2005). The spatial arrangement of plant material also creates a complex pattern of light components (direct, diffuse and transmitted), typically resulting in progressively lowered light levels superimposed with high light patches or ‘light flecks’. There is also a predictable temporal effect caused by solar movement, which results in a spatial shifting of this pattern according to time of day. However, the true pattern of light within a canopy will depend upon these factors in combination with displacement brought about by wind. Early work predicted that alterations in leaf angle caused by wind can influence canopy photosynthesis (Caldwell, 1970). Roden and Pearcy (1993a,b) and Roden (2003) showed that fluttering leaves at the top of an Aspen tree canopy created an understory light environment that was more dynamic with a more even spatial distribution of light and enhanced photosynthesis in lower leaves that were adapted to utilisation of rapid light flecks, plus reduced light interception at the top of the canopy. If mechanical canopy excitation is able to increase the probability of a photon penetrating into deeper canopy layers then it can be hypothesised that it can provide a method to increase photosynthesis. Such concepts have great significance for crop productivity but have not been explored in depth. Within the rest of this paper we will focus on small to moderate wind speeds (8-10 km h⁻¹; 2-3 m² s⁻¹), which are capable of facilitating mechanical canopy excitation, and thus potential photon penetration.

The ‘mosaic’ of light patterns within a canopy can be predicted by ray tracing (e.g. Song *et al.*, 2013) if one has a 3-dimensional computed reconstruction of the plant canopy. Recent developments in measuring 3-dimensional plant architecture at high resolutions are an essential tool in understanding canopy photosynthesis and crop improvement and can be used to predict dynamic responses of photosynthesis at the leaf level that scale up to the canopy (e.g. Falster and Westoby, 2003; Watanabe *et al.*, 2005; Wang and Li, 2006; Sinoquet *et al.*, 2007; Zheng *et al.*, 2008; Pound *et al.*, 2014; Burgess *et al.*, 2015). However these methods are currently limited to static plant descriptions and thus do not take into account mechanical perturbations to the canopy, such as those resulting from wind, despite it being a ubiquitous phenomenon.

In previous work we produced highly realistic 3-dimensional plant canopies of cereal plants and used these to predict light patterns and photosynthetic productivity (based on parameterisation with measured gas exchange data and an empirical model of photosynthesis) of architecturally contrasting lines (Burgess *et al.*, 2015). High-resolution canopy descriptions have never been used to test the influence of mechanical canopy excitation on photosynthesis. Here we produce the first such simulation using a simple, solid body rotation as a first step towards providing the tools needed to predict the effect of wind on light patterning and photosynthesis. Within this study we aim to test the theory that mechanical canopy excitation may promote photosynthesis within crop canopies through altered light dynamics and that the effect is dependent on the amplitude and frequency of motion, thus could provide a route for future crop improvement.

If we assume that the number of possible 3-dimensional configurations is substantially increased by movement, then we hypothesise that it would result in an altered probability of direct photon penetration to lower layers (more potential routes for transmission). Previous work with leaf flutter in trees suggests that leaf motion would substantially increase the rate of light penetration (Roden and Pearcy, 1993). We also hypothesise that a given surface area of leaf within the canopy is more likely to experience high light as a result of wind-induced perturbations. We discuss the impact these processes may have on the metabolism and physiology of leaves at the local scale, caused by an increase in the frequency of high light events.

Materials and Methods

Growth of rice plants

We selected the commonly used rice variety IR64 for this study because it has a relatively upright leaf structure, which is likely to show typical responses to movement. This experiment took place during the summer of 2014 in a south – facing glasshouse at Sutton Bonington campus, University of Nottingham (52°49'59" N, 1°14'50" W) designed and built by CambridgeHOK (Brough, UK) for the growth of crop stands within a controlled environment. It consisted of a concrete tank 5 m x 5 m x 1.25 m positioned at ground level. The tank was filled entirely with a sandy loam soil, extracted from local fields and sieved through a fine mesh. Plants (cultivar IR64) were provided with adequate macro and micronutrients. Following soil analysis pre-experiment, additional elements supplied throughout the experiment were mostly N, P, K and manganese. Plants were grown in nine plots, arranged in a 3 x 3 arrangement with 10 cm spacing between adjacent plants, a 1 m x 1 m plot size and 10 cm spacing between adjacent plots. Watering took place via automated trickle tape application for 15 minutes twice a day. Supplementary sodium lighting was supplied (SON-T agro, Philips) at a position of approximately 3 m above ground level. Photoperiod in the glasshouse was regulated to 12 hours using automated black out blinds. Temperature in the glasshouse was regulated to 30°C ± 3°C by automated venting and two gas-fired boilers. Humidity in the glasshouse was not regulated and typically varied between 60 and 70%.

3D reconstruction and modelling

A rice plant, grown as above, was subjected to 3D analysis (imaging and reconstruction) during a vegetative growth stage. This was to focus on the effects of wind-induced movement on light patterning predominantly on leaf surfaces, but also to prevent errors with inaccurate reconstruction of panicles or inappropriate movement. This was made according to the protocol of Pound *et al.* (2014), which uses multiple RGB images as a basis for reconstruction. Topogun (2012) was then used to convert the rudimentary mesh into a cleaner

mesh consisting of 600 triangles. The rice plant was duplicated and each of the 9 duplicates were randomly rotated and assigned an identification number that referred to their layout on a 3 x 3 canopy grid (with set 10 cm spacing between plants). All duplicates were then distorted by solid body rotation, 1-10° about a set axis as shown in Fig. 5.1 using Meshlab (2014). This was used to simulate wind from a set direction. A forward ray-tracing algorithm, fastTracer (fastTracer version 3; PICB, Shanghai, China from Song *et al.*, 2013), was used to calculate total light per unit leaf area throughout the canopies. Latitude was set at 14 (for the Philippines), atmospheric transmittance 0.5; light scattering 7.5%; light transmittance 7.5%; day 181 (30th June). To avoid interference from boundaries, we positioned the ray-tracing boundaries at centres of the outer plants. The software fires rays through a box with defined boundaries; when they exit one boundary (i.e. the side), they enter again from the opposite side.

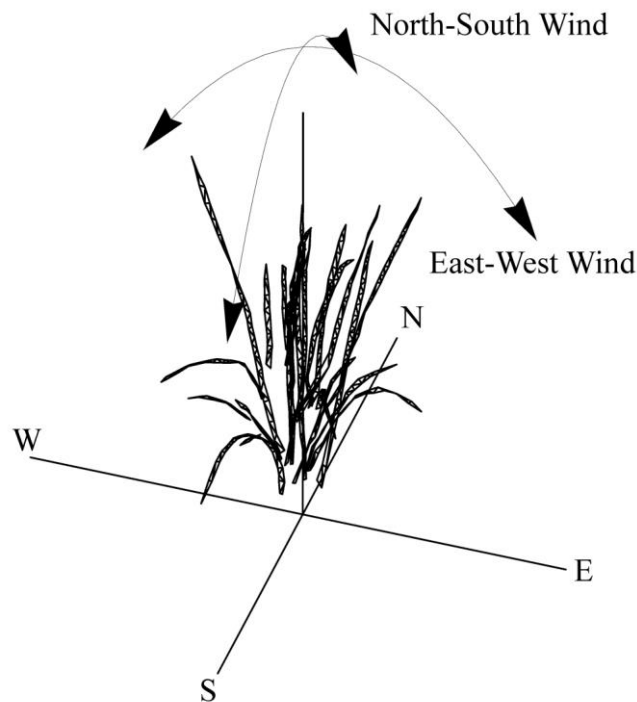


Figure 5.1: Overview of solid body rotation distortion method. Following distortion, 3x3 canopies were made.

Two different scenarios were modelled; firstly a constant distortion in which the canopy is subject to a constant wind causing a 6° distortion (equivalent to 7.6 cm displacement at the top of the canopy) throughout the whole day and; secondly a dynamic situation where the canopies were subject to a 0-10° (equivalent of 0 – 12.7 cm displacement) distortion (with 1° increments) at three time points throughout the day. For the constant displacement, the diurnal course of light intensities over a whole canopy was recorded in 1 min intervals and for the dynamic displacement, light intensities were recorded at 9:00 h, 12:00 h and 15:00 h.

All modelling was executed in Mathematica (Wolfram).

Total canopy light interception per unit leaf area was calculated according to Eq 1.

$$TL_{LA} = \frac{\sum_{i=1}^n S_i \int_6^{18} L_i(t) dt}{\sum_{i=1}^n S_i} \quad (1)$$

where S_i is the area of triangle i .

The response of photosynthesis to light irradiance, L , was calculated using a nonrectangular hyperbola given by Eq. 2:

$$F_{NRH}(L, \phi, \theta, P_{max}, \alpha) = \frac{\phi L + (1 + \alpha) P_{max} - \sqrt{(\phi L + (1 + \alpha) P_{max})^2 - 4\theta \phi L (1 + \alpha) P_{max}}}{2\theta} - \alpha P_{max} \quad (2)$$

The nonrectangular hyperbola is defined by four parameters: the quantum use efficiency, ϕ ; the convexity, θ ; the maximum photosynthetic capacity, P_{max} and; the rate of dark respiration, R_d . We assumed that the rate of dark respiration is proportional to the maximum photosynthetic capacity, according to the relationship $R_d = \alpha P_{max}$ (Givnish, 1988; Niinemets and Tenhunen, 1997; Retkute *et al.*, 2015). To maintain realism for the field we used the P_{max} photosynthetic parameter from IR72 canopies (Murchie *et al.* 2002; 32 for top layer, 21 middle layer and 5 bottom layer). IR72 and IR64 lines give highly similar photosynthetic values (data not shown). ϕ was fixed at 0.052, θ at

0.845 and α to 0.1 for all canopy layers as these values represent the maximal value possible based on an uninhibited state (Leverenz 1994; Werner *et al.*, 2001; Burgess *et al.*, 2015). The light response curves for all three canopy layers are given in Supplementary Figure S5.2.

For the constant wind scenario, the carbon assimilation at triangle i was calculated by combining Eq. 2 with the predicted Photosynthetic Photon Flux Density (PPFD) at triangle i for each minute. Daily carbon assimilation, P_i (Eq. 3), was then calculated by integrating the rate of photosynthetic carbon uptake over the day and multiplying by the area of the triangle, S_i .

$$P_i = S_i \int_6^{18} F_{NRH}(L_i(t), \phi, \theta, P_{max}, \alpha) dt \quad (3)$$

As each canopy was divided into 3 layers, each triangle from the digital plant reconstruction was assigned to a particular layer, m , according to the triangle centre (i.e. with triangle centre between upper and lower limit of a layer depth). Carbon gain per unit leaf area was calculated as daily carbon assimilation over a whole canopy divided by the total surface area of the canopy according to Eq. 4.

$$C = \frac{\sum_{i=1}^n P_i}{\sum_{i=1}^n S_i} \quad (4)$$

For the dynamic wind scenario, carbon gain was calculated from PPFD values using the light response curves as described by the non-rectangular hyperbola (Eq. 2).

Data presented in Figs. 5.2-5.5 uses a simulated easterly wind, the predominant wind direction in the Philippines.

Results

An overview of the distortion method is given in Figure 5.1. The before and after positions of each location in the rice canopy subject to a 6° distortion by

an easterly wind is given in Figure 5.2A. We used ray tracing (FastTracer3; Song *et al.*, 2013) and an empirical model of photosynthesis parameterised by measurements of photosynthetic gas exchange (see Materials and Methods) to determine the differences in light dynamics and overall carbon gain of the canopy.

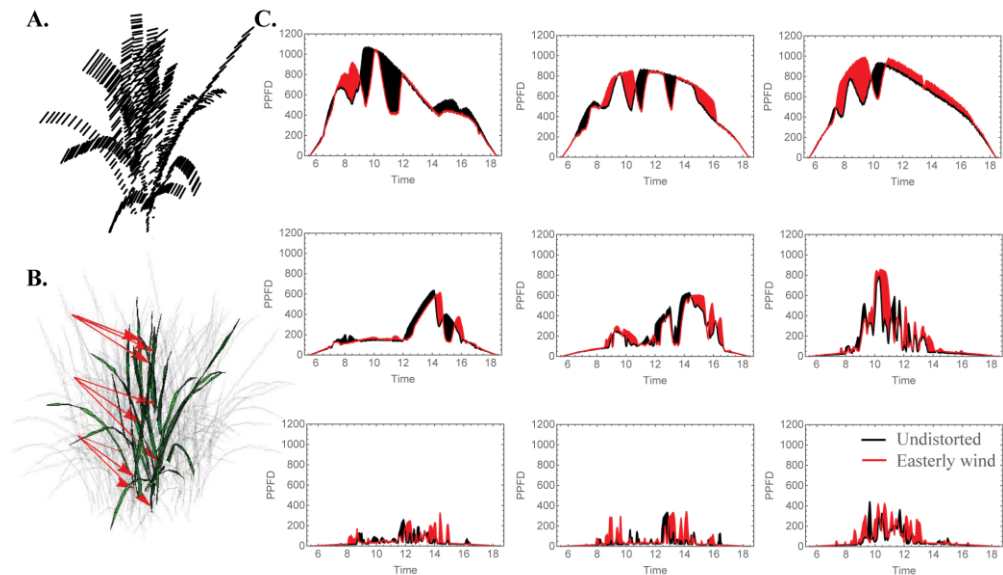


Figure 5.2: Changing Light Patterns due to simulated Easterly wind. (A) Schematic of plant distortion indicating centre of each triangle before and after simulated mechanical canopy excitation, (B) leaf locations analysed for light patterns given in (C): the selected light patterns over the whole day where black shaded regions indicate a period of higher light intensity in the undistorted orientation (no wind) and red indicates a period of higher light intensity for the distortion corresponding to an easterly wind. N.B. The three grid strata in C. correspond to the canopy strata as indicated by the arrows in B.

The number of possible canopy configurations is extremely large. To introduce as much sensitivity into the analysis as possible we have modelled two different scenarios; a constant wind inducing canopy displacement over the whole day and a dynamic wind, inducing varying degrees of displacement at three set time points during the day.

Constant displacement

Under all wind directions tested, the moderate displacement (6° ; equivalent to 7.6 cm displacement at the top of the canopy) resulted in changes in the light patterning at different canopy depths. Figure 5.2C shows the light signatures from 9 different locations (those denoted by arrows in Fig. 5.2B) in an undistorted (upright) canopy relative to a canopy subject to an easterly wind, where black shading indicates periods where there is a greater light intensity received in the undistorted canopy and red shading indicates a period of greater light intensity received by the distorted canopy. To explore this further, the frequency of PPFD values according to the fraction of surface area received by the central plant in the 3x3 canopy is shown for 9:00 h, 12:00 h and 15:00 h (Figure 5.3). For all three time points and canopy layers shown, there is a shift in the distribution towards a higher amount of intercepted light for the canopy subject to a constant moderate easterly wind relative to the undistorted canopy. This can also be seen over the course of the whole day as an increased total canopy light interception and translates into increases in total canopy carbon gain (Table 1; see Materials and Methods). The results obtained are dependent upon latitude, time of year, exact wind direction and the exact configuration achieved for a given wind speed. The percentage difference in canopy surface area receiving a set PPFD relative to the undistorted canopy at each time point was also calculated (Fig. 5.3D) where positive values indicate a higher surface area of the easterly wind distorted canopy receiving that set level of PPFD and negative values indicate a higher surface area of the undistorted canopy. This indicates that a greater surface area of the distorted canopy is under higher irradiance values relative to the undistorted canopy. These results support the hypothesis above that a mechanically excited canopy alters the light distribution patterns, here by altering the probability of a photon penetrating the canopy and being absorbed by leaves lower in the canopy.

Wind Direction	Daily Carbon Gain per unit leaf area (mol m⁻² d⁻¹)	Total Canopy Light Interception per unit leaf area (mol m⁻² d⁻¹)
None	0.262	7.548
West	0.279	8.014
East	0.307	9.325
South	0.301	8.905
North	0.285	8.297

Table 5.1: Daily carbon gain per unit leaf area and total canopy light interception for each of the simulated wind directions

Whilst it is not clear what is causing the increased interception of light in the distorted canopies we can speculate that it will be due to the more favourable leaf orientations. To assess whether this is the case, leaf angle distributions (Figure 5.4) were calculated relative to vertical (i.e. 0° represents an upright leaf and 90° a horizontally orientated leaf). These distributions do indicate a tendency towards more horizontal leaf orientations in the canopy subject to an easterly wind relative to an undistorted canopy (Figure 5.4A), which could be beneficial in this canopy where LAI is approximately 4. Distributions can also be calculated as a function of depth (Figure 5.4B), which, though difficult to interpret, indicate the possibility of more vertical leaves at the top of the canopy and more horizontal leaves at the bottom of the canopy in the easterly wind distortion. This trait (i.e. erect leaves at the top of the canopy and horizontal leaves at the bottom) represents the theoretical optimal structure for enhancing light interception and canopy photosynthesis as it provides a structure in which incident radiation can be uniformly distributed throughout all canopy layers (e.g. Duncan, 1971; Nobel *et al.*, 1993). This indicates that the increase in light interception and carbon gain witnessed under a constant distortion could be a result of more favourable orientations of leaf material for the interception of light although the next section will be able to determine this further.

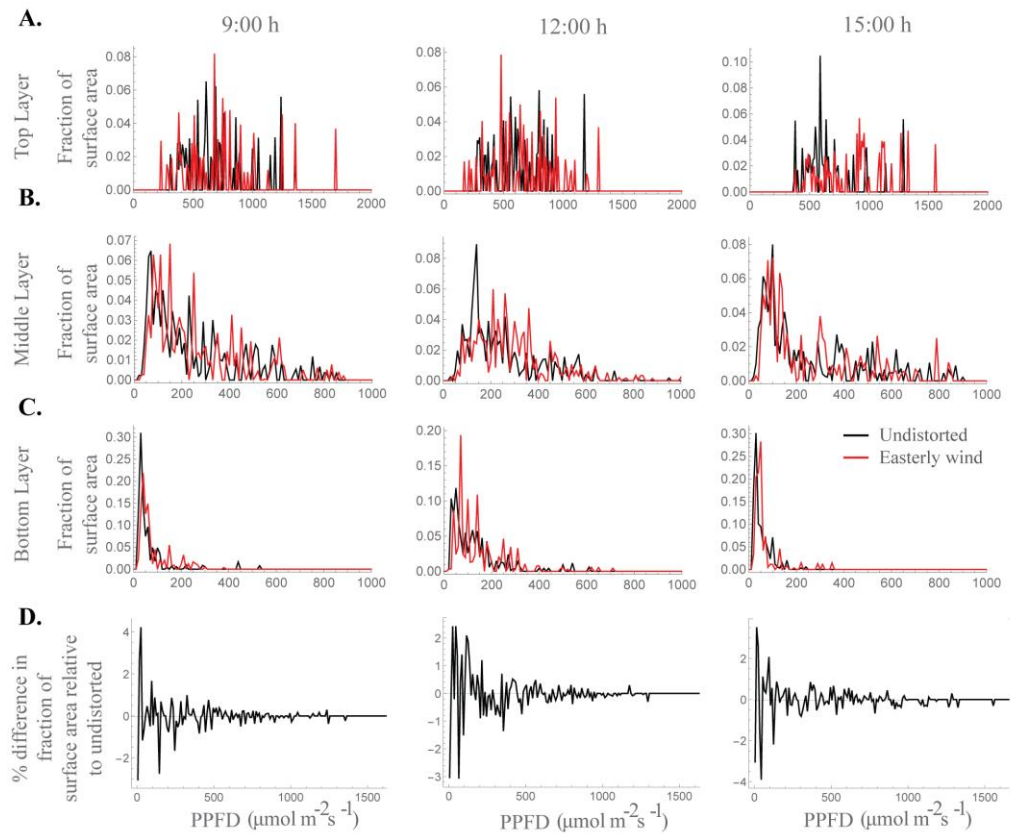


Figure 5.3: Frequency of PPFD values according to the fraction of surface area received at by a whole plant within a canopy at 9:00 h, 12:00 h and 15:00 h. (A) Top layer, (B) middle layer and (C) bottom layer where black is the undistorted canopy and red is the distortion equivalent to an easterly wind. (D) Percentage difference in the fraction of the total surface area receiving each PPFD value relative to the undistorted state; i.e. positive values indicate a higher surface area of the easterly wind distorted canopy receiving that set level of PPFD and negative values indicate a higher surface area of the undistorted canopy.

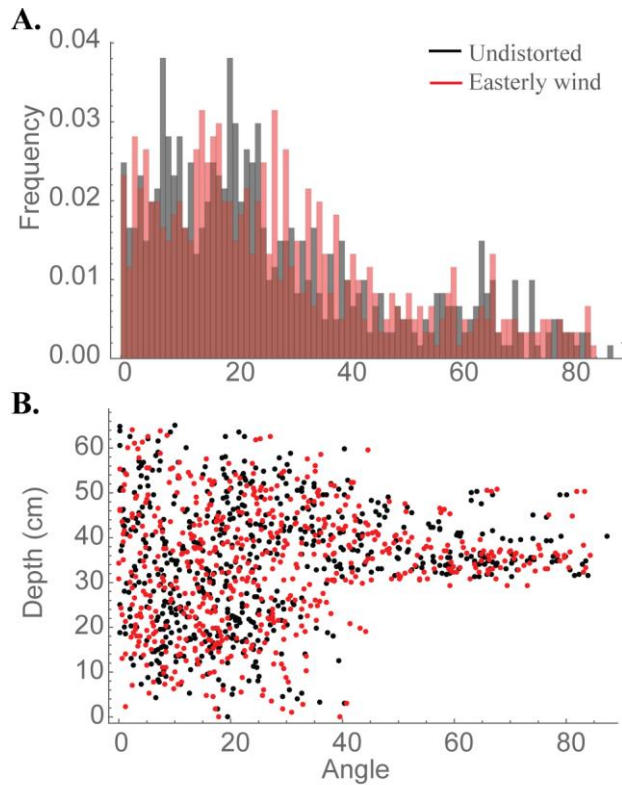


Figure 5.4: Angle distributions relative to vertical, whereby 0 indicates a vertically inclined leaf section and 90 represents horizontally inclined leaf sections. Data are shown for all canopy locations in the central plant of an undistorted canopy (black) versus a canopy subject to an easterly wind (red) where (A) frequency of different leaf orientations and (B) distribution of individual leaf sections with depth through the canopy from the top.

Dynamic displacement

The ‘constant’ displacement used above is useful but only partly representative of natural conditions. It represents states at either side of a continuum of movement. Significant computing power would be needed to calculate the effect of continually shifting between intermediate states over the course of the day since the number of configurations is so large. In our experiment we can anticipate that the actual values for carbon gain and total canopy absorption would be within this range of values. However, to assess how dynamic movements could affect the light environment and photosynthetic productivity, we have distorted the canopy by 1° increments

from 0 - 10° (equivalent to 0 – 12.7 cm displacement at the top of the canopy) at three set time points throughout the day. We assume that the canopy will move through these positions within seconds consistent with the measured frequency under a light wind (data not shown) and too fast for a change solar angle to have a measurable effect. Supplementary Movie S5.1 shows a short animation of the modelled dynamic mechanical excitation with a single, central plan in bold and coloured according to the maximum PPFD ranges each leaf portion is subject to. To indicate how degree increments in distortion can affect the light environment throughout the canopies three leaf locations per layer (located near those denoted in arrows in Fig 5.2B) were selected and the average of five PPFD values of adjacent triangles (taken from ray tracing data) was calculated (Figure 5.5A). Each PPFD value was translated into a carbon gain value using the light response curve as described by the non-rectangular hyperbola (Figure 5B; see Materials and Methods). These results show similar patterns as an increase in PPFD translates into an increase in carbon gain, although the magnitude of change will depend upon the region of the light response curve in which the point falls (i.e. a small change in PPFD can lead to a large change in carbon gain during the initial, linear phase of a light curve but will result in small differences in the saturating portion of the light curve; see Supplementary Figure S5.2 for the light response curves used in this study).

To see whether any orientation provides more favourable conditions, the normalised value of carbon gain was calculated (Figure 5.5C). This was calculated per individual triangle; each line represents the average of 5 triangles in close proximity on the same leaf. Values approaching 0 indicate the least favourable orientation in terms of carbon gain and 1 indicates the most favourable (N.B. each line represents the average of 5 measurements so does not reach the maximal limits). Whilst there is a lot of variation within the different canopy locations, there is a trend for an increase in the normalised values at 9:00 h and 12:00 h but a decrease at 15:00 h from 0 - 10°. The full impact on carbon gain in different regions of the canopy can be seen by calculating the percentage difference in carbon gain of each distortion relative to the undistorted state (i.e. at 0°; Figure 5.5D). Negative values indicate where

the distortion achieves a lower carbon gain relative to the undistorted state and can be seen most easily at 12:00 h at a position in the top of the canopy. The areas under the lines indicate the extra carbon gained as a result of shifting between 0 and 10°. The largest differences in carbon gain are found in leaf portions in the centre and bottom of the canopy (as indicated by the dark grey and light grey lines, respectively), with an increase of 350% for a section of leaf from the middle of the canopy at 9:00 h. These results indicate that, using the wind-induced canopy configurations shown here, movement would result in the greatest alterations at the middle and the bottom of the canopy consistent with the hypothesis that foliage movement will increase the probability of photon penetration through to lower canopy layers. These simulations also indicate the importance of solar angle in determining how beneficial movement will be, with results from 15:00 h showing less beneficial effects relative to the other time points. Thus both the direction of movement and the solar angle will be important in determining the exact impact of wind on plant productivity.

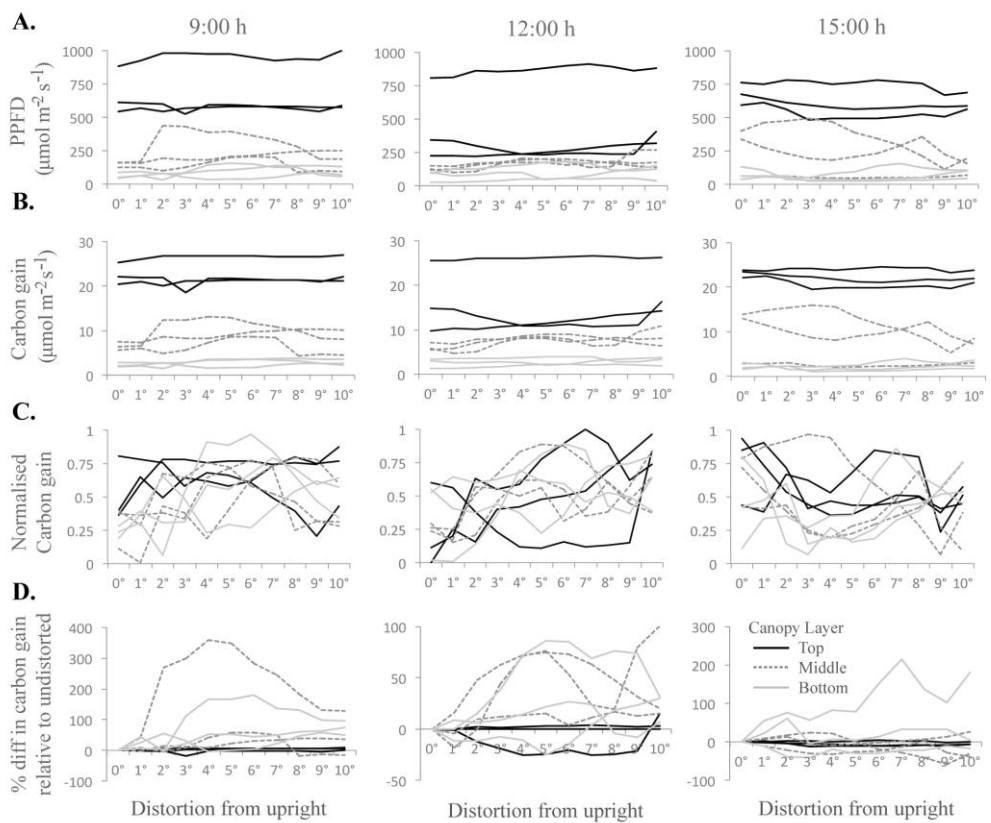


Figure 5.5: Changes as a result of dynamic movement at three time points throughout the day and nine canopy locations (A) PPFD, (B) Carbon gain, (C) normalised carbon gain and (D) percentage difference in carbon gain relative to the undistorted state; where each line represents the average of five measurements from adjacent triangles on the same section of leaf; from the top (black line), the middle (dark grey and dashed line) and the bottom of the canopy (light grey line). Normalised carbon gain was calculated per individual location and averaged across the 5 locations in close proximity on the same leaf (i.e. the 5 locations represented by a single line). Data is presented for 3 different locations (i.e. 3 different leaves) per canopy layer. Values approaching 0 indicate the least favourable orientation in terms of carbon gain and 1 indicates the most favourable.

Discussion

From these findings we can deduce an impact on canopy light distribution resulting from a moderate wind. Our first hypothesis for the effect of mechanical canopy excitation was the increased probability of light penetration through canopy layers in a given time period, with more frequent movements leading to a higher probability of penetration. In the case of the data shown here for the constant scenario, the undistorted configuration (i.e. a canopy in its resting state) had substantially lower total canopy light interception and canopy carbon gain than the distorted configurations. However, this was not necessarily expected and whether a configuration is favourable or not is likely to result from the original characteristics of the undistorted canopy. A canopy may constantly shift between less and more favourable configurations the likelihood of each being, in turn, dependent on solar angle and wind characteristics. To test this hypothesis further we used a simplified simulation of a dynamic canopy which also showed that summing the incremental degrees of movement from the upright position can indeed lead to increased light interception, with the most profound positive effects being seen in the middle and bottom layers of the canopy (Fig 5.5D). Whilst we found no single leaf orientation to be the most favourable for all areas of the canopy explored, in our case the distortions were, in the most part, beneficial. This simulation also agrees with our second hypothesis: that a given surface area of leaf within the canopy is more likely to experience, on average, higher light levels than if the canopy were not able to move. However for a full picture, the frequency of movement between states will ultimately determine productivity.

The effects of wind are likely to be very different for different canopy types. A planophile canopy with flatter leaves and a high extinction coefficient (Hirose, 2005) should offer less opportunity for light penetration since distortion is unlikely to alter leaf angle substantially. An erectophile canopy with a low extinction coefficient, like rice, is different: here upright leaves will absorb more or less light dependent on their angle and hence position relative to the sun and importantly are more likely to influence penetration to lower layers. The canopy selected here has upright leaves at the top, progressing to

more horizontal at the base, hence we were more likely to see the impact of displacement over time on the lower leaves. The next factor to consider is the biomechanical properties of the leaves and stems e.g. ‘stiffness’, which determines the frequency and amplitude of movement.

We have so far considered the probability of penetration of light into the canopy over time. For a given leaf surface, mechanical canopy excitation is likely to alter the dynamics of light patterning in terms of frequency, duration and amplitude of high light periods. A high light event becomes more likely as the canopy starts to move but the average duration may be lower. The effect (and possibly biological function) of movement, especially in upper layers, then becomes one of light scattering and distribution. A simple analogy is that of a dance-room ‘mirrorball’ spinning at fast or slow speeds. The faster it spins the more likely any area will receive a brief period of high light. In the next section we consider how such fluctuations will affect photosynthesis at the leaf level and how this can be manipulated in order to improve crop productivity.

Mechanical canopy excitation: a means to manipulate photosynthesis?

Photosynthesis is considered to be a significant trait for crop improvement (Zhu *et al.*, 2010). Since it is a dynamic process, any changes in local frequency or amplitude of illumination are linked directly to metabolic and physiological processes (such as stomatal opening, Rubisco activation and photoprotection), governing the efficiency with which photosynthesis tracks the light in the plant canopy. The potential impact of mechanical canopy excitation on photon penetration leads to the exciting possibility that traits associated with movement, or response to movement, can be manipulated as a means to improve productivity of our cropping systems. This could be targeted at two core areas; firstly at metabolic features of the crop plants that enable them to exploit the short-term peaks in light intensity and respond rapidly to a change in light levels or; secondly at mechanical or architectural features of the crop stand that increase the probability of these high light events.

It has been shown both empirically (Hubbart *et al.*, 2012; Lawson and Blatt, 2014) and theoretically (Zhu *et al.*, 2004) that the speed of photosynthetic induction to and recovery from high light determines photosynthesis and water use efficiency. Genetic variation in photosynthetic induction rates means that the overall effect of this process will differ between species and lines, and be influenced by the frequency and intensity of high light events. In the understorey, such light flecks can make up 90 % of available light (Percy, 1990). Higher frequency light should reduce the wastage caused by slow induction and relaxation (Murchie *et al.*, 2009).

Our data suggests that mechanical canopy excitation could also provide a means to substantially alter and even improve light penetration in crops relative to canopy structures that do not facilitate movement. The distribution of light in a canopy is a determinant of photosynthesis and productivity (Zhu *et al.*, 2010; Song *et al.*, 2013). Past studies indicate that the ideal canopy system is one with a high leaf area index but efficient light penetration in order to avoid saturation of photosynthesis at the top and avoid severe light limitation at the base. This established principle has led to the suggestion that to improve crop yield, leaf chlorophyll concentration at the top of the canopy should be lowered to aid light penetration whilst efficient light harvesting should be maintained at the bottom (Ort *et al.*, 2015). However, improved light distributions within the canopy could also be achieved by manipulating the biomechanical properties of the crop. This is consistent with the fluttering leaves example in Aspen trees of Roden and Percy (1993a,b) and Roden (2003). The implication is that the more rapid the leaf movement the greater the probability of light penetration. This is consistent with our work, and suggests that we should select for leaf properties in crops that permit small but rapid movements in light winds, similar to leaf flutter, although the exact traits will depend upon the canopy type (e.g. see planophile versus erectophile canopies above) although could include traits such as sheath or petiole flexibility, stem strength plus altered leaf blade length and width. It would be anticipated that stiffer stems and leaves would lead to lower frequencies and amplitudes of movement in light winds. Substantial variation for biomechanical properties exists in cereals and

can result from such properties as stem wall thickness and non-structural carbohydrate content (Kashiwagi *et al.*, 2008). Within the Aspen studies, the lower leaves were typically acclimated to high light with fast photosynthetic induction times, limited largely by Rubisco activation rather than stomata. This last point is important since the frequency of switching between high and low light will determine the ‘drag’ effect of photosynthetic induction: a higher frequency can lead to a higher integrated photosynthetic rate. Such improvements could be incorporated into crop plants by using existing variation in biomechanical properties (Berry *et al.*, 2004). Under moderate wind speeds this can be achieved without a risk to stem failure: our suggested changes need not involve a compromise to stem strength since they could be achieved by changes to upper part of the canopy alone.

The evolutionary or ecological significance of divergent groups of plants could be explored by studying differences in their modes of movement. For example, tree species have relatively solid trunks, thus movement is largely limited to the leaves. In contrast, cereal or other crop canopies could rely on wind to facilitate movement of the whole canopy although this should not be at the risk of increased stem failure. Crops have been cultivated under field conditions and so the selection process may already have incorporated wind. However there is no reason to assume this: it has been argued for a long time that photosynthesis per unit leaf area has not undergone genetic improvement as a result of ‘surrogacy’ by other physiological improvements and nutrients application (Reynolds *et al.*, 2000). There is no reason to assume that the same does not apply to wind. By studying model species such as rice and wheat with complex canopies and genetically altered canopy mechanical properties as well as wild relatives it will be possible to empirically test such theories further. However, for precise predictions of the effect of wind-induced movement on canopy photosynthesis we need to build more realistic distortions of the plant that are informed both by mechanical models and observations of real canopy motions described below.

The technology required for simulating the 4-dimensional canopy

Here, we have used a simple distortion based on solid body rotation as a means to predict the effect of mechanical canopy excitation on the resulting light environment. However this type of movement is far from realistic and does not reflect the unique and complex perturbations that plant material is subject to. Whilst the technology to reproduce this form of movement for these purposes is not currently available, we can predict what would be required. In order for mechanical canopy excitation to be incorporated into studies of canopy photosynthesis it is necessary to have a model that can accurately mimic a wide range of movements. Whilst movement may at first appear simple, in reality wind-induced displacement is highly complex and involves interactions between the individual mechanical properties of organs and plant, the characteristics of the wind and the physical proximity of other plants. For example: leaves may bend in different ways (partly dependent on growth angle); leaves are displaced at different rates in relation to each other; wind speed and direction are very complex and can change rapidly over short time scales; the characteristic features of canopy architecture can change throughout growth and development; solar angle changes throughout the day and year meaning that the light patterns will alter even if wind speed and direction remains the same.

For accurate modelling of movement, mechanical properties of individual organs and the canopy as a whole must be incorporated (de Langre, 2008). Firstly, one needs to mimic the distortion of leaves that are thicker and stiffer at their base. A simple representation of a leaf is as a tapered inextensible elastic rod that resists bending and that is anchored at its base. The rod can have an intrinsic curvature and is also bent by gravity. In the presence of wind, the rod will distort under drag forces from the air. These are likely to fluctuate because of turbulence. Furthermore, interactions between fluid and structural forces are likely to induce instabilities of the rod (via a form of aerodynamic flutter), which can typically be described using a small number of characteristic modes of oscillation of the rod. So the distortion of leaves in a real airflow will (a) be greater towards the more flexible tips of leaves, (b) will typically be unsteady

and (c) will be complicated by leaf-leaf interactions. These mechanical properties will differ based upon the crop used for study and its specific architecture. For example, the majority of rice leaves will be anchored towards the centre and base of the plant whereas wheat leaves will be anchored to a specific point on a stem- an organ, which will also have its own mode of movement, separate to those of the leaves.

Before accurate mathematical models can be produced, plant movement must first be captured. Methods and tools are required that are capable of characterising the motion of individual plant components in response to wind. This can be achieved through the development and application of appropriate visual tracking technologies. Visual tracking methods seek to maintain a description of the identity and movement of one or more target objects through a time-ordered image sequence (Yang *et al.*, 2011). Classic applications of visual tracking involve tracking hands and faces for human-computer interaction, and whole bodies for security and surveillance. Tracking can occur in any number of dimensions; one method might track the apparent movement of a leaf across the (2D) image, another the motion of a (3D) surface patch describing that leaf. Tracking methods can consider the whole object of interest, or a number of distinct parts (e.g. limbs, torsos) separately, combining results to give a final description of the target's motion.

Characterisation of individual and plant canopies' response to wind requires the position and orientation of surface patches extracted from multiple views to be tracked in 3-dimensional space. Hypothesised patch properties must be verified by reference to the available image(s) (as used in Pound *et al.*, 2014). The similar appearance of plant components make this a challenging task, but one that is within reach given current computer vision methods. To provide a full description of the effects of wind, differences in leaf shape and stalk shape must be recovered by comparison of the 3-dimensional plant descriptions obtained, and tracked, over time. Again, this is challenging, but within reach of current methods. By careful consideration of individual and sets of 2-dimensional images of wind-excited plants over time we can aim to provide the

rich descriptions of canopy motion that are needed to understand its effect on photosynthesis. Such methods, when combined with light (or other environmental) modelling could be used to build a true “four-dimensional plant”.

The concept of a “four-dimensional plant model” may not be as far into the future as we think. Whilst both the mathematical and computational methods are attainable with current technology, biologically relevant data are also integral. For example, details on wind speed and direction will be critical for accurate modelling, as well as the growth conditions and management practices of the crops under investigation (e.g. Sterling *et al.*, 2003). Whilst knowledge of the physical conditions of the canopies is required, the biological and biochemical properties of the crops are also important. Whilst this study has mainly focused on the altered light dynamics brought about by wind-induced movement, there are other environmental variables that would also be influenced. For example, turbulent airflow throughout canopy structure will have implications in terms of altered CO₂ and O₂ flux to leaves. Canopy CO₂ depression may be mitigated and similarly, transpiration rate and vapour pressure deficit in different canopy regions could also be altered.

The extent to which productivity will be affected will depend upon the local environmental conditions. Here we looked at latitude 14 (corresponding to the Philippines) but as solar angle and intensity is determined by latitude and the time of year, the location and season under study could influence the final productivity, and different modes of movement may be more suitable for a set location. For example an upright canopy (static) is particularly efficacious at lower altitudes due to the enhanced light penetration. However we would predict that movement will become more beneficial for upright canopies as we move to higher latitudes with low solar elevation. Furthermore, *fastTracer3* (i.e. ray tracing; Song *et al.*, 2013) assumes a constantly sunny day thus the values presented in this study are likely to represent the extremes for direct light. However, in reality cloud cover will alter the intensity and spectral composition of light reaching the top of a canopy, for example through an

increase in the proportion of diffused light. In some environments the development of cloud cover throughout the day is predictable. Therefore models informed by both weather data and the biological response of acclimation state; to the effect of altered light patterning and; to changes in airflow on photosynthetic productivity, will be essential for fully assessing the influence of wind at the whole canopy level.

There are a number of applications for high-resolution models of mechanical canopy excitation that mean that such 4-dimensional modelling techniques will be the foundation for detailed studies in a number of different areas. For example, such models can be used to better investigate how authentic, rapid oscillations between high- and low- light intensities affect the biochemical and physiological properties of plants, or how such changes alter the quality and quantity of different light components reaching leaves (e.g. direct, diffuse and scattered light or the light spectrum at different canopy layers). They could also be used to explore the effect of different architectural types on movement and light patterning. Information could also be used to inform ideal plant types; it may be that leaves that have specific mechanical properties enabling greater movement during wind (especially light intensity wind) could enable greater light penetration under certain conditions and therefore such plants could better exploit the environment in which they are grown. This could further be adapted to better inform structural modelling to inform lodging models of the structural properties required to resist certain wind speeds or directions and thus engineer a more resilient plant. Applications may also extend to other areas such as making predictions on the effect of future climate change scenarios or extreme weather events on cropping systems (e.g. Willenbockel, 2012; Lizumi and Ramankutty, 2015) or predicting the effect of disease spread for wind- and water- dispersed pathogens during outbreaks (e.g. Legg, 1983; Shaw, 2012).

The modelling work carried out here indicates that relatively small perturbations within the canopy can substantially alter the light environment and associated productivity in a cereal canopy. However, for accurate predictions of the effect of wind-induced movement on canopy photosynthesis

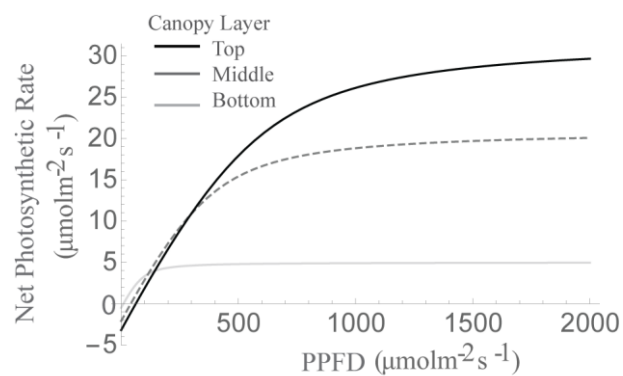
we need to build more realistic distortions of the plant that are informed both by mechanical models and observations of real canopy motions. Such approaches will be critical in accurately predicting whole canopy photosynthesis and exploring the effects of rapid changes in light intensity (i.e. those brought about by light flecks). This leads to the intriguing new possibility that manipulating the plant's mechanical movement properties in relation to wind, or the plant's response to rapid high light events, can be used as a means to optimise photosynthesis at the canopy level and therefore provide a route for crop improvement.

Supplementary Material

Supplementary Movie S5.1

Supplementary Movie S5.1: Change in overall canopy light distribution due to an Easterly wind at 12:00 h between 0-10° distortion

Supplementary Figure S5.2



Supplementary Figure S5.2: Light response curves used to calculate canopy carbon gain for the top (black), middle (dark grey, dashed), and bottom (light grey) layers. P_{max} values were taken from Murchie et al. (2002) and other parameters fixed as the maximal attainable value given an uninhibited state.

Chapter 6: The effect of nitrogen on rice growth, development and photosynthesis

Chapter 6 uses the plant reconstruction method and physiological measurements as a means to explore the effect of nitrogen on canopy architecture between three contrasting rice lines (IR64, MR219 and MR253). This has been written as a manuscript for future journal submission, so is presented in “paper format”.

Author contribution:

Project supervision performed by EH Murchie

Experimental work including measurements (physiology in the form of SPAD, plant height, chlorophyll assays and tiller number) and paper reconstruction performed by T Herman

Experimental work including measurements (gas exchange, ceptometer), plant reconstruction timecourse, modeling and paper reconstruction performed by AJ Burgess

The effect of nitrogen nutrition on rice canopy architecture and photosynthesis; assessed using high resolution reconstruction and modelling

Alexandra J. Burgess, Tiara Herman and Erik H. Murchie

Abstract

- *Backgrounds and Aims:* Rice yield must increase if it is to meet food security demands yet this rise must come with a concurrent limitation of the area of land under cultivation. Whilst nitrogenous (N) fertilisers are required for high crop yields, their economic costs and environmental consequences of use mean that seeking varieties that have a higher nitrogen use efficiency and / or are better able to cope with N deficiency is a key target for yield improvements.
- *Methods:* A combination of manual morphological measurements, physiological measurements and a high-resolution method of imaging and reconstructing 3-dimensional plant canopies was employed to investigate the effect of nitrogen availability on canopy architecture and light distribution. Three contrasting rice lines: two Malaysian rice varieties (MR219 and MR253) and a Philippine high-yielding cultivar (IR64) were grown under high N and moderate deficiency.
- *Results:* Both physiological and whole canopy modelling approaches indicate that whilst maximum photosynthetic capacity did not differ greatly between the high and low N treatments for all three lines, the high N treatment led to a greater accumulation of biomass. The whole canopy predicted carbon gain measurements indicated a higher carbon gain per unit leaf area for the

lower N treatment that partially offsets the lowered leaf area index (LAI) but a higher carbon gain per unit ground area for the higher N treatment.

- *Conclusions:* Understanding the physiological response to N availability will be critical in optimising nitrogen use efficiency (NUE) and preventing adverse effects of fertiliser use on the environment. High-resolution reconstruction and modelling techniques provide a useful tool in exploring the physiological response to N availability. Within the three rice varieties tested, additional fertiliser above the recommended values (the HN treatment) is not advantageous to an increase in photosynthetic productivity at the leaf level but is at the whole canopy level as a result of increased LAI.

Introduction

Increased crop yields per hectare will be needed to sustain the growing global population. However, this is increasingly difficult, as yield barriers are imposed by the decreasing availability of land and resources as well as a rapidly changing climate (Sheehy and Mitchell, 2015). Nitrogen (N) is one of the most costly resources globally, both in terms of production and environmental impact, despite being one of the most important mineral nutrients in terms of amount applied. Plants in both natural and agricultural systems are often deficient in N (Makino, 2003). Field grown crops therefore require an external input of N, which is usually in the form of fertiliser. Large amounts of N fertilisers are used to increase yield and to prevent fluctuating resources from affecting production (Kant *et al.*, 2011), however growing concerns over the environmental consequences of mineral N use, and its potential contamination when not used efficiently, has led to the need for research in the interactions between availability and crop growth (Birch *et al.*, 2003).

Rice is a staple food in many countries, accounting for more than 40% of global food production. The impact of rice on health and livelihoods is even greater in South East Asia, where rice provides the main source of nutrition as well as income and employment (Makino, 2011; GRiSP, 2013). The most productive systems are those which contain irrigated rice, where multiple

harvests occur per year and yield is high (Redfern *et al.*, 2012). Irrigated rice accounts for approximately 45% of rice cultivation areas (Redfern *et al.*, 2012). The potential for expanding crop area under cultivation is limited within most countries, with a concurrent reduction in the rate of expansion in irrigated land, damage to current cultivated land (e.g. salinization, waterlogging, and intensification-induced degradation of soil) plus transfer of cultivated land to other uses. Therefore, increases in rice yields must come with a concurrent reduction in the amount of land under cultivation.

Increased use of N fertilisers could enhance rice yields to some extent (Kropff *et al.*, 1993; Murchie *et al.*, 2009) and there has been a general trend for increased use of N fertiliser consumption in SE Asia (Supplementary Figure S6.1). However, the use of N fertilisers is not economical and the increased N levels do not improve the crop's tolerance to uncertain climatic conditions. Furthermore, studies indicate that at any given soil N level, significantly lower yields were achieved towards the end of the 21st century than the preceding 3 decades (Cassman & Pingali, 1995; Cassman *et al.*, 1997). The negative impact of N fertiliser use on the environment has also led to increasing concerns over its use and lobby pressure to restrict or even ban use in certain countries (e.g DEFRA & Environment Agency, 2015). However, despite these concerns, overdependence on fertiliser application is still a common practice in rice farming. In some instances, increases in N fertilisation can negatively affect yields. Application of N fertiliser in excess of that required can lead to increased growth and biomass production leading to mutual shading, lodging and pest damage (Peng *et al.*, 2006). Thus understanding the crop response to a change in N levels, and selecting varieties that are capable of outperforming others will be critical to reduce overreliance on fertilisers.

Nitrogen, canopy architecture and photosynthesis

Among agronomic and management practices, fertilisation with N plays a major role in determining productivity. As a primary constituent of essential proteins and enzymes that are involved in important plant metabolic processes,

N is essential in the formation of the plant canopy and increasing the leaf photosynthetic area. Photosynthetic components are a significant sink for leaf N: chloroplasts account for up to 80 % of total leaf N with Rubisco being the dominant enzyme (Makino & Osmond, 1991). Leaf photosynthetic capacity and Rubisco content per unit leaf area is highly correlated with leaf N both within and between species (Evans, 1989; Theobald *et al.*, 1998). Nitrogen affects a number of developmental traits including plant height, panicle number, leaf size and the spikelet number: all of which contribute to the yield potential of the crop. During the vegetative growth stage, absorbed N primarily promotes early growth and increases the number of tillers (Mae, 1997). For the formation of dense canopies, large concentrations of N are required (Connor *et al.*, 2011). In N deficient conditions, the plant counterbalances the lack of N by producing a lower number of tillers, this compensations step allows for fewer but fully functional leaves, instead of a higher number of leaves that are only semi-functional. In addition to this, N deficiency generally reduces leaf area index, plant height and overall crop photosynthesis, which is itself limited by leaf area and leaf capacity for photosynthesis (Connor *et al.*, 2011). This in turn leads to a lower amount of radiation intercepted, leading to lower radiation use efficiency. Spikelet number and the amount of filled spikelets are largely determined during the reproductive phase. Thus, even mild N deficiency can make moderate changes to architecture that will have a large impact on the light distributions and thus productivity of canopies. However, the effects of N on morphology have not been tested by looking at detailed canopy descriptions; for example through the use of sophisticated canopy reconstruction techniques.

Assessing the productivity of crops is confounded by heterogeneous nature of canopies; i.e. they consist of multiple plants exhibiting different growth and developmental patterns (Kozłowska-Ptaszyńska, 1993; Godin, 2000). Therefore understanding plant response to changes in N levels will require experimental data combined with high-resolution data on the physiological response of canopy architecture. This could be achieved through modelling approaches that can make more accurate predictions of the canopy light

environment, and thus the influence of architecture, compared to manual measurements. Estimating canopy photosynthesis and modelling plant growth in the field on a larger scale is a complex task. Whilst some research has been carried out to study the effects of varying nitrogen treatments on crop systems (e.g. Harasim *et al.*, 2016 for wheat) and on isolated rice varieties within hydroponic solutions with varying concentrations of N (e.g. Herman *et al.*, 2015), few studies exist to investigate how different varieties respond to varying nitrogen treatments in terms of changes to their canopy architecture and photosynthetic properties, particularly using high resolution modelling techniques. Mathematical modelling has been typically used to estimate canopy carbon dioxide (CO₂) uptake rate in optimal field conditions. Using gas exchange measurements together with the three-dimensional modelling of crop canopies, we can explore plant structure and estimate crop productivity at the whole canopy scale, which would not be feasible using manual measurements (Song *et al.*, 2013; Burgess *et al.*, 2015). Under high resolution, detailed representations of leaf and canopy microclimates can be made, both spatially and temporally.

Here we focus on rice cultivation in Malaysia. Despite rice being the most common grain for production and consumption, Malaysian rice production only accounts for a fraction of the total yields across SE Asia (~10% in 2014, Supp. Fig S6.1; FAOSTAT, 2014). Furthermore, evidence suggests that in recent years the average local rice yield is less than half (30-50%) of achievable potential based on the Malaysian Agricultural and Development Institute (MARDI) local verification trials (Omar, 2008). The current average rice yield has been reported at 4.5-5 t ha⁻¹, however this average is mostly as a result of application of more than the recommended 170 kg ha⁻¹ of N (Nori *et al.*, 2008). Nevertheless, increases in yield by 50% are estimated to be required in all rice growing countries to meet demand by 2050 (Sheehy & Mitchell, 2013). Crop breeding within Malaysia has led to the production of rice cultivars that have the potential to increase yields under poor conditions. This necessitates the need for studies to understand the performance of a wide range of cultivars under different conditions.

In this study, we employ a practical glasshouse approach combined with a high-resolution method of imaging and reconstructing 3-dimensional plant canopies (Pound *et al.*, 2014) in order to investigate the effect of N availability on three contrasting rice lines. Two Malaysian rice varieties, MR219 and MR253, were selected for study due to their potential biotic and abiotic resistance (e.g. MR253 is resistant to leaf blast) and performance in marginal soils. A high yielding Philippine cultivar, IR64, was also chosen as a control due to its high yielding potential, tolerance to multiple diseases and pests plus wide adaptability, as well as previous studies on its response to varied N application (Morris *et al.*, 1989; Diekmann *et al.*, 1996).

Materials and Methods

Plant Material and experimental design

Three rice varieties were selected for analysis, the popular widely grown Philippine variety IR64 from IRRI (International Rice Research Institute) and two Malaysian varieties, MR219 and MR253, both from MARDI (Ministry of Agriculture Research and Development Institute, Malaysia). Seeds were sown into module trays containing Levington Module compost (+ sand) in the FutureCrop Glasshouse facilities, University of Nottingham Sutton Bonington Campus, UK on the 8th May 2014. The seedlings were transplanted into soil beds 7 days after root establishment. The three rice varieties were assigned in a completely randomised design. The experimental plot was divided into 18 microplots, with each microplot containing 42 plants of the same variety (7 x 6 plants). The high nitrogen plots contained 350 kg N ha⁻¹ and the low nitrogen plots contained 250 kg N ha⁻¹. Additional fertiliser was not supplied throughout the duration of the experiment. Irrigation was supplied using drip irrigation for 15 minutes, twice daily. Metal halide lamps provided supplementary lighting when an external light sensor detected intensity below 300 $\mu\text{mol m}^{-2} \text{s}^{-1}$. A 12-h photoperiod (07:00 to 19:00) was maintained in the glasshouse using blackout blinds with a constant temperature of 30°C and relative humidity (RH) of 50–60%.

Physiological Measurements

Five replicate measurements per plot for plant heights and SPAD measurements were obtained weekly, from 20 days after transplanting (DAT) until the start of the flowering stage. Five replicate measurements per plot were also taken for tiller numbers between 14 and 35 DAT. Light levels at the top and bottom of the plant canopies were also measured weekly using a ceptometer (AccuPAR).

Leaf thickness and length between major veins were obtained using leaf sectioning as follows. Sections of the penultimate leaf on the main stem were cut from the widest part of the leaf using a razor blade and mounted on

microscope slides. The leaf sections were then cleared using 85% (w/v) lactic acid saturated with chloral hydrate. The slides were heated in a water bath at 70°C for an hour. After clearing, the leaf sections were washed with distilled water and stained using 1% toluidine blue dye in 1% (w/v) disodium tetraborate (as in Smillie *et al.*, 2012). A few drops of glycerol were added to the leaf sections to preserve the samples before being viewed under a calibrated light microscope and images captured using a digital camera (Nikon DXM 1200). All images were analysed using the analytical software ImageJ. The stomatal density and length were determined using leaf impressions of both the adaxial and abaxial surfaces on the widest part of the flag leaf. Impressions were made using Coltène® PRESIDENT Plus silicone-based impression putty (as in Hubbart *et al.*, 2013). Clear nail varnish was then applied to the hardened putty and later peeled and mounted on microscope glass slides for view under a 40x-magnification confocal light microscope. Images of six fields of view were taken for each variety under each treatment for analysis.

Chlorophyll a and b content were determined through chlorophyll assays. Frozen leaf samples of known area were ground in 80% acetone to extract the pigment. The samples were then centrifuged for 5 minutes at 300 rpm and the absorbance (at 663 and 645 nm) of the supernatant was measured using a spectrophotometer. Chlorophyll a and b content plus a:b ratios were calculated using the protocol of Porra *et al.* (1989).

Reconstruction and Ray Tracing

3D analysis of plants was made according to the protocol of Pound *et al.* (2014) and Burgess *et al.* (2015). Every two weeks and following photosynthesis measurements, the rice plants (roots and shoots) were carefully removed from the plots, placed into pots and moved to the imaging studio located next to the glasshouse to prevent excessive movement and damage to leaves. Roots were supplied with water to prevent wilting. It was found that this process did not alter the key architectural features of the plants. They were imaged within 10 minutes using three fixed Canon 650D cameras, with a

minimum of 40 images per plant. Images were captured using a revolving turntable, including a calibration target of set width (397mm). An initial point cloud was obtained using the PMVS software (Furukawa & Ponce, 2010; Wu, 2011). The PMVS photometric-consistency threshold (Furukawa & Ponce, 2010: Eq. 2) was set at 0.45 to optimise the amount of plant material recognised in the point cloud. Default parameters were used within the Reconstructor software, except for maximum cluster size and boundary sample rate that were changed to 120 and 15, respectively.

One plant per plot was removed at each growth stage leading to 3 replicates per line; at least 2 of these were used to form the final canopies. As only one plant was removed per plot, per growth stage, removal was expected to have minimal effect on the remaining plants however, to ensure this; care was taken to leave a buffer plant (i.e. the edge plant) next to removal sites. Duplicating and randomly rotating the individual reconstructed plants into a 3x3 grid with 10 cm within and between rows formed reconstructed canopies. Reconstructed canopies consist of a number of triangles within a mesh. Total light per unit leaf area for each triangle at a given time point was predicted using a forward ray-tracing algorithm implemented in fastTracer (fastTracer version 3; PICB, Shanghai, China; Song *et al.*, 2013). Latitude was set at 3 (for Kuala Lumpur, Malaysia), atmospheric transmittance 0.5, light reflectance 7.5%, light transmittance 7.5%, day set at the day of the imaging. The diurnal course of light intensities over a whole canopy was recorded in 30 minute intervals. The ray tracing boundaries were positioned within the outside plants so as to reduce boundary effects. The software fires rays through a box with defined boundaries: when they exit one boundary (i.e. the side) they enter again from the opposite side.

Gas Exchange

Data was taken from the glasshouse grown rice in plots in the same weeks in which the imaged plants were taken on Sutton Bonington Campus, UK. For light response and ACi response curves, leaves were not dark-adapted prior to measurements. Leaf gas exchange measurements (LRC and ACi) were taken

with a LI-COR 6400XT infra-red gas-exchange analyser (LI-COR, Nebraska). The block temperature was maintained at 30 °C using a flow rate of 500 ml min⁻¹. For light response curves, light was provided by a combination of in-built red and blue LEDs. Illumination occurred over a series of 7 photosynthetically active radiation values, prior to flowering and a series of 12 values post flowering, between 0 and 2000 $\mu\text{mol m}^{-2} \text{s}^{-1}$, with a minimum of 2 minutes at each light level. The light-response curves were taken at 2 different canopy heights; labelled top and bottom, where the top layer refers to the last fully expanded leaf and the bottom layer refers to a fully expanded leaf in the bottom half of the canopy that does not show signs of senescence. For the ACi curves, leaves were exposed to 1000 $\mu\text{mol m}^{-2} \text{s}^{-1}$ throughout. They were placed in the chamber at 400 p.p.m. CO₂ for a maximum of 2 min and then CO₂ was reduced stepwise to 40 p.p.m. CO₂ was then increased to 1500 p.p.m., again in a stepwise manner. At least one replicate was taken per treatment plot but with 5 replicates taken for each of the 6 treatments. For the induction curves, leaves were dark-adapted and placed into the chamber for a minimum of 2 minutes in the dark state. PAR was then increased to 2000 $\mu\text{mol m}^{-2} \text{s}^{-1}$ and measurements taken every 2 minutes.

Statistical Analysis

Analysis of variance (ANOVA) was carried out using GenStat for Windows, 17th Edition (VSN International Ltd.). All individual and interaction terms were considered in the model. Data was checked to see if it met the assumption of constant variance and normal distribution of residuals. For P_{max}, only data for GS5 was considered (i.e. at the flowering stage).

Modelling

All modelling was carried out using Mathematica (Wolfram).

Cumulative leaf area index (cLAI; leaf area per unit ground area as a function of depth) was calculated from each of the canopy reconstructions. For

each depth (d ; distance from the highest point of the canopy), we found all triangles with centres lying above d (Eq. 1).

$$d_i = \max_{j=1,2,3; 1 \leq i \leq n} z_i^j - (z_i^1 + z_i^2 + z_i^3)/3 \quad (1)$$

We then calculated the sum of the areas of these triangles and then divided this sum by ground area. The cumulative LAI as a function of depth through the canopy was calculated using Eq. 2.

$$cLAI(d) = \frac{\sum_{i=1}^n I(d_i \leq d) S_i}{\left(\max_{1 \leq i \leq n} x_i - \min_{1 \leq i \leq n} x_i \right) \left(\max_{1 \leq i \leq n} y_i - \min_{1 \leq i \leq n} y_i \right)}, \quad (2)$$

where $I(A)=1$ if condition A is satisfied and S_i is the area of a triangle i .

The light extinction coefficient of the canopy was calculated using the 3D structural data and the light distribution obtained from ray tracing. In order to calculate fractional interception within a canopy as a function of depth at time t , we first identified all triangles lying above depth, d (Eq. 1). We then calculated their contribution to intercepted light by multiplying PPF_D received per unit surface area (ray tracing output) by the area of triangle. The light intercepted was summed for all triangles above the set d , and divided by light intercepted by ground area according to Eq. 3.

$$F(d, t) = \frac{\sum_{i=1}^n I(d_i \leq d) S_i L_i(t)}{L_0(t) * \text{ground area}}, \quad (3)$$

where $L_0(t)$ is light received on a horizontal surface with a ground area $\left(\max_{1 \leq i \leq n} x_i - \min_{1 \leq i \leq n} x_i \right) \left(\max_{1 \leq i \leq n} y_i - \min_{1 \leq i \leq n} y_i \right)$ and $L_i(t)$ is light intercepted by a triangle i .

The light extinction coefficient, k , was calculated by fitting (by least squares) the function

$$f(x) = a(1 - e^{-kx}) \quad (4)$$

to the set of points $\{cLAI(d), F(d, t)\}$ calculated by varying depth from 0 to the height at total $cLAI$ with step $\Delta d = 1$ mm (Supplementary Figure S6.4), a in Eq.(4) is a fitted parameter.

The response of photosynthesis to light irradiance, L , was calculated using a nonrectangular hyperbola given by Eq. 5:

$$F_{NRH}(L, \phi, \theta, P_{max}, \alpha) = \frac{\phi L + (1 + \alpha)P_{max} - \sqrt{(\phi L + (1 + \alpha)P_{max})^2 - 4\theta\phi L(1 + \alpha)P_{max}}}{2\theta} - \alpha P_{max} \quad (5)$$

The nonrectangular hyperbola is defined by four parameters: the quantum use efficiency, ϕ ; the convexity, θ ; the maximum photosynthetic capacity; P_{max} , and the rate of dark respiration, R_d . We assumed that the rate of dark respiration is proportional to the maximum photosynthetic capacity, according to the relationship $R_d = \alpha P_{max}$ (Givnish, 1998; Niinemets and Tenhunen, 2007; Retkute *et al.*, 2015). Values for P_{max} were determined from leaf gas exchange measurements. For GS1-4 (prior to flowering), the light response curve data was averaged prior to LRC fitting, as the shorter 7-point curves (see Materials and Methods: Gas Exchange) do not give a good fit. For GS5, all individual curves were fit; the mean \pm SEM is presented in Table 6.3. Curve fitting was carried out using the Mathematica command **FindFit** with a minimum constraint on dark respiration at 0.05 and convexity at 0.7.

As each canopy was divided into 2 layers, each triangle from the digital plant reconstruction was assigned to a particular layer m according to the triangle centre (i.e. with triangle centre between upper and lower limit of a layer depth). Carbon gain per unit canopy area was calculated as daily carbon assimilation over a whole canopy divided by the total surface area of the canopy according to Eq. 6.

$$C = \frac{\sum_{i=1}^n P_i}{\sum_{i=1}^n S_i} \quad (6)$$

Results

Physiological Measurements

The canopy reconstructions for each treatment at each growth stage are given in Fig. 6.1. Visually, differences can be seen between the lines and between treatments. All lines show a greater amount of plant material under the high N treatment relative to the low N treatment. This is particularly noticeable at the bottom of each of the canopies where tillers and leaves are directly vertical under low N. An overview of key physiological measurements (measured plant height and modelled LAI over time and average leaf angle distributions; GS5 only) is given in Fig. 6.2. Over the course of the whole experiment, plant height and leaf area index (LAI; leaf area per unit ground area) was greater in the high N treatment. ANOVAs were performed on plant height at each of the 5 growth stages studied. Plant height varied between N treatment for all growth stages ($P < 0.05$), the lower N treatment leading to a shorter height for all lines (Table 6.1). There was no significant difference between lines at any growth stage. During the days measured, tiller number was higher in the high N treatment relative to the low N treatment (data not shown). Dry weight measurements were also taken from GS2 (Table 6.2) however there was no significant difference in dry weight between lines or treatment at any growth stage. At the final harvest there was a significant difference in plant dry weight between treatments ($P = 0.001$) and in seed dry weight per plant ($P = 0.031$) with lower weights for the low N treatment. For leaf angle distributions (Fig. 6.2C), the average triangle inclination angle throughout the horizontal subsection was calculated with respect to vertical, where a leaf inclination angle towards 0 indicates a more horizontal leaf and an inclination angle of 90 indicates a more vertical leaf. Whilst the two Malaysian varieties do not exhibit much difference in angle distributions between the high- and low- N treatments, IR64 exhibits more erect structure under high N.

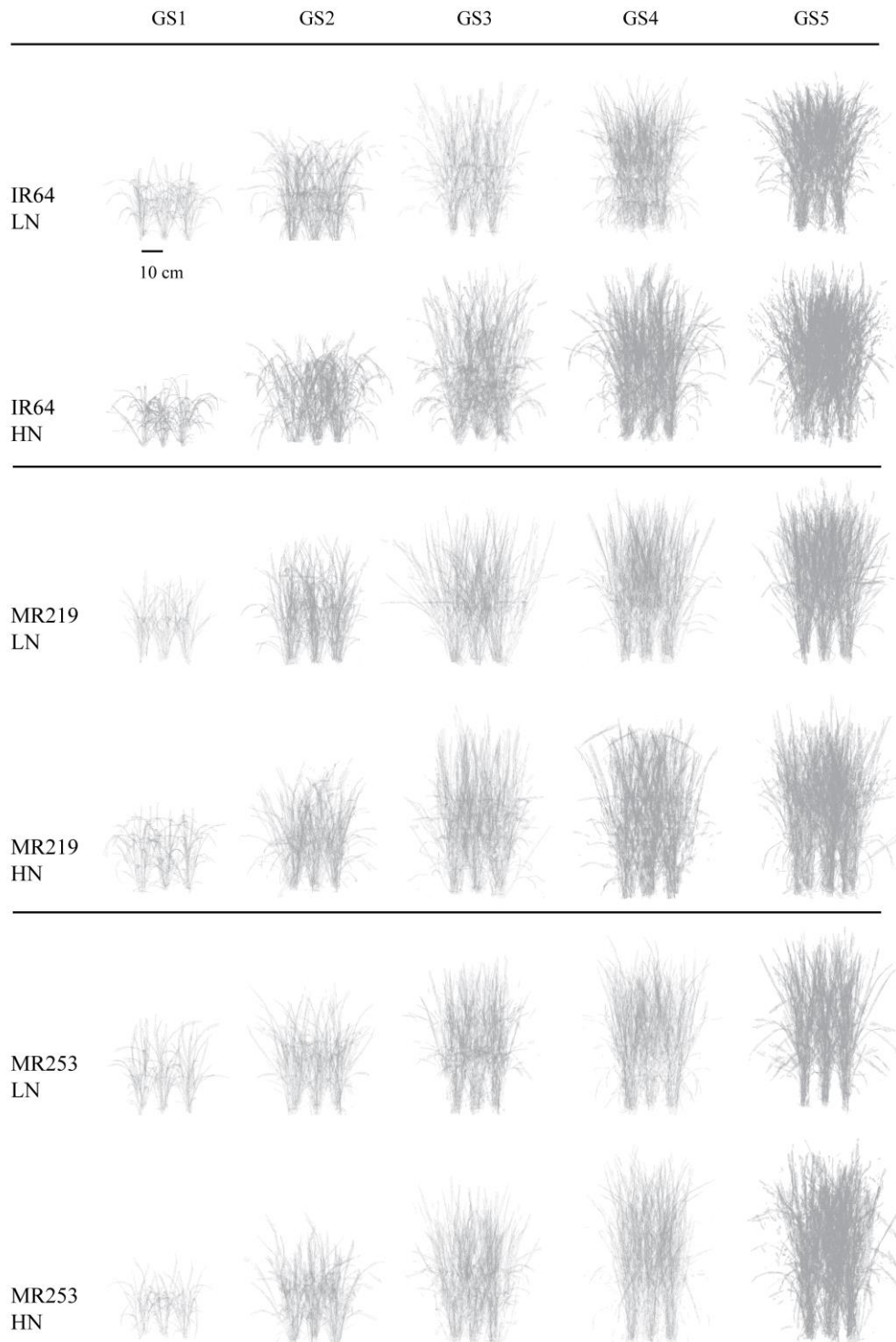


Figure 6.1: Whole canopy reconstruction developmental time course. Each of the reconstructed canopies for all growth stages is presented. Plants were imaged and reconstructed as a single plant according to the protocol of Pound et al. (2014). These were then duplicated and rotated and arranged on a 3 x 3 canopy grid.

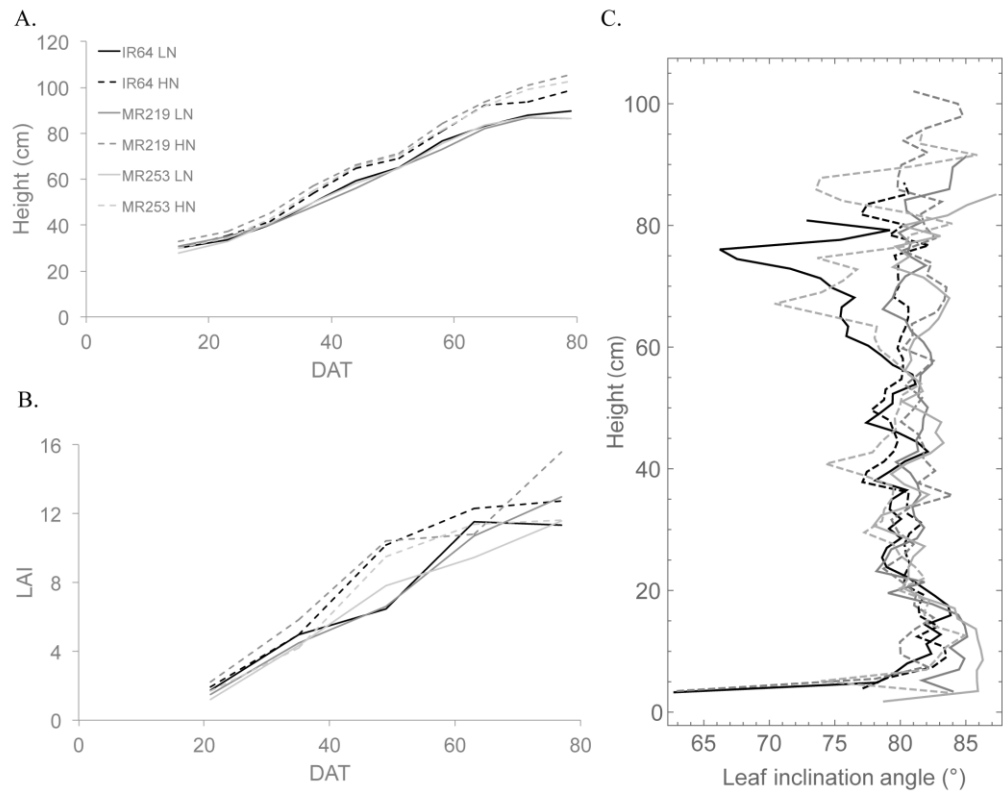


Figure 6.2: Physiological Measurements of individual lines (A) Measured plant height over time. Mean $n=3$, (B) Modelled LAI over time. LAI was calculated as mesh area inside the designated ray tracing boundaries (see Materials and Methods). (C) Modelled average leaf angle distribution as a function of height in the canopy. The average triangle inclination angle throughout the horizontal subsection was calculated with respect to vertical, where a leaf inclination angle towards 0 indicates a more horizontal leaf and an inclination angle of 90 indicates a more vertical leaf.

Treatment		GS1 (cm)	GS2 (cm)	GS3 (cm)	GS4 (cm)	GS5 (cm)
IR64 LN		33.5±0.4	59.3±0.7	76.6±3.8	88.0±3.4	90.0±2.9
IR64 HN		35.3±1.6	64.6±1.0	81.2±3.0	93.6±3.5	96.7±3.3
MR219 LN		35.1±0.4	56.0±2.0	73.2±2.4	87.0±3.3	91.7±6.0
MR219 HN		37.4±1.4	66.1±3.3	84.2±3.0	101.1±4.7	105.0±5.0
MR253 LN		32.9±0.9	58.4±3.0	75.7±3.7	87.3±5.3	91.7±4.4
MR253 HN		34.3±0.5	65.5±1.9	81.4±2.6	99.3±4.3	103.3±1.7
Grand Mean		34.8	61.6	78.7	92.7	96.4
Line	P	0.058	0.902	0.993	0.722	0.456
	SED	0.99	2.21	3.15	4.14	4.14
N	P	0.044	0.001	0.018	0.009	0.009
Treatment	SED	0.81	1.80	2.57	3.38	3.38
Interaction	P	0.909	0.563	0.567	0.574	0.711
	SED	1.41	3.12	4.45	5.85	5.85

Table 6.1: Plant Height at each of the studied growth stages. Mean± SEM, n=3. P values correspond to ANOVA.

Treatment		GS2 (g)	GS3 (g)	GS4 (g)	GS5 (g)	Harvest (g)	Seed Dry Weight (g plant⁻¹)
IR64 LN		2.40±0.35	8.94±2.53	16.35±7.18	18.64±3.58	18.59±1.98	14.74±1.67
IR64 HN		2.41±0.41	10.75±1.13	10.60±1.20	27.07±7.68	19.36±1.86	14.42±1.40
MR219 LN		2.57±0.42	13.13±3.64	14.94±3.37	16.72±4.33	15.14±1.50	16.45±1.86
MR219 HN		3.27±0.82	8.50±2.82	15.04±0.89	25.75±8.58	27.23±3.22	22.82±3.04
MR253 LN		2.06±0.49	6.13±1.26	11.44±0.35	9.99±1.50	17.46±1.85	14.79±2.18
MR253 HN		2.19±0.69	11.77±0.86	13.63±2.32	18.47±2.98	29.99±3.44	27.06±4.34
Grand Mean		2.48	9.87	13.7	19.4	21.3	18.4
Line	P	0.376	0.722	0.775	0.275	0.207	0.134
	SED	0.56	2.28	3.43	5.40	2.50	3.05
N	P	0.549	0.623	0.688	0.074	0.001	0.031
Treatment	SED	0.45	1.86	2.8	4.41	2.04	2.49
Interaction	P	0.809	0.116	0.507	0.998	0.061	0.159
	SED	0.79	3.22	4.85	7.64	3.54	4.32

Table 6.2: Dry weight measurements. Mean±SEM, n=3. P values correspond to ANOVA.

Cumulative leaf area index (cLAI) was calculated through canopy depth (i.e. from top-down; see Materials and Methods: Modelling) for each of the canopies at each growth stage (see Fig. 6.3A for results from GS5, Supp. Fig S6.3 for all growth stages). At growth stages 1-3, there was a more rapid rise in cLAI throughout the middle portion of the canopies in the higher N treatment for all lines but by GS4, this switched in favour of the lower N treatment, with mixed patterning for GS5. This pattern is associated with greater accumulation of leaf area within this mid-canopy region. Similar results can be seen for fractional interception (Fig 6.3B for results from GS5 and Supp. Fig S6.4) and total LAI (i.e. the cLAI at total depth within the canopy), with tendency towards increased interception of light within mid-canopy regions and a higher LAI in the higher N treatment at the earlier growth stages and mixed patterns by GS4 and 5. The architectural changes brought about by the differences in N levels contribute to the locations in the canopy in which the majority of photosynthesis is occurring. Fig. 6.3B indicates that at GS5 50% of light is intercepted in the top 30 cm of the canopy for all treatments except for MR253 LN and by 60 cm depth, almost all light ($F \sim 1.0$) is intercepted, again apart from MR253 LN. A lower extinction coefficient (k) value (see Materials and Methods: Modelling) indicates that light attenuation through the canopy is different between the N treatments, due to differences in leaf orientations, and contributes to the higher LAI of the canopies. The modelled canopy k values are given in Supp. Table S6.3. For all growth stages, there is a reduced k value for the HN treatment relative to the LN treatment (excepting MR253, GS5). MR219 has the lowest k values of all the varieties tested. To visualise whether the altered canopy architecture influenced the levels of light reaching leaf material, the light level per fraction surface area of the canopy was calculated. The values for the top third of the canopy are given in Fig. 6.5. This indicates the general light status of a set portion of canopy. The large peak in distribution under low PPFd for IR64 LN indicates that a large portion of that canopy is receiving low levels of light relative to the other canopies. Arrows indicate the average irradiance of each line in the top portion of the canopy (Fig. 6.4). The averaged value is similar for all lines; with the exception of MR219 HN, which is slightly shifted towards a higher value. This

suggests that despite an increase in LAI for all lines under high N, the leaf material is receiving similar levels of light in the top third of the canopy. Similar results are seen in the bottom two-thirds of the canopy (data not shown).

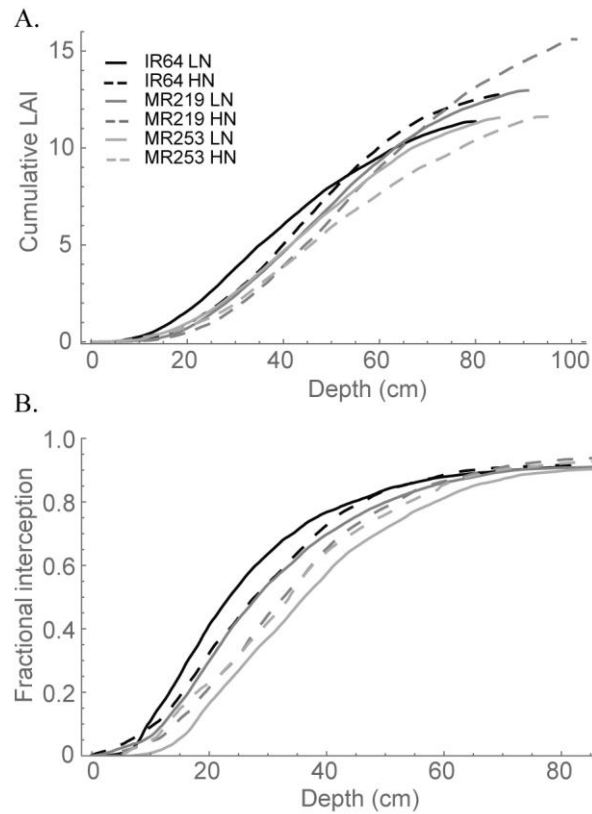


Figure 6.3: Modelled depth distributions of leaf material and light interception (A) cumulative leaf area index (cLAI; leaf area per unit ground area as a function of depth- i.e. from the top of the canopy) for all treatments (GS5) and (B) Fractional interception as a function of depth (i.e. from the top of the canopy) for all treatments (GS5).

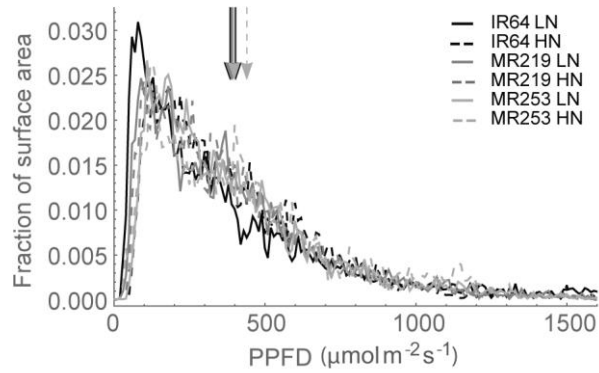


Figure 6.4: Modelled averaged light as a fraction of surface area in the top third of each canopy at 12:00 h. The average irradiance of each line is indicated by the arrow.

Leaf green-ness values (SPAD) was calculated measured weekly over the course of the experiment (Fig. 6.5A). These values often correlate with leaf N content (Peterson *et al.*, 1993). Values rise rapidly up to 30 DAT before decreasing for all lines and rising again. At 50 DAT the SPAD values reach their maximum and remain approximately constant for the remainder of the days tested. For all lines, there is a trend for an increased SPAD value in the high N treatment. Of all treatments, MR219 LN has the consistently lowest values. This is largely in agreement with chlorophyll content analysis (Fig. 6.5B), which indicates a higher content in the high N treatment for IR64 and MR219 but not for MR253.

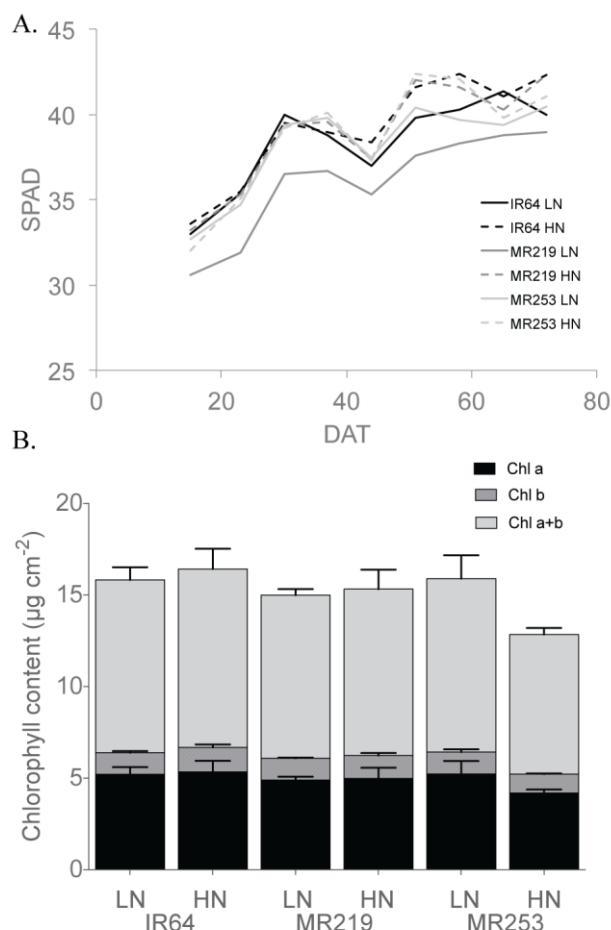


Figure 6.5: (A) Change in SPAD over time. (B) Chlorophyll content analysis. Mean \pm SEM $n=3$.

Photosynthesis

P_{max} taken from fitted light response curves at GS5 for the top, middle and bottom layers are given in Table 6.3. Significant differences can be seen between the lines for the top layer ($P<0.001$) but not for the bottom and middle layers. There was no significant difference between N treatments. An empirical model of photosynthesis was employed to calculate the total canopy carbon gain per unit leaf area and per unit ground area (see Materials and Methods using P_{max} values in Supp. Table S6.2); results are presented in Fig. 6.6. Throughout each of the growth stages (1-5) there is a trend for a decrease in carbon gain per unit leaf area and increase in carbon gain per unit ground area for all of the canopies. For growth stages 3 to 5, all three varieties show a reduced carbon gain per unit leaf area in the high N treatment relative to the low N counterpart. The opposite pattern is seen for most treatments for carbon

gain per unit ground area, with a higher carbon gain in the higher N treatments (apart from MR219 at GS4 and MR253 at GS5). These differences can be attributed to the differences in leaf area (given as LAI) between the different canopies. When considering carbon gain per unit leaf area, the reduced LAI of the low N canopies enables higher light intensities over a greater surface area of the canopy (Fig. 6.4) which, when combined with similar photosynthetic parameters, leads to a greater carbon gain. However, the greater LAI of the high N treatment means that per unit ground area basis, carbon gain is higher. To confirm these differences, correlations were carried out using a linear line of best fit. Carbon gain per unit leaf area is negatively correlated to LAI ($R^2=0.557$), however there is no clear correlation between LAI and carbon gain per unit ground area. There is a positive relationship between P_{max} (top layer) and carbon gain per unit ground area ($R^2=0.610$). Similarly to the P_{max} data, there were no significant differences between any of the ACi curve parameters (V_{cmax} , J and TPU) at either growth stage measured (GS2 and 3; see Table 6.4).

Treatment		Top	Middle	Bottom
IR64 LN		31.10±1.06	18.93±1.99	8.30±0.90
IR64 HN		28.55±0.76	15.48±1.82	7.74±1.63
MR219 LN		29.71±0.91	23.17±1.25	7.48±0.85
MR219 HN		26.31±0.28	18.97±3.69	8.72±0.71
MR253 LN		21.69±2.27	15.92±0.60	9.47±1.77
MR253 HN		23.08±1.49	18.33±4.16	9.00±0.33
Grand Mean		26.74	18.50	8.45
Line	P	<0.001	0.259	0.518
	SED	1.29	2.59	1.15
N	P	0.174	0.425	0.941
Treatment	SED	1.05	2.11	0.94
Interaction	P	0.182	0.403	0.685
	SED	1.82	3.66	1.63

Table 6.3: P_{max} values ($\mu\text{mol m}^{-2} \text{s}^{-1}$) taken from fitted LRCs at GS5.

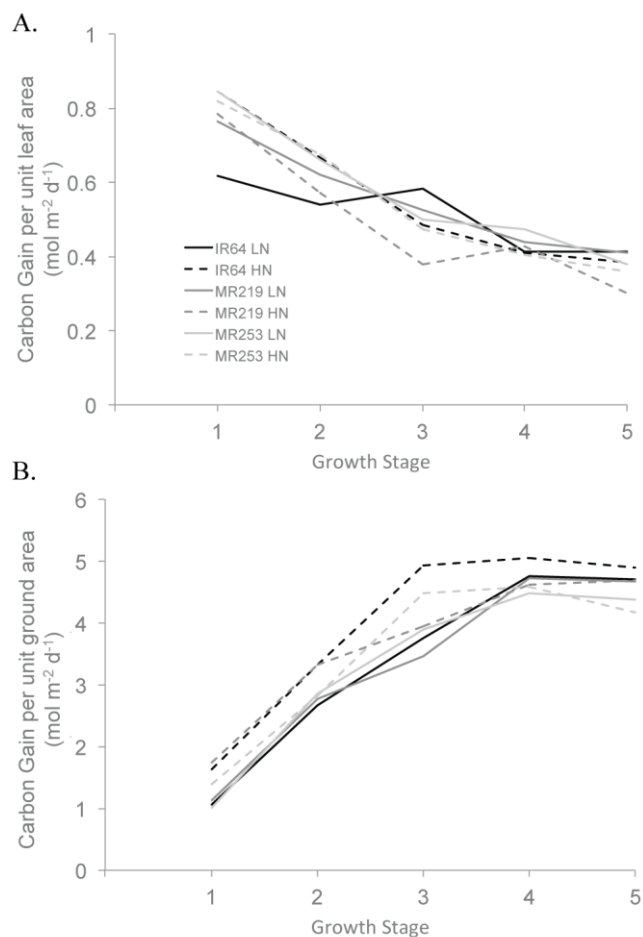


Figure 6.6: Modelled predicted carbon gain per unit leaf and ground area for each growth stage. An empirical model of photosynthesis was employed that calculates carbon gain from ray tracing values, parameterised from measured light response curves. This is integrated over the whole canopy over the course of the day.

To see whether the leaf anatomy changed as a result of N treatment, stomatal impressions and leaf sectioning was carried out (Materials and Methods: Physiological Measurements). There were no significant differences in stomatal density or length between all treatments and varieties with the exception of MR219, which showed a significant difference in stomatal density on the abaxial leaf surface between the different N treatments ($P < 0.05$; Supp. Table S6.1). The distance between major veins in each of the treatments is given in Supp. Fig. S6.3. Whilst no differences were seen in IR64 and MR253, there was a significant difference in N treatment in MR219 ($P < 0.05$) with a smaller distance between major veins under the low N treatment. The distance

between major veins under the high N treatment also differed, with significant difference between IR64 and MR219 ($P < 0.05$).

Growth Stage	Line	Vcmax	J	TPU
2	IR64 LN	57.60±12.16	125.12±1.56	7.97±0.85
	IR64 HN	57.27±9.46	99.59±6.75	6.88±0.65
	MR219 LN	61.52±15.73	94.61±15.40	7.32±0.80
	MR219 HN	70.71±10.57	112.12±3.04	7.39±0.42
	MR253 LN	65.41±11.18	100.21±20.11	7.90±0.81
	MR253 HN	89.45±13.53	112.90±12.02	8.07±1.01
	Grand Mean		67.00	107.40
Line	P	0.3	0.749	0.682
	SED	12.28	11.86	0.777
N	P	0.295	0.875	0.665
Treatment	SED	10.03	9.68	0.634
Interaction	P	0.619	0.181	0.675
	SED	17.37	16.77	1.099
3	IR64 LN	99.67±7.05	117.59±3.95	8.77±0.16
	IR64 HN	96.70±7.51	115.88±5.30	8.29±0.47
	MR219 LN	94.13±8.53	107.60±8.16	8.02±0.41
	MR219 HN	87.84±3.03	113.37±3.72	8.31±0.39
	MR253 LN	90.48±14.60	127.93±22.27	7.88±0.58
	MR253 HN	90.05±5.09	112.07±3.29	7.46±0.36
	Grand Mean		93.10	115.70
Line	P	0.590	0.646	0.137
	SED	8.44	10.25	0.42
N	P	0.643	0.643	0.553
Treatment	SED	6.89	8.37	0.34
Interaction	P	0.941	0.571	0.592
	SED	11.94	14.5	0.59

Table 6.4: Parameters taken from ACi curve fitting using Sharkey et al. (2007; fitting at 30°C). Mean ± SEM is presented, n=6. P value corresponds to ANOVA.

Discussion

Use of modelling approaches within nutrient or stress studies

The productivity of a stand of crops depends on a number of factors including the structure of both a single plant and the combined features of the whole canopy. As an essential component of the canopy, N is critical in determining the structure and thus the light environment. A high-resolution, low-tech method for canopy reconstruction and modelling aimed at assessing the relationship soil N and whole canopy photosynthesis was presented in this paper. Here, the architectures of three diverse rice cultivars at five different growth stages were captured under two different levels of soil N. This technique offers a substantial advance from previous work, because we are able to (1) explore the effect of N availability of architectural traits in high-resolution for “field-grown” plants; (2) define key structural and photosynthetic features throughout the canopy structure throughout growth and development; (3) extract traditional and unique canopy measurements that are difficult, if not impossible, to obtain in the field (for example, cLAI, vertical profiling, and leaf tissue angle distributions); and (4) make estimations of whole canopy productivity (i.e. canopy carbon gain). Such measurements can be extracted directly from 3D data, and thus does not require existing knowledge of the plant variety, and does not require the of field measurements using light sensors and geometric measuring tools that are prone to error according to weather and user.

Figure 6.1 shows the 3D mesh for each of the rice lines at each growth stage and N treatment, thus representing a time course of development. This reconstruction method has previously been shown to provide an accurate representation of the plants with replication of leaf area between 1-4 % of that of measured data and accurate capture of leaf angles (Pound *et al.*, 2014; Burgess *et al.*, 2015). The method used for reconstruction also enables development of *in silico* canopies with the same LAI as the real canopies (see Materials and Methods). Combining the reconstruction method with ray tracing provides an accurate depiction of the light gradients found within real life canopies in field settings (Burgess *et al.*, 2015). In this study we have utilised

the method for capturing and quantifying the unique architectural differences between contrasting rice lines as a result of differences in soil N. Using high-resolution techniques are important as the mild N deficiency used here produced small unique differences that would be difficult to measure manually and structural differences (i.e. cLAI and leaf angle distributions) and their relationship to whole canopy photosynthesis can be explored in more depth.

Image-based reconstruction approaches are more likely to capture the heterogeneity of crops within a field because they digitise existing crops. This can be compared to rule-based methods, which create an averaged crop that may capture the general features of the variety/line/species but will not capture unique differences between crops of the same type and thus, may not be as representative or realistic. Furthermore, such rule-based approaches are labour and data intensive and would need to be carried out for each individual variety and N treatment in this case, whereas this approach may give useable representative canopies within a very short time span.

The ease of the image-based reconstruction approach used in this study indicates that similar studies could be used to assess the effect of N deficiency on canopy architecture and photosynthesis under other conditions, or for studies of the effect of N availability on photosynthetic processes. The approach has previously been combined with an empirical model of photosynthetic acclimation to study the effect of canopy architecture on the distribution of photosynthesis throughout field grown wheat canopies (Chapter 10). The study indicated the consequences of nutrient budgeting on photosynthetic productivity of the canopies, with a witnessed accumulation of N at the bottom of the wheat canopies contributing to a higher photosynthetic productivity than would be expected based on light levels. Under the conditions studied, it was expected that accumulation and retention of N in lower leaves of the canopy was not used to promote carbon gain at the canopy level and thus was dominant over the regulation of key components of optimal photosynthetic acclimation (Chapter 10). The accumulation and storage of N in lower canopy layers could be desirable if the opportunities to exploit sun flecks

are high or if the N can later be remobilised for use in the grain. This was further explored in contrasting rice varieties (Chapter 4) whereby the upright and open canopy structure of variety Inia Tacuari led to a higher photosynthesis distribution throughout canopy depth (Fig. 4 in Chapter 4). Sinclair & Sheehy (1999) indicated that the erect nature of rice leaves could improve the capacity of the lower leaves for the storage of N and facilitate later remobilisation to the grain. Such approaches would be indispensable to the study of N availability to crop plants through the use of realistic fluctuating light as a means to predict NUE at both leaf and canopy level. This could indicate improvements to varieties based on N availability; for example, to canopy architecture to facilitate light penetration). Image-based reconstruction has also been used to assess architectural traits that prevent damage caused by high light levels (Burgess *et al.*, 2015: Chapter 7). This applies to studies of N nutrition if availability leads to altered architectural or photosynthetic features that increase susceptibility of the crop to further stressors (see below).

The effect of N availability on crop physiology

Previous studies using hydroponic solutions indicate differing consequences of reduced N on light saturated photosynthesis (P_{\max}) values using two of the same rice varieties (Herman *et al.*, 2015), with one rice variety capable of maintaining high levels of P_{\max} under reduced N, and with the ability to outperform other varieties under certain deficient N conditions. This improved P_{\max} within MR253 under reduced N conditions (Herman *et al.*, 2015) indicated a potential for improved nitrogen uptake and allocation relative to IR64 (Foulkes & Murchie, 2011). However, within this study we did not find a significant difference in P_{\max} values based on N treatment (Table 6.3). This could be a result of the relatively high residual soil N levels and indicates that excess N levels does not improve the photosynthetic rate for these three varieties. However, the excess levels do indicate an improvement to whole canopy productivity with greater carbon gain achieved per unit ground area in the higher N treatment attributed to a greater LAI, despite a reduction in carbon gain per unit leaf area. This suggests that the lower N treatment may be

offsetting carbon gain by maintaining higher leaf photosynthesis levels over a smaller surface area.

Increased LAI corresponds to taller height and higher biomass (measured as dry weights; Table 6.2). The two Malaysian varieties exhibit increased weight at the higher N treatment however, although there is a small difference, the magnitude of weight increase for IR64 is not as large. Due to the small scale of this trial we are unable to accurately predict the grain production and yield in a field setting for our varieties. However, similar patterns can be seen for seed dry weight per plant: with IR64 exhibiting similar values under both N treatments but a large increase for both MR219 and MR253. These results are in line with previous studies on the effect of N application on IR64, which indicated that applications above 90-100 kg N ha⁻¹ (using green manure) did not increase the agronomic efficiency of the system (Morris *et al.*, 1989; Diekmann *et al.*, 1996) and on MR219 where increases in the N application rate led to concurrent increases in the grain (Nori *et al.*, 2008). The residual N levels in this trial were similar (LN) and in excess (HN) of the recommended application levels for rice production (Rice Knowledge Bank, 2015). This may have contributed to the results witnessed here; namely no change in light saturated photosynthesis but an increase in biomass production. The response of IR64, in particular, to an increased soil N level indicates that increases in N application beyond this recommended value would not be advantageous to productivity. The results presented here indicate contrasting N uptake and utilisation responses of the 3 varieties, with MR219 and MR253 capable of utilising the extra N available in the soil.

Contrasting strategies can be seen in different crops in relation to N availability. In Potato (*Solanum tuberosum* L.), excess N led to enhanced apical branching and prolonged production of vegetative organs leading to a greater number of leaves per plant (Vos and Biemond, 1992; Biemond and Vos, 1992). Conversely, under N limitation leaf size was reduced (via reduced leaf expansion rates) in order to maintain N concentration per unit leaf area and the photosynthetic capacity of the leaf (Vos and Van der Putten, 1998). In

contrast, Maize (*Zea Mays* L.) exhibits a more conservative response to changes in leaf size relative to potato and reduces total leaf area by approximately 30% (Vos *et al.*, 2005). Furthermore, maintaining leaf area comes at the expense of decrease N per unit leaf area and a decrease in photosynthetic capacity. This reflects two opposing strategies to N availability: the maintenance of photosynthetic productivity per unit leaf area at the expense of total leaf area or; the maximisation of light interception per unit leaf area at the expense of photosynthetic productivity. It is broadly expected, with some exceptions, that these contrasting strategies represent the dicot versus the Gramineae response (see Vos *et al.*, 2005 and references within). Whilst this study did not use limiting amounts of N availability, results suggest that under excess N conditions, N is used for the production of increased tiller number, a greater leaf area and maintenance of photosynthetic capacity per unit leaf area in rice.

There is also an effect of N on the erectness of each of the canopies (i.e. the leaf angles; Figures 6.1 and 6.2). The maintenance of a similar stature for the two Malaysian lines under both N treatments but a difference in the stature of IR64 may relate to the conditions in which they were originally developed; with IR64 developed under high input agriculture and the Malaysian lines developed in marginal lands. The leaf inclination angle is critical in determining the flux of solar radiation per unit leaf area (Ehleringer and Werk, 1986; Ezcurra *et al.*, 1991; Falster and Westoby, 2003). Plants containing steep leaf inclination angles leads to a decreased light capture when the sun is directly overhead (i.e. during midday hours or during summer) but increases light capture at lower solar angles (i.e. start/ end of the day or during seasonal changes in the higher latitude regions). This feature has a number of practical applications including the decrease in susceptibility to photoinhibition (Burgess *et al.*, 2015; Ryel *et al.*, 1993; Valladares and Pugnaire, 1999; Werner *et al.*, 2001); reduced risk of overheating due to reduction in mid-day heat loads (King, 1997); and minimised water-use relative to carbon gain (Cowan *et al.*, 1982). This may therefore confer a stress tolerance mechanism to the Malaysian rice lines, whereby N is used to maintain an upright structure.

These results indicate the importance of selecting varieties based on the constraints of the agricultural setting in which they are to be grown. The increase in seed yield and canopy photosynthesis of the two Malaysian varieties indicate that they are responsive to increased fertiliser input, however the maintenance of leaf level photosynthesis over a smaller surface area can partially offset N deficiency. Furthermore, the maintenance of leaf stature by the Malaysian lines could confer stress tolerance to high light and heat, thus could provide a means of stabilising yields under adverse conditions.

Concluding Remarks

Understanding the relationships between the availability of resources, plant development and productivity will be critical in optimising cropping systems, reducing overreliance on external inputs and for selecting appropriate varieties for the local conditions. Here we show the importance of residual soil N levels on rice performance using a high-resolution method of reconstruction and modelling. Such methods are able to accurately capture unique differences in canopy structure and the canopy light environment brought about by mild N deficiency. Results indicate that increases in N above the suggested levels does not translate into increased photosynthesis at the leaf level but can at the whole canopy level as a results of increased leaf area.

Supplementary Material

Supplementary Table S6.1

	Stomata Density (mm ⁻²)		Stomatal Length (μm)	
	Adaxial	Abaxial	Adaxial	Abaxial
IR64 LN	492.86±30.96	640.71±19.55	20.29±0.51	20.17±0.33
IR64 HN	479.71±56.15	673.57±25.66	21.02±0.65	19.88±0.50
MR219 LN	594.71±47.59	732.71±48.40*	20.86±0.56	20.23±0.39
MR219 HN	469.86±18.64	571.71±34.90*	21.78±0.44	18.86±0.55
MR253 LN	548.71±35.05	640.71±19.55	20.74±0.51	19.70±0.61
MR253 HN	512.57±17.63	627.57±25.66	20.91±0.54	18.59±0.57

Supplementary Table S6.1: Stomatal Physiology. Stomata density and lengths on adaxial and abaxial sides for all lines and treatments. Mean ± SEM, n=6 (number), n= 10 (length)

Supplementary Table S6.2

Line	Layer	P _{max}			
		GS1 & 2	GS3	GS4	GS5
IR64 LN	Top	24.92	31.30	26.66	31.10
	Bottom	11.36	14.96	12.89	18.93
IR64 HN	Top	23.49	28.88	30.26	28.55
	Bottom	22.42	21.92	9.83	15.48
MR219 LN	Top	28.41	24.81	26.58	29.71
	Bottom	13.31	16.18	22.54	23.17
MR219 HN	Top	28.41	24.81	28.00	26.31
	Bottom	16.00	10.00	13.00	18.97
MR253 LN	Top	29.27	28.59	26.39	21.69
	Bottom	16.74	15.17	22.49	15.92
MR253 HN	Top	28.40	29.97	25.10	23.08
	Bottom	17.37	12.94	16.97	18.33

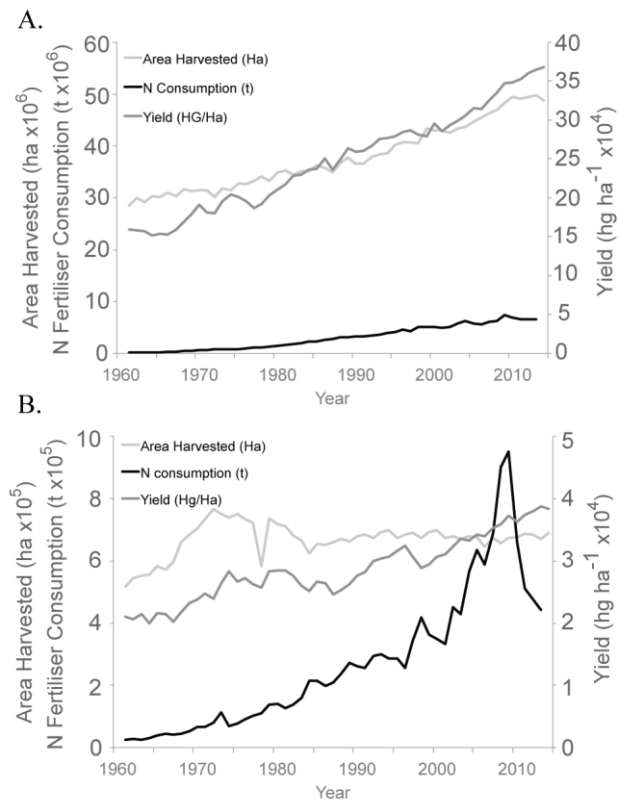
Supplementary Table S6.2: P_{max} values (μmol m⁻² s⁻¹) taken from fitted LRCs, used to calculate canopy carbon gain.

Supplementary Table S6.3

	GS1	GS2	GS3	GS4	GS5
IR64 LN	1.04574	0.729859	0.477377	0.41721	0.421619
IR64 HN	1.01216	0.558776	0.423337	0.322493	0.333194
MR219 LN	0.991188	0.633413	0.511834	0.415182	0.337057
MR219 HN	0.889662	0.560244	0.417877	0.433973	0.310883
MR253 LN	1.38772	0.679136	0.419393	0.437374	0.329098
MR253 HN	0.838208	0.625027	0.419121	0.393529	0.388188

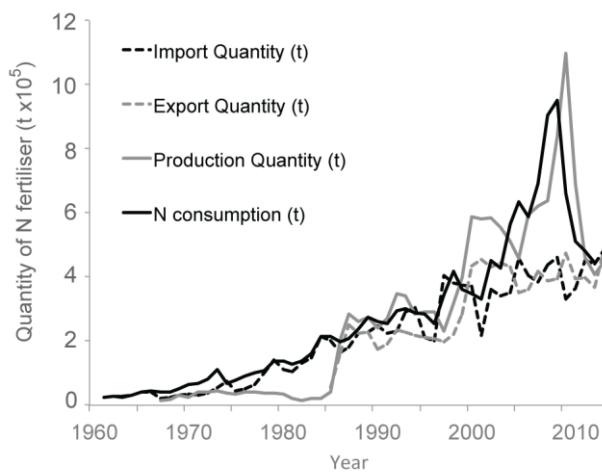
Supplementary Table S6.3: Canopy k Values

Supplementary Figure S6.1



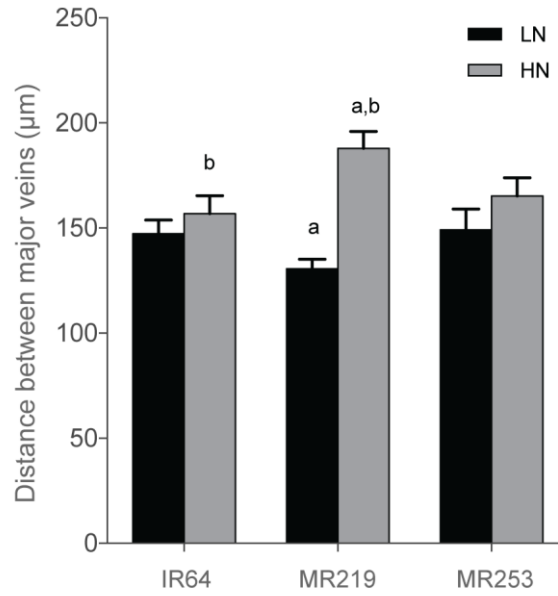
Supplementary Figure S6.1: SE Asian versus Malaysian Rice production (data from FAOStat).

Supplementary Figure S6.2



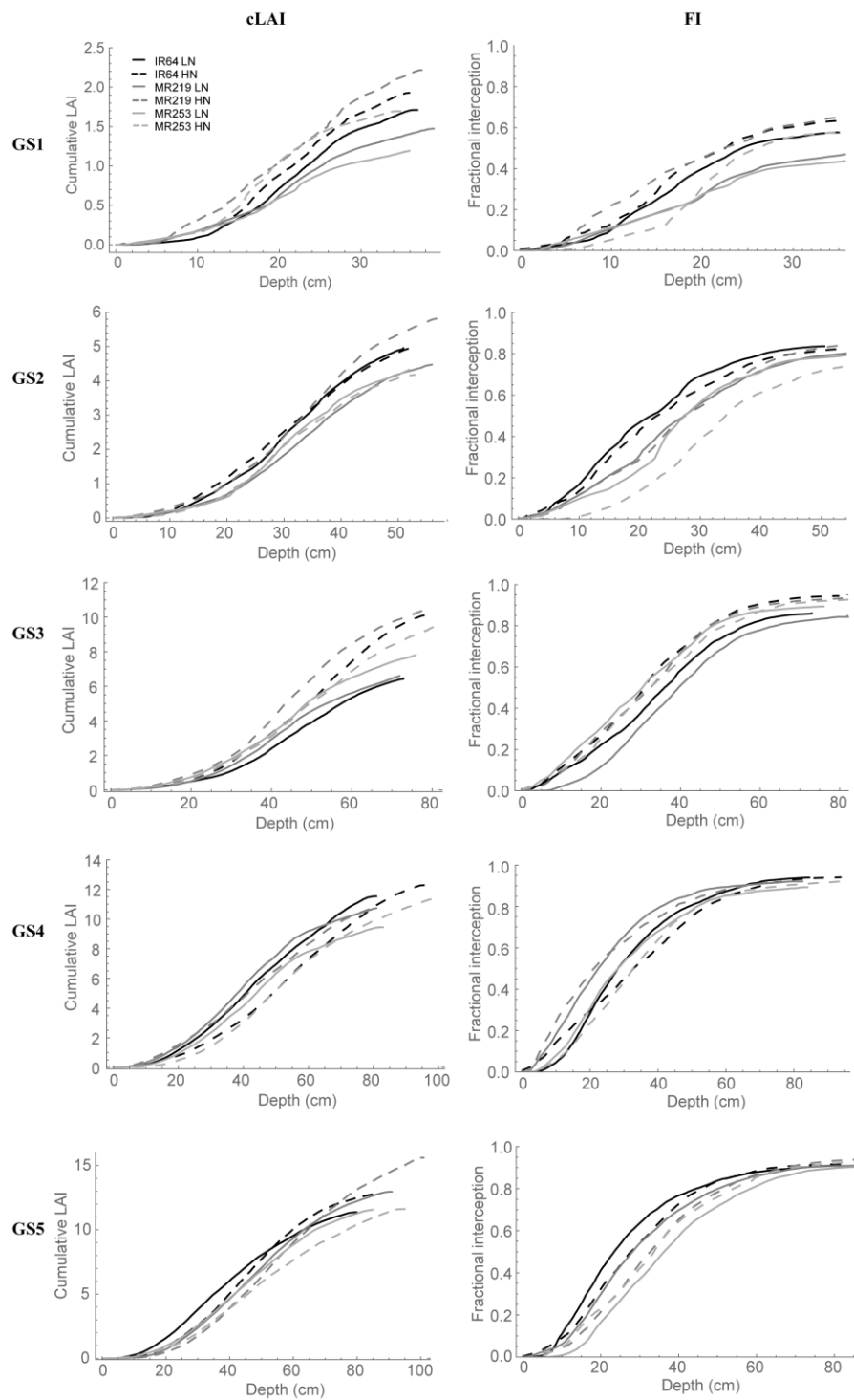
Supplementary Figure S6.2: Trends in Nitrogen fertiliser production, import, export and consumption dynamics in Malaysia.

Supplementary Figure S6.3



Supplementary Figure S6.3: Distance between major veins in each of the treatments. Letters indicate the relationships with a significant difference ($P < 0.05$).

Supplementary Figure S6.4



Supplementary Figure S6.4: Depth distributions of leaf material and light interception for all growth stages. Left Panel: Cumulative Leaf Area Index (cLAI; leaf are per unit ground area as a function of depth). Right Panel: Fractional interception (FI) as a function of depth.

Part II:
The Effect of Variable Light on
Photosynthetic Processes

Overview

The previous section has looked at how canopy composition leads to a heterogeneous light environment. This section will look at how this variable light environment impacts upon individual photosynthetic processes, and thus contribute to overall productivity and canopy carbon gain. The section consists of experimental papers looking at the processes of photosynthetic acclimation and photoprotection.

Chapter 7: Modelling the effect of photoinhibition in a wheat canopy

Paper as published in *Plant Physiology*

Chapter 7 uses a digital reconstruction method combined with a mathematical model of photosynthesis to quantify the effect of photoinhibition on canopy photosynthesis in three wheat lines differing in canopy structure. This has been published in the *Plant Physiology* (Burgess AJ*, Retkute R* *et al.* 2015. 169(2): 1192-1204) so is presented in “paper format”.

Author contribution:

Experiment conceived by EH Murchie and AJ Burgess

Work coordinated by EH Murchie

Three-dimensional reconstruction methodology developed by MP Pound and TP Pridmore

Technique for reconstruction of whole canopies from individual plant reconstructions and the model for the impact of photoinhibition on canopy carbon gain developed by AJ Burgess and R Retkute

Reconstructions performed by AJ Burgess with assistance of MP Pound.

Ray tracer applied by AJ Burgess whilst SP Preston, OE Jensen, and R Retkute and helped to devise the modelling approaches

Field measurements supervised by EH Murchie, AJ Burgess, and J Foulkes

The first draft of the article was written by EH Murchie, AJ Burgess, and R Retkute with input on later drafts by MP Pound, SP Preston, and OE Jensen

High-resolution three-dimensional structural data quantify the impact of photoinhibition on long-term carbon gain in wheat canopies in the field

Alexandra J. Burgess*, Renata Retkute*, Michael P. Pound, John Foulkes, Simon P. Preston, Oliver E. Jensen, Tony P. Pridmore, and Erik H. Murchie

Abstract

Photoinhibition reduces photosynthetic productivity; however, it is difficult to quantify accurately in complex canopies partly because of a lack of high-resolution structural data on plant canopy architecture, which determines complex fluctuations of light in space and time. Here, we evaluate the effects of photoinhibition on long-term carbon gain (over 1 d) in three different wheat (*Triticum aestivum*) lines, which are architecturally diverse. We use a unique method for accurate digital three-dimensional reconstruction of canopies growing in the field. The reconstruction method captures unique architectural differences between lines, such as leaf angle, curvature, and leaf density, thus providing a sensitive method of evaluating the productivity of actual canopy structures that previously were difficult or impossible to obtain. We show that complex data on light distribution can be automatically obtained without conventional manual measurements. We use a mathematical model of photosynthesis parameterized by field data consisting of chlorophyll fluorescence, light response curves of carbon dioxide assimilation, and manual confirmation of canopy architecture and light attenuation. Model simulations show that photoinhibition alone can result in substantial reduction in carbon gain, but this is highly dependent on exact canopy architecture and the diurnal dynamics of photoinhibition. The use of such highly realistic canopy reconstructions also allows us to conclude that even a moderate change in leaf

angle in upper layers of the wheat canopy led to a large increase in the number of leaves in a severely light-limited state.

Introduction

Plant canopy characteristics result from several factors, including genetically determined patterns of development, environmental influence on key developmental events (such as cell division), and population density. This means that plant canopies, whether considered as single plants or at the community scale, are spatially complex, resulting in a heterogeneous light environment (Russell *et al.*, 1989). Because photosynthetic rate is light intensity dependent, it is convenient to consider canopies as populations of leaves each consisting of surface areas with different characteristics and varying states of photosynthesis at any single time point. High-resolution three-dimensional (3D) representations of plant canopies have previously been difficult to obtain, and this has hampered predictions of canopy photosynthesis.

One of the consequences of canopy complexity is spatial and temporal variability in the onset of high light effects, such as photoinhibition. Here, we approach this problem by using unique techniques for high-resolution reconstruction of crop canopies in the field combined with an empirical model of photoinhibition. We consider photoinhibition as a light-dependent decline in the maximal quantum yield of photosynthesis, which can be monitored by a decrease in the chlorophyll fluorescence ratio of variable fluorescence (F_v) to maximal fluorescence (F_m ; Powles, 1984; Long *et al.*, 1994; Raven, 2011; Takahashi and Badger, 2011). The effect of photoinhibition on biomass production is not a unique concept, but very few techniques exist that are able to quantify its impact on long-term carbon gain at the canopy scale. The effect of photoinhibition on shaping parameters of the photosynthesis light response curve is already well characterized, and previous empirical models have looked at the effects of distorting such shaping parameters to empirically quantify values for reduction in carbon gain (Ögren and Sjöström, 1990; Werner *et al.*, 2001; Zhu *et al.*, 2004; Valladares *et al.*, 2005).

The effect of photoinhibition on productivity is, to a large extent, dependent upon the capacity of a leaf to utilize incident photosynthetic photon flux density (PPFD) as described by the shape of the light response curve. Two shaping parameters determine a light response curve as defined by the nonrectangular hyperbola, namely the quantum yield of PSII (Φ) and convexity (θ). The quantum yield (Φ) describes the initial linear portion (under low light intensities) of the light response curve and defines the maximum efficiency with which light can be converted to fixed carbon. The primary effect of photoinhibition is the reduction in Φ , which is important under low light conditions (Powles, 1984; Björkman and Demmig, 1987; Krause and Weis, 1991). Chlorophyll fluorescence measurements are often used to predict changes in Φ for a given location within a canopy (as dark-adapted F_v/F_m), because this is a measurement of actual maximum yield of PSII. Gas exchange and oxygen evolution data indicate a near-equal (1:1) relationship between changes in F_v/F_m and changes in Φ (Björkman and Demmig, 1987; Genty *et al.*, 1989).

The convexity (θ) describes the curvature of a light response curve. The optical properties of leaves and acclimation of individual cells result in convexity values of around 0.85. Higher values of convexity ($\theta < 0.96$) can be found within unicellular algae (*Coccomyxa* spp.; Terashima and Saeki, 1985; Ögren and Sjöström, 1990; Evans *et al.*, 1993; Leverenz, 1994).

Under conditions causing photoinhibition, a reduction in Φ is often accompanied by a similar reduction in θ (Ögren and Sjöström, 1990; Leverenz, 1994). However, the main difference between the two parameters is that a reduction in Φ will also reduce photosynthesis at intermediate light levels and not only under low light conditions. A reduction in both parameters is of particular importance under natural conditions, because light is thought to be a limiting resource to photosynthesis most of the time in a large number of environments (Long and Hällgren, 1985; Ort and Baker, 1988). The effect of photoinhibition on the light response curve can, therefore, be used to quantify its influence on long-term carbon gain by distorting the curve from a

theoretical maximal value and calculating how the results differ from an undistorted curve.

Plant canopies represent an intriguing model for studies in photoinhibition, because for a given leaf, the 3D structure results in a pattern of light that frequently shifts between high and low irradiance as a result of solar movement and other factors, such as plant movement. Hence, photoinhibited leaves are frequently and momentarily exposed to a range of light intensities. Architecture, therefore, determines both the pattern of onset and the cost to productivity.

In previous studies, the reduction in F_v/F_m for a given leaf area was considered to be a function of the weighted PPFD exposure over the previous 6 h (Werner *et al.*, 2001; Valladares *et al.*, 2005) or the cumulative weighted PPFD over the previous 24 h (Zhu *et al.*, 2004). We considered that this approach is not appropriate for comparisons between species and lineages where there may be variation in the quantum requirements for photoinhibition. There are known genotype-dependent differences in cereal species (Kasajima *et al.*, 2011); therefore, we derived a scaling factor (SF) directly from F_v/F_m data taken in the field measured at different canopy levels.

As described above, the photosynthetic rate depends on the shape of the light response curve as well as local light conditions. Plants are complex 3D objects with a great variability in leaf size, shape, area, angle, curvature, twisting, and clumping. Moreover, plants show emergent morphological and physiological properties as a result of being grown as a community in the field and not as single plants in pots. Therefore, an accurate estimation of light environment inside a crop canopy requires both image-based high-resolution 3D plant reconstruction (Pound *et al.*, 2014) and a ray-tracing algorithm (Song *et al.*, 2013) from plants grown in realistic field scenarios. Combining the techniques allows prediction of a precise local PPFD at multiple positions for any given time point, which would be difficult to achieve using manual measurements.

Furthermore, image-based reconstruction is more sensitive to small differences in plant architecture.

The empirical model that we propose uses the distortion of the light response curve from a maximal state parameterized by field-measured gas exchange and fluorescence data combined with detailed 3D structural data, where leaves are represented as a set of triangles. Ray tracing is used to assess the productivity of three field-grown wheat (*Triticum aestivum*) lines that contrast in plant architecture. Such a method can be used to assess the link between existing canopy architecture and carbon gain or could be used as a tool and platform for creating unique ideal plant types. Three wheat lines were selected for analysis in this study from an ongoing field trial at the University of Nottingham farm: cv Ashby, cv 32-129bc, and cv 23-74bc, which are referred to as the parent line, line 1, and line 2, respectively. We show that (1) variation in wheat canopy architecture measured using unique high-resolution 3D imaging affects both photoinhibition and canopy photosynthesis; (2) 3D reconstruction of entire canopies provides a convenient and accurate way of recovering descriptive features used in canopy analysis for light interception and crop production that were previously difficult, if not impossible, to obtain; and (3) the distribution of light levels in contrasting canopies shows unique features in terms of the degree of saturation of photosynthesis according to canopy position.

Materials and Methods

Plant Material

Wheat (*Triticum aestivum*) lines with contrasting canopy architectures were selected from an ongoing field trial at the University of Nottingham farm; 138 double-haploid lines were developed jointly by Nottingham and the International Maize and Wheat Improvement Centre from a cross between the International Maize and Wheat Improvement Centre large-ear phenotype spring wheat advanced line LSP2 and the United Kingdom winter wheat 'Rialto.' Back crossed 3 (BC3) lines were generated from three backcrosses between selected double-haploid lines as donors and a spring elite cultivar (cv Ashby) or a winter cultivar (cv Humber) as recipient. The BC3 lines were then self-fertilized for five generations to produce BC3S5 lines used in this experiment. This approach resulted in the formation of a large number of stable lines with contrasting canopy architecture but photosynthetic responses consistent with the United Kingdom environment (Driever *et al.*, 2014). Three wheat lines were selected for analysis: cv Ashby (parent line), cv 32-129bc (line 1), and cv 23-74bc (line 2).

A field experiment was carried out at Sutton Bonington (52° 839 N, 1° 259 W) in 2013 and 2014 on BC3S5 lines and the recurrent parents cv Ashby and cv Humber. The soil was a medium sandy loam 0.8-m deep over clay (Dunington Heath Series). The experiment used a randomized block design with two replicates, and the plot size was 1.65 x 6 m; there were 12 rows with a row width of 13.2 cm. The previous crop was oilseed rape (*Brassica napus*). The plots were sown on November 18, 2013 at a seed rate of 300 seeds m⁻². In each plot, 220 kg N ha⁻¹ nitrogenous fertilizer as ammonium nitrate was applied in a three-split program; 40 kg N ha⁻¹ was applied in early March, 100 kg N ha⁻¹ was applied in late March, and 80 kg N ha⁻¹ was applied in early May. Plant growth regulator chlormequat was applied at growth stage 31 (stem elongation and first node detectable). Prophylactic applications of fungicides were given at growth stages 31, 39, and 59 (Tottman, 1987) to keep diseases to very low levels. Pesticides and herbicides were used as necessary to minimise the effects of pests and weeds.

Imaging and Ray Tracing

3D analysis of plants was made according to the protocol by Pound *et al.* (2014). The developmental stage of each of the lines was the same. At anthesis and after photosynthesis measurements, wheat plants (roots and shoots) were carefully removed from the field, taken to a laboratory, and packed in a box to avoid excessive movement or damage to leaves. Roots were supplied with water to prevent wilting. It was found that this process did not alter the key architectural features of the plants. They were imaged within 2 h using three fixed Canon 650D cameras, with a minimum of 40 images per plant. Images were captured using a revolving turntable, including a calibration target of set width (397 mm) that was used to both aid with automatic camera calibration and enable scaling of the model to the correct size after reconstruction. An initial point cloud was obtained using the PMVS software (Furukawa and Ponce, 2010; Wu, 2011). The PMVS photometric consistency threshold (Furukawa and Ponce, 2010; Eq. 2) was set at 0.45 to optimize the amount of plant material recognized in the point cloud. Default parameters were used within the Reconstructor software, except for maximum cluster size and boundary sample rate, which were changed to 120 and 15, respectively. These parameters were chosen, because they reduce the number of triangles in the output mesh but give the most accurate mesh (in terms of both total area and Hausdorff distance) in optimization tests (data not shown).

Three replicate plants representative of the morphology of each line were taken from each line and reconstructed; however, for lines 1 and 2, two plants were used to form the final canopy. The wheat ears were manually removed from the resultant mesh, because the reconstructing method is unable to accurately represent their form. Canopies were created for each of the three plots by duplicating and randomly rotating the reconstructions in a 3 x 3-grid pattern. The orientations were altered until the cLAI of the plot matched the average value given from leaf and stem area measurements of the sampled plants (Supplemental Table S7.2). Reconstructed canopies consist of n triangles with coordinates of the i th triangle given by a vector $\{x_i^1, y_i^1, z_i^1, x_i^2, y_i^2, z_i^2, x_i^3, y_i^3, z_i^3\}$, where coordinates x and y correspond to the coordinates on the ground and coordinate z corresponds to height above the ground.

Total light per unit leaf area for the i th triangle at time t , $Li(t)$, was predicted using a forward ray-tracing algorithm implemented in fastTracer (fastTracer, version 3; PICB; Song *et al.*, 2013). Latitude was set at 53 (for Sutton Bonington, United Kingdom), atmospheric transmittance was 0.5, light reflectance was 7.5%, light transmittance was 7.5%, and day was 181 (June 30), with sunrise and sunset of 5 AM and 10 PM, respectively. The diurnal course of light intensities over a whole canopy was recorded in 1-h intervals. To prevent the boundary effect, we positioned the ray-tracing boundaries at centers of the outer plants. The software fires rays through a box with defined boundaries; when they exit one boundary (i.e. the side), they enter again from the opposite side.

Leaf angle, dry weight and leaf area measurements

Leaf angles were measured in two different ways. Leaf angles were measured in the field using a protractor (Pask *et al.*, 2012), with the average of five measurements per layer per line. These values were then compared with those obtained on the reconstructed plants using a mesh editing software (Meshlab. sourceforge.net; Supplemental Table S7.1). Plant dry weight and area were analyzed by separating shoot material into stem, flag leaf, and all other leaves before passing them through a leaf area meter (LI3000C; Licor) followed by drying each component individually in an oven at 80°C for 2 d until no more weight loss was noted. Plants were weighed immediately. Leaf and stem areas were also calculated for the reconstructions using Meshlab for comparison.

Field Data: Gas Exchange and Fluorescence

Data were taken from the field-grown wheat in plots in the same week in which the imaged plants were taken on Sutton Bonington Campus. Leaf gas exchange measurements were taken with a LI-COR 6400XT IR Gas-Exchange Analyzer (LI-COR). The block temperature was maintained at 20°C using a flow rate of 500 m⁻¹ min⁻¹. Light was provided by a combination of in-built red and blue light-emitting diodes. Light response curves were taken on leaves that had not been dark-adapted. Illumination occurred over a series of six

photosynthetically active radiation values between 50 and 2,000 $\mu\text{mol m}^{-2} \text{s}^{-1}$, with a minimum of 2 min at each light level. Light response curves were taken at three different canopy heights: labeled top, middle, and bottom referring to flag leaf, second leaf (Flag leaf -1 [FL -1]), and third leaf (FL -2), respectively, with height above ground being noted. Leaves in the middle and bottom layers were additionally exposed to a photosynthetically active radiation level of 500 $\mu\text{mol m}^{-2} \text{s}^{-1}$ for 3 min before the light response curve measurements. Four replicates were taken per plot for each canopy layer.

A Walz (EffeLtrich) MiniPam Fluorometer was used to measure dark-adapted values of Fv/Fm in the field wheat at midday. Leaves were dark-adapted using clips (DLC-08; Walz) for 20 min, and initial (minimum) PSII fluorescence in the dark-adapted state and Fm were measured by applying a saturating pulse (0.8 s at 6,000 $\mu\text{mol m}^{-2} \text{s}^{-1}$). Four replicates were taken per plot per layer, but as values for the middle layer were approaching or at the maximal value expected (Fv/Fm max = 0.83), measurements were not taken for the bottom layer.

cLAI and the Light extinction coefficient

Cumulative leaf area index (cLAI; leaf area per unit ground area as a function of depth) was calculated from each of the canopy reconstructions. For each depth (d ; distance from the highest point of the canopy), we found all triangles with centers lying above d (Eq. 1).

$$d_i = \max_{j=1,2,3; 1 \leq i \leq n} z_i^j - (z_i^1 + z_i^2 + z_i^3)/3 \quad (1)$$

We then calculated the sum of the areas of these triangles and then divided this sum by ground area. The cumulative LAI as a function of depth through the canopy was calculated using Eq. 2.

$$cLAI(d) = \frac{\sum_{i=1}^n I(d_i \leq d) S_i}{\left(\max_{1 \leq i \leq n} x_i - \min_{1 \leq i \leq n} x_i \right) \left(\max_{1 \leq i \leq n} y_i - \min_{1 \leq i \leq n} y_i \right)}, \quad (2)$$

where $I(A)=I$ if condition A is satisfied and S_i is the area of a triangle i .

The light extinction coefficient of the canopy was calculated using the 3D structural data and the light distribution obtained from ray tracing. In order to calculate fractional interception within a canopy as a function of depth at time t , we first identified all triangles lying above depth, d (Eq. 1). We then calculated their contribution to intercepted light by multiplying PPFD received per unit surface area (ray tracing output) by the area of triangle. The light intercepted was summed for all triangles above the set d , and divided by light intercepted by ground area according to Eq. 3.

$$F(d, t) = \frac{\sum_{i=1}^n I(d_i \leq d) S_i L_i(t)}{L_0(t) * \text{ground area}}, \quad (3)$$

where $L_0(t)$ is light received on a horizontal surface with a ground area $\left(\max_{1 \leq i \leq n} x_i - \min_{1 \leq i \leq n} x_i \right) \left(\max_{1 \leq i \leq n} y_i - \min_{1 \leq i \leq n} y_i \right)$, and $L_i(t)$ is light intercepted by a triangle i .

The light extinction coefficient, k , was calculated by fitting (by least squares) the function

$$f(x) = a(1 - e^{-kx}) \quad (4)$$

to the set of points $\{cLAI(d), F(d, t)\}$ calculated by varying depth from 0 to the height at total cLAI with step $\Delta d = 1$ mm (Supplementary Figure S7.4), a in Eq.(4) is a fitted parameter.

Model Set up

A simplified overview of the modelling process is given in Figure 7.6.

All modeling was carried out using Mathematica (Wolfram). The response of photosynthesis to light irradiance, L , was calculated using a nonrectangular hyperbola given by Eq. 5:

$$F_{NRH}(L, \phi, \theta, P_{max}, \alpha) = \frac{\phi L + (1 + \alpha)P_{max} - \sqrt{(\phi L + (1 + \alpha)P_{max})^2 - 4\theta\phi L(1 + \alpha)P_{max}}}{2\theta} - \alpha P_{max} \quad (5)$$

The nonrectangular hyperbola is defined by four parameters: the quantum use efficiency, ϕ ; the convexity, θ ; the maximum photosynthetic capacity; P_{max} , and the rate of dark respiration, R_d . We assumed that the rate of dark respiration is proportional to the maximum photosynthetic capacity, according to the relationship $R_d = \alpha P_{max}$ (Givnish, 1998; Niinemets and Tenhunen, 2007; Retkute *et al.*, 2015), where $\alpha = 0.1$.

Values for P_{max} were determined from leaf gas exchange measurements (see section “Field Data; gas exchange and fluorescence”). Curve fitting was carried out using the Mathematica command **FindFit** with a minimum constraint on dark respiration at 0.05 and convexity at 0.6. Data and fitted curves are shown in Figures 7.7A (line 2) and Supplementary Figure S7.2 (parent and line 1). Estimated values of P_{max} for each layer and each canopy are given in Table 7.1. As the plants were photoinhibited and the model works by distorting the light response curve from an “uninhibited” state, the values for quantum use efficiency and convexity could not be taken from the fitted light response curves. Instead, maximal values were taken from the literature; quantum use efficiency was set at 0.052 and convexity at 0.845 (table 7.1).

Layer	Fv/Fm	SF ₁₂	P _{max}
Parent Line			
Top Layer	0.772 ± 0.016	0.931	22.3
Middle Layer	0.814 ± 0.001	0.980	13.6
Bottom Layer	-	-	4.6
Line 1			
Top Layer	0.744 ± 0.014	0.896	25.8
Middle Layer	0.813 ± 0.003	0.980	16.9
Bottom Layer	-	-	6.3
Line 2			
Top Layer	0.712 ± 0.024	0.857	28.6
Middle Layer	0.802 ± 0.012	0.966	12.6
Bottom Layer	-	-	4.7
Maximal LRC values			
Φ			0.052
θ			0.845
α			0.1

Table 7.1: Parameters used in the model

To account for photoinhibition, we assumed that the quantum use efficiency and convexity change during the course of a day (see Figure 7.7C), i.e. each or both are reduced according to the scaling factor, which is parameterized using Fv/Fm measurements taken in the field (Genty *et al.*, 1988, Leverenz, 1994). The maximum photoinhibition was assumed to be present at 12:00 (see section “Field Data; gas exchange and fluorescence”), giving the scaling factor

$$SF_{12} = \frac{(Fv/Fm)}{(Fv/Fm_{max})} \quad (6a)$$

Two different scenarios of diurnal changes in photoinhibition were modelled to represent different responses to photoinhibition (Demmig-Adams *et al.*,

2012). Scenario 1 showed a depression in Fv/Fm over the 6 hours around midday which may be more appropriate for herbaceous fast-growing plants such as cereals (Murchie *et al.*, 1999) whereas scenario 2 showed a depression in Fv/Fm starting at sunrise, peaking in the middle of the day and ending at sunset. To represent these dynamics, we fitted a parabola (Eq. 6b) using least squares method through points $\{t_0, 1\}$, $\{12, SF_{12}\}$, $\{t_N, 1\}$, where t_0 and t_N indicate the onset and ending of the photoinhibition period ($t_0 = 09:00$ and $t_N = 15:00$ for photoinhibition scenario 1 and $t_0 = 05:00$ and $t_N = 22:00$ for photoinhibition scenario 2).

$$SF(t) = a t^2 + b t + c \quad (6b)$$

The dynamics of each of the photoinhibition scenarios for each canopy is given in Supplementary Figure S7.3.

The carbon assimilation at triangle i was calculated by combining Eq.(5) with the predicted PPFD at triangle I for each hour. Daily carbon assimilation, P_i (Eq. 7), was then calculated by integrating the rate of photosynthetic carbon uptake over the day (from 05:00 to 22:00) and multiplying by the area of the triangle, S_i :

$$P_i = S_i \int_5^{22} F_{NRH}(L_i(t), \phi, \theta, P_{max}, \alpha) dt \quad (7)$$

The daily carbon assimilation under photoinhibition, P_i^{PIH} , was calculated by scaling the appropriate parameters in Eq.(5) according to a scaling factor value at time t (Eqs. 8a-c), namely

- a) reduction in quantum use efficiency (only ϕ multiplied by the scaling factor)

$$P_i^{PIH} = S_i \int_5^{22} F_{NRH}(L_i(t), SF(t) * \phi, \theta, P_{max}, \alpha) dt; \quad (8a)$$

- b) reduction in convexity (only θ multiplied by the scaling factor)

$$P_i^{PIH} = S_i \int_5^{22} F_{NRH}(L_i(t), \phi, SF(t) * \theta, P_{max}, \alpha) dt; \quad (8b)$$

c) reduction in quantum use efficiency and convexity (both θ and ϕ multiplied by the scaling factor

$$P_i^{PIH} = S_i \int_5^{22} F_{NRH}(L_i(t), SF(t) * \phi, SF(t) * \theta, P_{max}, \alpha) dt. \quad (8c)$$

As each canopy was divided into 3 layers, each triangle from the digital plant reconstruction was assigned to a particular layer, m , according to the triangle centre (i.e. with triangle centre between upper and lower limit of a layer depth). Carbon gain per unit canopy area was calculated as daily carbon assimilation over a whole canopy divided by the total surface area of the canopy according to Eq. 9.

$$C = \frac{\sum_{i=1}^n P_i}{\sum_{i=1}^n S_i}. \quad (9)$$

The reduction in carbon gain due to the photoinhibition for a layer m , (where $m=1$ or 2 ; referring to the top and middle layer, respectively), was calculated as the percentage difference between daily carbon gain without photoinhibition (using the unscaled light response curve) and with photoinhibition (scaled light response curve) summed over all the triangles belonging to the layer m according to Eq. 10.

$$\Delta C_m = 100 \frac{\sum_{i=1}^n I(d_m^L \leq d_i < d_m^U) (P_i - P_i^{PIH})}{\sum_{i=1}^n P_i} \quad (10)$$

where P_i is calculated using Eq. 7 and P_i^{PIH} is calculated using Eq. 8a-c.

The reduction in whole-plant daily carbon gain due to photoinhibition is obtained as a sum over the top two layers,

$$\Delta C = \Delta C_1 + \Delta C_2. \quad (11)$$

Results

The Light Environment in a Leaf Canopy

A major determinant of light environment in a leaf canopy is plant architecture, the general descriptors of which are leaf area, leaf inclination, and arrangement in space. Traditionally, theoretical work on photosynthesis considers canopies with randomly distributed leaves and leaf angles defined by a particular distribution to account for spatial heterogeneity (Werner *et al.*, 2001; Zhu *et al.*, 2004; Song *et al.*, 2013). Our study is based on an accurate high-resolution digital reconstruction of real wheat canopy structure; therefore, it represents subtle features without the need to parameterize structural properties. Figure 7.1 shows two examples of the reconstruction process of single contrasting wheat plants, and Figure 7.2 shows the final three different reconstructed canopies (3 x 3- plant plots) designed to accurately represent the canopies from which each of the individual plant reconstructions was derived.

Clear visual differences between canopy geometrical measures of the three reconstructed canopies are apparent in Figure 7.2. The parent line has distinct upright leaves compared with the more curved and curled leaves of lines 1 and 2. This was confirmed by manual measurements of leaf angle (as the angle with which the leaf subtends the stem; Supplemental Table S7.1). It was also confirmed by calculating the distributions of angles of the reconstructed leaf elements (also known as individual triangles; “Imaging and Ray Tracing”) relative to the vertical axis (Supplemental Fig. S7.1).

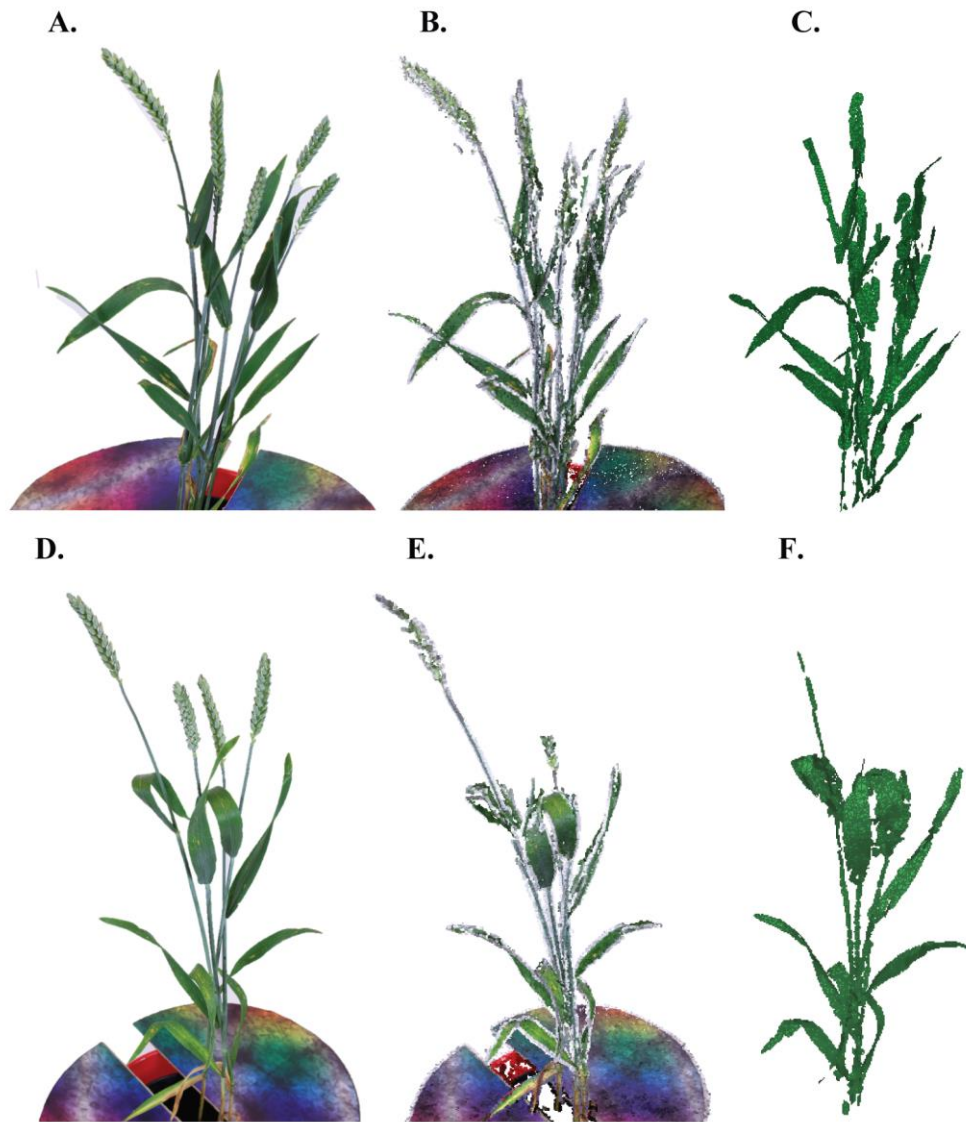


Figure 7.1: Stages of the reconstruction of a single plant from multiple color images. (A) and (D), An example photograph of a wheat plant including the calibration target, from one viewpoint, of the parent line (upright leaves) and line 2 (more curled leaves), respectively. (B) and (E), Point cloud reconstruction: the output when each set of images is run through VisualSFM (Wu, 2011). (C) and (F), The final output mesh after using the reconstructor software (Pound et al., 2014) with the ears removed.

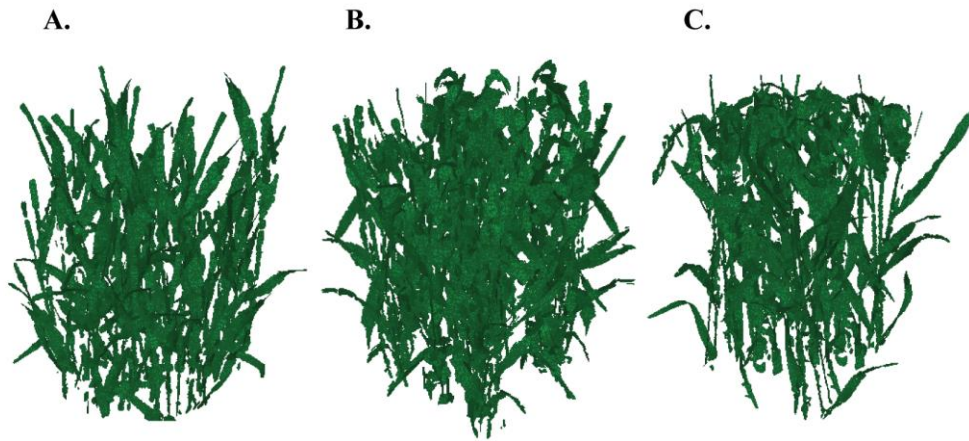


Figure 7.2. Wheat canopy reconstructions. All plots were made from single-plant reconstructions (as in Fig. 7.1), duplicated, randomly rotated, and spaced on a 3 x 3-plant grid. (A), Parent line. (B), Line 1. (C), Line 2.

We found substantial differences in vertical profiles of leaf material between the three canopies. We calculated the reconstructed leaf and stem area index to be 4.34 for the parent line, 5.33 for line 1, and 5.27 for line 2. Figure 7.3A shows cumulative leaf area index (cLAI) calculated as a function of depth using Equation 1 (see “Materials and Methods”). Although both lines 1 and 2 have a similar total canopy cLAI, line 2 accumulates more biomass at equivalent lower depths compared with line 1. The parent line has the lowest vertical distribution of biomass with depth. At the depth of 100 mm, cLAI is 0.66 for the parent line, 1.1 for line 1, and 1.8 for line 2.

Similar trends can be seen in plots indicating the fraction of solar incident radiation intercepted (F ; Eq. 3; see “Materials and Methods”) at midday, with each canopy exhibiting distinct dependence on depth (Fig. 7.3B). F accumulates more gradually in the parent line than in lines 1 and 2, with line 1 being intermediate between three canopies. For example, one-half of above-canopy PPFD is intercepted at the depths of 74 mm in line 2, 132 mm in line 1, and 201 mm in the parent line.

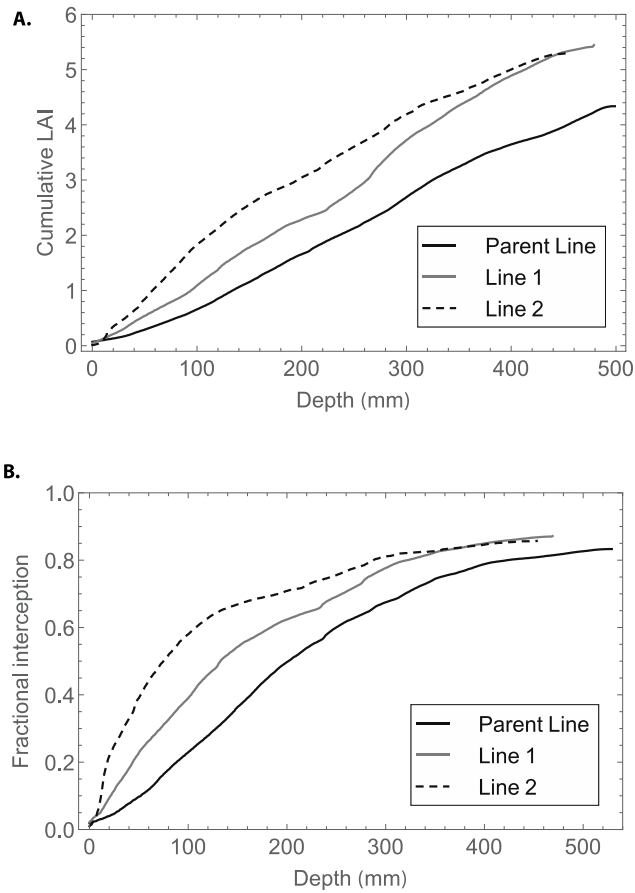


Figure 7.3. Properties of each canopy. (A), $cLAI$ (Eq. 1): the area of leaf material per unity ground as a function of depth through the canopy at 12 PM. (B), Fractional interception (Eq. 3) as a function of depth in the canopy at 12 PM. Curves were calculated with step $\Delta d=1mm$.

Simulations of the light environment show that the daily PPFD on average decreases with depth in all three plots, but the light environment has considerable spatial heterogeneity in PPFD at a fixed depth. Figure 7.4A shows a distribution of the logarithm of the ratio between PPFD absorbed at a point within a canopy and above-canopy PPFD at midday. The PPFD at any depth into the canopy can have a wide range of values, and Figure 7.4 shows that this variability increases with depth. Therefore, it is possible for a lower part of the canopy to have surface areas that receive higher PPFD than surface areas within upper parts of the canopy because of self-shading or shading by

neighboring plants. This gives rise to the phenomenon termed sun-flecks (Pearcy, 1990). Figure 7.4B takes this further, comparing the frequency of PPFD values according to the fraction of surface area in the top layer. Stark differences are seen between the lines, with the contrasting curled canopy (line 2) having a large proportion of leaf area in low light (below $150 \mu\text{mol m}^{-2} \text{s}^{-1}$) compared with line 1 and the parent line. This high-resolution analysis is valuable when comparing light distributions against photosynthetic light response curves. Similar differences are present during the whole day (Supplemental Fig. S7.2).

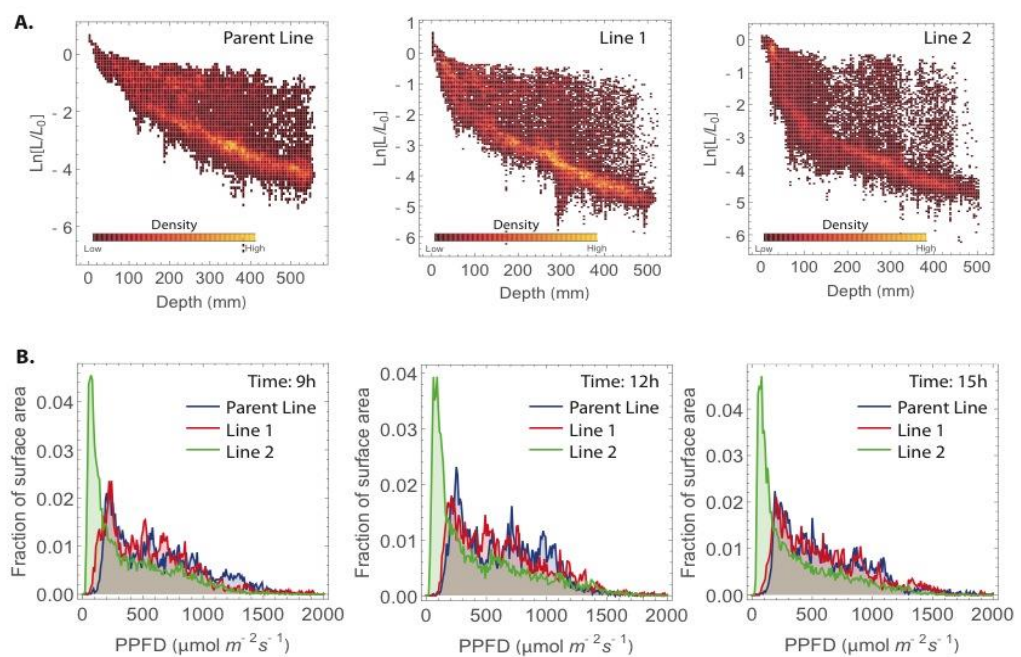


Figure 7.4. Diagrams depicting the heterogeneity of light environment of the three contrasting wheat canopies. (A), Density histogram showing the predicted light levels at 12 PM within each canopy described as the logarithm of the ratio of light received on a horizontal surface to light intercepted by a point on a leaf as a function of depth: parent line (left), line 1 (center), and line 2 (right). (B), Frequency of PPFD values according to the fraction of surface area received at the top layer within each canopy: at 9 AM (left), 12 PM, and 3 PM (right).

Based on fractional interception as a function of cLAI, we calculated light extinction coefficients (k ; Hirose, 2005) for the three canopies (Eq. 4; see “Materials and Methods”). Values of k are used in canopy analysis as a convenient way of mathematically describing the attenuation of light defined by architecture and dependent on the interaction between cLAI accumulation and fractional interception. The simulated values of k obtained are 0.40 for the parent line, 0.49 for line 1, and 0.61 for line 2. This corroborates findings from manually measured ceptometer data measured in the field (Fig. 7.5, line 2).

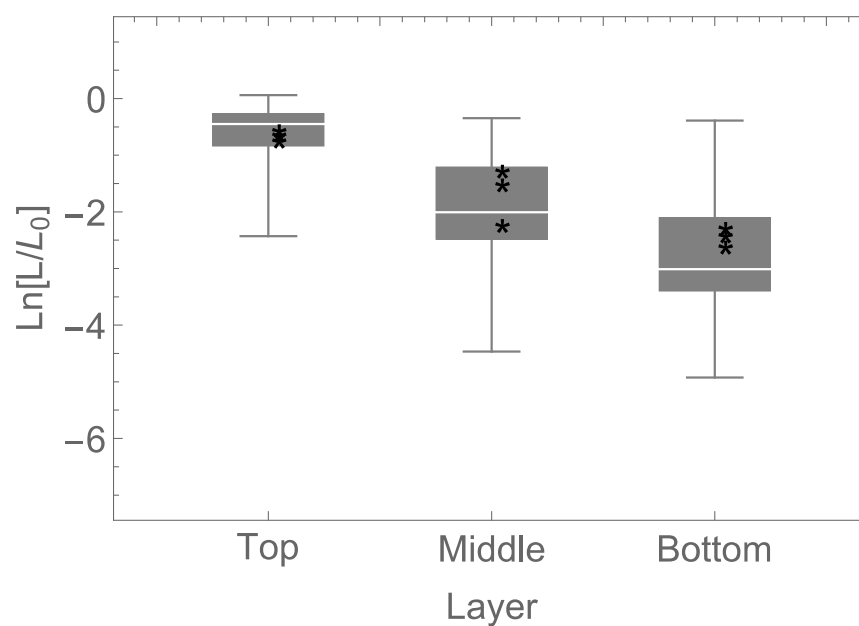


Figure 7.5. Experimental validation of the predicted light levels. The logarithm of the ratio of light received on a horizontal surface to light intercepted by a point of a leaf ($\text{Ln}[L/L_0]$) predicted by ray tracing (box and whiskers) is compared with measurements made manually using a ceptometer (asterisks). Leaves were not all horizontal. Predicted and measured data are for line 2 in top, middle, and bottom layers in the canopy at 12:00 h.

Incorporating Physiological Measurements into the Photoinhibition Model

An overview of the modeling process can be seen in Figure 7.6. Light response curves and F_v/F_m were measured at 12 PM at three levels within each canopy. The nonrectangular hyperbola given by Equation 5 (see “Materials and Methods”) was fitted to experimental data to determine the maximum photosynthetic capacity, quantum use efficiency, and convexity. Measurements and fitted curves for line 1 are shown in Figure 7.7A. The maximum photosynthetic capacity decreased (Fig. 7.7A; Supplemental Fig. S7.3) and F_v/F_m increased (Fig. 7.7B) with the depth in the canopy. The differences between photosynthetic light response curves are typical of the canopy depth-dependent changes caused by light acclimation and leaf ageing (Murchie *et al.*, 2002). Daily net photosynthesis per unit canopy area was higher for the parent line ($0.2583 \text{ mol m}^{-2} \text{ d}^{-1}$) compared with line 1 ($0.2166 \text{ mol m}^{-2} \text{ d}^{-1}$) or line 2 ($0.2163 \text{ mol m}^{-2} \text{ d}^{-1}$; see “Materials and Methods”).

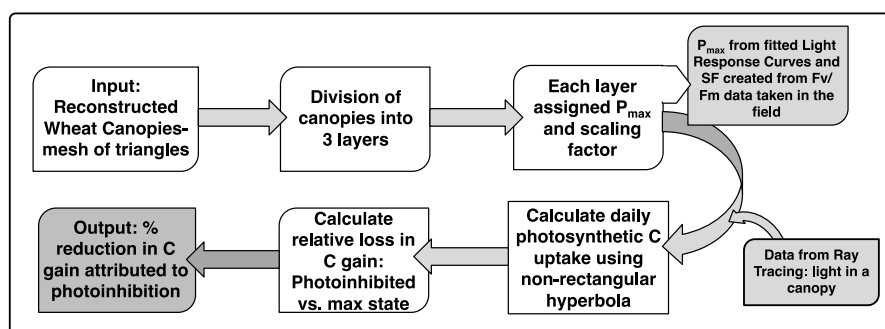


Figure 7.6. Simplified overview of the modelling method.

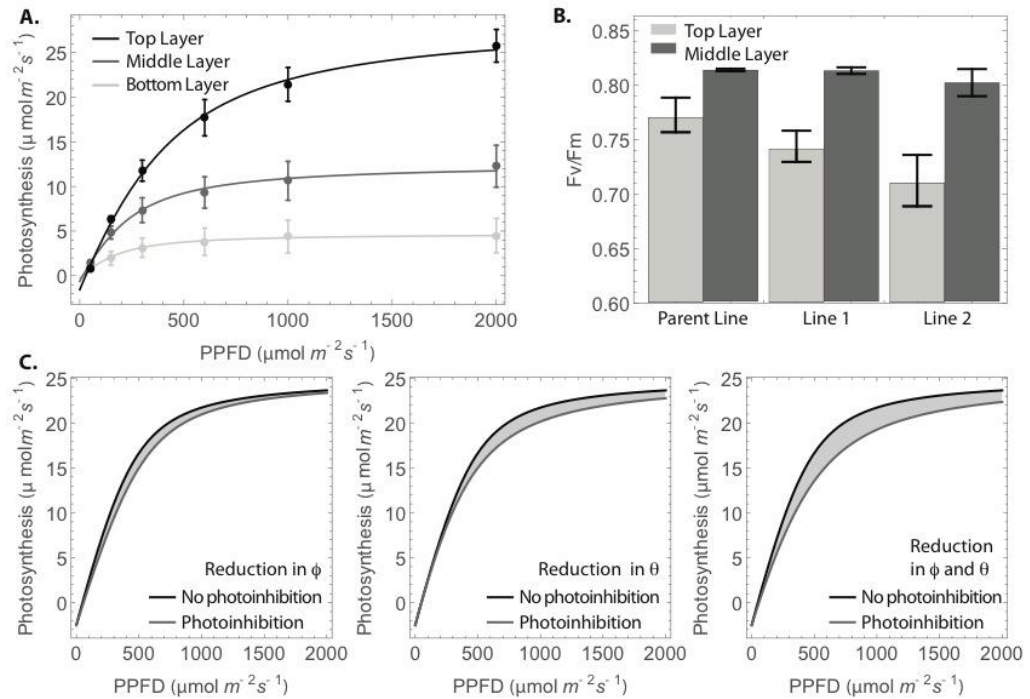


Figure 7.7. Data used for the parameterization of the photoinhibition model. (A), Example light response curves from the top (flag leaf; black), middle (FL-1; dark gray), and bottom (FL-2; light gray) layers of line 2 (light response curves for the parent line and line 1 can be found in Supplemental Fig. S7.3). Values of the maximum photosynthetic capacity for each layer were obtained from fitting the nonrectangular hyperbola (Eq. 5) to each of the curves. The graph shows the experimental data (mean $6 \pm \text{SEM}$ of three measurements) and fitted curves. (B), Dark-adapted F_v/F_m data per plot and layer measured at 12 PM. The means of five replicates are presented with SEM. (C), Distortion of Equation 5 based on parameters from top layer of line 2 and scenario 1 at 12 PM: reduction in Φ (left), reduction in θ (center), and reduction in Φ and θ (right).

The probability of photoinhibition diminishes in lower parts of the canopy because of the lower photon flux density, and this is reflected in the F_v/F_m values, with the middle layer (second leaf) approaching the maximal value (0.83; Fig. 7.7B; Table 7.1). Therefore, the influence of photoinhibition on the

top and middle layers only was considered within the model. The strongest photoinhibition (highest reduction in Fv/Fm) was found in the top layer of line 2 followed by line 1 and then, the parent line, whereas the middle layer for all three canopies showed similar Fv/Fm values (Table I). There was a statistically significant difference in Fv/ Fm between layers for all lines ($P < 0.001$) and no evidence of a significant difference between lines ($P = 0.053$).

The difference between measured Fv/Fm and theoretical maximal Fv/Fm (0.83) was used to calculate a maximal SF according to Equations 6a and 6b (see “Materials and Methods”). Photoinhibition in crops tends show a diurnal pattern from nonexistent at sunrise and sunset to maximal at midday when light levels are in excess. To account for these dynamics, we have fitted parabolas for each layer, with its vertex corresponding to SF₁₂ (Supplemental Fig. S7.2). This SF was used to distort the light response curve as shown in Figure 7.7. We used the light response curves of CO₂ assimilation for these calculations. It was not possible to use light response curves as a measurement of photoinhibition or quantum yield itself, because a measurement of leaf absorptance would be required.

We applied the SF according to two different scenarios in a manner that describes two contrasting diurnal changes in photoinhibition. In scenario 1, photoinhibition occurs over 6 h over the middle of the day, reaching the maximum value at 12:00 PM (Supplemental Fig. S7.4A). In scenario 2, photoinhibition starts at sunrise, peaks in the middle of the day, and decreases until sunset (Supplemental Fig. S7.4B). Such changes are consistent with those observed across different species, and previous responses for rice (*Oryza sativa*) followed a parabolic-type behavior (Murchie *et al.*, 1999; Demmig-Adams *et al.*, 2012). This approach uses existing knowledge on photoinhibition dynamics under different scenarios as the most effective way of meeting the objectives set out in this study.

The gas exchange and fluorescence parameters used in the model are given in Table 7.1. The values for P_{max} were similar at each level between each of the

three plots, with around a 2-fold decrease from upper layer to middle layer and around a 3-fold decrease from middle layer to bottom layer. Because we could not detect photoinhibition in the bottom layer, the F_v/F_m and SF data for layer 3 have been omitted from Table I and thus, will not contribute to the modeled reduction in carbon gain of each of the canopies in this model.

Effect of Photoinhibition on Carbon Gain: Model Output

The mathematical model predicted and compared the simulated daily carbon assimilation under different photoinhibition scenarios as described by Equations 7 to 10 (see “Materials and Methods”). The contribution of the top two layers to a reduction in simulated carbon gain can be seen in Figure 7.8, A (photoinhibition scenario 1) and B (photoinhibition scenario 2). There is interdependence between distorting both the convexity and the quantum use efficiency values, because light distribution takes a range of values: some of these are more sensitive to the reduction in yield, and some are more sensitive to the reduction in convexity (Long *et al.*, 1994). The strongest effect on net photosynthesis is achieved by a concomitant reduction in both parameters. For scenario 1, reduction in Φ alone resulted in approximately 1.1%, 2.3%, and 3% reductions in canopy carbon gain in parent line, line 1, and line 2, respectively, and this rose to 2.6%, 4.4%, and 5.6% when combined with θ (Fig. 7.8A). These represent substantial reductions in potential biomass productivity. These values are increased even further when considering the diurnal dynamics of photoinhibition represented by scenario 2 (Fig. 7.8B), with reductions in canopy carbon gain rising to 6.8%, 10.2%, and 13.7%, respectively, for a reduction in both Φ and θ .

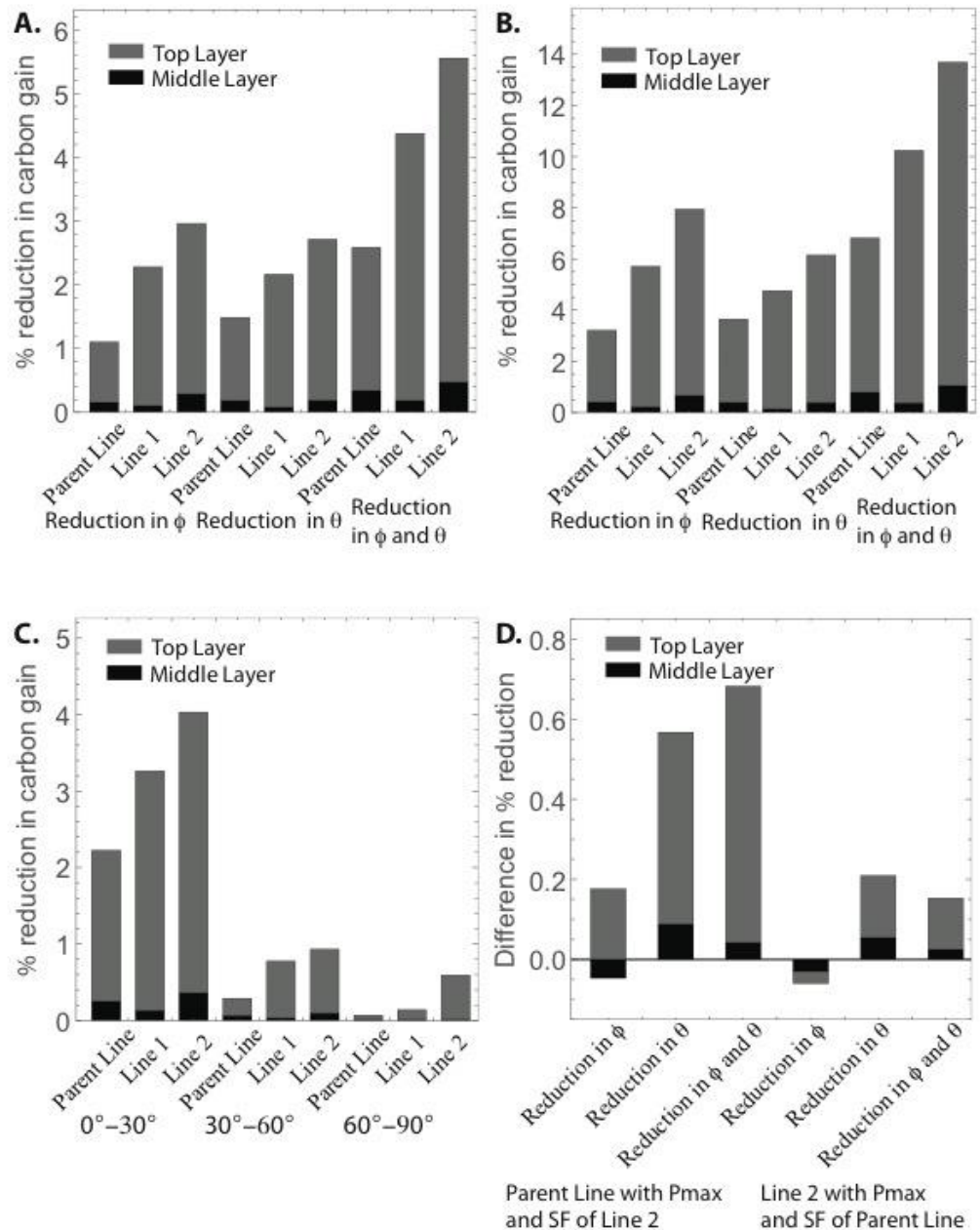


Figure 7.8. Results of the model: the predicted effect of photoinhibition on carbon gain (Eq. 10). (A), Percentage reduction in carbon gain relative to a non-inhibited canopy based on photoinhibition scenario 1, with depression in F_v/F_m occurring for 6 h around midday according to a hyperbolic relationship. (B), Percentage reduction in carbon gain relative to a nonphotoinhibited canopy based on photoinhibition scenario 2, with depression in F_v/F_m beginning at dawn and ending at dusk according to a hyperbolic relationship. (C), Percentage reduction in carbon gain relative to a nonphotoinhibited canopy based on photoinhibition on scenario 1 as a function of the triangle angle relative to vertical. Results are for a distortion in both Φ and

θ. (D), Graph indicating the importance of canopy architecture on the model output. The P_{max} and SF according to photoinhibition scenario 1 of line 2 were applied to the canopy and ray-tracing output of the parent line and vice versa. The difference in the percentage reduction in carbon gain was then calculated relative to the results obtained from the donor line. Positive values indicate a greater reduction in carbon gain for the parent line, whereas negative values indicate a greater reduction for line 2.

The large differences in canopy photosynthesis observed between different lines could result from differences in canopy architecture or differences in susceptibility to photoinhibition on a biochemical level. To investigate, the model was split dependent upon leaf angle within the canopy, which we calculate in a unique way using the triangle surface angle relative to vertical (see “Materials and Methods”; Supplemental Fig. S7.1A). Rather than a simple measurement of leaf angle subtending the stem and a visual assessment of leaf curvature, this approach allows triangles to form a population derived from every part of the leaf, therefore giving detailed empirical data that can be used against other canopy and physiological data. Results for simulated photoinhibition scenario 1 are shown in Figure 7.8C, confirming a strong relationship between triangle angle and loss of carbon gain, with line 2 (more visually horizontal leaves) possessing a higher proportion of triangles with higher angles (more horizontal) and suffering more than line 1 or parent lines. This compares well with Figures 7.3 and 7.4, which show the upright leaves of lines 1 and 2 with better light penetration and in which a lower proportion of leaf area is photo- inhibited (Fig. 7.7B).

To assess the effects of canopy architecture on the model outputs and determine the predominant drivers, the model was run again on the distribution of PPFD for parent line but this time using the P_{max} and SF values of line 2 and vice versa for comparison. The results can be seen in Figure 7.8D; positive values indicate a larger percentage reduction in carbon gain in the parent line relative to line 2, whereas negative values indicate a greater reduction in line 2

relative to the parent. The larger percentage reduction when the parent is given the level of photoinhibition shown by line 2 indicates that, although line 2 was probably more susceptible to leaf photoinhibition at least partly as a result of the canopy architecture, the impact of this on a whole-canopy level was in fact minimized by the less vertical leaf structure. The more open erect structure of the parent is less susceptible to photoinhibition, but in fact, the impact at canopy level will be greater should photoinhibition occur.

Figure 7.9 combines influence of canopy architecture on the distribution of PPFD (at 12 PM; Fig. 7.4) with light response curves showing effect of photoinhibition on carbon gain. The strongest effect of photoinhibition is shown, with the largest accumulated distortion between light response curve without and with photoinhibition (grey area in Fig. 7.9). The average light intensity received by the parent line corresponds to a region of the light response curve that received a greater distortion relative to line 2. It is also positioned higher on the light response curve than line 2. We conclude that the average light-saturated state of a canopy with upright leaves is higher and that the curled nature of leaves at the top of the canopy in line 2 has the effect of oversaturating leaves at the top and overshading at the bottom. The state of light saturation is, therefore, dependent on the relative distribution of leaf area in each layer. This corroborates previous findings and suggests that cLAI will have a strong influence on the tradeoff between photoinhibition susceptibility and impact on long-term canopy carbon gain (Long *et al.*, 2006; Murchie and Reynolds, 2012).

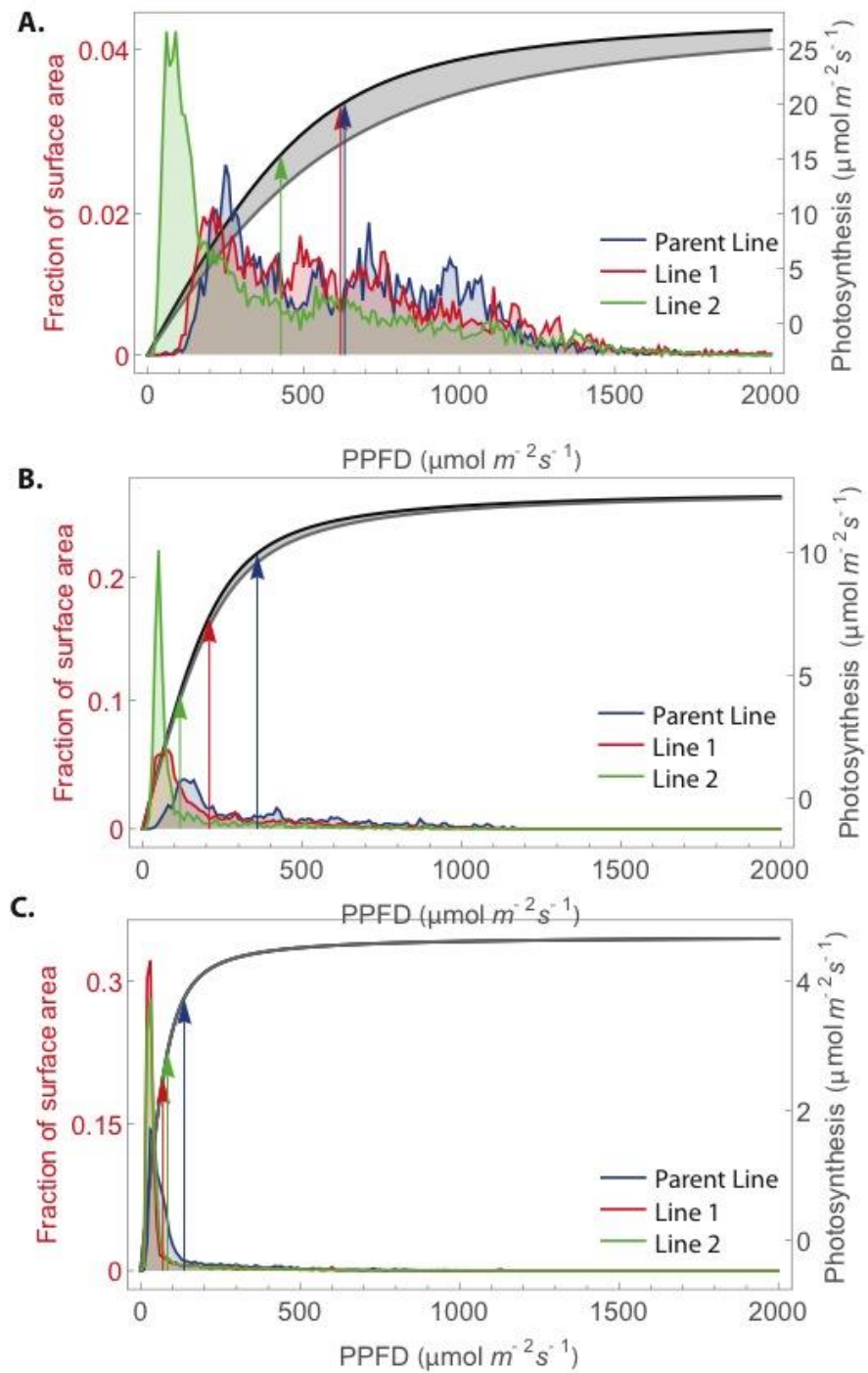


Figure 7.9: Graph indicating the frequency of light levels received at midday by the top layer (A), middle layer (B) and bottom layer (C) in each canopy and the average, indicated by the arrow, overlaid on the LRC and distorted LRC of Line 2.

Discussion

High-Resolution Digital Reconstruction of Field-Grown Plants as a Unique Tool

Here, we describe for the first time, to our knowledge, an accurate high-resolution (and rapidly obtained) structural description of canopy geometry from field-grown wheat plants using readily available standard photography techniques (SLR Digital Cameras). This marks a substantial advance from previous work, because we are able to (1) define key structural and photosynthetic features within the canopy and not simply on the upper canopy surface; (2) incorporate features of leaves, such as leaf curvature and twisting; and (3) extract traditional (e.g. extinction coefficient and fractional interception) and unique (e.g. average triangle angle and surface area fraction) canopy measurements that are difficult, if not impossible, to obtain in the field (for example, cLAI, vertical profiling, and leaf tissue angle distributions). These can be extracted directly from the 3D data and not from field measurements using light sensors and geometric measuring tools that are prone to error according to weather and user.

Construction of 3D plants *in silico* would require knowledge of plant topology and properties, such as leaf and stem length, blade width, tiller number, leaf laminae curvature, or inclination angle. A few models representing 3D canopy architecture for different crops have been developed in recent years; however, these models either simplify the representation of the plants to include only the essential features (Evers *et al.*, 2005) or deduce average architectural parameters from a number of representative plants (Valladares *et al.*, 2005; Song *et al.*, 2013). These methods can be highly time consuming because of the rigorous measurements required (Fourcaud *et al.*, 2008; Vos *et al.*, 2010), and based upon the parameters used, inputting standard leaf angle distributions into a photosynthesis model can lead to a 4% to 15% difference in output compared with models with explicitly described leaf angles (Sarlikioti *et al.*, 2011). Parameterization of functional-structural

plant models for wheat was carried out for contrasting densities (Baccar *et al.*, 2011) but not for cultivars with a contrasting architecture.

Our image-based approach is more likely to capture the heterogeneity of crops within a field, because image-based approaches such as this digitise existing crops, whereas other rule-based methods will create an averaged crop that may capture the general features of the variety/line/species but will not capture unique differences between crops of the same type and thus, may not be as representative or realistic. Furthermore, such rule-based approaches are labour and data intensive and would need to be carried out for each individual line in this case (or species/varieties), whereas this approach may give useable representative canopies within a very short time span.

There was good correspondence between manual and digitized canopy structural measurements, notably the extinction coefficient k . The differences in k seen here are within the range expected for wheat but still show variation that would be expected to result in differences in the relationship between intercepted light and potential productivity (Murchie and Reynolds, 2012). The percentage difference in leaf area between real and reconstructed plants using this method has previously been found to be low (4%; Pound *et al.*, 2014), and a value of 1% was found here (data not shown). The reconstruction method was also able to accurately reproduce similar percentages of stem versus leaf material (around 30% stem content by area for each of the three lines).

The predicted light distribution taken from ray- tracing data shows the spatial and temporal heterogeneity within all three wheat canopies resulting from their differences in architecture. Achieving such high resolution with measurements in the canopy would not be possible, and any attempt would require vast amounts of sensors and data processing. This tool could provide a low-cost but detailed method for phenotyping for both small-scale and advanced systems.

Accounting for Carbon Loss at the Whole-Canopy Level

We have used the highly accurate digitized 3D reconstructions to scale up photosynthetic processes to the whole-canopy level. Because the ray-tracing parameters day and latitude were kept the same and all gas exchange and fluorescence measurements were taken within the same period, any observed differences in photosynthetic activity were associated with genetically determined differences (e.g. plant architecture) and not with diurnal solar movement.

Susceptibility to photoinhibition and its dynamics is dependent on species, cultivar, and conditions, and thus, changes in Fv/Fm are not fixed (Murchie *et al.*, 1999; Demao and Xia, 2001; Demmig-Adams *et al.*, 2012). Values of photosynthetic capacity and the dark- adapted fluorescence parameters were used for model parameterization. Previous models used a photon dose effect to predict levels of photoinhibition (Werner *et al.*, 2001; Zhu *et al.*, 2004). We did not adopt this approach, because we wished to avoid potential genotype-specific differences in required dosage. We chose instead to use field measurements of Fv/Fm to predict photoinhibition at different canopy positions and times of day (Leverenz, 1994), because Fv/Fm is an actual measure of PSII quantum yield (Murchie and Lawson, 2013). To present a realistic picture of the potential for the impact of photoinhibition on canopy photosynthesis, variation in the dynamics of photoinhibition was explored in two different scenarios (results in Fig. 7.8, A and B; dynamics in Supplemental Fig. S7.4). In the first scenario, we restricted simulated photoinhibition to the hours surrounding midday (commonly seen for fast- growing plants, such as cereals; Murchie *et al.*, 1999), and in the second scenario, we assumed that it would start from the hours after dawn, which is more commonly seen in slower-growing stress-tolerant plants. When the dynamics are altered to represent depression in Fv/Fm over the whole day (scenario 2), the percentage reduction in carbon gain is much greater (Fig. 7.8B). These results indicate the flexibility of this modelling technique and highlight the impact of precise architecture for different photoinhibition dynamics.

Using measured photoinhibition data in the field, we have found up to a 5.6% (scenario 1) or 13.7% (scenario 2) reduction in carbon gain solely because of photoinhibition with the parent line exhibiting the smallest amount of carbon loss (line 2 had the greatest amount, and line 1 had an intermediate amount). This loss is largely caused by the measured differences in Fv/Fm and thus, the resultant SF between lines in the uppermost layer. The parent line has a more upright, straight-leaved phenotype, whereas line 2 exhibits a greater amount of leaf curling, particularly in the top layer, with line 1 exhibiting an intermediate phenotype. It is highly likely that this was a result of the canopy architecture and not inherent genetic differences in photoinhibition susceptibility between the lines, which are shown by Figure 7.8D. It is established that the leaf angle in relation to solar position is a strong determinant of radiation and heat load (He *et al.*, 1996; Murchie *et al.*, 1999).

The higher potential productivity of canopies with vertical leaves has been well documented and is largely because of a combination of higher optimal cLAI and a lowered overall state of photosynthetic saturation of the crop canopy (Murchie and Reynolds, 2012; Song *et al.*, 2013). Our data provide a more sophisticated analysis of real in-canopy light distribution, and we conclude that the state of light saturation of the upright canopy (parent line) was actually higher than that of the closed canopy (line 2). The proportion of leaves in a severely light-limited state is, therefore, of critical importance (Murchie *et al.*, 2002; Long *et al.*, 2006). Figure 7.8 shows that the parent line is closer to saturation at the top and middle layers (compared with line 2), has a higher canopy photosynthesis, and also, has spare capacity for increasing the overall canopy photosynthetic rate in all layers regardless of photoinhibition.

It is important to calculate percentage carbon loss caused by lowered quantum yield. Our three contrasting wheat canopies have inherent differences in potential canopy photosynthesis (shown above). The values observed are generally in line with a numerical study based on artificially constructed canopies that observed a decline of daily photosynthesis of 6% to 8% (Werner *et al.*, 2001). Zhu *et al.* (2004) found a 12% to 30% decrease of daily integral

carbon uptake because of thermal dissipation of absorbed light energy with the largest reduction from a top layer.

Managing and Mitigating Photoinhibition

Here, we extend earlier work on the impact of photoinhibition at the canopy scale, and we reveal how canopy structure, photosynthesis, and photoinhibitory loss are intimately connected within unique highly accurate 3D reconstructions of field-grown plants. We use the light-induced lowering of quantum yield in optimal conditions where there is no other stress factor present that may preinduce a lowered F_v/F_m value. Accumulation of carbohydrate has been suggested in some species to precede photoinhibition. However, this is highly unlikely in fast-growing unstressed cereals where diurnal patterns of leaf carbohydrate do not follow patterns of photoinhibition (Murchie *et al.*, 2002; Demmig-Adams *et al.*, 2012). In terms of productivity, the best strategy is of course to minimize photoinhibition in all circumstances at the biochemical level. Photoprotective mechanisms, such as the xanthophyll cycle and PsbS-dependent quenching, are known to reduce the level of photoinhibition in leaves (Li *et al.*, 2002; Niyogi *et al.*, 2005). It has been pointed out that such approaches may need to consider costs as well as benefits of high levels of thylakoid-level photoprotection (Hubbart *et al.*, 2012). If this is the case, then the role of canopy architecture in this tradeoff needs to be carefully considered.

We can discern strategies for dealing with the effects of photoinhibition at this level: restrict substantial levels of photoinhibition to the top layers by closing the canopy to protect the lower layers and ensure a high degree of saturation of the upper layers or attempt a higher overall productivity with a vertical structure but risk a greater impact on canopy carbon gain should photoinhibition occur. The former will result in a canopy with an inherently lower productivity that is still susceptible to localized photoinhibition in upper layers. Previously, it has been shown clearly that upright leaves have a lower susceptibility to photoinhibition (Murchie *et al.*, 1999), and this would seem to be synergistic with the higher inherent productivity of such architecture. However, our data suggest that the tolerance conferred by leaf posture is not

sufficient to avoid loss completely and that upright canopies should be selected to have a high tolerance to photoinhibition on a leaf level.

The importance of photoinhibition may come down to the level of sunshine hours that a crop canopy experiences during key yield-forming stages. For this study, we used sunny days to measure Fv/Fm, and we calculate that such days were restricted to less than 30 d of the total for the postanthesis period. Photoinhibition will be strongest in crops grown in high-yield potential, high-radiation environments, and these would see the greatest loss in yield as a result of photoinhibition alone. This will be true for many irrigated rice and yield environments. In the case of tropical rice, there is known genotypic diversity in susceptibility (Murchie *et al.*, 1999; Demao and Xia, 2001) that may be the result of genetically determined nonphotochemical quenching levels (Kasajima *et al.*, 2011). It is highly probable that we can improve biomass and yield by optimizing photoinhibition, and this requires understanding of the existing canopy architecture. The next step is to isolate genetic variation in photoprotection (e.g. resulting from PsbS expression) by incorporating the effect of canopy position.

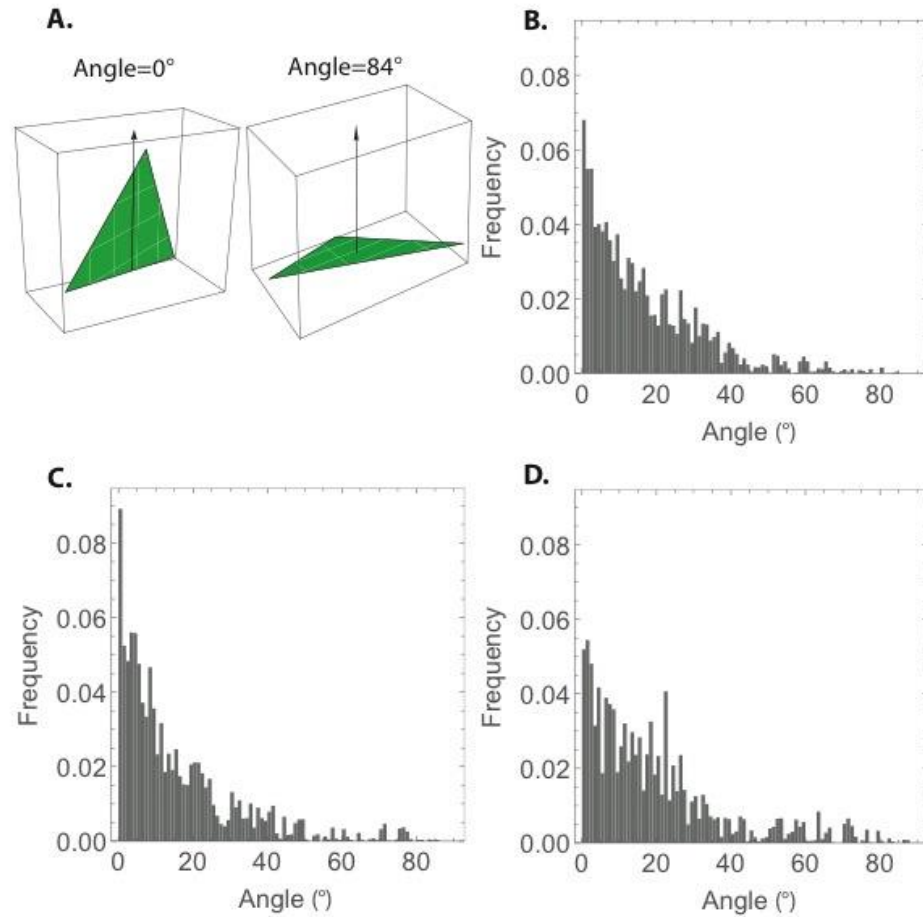
Conclusion

In this study, we used an empirical model to investigate the interactions between plant architecture and solar irradiance. Unique highly realistic digital reconstruction combined with simulation of light intercepted by leaves and prediction of carbon assimilation represent a unique method to investigate complex plant- environment interactions and provide a method of scaling up to the whole-canopy level and exploring the importance of canopy architecture.

Plant phenotyping is an important tool in screening crops for future breeding. As we show in this study, image-based 3D plant reconstruction was successfully applied to test how plant architecture influences photosynthesis and photoinhibition. The extracted features (cLAI, vertical profile, and angle distribution) showed clear differences between three contrasting wheat lines. In a similar way, all wheat lines showed differences in canopy light distribution. We found that larger carbon losses were associated with a higher light extinction coefficient. Whole-canopy carbon gain can be protected (under photoinhibition) if spatial distribution of light in the lower canopy is improved.

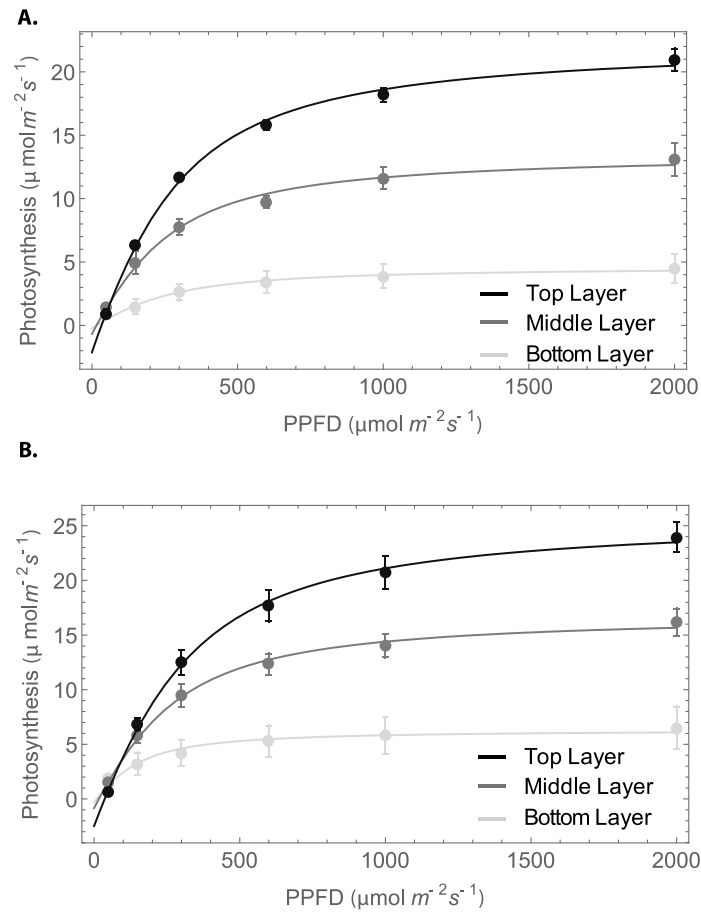
Supplementary Material

Supplementary Figure S7.1



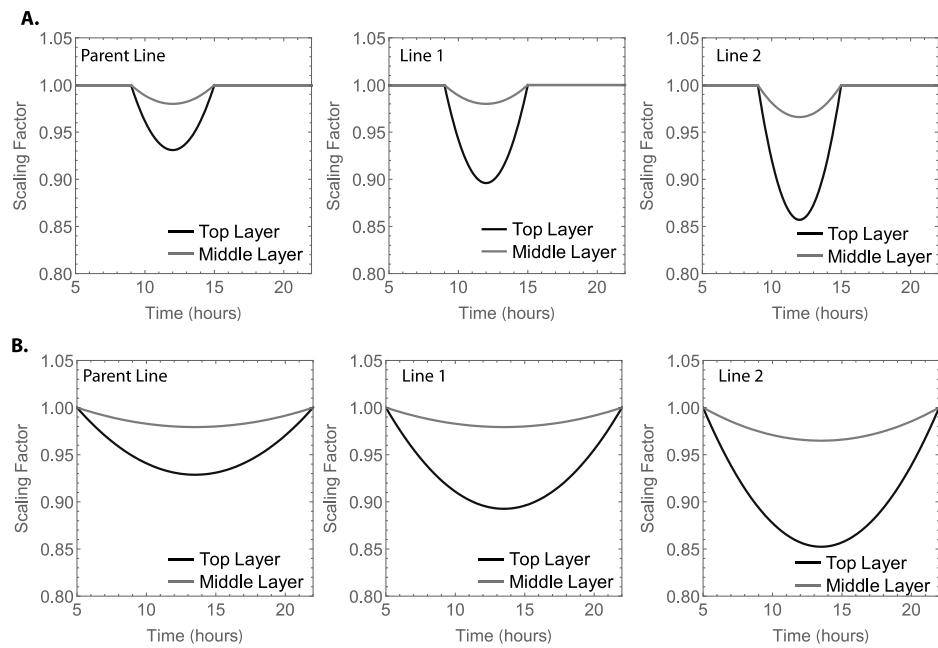
Supplementary Figure S7.1: (A) The triangle angle was determined with respect to vertical: two triangles with angles 0° and 84° are shown. (B-D) Histograms showing the frequency of triangle angle in each canopy, relative to the vertical: Parent Line (B), Line 1 (C), and Line 2 (D).

Supplementary Figure S7.2



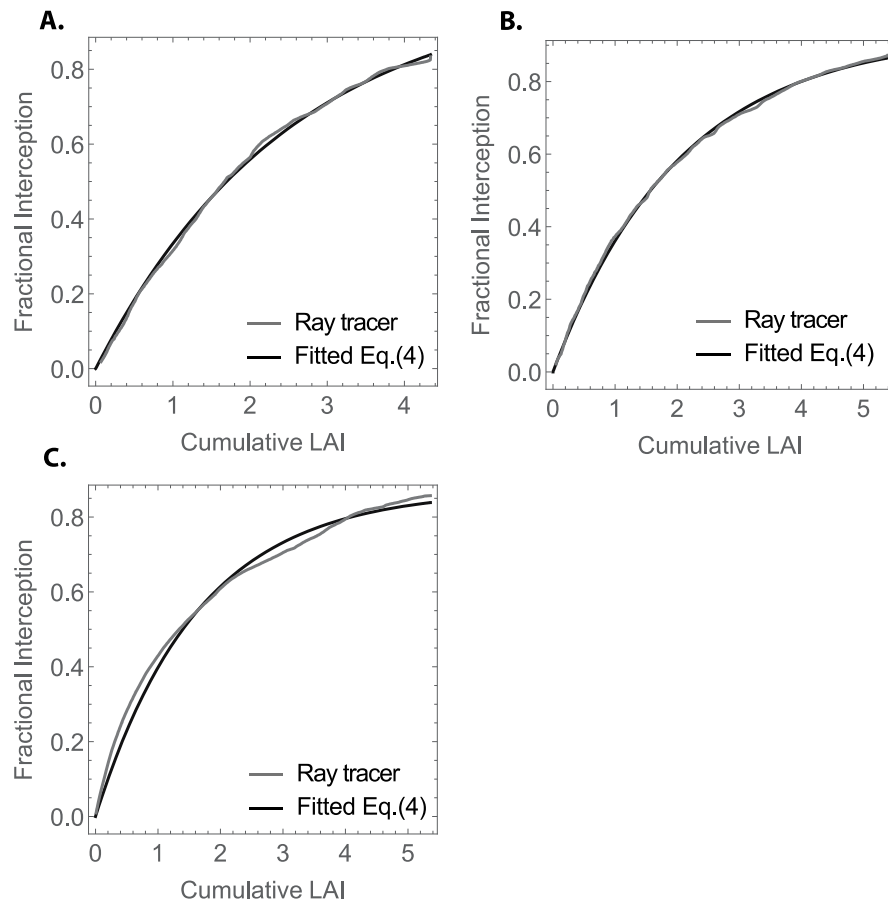
Supplementary Figure S7.2: Values of the maximum photosynthetic capacity for each layer were obtained from fitted Light Response Curves. Graph shows experimental data (mean \pm se of 3 measurements) and fitted curves (Eq.5) for: (A) Parent Line, (B) Line 1.

Supplementary Figure S7.3



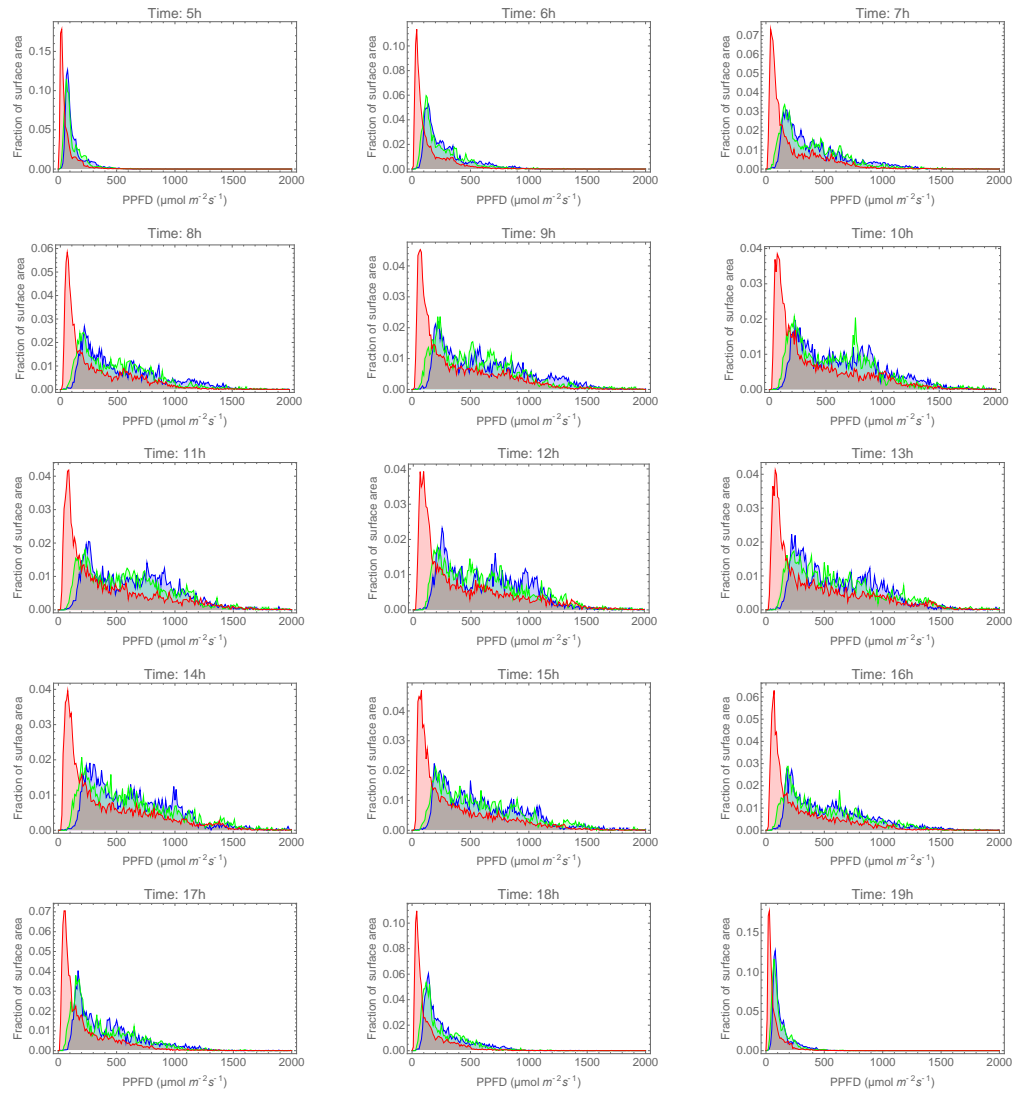
Supplementary Figure S7.3: Changes in scaling factor over the course of the day for the top (black) and middle (grey) layers: (A) Scenario 1. (B) Scenario 2. Left column corresponds for Parent Line, middle column- Line 1, and right column- Line 2.

Supplementary Figure S7.4



Supplementary Figure S7.4: Fractional interception as a function of cumulative LAI: data from canopy reconstruction and ray tracing (grey) and fitted Eq.(4) (black). (A) Parent Line. (B) Line 1. (C) Line 2.

Supplementary Figure S7.5



Supplementary Figure S7.5: Frequency of PPFD values according to the fraction of surface area received at the top layer at different times during day. Blue=Parent Line, Green=Line 1, Red=Line 2

Supplementary Table S7.1

Leaf angle for measured versus reconstructed canopies

	Line	Top Leaf °	Middle Leaf °	Bottom Leaf °
Reconstructed	Parent	31.3	30.1	32.7
Canopy	1	35.3	40.0	33.0
	2	31.5	35.5	34.0
Reconstructed	Parent	30.0	30.0	32.5
Canopy	1	36.2	37.2	34.6
	2	32.8	35.6	31.2

Supplementary Table S7.2

Reconstruction and Canopy details

Line	Reconstructed LAI vs. Real canopy LAI (%)	Canopy K (from reconstructions)
Parent	-1.72	0.40
1	-3.25	0.49
2	-0.90	0.61

Supplementary Table S7.3

Leaf versus stem area for measured and reconstructed canopies

	Total Leaf area	Stem area	% Stem	Average%
Parent Line				
R1	271.3	79.6	22.67	26.638
R2	348.3	153.6	30.61	
Line 1				
R1	425.7	149.9	26.04	26.245
R2	550.9	198.1	26.45	
Line 2				
R1	328.2	129.3	28.27	27.678
R2	384.1	142.7	27.09	

Supplementary Table S7.4

Symbol definitions.

Symbol	Definition	Values/units
$cLAI$	Cumulative Leaf Area Index	
d	Depth through the canopy	mm
d_i	Depth of triangle i	mm
d_k^L	Lower limit of depth for k th layer	mm
d_k^U	Upper limit of depth for k th layer	mm
Δd	Step for depth calculations	1 mm
k	Light extinction coefficient	
n	Number of triangles in 3D-reconstruction	
t	Time	hours
t_0	Onset of photoinhibition period	hours
t_N	Finish of photoinhibition period	hours
x_i^k, y_i^k, z_i^k	Spatial coordinates of k th point on i th triangle	mm
C	Carbon gain per unit leaf area	$\text{mol m}^{-2} \text{s}^{-1}$
F	Fractional interception	
F_0	Minimal level of florescence	
F_m	Maximum level of florescence	
F_v/F_m	Ratio between variable and maximum florescence	
$F_v/F_{m_{max}}$	The maximum value of F_v/F_m	0.83
I	Indicator function	
$L_i(t)$	Instantaneous photosynthetic photon flux density (PPFD) for i th triangle	$\mu\text{mol m}^{-2} \text{s}^{-1}$
$L_0(t)$	Instantaneous photosynthetic photon flux density received on a horizontal surface	$\mu\text{mol m}^{-2} \text{s}^{-1}$
P_{max}	Maximum photosynthetic capacity	$\mu\text{mol m}^{-2} \text{s}^{-1}$
P_i	Daily carbon assimilation at i th triangle	$\mu\text{mol m}^{-2} \text{s}^{-1}$
P_i^{PIH}	Daily carbon assimilation under photoinhibition at i th triangle	$\mu\text{mol m}^{-2} \text{s}^{-1}$
R_D	The rate of dark respiration	$\mu\text{mol m}^{-2} \text{s}^{-1}$

S_i	Area of triangle i	mm^{-2}
$SF(t)$	Scaling factor at time t	
SF_{12}	Scaling factor value at noon	
α	Fraction of the maximum photosynthetic capacity used for dark respiration	0.1
θ	Convexity of light response curve	
Φ	Maximum quantum yield	

Chapter 8: Modelling the effect of dynamic acclimation on photosynthesis

Paper as published in the Journal of Experimental Botany

Chapter 8 uses an empirical model of dynamic acclimation in order to predict the optimal P_{\max} based on the past light history. This has been published in the Journal of Experimental Botany (Retkute *et al.* 2015. 66: 2437–2447), so is presented in “paper format”.

Author contribution:

Project supervision performed by OE Jensen, SP Preston and EH Murchie

Concept development by R Retkute, SE Smith-Unna, RW Smith, OE Jensen, SP Preston and EH Murchie

Model creation performed by R Retkute

Biological advice and model aid provided by AJ Burgess

Experimental data and advice provided by GN Johnson

Paper construction performed by R Retkute, OE Jensen, SP Preston and EH Murchie with assistance of all authors

Paper editing performed by AJ Burgess

Exploiting heterogeneous environments: does photosynthetic acclimation optimize carbon gain in fluctuating light?

Renata Retkute, Stephanie E. Smith-Unna, Robert W. Smith, Alexandra J. Burgess, Oliver E. Jensen, Giles N. Johnson, Simon P. Preston and Erik H. Murchie

Abstract

Plants have evolved complex mechanisms to balance the efficient use of absorbed light energy in photosynthesis with the capacity to use that energy in assimilation, so avoiding potential damage from excess light. This is particularly important under natural light, which can vary according to weather, solar movement and canopy movement. Photosynthetic acclimation is the means by which plants alter their leaf composition and structure over time to enhance photosynthetic efficiency and productivity. However there is no empirical or theoretical basis for understanding how leaves track historic light levels to determine acclimation status, or whether they do this accurately. We hypothesized that in fluctuating light (varying in both intensity and frequency), the light-response characteristics of a leaf should adjust (dynamically acclimate) to maximize daily carbon gain. Using a framework of mathematical modelling based on light-response curves, we have analysed carbon-gain dynamics under various light patterns. The objective was to develop new tools to quantify the precision with which photosynthesis acclimates according to the environment in which plants exist and to test this tool on existing data. We found an inverse relationship between the optimal maximum photosynthetic capacity and the frequency of low to high light transitions. Using experimental data from the literature we were able to show that the observed patterns for acclimation were consistent with a strategy towards maximizing daily carbon gain. Refinement of the model will further determine the precision of acclimation.

Introduction

Light is one of the most variable resources for plants and is capable of changing by several orders of magnitude within fractions of a second. Solar movement, climate, clouds, canopy movement in the wind and canopy architecture can combine to produce a complex pattern of light in time and space. This has profound consequences for photosynthetic carbon assimilation in leaves, which can be slow to respond to changes in light. Light can rapidly shift from being limiting for photosynthesis to high levels that are sufficient to saturate the photosynthetic apparatus. Over the short term (seconds and minutes), the mechanisms that plants use to deal with these changes are relatively well understood: it is possible to invoke enzyme activation states, metabolite concentrations and the state of energisation of the thylakoid membrane as a 'memory' of short-term past light history (Murchie *et al.*, 2009; Garcia-Plazaola *et al.*, 2012; Horton and Ruban, 2004). Short-term responses are regulated by processes such as phosphorylation of thylakoid components, allosteric regulation of enzymes and the physical state of the thylakoid (Tikkanen *et al.*, 2010, 2012; Ruban *et al.*, 2012). Two examples of processes on such short timescales are photosynthetic induction – the delay in the rise in carbon assimilation immediately following a light increase (Percy *et al.*, 1997) - and thylakoid photoprotective processes which result in a decline in quantum efficiency of photosynthesis as a response to excess light (Demmig-Adams and Adams, 1992; Murchie and Niyogi, 2011).

Longer-term responses, which occur over the timescale of days in response to changes in environmental conditions, are termed acclimation and are characterised by changes in leaf phenotype. Acclimation describes the alterations in quantity and stoichiometry of photosynthetic components - including Rubisco, cytochrome-b/f complexes, light harvesting complexes, ATPase and enzymes involved in carbohydrate synthesis - resulting in long-term changes to leaf properties such as photosynthetic capacity, dark respiration and the light compensation point (Bjorkman, 1981; Murchie and Horton, 1997, 1998; Yano and Terashima, 2001; Walters, 2004; Anderson *et al.*, 1995; Athanasiou *et al.*, 2012). One can consider 'sun' and 'shade' leaf

physiology as two extreme states of acclimation (Björkman, 1981; Murchie and Horton, 1997) and a scale of response between them is not necessarily linear (Bailey *et al.*, 2001). Exploration of the adaptive significance of acclimation under complex light patterns has however been little studied but is key to understanding the limits placed on plants in natural environments.

Two types of acclimation can be distinguished: the first refers to responses during leaf development and plastid biogenesis that determine cell numbers and size and leaf shape, that are largely irreversible (Weston *et al.*, 2000; Murchie *et al.*, 2005); the second type, here termed dynamic acclimation, is defined as the reversible changes that can occur in mature tissues in response to changes in the environment (Walters and Horton, 1994). The extent of the propensity to acclimate will depend on the plant's genotype, which will, to a greater or lesser extent, match the environment to which it is adapted through evolution. Species from different ecological niches show differing abilities to acclimate (Murchie and Horton, 1997, 1998; Anderson *et al.*, 1995).

The acclimation state of a leaf can be readily defined in terms of its light response curve for photosynthesis. In the absence of light the net rate of CO₂ exchange will be negative and correspond to a dark respiration rate R_D . With increasing amounts of light, the rate of photosynthesis, measured as the rate of CO₂ uptake from the atmosphere, will increase, until a saturation point is reached. Experimentally, such responses are typically measured over a period of minutes as a light-response curve and can be modelled in C₃ leaves using a non-rectangular hyperbola (Fig. 8.1A; see also Ogren *et al.*, 1993; Leverenz *et al.*, 1992; Sharkey *et al.*, 2007) to relate net photosynthetic rate, P , (photosynthetic CO₂ uptake minus respiration rate) to photosynthetic photon flux density (PPFD), L . This curve is a useful reflection of the leaf's current acclimation state and can be used to calculate its productivity. The slope of the light-response curve at $L=0$ describes the maximum efficiency with which light can be converted into fixed carbon. This is called the maximum quantum yield, ϕ . The net photosynthesis rate, P , rises until it reaches a maximum, P_{\max} . The dark respiration rate R_D is the net rate of CO₂ exchange in darkness (i.e. at $L=0$,

where the curve meets the vertical axis). The value of L at which the curve crosses the horizontal axis (i.e. where the respiration rate equals the photosynthesis rate) is termed the light compensation point, where the PPFD takes the value L_c .

The non-rectangular hyperbola depends on parameters P_{\max} , R_D , ϕ and a convexity parameter, θ , which enable it to model C_3 leaves, whether acclimated to low or to high light intensities. The shape of this curve will depend on the light absorption properties of the leaf (chlorophyll content, leaf thickness, etc.) and the relative concentrations of the different structures (proteins, cofactors) involved in assimilating the light energy (Murchie and Horton, 1997; Adamson *et al.*, 1991; Chow *et al.*, 1991). Despite the variation seen between and within species there are conserved trends that are useful for acclimation modelling approaches. The maximum quantum yield is unaffected by (non-stressful) growth conditions (Long and Drake, 1991). The leaf absorptance is unlikely to be substantially altered during dynamic acclimation (Percy and Sims, 1994). The rate of dark respiration R_D is known to vary depending on acclimation state, with low-light-acclimated leaves having lower R_D than high-light-acclimated leaves. R_D can be treated as being dependent on P_{\max} according to the relationship $R_D = -\alpha P_{\max}$, where α is assumed to be constant (Givnish, 1998; Niinemets and Tenhunen, 2007). Furthermore, in this paper we consider experimental conditions where the basic photosynthetic responses (maximum quantum yield, ϕ , and convexity, θ) for a given species are known and therefore we assume that a leaf's acclimation state can be characterised using the value of P_{\max} .

To account for the change in incident light, leaves presumably set their acclimation state based on a combination of current environmental signals and accumulated information from the past. When plants are transferred from low to high light, they typically acclimate to increase their maximum photosynthetic capacity (P_{\max}), *i.e.* the light-saturated rate of photosynthesis. This process takes place over a period of 5-10 days, depending on species (Athanasίου *et al.*, 2010). Transfer from high to low light results in the

opposite response, *i.e.* reducing P_{\max} (Walters, 2005). Dynamic acclimation is, at least to some extent, mechanistically different from developmental acclimation (Athanasίου *et al.*, 2010, Murchie and Horton, 1997). However, little is known about the way in which light signals are integrated through time to drive the acclimation response.

Optimal dynamic acclimation would track environmental conditions in real time, and match maximum photosynthetic capacity to the light level that the leaf directly experiences. However, as discussed above, acclimation is not an instantaneous process, and there is a time lag before the leaf fully responds to changes (Walters and Horton, 1994; Athanasίου *et al.*, 2010). The lag for increasing P_{\max} is thought to be longer than that for decreasing P_{\max} , reflecting the fact that more proteins must be synthesised and maintained. Hence, the plant must invest carbon, nitrogen and other resources in order to sustain a higher photosynthetic capacity (Athanasίου *et al.*, 2010).

Mathematical models have been proposed to describe the response of plant photosynthetic processes to changes in external light conditions. These models have addressed the behaviour of key biochemical processes and plant physiology under variable light (Gross, 1982; Kirschbaum *et al.*, 1988, 1998; Pearcy, 1990; Pearcy *et al.*, 1997), and changes in the dynamics of photosynthetic machinery due to environmental changes (Ebenhoeh *et al.*, 2011; Stegemann *et al.*, 1999; Zaks *et al.*, 2012), to activation of enzymes and sucrose synthesis (Zhu *et al.*, 2013), and the role of crop canopy architecture on canopy photosynthesis (Song *et al.*, 2013; see Porcar-Castell and Palmroth, 2012 for a review of modelling photosynthesis under temporal variation in sunfleck activity). However, all of these models focus on time scales of seconds to minutes and all assume that the photosynthetic apparatus of the system modelled is constant.

It is often assumed that acclimation involves a strategy of optimisation geared toward maximum carbon gain in a given environment (Pons, 2012) but here we argue that our understanding is incomplete for complex light patterns.

There are few empirical experiments in the literature that explored how changes in light pattern influence the changes in P_{\max} (Chabot *et al.*, 1979; Watling *et al.*, 1997) and even fewer that utilised light response curves (Yin and Johnson, 2000). Two of the available mechanisms discussed in the literature involve peak PPFD and integrated PPFD (Niinemets and Anten, 2009). No statistically significant differences in P_{\max} were found between plants grown under either constant or fluctuating light of the same integrated PPFD (Watling *et al.*, 1997). Extensive study under conditions of either constant integrated PPFD, but variable peak PPFD, or constant peak PPFD, but variable integrated PPFD, concluded that the integrated PPFD was a stimulus for photosynthetic acclimation to light (Chabot *et al.*, 1979). However later work noted that photosynthetic capacity changed in response to growth in fluctuating light patterns under the same integrated and peak PPFD, but varying duration of the high and low light period (Yin and Johnson, 2000). Therefore, the strategies that plants use are not completely understood and future studies should move beyond the concept of integrated vs peak PPFD.

In this study, we use mathematical modelling to investigate the optimal acclimation state for leaves that are subjected to a light pattern that varies. We propose a new approach that can be used to empirically determine how successful plants are at optimising carbon gain in such conditions. We do not attempt to model how acclimation state changes with time, but our aim is instead to determine the efficiency of different fixed acclimation states for given light patterns.

Materials and Methods

Theoretical framework

The net photosynthetic rate, P , as a function of PPFD, L , and maximum photosynthetic capacity, P_{\max} , can be described by different mathematical formulas, for details see Supplementary Text. In this study we use a non-rectangular hyperbola model proposed by Prioul and Chartier (1977) see Fig. 8.1A and Eq. (1).

$$P(L, P_{\max}) = \frac{fL + (1+a)P_{\max} - \sqrt{(fL + (1+a)P_{\max})^2 - 4qfL(1+a)P_{\max}}}{2q} - aP_{\max} \quad (1)$$

Here L is the PPFD incident on a leaf ($\mu\text{mol m}^{-2} \text{s}^{-1}$), ϕ is the maximum quantum yield, α corresponds to the fraction of the maximum photosynthetic capacity used for dark respiration, and the parameter θ determines the curvature of the light-response curve.

We define the daily carbon gain, C , (mol m^{-2}), in a fluctuating or constant environment as the integrated carbon over the time period $t \in [0, T]$:

$$C(L(t), P_{\max}) = \int_0^T P(L(t), P_{\max}) dt \quad (2)$$

In this study we have sought to predict a maximum photosynthetic capacity, P_{\max}^{opt} , as the P_{\max} which represents maximum daily carbon gain for a given light pattern. We compared P_{\max}^{opt} with \bar{P}_{\max} , which is defined as the P_{\max} at which the maximum daily carbon gain would be attained if the variable light pattern, $L(t)$, were replaced by its average \bar{L} over the time T .

The rate of photosynthesis at any instant is also determined by the state of induction of photosynthesis, which is a complex condition that represents the overall activation state of enzymes and electron carriers, pool sizes of photosynthetic metabolites and stomatal conductance (Kuppers and Pfiz, 2009;

Gross, 1982). Induction state will determine the time taken to reach a steady state following an increase in light intensity.

Experimental data show that responses of photosynthesis to increases in irradiance are not instantaneous (Pearcy *et al.*, 1997). However, the available data is too limited for us to incorporate and parameterise accurately within our own model e.g. using an induction model such as that of Pearcy *et al.*, (1997). Instead, as a simple way to capture ‘fading memory’ of the recent light pattern, we introduce a time-weighted average for the light:

$$\check{L}_\tau(t) = \frac{1}{\tau} \int_{-\infty}^t L(t') e^{-(t-t')/\tau} dt'. \quad (3)$$

Here we have used an exponentially decaying weight. This represents the concept that the leaf response to the previous light pattern is more strongly dominated by recent events. Thus for $\tau=0$ the time-weighted averaged light pattern corresponds to its instantaneous value, whereas for $\tau>0$, the time-weighted averaged light pattern relaxes over a timescale τ following a sudden change in $L(t)$.

Experimental data

In Yin and Johnson (2000), plants of *Arabidopsis thaliana* were grown for 4-6 weeks at light intensity of $100 \mu\text{mol m}^{-2} \text{s}^{-1}$, then transferred to either a light environment that was constant during the photoperiod or an environment in which the light fluctuated between periods of low light intensity ($100 \mu\text{mol m}^{-2} \text{s}^{-1}$) and high light intensity ($475 \mu\text{mol m}^{-2} \text{s}^{-1}$) lasting 15 min, 1 h or 3 h, for 7 days. The integrated PPFD for all fluctuating light patterns was $12.42 \text{ mol m}^{-2} \text{d}^{-1}$. As described by Yin and Johnson (2000), light response curves for oxygen evolution in leaf discs were taken in saturated CO_2 (5%) at 20°C on leaf discs from dark-adapted leaves and therefore it is likely that light was the dominant limiting factor for photosynthesis in this experiment.

Model parameterisation

Parameters were estimated from light response curves of *A. thaliana* grown under constant light conditions at $100 \mu\text{mol m}^{-2} \text{s}^{-1}$ and $475 \mu\text{mol m}^{-2} \text{s}^{-1}$ with a 12h photoperiod (Yin and Johnson, 2000). The non-rectangular hyperbola in Eq. (1) was fitted to the means of 5-12 measurements using a least-squares method. We inferred the following values: $\alpha = 0.2$, $\phi = 0.055$ and $\theta = 0.96$. Experimental data together with the fitted light response curves are shown in Fig. 8.1A. These values are comparable with other experimental studies: $\phi = 0.043$ for *A. thaliana* grown in controlled environment chambers with a 12 h photoperiod at a PPFD of $250 \mu\text{mol m}^{-2} \text{s}^{-1}$ (Donahue *et al.*, 1997); and $\alpha = 0.15$ was found in Niinemets and Tenhunen (2007). All model analysis and model validation is done using these fitted parameter values.

As the same parameter values fitted both data sets (i.e. at $100 \mu\text{mol m}^{-2} \text{s}^{-1}$ and $475 \mu\text{mol m}^{-2} \text{s}^{-1}$), this suggests that photosynthetic acclimation to different growth conditions can be described using changes in P_{max} .

We calculated the time-weighted average of a given light pattern according to Eq.(3) with τ from 0.1h to 1h and calculated daily carbon gain using Eq.(2) for P_{max} values from 0 to $80 \mu\text{mol m}^{-2} \text{s}^{-1}$ with step 0.01. We assigned $P_{\text{max}}^{\text{opt}}$ as a value that gives the highest daily carbon gain. To determine the best fit for τ we calculated a mean squared error between predicted and experimentally measured light response curves for plants grown under 6 h switching period. This gave value $\tau = 0.3\text{h}$.

Symbol	Definition	Units
k	Fraction of time period spend under L .	[0,1]
C	Daily carbon gain	mol m ⁻²
L	Instantaneous photosynthetic photon flux density (PPFD)	μmol m ⁻² s ⁻¹
\bar{L}	Average of $L(t)$ over the day	μmol m ⁻² s ⁻¹
L_c	Light compensation point	μmol m ⁻² s ⁻¹
L_-	Lower PPFD for two-level fluctuating light	100 μmol m ⁻² s ⁻¹
L_+	Higher PPFD for two-level fluctuating light	475 μmol m ⁻² s ⁻¹
$\check{L}_\tau(t)$	Time-weighted average $L(t)$ calculated for a given τ	μmol m ⁻² s ⁻¹
P	Net photosynthetic rate	μmol m ⁻² s ⁻¹
P_{\max}	Maximum photosynthetic capacity	μmol m ⁻² s ⁻¹
P_{\max}^{opt}	Predicted P_{\max} for a given $L(t)$ over a day	μmol m ⁻² s ⁻¹
\bar{P}_{\max}	Predicted P_{\max} for \bar{L}	μmol m ⁻² s ⁻¹
R_D	Dark respiration rate	μmol m ⁻² s ⁻¹
S	Switching period	h
T	Length of day	24h
α	Fraction of the maximum photosynthetic capacity used for dark respiration	0.2
θ	Convexity of light response curve	0.96
τ	Scale of a time weighted averaging	h
ϕ	Maximum quantum yield	0.055

Table 8.1: Symbol definitions.

Results

Quasi-steady net photosynthetic rate

First we look at a quasi-steady state, where leaves are subjected to a given ‘constant’ light intensity. Under such conditions, we model the relationship between net photosynthetic rate, P (L , P_{\max}), maximum photosynthetic capacity, P_{\max} , and the instantaneous PPFD, L , without considering the effect of photosynthetic induction.

The contours of constant P in the positive quadrant of the (L, P_{\max}) -plane represent what can be termed the *light-response surface*. Fig. 8.1B shows contours for Eq. (1) for both varying P_{\max} and L . Traversing such surface horizontally at a fixed value of P_{\max} gives a light response curve similar to ones shown in Fig. 8.1A. If instead one follows the light-response surface for a fixed light PPFD (the grey line in Fig. 8.1B at $L=200 \mu\text{mol m}^{-2} \text{s}^{-1}$) this will give P as a function of P_{\max} . Fig. 8.1C shows that there is a value of P_{\max} that maximises P ; in this case it is $11.8 \mu\text{mol m}^{-2} \text{s}^{-1}$. This is a hypothetical example to help us illustrate a mechanism behind photosynthetic acclimation.

Acclimation is a long-term process in which we assume maximum photosynthetic capacity is adjusted to a particular light intensity, *i.e.* if PPFD is set to any fixed value L , acclimation involves moving vertically in Fig. 8.1B until the value of P_{\max} maximises the net photosynthetic rate, P . For any L there is a well-defined P_{\max} that maximises P (Fig. 8.1C); this corresponds to a point at which a contour of constant P in the (L, P_{\max}) -plane is vertical, as indicated by the black diagonal line in Fig. 8.1B. Under higher light conditions, the P_{\max} that maximises P for a given L is larger (moving along the black diagonal line in Fig. 8.1B).

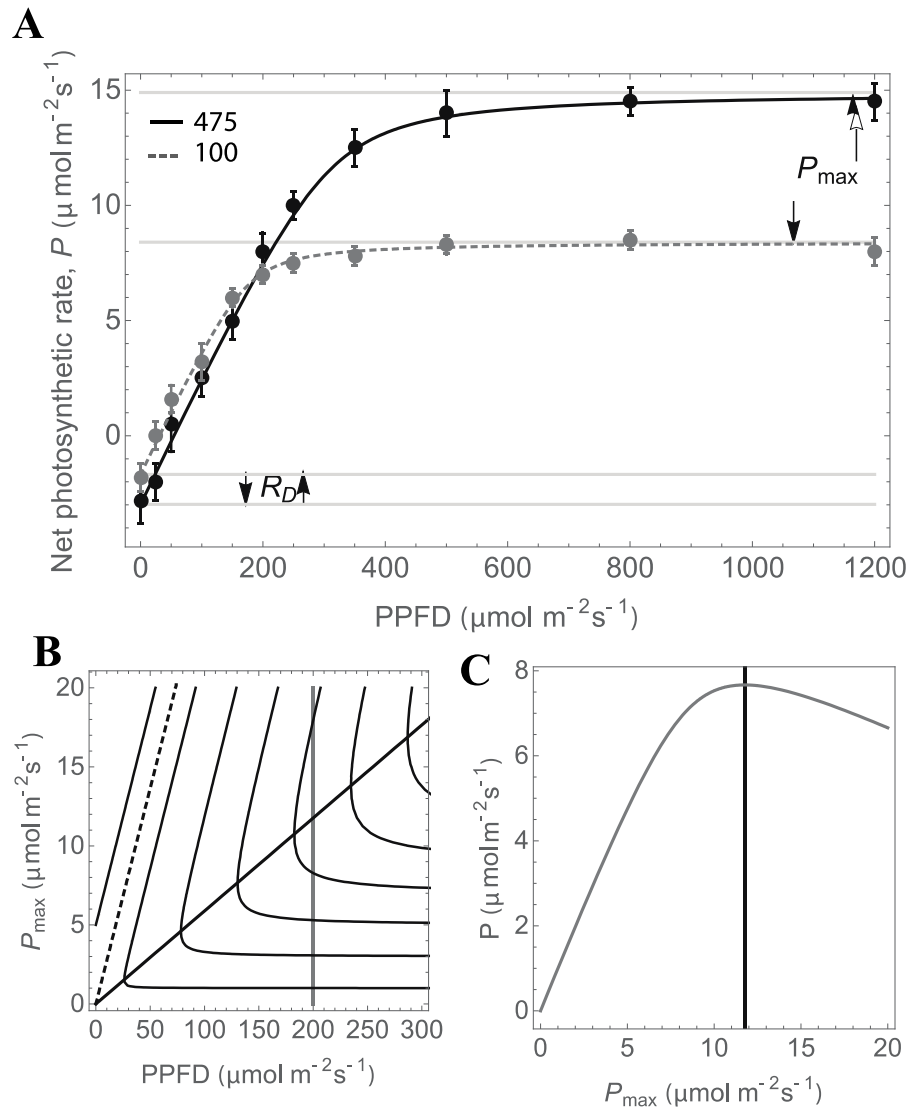


Figure 8.1: (A) Experimental data (Yin and Johnson, 2000) and fitted Eq.(1) for *A.thaliana* grown under 475 $\mu\text{mol m}^{-2}\text{s}^{-1}$ (black) and 100 $\mu\text{mol m}^{-2}\text{s}^{-1}$ (grey) PPFDs. Data are mean \pm SE of 5-12 measurements. The light compensation point is where the curves cross the horizontal axis $P = 0$. (B) The light-response surface: contours of constant net photosynthetic rate P are plotted in the positive quadrant of the (L, P_{max}) -plane. The dotted line indicates the light compensation point along which $P=0$ and the solid diagonal line is the locus of points for which P is maximised for fixed L . (C) P as a function of P_{max} for a fixed L , corresponding to the vertical (grey) line in (B).

Light pattern: alternation between two light levels

Suppose that light fluctuates between two different intensities, such that, for given time, t , PPFD equals either L_- or L_+ , where $L_- \leq L_+$. In the time period $0 \leq t \leq T$, let the total time for which $L(t) = L_-$ be kT and the total time for which $L(t) = L_+$ be $(1-k)T$, where $0 \leq k \leq 1$. The light pattern with $k=0.7$, $L_- = 100 \mu\text{mol m}^{-2}\text{s}^{-1}$ and $L_+ = 475 \mu\text{mol m}^{-2}\text{s}^{-1}$ is shown in Fig. 8.2A.

Fig. 8.2B shows how the P_{\max}^{opt} under fluctuating light depends on the value of k . The P_{\max}^{opt} under the average light intensity, $\bar{L} = kL_- + (1-k)L_+$, decreases linearly with increasing k , however, the P_{\max}^{opt} under alternation between two light levels responds in a nonlinear manner with respect to the parameter k . The highest rate of change in P_{\max}^{opt} is attained for values of $k < 1/(1+\alpha)$ (for details see the Supplementary text). It is important to observe that P_{\max}^{opt} is larger than \bar{P}_{\max} for $k < 1/(1+\alpha)$ indicating that P_{\max} must typically be elevated in order to attain an optimised response in fluctuating light conditions.

Next, we analysed how the amplitude of fluctuations influences P_{\max}^{opt} by keeping the averaged light intensity constant and setting $k=1/2$, but changing the light intensities L_- and L_+ . We defined intensities as $L_{\pm} = \bar{L}(1 \pm x)$, where $0 \leq x \leq 1$, so that for $x = 1$, for example, light intensity switches between zero and $2\bar{L}$. Figs. 8.2C, D show the fluctuating light pattern and P_{\max}^{opt} as a function of x . In this case, P_{\max}^{opt} is consistently greater than \bar{P}_{\max} by an amount that increases with the amplitude of the light fluctuation.

Light in nature is much more heterogeneous and unpredictable than that considered so far. One simple optimisation problem is to consider how to maximise daily carbon gain given that L is a fluctuating quantity. Analysis based on a small-amplitude approximation (details of which are given in the Supplementary text) shows how P_{\max}^{opt} rises in proportion to x^2 for small values

of x ; this approximation is indicated by the dashed line in Fig. 8.2D. It captures predictions of the numerically computed P_{\max}^{opt} in this example for values of light intensity up to approximately $100 \mu\text{mol m}^{-2} \text{s}^{-1}$.

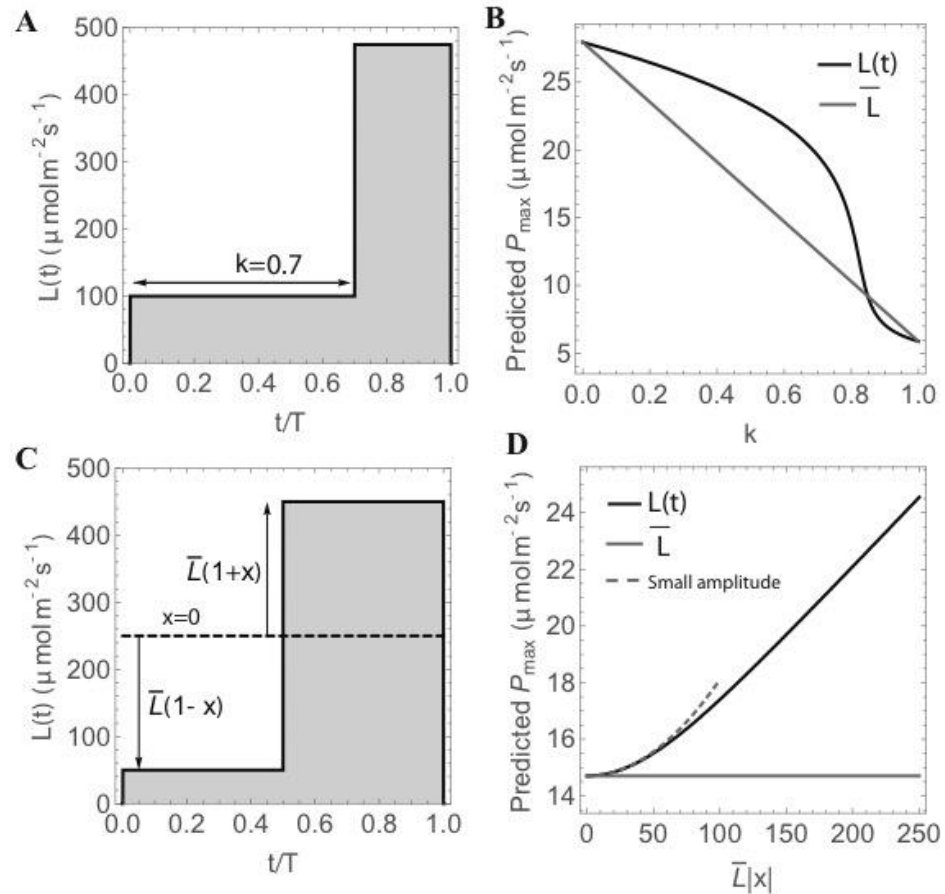


Figure 8.2: (A) Fluctuating light pattern for $k=0.7$; (B) predicted P_{\max} as a function of low light duration, k ; for $L_{-}=100 \mu\text{mol m}^{-2} \text{s}^{-1}$ and $L_{+}=475 \mu\text{mol m}^{-2} \text{s}^{-1}$ (C) Fluctuating light pattern for $k=0.5$ and varying low/high PPFDs; (D) predicted P_{\max} as a function of the amplitude of fluctuations. Light intensity fluctuates between L_{-} and L_{+} , where $L_{-}=100 \mu\text{mol m}^{-2} \text{s}^{-1}$ and $L_{+}=475 \mu\text{mol m}^{-2} \text{s}^{-1}$. In (B) and (D), the grey line corresponds to an averaged light intensity and the black line to the fluctuating light. In (D), the dashed grey line gives a small-amplitude approximation (see Supplement).

Influence of the light intensity switching period

We have considered so far that the leaf reacts to light intensity dynamics in a cumulative manner by determining the fraction of time it has been exposed to various intensities of light. Experimental evidence shows maximum photosynthetic capacity depends on the pattern of switching between high and low light intensity (Yin and Johnson, 2000). To account for this we apply a time-weighted average to the light pattern (see Eq. (3)). We now consider how the light-switching period influences the optimal photosynthetic rate when the leaf has a fading memory.

We set $k = 1/2$, so that $L(t)$ equals L_- or L_+ for equal amounts of time in total, but now vary the number of L_- to L_+ switches within a photoperiod of duration T . The switching period, S , specifies the time required to have a single continuous low light to continuous high light cycle, so that $S=T$ indicates no repeats of the light pattern.

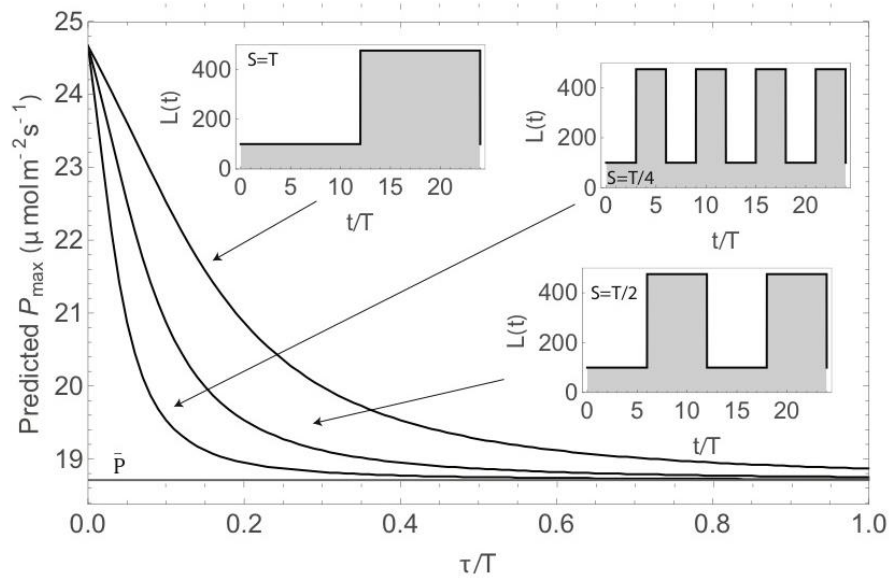


Figure 8.3: Influence of the light switching period, S , and time-weighted average timescale, τ , on P_{\max}^{opt} . Light fluctuated between $L_- = 100 \mu\text{mol m}^{-2}\text{s}^{-1}$ and $L_+ = 475 \mu\text{mol m}^{-2}\text{s}^{-1}$ for periods $S=T$, $S=T/2$ and $S=T/4$ (black lines). The grey line shows the predicted P_{\max} for $\bar{L} = 287.5 \mu\text{mol m}^{-2}\text{s}^{-1}$.

Fig. 8.3 shows how photosynthetic capacity changes as a function of τ for three fluctuating light patterns with switching period $S = T, T/2$ and $T/4$, i.e. the low/high light pattern changes one, twice or four times. As τ increases, P_{\max}^{opt} decreases steadily until it reaches \bar{P}_{\max} , the optimal value when the light pattern is replaced with its average. For a fixed time-averaging timescale τ , the light patterns with shorter switching periods are closer to \bar{L} after the time averaging than the longer switching periods, making P_{\max}^{opt} closer to \bar{P}_{\max} .

Fluctuating light

As a proof of concept we applied our proposed mathematical framework to a light pattern corresponding to a typical diurnal variation in PPFD at a particular point inside a canopy. The direct component of PPFD fluctuates due to the solar movement and canopy architecture; a detailed pattern of PPFD can be obtained using a direct ray-tracing algorithm (Song *et al.*, 2013). Figure 8.4 shows a fluctuating light pattern and a pattern with fixed $L=251.7 \mu\text{mol m}^{-2} \text{s}^{-1}$ over 16 hours, both having the same integrated PPFD. Again, as we increase value of τ , the P_{\max}^{opt} decreases; however, it is higher for fluctuating light compared to the fixed PPFD because of the differing patterns of variation in the light intensity on timescales longer than τ .

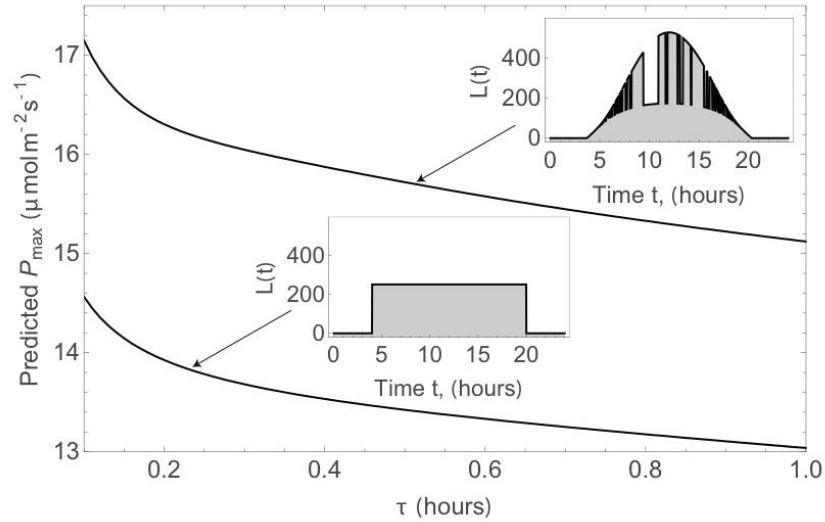


Figure 8.4: Predicted P_{max} as a function of τ for a typical diurnal variation in PPFD at a particular point inside a canopy and a pattern with a fixed $L=251.7 \mu\text{mol m}^{-2} \text{s}^{-1}$ over 16 h.

Comparison with experimental data

Model predictions were calculated for light fluctuating for 12 hours between 100 and 475 $\mu\text{mol m}^{-2}\text{s}^{-1}$ at switching periods $S = 0.5\text{h}, 1\text{h}, 2\text{h}, 4\text{h}, 6\text{h}$ and 12h, which correspond respectively to 24, 12, 6, 3, 2 and 1 switches from low to high light. All light patterns have the same integrated PPFD of 12.42 $\text{mol m}^{-2} \text{d}^{-1}$. Fig. 8.5A show light patterns for $S=0.5\text{h}, 2\text{h}$ and 6h.

By numerically optimising daily carbon gain for a time-weighted averaged light patterns over 24 hours as given in Eq. (2), we calculated the optimal maximum photosynthetic capacity as a function of S for values of τ in the range from 0.1h to 1h with a step of 0.1h (Fig. 8.5B). We found an inverse relationship between the maximum photosynthetic capacity and the frequency of low to high light transitions.

In Fig. 8.5C we plotted predicted P_{max}^{opt} versus experimentally measured P_{max} (Yin and Johnson, 2000) for light patterns given in Fig. 8.5A. With $\tau=0.3\text{h}$ there is good agreement between experiment and theory for the 6h switching period (RMSE=0.89). Although the model predicts the correct trend in light

response curves for $S=2\text{h}$ and $S=0.5\text{h}$, it predicts higher values of P_{max} compared to experimentally measured light response curves. Nevertheless, the model is valuable in providing a mechanistic explanation for the observed general increase in P_{max} with switching period.

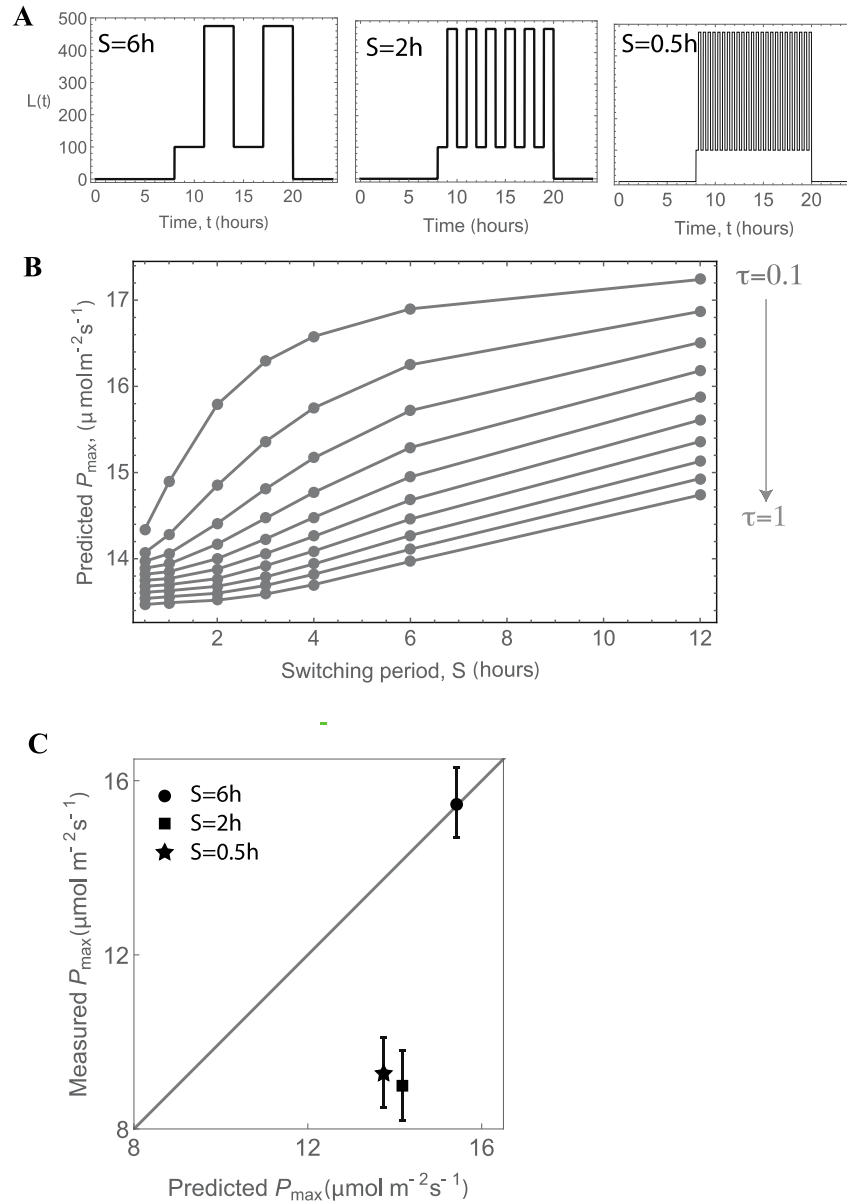


Figure 8.5: (A) Experimental set-up for 0.5h, 2h and 6h PPF switching. (B) Predicted P_{max} as a function of switching period for τ values from 0.1h to 1h. (C) Comparison between measured and predicted ($\tau=0.3\text{h}$) maximum photosynthetic capacity; gray line shows 1:1 values.

Discussion

We have formulated a mathematical framework of dynamic acclimation in order to define the optimal adjustments to net photosynthesis under fluctuating light conditions. We have found that the effect of different light patterns on maximum photosynthetic capacity has two main features: (i) for a light pattern with two levels of irradiance, the increase in optimal P_{\max} depends on the fraction of time under low light versus high light; and (ii) for a light pattern switching between low and high light at different frequencies, optimal P_{\max} is greater under a lower frequency of low light and high light transitions. These predictions offer a practical way of assessing whether the acclimation status of any given leaf is best adapted to its dynamic environment. However it is currently difficult to test this model with a broad range of data: the majority of experimental work carried out so far on acclimation has used steady-state conditions that do not reflect natural or agricultural environments accurately.

Previous empirical work showed that ability to undergo dynamic acclimation can affect biomass and fitness (Athanasίου *et al.*, 2010). Similarly, optimisation of short-term photoprotective responses to light dynamics can influence fitness (Kulheim *et al.*, 2002). However, regulatory aspects of acclimation and how they adapt under highly variable light patterns are less well understood. This paper represents the first step to addressing this problem. The quasi-steady net photosynthetic rate model we present here offers a clear framework that explains how dynamic acclimation may function in a complex light environment. This approach, where dynamic leaf responses are linked to environmental change in a quantitative manner in order to define optimal responses for productivity, has practical applications. For example there are implications for crop biomass and yield although any improvement would need a firm genetic basis.

Daily carbon gain cannot be derived from the average values of light due to the highly non-linear response of photosynthesis to light (Niinemets and Anten, 2009). Indeed measured profiles of photosynthetic capacity in plant crowns typically do not match those of average irradiance (Buckley *et al.*, 2013). The

results of the present study indicate that the optimal maximum photosynthetic capacity under fluctuating light patterns is different compared to those obtained from averaged light intensity. When comparing light patterns with the same integrated and peak PPFD, but with different intensity patterns, we found that the maximum photosynthetic capacity was reduced when the frequency of transitions was increased. This is in agreement with the dynamic acclimation data in existence for *A. thaliana*, grown under light patterns alternating for 12 hours between $100 \mu\text{mol m}^{-2} \text{s}^{-1}$ and $475 \mu\text{mol m}^{-2} \text{s}^{-1}$ over time periods of 30min, 2h and 6h (Yin and Johnson, 2000). Furthermore, a value of τ about 0.3h broadly agrees with the experimentally observed decrease in P_{max} .

We show here that the optimal maximum photosynthetic capacity was higher than that obtained for the averaged light intensity if the fraction of higher light intensity was large enough (Fig. 8.2B), even under small-amplitude light fluctuations. The relative advantage of $P_{\text{max}}^{\text{opt}}$ over \bar{P}_{max} increased with increasing difference between two levels of irradiance (Fig. 8.2D). Our study extends early work by Takenaka (1989), which employed a broadly similar mathematical approach but was based on optimal photosynthetic capacity of a leaf maximizing daily carbon gain estimated over an entire leaf lifetime, and found that the relative frequency distribution of irradiance rather than its average was critical when predicting optimal P_{max} .

Early notable work by Robert Pearcy and others (Pearcy, 1990) showed how light dynamics in plant canopies can contribute to productivity. The acclimation status of leaves within a canopy determines their ability to utilise light flecks effectively. However there are other factors that are thought to interact with acclimation to determine the final photosynthetic properties of a leaf, for example nitrogen (N) content. A long-established theory of optimal distribution of photosynthetic resources predicts that for a given total canopy N content, there is a 1:1 relationship between P_{max} and the light intensity (Field, 1983). However, experimental data indicates that maximum photosynthetic capacity does not precisely match the light vertical gradient within a canopy (Kull, 2002). One of the assumptions of canopy optimisation theory is that the

distribution of light absorption among leaves is constant (Niinemets, 2012; Foulkes and Murchie, 2011). But this ratio changes depending on various factors such as time of day, solar elevation and cloud cover (Terashima, 2005). Therefore the temporal fluctuations in PPFD should be explicitly considered when establishing the distribution of P_{\max} (Posada, 2009). To the best of our knowledge, methods for determining the efficiency of light acclimation for given complex patterns of light history have not been proposed in the literature. In addition there may be genetic constraints on the capacity of particular species to acclimate (Anderson *et al.*, 1995; Murchie *et al.*, 1998; Athanasiou *et al.*, 2010). This is the case for shade-adapted or sun-adapted species for example. However empirical knowledge of the optimal photosynthetic response for a given environment will allow acclimation to light to finally be placed in proper context, with limitations placed by other biotic and abiotic factors.

Previously, the acclimation status of leaves within a given plant canopy has been compared to average light level (Niinemets and Anten, 2009). We can now test the hypothesis that it is defined by the dynamic properties of the canopy and discover the limitations placed by other biological properties such as nitrogen remobilisation dynamics discussed above. With knowledge of canopy architecture, we can define the pattern of light via ray-tracing algorithms such as those used by Song *et al.* (2013) and calculate the predicted light history for canopy positions and layers. We applied our proposed mathematical framework to a typical diurnal variation in PPFD at a particular point inside a canopy (Fig 8.4). However it is first necessary to verify predictions of an optimal P_{\max} under a realistic variation in light environment and this requires experiments conducted under controlled conditions with precisely regulated complex light patterns and appropriate photosynthesis measurements. The final verification will arise from field testing.

There are very few experimental investigations producing data that would allow us to understand the influences of light pattern on dynamic acclimation. This may be partly due to past difficulties in developing lighting systems that

could cope with rapid switching between light levels of greatly differing magnitude. Recent developments with LED lighting have overcome such problems and it is now possible to accurately replicate light dynamics from virtually any environment. The model we present here should be considered a tool for the analysis of optimal leaf acclimation to variable light environments.

We have considered one factor, light energy input, and we view this method as a basis for more complex assessments that would parameterise the model with data affecting photosynthesis *in situ* such as leaf temperature, humidity and nutrients. We have not incorporated photosynthetic induction, i.e. the overall relative induction state (Stegemann *et al.*, 1999; Kupperts and Pfiz, 2009), into our model; instead we introduced a time-weighted average for the light pattern. A model that incorporates induction would need to be supported by data from light-fleck acclimation experiments. Full parameterisation of such a model will require high-resolution measurements of a time course of PPFD, as well as photosynthesis rates.

Another aspect, which will require future experimental data and model testing, is the inhibition of R_d in the light. For a given light intensity and temperature the level of inhibition is reasonably constant between species (Atkin *et al.*, 1997). Whether there is a variation in the level of inhibition according to the growth light treatment is in itself an interesting point.

Conclusion

Acclimation, sometimes referred to as plasticity, is an essential component of environmental adaptation but assessment of 'effectiveness' in a complex temporal and spatial environment can be difficult. There is a need to determine how efficiently leaves utilise light for photosynthesis in fluctuating conditions for ecological understanding and agricultural improvements. Our straightforward approach to develop a model for determining the efficiency of light acclimation in a given environment is a significant step forward and we propose it as the basis for a new physiological tool. We show that it is possible to take into account complex patterns of light history, the behaviour of processes such as induction state and for such a model to be consistent with available data. We anticipate that future experimental investigations will produce data necessary for further validation and refinement of the model.

Supplementary Material

Exploiting heterogeneous environments: does photosynthetic acclimation optimise carbon gain in fluctuating light?

R. Retkute, S. Unna, R. Smith, A.J. Burgess, O.E. Jensen, G.N. Johnson, S.P. Preston, E.II. Murchie

August 31, 2014

A Quasi-steady net photosynthetic rate model

The relationship between the net photosynthetic rate P and light intensity L (Fig. 1) possesses the following properties: $P \rightarrow P_{\max}$ for large L (saturation); $P(0, P_{\max}) = R_D < 0$ where $-R_D = \square P_{\max}$ for some $\square > 0$; $P(L_c, P_{\max}) = 0$, where L_c is the light compensation point; and $\frac{\partial P}{\partial L}(L_c, P_{\max}) = \varphi$. In this study, baseline parameters are $\square = 0.1$ and $\varphi = 0.0124$ mol CO_2 per mol photons.

Two simple models for P versus L are

$$P^{(1)}(L, P_{\max}) = \begin{cases} -\square P_{\max} + \varphi L & \text{if } 0 < L \leq \frac{(1+\square)P_{\max}}{\varphi}, \\ P_{\max} & \text{if } L > \frac{(1+\square)P_{\max}}{\varphi}, \end{cases} \quad (1a)$$

$$P^{(3)}(L, P_{\max}) = \frac{\varphi L + (1+\square)P_{\max} - \sqrt{(\varphi L + (1+\square)P_{\max})^2 - 4\varphi(1+\square)L P_{\max}}}{2\sqrt{}} - \square P_{\max}. \quad (1b)$$

The parameter $\sqrt{}$ determines the curvature of the response curve (1b). For $\sqrt{} = 1$, (1b) becomes $P^{(3)}(L, P_{\max}) = \frac{1}{2}(P_{\max}(1-\square) + L\varphi - |P_{\max}(1+\square) - L\varphi|)$, which is equivalent to (1a).

The value of P_{\max} , which we denote P_{\max}^{\square} , that maximises P for given L satisfies

$$P_{\max}^{\square(1)}(L) = \frac{\varphi L}{1+\square}; \quad (2a)$$

$$P_{\max}^{\square(3)}(L) = \frac{L\varphi - \square(-1+\square(\sqrt{}-1))(2\sqrt{}-1) - (1+\square-2\square\sqrt{})^{\frac{3}{2}} \square(-1+\square(\sqrt{}-1))(\sqrt{}-1)}{\square(1+\square)(-1+\square(\sqrt{}-1))}. \quad (2b)$$

Here $\frac{\partial P}{\partial L} = 0$ defines P_{\max}^{\square} in (2b); (2a) is then determined from the limit $\sqrt{} \rightarrow 1$.

B Light intensity regime under alternation between two light levels

Suppose that the light intensity $L(t)$ switches with period T between two different intensities L_{\pm} , where $L_- \leq L_+$. For $0 \leq t \leq kT$, $L(t) = L_-$, where $0 \leq k \leq 1$; $L(t) = L_+$ otherwise.

The net carbon assimilation rate for such an $L(t)$ is

$$C(k, L_-, L_+) = \frac{1}{T} \int_0^{kT} P(L_-, P_{\max}) dt + \frac{1}{T} \int_0^{(1-k)T} P(L_+, P_{\max}) dt, \quad (3)$$

giving

$$C^{(1)}(k, L_-, L_+) = \begin{cases} -\square P_{\max} + \varphi(kL_- + (1-k)L_+), & \text{if } L_+ \leq \frac{(1+\square)P_{\max}}{\varphi}, \\ k(-\square P_{\max} + \varphi L_-) + (1-k)P_{\max}, & \text{if } L_- \leq \frac{(1+\square)P_{\max}}{\varphi} < L_+, \\ P_{\max}, & \text{if } \frac{(1+\square)P_{\max}}{\varphi} < L_-, \end{cases} \quad (4a)$$

$$C^{(3)}(k, L_-, L_+) = k \frac{L_- \varphi - \sqrt{L_-^2 \varphi^2 - 4L_- P_{\max}(1+\square)\varphi + (P_{\max}(1+\square) + L_- \varphi)^2}}{2\varphi} + (1-k) \frac{L_+ \varphi - \sqrt{L_+^2 \varphi^2 - 4L_+ P_{\max}(1+\square)\varphi + (P_{\max}(1+\square) + L_+ \varphi)^2}}{2\varphi} - P_{\max} \square + \frac{P_{\max}(1+\square)}{2\varphi}. \quad (4b)$$

According to (4a), the maximum net carbon assimilation rate is attained for $P_{\max} = \varphi L_{\pm} / (1 + \square)$ (depending on the value of k), with the transition between the two states arising for $C' / C_{\max} = 0$, with

$$k = \frac{1}{1 + \square}. \quad (5)$$

Thus for $0 < k < 1/(1 + \square)$, $P_{\max}^{opt} = P_{\max}^{\square}(L_-) > \bar{P}_{\max}$, whereas for $1/(1 + \square) < k < 1$, $P_{\max}^{opt} = P_{\max}^{\square}(L_+) < \bar{P}_{\max}$. This step-like property remains evident in Figure 3, for which $\sqrt{\cdot} = 0.99$, although in this case P_{\max}^{opt} is typically larger than P_{\max} , indicating that P_{\max} must be elevated in order to attain an optimised response in fluctuating light conditions.

C Small amplitude light fluctuations

Light in nature is much more heterogeneous and unpredictable than that considered in previous sections. Here we consider how to maximise C when L is a fluctuating quantity. Specifically, suppose that $L = \bar{L} + \hat{L}$, where the bar denotes a time average and by definition $\bar{\hat{L}} = 0$. If the fluctuations are infinitesimal, we anticipate that C is maximised by $P_{\max} = P_{\max}^{\square}(\bar{L})$. We now determine how P_{\max}^{opt} must change in order to accommodate the fluctuations. We write the change as the constant \hat{P}_{\max} . For clarity of notation we express the response curve as $P = F(L, P_{\max})$ for some function F .

Setting $P_{\max} = \bar{P}_{\max} + \hat{P}_{\max}$, where \hat{P}_{\max} is to be determined, we Taylor expand F , treating \hat{P}_{\max} as being of comparable magnitude to \hat{L}^2 :

$$P = F(\bar{L}, \bar{P}_{\max}) + F_L(\bar{L}, \bar{P}_{\max})\hat{L} + F_P(\bar{L}, \bar{P}_{\max})\hat{P}_{\max} + \frac{1}{2}F_{LL}(\bar{L}, \bar{P}_{\max})\hat{L}^2 + \dots \quad (6)$$

where $F_P \neq C' / C_{\max}$. Evaluating C for large T , so that C is the time-average of P , it follows that

$$C = F + F_P \hat{P}_{\max} + \frac{1}{2}F_{LL} \bar{\hat{L}}^2 + \dots \quad (7)$$

Maximising C over P_{\max} requires $C_P = 0$, i.e. $F_P + F_{PP} \hat{P}_{\max} + \frac{1}{2}F_{PLL} \bar{\hat{L}}^2 + \dots = 0$. However derivatives are evaluated at $L = \bar{L}$, $P_{\max} = \bar{P}_{\max}$ and $F_P(\bar{L}, \bar{P}_{\max}) = 0$, implying that

$$\hat{P}_{\max} = -\bar{\hat{L}}^2 \frac{F_{PLL}}{2F_{PP}}, \quad (F_{PP} \neq 0). \quad (8)$$

For the light saturation model given by (1b), (8) gives

$$P_{\max}^{opt} = \bar{P}_{\max} + \frac{\bar{\hat{L}}^2 \bar{P}_{\max}}{2} \frac{P_{\max}^2(1+\square)^2 + \bar{L}P_{\max}(1+\square)(2\sqrt{\cdot}-1)\varphi - 2\bar{L}^2\varphi^2}{P_{\max}^2(1+\square)^2 - 2\bar{L}P_{\max}(1+\square)(2\sqrt{\cdot}-1)\varphi + \bar{L}^2\varphi^2}. \quad (9)$$

Numerical calculations over range of parameter values show that second term in the above expression is positive, therefore $P_{\max}^{opt} > \bar{P}_{\max}$ if $\bar{\hat{L}}^2 > 0$. This is illustrated in Fig. 4. Thus P_{\max}^{opt} must increase in the presence of fluctuations as a consequence of the shape of the underlying light-response surface.

Chapter 9: The effect of fluctuating light on acclimation in *Arabidopsis thaliana*

Chapter 9 uses a controlled LED cabinet experiment to assess photosynthetic acclimation within *Arabidopsis* lines compared to a results of an acclimation model presented in Chapter 8. This has been written for possible publication so is presented in “paper format”.

Author contribution:

Experiment conceived by AJ Burgess

Project supervision performed by EH Murchie

General advice and model aid performed by R Retkute

Practical work (rosette area, chlorophyll assays) assistance performed by C Simpson

Practical work (all assays), data analysis, model implementation and paper construction performed by AJ Burgess

The effect of fluctuating light on acclimation in *Arabidopsis thaliana*

Alexandra J. Burgess, Renata Retkute, Conor Simpson and Erik H. Murchie

Abstract

Dynamic acclimation is the process by which mature plants and organs can adjust their structure and composition in order to respond to a change in their environment. In contrast, developmental acclimation is largely irreversible and describes changes in cell number, size and shape which is set early in development. Recent work has indicated the importance of acclimation to irradiance and the fitness advantage it provides. However, the conditions that induce acclimation under natural conditions, in particular under fluctuating light, are poorly understood. In order to explore this process further, acclimation responses of *Arabidopsis thaliana* were subjected to a fluctuating light (FL) pattern relative to a constant light (CL) pattern of the same light intensity ($266 \mu\text{mol m}^{-2} \text{s}^{-1}$). The Wassilewskija-4 (Ws) and Landsberg erecta (Ler) accessions were chosen for their ability to undergo dynamic and developmental acclimation, and a GPT2 (encoding a Glucose-6-P/phosphate translocator) knock out mutant on a Ws background (*gpt2*⁻) was used as it lacks the ability to undergo dynamic acclimation. Our results indicate that following exposure to a series of predetermined and repeating fluctuating light motifs, plants adjust different components of acclimation to high and low light independently. This leads to an increase in the maximal photosynthetic capacity (P_{max}) of the wild type plants but a slight decrease in the *gpt2*⁻ mutant. Simultaneously rates of photosynthesis at low light were enhanced enabling better exploitation of the low light periods with no apparent reduction in dark respiration rate. An empirical model of acclimation was tested and, in general, modelled results show good agreement to measured data. Past experiments have found that the photosynthetic capacity is dependent on the number of switches from high to low irradiance and the amount of time spent under each

light level. Based on the data we present we conclude that acclimation is a complex process, involving more than one mechanism, that allows for plants to adjust to the light pattern that they are under in order to be most efficient under varying light.

Introduction

Light drives photosynthesis and is arguably the most important environmental factor for plant growth and maintenance. As such, plants must find a way to optimise photosynthesis according to light availability. Optimising photosynthesis requires a balance between the efficiency under low light whilst simultaneously preventing harm caused by excess radiation. Achieving balance between these two states is critical to maximise both productivity and mitigate radiation-induced damage (Demmig-Adams *et al.*, 2012). In a plant canopy this is especially true: the position of leaves in relation to one another and to the sun plus the stochasticity of sun flecks means that an individual leaf can go from being in a light-limited state to a state in which photosynthetic apparatus is saturated within a short period of time. The heterogeneous light environments created by structurally complex plant canopies and weather patterns results in difficulty when assessing cellular level processes at the whole plant and canopy scale, however, these processes are so intrinsically linked to fitness that they could provide a means to optimise plant performance and productivity in a changing environment. Such responses are diverse and can occur on a magnitude from minutes to days or even weeks (Murchie *et al.*, 2009; Athanasiou *et al.*, 2010). Plants can be slow to respond to a change in light levels but the fittest plants will be those that can optimise their level of photosynthesis so as to track these changes in light. Acclimation refers to changes in the composition and organisation of photosynthetic apparatus and can be broadly split into two processes: developmental acclimation and dynamic acclimation.

Developmental acclimation is largely irreversible and is determined early in development. It describes changes to cell size, number and shape. This can arise as different leaves are exposed to varying light levels; as such they

develop differently in order to optimise photosynthetic efficiency. Differences in acclimation state can be seen as changes in the characteristics of the light response curve of photosynthesis. Leaves that developed under a higher light level will have a higher maximum photosynthesis rate (P_{\max}). However, leaves that developed under lower irradiance, will have a lower light compensation point (LCP) to improve carbon gain at low light intensities resulting in a shorter, but more sensitive, light limiting state, thus allowing improved exploitation of low light levels and a swift response to any influx of light due to a passing sun fleck or change in light availability (Yin & Johnson, 2000). These differences are observed due to changes in chlorophyll concentration, leaf thickness and molecular alterations such as changes in photosystem I (PSI) and photosystem II (PSII) structure and concentration plus changes in photosynthetic enzyme activities (Murchie & Horton, 1997; Walters, 2005).

The second form of acclimation is dynamic acclimation, which can be characterised as structural and biochemical changes in the photosynthetic machinery of a mature leaf (Walters & Horton, 1994). It involves reversible responses to light that occur >20 minutes following an irradiance increase or decrease (Müller *et al.*, 2001; Retkute *et al.*, 2015). Responses include changes to PSI and PSII levels or structure; changes in the regulation of electron transport components; changes in enzyme concentrations such as Rubisco and ATPase; changes in granal stacking and; the chloroplast avoidance/accumulative response (Walters & Horton, 1994; Anderson *et al.*, 1995; Murchie & Horton, 1997; Walters *et al.*, 1999; Walters, 2005; Li *et al.*, 2009; Dyson *et al.*, 2015). Dynamic acclimation can also effect the pigment composition found in a leaf, and adaptations to changes in irradiance can manifest themselves as changes in chlorophyll content and ratios. Chlorophyll a is found in the reaction centre of both photosystems, and its synthesis is dependent on the synthesis of photosystems, whereas chlorophyll b is an accessory pigment, part of the antenna complex and therefore is more readily synthesised when light levels drop in an attempt to harvest maximum light (Anderson, 1980; Anderson, 1986; Murchie & Horton, 1997; Walters *et al.*, 1999). Analysis of chlorophyll content and ratios can provide an alternative to

analysis of dark respiration rates, which can be difficult to accurately measure (Walters, 2005). Dynamic acclimation can also be seen through changes to the light response curve characteristics, particularly the impact on P_{\max} . Both developmental and dynamic acclimation are important under natural conditions but knowledge of how they interact together is poorly understood.

There has been extensive research on how plants acclimate to high light and to low light (Anderson, 1980; 1986; Demmig-Adams & Adams, 1992; Murchie & Horton, 1997; Yin & Johnson, 2000; Walters, 2004; 2005; Scheibe *et al.*, 2005; Athanasiou *et al.*, 2010; Kunz *et al.*, 2010; Suorsa *et al.*, 2012; Dyson *et al.*, 2015; Retkute *et al.*, 2015), however, few experiments have focused purely on the effect of controlled fluctuating light (Chabot *et al.*, 1979; Watling *et al.*, 1997; Yin & Johnson, 2000). Of those that have been carried out, experiments have predominantly focused on fluctuating light patterns that alternate between a fixed high and low value, thus they do not represent the varying irradiances that plants are subject to throughout the day. Furthermore, it is understood that the maximum photosynthetic capacity of a plant is dependent on the number of switches between high and low light intensity and the proportion of time spent under each irradiance (Yin & Johnson, 2000; Retkute *et al.*, 2015). Until recently, simulating accurate fluctuations of light were not possible but LED-based growth chambers enable us to subject plants to a predetermined and controlled pattern of irradiance.

Fluctuating light presents a potential challenge to the acclimation process: a high light acclimated leaf will not perform well under low light and vice versa. Photosynthetic capacity is considered to correlate with dark respiration (Givnish, 1988; Niinemets and Tenhunen, 1997; Retkute *et al.*, 2015). Therefore do you exploit high light via raising P_{\max} and / or do you enhance light capture and reduce respiratory loss under low light? This study was aimed at assessing the acclimation potential of *Arabidopsis thaliana* in a fluctuating light environment and investigate the possibility that acclimation is under the control of multiple pathways. The *A. thaliana* accessions, Wassilewskija-4 (Ws), Landsberg erecta (Ler) and a GPT2 knock out mutant on a Ws

background (*gpt2*-), were grown in a LED growth cabinet and were subject to either a constant light treatment for full growth or constant light followed by fluctuating light treatment for the final 9 days of growth in order to see how plants acclimate. It is predicted that full dynamic acclimation takes at least 7 days (Retkute *et al.*, 2015), thus, combined with the short life span of *Arabidopsis* under these conditions, this study aims to see the response of both dynamic and developmental acclimation. It has previously been shown that *Ws* and *Ler* are capable of undergoing dynamic acclimation, as witnessed through changes in their P_{\max} (Athanasidou *et al.*, 2010). GPT2 is thought to mediate dynamic acclimation responses via metabolic fluxes. It is responsible for the import of glucose-6-phosphate (G6P) into the chloroplast, from the cytosol (Kunz *et al.*, 2010). This has the net effect of increasing starch synthesis, resulting in the chloroplast's phosphate concentration increasing, leading to gene expression changes allowing the cell to sense changes in environmental signals (Walters, 2004; Dyson *et al.*, 2015). Whilst *gpt2* knock out mutants grow normally, and demonstrate developmental acclimation (Niewiadomski *et al.*, 2005) they do not exhibit dynamic acclimation (Dyson *et al.*, 2015), which means they can provide a negative control for demonstrating the fitness benefits of dynamic acclimation in *Arabidopsis*. Within this study, we use a fluctuating light pattern (Fig. 9.1), which represents a more realistic representation of the light patterns that plants would be subject to in nature and therefore provides a more accurate into the effects of fluctuating light on acclimation *A. thaliana*. Our results indicate that plants can demonstrate entrained responses based on past light history.

Materials and Methods

Plant Growth

A. thaliana ecotypes Landsberg erecta (Ler), Wassilewskija (Ws) and a *gpt2*-mutant (Ws WT background) were selected based on their differing abilities to undergo dynamic acclimation (Athanasidou *et al.*, 2010). The seeds were vernalised at 4°C in a water suspension for 48 hours, prior to transfer into 6.5 cm diameter pots containing Levington 3 compost. One week after germination, seedlings were transplanted into individual pots containing 25g of Levington 3 compost. A Fytoscope 3000 (PSI Systems, Czech Republic) was employed which uses a combination of red and blue LEDs (1:1 ratio throughout on a photon flux basis) plus far-red LEDs (on during day at a constant rate of around 10 $\mu\text{mol m}^{-2} \text{s}^{-1}$). The cabinet was set to a 12 hour photoperiod, with a 20°C day temperature, 16°C night temperature and 50% humidity; these conditions remained constant throughout the experiment. Plants were split into two groups and were subject to two different light treatments: Constant light (CL) and fluctuating light (FL). The CL plants were grown under $266 \pm 10 \mu\text{mol m}^{-2} \text{s}^{-1}$ (red line Fig. 9.1) for the full growth, i.e. up to 37 days. The FL group was subject to the same conditions (i.e. CL) for 28 days and then transferred into a fluctuating light pattern (black line Fig. 9.2), with the same amount of integrated light (average light intensity of $266 \pm 10 \mu\text{mol m}^{-2} \text{s}^{-1}$) for the remainder of the full growth (i.e. 9 days). 9 days was selected to ensure full dynamic acclimation. Due to the short growth span of *Arabidopsis* under these conditions, response to these treatments will represent a combination of developmental and dynamic acclimation. The fluctuating light treatment includes a light pattern motif of 3 h 20 min, which was repeated 3 times throughout the day (see arrows Fig. 9.1) to allow repeat measurements. Each light step was a minimum of 20 min long to discount changes as a result of induction. During growth, plants were kept well-watered. The experiment was repeated four times for Ws and *gpt2*- and three times for Ler.

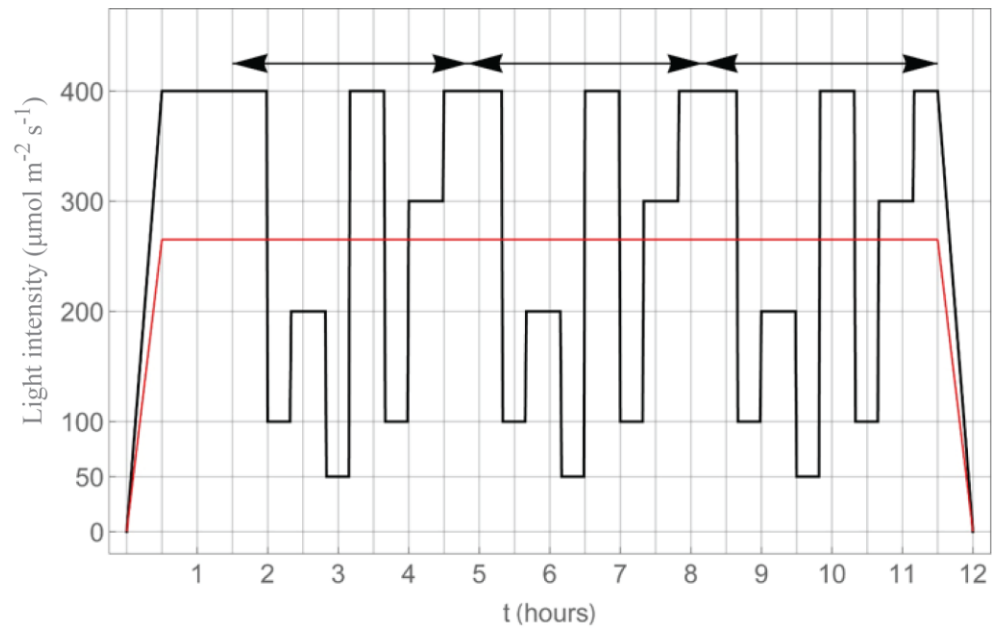


Figure 9.1: Light patterns used for the analysis of acclimation in Arabidopsis thaliana. A Fytoscope 3000 (PSI Systems, Czech Republic) was employed which uses a combination of 50:50 red: blue plus far-red LEDs. Plants were split into two groups and were subject to two different light treatments: Constant Light (CL: red) versus Fluctuating Light (FL: black) light patterns. The CL plants were grown under $266 \pm 10 \mu\text{mol m}^{-2} \text{s}^{-1}$ for the full growth, i.e. up to 37 days. The FL group was subject to the same conditions for 28 days and then transferred into the fluctuating light pattern, with the same average light intensity of $266 \pm 10 \mu\text{mol m}^{-2} \text{s}^{-1}$ for the remainder of the full growth (i.e. 9 days). The fluctuating light treatment includes a light pattern motif of 3 h 20 min (denoted by arrows), which was repeated 3 times throughout the day to allow repeat measurements. Each light step was a minimum of 20 min long to prevent changes resulting of induction.

Physiological Measurements

Both destructive and non-destructive measurements were made on plants. Analysis of rosette area were performed on all plants starting at 21 days after sowing (DAS). Plants were briefly removed from the Fytoscope 3000 growth cabinet into the adjoining room every other working day and were photographed using a RGB camera (Canon SLR) using ambient lighting and a

scale. Images were analysed using Image J for rosette area (Rasband, 2012). Following gas exchange measurements, chlorophyll assays were carried out. A size 4 leaf borer was used to take 2 leaf discs per plant from leaves in the 3rd whorl, which were placed immediately in cold, 80% acetone and kept dark. Leaf samples were ground in the 80% acetone and made up to 5 ml before being centrifuged for 5 min at 3000 r.p.m, 1600 g. The chlorophyll content and a:b ratios in the supernatant was determined according to Porra *et al.* (1989) using absorption with a spectrophotometer at 646.6, 663.6 and 750 nm.

Gas Exchange Measurements

Whole plant light response curves were taken using the LI-COR 6400XT using the whole plant chamber attachment (6400-17) and RGB Light source (6400-18A for LRCS) at the end of the experiment (36 DAS+). The small size of some of the leaves precluded the use of a single leaf chamber and measurement of the whole plant allows the response of both developmental and dynamic acclimation to be monitored. For all gas exchange measurements, plants were not dark-adapted prior to measurements. The block temperature was maintained at 20°C using a flow rate of 600 ml min⁻¹. For LRCs, light was provided by a combination of in-built red, blue and green LEDs, set to “white” light. Illumination occurred over a series of 12 photosynthetically active radiation values between 0 and 1500 $\mu\text{mol m}^{-2} \text{s}^{-1}$, with a minimum of two minutes at each light level. At least 6 replicates were taken per experimental repeat for both CL and FL plants. Curve fitting to the non-rectangular hyperbola (Eq. 1) was carried out using the Mathematica (Wolfram) command **FindFit** with a minimum constraint on dark respiration at 0.05 and convexity at 0.8.

During the light treatment period, changes in photosynthesis were measured using the LI-COR 6400XT with the whole plant chamber attachment and sun and sky lid. An “autologging” program was created that took measurements every 15 seconds throughout the light fluctuation program, thus could study photosynthesis induction during the fluctuations. The LI-COR was placed inside the Fytoscope chamber, with the chamber providing the light pattern to

the individual plant being measured, through the sun and sky lid. CO₂ was maintained at 400 p.p.m. throughout. Due to the repeating light signature (3 hours 20 minutes long; see Materials and Methods, Plant Growth) in the fluctuating light treatment pattern, 3 replicates were taken per day on days 1, 3, 5 and 8- post treatment (corresponding to 28, 30, 32 and 35 DAS). Autologging was carried out for two full repeat experiments of the WTs Ler and Ws (i.e. 6 replicates per post treatment day) and one full experiment for the *gpt2*- mutant (i.e. 3 replicates per post treatment day). The data was normalised according to the average photosynthesis during the last 10 time points at the end of the light pattern (Supplementary Fig. S9.1).

Statistics

Analysis of variance (ANOVA) was carried out using GenStat for Windows, 17th Edition (VSN International Ltd.). An unbalanced design was used to account for differences in the number of replicates each round (i.e. due to plant death). The data was checked to see if it met the assumption of constant variance and normal distribution of residuals. For all statistical analyses, data from each of the lines (Ws, Ler and *gpt2*) were treated independently because of their differing responses to a change in light. Rosette area was analysed at 28 DAS and 37 DAS. The former was carried out to ensure that plant growth was same in the CL treatment relative to FL treatment during the period of growth under which they were subject to the same light pattern (red line; Fig 9.2) whilst the latter was to determine whether the fluctuating light pattern influenced growth and final rosette area. Photosynthetic light response curve parameters P_{max}, quantum use efficiency (ϕ), LCP and α (see below) plus chlorophyll a:b ratio and total chlorophyll content was also analysed. ANOVAs were also carried out on the response of photosynthesis to a change in irradiance. The light motif can be divided into 8 stages, each stage representing a different light intensity (Supplementary Figure S9.2). For the stages 1-4 and 6 (corresponding to the steps at 400, 100, 200, 50 and 100 $\mu\text{mol m}^{-2} \text{s}^{-1}$, respectively), the average normalised photosynthesis value at the last 50 time points was compared. For stage 5 (the 50 - 400 $\mu\text{mol m}^{-2} \text{s}^{-1}$ step), the time taken to reach 0.7, 0.8 and 0.9 of the normalised photosynthesis value was

tested. This is a proxy to see if there are any differences in the rate of change (i.e. the response of photosynthesis) following a change in light level.

Curve fitting and modelling

All modelling was carried out using Mathematica (Wolfram).

Within this study the net photosynthetic rate, P , as a function of irradiance, L , and maximum photosynthetic capacity, P_{max} , was described using the non-rectangular hyperbola proposed by Prioul and Chartier (1977):

$$P(L, P_{max}) = \frac{\phi L + (1 + \alpha)P_{max} - \sqrt{(\phi L + (1 + \alpha)P_{max})^2 - 4\theta\phi L(1 + \alpha)P_{max}}}{2\theta} - \alpha P_{max} \quad (1)$$

The nonrectangular hyperbola is defined by four parameters: the quantum use efficiency, ϕ ; convexity, θ ; maximum photosynthetic capacity, P_{max} and; the rate of dark respiration, R_d . We assumed that the rate of dark respiration is proportional to the maximum photosynthetic capacity, according to the relationship $R_d = \alpha P_{max}$ (Givnish, 1988; Niinemets and Tenhunen, 1997; Retkute *et al.*, 2015). Curve fitting was carried out using the Mathematica command **FindFit** with a minimum constraint on α at 0.05 and θ at 0.8.

One purpose of this study was to test the acclimation model of Retkute *et al.* (2015). This model aims to predict the optimal maximum photosynthetic capacity, P_{max}^{opt} , for a given light pattern, in this case the FL treatment. This value can be compared with \bar{P}_{max} , which refers to the P_{max} if the fluctuating light pattern (FL) were replaced by its average, in this case the CL treatment. Whilst this model was originally developed based on dynamic acclimation data, P_{max}^{opt} can theoretically arise from either developmental or dynamic acclimation so can be applied to this study. The model incorporates a “fading memory” of the recent light pattern in the form of a time-weighted average for the light (see Eq. 3 in Retkute *et al.* 2015), to represent how plants will respond

more strongly to recent changes in light history. Full details of the model are given in Retkute *et al.* (2015) but in brief:

Carbon gain, C (mol m⁻²), was calculated over the time period $t \in [0, T]$ according to Eq. 2.

$$C(L(t), P_{max}) = \int_0^T P(L(t), P_{max}) dt \quad (2)$$

Experimental data indicates that the response of photosynthesis to a change in irradiance is not instantaneous and thus to incorporate this into the model Retkute *et al.* (2015) introduced a time-weighted average for light (Eq. 3).

$$L_\tau(t) = \frac{1}{\tau} \int_{-\infty}^T L(t') e^{-\frac{t-t'}{\tau}} dt' \quad (3)$$

This effectively accounts for photosynthetic induction state, which is very hard to quantify *in situ* as it varies according to the light history of the leaf. The more time recently spent in high light, the faster the induction response. The time-weighted average acts as a “fading memory” of the recent light pattern and uses an exponentially decaying weight. If $\tau = 0$ then a plant will be able to instantaneously respond to a change in irradiance, whereas if $\tau > 0$ the time-weighted average light pattern will relax over the timescale τ . The model was adapted so the time-weighted average was only applied during the transition from low to high light (to represent induction) but not from high to low light, during which photosynthesis can almost immediately respond (Supplementary Fig. S9.3). Previous data from *Arabidopsis* indicates that $\tau \sim 0.3$ (Retkute *et al.*, 2015). This value of τ (0.3) represents a maximum leaf ‘memory’ of around 18 minutes that exponentially declines according to time spent in the light (the effect of τ at 0.3 is given in Supplementary Fig. S9.3). For this study, different values of τ were selected and the model was allowed to try different combinations of light response curve parameters in order to find the best fit with the constant light data (i.e. \bar{P}_{max}). The same parameters were then used to calculate the optimal P_{max} for the fluctuating light treatment (i.e. P_{max}^{opt}).

Results

Growth

Figure 9.2 shows the change in rosette area over the course of the experiment. Two CL vs FL comparisons were performed on each accession in order to see if there were any differences in growth of the plants: first at 28 DAS make sure there were no differences in growth between each of the treatments prior to the start of the fluctuating light for FL plants and; secondly at 37 DAS. At 28 DAS there was no significant difference in rosette area between the treatments in any line, which suggests that up to that point the plants grew similarly. Similarly, at 37 DAS there was no significant difference in the rosette area for any line. These results suggest that the fluctuating light treatment used here had no impact on the growth of the plants.

Light Response Curves

Figure 9.3 shows the mean LRC representative of all plants throughout the study for each accession under CL and FL. In consensus with the literature the results showed a significant increase in P_{\max} for both the wild type accessions (Ws $P=0.023$; Ler $P<0.001$), indicative of acclimation to high light (Murchie & Horton, 1997; Yin & Johnson, 2000; Walters, 2005; Li *et al.*, 2009; Athanasiou *et al.*, 2010; Dyson *et al.*, 2015; Retkute *et al.*, 2015). The P_{\max} for the *gpt2*- mutant significantly decreased ($P=0.013$). Direct comparisons between Ws and *gpt2*- under CL showed no significant difference in P_{\max} but under FL P_{\max} in the mutant was significantly lower, demonstrating that GPT2 is essential for acclimation to high light (Dyson *et al.*, 2015).

Fitted values for QUE indicated that for both the WT accessions, QUE was significantly higher in plants under FL compared to those under CL ($P<0.001$ for Ws and $P=0.006$ for Ler), which is an indicator of high light acclimation. The QUE was not significantly difference for *gpt2*-. There was a significant decrease in LCP in the FL plants relative to CL plants for Ws ($P=0.012$) but not Ler or *gpt2*-. A decrease in LCP is an indicator of acclimation to low light (King, 1994). We did not find a significant difference in dark respiration for

any line, contrary to past experiments (Dyson *et al.*, 2015; Yin & Johnson, 2000), although this may be due to the difficulty in measuring dark respiration with the whole plant chamber.

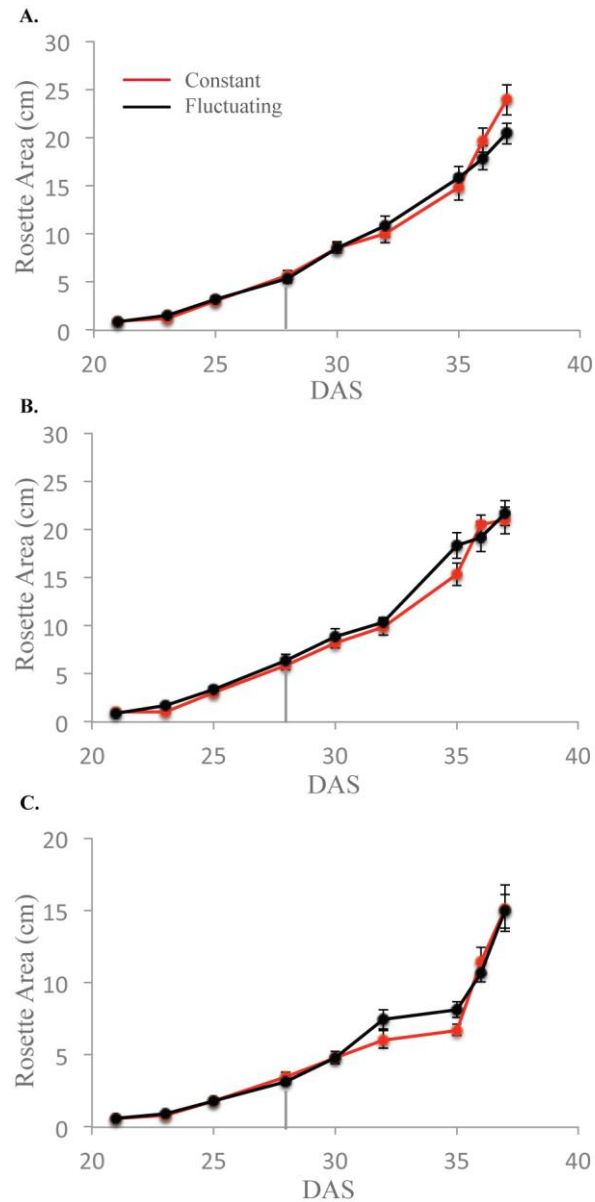


Figure 9.2: Rosette area timecourse. (A) *Ws* (B) *gpt2-* (C) *Ler*. Measurements began 21 days after sowing (DAS) for constant light (red) and fluctuating light (black) plants. For the fluctuating light treatment plants, the light pattern was changed at 28 DAS, as denoted by the grey vertical line.

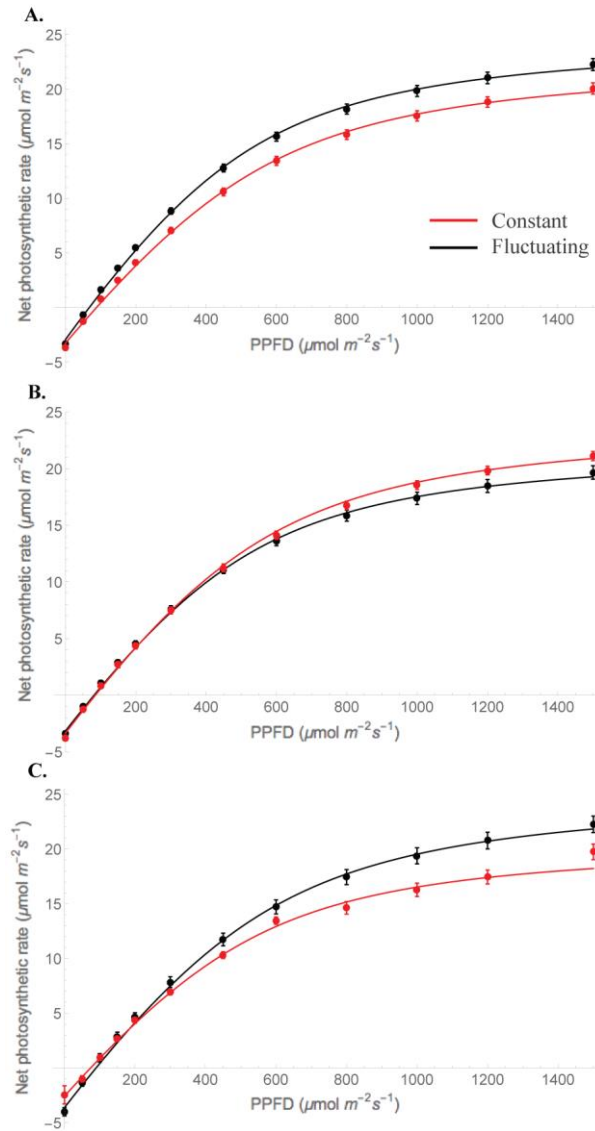


Figure 9.3: Light response curves for plants grown under constant light (red) versus fluctuating light (black). (A) *Ws* (B) *gpt2-* (C) *Ler*. Light response curves were measured 37 days after sowing, equivalent to 9 days after starting the fluctuating light pattern (FL plants). Curves were fitted using Mathematica (Wolfram) command *FindFit*. P_{max} , Q_{UE} , LCP and dark respiration comparisons were made using an ANOVA.

Chlorophyll Assays

Figure 9.4 shows the mean values from chlorophyll assays for each line. Based on LRC analysis, acclimation to high light was observed in *Ler* (FL) and *Ws* (FL). It was therefore expected that Chl a:b ratio would increase for these two accessions (Anderson, 1980; Anderson, 1986; Murchie & Horton, 1997;

Bailey *et al.*, 2001). There was no significant difference in chlorophyll a:b in Ws. However, for both Ler and *gpt2*- the chlorophyll a:b ratios were significantly lower in the FL plants compared to the CL plants ($P=0.049$ and $P=0.004$, respectively). These findings suggest that none of the plants were strictly acclimating to high light, and that Ler and *gpt2*- plants were able to acclimate to low light under FL conditions. For both Ws and *gpt2*- the total Chl was significantly lower in plants under FL compared to those under CL ($P<0.001$ and $P=0.002$, respectively). For Ler, no significant change was observed between total Chl amounts.

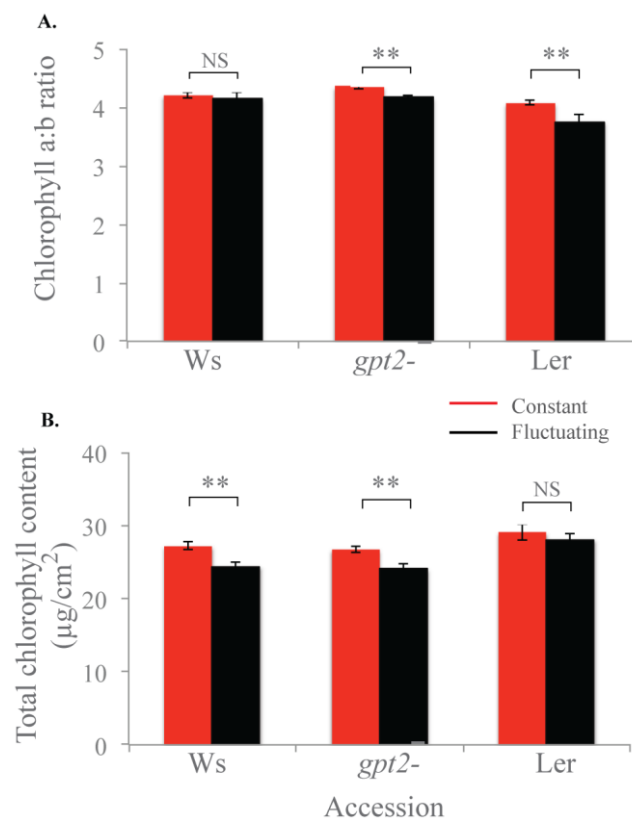


Figure 9.4: Chlorophyll analysis of plants. (A) Chlorophyll a:b ratio. (B) Total chlorophyll content. Comparisons were made in each case using an unbalanced ANOVA (NS=Not significant; * $p<0.05$ ** $p<0.01$).

Response of Photosynthesis to a change in irradiance

To monitor whether the plants are able to respond more rapidly to changes in light level with a greater number of days following the change to a fluctuating light pattern, photosynthesis measurements were made every 15 seconds throughout the light motif at days 1, 3, 5 and 8 post treatment (see Materials and Methods: Gas exchange). The results can be seen in Figure 9.5. To avoid errors associated with miscalculation of rosette area, the data was normalised according to the photosynthesis value at the final ($400 \mu\text{mol m}^{-2} \text{s}^{-1}$) stage (Supplementary Figure S9.1). The light motif was split into 8 stages according to the irradiance level (Supplementary Fig. S9.2); statistics was carried out on stages 1-6 during the light motif (Materials and Methods). For stages 1-4 and 6 (corresponding to the steps at 400 , 100 , 200 , 50 and $100 \mu\text{mol m}^{-2} \text{s}^{-1}$, respectively), the average normalised photosynthesis value of the last 50 time points during the step (i.e. at steady state) was calculated. For stage 5, the time taken to reach a normalised photosynthesis value of 0.7, 0.8 and 0.9 was calculated as a proxy for rate of change. A full summary of the normalised photosynthesis values at for stages 1-4 and 6 plus the time taken to achieve a normalised photosynthesis of 0.7, 0.8 and 0.9 following a change in light intensity in stage 5 is given in Supplementary Table S9.1. There was no significant difference in days post treatment for any of the lines at stages 1-3 and 6. For *gpt2*- and *Ws*, there was no significant difference during stage 4 (i.e. the step at $50 \mu\text{mol m}^{-2} \text{s}^{-1}$) or 5 (i.e. the step from 50 to $400 \mu\text{mol m}^{-2} \text{s}^{-1}$). However, for *Ler* there was a significant difference. For normalised photosynthesis at stage 4 (under $50 \mu\text{mol m}^{-2} \text{s}^{-1}$; $P=0.017$) and at stage 5 in the time taken to get to 0.8 ($P=0.044$) and 0.9 ($P=0.036$). This indicates that in the days following a change in the light environment, the plant is able to respond more quickly to a change in irradiance, thus indicating the importance of the light history.

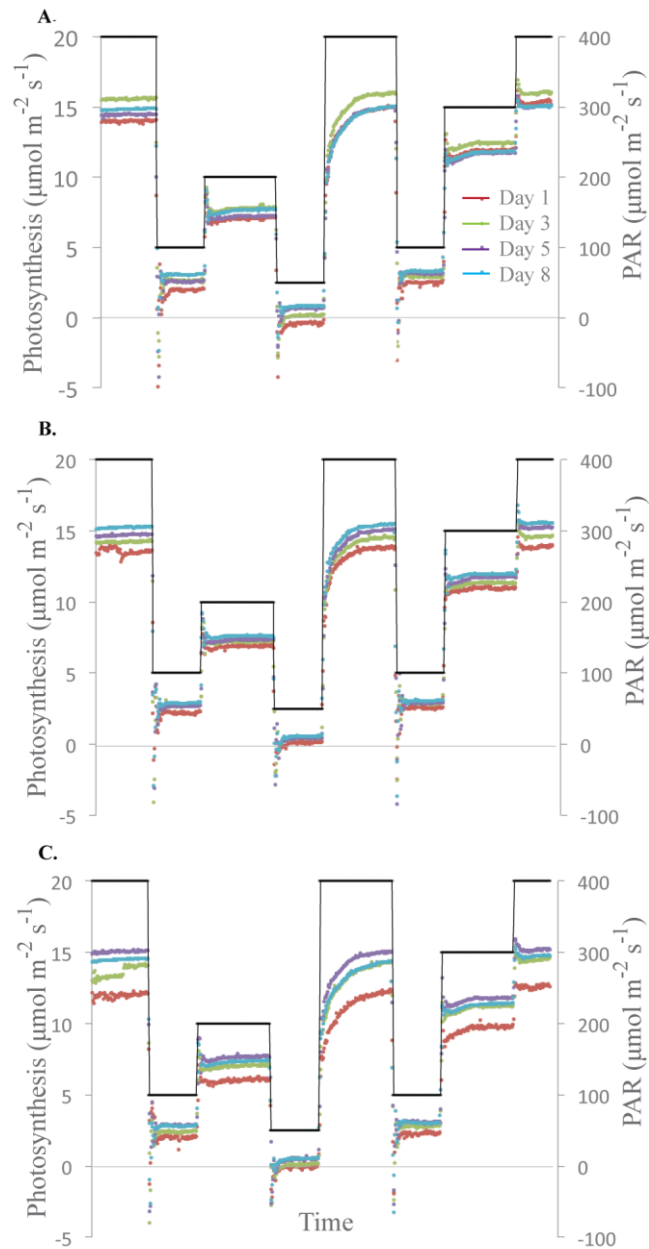


Figure 9.5: Induction data in the days following a change in the light pattern. (A) *Ws* (B) *gpt2-* and (C) *Ler*. During the light treatment period, changes in photosynthesis were measured using the LI-COR 6400XT with the whole plant chamber attachment and sun and sky lid. An “autologging” program was created that took measurements every 15 seconds throughout the light fluctuation program, thus could study photosynthesis induction during the fluctuations. The LI-COR was placed inside the Fytoscope chamber, with the chamber providing the light pattern to the individual plant being measured, through the sun and sky lid. Due to the repeating light signature (3 hours 20 minutes long; see Materials and Methods, Plant Growth) in the fluctuating

light treatment pattern, 3 replicates were taken per day on days 1, 3, 5 and 8-post treatment (corresponding to 28, 30, 32 and 35 DAS). Autologging was carried out for two full repeat experiments of the WTs Ler and Ws (i.e. 6 replicates per post treatment day) and one full experiment for the *gpt2*-mutant (i.e. 3 replicates per post treatment day).

Acclimation Model

As well as exploring the acclimation process of *Arabidopsis thaliana* to a fluctuating light pattern, this study was also carried out in order to test the acclimation model of Retkute *et al.* (2015). This model aims to predict the optimal maximum photosynthetic capacity, P_{max}^{opt} , for a given light pattern (i.e. the fluctuating light pattern) and can be compared to the optimal maximum photosynthetic capacity for the average of the light pattern, \bar{P}_{max} , (i.e. the constant light pattern). As the model was developed based on parameterisation from plants that can undergo dynamic acclimation, it has only been tested for Ws and Ler data in this study. The time-weighted average, τ (Eq. 3: Materials and Methods) describes the rate of response to a change in irradiance levels, with a $\tau=0$ indicating instantaneous response the plant to a change in light and $\tau>0$ indicates a relaxation in response over the timescale τ . Using the parameters taken from fitted LRCs and a τ of 0.3, the model predicts very low values of both \bar{P}_{max} and P_{max}^{opt} for both accessions (Ws: $10.4 \mu\text{mol m}^{-2} \text{s}^{-1}$ and $9.6 \mu\text{mol m}^{-2} \text{s}^{-1}$; Ler: $10.6 \mu\text{mol m}^{-2} \text{s}^{-1}$ and $9.9 \mu\text{mol m}^{-2} \text{s}^{-1}$, respectively). Decreasing τ to 0.1 (i.e. increasing the response time to a change in light levels) does not greatly improve this with values of $10.6 \mu\text{mol m}^{-2} \text{s}^{-1}$ and $10.7 \mu\text{mol m}^{-2} \text{s}^{-1}$ for Ws and $10.7 \mu\text{mol m}^{-2} \text{s}^{-1}$ and $11.2 \mu\text{mol m}^{-2} \text{s}^{-1}$ for Ler, for \bar{P}_{max} and P_{max}^{opt} , respectively. The slightly lower predictions for Ws relative to Ler indicate the low values given could be a result of differences in the parameters, with a lower α (0.143 and 0.124), θ (~ 0.8) and ϕ (0.0381 and 0.0357) values in this study relative to data used to initially develop the model ($\alpha= 0.02$, $\phi= 0.055$ and $\theta= 0.96$). Within the model, ϕ was predicted directly from light response curve fitting, however the value given is dependent upon the range of values considered for the fit. For example, if you constrain the fit for ϕ to be between 0 and $50 \mu\text{mol m}^{-2} \text{s}^{-1}$, the value of ϕ rises from 0.0381 to

0.0482 for Ws. This corresponds to a \bar{P}_{max} and P_{max}^{opt} of 14.3 $\mu\text{mol m}^{-2} \text{s}^{-1}$ and 13.4 $\mu\text{mol m}^{-2} \text{s}^{-1}$ for τ of 0.3 and 14.5 $\mu\text{mol m}^{-2} \text{s}^{-1}$ and 15.1 $\mu\text{mol m}^{-2} \text{s}^{-1}$ for τ of 0.1, respectively. Thus the conditions under which quantum use efficiency and the other light response curve parameters are determined will determine the output of the model.

To see whether the model is capable of predicting the magnitude of change witnessed in this study, different combinations of parameters were also tried. Model simulations were run at incremental values of τ between 0 and 1. For these simulations, different combinations of α and ϕ were trialed in order to find the closest correspondence to the P_{max} value for the constant light treatment (i.e. \bar{P}_{max}). θ remained fixed throughout in accordance with the value taken from the fitted LRCs (Fig. 9.3). The same parameters were then used to predict P_{max}^{opt} . Simulation results are shown in Fig. 9.6. Results indicate that for a $\tau < 0.1$, the value of P_{max}^{opt} is greater than the value of \bar{P}_{max} , but by a τ value of 0.2 this pattern is reversed. The model is capable of correctly predicting the magnitude of change in P_{max} for Ws, at a τ value of approximately 0.1, but is unable to predict the change for Ler. This may be due to different kinetics of induction between the two lines or genotypic differences allowing for a greater response of Ler relative to Ws. For Ws, the model output for τ value of 0.1 corresponds to values of α at 0.08 and ϕ at 0.06. This value of τ may be more representative of the plants used in this study, relative to the value of 0.3 found previously (Retkute *et al.*, 2015) as induction appears to be rapid during the change between irradiance levels (Fig. 9.5 and Supp. Fig. S9.1).

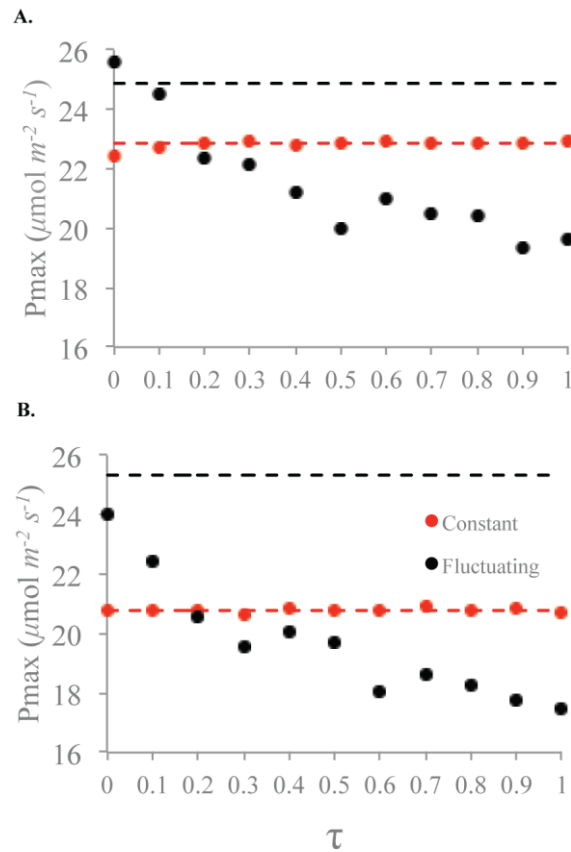


Figure 9.6: Acclimation Model output. (A) *Ws* (B) *Ler*. The acclimation model was run at incremental values of τ between 0 and 1. For these simulations, different combinations of α and Φ were trialed in order to find the closest correspondence to the P_{max} value for the constant light treatment (i.e. \bar{P}_{max} ; red points). θ remained fixed throughout in accordance with the value taken from the fitted LRCs (Fig. 9.3). The same parameters were then used to predict P_{max}^{opt} ; black points.

Discussion

Within this study, we have shown that the ability of *Arabidopsis* to acclimate under fluctuating light conditions. Our inclusion of the *gpt2*- mutant not only agrees with previous studies that indicate GPT2 is critical to the dynamic acclimation process and confers a fitness advantage for plants growing in a fluctuating light environment (Athanasίου *et al.*, 2010; Dyson *et al.*, 2015).

The acclimation response of increasing P_{\max} under high light is usually mirrored by a step-wise increase in Chl a:b ratio, due to loss of LHCII (Scheibe *et al.*, 2005 Bailey *et al.*, 2001). Interestingly, for the Ler ecotype, a lower Chl a:b ratio was observed in the FL treatment compared to CL treatment (Fig. 9.4), this combined with the fact it there was a significant increase in P_{\max} (Fig. 9.3C) plus a change in photosynthesis at $50 \mu\text{mol m}^{-2} \text{s}^{-1}$ in the days following a change in the light treatment (Fig. 9.5C) suggests that it was able to acclimate to both the high light and the low light under FL conditions (Anderson, 1980; 1986; Walters, 2005). This decrease in Chl a:b ratio under FL vs CL was also observed in the *gpt2*- mutants suggesting that the mutant was still able to acclimate to lower light. Whilst the FL treatment did appear to have an influence on chl a:b in Ws, the results were not consistent across all rounds however a low light adaptation can be seen in the change in photosynthesis at $50 \mu\text{mol m}^{-2} \text{s}^{-1}$ in the days following a change in the light treatment, although this is not significant, (Fig. 9.5A) and high light adaptation can be seen with the significant increase in P_{\max} (Fig. 9.3A). These findings suggest that the effect of fluctuating light on acclimation is to invoke multiple pathways that allow an acclimation response to both high and low irradiances.

Athanasίου *et al.* (2010) grew plants outdoors in unheated green houses, and found that under naturally fluctuating light, WT Ws had a higher fitness compared to *gpt2*- mutants and the Columbia (Col) accession. The same study also showed the inability for Col to dynamically acclimate to an increase in irradiance under controlled conditions (see Fig. 1 in Athanasίου *et al.*, 2010). The fact that Col expresses GPT2 but does not acclimate (Niewiadomski *et al.*, 2005) supports the hypothesis that alternative pathways, not involving GPT2,

are necessary for dynamic acclimation under fluctuating light. Further evidence for this is that *gpt2*- mutants have a higher photosynthesis rate at lower light levels than WT plants (Dyson *et al.*, 2015). However, these findings represented developmental acclimation, as the plants were grown under low light. Even so, this data combined with our findings that *gpt2*- plants had a significantly lower Chl a:b ratio (Fig. 9.5) provides evidence that acclimation to lower light is controlled by a different process to the GPT2-mediated acclimation to high light. The role of GPT2 is to translocate G6P into the chloroplast (Kunz *et al.*, 2010) in order to allow for starch synthesis. This results in an increased chloroplastic phosphate pool, causing changes in gene expression and enabling acclimation to high light. It would therefore make sense that a knock out in triphosphate translocator (TPT) (responsible for export of glyceraldehyde 6-phosphate, the precursor to G6P) would allow for a better acclimation response to higher light. Instead the opposite is seen (Walters, 2004), indicating that the full mechanism behind the acclimation response is not yet understood. In consensus with the literature, our findings suggest that dynamic acclimation to high- and low- light are controlled by at least two distinct mechanisms, and that both are utilised in *A. thaliana* in order to provide a fitness advantage under the fluctuating light patterns that plants are subject to in natural conditions (Athanasidou *et al.*, 2010; Suorsa *et al.*, 2012; Dyson *et al.*, 2015; Retkute *et al.*, 2015). Athanasidou *et al.* (2010) identified genes that were up/down regulated in response to high light; similar methods such as reverse genetics could be used to identify up/down regulated genes in response to low light, and identify candidates that are used in both mechanisms.

There is evidence that in developmentally acclimated plants, some species do not change their chlorophyll a:b ratios (Murchie & Horton, 1997; Zivcak *et al.* 2014). Furthermore, some changes in chlorophyll a:b ratio have been attributed to genes involved in LHCII distribution, which is a known induction response (Allen & Forsberg, 2001; Depège *et al.*, 2003; Bellafiore *et al.*, 2005; Vainonen *et al.*, 2005; Suorsa *et al.*, 2012; Mekala *et al.*, 2015; Retkute *et al.*, 2015). These genes could also be manipulated in order to eliminate induction-

induced changes and thus focus solely on the effects of acclimation. However, experiments would have to be done under relatively low light levels, since induction is vital for photoprotection (Demmig-Adams & Adams, 1992). This could be used to indicate the role of acclimation in low light adaptation. Other responses may also be involved in the acclimation response. For example, changes in Rubisco concentration and activity, along with molecular changes such as cytochrome-b/f activity and, as described, light harvesting complexes alter during switching from high to low light or vice versa (Murchie & Horton, 1997; Walters *et al.*, 1999; Yano & Terashima, 2001; Walters, 2005; Suorsa *et al.*, 2012). Thus, for further analysis of the affects of fluctuating light on acclimation in *A. thaliana* protein assays for Rubisco, cytochrome b/f and LHCs on would also be required.

Fluctuating light experiments have been performed on plants under natural conditions, these found that the ability to acclimate provided a fitness advantage (Athanasίου *et al.*, 2010; Suorsa *et al.*, 2012). However, in these experiments plants were grown constantly outside and were subject to fluctuations in temperature and humidity as well as light. Therefore these experiments did not distinguish between developmental and dynamic acclimation, nor did they distinguish between temperature and light acclimation, or rule out any other stressors to which the plants may have been subject to. The experiment we designed was a first that attempted to outline specifically the effect of fluctuating light on acclimating *A. thaliana*. By utilising a more realistic fluctuating light pattern than previous experiments (Chabot *et al.*, 1979; Watling *et al.*, 1997; Yin & Johnson, 2000), keeping all other conditions constant and performing direct comparisons with a *gpt2*-mutant known not to be able to acclimate at least to high light, we have demonstrated the advantage of dynamic and developmental acclimation to light.

The modelling approach used in this study shows that there is good agreement between the change in P_{\max} between the constant and fluctuating light pattern for τ values < 0.1 . Above this value, P_{\max}^{opt} is predicted to be lower

than \bar{P}_{max} . A value of τ at 0.1 corresponds to a maximum leaf ‘memory’ of 6 minutes. This suggests that to fully exploit a fluctuating light environment, plants must be able to respond rapidly to changes in light levels. The predicted values of P_{max} derived depend upon the parameters used to run the model. The accuracy of the model could be improved by a number of ways. Firstly, the model does not take into account a change in the other light response curve parameters following a change in light; for example, the data here indicates that quantum use efficiency is higher under the fluctuating light pattern relative to constant light. Secondly, the model does not take into account differences in the acclimation potential of the different lines (e.g. Athanasiou *et al.*, 2010), therefore whilst the model shows a good agreement to measured data for Ws, it is unable to predict the magnitude of change seen in Ler (Fig. 9.6). Finally, the model uses a time-weighted average of light to account for induction data (Eq. 3). Knowledge of actual induction times could be used to improve the accuracy of this aspect of the model, however this can be extremely difficult to measure with knowledge of the past light history critical. Nevertheless, the modelled data here shows good agreement to measured data. Two key conclusions were drawn by Retkute *et al.* (2015): i) the increase in optimal P_{max} depends on the fraction of time spent under low light compared to high light and ii) optimal P_{max} is greater under a lower frequency of low to high light transitions. Therefore, the actual light pattern a plant is subject to in nature will determine whether acclimation is beneficial or not in terms of carbon gain.

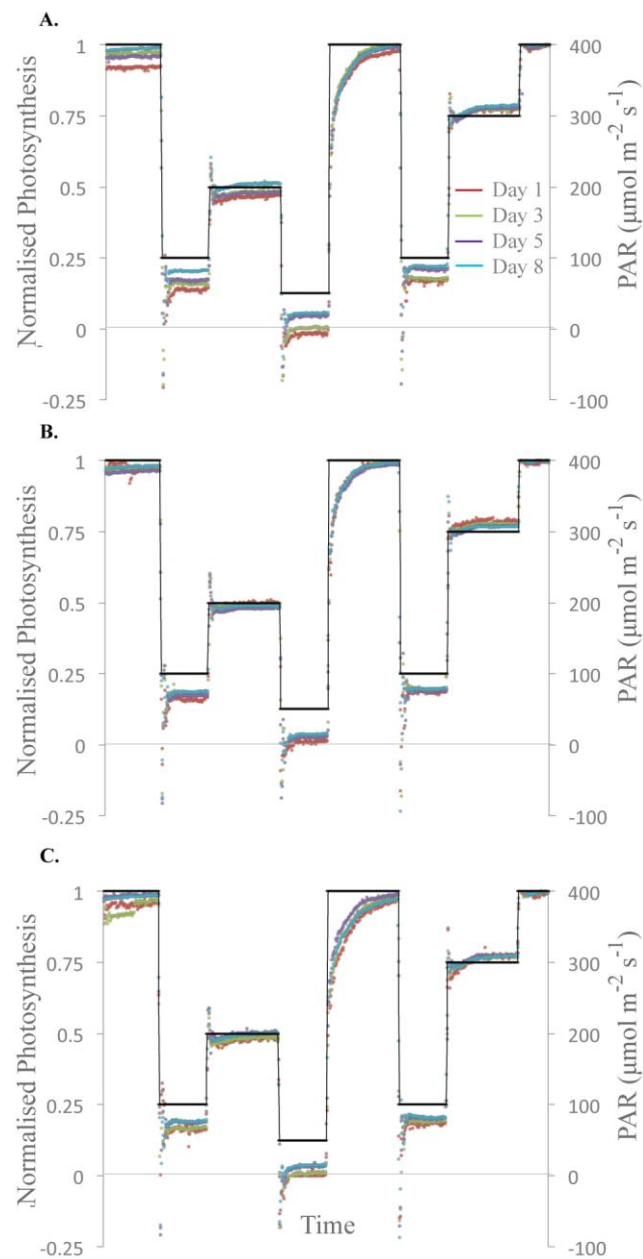
More realistic representations of the natural environment will be critical for determining the adaptive significance of acclimation and determining the limits placed on plants. Whilst we provide good evidence, based on gas exchange and chlorophyll assays, that acclimating under fluctuating light provides a fitness advantage, the equipment used for light response curve measurements (see Materials and Methods; Gas Exchange Measurements) is not sensitive enough to accurately measure dark respiration, which is a key indicator of acclimation to low light. Furthermore, the Fytoscope 3000 (PSI System, Czech Republic) used within this experiment uses a combination of red, blue and far-red LEDs, not white light, which plants would be subject to under natural conditions. We

used a 50:50 red:blue composition within this study in order to mimic natural conditions as closely as possible and whilst it would be more accurate to perform the experiment under white light (Walters, 2005), these wavelengths drive the major light dependent processes in a plant. Light response curves were taken using white light (from a combination of red, blue and green LEDs). A repeat of this experiment using more accurate methods of calculating gas exchange in *Arabidopsis* and white light could be performed to improve the accuracy of the results. Furthermore, more realistic light patterns could be achieved (see Fig. 4 Retkute *et al.*, 2015) by designing a light pattern based on natural conditions, in order to achieve results that better represent the effect of a natural fluctuating light pattern on acclimation in *A. thaliana*.

Acclimation is a complex process and experimental data indicates that the past light history of a leaf is critical in determining the optimal P_{\max} under a given light level (e.g. Retkute *et al.*, 2015). Whilst this can be controlled or determined relatively easily within small plants with simple structures, such as *Arabidopsis*, knowledge of the past light history is difficult to obtain for larger plants, or crop plants, like rice and wheat (Murchie *et al.*, 2002; 2009). The complex canopy structure of these plants combined with environmental factors such as weather conditions and wind, cloud or solar movement mean that a given section of leaf within the same plant will be subject to light changes that vary in frequency and longevity. Knowledge of the underlying mechanisms of this process, what fitness advantages acclimation provides and how it could be manipulated will therefore be critical in targeting crops for improved productivity and yield.

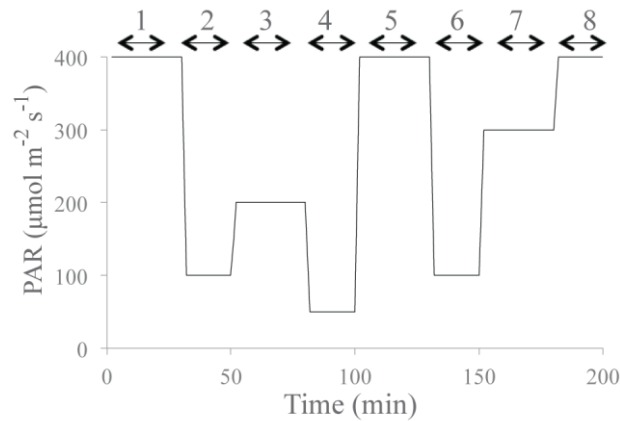
Supplementary Material

Supplementary Figure S9.1



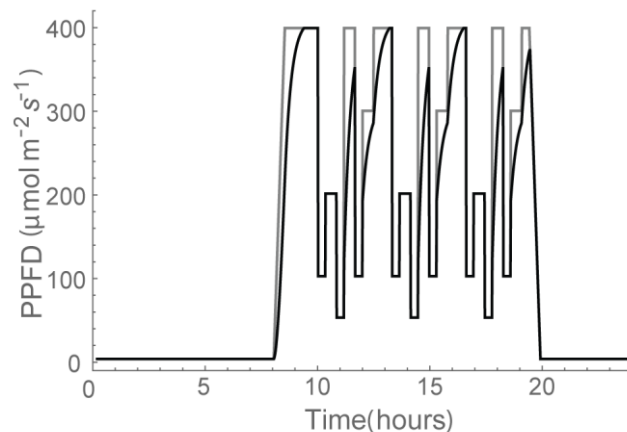
Supplementary Figure S9.1: Normalised response of photosynthesis to light levels in the days following a change in the light pattern. (A) Ws (B) gpt2- and (C) Ler. To avoid errors associated with miscalculation of rosette area, the data presented in Fig. 5 was normalised according to the photosynthesis value at the final ($400 \mu\text{mol m}^{-2} \text{s}^{-1}$) stage.

Supplementary Figure S9.2



Supplementary Figure S9.2: Light motif taken from the fluctuating light pattern. The light motif was separated out into sections, denoted by the numbers and arrows above the graph, in order to make comparisons in the change in photosynthesis in the days following a change in light level.

Supplementary Figure S9.3



Supplementary Figure S9.3: Example of a time-weighted light pattern at $\tau=0.3$ (black line) relative to a non-weighted line (i.e. $\tau=0$; grey line). The time weighted average (Eq. 3) is an exponentially decaying weight used to represent the fact that photosynthesis is not able to respond instantaneously to a change in irradiance levels. If $\tau=0$ then a plant will be able to instantaneously respond to a change in irradiance, whereas if $\tau>0$ the time-weighted average light pattern will relax over the timescale τ . Within this study, different values of τ were trialed.

Supplementary Table S9.1

Line	Days Post Treatment	Stage 1	Stage 2	Stage 3	Stage 4 (50	Stage 6 (100	Stage 5 (50 - 400 $\mu\text{mol m}^{-2} \text{s}^{-1}$)			
		(400 $\mu\text{mol m}^{-2} \text{s}^{-1}$)	(100 $\mu\text{mol m}^{-2} \text{s}^{-1}$)	(200 $\mu\text{mol m}^{-2} \text{s}^{-1}$)	$\mu\text{mol m}^{-2} \text{s}^{-1}$)	$\mu\text{mol m}^{-2} \text{s}^{-1}$)	Time taken to 0.7 (min)	Time taken to 0.8 (min)	Time Taken to 0.9 (min)	
		Normalised Photosynthesis								
Ws	Day 1	0.921±0.049	0.138±0.033	0.467±0.027	-0.015±0.031	0.170±0.023	1.625±0.308	3.417±0.641	9.500±2.426	
	Day 3	0.972±0.013	0.159±0.037	0.485±0.021	0.005±0.041	0.177±0.033	1.542±0.368	3.000±0.761	5.958±1.168	
	Day 5	0.959±0.026	0.171±0.026	0.479±0.024	0.046±0.012	0.120±0.009	1.400±0.332	3.300±0.677	6.950±1.062	
	Day 8	0.988±0.016	0.204±0.014	0.512±0.011	0.057±0.010	0.225±0.010	1.500±0.371	3.292±0.624	7.000±1.342	
	P Value	0.455	0.447	0.508	0.247	0.272	0.976	0.975	0.469	
<i>gpt2-</i>	Day 1	0.966±0.004	0.160±0.032	0.498±0.027	0.015±0.036	0.191±0.021	0.750±0.500	2.250±0.250	5.250±0.750	
	Day 3	0.974±0.018	0.184±0.020	0.495±0.019	0.031±0.016	0.199±0.014	1.000±0.381	2.417±0.667	5.333±1.609	
	Day 5	0.964±0.016	0.174±0.018	0.481±0.016	0.027±0.019	0.191±0.017	1.670±0.363	2.417±0.546	6.083±1.333	
	Day 8	0.981±0.009	0.186±0.015	0.490±0.011	0.039±0.018	0.201±0.015	1.000±0.289	2.083±0.712	5.167±1.202	
	P Value	0.836	0.827	0.906	0.861	0.958	0.905	0.974	0.957	
Ler	Day 1	0.954±0.030	0.162±0.011	0.483±0.017	0.0003±0.009	0.184±0.009	2.792±0.236	6.125±0.738	12.708±1.603	
	Day 3	0.954±0.026	0.167±0.015	0.486±0.014	0.010±0.015	0.193±0.008	2.250±0.479	4.167±0.826	9.333±1.125	
	Day 5	0.988±0.008	0.188±0.005	0.503±0.006	0.035±0.004	0.204±0.005	1.625±0.272	3.125±0.648	7.458±0.950	
	Day 8	0.984±0.010	0.191±0.004	0.499±0.005	0.039±0.004	0.209±0.004	1.833±0.154	4.292±0.522	10.958±1.046	
	P Value	0.533	0.135	0.544	0.017	0.068	0.068	0.044	0.036	

Supplementary Table S9.1: Normalised photosynthesis at stages 1-4 and 6 (corresponding to the steps at 400, 100, 200, 50 and 100 $\mu\text{mol m}^{-2} \text{s}^{-1}$, respectively) and the time taken to achieve a normalised photosynthesis value of 0.7, 0.8 and 0.9 following a change in light level from 50 to 400 $\mu\text{mol m}^{-2} \text{s}^{-1}$ (stage 5). $n=6$ (apart from gpt2- where $n=3$). To avoid errors associated with miscalculation of rosette area, the data presented in Fig. 5 was normalised according to the photosynthesis value at the final (400 $\mu\text{mol m}^{-2} \text{s}^{-1}$) stage. Mean \pm SEM presented plus P value following ANOVA.

Chapter 10: Whole canopy acclimation

Paper as resubmitted to New Phytologist

Chapter 10 adapts the acclimation model presented in Chapter 8 to the whole canopy level using field-grown wheat. This has been resubmitted to New Phytologist so is presented in “paper format”.

Author contribution:

Experiments designed by AJ Burgess, R Retkute and EH Murchie

Project supervision performed by EH Murchie

Field measurements by AJ Burgess, K Chinnathambi and JWP Randall

Rubisco Assays conducted by E Carmo-Silva

Model adaptation by R Retkute and all modelling carried out by AJ Burgess and R Retkute

Imaging and reconstruction, data analysis and paper construction performed by AJ Burgess

Sub-optimal photosynthetic acclimation in wheat is revealed by high resolution 3D canopy reconstruction

Alexandra J. Burgess, Renata Retkute, Kannan Chinnathambi, Jamie W.P. Randall, Elizabete Carmo-Silva and Erik H. Murchie

Summary

- Photosynthetic acclimation (photoacclimation) is the process whereby leaves alter their morphology and/or biochemistry to optimise photosynthetic efficiency and productivity according to long-term changes in the light environment. Three-dimensional (3D) architecture of plant canopies imposes complex light dynamics, causing leaves to frequently shift between light limitation and light saturation. The drivers for photoacclimation in such fluctuating environments are poorly understood.
- Here techniques for high-resolution 3D reconstruction of canopies were combined with photosynthesis modelling to test the effectiveness of photoacclimation according to in-canopy light. Three field-grown wheat lines were reconstructed. Ray tracing was used to simulate a daily time course of radiation. A model of photoacclimation predicted the optimal distribution of photosynthesis according to the complex fluctuating light patterns that occur within each canopy level.
- Whilst the acclimation model output showed good correlation with the field-measured gas exchange data at the top of the canopies, it predicts a lower optimal light saturated rate of photosynthesis (P_{\max}) at the base. Measured levels of Rubisco and protein content are consistent with the measured P_{\max} .
- We conclude that even when the fluctuating light patterns imposed by realistic 3D architecture are taken in to account, it's clear that lower

leaves retain a photosynthetic capacity greatly in excess of that required. These leaves are unable to exploit high light 'sun flecks'. This substantially reduces photosynthetic nitrogen use efficiency at the canopy level and has implications for photosynthetic productivity in low light environments.

Introduction

The arrangement of plant material in time and space can result in a heterogeneous and temporally unpredictable light environment. This is especially true within canopies, where unique and subtle variations in leaf and stem architectural features can lead to complex patterns of light according to solar movement, weather and wind. This has an effect on productivity because photosynthesis is highly responsive to changes in light intensity over short timescales (seconds to minutes). Leaf photosynthesis does not respond instantaneously to a sudden change in light level: the delay before steady state is reached is closely linked to the photosynthetic induction state, which is a physiological condition dependent on the leaf's recent 'light history'. Induction state is defined by factors including the activation state of photosynthetic enzymes (Yamori *et al.*, 2012; Carmo-Silva & Salvucci, 2013), stomatal opening (Lawson & Blatt, 2014) and photoprotection (Hubbart *et al.*, 2012). Together these determine the speed with which a leaf can respond to an increase in light intensity. It is thought that these processes are not always coordinated for optimal productivity in fluctuating light, as shown by the slow recovery of quantum efficiency for CO₂ assimilation (ϕ_{CO_2}) in low light (Zhu *et al.*, 2004), high non-photochemical quenching (NPQ) during induction (Hubbart *et al.*, 2012) and slow stomatal opening and closure (Lawson & Blatt, 2014).

Photosynthetic acclimation (photoacclimation) is the process by which plants alter their structure and composition over long time periods (days and weeks), in response to the environment they experience. Acclimation to light can be broadly split into two types: acclimation that is determined during leaf

development, including cell size and number plus leaf shape (Weston *et al.*, 2000; Murchie *et al.*, 2005) or acclimation that can occur within mature tissues (Anderson *et al.*, 1995; Walters, 2005; Retkute *et al.*, 2015). Whilst the former is largely irreversible, the latter, here termed dynamic acclimation, can be reversible. Differences include changes in light harvesting capacity (shown by chlorophyll a:b ratio), chlorophyll per unit nitrogen, electron transport capacity per unit chlorophyll and rate of electron transport capacity relative to Rubisco activity (Björkman, 1981; Evans, 1989; Evans & Poorter, 2001). This involves change in relative amounts of a number of primary components and processes including light harvesting pigment protein complexes (LHC), Calvin cycle enzymes and electron transport components such as the cytochrome b/f complex. It is normally considered that acclimation represents an economy of form and function, permitting higher capacity for carbon assimilation in high light whilst improving the quantum efficiency at low light (Björkman, 1981; Anderson & Osmund, 1987; Anderson *et al.*, 1995; Murchie & Horton, 1997).

Acclimation has typically been studied in experiments that use artificial growth room lighting, without the capability to simulate natural fluctuations. An important question concerns which features of natural light induce acclimation processes e.g. integrated light levels, duration of high / low light periods or the frequency of high / low light periods. Early work suggested that integrated PPFD could be an important driver of acclimation (Chabot *et al.*, 1979; Watling *et al.*, 1997) however later work, using well characterised artificial fluctuations, highlighted the importance of the duration of high and low light periods (Yin & Johnson, 2000; Retkute *et al.*, 2015). These questions are especially important when attempting to predict the efficacy of acclimation for productivity in a changeable environment such as a plant canopy. There is a cost to the organism in terms of investment of energy and resources (C, N) in acclimation which may explain why acclimation to high light (which requires *de novo* synthesis of proteins such as Rubisco to support higher P_{\max}) is slower than the response to low light (Athanasidou *et al.*, 2010). The concept of economy is important: the photosynthetic system represents a significant sink for leaf nitrogen and other soil-derived mineral elements and this sink will

increase in size as photosynthetic capacity of the leaf rises. This gives rise to the further concept that the plant must measure and predict changes in its environment to elicit the most efficient response.

Calculating the relative benefits of acclimation in natural fluctuating environments is therefore not straightforward and must take into account the patterns of naturally fluctuating light which has not so far been addressed. In addition to light, there are clear interactions with other factors for example photosynthetic nitrogen use efficiency (PNUE, photosynthesis per unit leaf N on an area basis). It has been previously shown that increasing growth irradiance leads to a change in nitrogen partitioning geared towards maximising photosynthesis in high light (Evans & Terashima, 1987; Terashima & Evans, 1988; Verhoeven *et al.*, 1997; Evans & Poorter, 2001; Terashima *et al.*, 2005; Niinemets & Anten, 2009). Changes in light levels shift biomass allocation between components which influences the investment of nitrogen (Evans & Poorter, 2001). Within canopies, a close relationship between light, N and photosynthesis is often observed that is partly driven by acclimation and this is termed canopy ‘optimisation’. However many plants (e.g. cereals) also remobilise N and C away from the leaf as part of a preprogrammed senescence, a process that occurs alongside an acclimation response to progressive shading and is linked to demands for grain nitrogen accumulation (Foulkes & Murchie, 2011; Pask *et al.*, 2012). Despite this, light is considered to be the dominant factor in determining N distribution (and therefore photosynthetic capacity) in most plant canopies (Hikosaka *et al.*, 1994; Anten *et al.*, 1995; Niinemets *et al.*, 2015). It needs to be noted that the correlation between light and nitrogen extinction coefficients seems to vary according to canopy size (Moreau *et al.*, 2012).

We know from previous work that leaves do not simply integrate light over time to determine acclimation status (e.g. Retkute *et al.* 2015). Progress is currently limited by a lack of understanding of the role of complex natural fluctuations caused by the difficulty of obtaining realistic 3D canopy reconstructions. Previous work has shown that even small alterations in

architecture result in substantial changes in light distribution (Burgess *et al.*, 2015). The importance of using natural light should be stressed here: it is axiomatic that in a fluctuating light environment the cost and benefit of investment of carbon, nutrients and energy will also change according to the light level, even over very short time periods. For example acclimation to high irradiance is often associated with an increase in the synthesis of Rubisco per unit leaf area (Evans & Terashima, 1987) and PNUE will thereafter remain high only if the high irradiance is sustained. It could be assumed that investing in a high photosynthetic capacity in low light environments would be advantageous in terms of exploiting brief periods of high light (Percy, 1990) but this has not been tested using realistic light patterns within a plant canopy.

To address this issue we have developed two novel techniques. First a model of acclimation that provides a quantitative indicator of carbon gain, predicting optimal maximal photosynthetic capacity levels (P_{max}^{opt}) for a given variable environment (Retkute *et al.*, 2015) but does not consider PNUE or the energy required to undergo acclimation. Secondly, a method for the 3-dimensional (3D reconstruction of plant canopies in high resolution that, with available ray tracing techniques (Song *et al.*, 2013), can characterise light in every point in the canopy over the course of a day (Pound *et al.*, 2014; Burgess *et al.*, 2015). Here we use these techniques in combination with manual measurements of photosynthesis to predict the optimal acclimation status throughout canopy depth according to the (variable) light it receives due to its canopy position. We show that the optimal P_{max} in all leaves in the bottom canopy layers is substantially lower than that measured, an observation that has implications for PNUE of the whole canopy.

Materials and Methods

Experimental and modelling strategy

The complexity of a crop canopy combined with the intricacy of the processes that lead to acclimation means that scaling up to the whole canopy level is difficult. However, recent advances have led to new techniques for high-resolution reconstruction of crop canopies, and methods for accurately simulating the light environment (e.g. Song *et al.*, 2013; Pound *et al.*, 2014). Combining the two techniques allows the prediction of precise local PPFD at multiple time points. The empirical model employed (Retkute *et al.*, 2015) uses parameterisation in the form of gas exchange data taken in the field to predict a distribution of optimal photosynthetic capacities within each of the canopies, based on the levels of light experienced within the canopy over the whole day.

Plant Material

Wheat lines with contrasting canopy architectures were selected from an ongoing field trial at the University of Nottingham farm (Sutton Bonington Campus) in 2015. 138 Double haploid (DH) lines were developed jointly by Nottingham and CIMMYT from a cross between the CIMMYT large-ear phenotype spring wheat advanced line LSP2 and UK winter wheat cultivar Rialto, as described in Burgess *et al.* (2015). This approach resulted in the formation of a large number of stable lines with contrasting canopy architecture but with photosynthetic responses consistent with the UK environment (Driever *et al.*, 2014). Three wheat lines were selected for analysis: Ashby (one of the parent lines), 32-129bc (Line 1) and 23-74bc (Line 2). All field conditions and N applications were the same as described for the previous growing season in Burgess *et al.* (2015). Two growth stages were analysed: preanthesis and postanthesis (equivalent to GS55-59; Zadoks *et al.*, 1974).

Plant Physical Measurements

Physical measurements were made on plants in the field (see Table 10.1 plus Supporting Information Table S10.1). The number of plants and tillers within a

1 m section along the middle of each row were counted and averaged across the three replicate plots. This average value was used to calculate the planting density within the plots and thus used to ensure that the reconstructed canopies were representative of field conditions.

Plant dry weight and area was analysed by separating shoot material into stem, flag leaf and all other leaves before passing them through a leaf area meter (LI3000C, Licor, Nebraska) for 6 replicate plants (2 per plot; those used for the reconstruction of canopies below). Each component was then dried individually in an oven at 80°C for 48 hours or until no more weight loss was noted. Plants were weighed immediately. Measured LAI (leaf area per unit ground area: m²) was calculated as the total area (leaf + stem) divided by the area of ground each plant covered (distance between rows x distance within rows) and averaged across the 6 replicate plants. The LAI of each reconstructed canopy was calculated as the area of mesh inside the ray tracing boundaries divided by the ground area. The LAI of the plots were then compared to the LAI for each of the reconstruction plots; see Table 2.

Imaging and Ray Tracing

3D analysis of plants was made according to the protocol of Pound *et al.* (2014) and further details are given in Burgess *et al.* (2015). An overview of this process is given in Fig. 10.1. From the sampled and reconstructed plants, canopies were made in *silico* according to Burgess *et al.* (2015). Two replicate plants representative of the morphology of each wheat line were taken per plot, giving 6 replicates per line, and reconstructed; at least 4 of these were used to form each the final canopies (Fig. 10.2). The wheat ears (present postanthesis) were manually removed from the resultant mesh as the reconstructing method is unable to accurately represent their form. Reconstructed canopies were formed by duplicating and randomly rotating the plants in a 3 x 4 grid, with 13 cm between rows and 5 cm within rows (calculated from field measurements).

Total light per unit leaf area was predicted using a forward ray-tracing algorithm implemented in fastTracer (fastTracer version 3; PICB, Shanghai,

China; Song *et al.*, 2013). Latitude was set at 53 (for Sutton Bonington, UK), atmospheric transmittance 0.5, light reflectance 7.5%, light transmittance 7.5%, day 155 and 185 (4th June and 4th July, Preanthesis and Postanthesis respectively). FastTracer3 calculates light as direct, diffused and transmitted components separately; these were combined together to give a single irradiance levels for all canopy positions. The diurnal course of light intensities over a whole canopy was recorded in 1 minute intervals. The ray tracing boundaries were positioned within the outside plants so as to reduce boundary effects.

Gas Exchange and Fluorescence

Measurements were made on field grown wheat in plots in the same week in which the plants were imaged. For light response curves (LRC) and A_{Ci} response curves of photosynthesis, leaves were not dark-adapted. Leaf gas exchange measurements (LRC and A_{Ci}) were taken with a LI-COR 6400XT infra-red gas-exchange analyser (LI-COR, Nebraska). The block temperature was maintained at 20°C using a flow rate of 500 ml min⁻¹. Ambient field humidity was used. LRCs were measured over a series of 7 photosynthetically active radiation (PAR) values between 0 and 2000 μmol m⁻² s⁻¹, with a minimum of 2 minutes at each light level moving from low to high. LRCs were measured at 3 different canopy heights; labelled top (flag leaf), middle and bottom, with height above ground being noted. Three replicates were taken per treatment plot per layer, thus leading to 9 replicates per line. For the A_{Ci} curves, leaves were exposed to 1500 μmol m⁻² sec⁻¹ throughout. They were placed in the chamber at 400 p.p.m. CO₂ for a maximum of 2 min and then CO₂ was reduced stepwise to 40 p.p.m. CO₂ was then increased to 1500 p.p.m., again in a stepwise manner. At least one replicate was taken per treatment plot per layer but with 5 replicates taken for each of the 3 lines. Individual A_{Ci} curves were fitted using the tool in Sharkey *et al.* (2007) to derive values for maximum catalytic activity of Rubisco (V_{cmax}), maximum electron transport activity (J) and triose phosphate utilisation (TPU).

A Walz (Effeltrich, Germany) MiniPam fluorometer was used to measure dark-adapted values of F_v/F_m in the field wheat every hour between 09:00 and 17:00 h. Leaves were dark-adapted using clips (DLC-08; Walz) for 20 min and F_0 and F_m were measured by applying a saturating pulse (0.8 s, $6000 \mu\text{mol m}^{-2} \text{s}^{-1}$). Four replicates were taken per plot per layer but as values for the middle layer were approaching or at the maximal value expected ($F_v/F_{m_{max}} = 0.83$) measurements were not taken for the bottom layer.

Rubisco quantification

Leaf samples were taken from the same leaves and same region of the leaf as the gas exchange measurements. One day was left between gas exchange and sampling. Leaf samples (1.26 cm^2) were ground at 4°C in an ice-cold pestle and mortar containing 0.5 mL of 50 mM Bicine-NaOH pH 8.2, 20 mM MgCl_2 , 1 mM EDTA, 2 mM benzamidine, 5 mM ϵ -aminocaproic acid, 50 mM 2-mercaptoethanol, 10 mM DTT, 1mM PMSF and 1% (v/v) protease inhibitor cocktail (Sigma-Aldrich Co., St Louis, MO, USA). The homogenate was clarified by centrifugation at $14700g$ and 4°C for 3 min. Rubisco in 150 μL of the supernatant was quantified by the [^{14}C]-CABP binding assay (Parry *et al.*, 1997), as described previously (Carmo-Silva *et al.* 2010). The radioactivity due to [^{14}C]-CABP bound to Rubisco catalytic sites was measured by liquid scintillation counting (PerkinElmer, Waltham, MA, USA). Total soluble protein content in the supernatants was determined by the method of Bradford (1976) using bovine serum albumin as a standard. Chlorophylls in 20 μL of the homogenate (prior to centrifugation) were extracted in 95% ethanol for 4-8 hours in darkness (Lichtenthaler, 1987). After clarifying the ethanol-extracted samples by centrifugation at $14000g$ for 3 min, the absorbance of chlorophylls in ethanol was measured at 649 and 665 nm. Chlorophyll *a* and *b* contents were estimated using the formulas $C_a = (13.36 \cdot A_{664}) - (5.19 \cdot A_{649})$ and $C_b = (27.43 \cdot A_{649}) - (8.12 \cdot A_{664})$.

Modelling

All modelling was carried out using Mathematica (Wolfram) using the techniques described in more detail in Retkute *et al.*, (2015) and Burgess *et al.*, (2015). The acclimation model, here adopted for use in the canopy setting, was originally developed based on the observation that *Arabidopsis thaliana* plants subject to a fluctuating light pattern exhibit a higher P_{max} than plants grown under a constant light pattern of the same average irradiance (Yin & Johnson, 2000; Athanasiou *et al.*, 2010). The main model assumption is that plants will adjust P_{max} from a range of possible values in such a way as to produce the largest amount of daily carbon gain. The model predicts an optimal maximum photosynthetic capacity, P_{max}^{opt} , for a given light pattern from light response curve parameters (ϕ , θ and α ; explained below).

In this study we sought to predict the maximum photosynthetic capacity, P_{max}^{opt} , as the P_{max} that represents maximal carbon gain at a single point within the canopy, based on the light pattern that point has experienced (i.e. using the light pattern output from ray tracing; as in right hand panel, Fig. 10.3). This was predicted across 250 canopy points, thus leading to distribution of P_{max}^{opt} values throughout each of the canopies. These 250 canopy points (triangles) from each of the canopies were chosen as a subset of triangles that were of similar size (i.e. area) and constitute a representative sample distribution throughout canopy depth.

The net photosynthetic rate, P , as a function of PPFD, L , and maximum photosynthetic capacity, P_{max} , was calculated using the non-rectangular hyperbola (Eq. 1).

$$F_{NRH}(L, \phi, \theta, P_{max}, \alpha) = \frac{\phi L + (1 + \alpha)P_{max} - \sqrt{(\phi L + (1 + \alpha)P_{max})^2 - 4\theta\phi L(1 + \alpha)P_{max}}}{2\theta} - \alpha P_{max} \quad (1)$$

Where L is the PPFD incident on a leaf ($\mu\text{mol m}^{-2} \text{s}^{-1}$), ϕ is the quantum use efficiency, θ is the convexity and α corresponds to the fraction of maximum

photosynthetic capacity (P_{max}) used for dark respiration according to the relationship $Rd = \alpha P_{max}$ (Givnish, 1988; Niinemets & Tenhunen, 1997; Retkute *et al.*, 2015). The value of α was obtained by fitting a line of best fit between all measured P_{max} and Rd values. Therefore the relationship between P_{max} and Rd used in modelling is based on observation rather than assumption of linear fit. All other parameters (e.g. P_{max} , ϕ and θ) were estimated from the light response curves for three canopy layers using the Mathematica command **FindFit**.

As each canopy was divided into 3 layers, each triangle from the digital plant reconstruction was assigned to a particular layer, m , according to the triangle centre (i.e. with triangle centre between upper and lower limit of a layer depth). For each depth (d ; distance from the highest point of the canopy), we found all triangles with centres lying above d (Eq. 2).

$$d_i = \max_{j=1,2,3; 1 \leq i \leq n} z_i^j - (z_i^1 + z_i^2 + z_i^3)/3 \quad (2)$$

Each triangle within a specific layer was assigned the light response curve parameters from the corresponding measured data.

Carbon gain, C (mol m⁻²) was calculated over the time period $t \in [0, T]$ (Eq. 3).

$$C(L(t), P_{max}) = \int_0^T P(L(t), P_{max}) dt \quad (3)$$

Experimental data indicates that the response of photosynthesis to a change in irradiance is not instantaneous and thus to incorporate this into the model Retkute *et al.* (2015) introduced a time-weighted average for light (Eq. 4).

$$L_\tau(t) = \frac{1}{\tau} \int_{-\infty}^T L(t') e^{-\frac{t-t'}{\tau}} dt' \quad (4)$$

This effectively accounts for photosynthetic induction state, which is very hard to quantify *in situ* as it varies according to the light history of the leaf. The more time recently spent in high light, the faster the induction response. The time-weighted average effectively acts as a “fading memory” of the recent light pattern and uses an exponentially decaying weight. If $\tau = 0$ then a plant will be able to instantaneously respond to a change in irradiance, whereas if $\tau > 0$ the time-weighted average light pattern will relax over the timescale τ . Within this study, τ was fixed at 0.2 (unless otherwise stated) in agreement with previous studies and fit with past experimental data (Percy and Seemann, 1990; Retkute *et al.*, 2015). The time-weighted average only applies to the transition from low to high light, but from high to low, response is here considered to be virtually instantaneous and the time-weighted average is not applied. The effect of this decaying weight effectively acts as a “filter” for irradiance levels, with photosynthesis as slow to respond from a transition from low to high light but quick to respond following a drop in irradiance. This can be seen in Supporting Information Fig. S10.2. This value of τ (0.2) represents a maximum leaf ‘memory’ of around 12 minutes that exponentially declines according to time spent in the light. We also tested the model at a lower value of τ to account for leaves capable of faster induction or a longer ‘memory’.

Results

The Canopy Light Environment

Canopy architectural features such as leaf number, area and angle are key determinants of the in-canopy light environment. Past theoretical work has tended to focus upon canopies with randomly distributed leaves in space (Werner *et al.*, 2001; Zhu *et al.*, 2004) with few recent models using more complex architectural features to simulate canopies (Song *et al.*, 2013; Burgess *et al.*, 2015). The method we employ during this study enables high-resolution accurate reconstruction of the wheat canopies, which represent small differences in architectural features without the need to parameterise structural models. Fig. 10.1 shows an example of the reconstruction process whilst Fig. 10.2 shows the final six canopies (three per growth stage) used within this study.

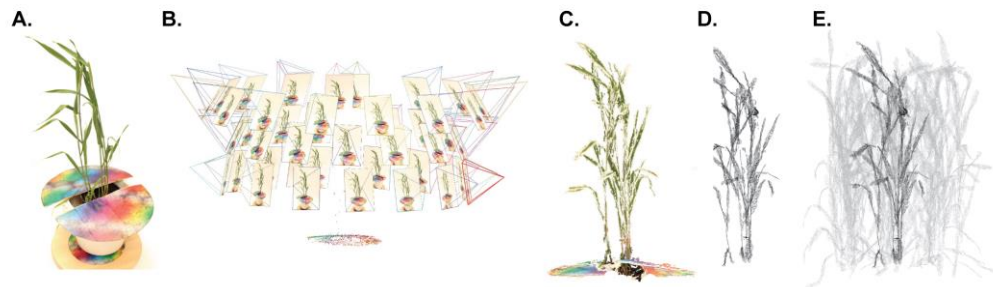


*Figure 10.1: Overview of the Reconstruction Process (A) original photograph, (B) point cloud reconstruction process from stereocameras (Wu, 2011), (C) output point cloud, (D) mesh following reconstruction method (Pound *et al.*, 2014) and (E) final canopy reconstruction. N.B. The multi-coloured disc in panels A-C is a calibration target, used to optimise the reconstruction process and scale the final reconstructions back to their original units.*

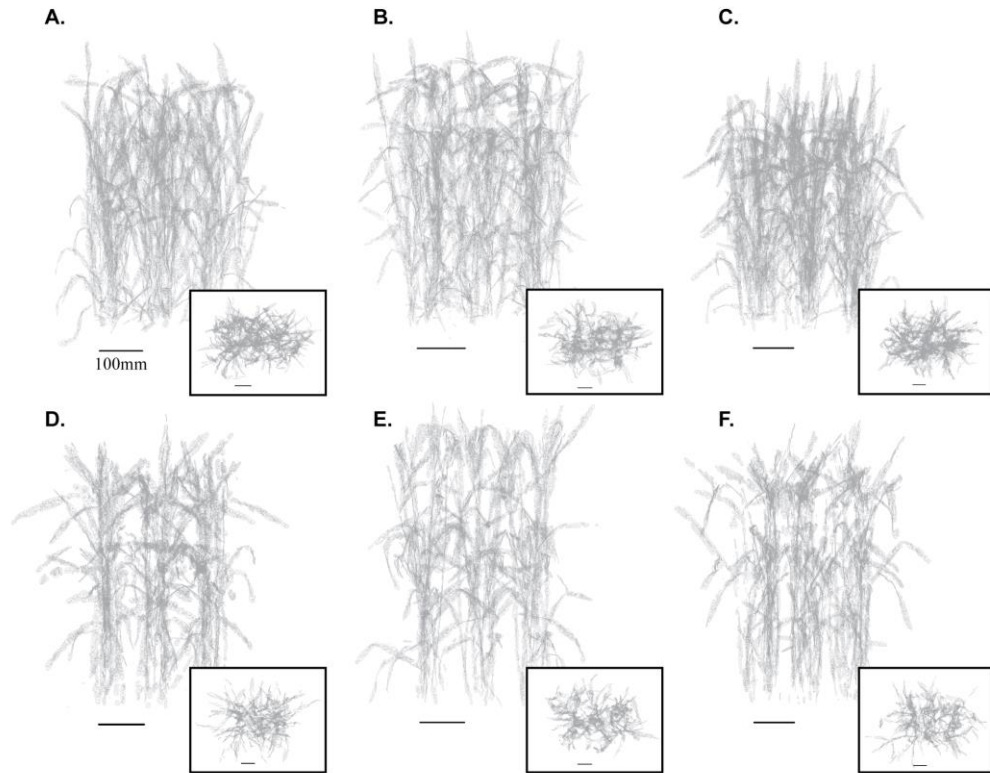


Figure 10.2: Example Canopy Reconstructions from front and top down views. (A-C) Preanthesis and (D-F) Postanthesis. (A,D) Parent Line, (B,E) Line 1 and (C,F) Line 2.

The wheat lines selected were the same as those used for a previous study examining photoinhibition within canopies under field conditions during the 2013/14 growing season (Burgess *et al.*, 2015). The three lines were selected due to their contrasting architectural features; the Parent line contains more upright leaves, Line 2 more curled leaves and Line 1 with an intermediate phenotype. Similar features were observed during the 2014/15 growing season used in this study, with the exception of a more curled leaf phenotype of Line 1 relative to the previous year and altered Leaf Area Index (LAI; leaf area per unit ground area (Table 10.1 and 10.2; measured physical plant measurements and reconstruction LAI values). Burgess *et al.* (2015) showed that manually measured leaf area corresponded well to reconstructed values. Here we find that LAI was slightly higher in all the reconstructions compared to the measured values which was likely due to differences in the way in which stem and leaf area is accounted for in each method: in particular, the manual method

did not account for all stem material and reconstruction method slightly over estimated stem area. Nevertheless, the overestimation was consistent for all lines. Plant density, tillering and plant height were equivalent in Lines 1 and 2 but slightly higher in the Parent line.

Line	Average Number of Plants m ⁻¹	Average Number of Tillers m ⁻¹	Number of Tillers of plant ⁻¹	Average Resting Plant height (cm)	
				Preanthesis	Postanthesis
Parent	25.3±1.5	69.0±3.1	4.0±0.0	72.1±3.2	84.7±0.3
Line 1	21.3±3.2	61.0±2.3	3.5±0.3	68.3±2.0	90.7±1.6
Line 2	20.7±0.3	62.7±2.7	4.1±0.9	69.5±2.7	94.1±5.5
P value	0.287	0.170	0.675	0.579	0.063

Table 10.1: Physical canopy measurements of each Line. Mean ± SEM, n=3. The number of plants and tillers within a 1 m section along a row at the preanthesis stage were counted and averaged across 3 plots. The number of tillers for each of the plants used for reconstructions at preanthesis was counted. The resting plant height of 5 plants per plot was calculated. P value corresponds to ANOVA.

Simulations of the light environment within each of the canopies indicate that the daily photosynthetic photon flux density (PPFD) decreases with depth in all three plots at both growth stages, however there is considerable heterogeneity at each depth that needs to be accounted for in the model application. Fig. 10.3 shows how PPFD varies with depth in 3 randomly selected triangles at each of the three depth positions where samples and gas exchange measurements were made. To validate the predicted light levels in each of the canopies using ray tracing, we compared the model data (as the logarithm of the ratio of light received on a horizontal surface and light intercepted by a point on the leaf ($\ln[L/L_0]$) to manual measurements taken in the field with a ceptometer (Fig. 10.4). We calculated light interception coefficients (k) (Monsi & Saeki, 1953; Hirose 2005) based on fractional interception and cumulative LAI (calculated

as the area of triangles in the mesh with each depth in the canopy; see Burgess *et al.*, 2015 for more details).

Line	Measured			Reconstruction	
	Leaf Area	Stem Area	Total Area	LAI	LAI
Parent	318±20	93±4	799±73	7.22±1.23	8.55
Line 1	312±27	66±10	807±42	6.71±1.30	8.39
Line 2	411±70	82±10	1118±113	8.78±1.90	9.75
P value	0.290	0.167	0.520	0.520	

Table 10.2: Plant and canopy area properties. Mean ± SEM, n=3. Plants were separated into leaf and stem material and measured using a leaf area meter (LI3000C, Licor, Nebraska). Measured LAI was calculated as the total area (leaf + stem) divided by the area of ground each plant covered (distance between rows x distance within rows). The reconstructed LAI was calculated as mesh area inside the designated ray tracing boundaries (see Materials and Methods: Imaging and Ray Tracing). P value corresponds to ANOVA.

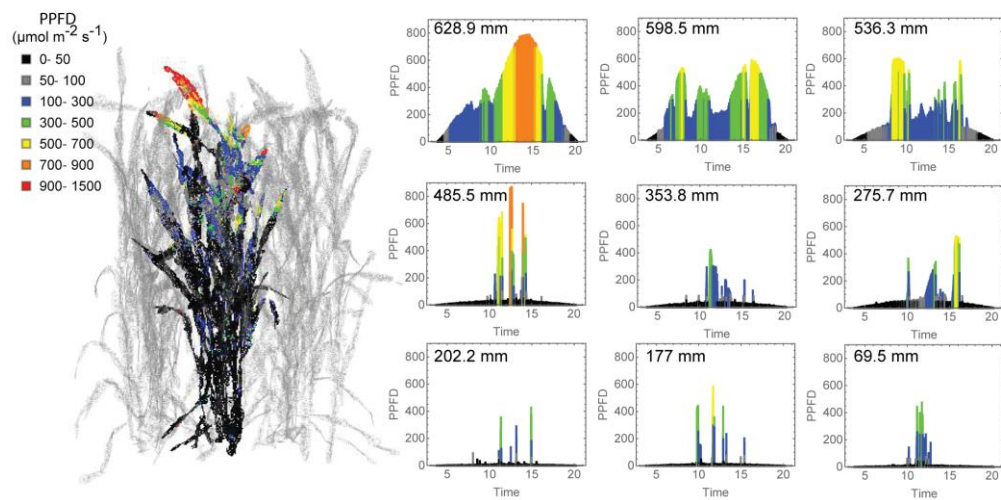


Figure 10.3: Progressive lowering of the canopy position in a canopy results in a reduction in daily integrated PPFD ($\mu\text{mol m}^{-2} \text{s}^{-1}$) but also the pattern and incidence of high light events within the canopy. The left-hand panel shows a representative reconstructed preanthesis wheat canopy with a single plant in bold: Maximum PPFD ranges are colour coded. The right-hand panels show PPFD during the course of a day at 9 representative and progressively lower canopy positions (the height of each canopy location from the ground given in the top left corner of each graph) calculated using ray tracing techniques.

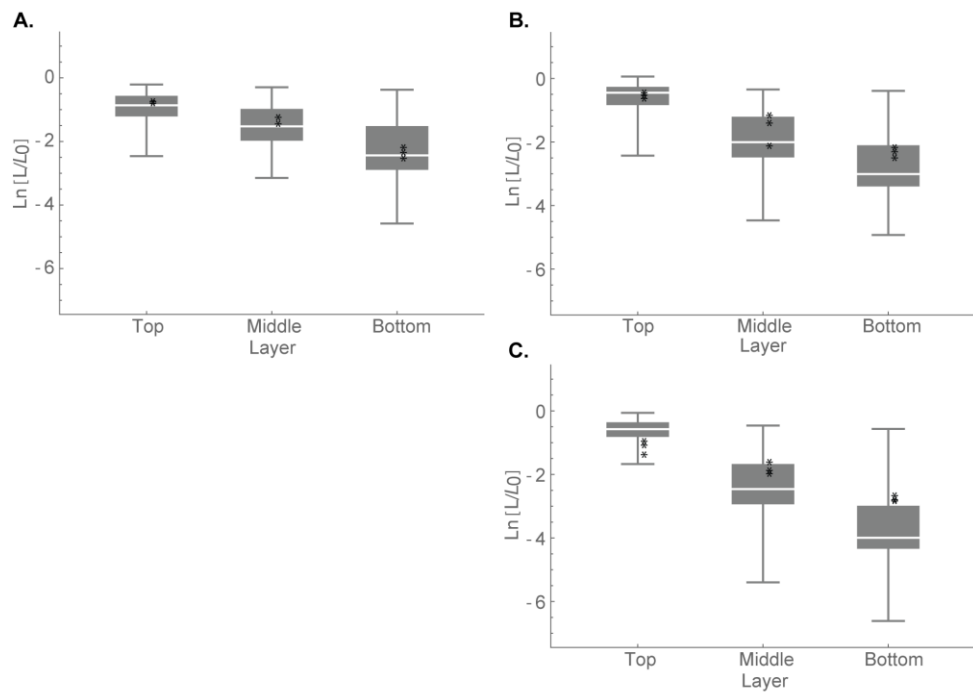


Figure 10.4: Experimental validation of the predicted light levels. The logarithm of the ratio of the light received on a horizontal surface and light intercepted on a point on a leaf ($\ln[L/L_0]$) predicted by ray tracing (box and whisker) is compared to manual measurements made using a ceptometer (stars). Predicted and measured data for (A) Parent Line, (B) Line 1 and (C) Line 2; top, middle and bottom layers of the canopy at 12:00 h.

Effect of Light Levels on Acclimation: Model Output

Fig. 10.5 shows light response curves of photosynthesis for each of the lines at 3 canopy levels. Typical responses are seen: a decline in both P_{\max} and dark respiration rate with increasing canopy depth. A significant lowering of P_{\max} was observed within the two lower layers at postanthesis. A comparison of photosynthesis rates with light levels (Fig. 10.3) shows that all leaves would remain above the light compensation point and positively contribute to carbon gain.

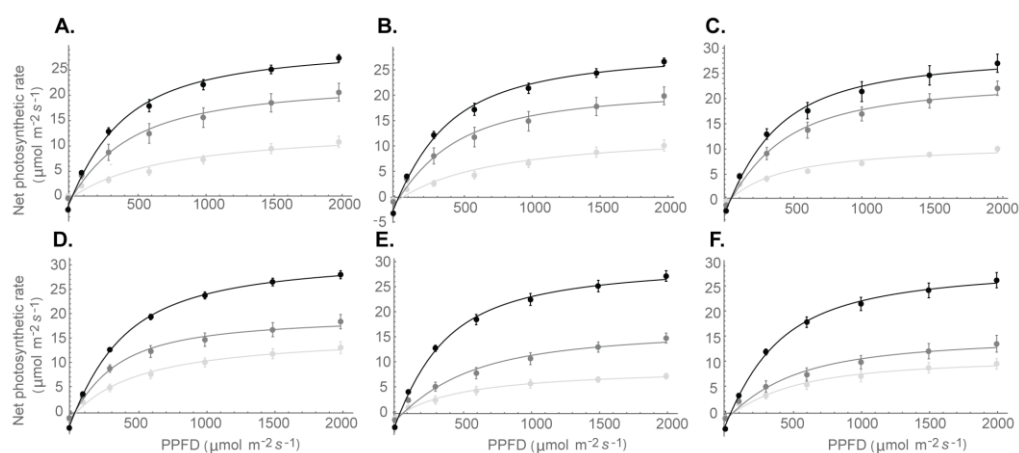


Figure 10.5: Fitted Light response curves for (A-C) Preanthesis; Parent Line, Line 1 and Line 2, respectively. Layer top (black), middle (dark grey) and bottom (light grey). (D-F) Postanthesis; Parent Line, Line 1 and Line 2, respectively. Layer top (black), middle (dark grey) and bottom (light grey).

An empirical model of acclimation was applied (Retkute *et al.*, 2015) as described above in order to predict the optimal P_{\max} (P_{\max}^{opt}) for 250 canopy positions. The model includes the time weighted average (τ), a calculation of the effect of a variable induction state which manifests as a gradually ‘fading memory’ of a high light event (see Materials and Methods: Modelling). Fig. 10.6 shows the result of the modelled optimal P_{\max} against measured P_{\max} . Strikingly, the measured P_{\max} was substantially higher than predicted except in the upper parts of the canopy, which showed good correspondence. This was consistently the case for all lines and both growth stages. In the lowest canopy positions (below 300 mm from the ground) the measured values of P_{\max} were

several times higher than the lowest predicted values : $1 - 2 \mu\text{mol CO}_2 \text{ m}^{-2} \text{ s}^{-1}$. In these positions the important features were those that support a positive carbon gain in extremely low light environments notably a very low dark respiration level (measured at less than $0.5 \mu\text{mol m}^{-2} \text{ s}^{-1}$) and light compensation point. In other words, the measured P_{max} would rarely be achieved *in situ* largely due to the brevity of the high light periods and the slow induction of photosynthesis. A comparison with Fig. 10.3 shows that light levels in this part of the canopy were extremely low: $10 - 30 \mu\text{mol m}^{-2} \text{ s}^{-1}$ punctuated by rare short lived high light events with a large variation in frequency and intensity. The decay of modelled P_{max} was exponential (Fig. 10.6) consistent with that of light (Hirose, 2005) in contrast with the measured P_{max} which appeared linear. It was also notable that the different canopy architectures affected the acclimation responses: the disparity between measured and modelled was greater in line 2 (non erect leaves) which had a higher rate of light extinction. A comparison of the modelled and measured P_{max} versus PPFD at 12:00 h, plus modelled P_{max} versus daily PPFD is given in Supporting Information Fig. S10.3. This shows a similar spread of modelled versus measured P_{max} values and a linear relationship between modelled P_{max} and daily PPFD. We also tested the model at a substantially lower value of τ (0.1; Supporting Information Fig. S10.4), which results in a more rapid response to light flecks (equivalent to maximum leaf ‘memory’ of 6 minutes). Even using this parameter, the P_{max} was substantially over estimated in the bottom layer of the canopy.

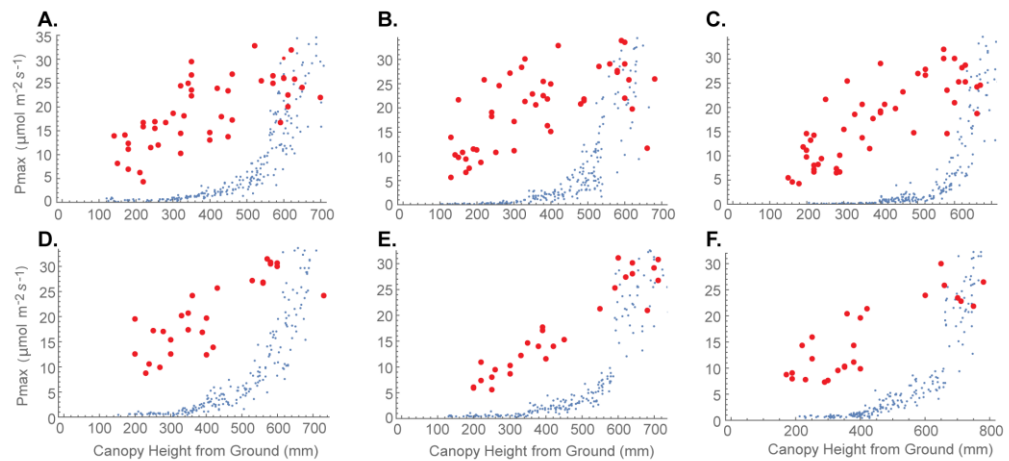


Figure 10.6: Whole canopy acclimation model output (blue) versus gas exchange measurement (red) graphs. The acclimation model was run at 250 locations throughout canopy depth to predict the optimal P_{max} at each location dependent upon the light environment that it experienced, calculated via ray tracing. The time weighted average (Eq. 4) was fixed at $\tau=0.2$. This is an exponentially decaying weight used to represent the fact that photosynthesis is not able to respond instantaneously to a change in irradiance levels. If $\tau=0$ then a plant will be able to instantaneously respond to a change in irradiance, whereas if $\tau>0$ the time-weighted average light pattern will relax over the timescale τ . Model results are compared to field measured gas exchange. (A-C) Preanthesis and (D-F) Postanthesis. (A,D) Parent Line, (B,E) Line 1 and (C,F) Line 2.

During canopy development wheat leaves will normally emerge into high light and then become progressively more shaded by production of subsequent leaves. The higher than expected measured P_{max} at the base of the canopy indicates retention of the enzymes and components of photosynthesis to a level that was excessive when compared to the properties of the light environment. The difference between measured and modelled P_{max} became progressively lower, moving from the bottom of the canopy to the top until there was complete correspondence at the top of the canopy. It is therefore important to confirm the activity of specific components of photosynthesis and compare them to both P_{max} values. One important rate-limiting enzyme is Rubisco: to

understand how Rubisco activity might be changing we measured ACi responses and performed curve fitting to separate the maximum rate of carboxylation (V_{cmax}), electron transport (J) and end product limitation (TPU; see Table 10.3). V_{cmax} values at the top of the canopy are consistent with those observed in other studies (e.g. Theobald *et al.*, 1998). As we descend the canopy V_{cmax} declines in a proportion that is consistent with measured, not modelled, P_{max} .

Growth Stage	Line	Layer	P_{max} ($\mu\text{mol m}^{-2} \text{s}^{-1}$)	V_{cmax}	J	TPU	
Preanthesis	Parent	Top	30.10±2.19	224.67±13.67	304.68±4.72	23.95±0.37	
		Middle	25.02±2.00	124.26±8.40	232.48±16.88	18.19±1.30	
		Bottom	15.64±0.81	80.39±8.42	168.59±15.59	13.54±1.09	
	Line 1	Top	32.29±0.72	184.54±19.21	313.08±24.12	24.21±1.90	
		Middle	23.59±1.77	149.89±37.42	259.13±34.38	19.91±2.85	
		Bottom	12.43±1.36	64.05±24.37	102.73±14.22	8.29±1.12	
	Line 2	Top	30.26±2.50	200.29±45.87	289.81±24.35	23.07±2.50	
		Middle	25.83±2.08	111.12±14.29	245.81±25.01	18.99±1.73	
		Bottom	10.97±0.74	72.47±13.26	124.90±15.03	10.14±1.24	
		P between Lines	0.638	0.733	0.718	0.691	
		Mean	Top	30.91	203.20	302.50	23.74
			Middle	24.81	128.40	245.80	19.03
	Bottom		13.01	72.90	134.20	10.83	
	P between layers	<0.001	<0.001	<0.001	<0.001		

Postanthesis	Parent	Top	33.84±1.01	154.26±13.66	250.60±24.82	19.32±2.02
		Middle	21.92±1.77	111.42±9.56	206.73±20.34	16.06±1.55
		Bottom	16.07±1.61	70.32±30.07	105.80±19.04	8.61±1.42
	Line 1	Top	32.26±1.26	150.58±10.50	253.34±16.14	19.83±1.19
		Middle	17.61±1.42	71.31±2.43	132.31±6.36	10.32±0.53
		Bottom	9.60±0.88	31.54±2.68	64.96±6.71	5.42±0.40
	Line 2	Top	31.69±1.92	156.31±21.80	262.04±14.76	20.70±0.94
		Middle	16.24±1.78	91.78±15.14	186.58±22.57	14.60±1.71
		Bottom	9.28±0.82	44.66±8.85	90.23±7.93	7.46±0.48
P between Lines			<0.001	0.106	0.027	0.024
Mean	Top	32.60	153.70	255.30	19.95	
	Middle	18.59	91.50	175.20	13.66	
	Bottom	11.65	49.50	86.50	7.12	
P between Layers			<0.001	<0.001	<0.001	<0.001

Table 10.3: Parameters taken from curve fitting. P_{max} taken from light response curves and V_{cmax} , J and TPU taken from AC_i curves (fitting at 25°C; $I= 3.74$ using Sharkey et al., 2007). Mean \pm SEM, $n=9$ for P_{max} and $n=5$ for AC_i parameters. P value corresponds to ANOVA.

To analyse acclimation further in terms of leaf composition, amounts of Rubisco, total soluble protein and chlorophyll were quantified (Table 10.4). Rubisco amounts at the top of the canopy were consistent with those towards the upper end for wheat (e.g. Theobald *et al.*, 1998) and are highly correlated with measured P_{\max} and V_{cmax} (Fig. 10.7) within the canopy indicating that Rubisco content accounts for all values of measured P_{\max} and V_{cmax} and not the modelled P_{\max} values. Other work using similar techniques to characterise rice canopies indicates that measured P_{\max} values are consistent with the measured Rubisco contents (Murchie *et al.*, 2002).

Line	Layer	Rubisco (g m⁻²)	TSP (g m⁻²)	Chlorophyll (mg m⁻²)	Chlorophyll a:b	Rubisco : Chlorophyll
Parent	Top	2.49±0.16	10.71±0.81	844.27±49.34	1.93±0.04	2.95±0.11
	Middle	1.36±0.08	5.89±0.24	723.32±21.01	1.79±0.03	1.88±0.09
	Bottom	0.98±0.12	4.61±0.55	602.02±46.32	1.79±0.02	1.61±0.01
Line 1	Top	2.92±0.16	12.43±0.54	819.79±28.27	1.98±0.05	3.58±0.23
	Middle	1.30±0.17	6.04±0.80	666.56±38.70	1.79±0.02	1.92±0.15
	Bottom	0.94±0.14	4.09±0.77	532.09±54.72	1.68±0.03	1.74±0.16
Line 2	Top	2.29±0.10	10.45±0.51	733.63±36.25	1.99±0.04	3.13±0.10
	Middle	1.12±0.07	5.14±0.40	617.79±19.68	1.75±0.03	1.81±0.07
	Bottom	0.62±0.07	2.85±0.32	439.75±50.62	1.72±0.05	1.41±0.07
P between Lines		0.002	0.019	0.002	0.763	0.015
Mean	Top	2.566	11.2	799	1.963	3.222
	Middle	1.26	5.69	669	1.779	1.868
	Bottom	0.845	3.85	525	1.729	1.584
P between Layers		<0.001	<0.001	<0.001	<0.001	<0.001

Table 10.4: Rubisco, total soluble protein and chlorophyll content plus chlorophyll a:b and Rubisco: chlorophyll ratios with each layer through the canopy at the postanthesis stage. Means ± SEM, n=6. P value corresponds to ANOVA.

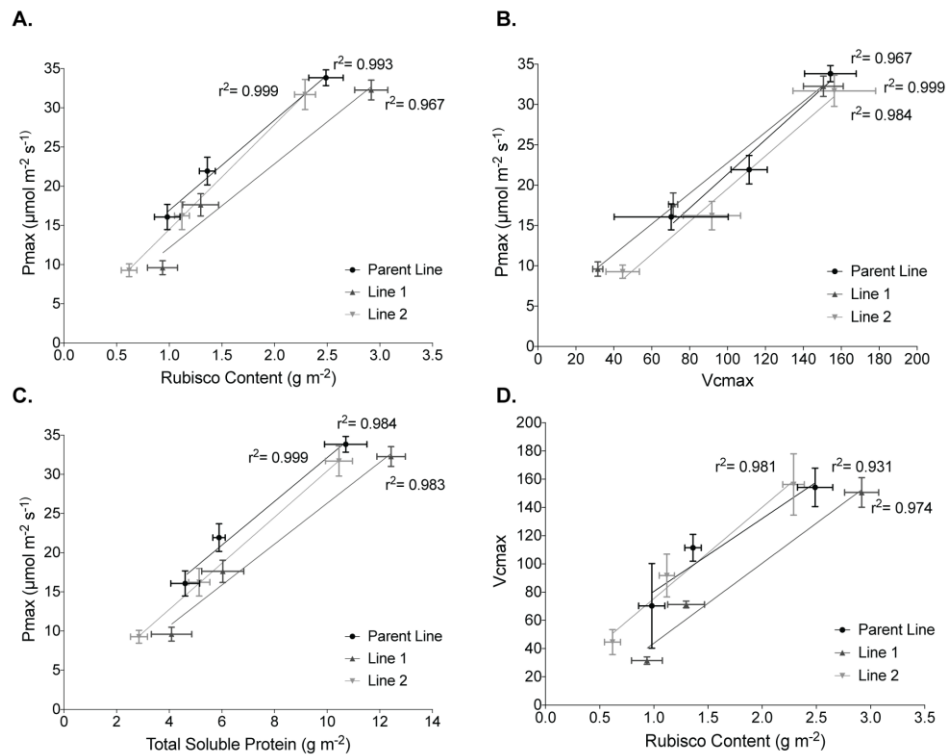


Figure 10.7: Relationships between photosynthesis (P_{max} taken from fitted light response curves) and Rubisco properties (V_{cmax} from fitted AC_i curves and Rubisco/ total soluble protein (TSP) amount) throughout canopy depth; (A) P_{max} and Rubisco content; (B) P_{max} and V_{cmax} ; (C) P_{max} and Total Soluble Protein and; (D) V_{cmax} and Rubisco content. Where black (round symbol) in the Parent Line, dark grey (triangle symbol) is Line 1 and light grey (upside down triangle symbol) is Line 2.

The changes in chl a:b are consistent with those expected for acclimation of light harvesting complexes (LHC), with a lowered ratio indicating a greater investment into peripheral LHCII (Murchie & Horton, 1997). Interestingly the largest change in chl a:b occurs in the upper half of the canopy where the greatest proportional change in light level occurs. Chl a:b is important because it is a reliable indicator of dynamic acclimation i.e. fully reversible changes occurring at the biochemical level that are not the result of morphological alteration.

Discussion

Photosynthesis in nature responds largely to fluctuating light, not the unchanging or ‘square waves’ commonly used for studies in acclimation. Here we analyse the responses of leaves within a wheat canopy to predict the optimal state of acclimation using light history as a natural dynamic, rather than fixed or artificially fluctuating, parameter. To do this we used a framework of image-based 3D canopy reconstruction and ray tracing combined with mathematical modelling to predict the optimal distribution of photosynthetic acclimation states throughout a field grown wheat canopy based on the realistic dynamic light environment. The field measured data and modelled data indicate two key features: (i) photosynthesis can vary greatly at the same canopy height according to both acclimation and instantaneous irradiance shifts and (ii) whilst the model indicates good correspondence to field data at the top of the canopy, the model consistently predicts lower optimal P_{\max} values in the bottom canopy layers relative to measured data. These predictions are important because they take into account the effects of fluctuating light in each layer, in particular the high light events at the base of the canopy, which are too short and infrequent to represent a substantial carbon resource. From this we conclude that plants are not optimising leaf composition in response to the long term light levels they are experiencing, but rather are retaining excessive levels of photosynthetic enzymes at lower canopy levels.

The regulatory aspects of acclimation and how it is triggered by changing light levels are little understood, but recent work has begun to address this and attempt to elucidate the link between variations in light and the resulting biomass and fitness (e.g. Külheim *et al.*, 2002; Athanasiou *et al.*, 2010; Retkute *et al.*, 2015). This paper builds on this work and reveals for the first time the relationship between ‘real’ canopy architecture, the resulting dynamic light environment and its effect on photoacclimation. In addition to fundamental understanding of photoacclimation, this work has consequences in terms of nutrient usage within our agricultural systems, which we discuss below.

Influence of Canopy Architecture on Acclimation

Mono-species crop canopies have more consistent structural patterns in comparison with natural systems and are useful models for this type of work since data can be classified according to stratification, but still include spatial complexity and an inherent stochastic component. Photoacclimation according to canopy level is an expected property (Fig. 10.4). The dynamic nature of the in-canopy light environment means that any leaf may be exposed to a range of conditions; from light-saturation to light limitation but with varying probability of either according to canopy depth. Fig. 10.3 shows clearly how leaves at the top of the canopy experience high likelihood of direct radiation with fluctuations ranging from 2 – 3 fold depending on leaf position. Lower in the canopy, occlusion results in an increasing dominance of diffuse and low levels of radiation punctuated by brief and rare high light events (sun flecks) that can be 10 – 50 times the mean level. Both the measured and modelled canopy light levels indicate that the P_{\max} values predicted by the model are expected based upon the low, basal, levels of light the lower canopy layers receive. The key question is whether acclimation of (i.e. higher) P_{\max} is needed to exploit sun flecks.

Much previous literature has discussed the importance of exploiting sun flecks as a carbon resource in light-limited environments such as forest understoreys (Pearcy, 1990). However the response seems to be variable, depending on physiological acclimation of each species and stresses associated with higher temperatures and high light (Watling *et al.*, 1997; Leakey *et al.*, 2005). Here, the use of a novel acclimation model allows us to assess the effectiveness of acclimation in terms of carbon gain at each position. As sun flecks become increasingly rare in the lower portions of the canopy, the model predicts that acclimation of P_{\max} towards higher values becomes an increasingly ineffective strategy in terms of exploiting them for carbon gain.

To efficiently exploit the light flecks in the lower canopy positions it is necessary to have a high photosynthetic capacity (P_{\max}), a rapid rate of photosynthetic induction and a degree of photoprotective tolerance to avoid

photoinhibition. The latter point is not accounted for in this paper but has been noted in other species, especially where much higher leaf temperatures are involved (Leakey *et al.*, 2005). Photoinhibition in lower parts of wheat canopies in the UK was not observed in this study or in a previous study (Burgess *et al.*, 2015) and in our temperate system we do not expect excessive leaf temperatures. Photosynthetic induction state is determined by the previous light history of the leaf; by stomatal dynamics and the activation state of key enzymes such as Rubisco. Acclimation of P_{\max} becomes more effective in terms of overall carbon gain where there is a lower frequency of light transitions but increasing duration of high light events (Retkute *et al.*, 2015). This is consistent with the light data (Fig. 10.3), which shows rare, brief high light events lower in the wheat canopy.

Such very low levels of light within a crop canopy are comparable with forest floors where morphological and molecular adaptations are used to enhance light harvesting, carbon gain and avoid photoinhibition during high light periods (Powles & Bjorkman, 1981; Raven, 1994; Sheue *et al.*, 2015). The interesting feature of cereal canopy development is the fact that leaves initially develop in high light and then are progressively shaded as the canopy matures. Since the morphology of the leaf is determined prior to emergence, all acclimation to low light, post emergence, must be at the biochemical level as shown by the Chl a:b ratio (Murchie *et al.*, 2005).

The low light levels within the wheat canopy also require effective acclimation of respiration rates in order to maintain positive carbon gain and this was observed here (Fig. 10.5). Leaf respiration is a critical aspect of photoacclimation, permitting lowered light compensation points and positive carbon balance in low light. The relatively low rates of dark respiration in the lower layers and the very low measured light levels at the base of the canopy indicate that leaves maintain their (measured) high P_{\max} alongside low respiration rates and light compensation points. Therefore there must be some decoupling of P_{\max} from these other acclimation processes at lower light levels.

We conclude perhaps surprisingly that the optimal strategy in lower parts of the wheat canopy where light is extremely low ($<50 \mu\text{mol m}^{-2} \text{s}^{-1}$) should not be geared towards exploiting sun flecks (previously seen as an important carbon resource) but towards light harvesting, maintenance of low leaf respiration and low light compensation point. Indeed the acclimation of P_{max} to higher levels requires substantial investments of resources such as energy, nitrogen and carbon. It is still possible that the high measured P_{max} may allow a greater ability to exploit some sun flecks of increased duration where they do not lead to substantial photoinhibition (Raven, 2011). It is likely that the planting density has an effect: in this experiment we have used standard sowing rates for the UK where the LAI is reasonably high leading to a dense canopy. The excessive accumulation of Rubisco in lower leaves may be more useful for exploiting planting systems where spacing is greater and light penetration is higher (Parry *et al.*, 2011).

Implications in terms of Nutrient Budgeting

The disparity between model data and manually measured data has consequences in terms of the canopy nutrient budget. Photosynthetic components are a significant sink for leaf N: chloroplasts account for up to 80 % of total leaf N with Rubisco being the dominant enzyme (Makino & Osmond, 1991). Leaf photosynthetic capacity and Rubisco content per unit leaf area is highly correlated with leaf N both within and between species (Evans, 1989; Theobald *et al.*, 1998). Wheat plants and other cereals exhibit a pattern of storage of N in leaves, leaf sheaths and stems prior to grain filling whereby a substantial proportion of stored N is remobilised toward the grain where it contributes to protein synthesis (Foulkes & Murchie, 2011; Gaju *et al.*, 2011; Moreau *et al.*, 2012). For bread wheat this is especially important for grain quality. Similar mechanisms occur in many plant species to conserve nutrients. Therefore the retention of N in leaves represents a strategy for storage in the latter part of the plant life. Since wheat leaves develop in high light and become progressively shaded their net lifetime contribution to canopy photosynthesis within the shaded environment will still be substantial. This secondary property of photosynthetic enzymes for N storage has been

discussed previously e.g. Sinclair & Sheehy (1999). It is clear that this role is valid but it is still not certain how it is effectively coordinated with photosynthetic productivity since remobilisation and subsequent senescence represent a compromise to canopy carbon gain in the latter grain filling periods. In this case it is clear that the accumulation and retention of N in lower leaves of the wheat canopy is dominant over the regulation of key components of optimal photosynthetic acclimation, especially P_{\max} and this N is not used to promote carbon gain at the canopy level. Therefore, questions must be raised as to the cost of this accumulation and whether all of this N is efficiently remobilized to improve grain quality. Recent data for UK wheat shows that only 76 % of leaf N is remobilized, indicating that a substantial improvement in NUE could be achieved with no penalty for photosynthesis or grain quality (Pask *et al.*, 2012). Altering the acclimation responses of the lower leaves to fluctuating light could bring about this improvement.

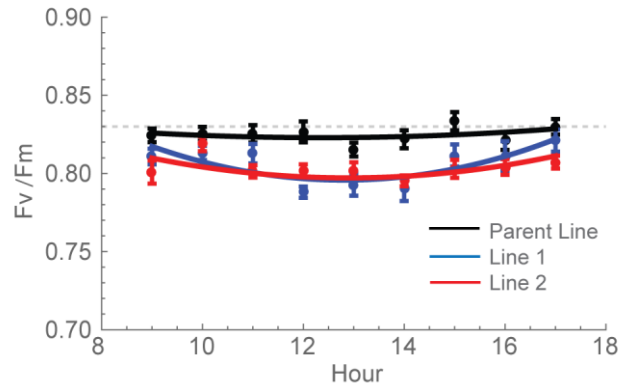
Cross-species correlations between leaf N content and dark respiration have been observed raising a further question over the respiratory cost of accumulating leaf N in such low light levels where the opportunities to exploit sun flecks are not high, nor are warranted in terms of acclimation of P_{\max} (Reich *et al.*, 1998). Sinclair & Sheehy (1999) pointed out that the erect nature of rice leaves had an important effect in terms of improving the capacity of the lower leaves to store N for remobilisation. Further, we suggest that even small changes in canopy architecture analysed by Burgess *et al.* (2015) would permit lower leaves to operate more efficiently as N storage organs in addition to their role as net carbon contributors.

Concluding remarks

Photosynthetic acclimation permits photosynthesis to remain optimal but its regulation in natural fluctuating light is poorly understood. We have shown an uncoupling between the responses that are required to maintain optimal photosynthetic efficiency and other processes that drive plant function. In this case we conclude that the accumulation of excessive photosynthetic capacity is not optimal for exploiting the wheat canopy light environment and that levels of canopy nutrients (especially N) could be reduced with no detrimental impact on either carbon gain or grain protein content.

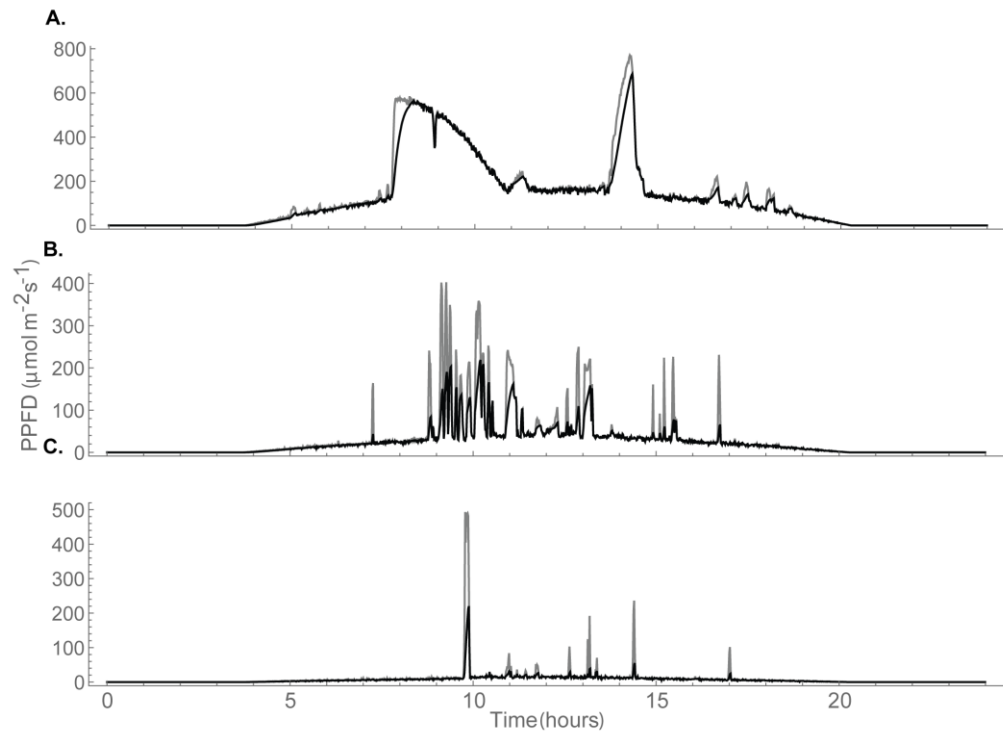
Supplementary Material

Supplementary Figure S10.1



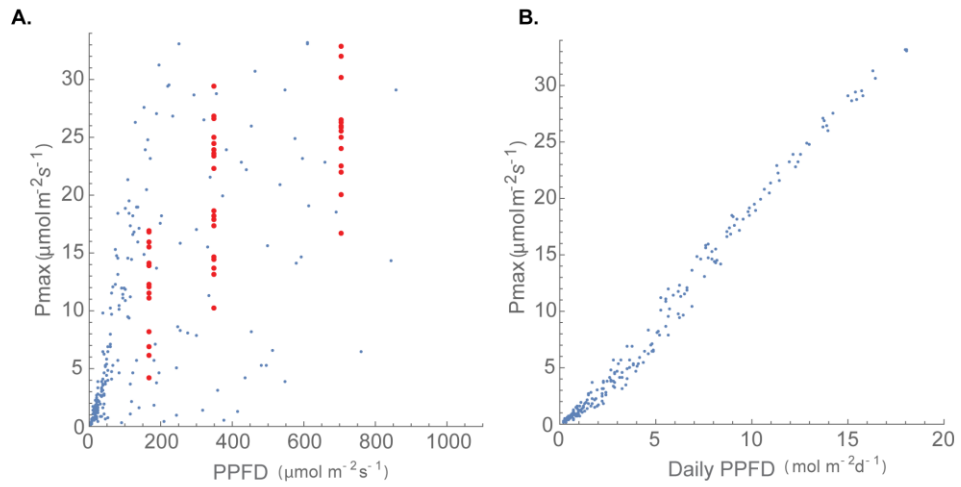
Supplementary Figure S10.1: Diurnal dynamics of F_v/F_m over the whole day. Grey dotted line indicates the maximal F_v/F_m value in the uninhibited state (0.83).

Supplementary Figure S10.2



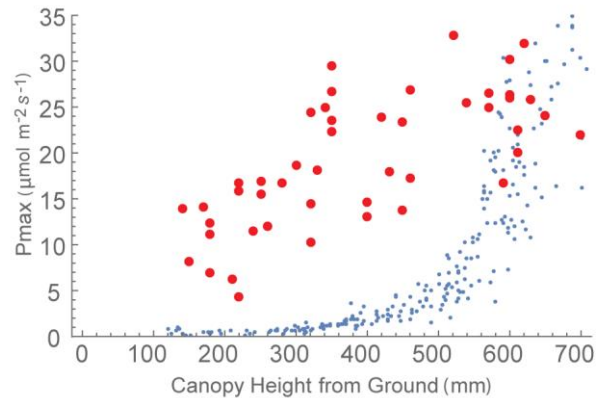
Supplementary Figure S10.2: Example of a time-weighted light pattern at $\tau=0.2$ (black line) relative to a non-weighted line (i.e. $\tau=0$). Light patterns for (A) top, (B) middle and (C) bottom canopy layers (as shown in Fig. 10.3). The time weighted average (Eq. 4) is an exponentially decaying weight used to represent the fact that photosynthesis is not able to respond instantaneously to a change in irradiance levels. If $\tau=0$ then a plant will be able to instantaneously respond to a change in irradiance, whereas if $\tau>0$ the time-weighted average light pattern will relax over the timescale τ . Within this study, τ was fixed at 0.2 unless otherwise stated.

Supplementary Figure S10.3



Supplementary Figure S10.3: Model output (blue) versus gas exchange measurement (red) graphs for the Parent Line, preanthesis. (A) P_{max} against the PPFD at 12:00 h. Modelled PPFD is taken from the ray tracing output whereas measured PPFD is taken from ceptometer data in the field; N.B. ceptometer measurements were taken at a quarter, half and three quarters up the canopy, relating to bottom, middle and top layers, respectively, so the data was grouped accordingly. (B) Modelled daily integrated PPFD versus modelled P_{max} .

Supplementary Figure S10.4



Supplementary Figure S10.4: Whole canopy acclimation model output (blue) versus gas exchange measurement (red) graphs. The acclimation model was run at 250 locations throughout canopy depth to predict the optimal P_{max} at each location dependent upon the light environment that it experienced, calculated via ray tracing. The time weighted average (Eq. 4) was fixed at $\tau = 0.1$. This is an exponentially decaying weight used to represent the fact that photosynthesis is not able to respond instantaneously to a change in irradiance levels. If $\tau = 0$ then a plant will be able to instantaneously respond to a change in irradiance, whereas if $\tau > 0$ the time-weighted average light pattern will relax over the timescale τ . Results shown for the Parent Line, Preanthesis.

Chapter 11: Discussion

This thesis has demonstrated the influence of canopy architectural traits on the resulting light environment within the canopy, and how this may influence photosynthetic processes and therefore the productivity of different canopy structures. The use of 3-dimensional reconstruction of plants combined with ray tracing has provided a high-resolution method of exploring unique architectural traits; this process of digitising preexisting and “naturally” field-formed canopy structures means that small variations between plants can be preserved. This can be applied to different areas of research including multiple cropping systems (Chapter 3), phenotyping (Chapter 4 and 7) or the influence of external inputs on growth and development (Chapter 6). The method also provides a means to scale up leaf level responses to the whole canopy scale (Chapters 7 and 10). Chapter 5 has shown that other environmental variables, in this case wind, will determine the exact canopy configuration at a given time, whilst Chapters 8 and 9 highlight the importance of the response time of photosynthesis and influence of the previous light history in determining the productivity of a plant.

The following key conclusions can be drawn from this study:

- The physical structure of a plant canopy depends upon a number of different factors including the cropping system adopted; the variety selected; the planting pattern; the addition of external inputs; and the biotic and abiotic environment in which the canopy is subject to. Plasticity of plants to their growing conditions means that broad generalisations are difficult to make.
- The architectural characteristics of a plant are critical in determining the light distribution throughout a canopy and, in combination with photosynthetic traits of the plant, will determine the ultimate

productivity of the canopy. Whilst a more upright canopy structure may lead to a greater distribution of light throughout depth, it can also provide a method to prevent radiation-induced damage (Chapter 7) or can lead to benefits such as heat tolerance (discussed in Chapter 4).

- Traditional theories regarding light attenuation through a canopy often do not hold, particularly for structurally complex canopies as they rely on two main assumptions; leaves are small and they are evenly dispersed throughout canopy structure (Ross, 1981). However, homogeneity is rarely attainable in the field both in sole cropping and multiple cropping systems and departure from random leaf dispersion (i.e. through clumping) is common. Furthermore, these traditional theories simplify both plant architecture and light interception. For accurate prediction of light interception and photosynthetic processes at the canopy level, models must take into account the heterogeneity of canopy structure (Vos *et al.*, 2010) and the differences in photosynthetic potential within a canopy. Predicting whole canopy photosynthesis requires two steps: first the calculation of the PPFD profile within the canopy and secondly, its relation to the distribution in photosynthetic capacity. Detailed descriptions of canopy architecture are integral to this due to the spatial and temporal differences in PPFD profiles between canopies.
- Image-based reconstruction combined with ray tracing provides high-resolution information on canopy structure and the light environment at a low cost, with little prior knowledge of the plant under study and without extensive data collection and analysis required for alternative reconstruction methods (i.e. functional structural plant models- Chapters 1 and 3). Furthermore, image-based methods are able to accurately represent unique differences in architectural traits and thus can capture heterogeneity in canopy structure. Using these methods to calculate light interception and photosynthesis are therefore not restricted by assumptions (as above). Combined with gas exchange and/

or fluorescence data, mathematical models can be used to scale up cellular processes to the whole canopy level. This enables predictions of whole canopy carbon gain and the estimation of the distribution of photosynthetic potential throughout canopy depth.

- External inputs of nitrogen (N) fertiliser are able to alter the productivity of a cropping system. An increase in residual soil N can lead to an increase in carbon gain per unit ground area, but can decrease carbon gain per unit leaf area. This is due to the increased leaf area index (LAI) and biomass production of the high N plants. Uptake of N can also lead to higher photosynthesis than would be expected based on light levels, as assessed using an empirical model of photosynthetic acclimation based on realistic fluctuating light. This is likely due to the storage of N in the lower canopy layers. This has implications in terms of the nitrogen use efficiency (NUE) of the crops and provides a target for future improvements (see below).
- Multiple pathways control the response of a plant to a change in irradiance level. There is an intricate relationship between light regime and P_{\max} which cannot be deduced from such light properties as integrated PPFD or peak PPFD (Chapter 8). Furthermore, the relative frequency distribution of PPFD plays a crucial role in determining P_{\max} , which maximises carbon gain (Takenaka, 1989).

Limitations of work presented in this thesis

There are a number of limitations of this work that means a full picture of canopy function is not yet possible. These will be discussed further below but briefly: the plasticity of plants means that canopy architecture is dependent on many different factors, not all of which are known or can be predicted; limited space or access to varieties meant that the full relationships between canopy architecture and photosynthesis cannot be fully discerned; the complexity of a canopy means that models must be simplified (e.g. the use of empirical models) which may not be representative; and for more accurate reconstruction

of dense canopies, the plants must be removed and imaged which means they cannot be followed over the growing season.

11.1 Improving Agricultural Productivity

Increases in food production are an important component of future agricultural systems, but they will be constrained by the finite resources available (Freibauer *et al.*, 2011). A threefold challenge now faces the world (von Braun, 2007): to match the food demand to supply; achieve food production in an environmentally- and socially-sustainable way; and eradicate food insecurity. Previously, increases have been achieved through increasing the area of land under cultivation (World Bank, 2016), however, the area of land available for production is stagnating (World Bank, 2016); the most productive land for agriculture is already in use thus expansion would be need to be on marginal and vulnerable lands (Tilman *et al.*, 2002); and the competition for land for other uses is increasing (Rosegrant *et al.*, 2001; Foley *et al.*, 2005; World Bank, 2016). Thus, it is likely that more food will need to be produced from the same amount, or even less, land. This challenge will require changes to the way that food is produced, stored, processed, redistributed and accessed (Godfray *et al.*, 2010).

- **The Yield Gap**

There is a wide geographic variation in crop and livestock productivity, even in areas with similar climatic conditions (Godfray *et al.*, 2010). The difference between the actual yield and the best that can be theoretically achieved using optimal conditions is called the “yield gap” (Lobell *et al.*, 2009; Licker *et al.*, 2010; Neumann *et al.*, 2010; Van Ittersum *et al.*, 2013; Pradhan *et al.*, 2015). The best yields that can be obtained locally will depend on a number of factors including the capacity for farmers to access seeds, water, nutrients, pest management and knowledge. It has been estimated that in regions of South East Asia, actual rice yields are between 43% and 75% of the climatic yield

potential and 61% and 83% of the best farmers' yields (Laborte *et al.*, 2012). Similar yield gaps are found in other rice growing areas (Cassman, 1999) and for other cereals and crops worldwide (e.g. Mueller *et al.*, 2012). Low yields often occur because of technical or socioeconomic constraints (van Tran, 2001; Godfray *et al.*, 2010). For example, farmers may not have access to the knowledge and skills required to increase production (e.g. Kelly *et al.*, 2003; UNDP, 2012); the finances required to invest in higher production (e.g. irrigation, agro-chemicals, fertilizer, machinery; e.g. Hazell *et al.*, 2010; Ray *et al.*, 2012); or the crop and livestock varieties that maximise yields (Ray *et al.*, 2012). A yield gap may also exist because the high costs of inputs, or the low returns from increased production, means that it is economically suboptimal to raise production (Lobell *et al.*, 2009). For low-income farms, not investing in agricultural improvement is often seen as a rational decision against undue risk but can lead to a "poverty trap" (Barnett *et al.*, 2008).

The yield gap is not static and can vary from year to year and region to region (Lobell *et al.*, 2009). Maintaining and also increasing crop yields will depend on continued advances to combat weeds, diseases, insects and pests plus the creation of improved varieties (see above; e.g. van Tran, 2002; Tilman *et al.*, 2002; 2011). This will involve both the continued development of better agro-chemicals and management practices plus the use of traditional and advanced crop breeding. The maximum attainable yield in different regions will also shift through a change in climatic conditions (Rosenzweig & Parry, 1994; Trnka *et al.*, 2004; Kalra *et al.*, 2008; Ortiz *et al.*, 2008; Wheeler & von Braun, 2013). This may lead to the expansion of cultivation areas of certain crops, particularly northern temperate regions, but also the loss of currently productive regions due to excessive temperatures, drought, desertification, salinisation and extreme weather events. The following sections will look at improvements that can be made in our crop varieties and the systems and practices used to grow them in order to reduce the yield gap.

11.1.1 Targets for Improvement arising from this thesis

The work carried out in this thesis indicates a number of targets for potential improvement. This includes:

- Selection of species or varieties that allow spatial and temporal complementarity in multiple cropping systems (Chapter 3). Careful selection could enable resources to be more efficiently used over the whole growing season.
- Selection of varieties that contain optimal architecture for light acquisition (Chapter 4) yet prevent damage from excess light (Chapter 7). This is often seen as an erectophile canopy structure although will be situation specific (see below).
- Selection of architectural traits that permit leaf movement during moderate wind (Chapter 5). For example, altering the mechanical strength of stem of leaf material, altering petiole length or leaf blade length and width, so as to increase the likelihood of light penetration into the canopy.
- Selection of varieties that are able to respond well to an increase or decrease in inputs (i.e. N fertiliser: Chapter 6).
- Selection of biochemical traits that enable the photosynthetic machinery to respond rapidly to a change in light levels (Chapters 8-10).

Creation of site- and situation-specific cultivars

Chapter 3 indicated the importance of matching the traits of an individual crop plant to the environment or situation in which it is to be grown. Within the case of multiple cropping systems discussed, traits that confer benefits to the system are likely to be different to those that confer benefits to a monocropping system. Another example can be seen through the adoption of crop plants that stabilise yields for a given environment as opposed to maximise it (i.e. see section 11.1.3 below). This will be especially important within sub-optimal environments. Thus care should be taken to recognise the specific constraints

of an area of land and chose species or varieties that can adapt to those constraints.

It is often suggested that a plant ideotype containing erect leaves (particularly at the top of the canopy) will be more productive than that containing horizontal leaves due to the more uniform distribution of light. This trait is also expected to permit a higher amount of leaf material (i.e. LAI; Chapter 1), although the opposite was found within this project (Chapter 4). However, there may be other factors, not considered here, which may mean that this feature would not be optimal for productivity in a set environment. For example, the canopy structure leads to a microclimate due to boundary layers and the development of gradients within the canopy (i.e. gas, heat, light, water etc). Thus, specific canopy structures could permit an unfavourable environment, for example by facilitating pests or disease. Canopy structure will also determine the flow of air, or wind, through a canopy structure (Chapter 5). Therefore, in exposed environments, a more conservative canopy structure may limit mechanical damage to plants but not necessarily permit optimal light distributions for photosynthesis.

Alternatively, manipulation of traits involved in photosynthesis could also be situation-specific. As the light environment shifts during growth and development, or during the growing season, the requirements of the plants and the impact of the environment will also shift, thus the optimal strategy will differ. Therefore changes that can enhance productivity under one situation may not benefit another. For example, increasing photoprotective potential (discussed above) may be beneficial during vegetative development when the plants are relatively young and thus exposed to high irradiance levels, however once the canopy closes and the irradiance levels decrease, this enhanced photoprotection could negatively impact productivity (Hubbart *et al.*, 2012). If the canopy development stage is particularly limiting to productivity under certain environmental conditions then improvement to this stage at the expense of another would be beneficial overall.

The examples given here may alter the optimal canopy structure or metabolomic composition for a given environment and thus breeding efforts should be site- or situation-specific.

11.1.2 Genetic Improvement of Crop Plants

The wide range of existing genetic variation available in both canopy architectural features and traits associated with photosynthetic performance provides a great scope for both developing ideal plant types and improving knowledge on the interactions between plant growth and development and the environment. However, it is important to note that no single improvement pathway will be suitable for all locations and thus improvements will need to be site- and situation-specific (see above). As knowledge of the genes underlying control of architecture and photosynthetic traits increases, so does our ability to potentially manipulate such targets in order to optimise light interception and productivity.

11.1.2.1 Genetic Manipulation of Canopy Architecture

Historically, canopy structure in crop plants has altered greatly through breeding programs. The switch in plant height from tall to small varieties in the mid 20th century (part of the ‘Green Revolution’) was the first stage in optimising canopy architecture to improve biomass production. This change was brought about through the use of high-yielding cultivars of rice and wheat combined with improved cultivation practices including the use of fertilisers, herbicides, irrigation and mechanisation of cultivation. The cultivars conferred higher yields due to the introduction of dwarfing genes; genes that interfere with the action or production of plant hormones, predominantly gibberellin (GA) (Monna *et al.*, 2002; Hedden, 2003; Pearce *et al.*, 2011). This led to the increase in harvest index (HI) by increasing grain mass at the expense of stem mass, improved lodging resistance and increased responsiveness to nitrogen fertilisers without affecting panicle and grain quality. Other changes in

structure are, in part, due to adaptations to higher planting density (e.g. Duvick, 2005a, 2005b). For many crops, this was associated with changes in shoot morphology to permit greater light penetration to reduce the shading effects (Edwards *et al.*, 2011; Edwards, 2011). One example of this can be seen in I.R. rice varieties (varieties bred for disease resistance and increased productivity by IRRI), first achieved in IR8, so called ‘miracle rice’ (Peng *et al.*, 2010). Compared to the older varieties, the I.R. varieties achieve higher rates of photosynthesis attributed to canopy structure and greater light penetration to lower canopy layers. This was achieved through a semidwarf structure with a stiff culm, erect leaves, profuse tillering and a high harvest index (Chandler, 1969). The variety also responded well to N fertilisation and exhibited photoin sensitivity, thus broadening its cultivation range (Vergara & Chang, 1985). A gene responsible for the key domestication transition from wild rice species has been identified (Jin *et al.*, 2008). *PROG1* (*PROSTRATE GROWTH 1*) encodes a zinc-finger nuclear transcription factor, which is present in the rice wild relative (*Oryza rufipogon*) where it confers a prostrate growth habit with a wide tiller angle, short stature and multiple tillers. This architecture leads to leaf shading, thus reducing photosynthetic productivity and prohibits dense planting and thus was selected out during domestication. Similar genes are also present within other crop plants such as the *Reduced height* (*Rht*) genes of wheat, which encode DELLA proteins (transcriptional regulators) that confer dwarfing by repressing GA- responsive growth (Hedden, 2003; Pearce *et al.*, 2011).

Improving crop yield through altered canopy architecture continues to be a target for breeding programs. The study of different plant types dates back to the 1930s (Boysen Jensen, 1932). Since that time, research has been aimed at studying the relationship between plant type and grain yield. From this research, a number of ideal plant types (i.e. ideotypes) have been proposed for wheat (Donald, 1968), rice (Gao *et al.*, 2000; Khush, 1994; Lu *et al.*, 1991; Yuan, 1997; Zhou *et al.*, 1995) and other crops. For example, Zheng *et al.* (2008) showed that rice cultivars exhibiting steeper leaf angles allowed higher light penetration to deeper canopy layers and thus greater biomass production.

Super rice breeding programs use heterosis between *indica* and *japonica* subspecies in order to obtain varieties with upright leaves, small leaf angle and appropriately curled leaves (Khush, 1994; Liu *et al.*, 2005; Yuan, 1997). The idealised rice plant should contain a leaf area index of between 7 and 8 (Ning *et al.*, 2013). A number of genes controlling plant architectural traits have been identified which could provide targets for manipulation or breeding studies; for example, *Tiller Angle Control 1 (TAC1)* in rice. Mutants lacking *tac1* have a compact plant architecture with erect tillers. *Monoculm1 (MOC1)* in rice encodes a putative GRAS family nuclear protein that is expressed mainly in the axillary buds and controls tiller initiation and outgrowth (Li *et al.*, 2003). Mutant plants lacking *MOC1* grow with only a main culm without any tillers. For a full review of genes controlling branching, plant height and inflorescence morphology see Wang & Li (2006). Many of these genes are conserved between monocotyledonous and dicotyledonous plants, suggesting similar regulatory pathways control plant architecture in all plants.

11.1.2.2 Genetic Manipulation of plant processes

If light interception throughout a growing season has already been fully exploited (i.e. through optimal canopy architecture and growth), then further increases in biomass requires that photosynthesis must be improved (Evans, 2013). In reviews of methods to increase photosynthesis, Evans (2013) and Ort (2015) identified a number of key targets including: i) improving Rubisco kinetic properties, ii) introducing the C₄ pathway into C₃ crops, iii) manipulating photoprotection kinetics and iv) improving canopy architecture (discussed above).

Rubisco is a critical enzyme in the process of photosynthesis as it catalyses the first step of the Calvin–Benson cycle, fixing CO₂ via the carboxylation of ribulose-1,5-bisphosphate (RuBP). However, a second, competing reaction with oxygen (known as photorespiration) is also catalysed by Rubisco, which leads to the net loss of energy and carbon. Rubisco is a slow acting enzyme, with large quantities required to support adequate photosynthetic rates. In

addition, repeated conformational remodelling is required for Rubisco to stay active (Parry *et al.*, 2003; 2013). There is natural variation in the catalytic properties of Rubisco among higher plants (Prins *et al.*, 2016) with further variations in Rubisco turnover rate, affinity or specificity for CO₂ expected, but not yet identified (Parry *et al.*, 2013). It is possible that these improved Rubiscos could be introduced to commercial crops through conventional breeding. Alternatively biotechnological approaches could be used to manipulate the enzyme directly (e.g. by altering content, activation, specificity or kinetics) or indirectly (i.e. the improvement of thermal tolerance of Rubisco activase; von Caemmerer & Evans, 2010). Rubisco accounts for up to 50% of leaf soluble protein and 25% of leaf N, therefore lowering its abundance in crop plants could also provide a means to increase nitrogen-use efficiency (Parry *et al.*, 2003; 2013). Evidence from antisense plants indicates that a 15-20% reduction in Rubisco levels could confer a 10% reduction in N demand under low-moderate light intensities without negatively impacting CO₂ fixation (Stitt & Schulze, 1994). Manipulation of Rubisco indicates that improvements cannot only be made through the process of photosynthesis and the conversion of light energy, but also through the mobilisation of nutrients into the harvestable organs of the plant. For example, Chapter 10 shows the storage of large quantities of nitrogen (N) in the bottom layers of a wheat canopy as Rubisco, and how this drives higher levels of photosynthesis than would be expected based on light levels. This excess N storage could be converted into grain yield through the selection of varieties with improved N partitioning and remobilization. This would help to achieve greater photosynthetic nitrogen-use efficiencies (PNUE) (Barraclough *et al.*, 2014; Gaju *et al.*, 2014).

Due to the improved efficiency of the C₄ photosynthetic pathway over C₃ (e.g. see Fig 2 in Zhu *et al.*, 2010), introducing the pathway into C₃ crops could provide a key target, particularly within hotter or drier environments (Gowik & Westhoff, 2011; Sage & Zhu, 2011). This will require manipulation of multiple gene targets, the modification of approximately 3% of the mature leaf transcriptomes (Bräutigam *et al.*, 2010) and changes to leaf anatomy (Furbank *et al.*, 2009; Zhu *et al.*, 2010; Kajala *et al.*, 2011). Introducing the C₄ pathway

into rice is postulated to have a number of benefits including a doubling of water-use efficiency (WUE) and improved nitrogen-use efficiency (NUE) (IRRI, 2006). Based on comparative studies between rice and maize, models predict that this can translate into a yield gain of 30-50% and the cost-benefit ratio could be of a similar magnitude to that achieved through the introduction of dwarfing genes during the green revolution (IRRI, 2006). Alternatively, achieving the efficiency of C₄ photosynthesis without the full genetic and morphological changes required could similarly be achieved through processes that concentrate CO₂ in the chloroplast. This could be accomplished through introducing cyanobacterial membrane transporters (e.g. BicA and SbtA; Price *et al.*, 2008; 2011; 2012) and by preventing CO₂ leakage.

Manipulating photosynthesis at the organ or leaf level will only confer benefits if it also improves photosynthesis at the whole canopy level (Evans, 2013). This requires an understanding of how cellular level processes scale up and impact the whole organism or community. As the plants develop and canopy closure occurs, the light environment will dramatically shift and the majority of the canopy will be under low light environments with infrequent peaks in irradiance caused by sun flecks. Thus improvements must be geared towards the specific environment in which the plant will be exposed to. This can be exemplified by improvements that can be made to photoprotective processes. Light may frequently be in excess of that required by photosynthesis; this excess excitation energy can cause damage to the plants through the production of reactive oxygen species (ROS) and lead to a sustained decrease in quantum yield, however photoprotection acts to mitigate this damage. As photoprotection is so entwined with carbon gain, manipulation of the pathways involved could provide a means to enhance productivity; although the maximal benefits available may also require a balance with the need to limit damage (Murchie *et al.*, 2009; Murchie & Niyogi, 2011). Targets for improvement could include light avoidance strategies (e.g. Raven, 1994), improved photoacclimation (Murchie *et al.*, 2009; Part II of this thesis), optimising pathway component amounts e.g. PsbS or Xanthophyll (Hubbart *et al.*, 2012; Ware *et al.*, 2014; 2015; 2016) or increasing the relaxation time of

photoprotection. For a full review on the photoprotective targets that could be manipulated to improve photosynthesis see Murchie & Niyogi (2011). Improvements could also be made to the processes that determine how a plant responds to a change in light levels; photosynthetic induction and acclimation (Chapters 8-10). For example, improvements to the speed of response to a change in irradiance level (i.e. through induction) could increase the maximum capacity for photosynthesis throughout the canopy profile and enable exploitation of peaks in irradiance (e.g. Chapter 10). Thus improvements can be based on existing genetic variation in photosynthetic induction rates.

Another consideration is the effect of wind on plant productivity (Chapter 5) and provides further targets for crop improvement. Wind is a ubiquitous property of field crop cultivation yet has a major effect on canopy carbon gain. Knowledge of how wind effects plant structure and photosynthetic potential is poorly understood. Improvements could be aimed at two different targets; firstly, at the response of photosynthesis to a change in irradiance (discussed above) and, secondly, at structural properties that may facilitate movement that brings about a more favourable light environment. Structural properties may include stem strength and flexibility or leaf properties in crops that permit small but rapid movements in light winds, similar to leaf flutter, such as sheath or petiole flexibility or altered leaf blade length and width.

The potential gains associated with each target will differ depending on the process affected and the biotic and abiotic environment to which the plant is exposed (Evans, 2013). The technical requirements associated with manipulation of each target will also differ. Greater benefits could be achieved by combining multiple approaches together, however the full impact of manipulation cannot be accurately estimated from models and unknown side effects are possible (Evans, 2013; Lüttge *et al.*, 2016). Plants containing multiple transgenes (called stacked gene hybrids) are already being cultivated, such as maize or cotton plants containing multiple genes for insect or herbicide resistance (Que *et al.*, 2010; D'Halluin *et al.*, 2013), and others for improved photosynthesis are being developed (Simkin *et al.*, 2015).

As well as identification and manipulation of specific gene targets, breeding programs also focus on the introgression of multiple desirable traits (termed ‘Alien Introgression’). Crop monoculture and domestication processes have led the narrowing of germplasm, leading to susceptibility to pests, pathogens and little resilience to cropping systems. Increasing genetic diversity is a common aim of crop breeding, and distant wild relatives and landraces are commonly used as a source (Zamir, 2001; Gill *et al.*, 2011; King *et al.*, 2013). Alien introgression provides the means to improve a number of agronomic traits (King *et al.*, 2013) including root architecture and drought tolerance (Humphreys *et al.*, 2005; Placido *et al.*, 2013), biomass and resource use efficiency (Gaju *et al.*, 2011) and disease resistance (Roderick *et al.*, 2003).

11.1.3 Underutilised Crops

Global cropping systems are dominated by approximately 30 core crop varieties, termed the major or staple crops, which provide 95% of the world's food energy (Williams & Haq, 2002). However, diversification away from the over-reliance on these major crops will be an important part of our future agricultural systems. It is estimated that approximately 7000 species are currently grown for food, with the majority being either partly or fully domesticated (Williams & Haq, 2002). Underutilised or neglected crop species are crops that are predominantly used at the local level but have the potential to be used at the international level (Mayes *et al.*, 2012). They are considered “minor crops” as they are less important in terms of global production and market value relative to the major or staple crops (IPGRI, 2002). However, underutilised and neglected species can contribute to global food security and improvement of agricultural systems. Firstly, many underutilised crop species are nutritionally rich and adapted to grow on damaged or marginal lands thus can contribute to food security, improved diets and ecosystem stability. Many underutilised fruit and vegetables contain more vitamins and minerals than commercial species; many grain species have a better protein profile and improved than commercial cereals (e.g. quinoa and fonio); and legumes can contain better amino acid profiles (e.g. Bambara groundnut) (e.g. IPGRI, 2002; Williams & Haq, 2002; Jansen Van Rensburg *et al.*, 2004; Andini *et al.*, 2013; Ebert, 2014; Chivenge *et al.*, 2015; Nyadanu & Lowor, 2015). Underutilised crops can also provide an income for the rural poor and growing demand for more varied diets have led to the creation of niche markets (Gruere *et al.*, 2006; Chivenge *et al.*, 2015). Finally, underutilised crop species can also be used to preserve and celebrate cultural diversity (IPGRI, 2002; Mayes *et al.*, 2012).

11.1.4 Cropping Systems and Management Practices

The cropping system, crop choice, the management practices adopted and local climatic environment will influence the architecture, resulting light environment and thus the productivity of our agricultural systems (see Chapter

3 for influence of cropping system, Chapter 4 for varietal selection and Chapter 6 for soil nitrogen levels). Whilst maximising crop production is important for reaching food security goals, other targets must also be addressed.

- **Sustainability**

Environmental concerns over agricultural lands combined with depleting natural resources has led to the importance of improving the sustainability of cropping systems. The key aims of sustainable agricultural practices are: integrate biological and ecological processes; minimise the use of non-renewable resources; and make productive use of knowledge and skills (Pretty, 2008). This could be achieved by a number of different methods (for a full review see Pretty, 2008) although one will be given here.

Case Study: Precision Agriculture

Precision agriculture (or satellite farming) is a management concept based on the observation and response to intra-field variation, with the aim to optimise returns whilst conserving resources (Bongiovanni & Lowenberg-Deboer, 2004; Gebbers & Adamchuk, 2010). The concept first arose in America in the 1980s; with the development of the first maps for the recommendation of fertiliser and pH corrections (Robert, 1999). Since that time, the emergence of new technologies such as satellite imagery, information technology, geospatial tools and location systems (such as GPS) have led to more informed management and mapping; whilst improved machinery has allowed more controlled implementation (Gebbers & Adamchuk, 2010). Precision agriculture is a four stage process: geolocation of data; characterisation of variability; decision-making; and implementation of practices to address the variability (Henkel, 2015). In the American Midwest, precision agriculture is common practice among mainstream farmers who vary the rate of fertiliser application across fields in order to maximise profits (e.g. Daberkow & McBride, 1998). However, the practice can also be used to ensure sustainability; by enabling the

application of the right amount of inputs in the right place at the right time (Bongiovanni & Lowenberg-Deboer, 2004; Gebbers & Adamchuk, 2010).

Because sustainable agriculture aims to make the best use of goods and services of each set location, the technologies and practices that are adopted must be suitable locally (Pretty, 2008). Thus the same sustainability practices will not be applicable to all situations. This can be seen with the above example of precision agriculture whereby high technology requirements and mechanisation may be suitable for areas of the developing world but could not be applied to low-input or subsistence agriculture. This suggests that no single configuration of technologies or practices will be suitable to all situations and that there will be multiple ways to achieve sustainability (Pretty, 2008).

- **Resilience**

The concept of sustainability can also be extended to include the resilience of system. The capacity for agricultural systems to buffer shocks and stresses will be integral for stabilising systems and maintaining any yield gains achieved. One example can be seen through cropping practices that help buffer crop losses from biotic or abiotic factors. Multiple cropping systems have a number of benefits including soil conservation (Anil, Park, Phipps, & Miller, 1998), pest and disease reduction (Paoletti, 2005; Perrin, 1977; Thresh, 1982), increased biodiversity (Wolfe, 2000; Lithourgidis *et al.*, 2011), reduced risk of total crop failure (Fukai & Trenbath, 1993) and improved yield stability (Horwith, 1985; Lithourgidis *et al.*, 2006). There is also the potential for the type of cropping system used to mitigate weather-induced damage; as seen in agroforestry systems (for case studies in coffee and rice see Lin *et al.*, 2015).

11.2 The use of plant reconstruction and modelling techniques in studies of crop processes and productivity

Given the complexity of the light environment within canopies, and the various mechanisms determining the absorption, utilisation and response to light energy, processes and mechanisms governing canopy productivity are poorly understood. This highlights the need for methods to quantify the effects of such processes on long-term carbon gain by taking into consideration the complexity of canopy architecture. Modelling provides one such approach by describing growth dynamics as a relationship between complex biophysical processes (Marcelis *et al.*, 1998; Heuvelink, 1999; Gayler *et al.*, 2006). Accurate predictions and quantifications of such processes will both enhance knowledge and provide the potential for a platform for targeted future breeding efforts to maximise canopy productivity (Fourcaud *et al.*, 2008). Successful modelling attempts may provide a number of uses including attempts to explain the link between phenotype and genotype; the effect of the environment on form and function; or provide the basis for growth or photosynthesis modelling (Kawamura *et al.*, 2014).

With increases in technology and production of more affordable equipment, digitising canopies for 3D modelling *in silico* will become increasingly accessible. Accompanied by methods for modelling the light environment (e.g. ray tracing, sunlit-shaded analysis, etc.) more accurate evaluation of the light environment within a canopy is possible. Progress in visual data acquisition and processing has enabled more accurate measurements of plants whilst 3D reconstruction techniques have allowed the modelling of whole-plant physiological function as an integration of organ level processes (Fourcaud *et al.*, 2008). *In silico* modelling enables the development of virtual experiments and measurements without the time, cost, space or feasibility constraints that are present under field or practical situations (Godin & Sinoquet, 2005). For example, detailed information on light partitioning and absorption within

heterogeneous canopy structures would not be possible to obtain from sensors. Also, modelling allows physiological measurements to be made which would be difficult if not impossible to achieve in the field (such as cumulative leaf area index; cLAI) (Allen *et al.*, 2005; Chapter 7). However, validation, wherever possible, should be included to provide confidence in results and enable the most accurate representation of models with real situations. Plant models have been applied to a number of areas including the analysis of plant architecture (e.g. Sinoquet *et al.*, 1997; Barthelemy & Caraglio, 2007), tree stability in winds as a result of crown architecture (Sellier & Fourcaud, 2005) plus light interception and photosynthesis modelling (e.g. Sinoquet *et al.*, 2001; Dauzat *et al.*, 2008).

Within this thesis, an image-based method for 3D plant reconstruction was presented and optimised which, combined with a ray tracing algorithm, enables high-resolution modelling of the light environment within any canopy structure. Empirical modelling was also carried out using parameterisation from light response curves. The light response curve, as described by the non-rectangular hyperbola, provides a means to empirically model photosynthetic processes such as acclimation and photoprotection and scale them up to the whole canopy level. The relative ease at which light response curves can be obtained and incorporated into models provides a means to adapt the model to any C₃ plant species or variety. Whilst the light response curve does not explicitly describe the underlying mechanisms, the shape of the curve can be used to deduce the biochemistry and status of the plant (see Chapter 1). Combined together, these methods provide a means to model light-based processes at a higher level of hierarchy (see Chapter 1) and can be adapted to multiple situations and locations.

- **Applicability of techniques for other situations**

Image-based reconstruction techniques have both practical and economic advantages over other methods for capturing plant structure. Firstly, image-based techniques can be applied quickly and easily to multiple crops and situations, without much prior knowledge. This can be compared to rule-based

systems, whereby the *de novo* construction of 3D plants *in silico* requires knowledge of plant topology and multiple, intensive measurements of architectural features (i.e. leaf and stem length, leaf angle distributions, etc.). Thus, these approaches tend to be both time- and parameter-intensive and may not necessarily reflect inter- or intra-field variation (i.e. due to averages in measurements). Image-based techniques can therefore be used for multiple different types of plants or situations. The reconstruction method used in this thesis also has advantages over other image-based techniques such as space carving. In the latter method, multiple images are taken and the object is treated as a block with the background in images effectively “carved away”, using the different image views, to reveal the ultimate shape. Whilst this may work for some objects, it will not work for others such as those that contain concave angles. Thus leaves that are concave in nature (i.e. Basil leaves) would be produced as a solid block. This is in contrast to the reconstruction method of Pound *et al.* (2014) where these complex shapes will be preserved. However, the former method cannot be applied to 3D structures, such as stems or ears, because of this reason (see below). Compared to other systems required for capturing plant structure (e.g. laser systems or phenotyping platforms), cameras are easily portable and can be used within the field or other inaccessible areas where more bulky or expensive equipment would not be feasible.

- **Applicability of techniques for use in developing countries**

Increasing affordability and accessibility of hardware and software means that modelling methods are more suitable for lower research budgets. RGB image-based reconstruction and analysis methods are already of use within other fields of research such as: the documentation of historical artefacts for inventory of cultural heritage and fast visualization of archaeological finds (Visnovcova *et al.*, 2001; Ioannides *et al.*, 2003; Schindler *et al.*, 2003; Hermon, 2011); for shape modelling research or the development robust and general computer vision algorithms (Snavely *et al.*, 2008) and; for the generation of geospatial databases of informal settlements for application for

improving living conditions (Mason & Baltsavias, 1997). RGB image techniques are often chosen due to their low relative cost, ease of use and speed of capture. Within this thesis, an image based method for the reconstruction of plants (Pound *et al.*, 2014) was optimised (Chapter 2) and used. This method relies on RGB images, which are readily attainable. Furthermore, optimisation tests (data not shown) indicate relatively low resolution images (i.e 8 MP) are suitable for use and thus more affordable, lower resolution cameras are acceptable. Whilst VisualSFM (required for the creation of the initial point cloud; Furukawa & Ponce, 2010; Wu, 2011) and the reconstructor software (Pound *et al.*, 2014) does allow user interaction for the selection of parameters used (see Chapter 2 for full details), they can run with minimal intervention and background knowledge. A minimal constraint on computer performance is set at 6-8 GB of RAM for the reconstruction process. This is due to the number of images contained in some datasets with RAM for high image counts.

11.2.1 Problems with modelling methods

The complexity of photosynthetic and other plant processes, plus the unknown mechanistic response to specific stimuli mean that scaling up processes to the whole system or canopy level in depth is difficult and currently impossible to do with complete accuracy. This is partly as a result of the lack of knowledge of the underlying processes and is confounded by insufficient or unrealistic experimental data. One example of this can be seen in studies of acclimation to a change in light level.

Case Study: Experimental problems with the prediction of Acclimation

Studies on acclimation and plant response to a change in irradiance levels often show dissimilarities to natural conditions (Walters, 2005). As well as experiments in which the light levels are not representative of natural conditions, the light spectrum may similarly be insufficient to promote an acclimation response. For example, fluorescent lights are often used in

controlled environment growth rooms but are lacking in blue wavelengths, which are needed to trigger responses by blue photoreceptors. Furthermore, actinic lights used for measurements (i.e. gas exchange or fluorescence) are almost always of a different spectrum to sunlight or growth conditions.

Responses may be hidden in plants that are grown at the limits of their acclimation range (Walters, 2005), thus knowledge of the acclimation process for the specific plant species or variety is important. However, the growth conditions of a plant may place limits on the ability to acclimate, even if the conditions are theoretically within the acclimation range (Walters, 2005). For example, transferring *Arabidopsis* from low light levels to high light levels leads to only partial acclimation (Yin & Johnson, 2000). This may be a result of photoinhibition, however similar partial acclimation is also seen when transferring plants from high light to low light. This partial acclimation is likely to be a result of mechanical or structural constraints placed by the effect of previous light history (Walters, 2005). For example, anatomical features or specialized complexes may be difficult to alter once in place or growth conditions may limit the plant's ability to detect and respond to signals (Walters, 2005; Yin & Johnson, 2000). Thus whilst growth under uniform conditions (i.e. low or high light) may describe the limits to a plant's acclimation range, the actual response by the plant will depend on its previous light history and stage of development (e.g. age of the leaf). This highlights the complexity of the signalling network within plants and the interaction between different processes. As well as problems with growth conditions, the experimental data itself may not be sufficient to accurately predict the effect of changes in light level. The response will be a result of a number of different factors including light intensity, developmental age, spectral quality and duration of the light periods, including past light histories. The relationship between each of these factors and how they interact together must first be explored.

11.2.2 Improvements to the reconstruction and modelling techniques

- **Improvements to reconstruction techniques**

There are a number of areas which could be targeted in order to improve both the throughput and the accuracy of the reconstruction technique. Firstly, the technique could be automated in order to speed up the process, improve the accuracy of the final reconstruction and reduce human error. For example, using a robot arm and an automated turntable would allow application of a preprogrammed reconstruction “run” which can be optimised to specific plant material. This could include the rotation of the automated turntable by a set degree and the movement of the robot arm to be coordinated. Such a system would remove the need for calibration by VisualSFM (Chapter 2) as calibration would be automatic. This is likely to lead to improvements in both the point cloud and the final reconstruction. Through this method, a feedback loop could also be included, therefore if the reconstruction software finds that there is not enough image detail at a specific point on the plant, the robot arm could return back and another image could be taken. Use of an automated system such as this would also enable other sensors and instruments to be placed on the robot arm (i.e. fluorescence sensors, etc.) and measurements to be taken from known locations on the plant.

There are also areas of the reconstruction process itself that could be improved. During the method, the point cloud is segmented into a number of small patches which are then treated independently; partly to reduce complexity and allow a 3D reconstruction problem to be treated as multiple 2D problems. However, this can often lead to gaps in the final mesh, where these small surface patches do not meet up or touch each other (see Chapter 2, Figs 2.6 and 2.9). A reduction in these gaps would help optimise the overall reconstruction. This could be achieved by separating out the reconstruction into individual organs (i.e. individual leaves) and fitting a surface to each. This surface could then be triangulated; which is likely to reduce the overall number of triangles in the mesh and thus reduce the amount of time it will take for ray tracing and modelling (see Chapter 2).

When segmenting the canopy, the points that make up the section (from the point cloud) are flattened onto a single plane to reduce depth noise (arising from inaccurate camera calibration in VisualSFM) and create the 2D patches. This means that 3D structures, such as stems and ears, will not be preserved as they will be flattened onto a single plane. Thus for plants that contain a lot of 3D structures (i.e. stem material, ears or panicles, succulents with thick stems etc), the reconstruction process used in this thesis is not able to preserve their form. Furthermore, the ray tracing employed in this thesis (Song *et al.*, 2013) can similarly not be used on 3D organs due to the fate of a ray once it has hit a triangle (i.e. the part that will be transmitted through the triangle). Thus to study plants with 3D organs, improvements to both the reconstruction and the ray tracing method are required.

- **Improvements to modelling techniques**

For further improvements in accuracy and precision of plant modelling there are various knowledge gaps that must be addressed. There are multiple aspects of plant growth and development that are less understood such as the feedback between plant physiology and morphology over time, interactions between plants dependent upon cropping system, and interactions with both biotic and abiotic factors in the environment (Bazzaz, 1996; Lambers *et al.*, 2006; Prusinkiewicz & Rolland-Lagan, 2006; Buck-Sorlin *et al.*, 2008; Fourcaud *et al.*, 2008). Mechanistic modelling could be employed to help fill these knowledge gaps (see Chapter 1 for an overview of empirical versus mechanistic modelling and their advantages and drawbacks). This thesis focused on the use of empirical models due to their ease of use and easy applicability to the other techniques used here (i.e. reconstruction and ray tracing outputs). Whilst the models provide a general suggestion as to what we may be seeing in the field, they are unlikely to be accurately predicting the response of the plants (i.e. Part II in particular). Thus, existing mechanistic models of photosynthesis could be applied, or others could be developed that take into account the biochemical status of the plant under study. Concurrent improvements to the throughput of experiments (i.e. use of phenotyping and

screening platforms) and data processing will also be required. Integrating further knowledge over different scales and processes will be integral to not only improve knowledge of plant function but also provide links to other disciplines and services and enable manipulation of processes, for example to improve crop yields or mitigate the effects of climate change (Vos *et al.*, 2007; Fourcaud *et al.*, 2008; Lin *et al.*, 2015).

Chapter 5 discussed the potential impact of wind-induced movement on light patterning within a canopy. This provides one example of how increasing the complexity of the modelling approach could lead to more realistic representations of canopy function. The discussion of Chapter 5 talks about how achieving these moving models (or 4D plants) could arise. Accuracy of models could also be improved through considering further features of canopies, such as canopy gradients or air movements (i.e. eddies, etc.).

Any future advances will not only require development of new techniques but also the sharing of knowledge and ideas. In 1996 a functional structural plant modelling (FSPM) series of workshops was initiated with the aim to share knowledge on physiological- and environmental-models and processes plus advances in computer science and mathematics for the 3D modelling of plants, and in 2003 the Plant-growth Modelling and Applications (PMA) symposium series was commenced. Not only will knowledge sharing be important but also the creation of databases or analysis tools that can be adapted to different experimental data (e.g. analysis tool for the identification of homogeneous zones in tree structures; Durand *et al.*, 2005).

11.3 The Future of Canopy Research

Advances in technology and increased affordability of both hardware and software means that more tools are now available to study canopy structure and the resulting light environment. Combined with more information on the genetic and biochemical properties of processes and pathways, a more detailed understanding of plant form and function is developing. The approaches used in this thesis will be a cornerstone of this emerging field, due their affordability, ease of use and application to multiple situation and scenarios, although some improvements could be made (see section 11.2).

Following this work, there are a number of immediate steps that could be carried out:

- Within Chapter 3, the reconstruction technique was applied to a multiple cropping system. The results predict specific contributions of each component crop to the productivity of the whole system, but are these the results that will be seen if the same intercropping layouts were cultivated in the field? Furthermore, the system under study was interesting as Bambara groundnut and Proso millet are an untested intercrop pairing, yet each component contains features that would suggest they will be complementary. Therefore, a field trial would be able to assess whether the system could be productive. Furthermore, it would give the ability to test both spatial and temporal complementarity, and would provide an interesting case for the study of acclimation (for example: acclimation of the Bambara to a change in light during the cultivation and subsequent removal of the millet).
- Whilst some of the relationships between canopy architecture, the light environment and photosynthesis were discovered in Chapter 4, that trial was limited due to both space constraints and the availability of lines. Screening a much larger range of varieties or lines would help to see whether these traits hold across further germplasm. Furthermore, the study looked at rice, but are these relationships also seen within other species?

- Whilst the process of acclimation was studied here, difficulties in accurately modelling or measuring the process means that there are still large knowledge gaps on its impact on plant performance (see above). These could be filled by: improvements to experimental design and measurement techniques; the use of mutants to separate out different responses; or the use of weather or sensor data so that the influence of past light history can be accounted for.
- Part II discusses the importance of light quantity on photosynthetic processes. This could also be expanded to light quality, with the spectrum of light being critical in determining physiological and molecular processes. This requires understanding of how the arrangement of plant material leads to differences in spectrum, and how this then impacts on functioning.

11.4 Concluding Remarks

With the advent of new techniques that are able to quantitatively describe the distribution of vegetative organs in space and the development of models that can match plant processes to the environment in which the plant is grown, the future of agricultural research is promising. However, despite such advances there are still large knowledge gaps that need to be filled before an accurate picture of whole canopy photosynthesis, and the corresponding breeding platform to improve performance under variable environmental conditions, can be created. Section 11.2 looked at the use of modelling techniques for study plant productivity. Further advances in these technologies combined with improved experiments and data acquisition plus the identification and manipulation of targets (e.g. genes or systems; section 11.1) means that these knowledge gaps are being filled.

References

- Ackerly DD, Bazzaz FA. (1995).** Seedling crown orientation and interception of diffuse radiation in tropical forest gaps. *Ecology* **76**: 1134–1146
- Adamson HY, Chow WS, Anderson JM, Vesik M, Sutherland MW. (1991).** Photosynthetic Acclimation of *Tradescantia Albiflora* to Growth Irradiance Morphological, Ultrastructural and Growth-Responses. *Physiologia Plantarum* **82**: 353–359
- Aggarwal NA, Gaur A, Bhalla E, Gupta SR. (2010).** Soil aggregate carbon and diversity of mycorrhiza as affected by tillage practices in a rice-wheat cropping system in northern India. *International Journal of Ecology and Environmental Science* **36**: 233-243
- Ainsworth EA, Long SP. (2005).** What have we learned from 15 years of free-air CO₂ enrichment (FACE)? A meta-analytic review of the responses of photosynthesis, canopy properties and plant production to rising CO₂. *New Phytologist* **165**: 351–371
- Alarcon VJ, Sassenrath GF. (2011).** Modeling cotton (*Gossypium spp.*) leaves and canopy using computer aided geometric design (CAGD). *Ecological Modelling* **222**: 1951–1963
- Alenya G, Dellen B, Torras C. (2011).** 3D modelling of leaves from color and ToF data for robotized plant measuring. In *Proceedings -IEEE International Conference on Robotics and Automation* pp. 3408–3414
- Allen JF, Forsberg J. (2001).** Molecular recognition in thylakoid structure and function. *Trends in Plant Science* **6**: 317–326
- Allen M, Prusinkiewicz P, DeJong T. (2005).** Using L-systems for modeling source–sink interactions, architecture and physiology of growing trees, the L-PEACH model. *New Phytologist* **166**: 869–880
- Anderson JM, Chow WS, Park Y-I. (1995).** The grand design of photosynthesis: Acclimation of the photosynthetic apparatus to environmental cues. *Photosynthesis Research* **46**: 129–139
- Anderson JM, Osmond CB. (1987).** Shade-Sun responses: compromises between acclimation and photoinhibition. In: Kyle DJ, Osmond CB,

Arntzen CJ, Eds. *Photoinhibition*. Amsterdam: Elsevier Science bv. Amsterdam, Netherlands, pp. 1–38

- Anderson JM. (1980).** Chlorophyllprotein complexes of higher plant thylakoids: Distribution, stoichiometry and organization in the photosynthetic unit. *FEBS letters* **117**: 327-331
- Anderson JM. (1986).** Photoregulation of the composition, function, and structure of thylakoid membranes. *Annual Review in Plant Physiology* **37**: 93–136
- Anderson MC. (1971).** Radiation and Crop Structure. In Z Sesták, J Catsky, PG Jarvis eds., *Plant Photosynthetic Production. Manual of Methods*. The Hague, Netherlands. pp. 412–466
- Andini R, Yoshida S, Ohsawa R. (2013).** Variation in protein content and amino acids in the leaves of grain, vegetable and weedy types of amaranths. *Agronomy* **3**: 391–403
- Ando K, Grumet R, Terpstra K, Kelly J. (2007).** Manipulation of plant architecture to enhance crop disease control. *CAB Reviews: Perspectives in Agriculture, Veterinary Science, Nutrition and Natural Resources*, 2(8)
- Andrieu B, Ivanov N, Boissard P. (1995).** Simulation of light interception from a maize canopy model constructed by stereo plotting. *Agricultural and Forest meteorology* **75**: 103-19
- Anil L, Park J, Phipps RH, Miller FA. (1998).** Temperate intercropping of cereals for forage: A review of the potential for growth and utilization with particular reference to the UK. *Grass and Forage Science* **53**: 301–317
- Anten N. (1999).** Interspecific differences in above-ground growth patterns result in spatial and temporal partitioning of light among species in a tall-grass meadow. *Journal of Ecology* **87**: 583–597
- Anten NP, Schieving F, Werger MJ. (1995).** Patterns of light and nitrogen distribution in relation to whole canopy carbon gain in C3 and C4 mono- and dicotyledonous species. *Oecologia* **101**: 504-513
- Asner GP, Scurlock JMO, Hicke JA. (2003).** Global synthesis of leaf area index observations: Implications for ecological and remote sensing studies. *Global Ecology and Biogeography* **12**: 191–205

- Athanasίου K, Dyson BC, Webster RE, Johnson GN. (2010).** Dynamic acclimation of photosynthesis increases plant fitness in changing environments. *Plant Physiology* **152**: 366–373
- Atkin OK, Westbeek M, Cambridge ML, Lambers H, Pons TL. (1997).** Leaf respiration in light and darkness (A comparison of slow- and fast-growing poa species). *Plant Physiology* **113**: 961-965
- Aylor DE. (1990).** The Role of Intermittent Wind in the Dispersal of Fungal Pathogens. *Annual Review of Phytopathology* **28**: 73–92
- Azam-Ali S, & Squire, G. (2002).** Principles of Tropical Agronomy. Wallingford, UK: CABI.
- Azam-Ali S, Squire G. (2002).** *Principles of Tropical Agronomy*. Wallingford, UK: CABI
- Baccar R, Fournier C, Dornbusch T, Andrieu B, Gouache D, Robert C. (2011).** Modelling the effect of wheat canopy architecture as affected by sowing density on *Septoria tritici* epidemics using a coupled epidemic-virtual plant model. *Annals of Botany* **108**: 1179–1194
- Bailey S, Walters RG, Jansson S, Horton P. (2001).** Acclimation of *Arabidopsis thaliana* to the light environment: The existence of separate low light and high light responses. *Planta* **213**: 794–801
- Baker NR, Oxborough K. (2004).** Chlorophyll fluorescence as a probe of photosynthetic productivity. In GC Papageorgiou, Govindjee eds., *Chlorophyll a fluorescence: a signature of photosynthesis*. Springer. pp. 65–82
- Baldocchi D, Collineau S. (1994).** The physical nature of solar radiation in heterogeneous canopies: spatial and temporal attributes. In M Caldwell, R Pearcy eds. *Exploitation of Environmental Heterogeneity by Plants. Ecophysiology Processes- Above and Belowground*. San Diego, New York, Boston, London, Sydney, Toronto: Academic Press. pp. 21–71
- Baldocchi DD, Amthor J. (2001).** Canopy Photosynthesis: History, Measurements and Models. In *Terrestrial Global Productivity*. pp. 9–31
- Baldocchi DD, Hutchison BA, Matt DR, McMillen RT. (1985).** Canopy radiative-transfer models for spherical and known leaf inclination angle distributions – a test in an oak hickory forest. *Journal of Applied Ecology* **22**: 539–555

- Bandillo N, Raghavan C, Muyco PA, Sevilla MAL, Lobina IT, Dilla-Ermita CJ, et al. (2013).** Multi-parent advanced generation inter-cross (MAGIC) populations in rice: progress and potential for genetics research and breeding. *Rice* **6**: 1
- Barillot R, Escobar-Gutierrez AJ, Fournier C, Huynh P, Combes D. (2014).** Assessing the effects of architectural variations on light partitioning within virtual wheat – pea mixtures. *Annals of Botany Special Issue: Functional-Structural Plant Modelling*, **114**: 13
- Barillot R, Louarn G, Escobar-Gutiérrez AJ, Huynh P, Combes D. (2011).** How good is the turbid medium-based approach for accounting for light partitioning in contrasted grass–legume intercropping systems? *Annals of Botany* **108**: 1013-1024
- Barnett BJ, Barrett CB, Skees JR. (2008).** Poverty traps and index-based risk transfer products. *World Development* **36**: 1766–1785
- Barraclough P, Lopez-Bellido R, Hawkesford M. (2014).** Nitrogen partitioning and remobilization in relation to leaf senescence, grain yield and grain nitrogen concentration in wheat cultivars. *Field Crops Research* **156**: 242–248
- Barraclough PB, Kuhlmann H, Weir AH. (1989).** The effects of prolonged drought and nitrogen fertilizer on root and shoot growth and water uptake by winter wheat. *Journal of Agronomy and Crop Science* **163**: 352-360
- Barthelemy D, Caraglio Y. (2007).** Plant architecture: A dynamic, multilevel and comprehensive approach to plant form, structure and ontogeny. *Annals of Botany* **99**: 375–407
- Bazzaz F. (1996).** *Plants in Changing Environments: Linking Physiological, Population, and Community Ecology*. Cambridge University Press.
- Beadle CL, Long SP. (1985).** Photosynthesis — is it limiting to biomass production? *Biomass* **8**: 119-168
- Beets W. (1982).** *Multiple cropping and tropical farming systems*. Gower and Westview Press
- Bellafiore S, Barneche F, Peltier G, Rochaix J-D. (2005).** State transitions and light adaptation require chloroplast thylakoid protein kinase STN7. *Nature* **433**: 892–895

- Berry P, Sterling M, Spink J, Baker C, Sylvester-Bradley R, Mooney S, Tams A, Ennos A. (2004).** *Advances in Agronomy Volume 84*. Elsevier
- Bhattacharya A, Kourmpetli S, Davey MR. (2010).** Practical applications of manipulating plant architecture by regulating gibberellin metabolism. *Journal of Plant Growth Regulation* **29**: 249–256
- Biemond H, Vos J. (1992).** Effects of nitrogen on the development and growth of the potato plant. 2. The partitioning of dry matter, nitrogen and nitrate. *Annals of Botany* **70**: 37–45
- Birch CJ, Andrieu B, Fournier C, Vos, J, Room P. (2003).** Modelling kinetics of plant canopy architecture—concepts and applications. *European Journal of Agronomy* **19**: 519-533
- Björkman O. (1981).** Responses to different quantum flux densities. In: Lange OL, Nobel PS, Osmond CB, Ziegler H, Eds. *Physiological Plant Ecology*. Springer. pp. 57–107
- Björkman O, Demmig B. (1987).** Photon yield of O₂ evolution and chlorophyll fluorescence characteristics at 77 K among vascular plants of diverse origins. *Planta* **170**: 489–504
- Black JN. (1960).** The significance of petiole length, leaf area, and light interception in competition between strains of subterranean clover (*Trifolium subterraneum* L.) grown in swards. *Australian Journal of Agricultural Research* **11**: 277–291
- Black JN. (1961).** Competition between two varieties of subterranean clover (*Trifolium subterraneum* L.) as related to the proportions of seed sown. *Australian Journal of Agricultural Research* **12**: 810–820
- Blackshaw R, Anderson R, Lemerie D. (2007).** Cultural Weed Management. In: Upadhyaya M, Blackshaw R, eds. *Non-chemical Weed Management: Principles, Concepts and Technology*. CABI, pp. 35–48
- Bonan G. (2002).** *Ecological Climatology: Concepts and Applications* (1st ed.). Cambridge: Cambridge University Press.
- Bongiovanni R, Lowenberg-Deboer J. (2004).** Precision agriculture and sustainability. *Precision Agriculture* **5**: 359–387
- Borel CC, Gerstl SAW, Powers BJ. (1991).** The radiosity method in optical remote sensing of structured 3-D surfaces. *Remote Sensing of Environment* **36**: 13–44

- Boysen Jensen P. (1932).** *Die Stoffproduktion der Pflanzen*. Fischer.
- Bradford MM (1976)** A rapid and sensitive method for the quantitation of microgram quantities of protein utilizing the principle of protein-dye binding. *Analytical Biochemistry* **72**: 248-254
- Bräutigam A, Kajala K, Wullenweber J, Sommer M, Gagneul D, Weber KL, et al. (2010).** An mRNA blueprint for C4 photosynthesis derived from comparative transcriptomics of closely related C3 and C4 species. *Plant Physiology* **155**: 142–156
- Bréda NJJ. (2003).** Ground-based measurements of leaf area index: a review of methods, instruments and current controversies. *Journal of Experimental Botany* **54**: 2403–2417
- Brenner AJ. (1996).** Microclimate modifications in agroforestry. In CK Ong, P Huxley eds. *Tree-Crop Interactions: A physiological Approach*. CAB International/ ICRAF. pp. 157-187
- Broadbent FE, de Datta SK, Laureles EV. (1987).** Measurement of nitrogen-use efficiency in rice genotypes. *Agronomy Journal* **79**: 786–791
- Brodersen CR, Vogelmann TC, Williams WE, Gorton HL. (2008).** A new paradigm in leaf-level photosynthesis: Direct and diffuse lights are not equal. *Plant, Cell and Environment* **31**: 159–164
- Brooker RW, Bennett AE, Cong W-F et al. (2015).** Improving intercropping: a synthesis of research in agronomy, plant physiology and ecology. *New Phytologist* **206**: 107-117
- Brown PL, Doley D, Keenan RJ. (2000).** Estimating tree crown dimensions using digital analysis of vertical photographs. *Agricultural and Forest Meteorology* **100**: 199-212
- Buck-Sorlin G, Hemmerling R, Kniemeyer O, Burema B, Kurth W. (2008).** A rule-based model of barley morphogenesis, with special respect to shading and gibberellic acid signal transduction. *Annals of Botany* **101**: 1109–1123
- Buckley TN, Cescatti A, Farquhar GD. (2013).** What does optimization theory actually predict about crown profiles of photosynthetic capacity when models incorporate greater realism? *Plant Cell and Environment* **36**: 1547-1563

- Burgess AJ, Retkute R, Pound MP, Foulkes J, Preston SP, Jensen OE, Pridmore TP, Murchie EH. (2015).** High-resolution three-dimensional structural data quantify the impact of photoinhibition on long-term carbon gain in wheat canopies in the field. *Plant Physiology* **169**: 1192–1204
- Busov VB, Brunner AM, Strauss SH. (2008).** Genes for control of plant stature and form. *New Phytologist* **177**: 589–607
- Cabrera-Bosquet L, Molero G, Bort J, Nogués S, Araus JL. (2007).** The combined effect of constant water deficit and nitrogen supply on WUE, NUE and $\Delta^{13}C$ in durum wheat potted plants. *Annals of Applied Biology* **151**: 277-289
- Cai Y, Wang W, Zhu Z, Zhang Z, Lang Y, Zhu Q. (2006).** [Effects of water stress during grain-filling period on rice grain yield and its quality under different nitrogen levels]. *The journal of Applied Ecology* **17**: 1201-1206
- Caldwell MM. (1970).** Plant Gas Exchange at High Wind Speeds. *Plant Physiology* **46**: 535–537
- Campbell GS, Norman JM. (1989).** The description and measurement of plant canopy structure. In G Russell, B Marshall, PG Jarvis eds. *Plant Canopies Their Growth Form and Function*. Cambridge University Press. Vol. 31, pp. 1–19
- Carmo-Silva AE, Keys AJ, Andralojc PJ, Powers SJ, Arrabaça MC, Parry MA. (2010).** Rubisco activities, properties, and regulation in three different C4 grasses under drought. *Journal of Experimental Botany* **61**: 2355-2366
- Carmo-Silva AE, Salvucci ME. (2013).** The regulatory properties of Rubisco activase differ among species and affect photosynthetic induction during light transitions. *Plant Physiology* **161**: 1645–1655
- Carmo-Silva E, Scales JC, Madgwick PJ, Parry MAJ. (2015).** Optimizing Rubisco and its regulation for greater resource use efficiency. *Plant Cell and Environment* **38**: 1817–1832
- Cassman KG, Olk DC, Doberman A. (1997).** Scientific evidence of yield and productivity declines in irrigated rice systems of tropical Asia. *IRC Newsletter* **46**: 7 -27

- Cassman KG, Pingali PL. (1995).** Extrapolating trends from long-term experiments to farmers' fields: the case of irrigated rice ecosystem in Asia. IN: Barnett et al. Eds. *Agricultural Sustainability: Economic, Environmental and Statistical considerations*. John Wiley & Sons Ltd. NY
- Cassman KG. (1999).** Ecological intensification of cereal production systems: yield potential, soil quality, and precision agriculture. *Proceedings of the National Academy of Sciences of the USA* **96**: 5952–5959
- Cavazzoni J, Volk T, Tubiello F, Monje O. (2002).** Modelling the effect of diffuse light on canopy photosynthesis in controlled environments. In *IV International Symposium on Models for Plant Growth and Control in Greenhouses: Modeling for the 21st Century-Agronomic and 593*. pp. 39-45
- Cescatti A. (1998).** Effects of needle clumping in shoots and crowns on the radiative regime of a Norway spruce canopy. *Annales Des Sciences Forestieres* **55**: 89–102
- Cescatti A, Niinemets U. (2004).** Leaf to Landscape. In *Photosynthetic adaptation*. Springer, New York. pp. 42–85
- Cescatti A, Zorer R. (2003).** Structural acclimation and radiation regime of silver fir (*Abies alba Mill.*) shoots along a light gradient. *Plant Cell Environment* **26**: 429–442
- Chabot BF, Jurik TW, Chabot JF. (1979).** Influence of instantaneous and integrated light-flux density on leaf anatomy and photosynthesis. *American Journal of Botany* **66**: 940-945
- Chandler RJ. (1969).** Plant morphology and stand geometry in relation to nitrogen. In J Eastin, F Haskins, C Sullivan, C van Bavel eds., *Physiological Aspects of Crop Yield*. ASA, Madison, Wisconsin. pp. 265–285
- Chehab EW, Yao C, Henderson Z, Kim S, Braam J. (2012).** Arabidopsis touch-induced morphogenesis is jasmonate mediated and protects against pests. *Current Biology* **22**: 701–706
- Chelle M, Andrieu B. (2007).** Modelling the light environment of virtual crop canopies. In *Functional-structural modelling in crop production*. Vol. 22, pp. 75–89

- Chelle M, Bouatouch K, Andrieu B. (1998).** Nested radiosity for plant canopies. *The Visual Computer* **14**: 109–125
- Chelle M. (2005).** Phylloclimate or the climate perceived by individual plant organs: what is it? How to model it? What for? *New Phytologist* **166**: 781–790
- Chen JM, Blanken PD, Black TA, Guilbeault M, Chen S. (1997).** Radiation regime and canopy architecture in a boreal aspen forest. *Agricultural and Forest Meteorology* **86**: 107–125
- Chen JM, Rich PM, Gower ST, Norman JM, Plummer S. (1997).** Leaf area index of boreal forests: Theory, techniques, and measurements. *Journal of Geophysical Research* **102**: 29429
- Chitwood DH, Headland LR, Filaault DL, Kumar R, Jiménez-Gómez JM, Schrager V, et al.. (2012).** Native environment modulates leaf size and response to simulated foliar shade across wild tomato species. *PLoS One* **7**: e29570
- Chivenge P, Mabhaudhi T, Modi AT, Mafongoya P. (2015).** The potential role of neglected and underutilised crop species as future crops under water scarce conditions in Sub-Saharan Africa. *International Journal of Environmental Research and Public Health* **12**: 5685–5711
- Chow WS, Adamson HY, Anderson JA. (1991).** Photosynthetic acclimation of *Tradescantia albiflora* to growth irradiance: Lack of adjustment of light-harvesting components and its consequences. *Physiologia Plantarum* **81**: 175-182
- Chow WS. (1994).** Photoprotection and photoinhibitory damage. *Advanced Molecular Cellular Biology* **10**: 151–196
- Cieslak M, Lemieux C, Hanan J, Prusinkiewicz P. (2008).** Quasi-Monte Carlo simulation of the light environment of plants. *Functional Plant Biology* **35**: 837-849
- Clearwater M, Gould K. (1995).** Leaf orientation and light interception by juvenile *Pseudo-panax crassifolius* (Cunn) C. Koch in a partially shaded forest environment. *Oecologia* **104**: 363–371
- Clendon JHM, Millen GGM. (1979).** Leaf Angle: An Adaptive Feature of Sun and Shade Leaves. *Botanical Gazette* **140**: 437-442

- Collinson S, Berchie J, Azam-Ali S. (1999).** The effect of soil moisture on light interception and the conversion coefficient for three landraces of bambara groundnut (*Vigna subterranea*). *The Journal of Agricultural Science* **133**: 151–157
- Connor DJ, Loomis RS, Cassman KG. (2011).** *Crop ecology: productivity and management in agricultural systems*. Cambridge University Press. pp 286
- Cooper J. (1970).** *Potential production and energy conversion in temperate and tropical grasses*. Bureau of pastures and forage crops. Vol 1769
- Cornelissen R. (2005).** *Modelling variation in the physiology of Bambara Groundnut (Vigna subterranea (L.) Verdc.)*. PhD Thesis, Cranfield University at Silsoe, UK
- Corre-Hellou G, Faure M, Launay M, Brisson N, Crozat Y. (2009).** Adaptation of the STICS intercrop model to simulate crop growth and N accumulation in pea–barley intercrops. *Field Crops Research* **113**: 72-81
- Cowan IR, Lange OL, Nobel PS, Osmond CB, Ziegler H. (1982).** Regulation of water use in relation to carbon gain in higher plants. *Physiology and Plant Ecology* **3**: 589-613
- Coyne DP. (1980).** Modification of plant architecture and crop yield by breeding. *HortScience* **15**: 244–247
- D’Halluin K, Vanderstraeten C, Van Hulle J, Rosolowska J, Van Den Brande I, Pennewaert A, et al. (2013).** Targeted molecular trait stacking in cotton through targeted double-strand break induction. *Plant Biotechnology Journal* **11**: 933–941
- Daberkow S, McBride W. (1998).** Adoption of Precision Agriculture Technologies by U.S. Corn Producers. In P Robert eds., *Proceedings of the Fourth International Conference on Precision Agriculture*. St Paul, MN
- Darwin C. (1880).** *The power of movement in plants*. London: John Murray.
- Dauzat J, Clouvel P, Luquet D, Martin P. (2008).** Using virtual plants to analyse the light-foraging efficiency of a low-density cotton crop. *Annals of Botany* **101**: 1153–1166
- Davies J. (2013).** *Mechanisms of morphogenesis*. Academic Press

- de Datta SK, Broadbent FE. (1990).** Nitrogen-use efficiency of 24 rice genotypes on an N-deficient soil. *Field Crops Research* **23**: 81–92
- de Langre E. (2008).** Effects of Wind on Plants. *Annual Review of Fluid Mechanics* **40**: 141-168
- De Lucia EH, Shenoj HD, Naidu SL, Day TA. (1991).** Photosynthetic symmetry of sun and shade leaves of different orientations. *Oecologia* **87**: 51–57
- de Pury DGG, Farquhar GD. (1999).** A commentary on the use of a sun/shade model to scale from the leaf to a canopy. *Agricultural and Forest Meteorology* **95**: 257–260
- de Wit CT. (1958).** *Transpiration and crop yields*. Versl. Landbouwk. Onderz., vol. 64.6. Institute of Biological and Chemical Research on Field Crops and Herbage, Wageningen, The Netherlands.
- Deery D, Jimenez-Berni J, Jones H, Sirault X, Furbank RT. (2014).** Proximal Remote Sensing Buggies and Potential Applications for Field-Based Phenotyping. *Agronomy* **5**: 349–379
- DEFRA. (2015).** *Using nitrogen fertilisers in nitrate vulnerable zones*. Available at www.gov.uk
- DeJong TM, Da Silva D, Vos J, Escobar-Gutiérrez AJ. (2011).** Using functional–structural plant models to study, understand and integrate plant development and ecophysiology. *Annals Of Botany* **108**: 987-989
- Demao J, Xia L. (2001).** Cultivar differences in photosynthetic tolerance to photo-oxidation and shading in rice (*Oryza sativa* L.). *Photosynthetica* **39**: 167–175
- Demmig-Adams B, Adams WW. (1992).** Photoprotection and other responses of plants to high light stress. *Annual Review of Plant Physiology and Plant Molecular Biology* **43**: 599-626
- Demmig-Adams B, Cohu CM, Muller O, Adams WW. (2012).** Modulation of photosynthetic energy conversion efficiency in nature: from seconds to seasons. *Photosynthetic Research* **113**: 75–88
- Depège N, Bellafiore S, Rochaix J-D. (2003).** Role of chloroplast protein kinase Stt7 in LHCII phosphorylation and state transition in *Chlamydomonas*. *Science* **299**: 1572–1575

- Dhima K V., Lithourgidis AS, Vasilakoglou IB, Dordas CA. (2007).** Competition indices of common vetch and cereal intercrops in two seeding ratio. *Field Crops Research* **100**: 249–256
- Dias-Filho MB. (2002).** Photosynthetic light response of the C4 grasses *Brachiaria brizantha* and *B. humidicola* under shade. *Scientia Agricola* **59**: 65-68
- Diekmann KH, Ottow JCG, De Datta SK. (1996).** Yield and nitrogen response of lowland rice (*Oryza sativa L.*) to *Sesbania rostrata* and *Aeschynomene afрасpera* green manure in different marginally productive soils in the Philippines. *Biol Fertile Soils* **21**: 103-108
- Dietzel L, Pfannschmidt T. (2008).** Photosynthetic acclimation to light gradients in plant stands comes out of shade. *Plant Signaling Behavior* **3**: 1116–1118
- Dingkuhn M, Penning De Vries F, Van Laar H. (1991).** Concepts for a new plant type for direct seeded flooded tropical rice. *International Rice Research Institute* pp. 17-31
- Dobermann A, Witt C, Dawe D, Abdulrachman S, Gines HC, Nagarajan R. et al. (2002).** Site-specific nutrient management for intensive rice cropping systems in Asia. *Field Crops Research* **74**: 37-66
- Donahue RA, Poulson ME, Edwards GE. (1997).** A method for measuring whole plant photosynthesis in *Arabidopsis thaliana*. *Photosynthesis Research* **52**: 263-269
- Donald CM. (1968).** The breeding of crop ideotypes. *Euphytica* **17**: 385-403
- Dormann CF. (2007).** Promising the future? Global change projections of species distributions. *Basic and Applied Ecology* **8**: 387–397
- Driever SM, Lawson T, Andralojc PJ, Raines CA, Parry MAJ. (2014).** Natural variation in photosynthetic capacity, growth, and yield in 64 field-grown wheat genotypes. *Journal Experimental Botany* **65**: 4959–4973
- Duncan WG, Loomis RS, Williams WA, Hanau R. (1967).** A model for simulating photosynthesis in plant communities. *Hilgardia* **38**: 181–205
- Duncan WG. (1971).** Leaf Angles, Leaf Area, and Canopy Photosynthesis. *Crop Science* **11**: 482-485

- Durand J-B, Guédon Y, Caraglio Y, Costes E. (2005).** Analysis of the plant architecture via tree-structured statistical models: the hidden Markov tree models. *New Phytologist* **166**: 813–825
- Dutilleul P, Lontoc-Roy M, Prasher S. (2005).** Branching out with a CT scanner. *Trends in Plant Science* **10**: 411–412
- Duvick DN. (2005a).** Genetic progress in yield of United States maize (*Zea mays* L.). *Maydica* **50**: 193–202
- Duvick DN. (2005b).** The contribution of breeding to yield advances in Maize (*Zea mays* L.). *Advances in Agronomy* **86**: 83–145
- Dyson BC, Allwood JW, Feil R, Xu YU, Miller M, Bowsher CG, Goodacre R, Lunn JE, Johnson GN. (2015).** Acclimation of metabolism to light in *Arabidopsis thaliana*: The glucose 6-phosphate/phosphate translocator GPT2 directs metabolic acclimation. *Plant Cell and Environment* **38**: 1404–1417
- Ebenhoeh O, Houwaart T, Lokstein H, Schlede S, Tirok K. (2011).** A minimal mathematical model of nonphotochemical quenching of chlorophyll fluorescence. *Biosystems* **103**: 196-204
- Ebert AW. (2014).** Potential of underutilized traditional vegetables and legume crops to contribute to food and nutritional security, income and more sustainable production systems. *Sustainability* **6**: 319–335
- Edwards J, Knapp A, Brekke B. (2011).** Selection and adaptation to high plant density in the iowa stiff stalk synthetic Maize (*Zea mays* L.) population. *Crop Science* **51**: 2344-2351
- Edwards J. (2011).** Changes in plant morphology in response to recurrent selection in the iowa stiff stalk synthetic maize population. *Crop Science* **51**: 2352-2361
- Ehleringer J, Bjorkman O. (1977).** Quantum Yields for CO₂ Uptake in C₃ and C₄ Plants. *Plant Physiology* **59**: 86–90
- Ehleringer J, Forseth I. (1980).** Solar tracking by plants. *Science* **210**: 1094–1098
- Ehleringer J, Forseth I. (1990).** Diurnal Leaf Movements and Productivity in Canopies. In G Russell, M Bruce, PG. Jarvis eds., *Plant Canopies: Their Growth, Form and Function*. Cambridge University Press. pp.129–142

- Ehleringer J, Werk K. (1986).** Modifications of solar-radiation absorption patterns and implications for carbon gain at the leaf level. In T Givnish eds., *On the Economy of Plant Form and Function. Proceedings of the Sixth Maria Moors Cabot Symposium, "Evolutionary constraints on primary productivity: adaptive patterns of energy capture in plants"* Cambridge University Press. pp. 57–82
- Ehleringer JR. (1988).** Changes in leaf characteristics of species along elevational gradients in the Wasatch-Front, Utah. *American Journal of Botany* **75**: 680–689
- Ennos A. (1997).** Wind as an ecological factor. *Trends in Ecology & Evolution* **12**: 108–111
- Eschrich W, Burchardt R, Essiamah S. (1989).** The induction of sun and shade leaves of the European beech (*Fagus sylvatica* L.): anatomical studies. *Trees - Structure and Function* **3**: 1–10
- Estes LD, Bradley BA, Beukes H, Hole DG, Lau M, Oppenheimer MG, et al. (2013).** Comparing mechanistic and empirical model projections of crop suitability and productivity: Implications for ecological forecasting. *Global Ecology and Biogeography* **22**: 1007–1018
- Evans JR. (1989).** Photosynthesis and nitrogen relationships in leaves of C3 plants. *Oecologia* **78**: 9–19
- Evans JR. (2013).** Improving Photosynthesis. *Plant Physiology* **162**: 1780–1793
- Evans JR, Jakobsen I, Ogren E, (1993).** Photosynthetic light-response curves: 2. Gradients of light-absorption and photosynthetic capacity. *Planta* **189**: 191–200
- Evans JR, Poorter H. (2001).** Photosynthetic acclimation of plants to growth irradiance: the relative importance of specific leaf area and nitrogen partitioning in maximizing carbon gain. *Plant Cell and Environment* **24**: 755–767
- Evans JR, Seemann J. (1989).** The allocation of nitrogen in the photosynthetic apparatus: costs, consequences and control. In *Photosynthesis*. pp. 183–205

- Evans JR, Terashima I. (1987).** Effects of nitrogen nutrition on electron transport components and photosynthesis in spinach. *Functional Plant Biology* **14**: 59-68
- Evers JB, Vos J, Fournier C, Andrieu B, Chelle M, Struik PC. (2005).** Towards a generic architectural model of tillering in Gramineae, as exemplified by spring wheat (*Triticum aestivum*). *New Phytologist* **166**: 801–812
- Ezcurra E, Montana C, Arizaga S. (1991).** Architecture, light interception, and distribution of *Larrea* species in the Monte Desert, Argentina. *Ecology* **72**: 23–34
- Falster DS, Westoby M. (2003).** Leaf size and angle vary widely across species: What consequences for light interception? *New Phytologist* **158**: 509–525
- FAO. (2009).** *Global Agriculture towards 2050*. Rome, FAO. Rome: FAO.
- FAO. (2015).** *The state of food insecurity in the world*.
- FAOSTAT. (2014).** (available at: www.faostat.fao.org/)
- Farque L, Sinoquet H, Colin, F. (2001).** Canopy structure and light interception in *Quercus petraea* seedlings in relation to light regime and plant density. *Tree Physiology* **21**: 1257–1267
- Field CB, Mooney HA. (1983).** Leaf age and seasonal effects on light, water, and nitrogen use efficiency in a California shrub. *Oecologia* **56**: 348-355
- Field CB. (1981).** Leaf age effects on the carbon gain of individual leaves in relation to microsite. *Tasks for Vegetation Science* **4**: 41–50
- Field CB. (1983).** Allocating leaf nitrogen for the maximization of carbon gain: leaf age as a control on the allocation program. *Oecologia* **56**: 314-347
- Finger R. (2010).** Evidence of slowing yield growth – The example of Swiss cereal yields. *Food Policy* **35**: 175–182
- Foley JA, Defries R, Asner GP, Barford C, Bonan G, Carpenter SR, et al. (2005).** Global consequences of land use. *Science* **309**: 570–574
- Foulkes M, Murchie E. (2011).** Optimizing canopy physiology traits to improve the nutrient use efficiency of crops. In: Hawkesford MJ, Barraclough P, Eds. *The Molecular and physiological basis of nutrient use efficiency in crops*. Chichester: Wiley-Blackwell. pp. 65–83

- Fourcaud T, Zhang X, Stokes A, Lambers H, Körner C. (2008).** Plant growth modelling and applications: the increasing importance of plant architecture in growth models. *Annals of Botany* **101**: 1053–1063
- Fournier C, Andrieu B, Ljutovac S, Saint-Jean S. (2003).** ADEL-wheat: a 3D architectural model of wheat development. In Hu B-G & Jaeger M. Eds. *Plant Growth Modeling and Applications* pp.54-66
- Francis CA. (1986).** *Multiple Cropping Systems*. MP Company, Ed. New York.
- Freibauer A, Mathijs E, Brunori G, Damianova Z, Faroult E, Gomis JG, O'Brien L, Treyer S. (2011).** Sustainable food consumption and production in a resource-constrained world. *The 3rd SCAR (European Commission–Standing Committee on Agricultural Research) Foresight Exercise*
- Fukai S, Trenbath BR. (1993).** Processes determining intercrop productivity and yields of component crops. *Field Crops Research* **34**: 247–271
- Furbank RT, Von Caemmerer S, Sheehy J, Edwards G. (2009).** C₄ rice: A challenge for plant phenomics. *Functional Plant Biology* **36**: 845–856
- Furukawa Y, Ponce J. (2010).** Accurate, dense, and robust multiview stereopsis. *IEEE Transactions on Pattern Analysis and Machine Intelligence* **32**: 1362–1376
- Gaju O, Allard V, Martre P, Le Gouis J, Moreau D, Bogard M, et al. (2014).** Nitrogen partitioning and remobilization in relation to leaf senescence, grain yield and grain nitrogen concentration in wheat cultivars. *Field Crops Research* **155**: 213–223
- Gaju O, Martre P, Snape J, Heumez E, LeGouis J, Moreau D, et al. (2011).** Identification of traits to improve the nitrogen-use efficiency of wheat genotypes. *Field Crops Research* **123**: 139–152
- Gallais A, Coque M. (2005).** Genetic variation and selection for nitrogen use efficiency in maize: A synthesis. *Maydica* **50**: 531-537
- Gao L, Jin Z, Zhang G, Shi C, Ge D. (2000).** A numerical model to simulate the incident radiation and photosynthate for rice canopies with optimum plant type. *Jiangsu Journal of Agricultural Sciences* **16**: 1-9

- Garcia-Plazaola JI, Esteban R, Fernandez-Marin B, Kranter I, Porcar-Castell A. (2012).** Thermal energy dissipation and xanthophyll cycles beyond the Arabidopsis model. *Photosynthesis Research* **113**: 89-103
- Gayler S, Grams TEE, Kozovits AR, Winkler JB, Luedemann G, Priesack E. (2006).** Analysis of competition effects in mono- and mixed cultures of juvenile beech and spruce by means of the plant growth simulation model PLATHO. *Plant Biology* **8**: 503–514
- Gebbers R, Adamchuk VI. (2010).** Precision agriculture and food security. *Science* **327**: 828–31
- Geiger D. (1994).** General Lighting Requirements for Photosynthesis. *International Lighting in Controlled Environments Workshop*. pp. 3–18
- Genty B, Briantais JM, Baker NR. (1989).** The relationship between the quantum yield of photosynthetic electron transport and quenching of chlorophyll fluorescence. *Biochimica et Biophysica Acta* **990**: 87–92
- Gill BS, Friebe BR, White FF. (2011).** Alien introgressions represent a rich source of genes for crop improvement. *Proceedings of the National Academy of Sciences of the USA* **108**: 7657–7658
- Givnish TJ. (1986).** On the Economy of Plant Form and Function. *Proceedings of the Sixth Maria Moors Cabot Symposium, Evolutionary Constraints on Primary Productivity, Adaptive Patterns of Energy Capture in Plants*. Cambridge University Press.
- Givnish TJ. (1988).** Adaptation to Sun and Shade: a Whole-Plant Perspective. *Australian Journal of Plant Physiology* **15**: 63-92
- Givnish TJ, Vermeij GJ. (1976).** Sizes and Shapes of Liane Leaves. *The American Naturalist*: 743-778
- Godfray HCJ, Beddington JR, Crute IR, Haddad L, Lawrence D, Muir JF, et al. (2010).** Food security: the challenge of feeding 9 billion people. *Science* **327**: 812–818
- Godin C. (2000).** Representing and encoding plant architecture: a review. *Annals of Forest Science* **57**: 413–438
- Godin C, Sinoquet H. (2005).** Functional-structural plant modelling. *New Phytologist* **166**: 705–708

- Goel N, Rozehnal I, Thompson R. (1991).** A computer graphics based model for scattering from objects of arbitrary shapes in the optical region. *Remote Sensing of Environment* **36**: 73–104
- Gouache D, Gate P, Charmet G, Brisson N, Huard F, Oury F-X. (2010).** Why are wheat yields stagnating in Europe? A comprehensive data analysis for France. *Field Crops Research* **119**: 201–212
- Govindjee. (2012).** *Photosynthesis V2: Development, Carbon Metabolism, and Plant Productivity*. Elsevier.
- Gowik U, Westhoff P. (2011).** The path from C₃ to C₄ photosynthesis. *Plant Physiology* **155**: 56–63
- Grace J. (1977).** *Plant Responses to Wind*. Academic Press Limited
- Grace J. (1988).** Plant response to wind. *Agriculture, Ecosystems & Environment* **22-23**: 71–88
- Gridley H, Jones M, Wopereis-Pura M. (2002).** Development of new rice for Africa (NERICA) and participatory varietal selection. In *Breeding rainfed rice for drought-prone environments: integrating conventional and participatory plant breeding in South and Southeast Asia*. Proceedings of a DFID Plant Sciences Research Programme/IRRI Conference, pp. 12–15
- GRiSP (Global Rice Science Partnership). (2013).** *Rice almanac, 4th edition*. Los Baños (Philippines): International Rice Research Institute. pp. 283
- Gross LJ. (1982).** Photosynthetic dynamics in varying light environments, a model and its application to whole leaf carbon gain. *Ecology* **63**: 84-93
- Gruere G, Giuliani A, Smale M. (2006).** *Marketing Underutilized Plant Species for the Benefit of the Poor: A Conceptual Framework*. IFPRI Discussion Paper, 54
- Grumet R, Colle M, Ando K, Xie D, Havenga L, Switzenberg J. (2013).** Modified plant architecture to enhance crop disease control: genetic control and possible value of upright fruit position in cucumber. *European Journal of Plant Pathology* **135**: 545–560
- Gutschick V, Wiegand F. (1988).** Optimizing the canopy photosynthetic rate by patterns of investment in specific leaf mass. *The American Naturalist* **132**: 67–86

- Haefele SM, Jabbar SM, Siopongco JD, Tirol-Padre A, Amarante ST, Cruz PS, Cosico WC. (2008).** Nitrogen use efficiency in selected rice (*Oryza sativa L.*) genotypes under different water regimes and nitrogen levels. *Field Crops Research* **107**: 137-46
- Hanafi MM, Eltaib SM, Ahmad MB. (2000).** Physical and chemical characteristics of controlled release compound fertiliser. *European Polymer Journal* **36**: 2081-2088
- Harasim E, Wesolowski M, Kwiatowski C, Cierpiala R. (2016).** The effect of retardants and nitrogen fertilization on winter wheat canopy structure. *Romanian Agricultural Research* **33**: 29-39
- Hashim MM, Yusop MK, Othman R, Wahid SA. (2015).** Characterization of nitrogen uptake pattern in Malaysian rice MR219 at different growth stages using ¹⁵N isotope. *Rice Science* **22**: 250-254
- Haugaard-Nielsen H, Gooding M, Ambus P, Corre-Hellou G, Crozat Y, Dahlmann C, Dibet A, et al. (2009).** Pea-barley intercropping and short-term subsequent crop effects across European organic cropping conditions. *Nutrient Cycling in Agroecosystems* **85**: 141–155
- Hazell P, Poulton C, Wiggins S, Dorward A. (2010).** The future of small farms: trajectories and policy priorities. *World Development* **38**: 1349–1361
- He J, Chee C, Goh C. (1996).** “Photoinhibition” of *Heliconia* under natural tropical conditions: the importance of leaf orientation for light interception and leaf temperature. *Plant Cell Environment* **19**: 1238–1248
- Hedden P. (2003).** The genes of the Green Revolution. *Trends in Genetics* **19**: 5–9
- Henkel M. (2015).** *21st Century Homestead: Sustainable Agriculture I.*
- Herbert TJ. (1991).** Variation in interception of the direct solar beam by top canopy layers. *Ecology* **72**: 17–22
- Herbert TJ. (2003).** A latitudinal cline in leaf inclination of *Dryas octopetala* and implications for maximization of whole plant photosynthesis. *Photosynthetica* **41**: 631–633

- Herman T, Murchie EH, Ali A. (2015).** Rice production and climate change: a case study of Malaysian Rice. *Pertanika Journal of Tropical Agricultural Science* **38**: 321-328
- Hermon S. (2011).** Ancient Vase 3D Reconstruction and 3D Visualization. *Conference on Computer Applications and Quantitative Methods in Archaeology*. pp. 59–64
- Hesketh JD, Musgrave RB. (1962).** Photosynthesis under field conditions. IV. Light studies with individual corn leaves. *Crop Science* **2**: 311–315
- Heuvelink E. (1999).** Evaluation of a dynamic simulation model for tomato crop growth and development. *Annals of Botany* **83**: 413–422
- Hikosaka K, Terashima I, Katoh S. (1994).** Effects of leaf age, nitrogen nutrition and photon flux density on the distribution of nitrogen among leaves of a vine (*Ipomoea tricolor Cav.*) grown horizontally to avoid mutual shading of leaves. *Oecologia* **97**: 451-457
- Hikosaka K, Terashima I. (1995).** A model of the acclimation of photosynthesis in the leaves of C3 plants to sun and shade with respect to nitrogen use. *Plant Cell and Environment* **18**: 605–618
- Hikosaka K. (2005).** Leaf canopy as a dynamic system: ecophysiology and optimality in leaf turnover. *Annals of Botany* **95**: 521–533
- Hillocks RJ, Bennett C, Mponda OM. (2012).** Bambara nut: A review of utilisation, market potential and crop improvement. *African Crop Science Journal* **20**: 1–16
- Hirel B, Le Gouis J, Ney B, Gallais A. (2007).** The challenge of improving nitrogen use efficiency in crop plants: Towards a more central role for genetic variability and quantitative genetics within integrated approaches. *Journal of Experimental Botany* **58**: 2369-2387
- Hirel B, Tétu T, Lea PJ, Dubois F. (2011).** Improving nitrogen use efficiency in crops for sustainable agriculture. *Sustainability* **3**: 1452-1485
- Hirose T, Werger MJA. (1987).** Maximizing daily canopy photosynthesis with respect to the leaf nitrogen allocation pattern in the canopy. *Oecologia* **72**: 520–526
- Hirose T. (2005).** Development of the Monsi-Saeki theory on canopy structure and function. *Annals of Botany* **95**: 483–494

- Hodanova D. (1979).** Sugar beet canopy photosynthesis as limited by leaf age and irradiance. Estimation by models. *Photosynthetica* **13**: 376–385
- Hofle B. (2014).** Radiometric correction of terrestrial LiDAR point cloud data for individual maize plant detection. *IEEE Geoscience and Remote Sensing Letters* **11**: 94–98
- Hopkins R, Schmitt J, Stinchcombe JR. (2008).** A latitudinal cline and response to vernalization in leaf angle and morphology in *Arabidopsis thaliana* (Brassicaceae). *New Phytologist* **179**: 155-164
- Horn H. (1971).** *The Adaptive Geometry of Trees*. Princeton University Press.
- Horton P. (2000).** Prospects for crop improvement through the genetic manipulation of photosynthesis: morphological and biochemical aspects of light capture. *Journal of Experimental Botany* **51**: 475–485
- Horton P, Ruban A. (2005).** Molecular design of the photosystem II light-harvesting antenna: photosynthesis and photoprotection. *Journal of Experimental Botany* **56**: 365-373
- Horwith B. (1985).** A role for intercropping in modern agriculture. *BioScience* **35**: 286–291
- Houle D, Govindaraju DR, Omholt S. (2010).** Phenomics: the next challenge. *Nature Reviews. Genetics* **11**: 855–866
- Hubbart S, Ajigboye OO, Horton P, Murchie EH. (2012).** The photoprotective protein PsbS exerts control over CO₂ assimilation rate in fluctuating light in rice. *Plant Journal* **71**: 402–412
- Hubbart S, Bird S, Lake JA, Murchie EH. (2013).** Does growth under elevated CO₂ moderate photoacclimation in rice? *Physiologia plantarum* **148**: 297-306
- Humphreys J, Harper JA, Armstead IP, Humphreys MW (2005).** Introgression-mapping of genes for drought resistance transferred from *Festuca arundinacea* var. *glaucescens* into *Lolium multiflorum*. *Theoretical and Applied Genetics* **110**: 579–587
- Ioannides M, Stylianidis E, Stylianos S. (2003).** 3D reconstruction and visualization in cultural heritage. *Proceedings of the 19th International CIPA Symposium*. pp. 258–262
- IPGRI. (2002).** *Neglected and Underutilized Plant Species: Strategic Action plan*. Rome, Italy.

- IRRI. (2006).** *C4 Rice Project*.
- Ivanov N, Boissard P, Chapron M, Andrieu B. (1995).** Computer stereo plotting for 3-D reconstruction of a maize canopy. *Agricultural and Forest Meteorology* **75**: 85-102
- Jansen Van Rensburg WS, Venter SL, Netshiluvhi TR, Van Den Heever E, Vorster HJ, De Ronde JA. (2004).** Role of indigenous leafy vegetables in combating hunger and malnutrition. *South African Journal of Botany* **70**: 52–59
- Jaya I, Bell C, Sale P. (2001).** Modification of within- microclimate in maize for intercropping in the lowland tropics. *Australian Agronomy Conference*. Australia, pp. 123–133
- Jensen E, Hauggaard-Nielson H, Kinane J, Anderson M, Jornsgaard B. (2005).** Intercropping – The practical application of diversity, competition and facilitation in arable organic cropping systems. In: Kopke U, Niggli U, Neuhoﬀ D, Lockeretx W, Willer H, eds. *Researching sustainable systems*. Proceedings of the first scientific conference of the international society of organic agricultural research (ISO FAR). Bonn, Germany, pp. 22–25
- Jin J, Huang W, Gao J-P, Yang J, Shi M, Zhu M-Z, et al. (2008).** Genetic control of rice plant architecture under domestication. *Nature Genetics*, **40**: 1365–1369
- Johnson IR, Thornley JHM, Frantz JM, Bugbee B. (2010).** A model of canopy photosynthesis incorporating protein distribution through the canopy and its acclimation to light, temperature and CO₂. *Annals of Botany* **106**: 735–749
- Jonckheere I, Fleck S, Nackaerts K, Muys B, Coppin P, Weiss M, Baret F. (2004).** Review of methods for in situ leaf area index determination - Part I. Theories, sensors and hemispherical photography. *Agricultural and Forest Meteorology* **121**: 19–35
- Jung G, Coyne DP, Skroch PW, Nienhuis J, Arnaud-Santana E, Bokosi J, et al. (1996).** Molecular Markers Associated with Plant Architecture and Resistance to Common Blight, Web Blight, and Rust in Common Beans. *Journal of the American Society for Horticultural Science* **121**: 794–803

- Kabir Z, Rhamoun M, Lazicki P, Horwath W. (2008).** Cover crops and conservation tillage increase mycorrhizal colonization of corn and tomato roots. In *Sustainable Agriculture Farming System Project; Volume 9, No. 1*. University of California, Davis, CA, USA.
- Kajala K, Covshoff S, Karki S, Woodfield H, Tolley B, Dionora M, et al. (2011).** Strategies for engineering a two-celled C4 photosynthetic pathway into rice. *Journal of Experimental Botany* **62**: 3001–3010
- Kalos M, Whitlock P. (1986).** *Monte Carlo methods. Volume I: basics*. Chichester: Wiley.
- Kalra N, Chakraborty D, Sharma A, Rai HK, Jolly M, Chander S, et al. (2008).** Effect of increasing temperature on yield of some winter crops in northwest India. *Current Science* **94**: 82–88
- Kant S, Bi YM, Rothstein SJ. (2011).** Understanding plant response to nitrogen limitation for the improvement of crop nitrogen use efficiency. *Journal of Experimental Botany* **62**: 1499-1509
- Kasajima I, Ebana K, Yamamoto T, Takahara K, Yano M, Kawai-Yamada M, Uchimiya H. (2011).** Molecular distinction in genetic regulation of nonphotochemical quenching in rice. *PNAS* **108**: 13835-13840
- Kasanga H, Monsi M. (1954).** On the light transmission of leaves, and its meaning for the production of dry matter in plant communities. *Japan Journal of Botany* **14**: 304–324
- Kashiwagi T, Togawa E, Hirotsu N, Ishimaru K. (2008).** Improvement of lodging resistance with QTLs for stem diameter in rice (*Oryza sativa* L.). *Theoretical and Applied Genetics* **117**: 749–757.
- Kass D. (1978).** Polyculture cropping systems: review and analysis. Cornell International Agriculture Bulletin 32, New York State College of Agriculture and Life Sciences, Cornell University, Ithaca, N.Y.
- Katyal JC, Singh B, Vlek PLG, Craswell E. (1985).** Fate and efficiency of nitrogen fertilizers applied to wetland rice: II. Punjab, India. *Nutrient Cycle Agroecosystems* **6**: 279–290
- Kawamura K, Hibrand-Saint Oyant L, Foucher F, Thouroude T, Loustau S. (2014).** Kernel methods for phenotyping complex plant architecture. *Journal of Theoretical Biology* **342**: 83–92

- Keating BA, Carberry PS. (1993).** Resource capture and use in intercropping: solar radiation. *Field Crops Research* **34**: 273–301
- Kelly V, Adesina AA, Gordon A. (2003).** Expanding access to agricultural inputs in Africa: A review of recent market development experience. *Food Policy* **28**: 379–404
- Kempf J, Pickett S. (1981).** The role of branch length and angle in branching pattern of forest shrubs along a successional gradient. *New Phytologist* **88**: 111–116
- Khan MH, Dar ZA, Dar SA. (2015).** Breeding strategies for improving rice yield—A Review. *Agricultural Science* **6**: 467–478
- Khush GS. (1994).** Increasing the genetic yield potential of rice: prospects and approaches. *International Rice Commission Newsletter* **43**: 1–8
- Khush GS. (1996).** Prospects of and approaches to increasing the genetic yield potential of rice. In R Evenson, R Herdt, M Hossain eds., *Rice Research in Asia. Progress and Priorities*. Wallingford, UK: CABI. pp. 59–71
- Khush GS. (2005).** What it will take to feed 5.0 billion rice consumers in 2030. *Plant Molecular Biology* **59**: 1–6
- Kim HS, Palmroth S, Thérézien M, Stenberg P, Oren R. (2011).** Analysis of the sensitivity of absorbed light and incident light profile to various canopy architecture and stand conditions. *Tree Physiology* **31**: 30–47
- King DA. (1994).** Influence of light level on the growth and morphology of saplings in a Panamanian Forest. *American Journal of Botany* **81**: 948–957
- King DA. (1997).** The functional significance of leaf angle in eucalyptus. *Australian Journal Botany* **45**: 619–639
- King DA. (1998).** Relationship between crown architecture and branch orientation in rain forest trees. *Annals of Botany* **82**: 1–7
- King DA, Maindonald JH. (1999).** Tree architecture in relation to leaf dimensions and tree stature in temperate and tropical rain forests. *Journal of Ecology* **87**: 1012–1024
- King J, Armstead I, Harper J, Ramsey L, Snape J, Waugh R, et al. (2013).** Exploitation of interspecific diversity for monocot crop improvement. *Heredity* **110**: 475–483

- Kirschbaum MUF, Gross LJ, Pearcy RW. (1988).** Observed and modeled stomatal responses to dynamic light environments in the shade plant *Alocasia-Macrorrhiza*. *Plant Cell And Environment* **11**: 111-121
- Kirschbaum MUF, Kuppers M, Schneider H, Giersch C, Noe S. (1998).** Modelling photosynthesis in fluctuating light with inclusion of stomatal conductance, biochemical activation and pools of key photosynthetic intermediates. *Planta* **204**: 16-26
- Knight MR, Smith SM, Trewavas AJ. (1992).** Wind-induced plant motion immediately increases cytosolic calcium. *Proceedings of the National Academy of Sciences* **89**: 4967–4971
- Koyama K, Kikuzawa K. (2010).** Geometrical similarity analysis of photosynthetic light response curves, light saturation and light use efficiency. *Oecologia* **164**: 53-63
- Kozłowska-Ptaszyńska Z. (1993).** Changes in the structure and architecture of plant canopy of two- and six-rowed spring barley cultivars as influenced by seeding date. *Pam. Pul.* **102**: 53–63
- Krause GH, Weis E. (1991).** Chlorophyll fluorescence and photosynthesis: the basics. *Annual Review Plant Physiology and Plant Molecular Biology* **42**: 313–349
- Kropff MJ, Cassman KG, Van Laar HH, Peng S. (1993).** Nitrogen and yield potential of irrigated rice. *Plant and Soil* **155-156**: 391–394
- Kulheim C, Agren J, Jansson S. (2002).** Rapid regulation of light harvesting and plant fitness in the field. *Science* **297**: 91-93
- Kull O, Broadmeadow M, Kruijt B, Meir P. (1999).** Light distribution and foliage structure in an oak canopy. *Trees - Structure and Function* **14**: 55–64
- Kull O. (2002).** Acclimation of photosynthesis in canopies: models and limitations. *Oecologia* **133**: 267–279
- Kunz HH, Häusler RE, Fettke J, Herbst K, Niewiadomski P, Gierth M, et al. (2010).** The role of plastidial glucose-6-phosphate/phosphate translocators in vegetative tissues of *Arabidopsis thaliana* mutants impaired in starch biosynthesis. *Plant Biology* **12**: 115-128
- Kuppers M, Pfiz M. (2009).** Role of photosynthetic induction for daily and annual carbon gains of leaves and plant canopies. In: *Photosynthesis In*

Silico: Understanding Complexity From Molecules To Ecosystems, pp. 417-440

- Laborde AG, de Bie KC, Smaling EM, Moya PF, Boling AA, Van Ittersum MK. (2012).** Rice yields and yield gaps in Southeast Asia: past trends and future outlook. *European Journal of Agronomy* **36**: 9-20
- Lambers H, Chapin F, Pons TL. (2008).** *Plant Physiological Ecology*. Springer
- Lambers H, Shane MW, Cramer MD, Pearse SJ, Veneklaas EJ. (2006).** Root structure and functioning for efficient acquisition of phosphorus: Matching morphological and physiological traits. *Annals of Botany* **98**: 693-713
- Lantinga EA, Nassiri M, Kropff MJ. (1999).** Modelling and measuring vertical light absorption within grass–clover mixtures. *Agricultural and Forest Meteorology* **96**: 71-83
- Law BE, Cescatti A, Baldocchi DD. (2001).** Leaf area distribution and radiative transfer in open-canopy forests: implications for mass and energy exchange. *Tree Physiology* **21**: 777–787
- Lawson T, Blatt MR. (2014).** Stomatal Size, Speed, and Responsiveness Impact on Photosynthesis and Water Use Efficiency. *Plant Physiology* **164**: 1556–1570
- Leakey ADB, Scholes JD, Press MC. (2005).** Physiological and ecological significance of sunflecks for dipterocarp seedlings. *Journal of Experimental Botany* **56**: 469–82
- Leegood RC, Walker DA, Foyer CH. (1985).** Regulation of the Benson-calvin cycle. In: Barber JN, Baker NR, eds. *Photosynthetic mechanisms and the environment*. Elsevier Science. pp. 189-258
- Legg BJ. (1983).** Movement of plant pathogens in the crop canopy. *Philosophical Transactions of the Royal Society of London. Series B, Biological Sciences* **302**: 559-574
- Lemaire G, Gastal F. (1997).** Nitrogen uptake and distribution in plant canopies. In: Lemaire G. Ed. *Diagnosis of the Nitrogen Status in Crops*. Springer–Verlag, Berlin, pp. 3–43
- Leverenz JW. (1994).** Factors determining the nature of the light dosage response curves of leaves. In NR Baker, JR Bowyer eds. *Photoinhibition*

of Photosynthesis: From Molecular Mechanisms to the Field. Bios Scientific Publishing, Oxford. pp. 239–254

- Leverenz JW, Gunnar Oquist G, Wingsle G. (1992).** Photosynthesis and photoinhibition in leaves of chlorophyll b-less barley in relation to absorbed light. *Physiologia Plantarum* **85**: 495-502
- Li W, Guo Q, Jakubowski MK, Kelly M. (2012).** A New Method for Segmenting Individual Trees from the Lidar Point Cloud. *Photogrammetric Engineering & Remote Sensing* **78**: 75–84
- Li X, Qian Q, Fu Z, Wang Y, Xiong G, Zeng D, et al. (2003).** Control of tillering in rice. *Nature* **422**: 618-621
- Li XP, Muller-Moule P, Gilmore AM, Niyogi KK. (2002).** PsbS-dependent enhancement of feedback de-excitation protects photosystem II from photoinhibition. *Proceedings National Academy of Science USA* **99**: 15222–15227
- Li Z, Wakao S, Fischer BB, Niyogi KK. (2009).** Sensing and responding to excess light. *Annual Review of Plant Biology* **60**: 239–260
- Lichtenthaler HK. (1987).** Chlorophylls and carotenoids, the pigments of photosynthetic biomembranes. *Methods in Enzymology* **148**: 350-382
- Licker R, Johnston M, Foley JA, Barford C, Kucharik CJ, Monfreda C, Ramankutty N. (2010).** Mind the gap: How do climate and agricultural management explain the “yield gap” of croplands around the world? *Global Ecology and Biogeography* **19**: 769–782
- Lin B, Burgess AJ, Murchie EH. (2015).** Adaptation for climate-sensitive crops using agroforestry: case studies for coffee and rice. In C Ong, C Black, J Wilson eds., *Tree-Crop Interactions: Agroforestry in a Changing Climate*. Wallingford, UK: CABI. pp. 278–208
- Lithourgidis A, Dordas C, Damalas C, Vlachostergios D. (2011).** Annual Intercrops: An Alternative Pathway for Sustainable Agriculture. *Australian Journal of Crop Science* **5**: 396–410
- Lithourgidis AS, Vasilakoglou IB, Dhima KV, Dordas CA, Yiakoulaki MD. (2006).** Forage yield and quality of common vetch mixtures with oat and triticale in two seeding ratios. *Field Crops Research* **99**: 106–113

- Liu J, Yuan L, Deng Q, Chen L, Cai Y. (2005).** A study on characteristics of photosynthesis in super high-yielding hybrid rice. *Zhongguo nongye kexue* **38**: 258–264
- Liu Q, Chen L. (2003).** A radiation transfer model to predict canopy radiation in thermal infrared band. *Journal of Remote Sensing* **7**: 161–167
- Lizumi T, Ramankutty N. (2015).** How do weather and climate influence cropping area and intensity? *Global Food Security* **4**: 46-50
- Lobell DB, Cassman KG, Field CB. (2009).** Crop Yield Gaps: Their Importance, Magnitudes, and Causes. *Annual Review of Environment and Resources* **34**: 179–204
- Lobet G, Pagès L, Draye X. (2011).** A novel image-analysis toolbox enabling quantitative analysis of root system architecture. *Plant Physiology* **157**: 29-39
- Long SP, Drake BG. (1991).** Effect of the long-term elevation of CO₂ concentration in the field on the quantum yield of photosynthesis of the C₃ Sedge, *Scirpus olneyi*. *Plant Physiology* **96**: 221-226
- Long SP, Hällgren JE. (1985).** Measurement of CO₂ assimilation by plants in the field and in the laboratory. In J Coombs, DO Hall, SP Long, JMO Scurlock, eds, *Techniques in Bioproductivity and Photosynthesis*. Pergamon Press, Oxford, pp 62–94
- Long SP, Humphries S, Falkowski PG. (1994).** Photoinhibition of photosynthesis in nature. *Annual Review Plant Physiology and Plant Molecular Biology* **45**: 633–662
- Long SP, Zhu XG, Naidu SL, Ort DR. (2006).** Can improvement in photosynthesis increase crop yields? *Plant Cell and Environment* **29**: 315–330
- Lorenz AJ, Gustafson TJ, Coors JG, de Leon N. (2010).** Breeding maize for a bioeconomy: A literature survey examining harvest index and stover yield and their relationship to grain yield. *Crop Science* **50**: 1–12
- Loss SP, Siddique KHM. (1994).** Morphological and Physiological Traits Associated with Wheat Yield Increases in Mediterranean Environments. *Advances in Agronomy* **52**: 229–276

- Lowe DG. (1999).** Object recognition from local scale-invariant features. *Proceedings of the Seventh IEEE International Conference on Computer Vision*, 2
- Lu C, Gu F, Zou J, Lu M. (1991).** Studies on yielding potential and related characteristics of rice ideotype. *Scientia Agricultura Sinica* **24**: 15–22
- Lüttge U, Cánovas F, Matyssek R. (2016).** *Progress in Botany* 77. Springer.
- Mae T. (1997).** Physiological nitrogen efficiency in rice: nitrogen utilization, photosynthesis, and yield potential. In: *Plant nutrition for sustainable food production and environment*. Springer Netherlands. pp. 51-60
- Makino A. (2003).** Rubisco and nitrogen relationships in rice: leaf photosynthesis and plant growth. *Soil Science and Plant Nutrition* **49**: 319-27
- Makino A. (2011).** Photosynthesis, grain yield, and nitrogen utilization in rice and wheat. *Plant Physiology* **155**: 125–129
- Makino A, Osmond B. (1991).** Effects of nitrogen nutrition on nitrogen partitioning between chloroplasts and mitochondria in Pea and Wheat. *Plant Physiology* **96**: 355–362
- Malézieux E, Crozat Y, Dupraz C, Laurans M, Makowski D, Ozier-Lafontaine H, et al. (2009).** Mixing plant species in cropping systems: Concepts, tools and models. A review. *Agronomic Sustainability Development* **29**: 43-62
- Marcelis LF, Heuvelink E, Goudriaan J. (1998).** Modelling biomass production and yield of horticultural crops: a review. *Scientia Horticulturae* **74**: 83–111
- Mason S, Baltasvias EP. (1997).** Image-Based Reconstruction of Informal Settlements. In *Proceedings of 17 International Workshop Automatic Extraction of Man Made Objects from Aerial and Space Images*. Ascona Switzerland. pp. 97 – 108
- Matloobi M. (2012).** Light Harvesting and Photosynthesis by the Canopy. In M Najafpour eds., *Advances in Photosynthesis- Fundamental Aspects*. pp 235-256
- Mayes S, Massawe F, Alderson P, Roberts J, Azam-Ali S, Hermann M. (2012).** The potential for underutilized crops to improve security of food production. *Journal of Experimental Botany* **63**: 1075–1079

- McLean G, Paszkiewicz S, Messina C, Zinselmeier C, Doherty A, Schussler J, et al. (2009).** Can Changes in Canopy and/or Root System Architecture Explain Historical Maize Yield Trends in the U.S. Corn Belt? *Crop Science* **49**: 299-312
- McMurtrie R, Wolf L. (1983).** A model of competition between trees and grass for radiation, water and nutrients. *Annals of Botany* **52**: 449-58
- Mekala NR, Suorsa M, Rantala M, Aro E-M, Tikkanen M. (2015).** Plants actively avoid state transitions upon changes in light intensity: role of light-harvesting complex ii protein dephosphorylation in high light. *Plant Physiology* **168**: 721–34
- Meshlab. (2014).** <http://meshlab.sourceforge.net>
- Midmore DJ. (1993).** Agronomic modification of resource use and intercrop productivity. *Field Crops Research* **34**: 357–380
- Minorsky P V. (2010).** On the Inside. *Plant Physiology* **152**: 1–2
- Mock JJ, Pearce RB. (1975).** Ideotype of Maize. *Euphytica* **24**: 613–623
- Moncrieff GR, Lehmann CER, Schnitzler J, Gambiza J, Hiernaux P, Ryan CM, et al. (2014).** Contrasting architecture of key African and Australian savanna tree taxa drives intercontinental structural divergence. *Global Ecology Biogeography* **23**: 1235–1244
- Monna L, Kitazawa N, Yoshino R, Suzuki J, Masuda H, Maehara Y, et al. (2002).** Positional cloning of rice semidwarfing gene, sd-1: Rice “green revolution gene” encodes a mutant enzyme involved in gibberellin synthesis. *DNA Research* **9**: 11–17
- Monsi M, Saeki T. (1953).** Über den Lichtfaktor in den Pflanzengesellschaft- u ur die Stoffproduktion. *Japanese Journal of Botany* **14**: 22–52
- Monsi M, Uchijima Z, Oikawa T. (1973).** Structure of foliage canopies and photosynthesis. *Annual Review Ecological System* **4**: 301–327
- Monteith JL. (1965).** Light distribution and photosynthesis in field crops. *Annals of Botany* **29**: 17–37
- Monteith JL, Moss CJ. (1977).** Climate and the efficiency of crop production in Britain. *Philosophical Transactions of the Royal Society B: Biological Sciences* **281**: 277–294
- Moore G. (2007).** *Living with the Earth, Third Edition: Concepts in Environmental Health Science*. CRC Press.

- Moreau D, Allard V, Gaju O, Le Gouis J, Foulkes MJ, Martre P. (2012).** Acclimation of leaf nitrogen to vertical light gradient at anthesis in wheat is a whole-plant process that scales with the size of the canopy. *Plant Physiology* **160**: 1479–1490
- Morris RA, Furoc RE, Rajbhandari NK, Marqueses EP. (1989).** Rice response to waterlog-tolerant green manure. *Agronomy Journal* **81**: 803–809
- Moser D, Drapela T, Zaller JG, Frank T. (2009).** Interacting effects of wind direction and resource distribution on insect pest densities. *Basic and Applied Ecology* **10**: 208–215
- Moulia B, Coutand C, Lenne C. (2006).** Posture control and skeletal mechanical acclimation in terrestrial plants: implications for mechanical modeling of plant architecture. *American Journal of Botany* **93**: 1477–1489
- Mucheru-Muna M, Pypers P, Mugendi D, Kung'u J, Mugwe J, Merckx R, Vanlauwe B. (2010).** A staggered maize-legume intercrop arrangement robustly increases crop yields and economic returns in the highlands of Central Kenya. *Field Crops Research* **115**: 132–139
- Mueller ND, Gerber JS, Johnston M, Ray DK, Ramankutty N, Foley JA. (2012).** Closing yield gaps through nutrient and water management. *Nature* **490**: 254–257
- Müller P, Li XP, Niyogi KK (2001).** Non-photochemical quenching. A response to excess light energy. *Plant Physiology* **125**: 1558–1566
- Muraoka H, Takenaka A, Tang Y, Koizumi H, Washitani I. (1998).** Flexible leaf orientations of *Arisaema heterophyllum* maximize light capture in a forest understorey and avoid excess irradiance at a deforested site. *Annals of Botany* **82**: 297–307
- Murchie EH, Chen Y, Hubbart S, Peng S, Horton P. (1999).** Interactions between senescence and leaf orientation determine in situ patterns of photosynthesis and photoinhibition in field-grown rice. *Plant Physiology* **119**: 553–564
- Murchie EH, Horton P. (1997).** Acclimation of photosynthesis to irradiance and spectral quality in British plant species: Chlorophyll content,

photosynthetic capacity and habitat preference. *Plant Cell and Environment* **20**: 438–448

Murchie EH, Horton P. (1998). Contrasting patterns of photosynthetic acclimation to the light environment are dependent on the differential expression of the responses to altered irradiance and spectral quality. *Plant Cell and Environment* **21**: 139-148

Murchie EH, Hubbart S, Chen Y, Peng S, Horton P. (2002). Acclimation of rice photosynthesis to irradiance under field conditions. *Plant Physiology* **130**: 1999–2010

Murchie EH, Hubbart S, Peng S, Horton P. (2005). Acclimation of photosynthesis to high irradiance in rice: gene expression and interactions with leaf development. *Journal of Experimental Botany* **56**: 449–460

Murchie EH, Lawson T. (2013). Chlorophyll fluorescence analysis: a guide to good practice and understanding some new applications. *Journal Experimental Botany* **64**: 3983–3998

Murchie EH, Niyogi KK. (2011). Manipulation of photoprotection to improve plant photosynthesis. *Plant Physiology* **155**: 86–92

Murchie EH, Pinto M, Horton P. (2009). Agriculture and the new challenges for photosynthesis research. *New Phytologist* **181**: 532–552

Murchie EH, Reynolds MP. (2012). Crop radiation capture and use efficiency. In RA Meyers eds., *Encyclopedia of Sustainability Science and Technology*. Springer, New York, pp 2615–2638

Myneni RB, Ross J, Asrar G. (1989). A review on the theory of photon transport in leaf canopies. *Agricultural and Forest Meteorology* **45**: 1-53

Neeraja CN, Vemireddy LR, Malathi S, Siddiq EA. (2009). Identification of alternate dwarfing gene sources to widely used Dee-Gee-Woo-Gen allele of sd1 gene by molecular and biochemical assays in rice (*Oryza sativa* L.). *Electronic Journal Biotechnology* **12**: 7-8

Neumann K, Verburg PH, Stehfest E, Muller C. (2010). The yield gap of global grain production: A spatial analysis. *Agricultural Systems* **103**: 316–326

Newbold P. (1989). The use of nitrogen fertiliser in agriculture. Where do we go practically and ecologically? *Plant and Soil* **115**: 297–311

- Niewiadomski P, Knappe S, Geimer S, Fischer K, Schulz B, Unte US, et al. (2005).** The Arabidopsis plastidic glucose 6-phosphate/phosphate translocator GPT1 is essential for pollen maturation and embryo sac development. *The Plant Cell* **17**: 760–775
- Niinemets Ü. (2007).** Photosynthesis and resource distribution through plant canopies. *Plant Cell & Environment* **30**: 1052–1071
- Niinemets Ü. (2012).** Optimization of foliage photosynthetic capacity in tree canopies: towards identifying missing constraints. *Tree Physiology* **32**: 505–509
- Niinemets Ü, Anten N. (2009).** Packing the photosynthetic machinery: from leaf to canopy. In: Laisk A, Nedbal L, Govindjee. Eds. *Photosynthesis in silico: understanding complexity from molecules to ecosystems*. Dordrecht, Netherlands, pp. 363–399
- Niinemets Ü, Anten NP. (2009).** Photosynthesis in Canopies. In A Laisk, L Nedbal, Govindjee eds., *Photosynthesis in silico*. Springer. pp. 363–399
- Niinemets Ü, Cescatti A, Christian R. (2004).** Constraints on light interception efficiency due to shoot architecture in broad-leaved *Nothofagus* species. *Tree Physiology* **24**: 617–630
- Niinemets Ü, Cescatti, A., Lukjanova, A., Tobias, M., & Truus, L. (2002).** Modification of light-acclimation of *Pinus sylvestris* shoot architecture by site fertility. *Agricultural and Forest Meteorology* **111**: 121–140
- Niinemets Ü, Keenan TF, Hallik L. (2015).** A worldwide analysis of within - canopy variations in leaf structural, chemical and physiological traits across plant functional types. *New Phytologist* **205**: 973–993
- Niinemets Ü, Sparrow A, Cescatti A. (2005).** Light capture efficiency decreases with increasing tree age and size in the southern hemisphere gymnosperm *Agathis australis*. *Trees - Structure and Function* **19**: 177–190
- Niinemets Ü, Tenhunen JD. (1997).** A model separating leaf structural and physiological effects on carbon gain along light gradients for the shade-tolerant species *Acer saccharum*. *Plant Cell and Environment* **20**: 845–866

- Niinemets Ü, Tobias M, Cescatti A, Sparrow A. (2006).** Size - dependent variation in shoot light - harvesting efficiency in shade - intolerant Conifers. *International Journal of Plant Sciences* **167**: 19-32
- Niklas PJ. (1994).** Plant allometry: The scaling of form and process. *Trends in Ecology & Evolution (Vol. 10)*. University Of Chicago Press
- Ning H, Chuan-gen L, Ke-min Y, Jing C, Xiao-cui Z. (2013).** Analysis and simulation of plant type on canopy structure and radiation transmission in Rice. *Rice Science* **20**: 229–237
- Niyogi KK, Li XP, Rosenberg V, Jung HS. (2005).** Is PsbS the site of non-photochemical quenching in photosynthesis? *Journal Experimental Botany* **56**: 375–382
- Nobel P. (1991).** *Physiochemical and environmental plant physiology*. San Diego: Academic Press.
- Nobel P, Forseth I, Long S. (1993).** Canopy Structure and light interception. In: Hall D, Scurlock J, Bohlar-Nordenkamp H, Leegood R, Long S, eds. *Photosynthesis and Production in a Changing Environment: a field and laboratory manual*. pp. 79–90
- Nori H, Abdul Halim R, Ramlan MF. (2008).** Effects of nitrogen fertilization management practice on the yield and straw nutritional quality of commercial rice varieties. *Malaysian Journal of Mathematical Sciences* **2**: 61–71
- Norman J, Campbell G. (1989).** Canopy Structure. In *Plant Physiological Ecology. Field Methods and Instrumentation*. pp. 321–325
- Norman J. (1980).** Interfacing leaf and canopy light interception models. In *Predicting Photosynthesis for Ecosystem Models*. Vol. 2. pp. 49–67
- Normile D. (1999).** Crossing rice strains to keep Asia's rice bowls brimming. *Science* **80**: 283-313
- Nyadanu D, Lowor S. (2015).** Promoting competitiveness of neglected and underutilized crop species: comparative analysis of nutritional composition of indigenous and exotic leafy and fruit vegetables in Ghana. *Genetic Resources and Crop Evolution* **62**: 131–140
- Ofori F, Stern WR. (1987).** Cereal-Legume Intercropping Systems. *Advances in Agronomy* **41**: 41–90

- Ögren E. (1993).** Convexity of the photosynthetic light-response curve in relation to intensity and direction of light during growth. *Plant Physiology* **101**: 1013-1019
- Ögren E, Sjöström M. (1990).** Estimation of the effect of photoinhibition on the carbon gain in leaves of a willow canopy. *Planta* **181**: 560–567
- Oguchi R, Hikosaka K, Hirose T. (2003).** Does the photosynthetic light-acclimation need change in leaf anatomy? *Plant Cell and Environment* **26**: 505–512
- Oguchi R, Hikosaka K, Hirose T. (2005).** Leaf anatomy as a constraint for photosynthetic acclimation: differential responses in leaf anatomy to increasing growth irradiance among three deciduous trees. *Plant Cell and Environment* **28**: 916–927
- Oker-Blom P, Kellomäki S. (1982).** Effect of angular distribution of foliage on light absorption and photosynthesis in the plant canopy: Theoretical computations. *Agricultural Meteorology* **26**: 104–116
- Omar O. (2008).** *Rice production and potential for hybrid rice in Malaysia.* Paper presented at International Plantation Industry Conference & Exhibition (IPiCEX), Nov. 2008.
- Omasa K, Hosoi F, Konishi A. (2007).** 3D lidar imaging for detecting and understanding plant responses and canopy structure. *Journal of Experimental Botany* **58**: 881–898
- Onoda Y, Anten NPR. (2011).** Challenges to understand plant responses to wind. *Plant Signaling and Behavior* **6**: 1057-1059
- Orr D, Alcântara A, Kapralov M, Andralojc J, Carmo-Silva E, Parry M. (2016).** Surveying Rubisco diversity and temperature response to improve crop photosynthetic efficiency. *Plant Physiology*: pp.16.00750v1–pp.00750.2016
- Ort DR, Baker NR. (1988).** Consideration of the photosynthetic efficiency at low light as a major determinant of crop photosynthetic performance. *Plant Physiology and Biochemistry* **26**: 555–565
- Ort DR, Long SP. (2014).** Limits on yields in the corn belt. *Science*, **344**: 484-485
- Ort DR, Merchant SS, Alric J, Barkan A, Blankenship RE, Bock R, et al. (2015).** Redesigning photosynthesis to sustainably meet global food and

bioenergy demand. *Proceedings of the National Academy of Sciences of the United States of America* **112**: 8529–36

Ortiz R, Sayre KD, Govaerts B, Gupta R, Subbarao GV, Ban T, et al. (2008). Climate change: Can wheat beat the heat? *Agriculture, Ecosystems and Environment* **126**: 46–58

Pagès L, Drouet J.-L. (2007). GRAAL-CN: A model of GRowth, Architecture and ALlocation for Carbon and Nitrogen dynamics within whole plants formalised at the organ level. *Ecological Modelling* **206**: 231–249

Pagès L, Vercambre G, Gautier H, Najla S, Grasselly D, Génard M. (2009). Tomato plant architecture as affected by salinity: Descriptive analysis and integration in a 3-D simulation model. *Botany* **87**: 893–904

Palmer J, Wallace S, Hood C, Khalilian A, Porter P. (1993). Agronomic considerations for successfully relay intercropping soybeans into standing wheat in the southern United States. *1993 Southern Conservation Tillage Conference for Sustainable Agriculture*

Pan S, Liu C, Zhang W, Xu S, Wang N, Li Y, et al. (2013). The scaling relationships between leaf mass and leaf area of vascular plant species change with altitude. *PLoS One* **8**: e76872

Paoletti MG. (2005). Ecological engineering for pest management—advances in habitat manipulation for arthropods. *Austral Ecology* **30**: 613–614

Parkhurst DF, Loucks OL. (1972). Optimal leaf size in relation to environment. *Journal of Ecology* **60**: 505–537

Parry MAJ, Andralojc PJ, Mitchell RAC, Madgwick PJ, Keys AJ. (2003). Manipulation of Rubisco: the amount, activity, function and regulation. *Journal of Experimental Botany* **54**: 1321–1333

Parry MAJ, Andralojc PJ, Parmar S, Keys AJ, Habash D, Paul MJ, et al. (1997). Regulation of Rubisco by inhibitors in the light. *Plant Cell and Environment* **20**: 528–534

Parry MAJ, Andralojc PJ, Scales JC, Salvucci ME, Carmo-Silva AE, Alonso H, Whitney SM. (2013). Rubisco activity and regulation as targets for crop improvement. *Journal of Experimental Botany* **64**: 717–730

- Parry MAJ, Reynolds M, Salvucci ME, Raines C, Andralojc PJ, Zhu X-G, et al. (2011).** Raising yield potential of wheat. II. Increasing photosynthetic capacity and efficiency. *Journal of Experimental Botany* **62**: 453–467
- Pask AJD, Pietragalla J, Mullan, Reynolds MP. (2012).** *Physiological Breeding. II. A Field Guide to Wheat Phenotyping*. International Wheat and Maize Improvement Centre (CIMMYT), Mexico City, Mexico
- Pask AJD, Sylvester-Bradley R, Jamieson PD, Foulkes MJ. (2012).** Quantifying how winter wheat crops accumulate and use nitrogen reserves during growth. *Field Crops Research* **126**: 104–118
- Patterson MF, Wiseman PE, Winn MF, Lee SM, Araman PA. (2011).** Effects of photographic distance on tree crown attributes calculated using UrbanCrowns image analysis software. *Arboriculture & Urban Forestry* **37**: 173–179
- Paulus S, Dupuis J, Mahlein A-K, Kuhlmann H. (2013).** Surface feature based classification of plant organs from 3D laserscanned point clouds for plant phenotyping. *BMC Bioinformatics* **14**: 238
- Pearce S, Saville R, Vaughan SP, Chandler PM, Wilhelm EP, Sparks CA, et al. (2011).** Molecular characterization of Rht-1 dwarfing genes in hexaploid wheat. *Plant Physiology* **157**: 1820–1831
- Pearcy RW. (1990).** Sunflecks and Photosynthesis in Plant Canopies. *Annual Review of Plant Physiology and Plant Molecular Biology* **41**: 421–453
- Pearcy RW, Gross LJ, He D. (1997).** An improved dynamic model of photosynthesis for estimation of carbon gain in sunfleck light regimes. *Plant Cell And Environment* **20**: 411-424
- Pearcy RW, Seemann JR. (1990).** Photosynthetic induction state of leaves. *Plant Physiology* **94**: 628–633
- Pearcy RW, Sims DA. (1994).** Photosynthetic acclimation to changing light environments: scaling from the leaf to the whole plant. In Caldwell MM and Pearcy RW, eds. *Exploitation of environmental heterogeneity by plants: ecophysiological processes above and below ground*. Academic Press London. pp. 145-170

- Peltonen-Sainio, P., Jauhiainen, L., & Laurila, I. P. (2009).** Cereal yield trends in northern European conditions: Changes in yield potential and its realisation. *Field Crops Research* **110**: 85–90
- Peng S, Garcia FV, Laza RC, Sanico AL, Visperas RM, Cassman KG. (1996).** Increased N-use efficiency using a chlorophyll meter on high yielding irrigated rice. *Field Crops Research* **47**: 243–252
- Peng S, Huang J, Cassman KG, Laza RC, Visperas RM, Khush GS. (2010).** The importance of maintenance breeding: A case study of the first miracle rice variety-IR8. *Field Crops Research* **119**: 342–347
- Peng S, Khush GS, Virk P, Tang Q, Zou Y. (2008).** Progress in ideotype breeding to increase rice yield potential. *Field Crops Research* **108**: 32–38
- Peppe DJ, Royer DL, Cariglino B, Oliver SY, Newman S, Leight E, et al. (2011).** Sensitivity of leaf size and shape to climate: Global patterns and paleoclimatic applications. *New Phytologist* **190**: 724–739
- Perrin R. (1977).** Pest management in multiple cropping systems. *AgroEcosystems* **3**: 93-118
- Peterson TA, Blackmer TM, Francis DD, Scheppers JS. (1993).** *Using a chlorophyll meter to improve N management. A Webguide in soil resource management: D-13, fertility.* Cooperative Extension, Institute of Agriculture and Natural Resources, University of Nebraska, Lincoln, NE
- Phattaralerphong J, Sinoquet H. (2005).** A method for 3D reconstruction of tree crown volume from photographs: assessment with 3D-digitized plants. *Tree Physiology* **25**: 1229-1242
- Pinstrup-Andersen P, Pandya-Lorch R. (1994).** *Alleviating poverty, intensifying agriculture and effectively managing natural resources.* International Food Policy Research Institute
- Placido DF, Campbell MT, Folsom JJ, Cui X, Kruger GR, Baenziger PS, Walia H. (2013).** Introgression of novel traits from a wild wheat relative improves drought adaptation in wheat. *Plant Physiology* **161**: 1806–19
- Pons TL. (2012).** Interaction of temperature and irradiance effects on photosynthetic acclimation in two accessions of *Arabidopsis thaliana*. *Photosynthesis Research* **113**: 207-219

- Pons TL, Jordi W, Kuiper D. (2001).** Acclimation of plants to light gradients in leaf canopies: evidence for a possible role for cytokinins transported in the transpiration stream. *Journal of Experimental Botany* **52**: 1563–1574
- Porcar-Castell A, Palmroth S. (2012).** Modelling photosynthesis in highly dynamic environments: the case of sunflecks. *Tree Physiology* **32**: 1062–1065
- Porra RJ, Thompson WA, Kriedemann PE. (1989).** Determination of accurate extinction coefficients and simultaneous equations for assaying chlorophylls a and b extracted with four different solvents: verification of the concentration of chlorophyll standards by atomic absorption spectroscopy. *Biochimica et Biophysica Acta* **975**: 384–394
- Posada HM, Lechowicz MJ, Kitajima K. (2009).** Optimal photosynthetic use of light by tropical tree crowns achieved by adjustment of individual leaf angles and nitrogen content. *Annals of Botany* **103**: 795–805
- Poulson ME, De Lucia EH. (1993).** Photosynthetic and structural acclimation to light direction in vertical leaves of *Silphium terebinthinaceum*. *Oecologia* **95**: 393–400
- Pound MP, French AP, Murchie EH, Pridmore TP. (2014).** Automated recovery of three-dimensional models of plant shoots from multiple color images. *Plant physiology* **166**: 1688–1698
- Powles SB. (1984).** Photoinhibition of photosynthesis induced by visible light. *Annual Review Plant Physiology and Plant Molecular Biology* **35**: 15–44
- Powles SB, Björkman O. (1981).** Leaf movement in the shade species *Oxalis oregana*. II. Role in protection against injury by intense light. Year Book - Carnegie Institution of Washington (USA)
- Pradhan P, Fischer G, van Velthuisen H, Reusser D, Kropp J. (2015).** Closing yield gaps: how sustainable can we be? *PLoS One* **10**: e0129487
- Pretty J (2008).** Agricultural sustainability: concepts, principles and evidence. *Philosophical Transactions of the Royal Society of London. Series B, Biological Sciences* **363**: 447–465
- Price GD, Badger MR, von Caemmerer S. (2011).** The prospect of using cyanobacterial bicarbonate transporters to improve leaf photosynthesis in C₃ crop plants. *Plant Physiology* **155**: 20–26

- Price GD, Badger MR, Woodger FJ, Long BM. (2008).** Advances in understanding the cyanobacterial CO₂-concentrating- mechanism (CCM): Functional components, Ci transporters, diversity, genetic regulation and prospects for engineering into plants. *Journal of Experimental Botany* **59**: 1441–1461
- Price GD, Pengelly J, Forster B, Du J, Whitney S, von Caemmerer S, et al. (2012).** The cyanobacterial CCM as a source of genes for improving photosynthetic CO₂ fixation in crop species. *Journal of Experimental Botany* **3**: 753:768
- Prins A, Orr DJ, Andralojc PJ, Reynolds MP, Carmo-Silva E, Parry MAJ. (2016).** Rubisco catalytic properties of wild and domesticated relatives provide scope for improving wheat photosynthesis. *Journal of Experimental Botany* **67**: 1827–38
- Prioul JL, Chartier P. (1977).** Partitioning of transfer and carboxylation components of intracellular resistance to photosynthetic CO₂ fixation: a critical analysis of the methods used. *Annals of Botany* **41**: 789-800
- Prusinkiewicz P, Rolland-Lagan AG. (2006).** Modeling plant morphogenesis. *Current Opinion in Plant Biology* **9**: 83-88
- Pugnaire F, Valladares F. (1999).** *Handbook of Functional Plant Ecology*. CRC Press
- Quan L, Tan P, Zeng G, Yuan L, Wang J, Kang SB. (2006).** Image-based plant modeling. *ACM Transactions on Graphics* **25**: 599-604
- Que Q, Chilton M-DM, de Fontes CM, He C, Nuccio M, Zhu T, et al. (2010).** Trait stacking in transgenic crops: challenges and opportunities. *GM Crops* **1**: 220–229
- Rakocevic M, Sinoquet H, Christophe A, Varlet-Grancher C. (2000).** Assessing the geometric structure of a white clover (*Trifolium repens* L.) canopy using 3-D digitising. *Annals of Botany* **86**: 519–526
- Rasband, W. (2012).** *ImageJ*. U. S. National Institutes of Health, Bethesda, Maryland, USA, //imagej.nih.gov/ij/.
- Raven JA. (2011).** The cost of photoinhibition. *Physiol Plant* **142**: 87–104
- Raven JR. (1994).** The cost of photoinhibition to plant communities. In: Baker NR, Bowyer JR. Eds. *Photoinhibition of photosynthesis- molecular mechanisms to the field*. Oxford: Bios Sci

- Raven JR. (1994).** The cost of photoinhibition to plant communities. In NR Baker & JR Bowyer eds., *Photoinhibition of photosynthesis- molecular mechanisms to the field*. Oxford: Bios.Sci.
- Raviv M. (2010).** The use of mycorrhiza in organically- grown crops under semi arid conditions: A review of benefits, constraints and future challenges. *Symbiosis* **52**: 65-74
- Ray DK, Mueller ND, West PC, Foley JA. (2013).** Yield trends are insufficient to double global crop production by 2050. *PloS One* **8**: e66428
- Ray DK, Ramankutty N, Mueller ND, West PC, Foley JA. (2012).** Recent patterns of crop yield growth and stagnation. *Nature Communications* **3**: 1293
- Reddy MS, Willey RW. (1981).** Growth and resource use studies in an intercrop of pearl millet/groundnut. *Field Crops Research* **4**: 13–24
- Redfern S, Azzu N, Binamira J. (2012).** *Rice in Southeast Asia: facing risks and vulnerabilities to respond to climate change. Build Resilience Adapt Climate Change Agri Sector* 23
- Reich PB, Walters MB, Ellsworth DS, Vose JM, Volin JC, Gresham C, Bowman WD. (1998).** Relationships of leaf dark respiration to leaf nitrogen, specific leaf area and leaf life-span: a test across biomes and functional groups. *Oecologia* **114**: 471–482
- Rengel Z. (2002).** Breeding for better symbiosis. *Plant Soil* **245**: 147-162
- Retkute R, Smith-Unna SE, Smith RW, Burgess AJ, Jensen OE, Johnson GN, Preston SP, Murchie EH. (2015).** Exploiting heterogeneous environments: Does photosynthetic acclimation optimize carbon gain in fluctuating light? *Journal of Experimental Botany* **66**: 2437–2447
- Reynolds JF, Acock B. (1985).** Predicting the response of plants to increasing carbon dioxide: A critique of plant growth models. *Ecological Modelling* **29**: 107–129
- Reynolds MP, Van Ginkel M, Ribaut JM. (2000).** Avenues for genetic modification of radiation use efficiency in wheat. *Journal of Experimental Botany* **51**: 459-473
- Rice Knowledge Bank, IRRI. (2016).** Available at: <http://www.knowledgebank.irri.org/>

- Robert PC. (1999).** *Precision Agriculture: an information revolution in Agriculture.*
- Roden JS, Pearcy RW. (1993a).** Effect of leaf flutter on the light environment of poplars. *Oecologia* **93**: 201–207
- Roden JS, Pearcy RW. (1993b).** Photosynthetic gas exchange response of poplars to steady-state and dynamic light environments. *Oecologia* **93**: 208–214
- Roden JS. (2003).** Modeling the light interception and carbon gain of individual fluttering aspen (*Populus tremuloides* Michx) leaves. *Trees* **17**: 117–126
- Roderick HW, Morgan WG, Harper JA, Thomas HM. (2003).** Introgression of crown rust (*Puccinia coronata*) resistance from meadow fescue (*Festuca pratensis*) into Italian ryegrass (*Lolium multiflorum*) and physical mapping of the locus. *Heredity* **91**: 396–400
- Rosegrant MW, Paisner MS, Meijer S, Witcover J, Meijer Juliewitcover S. (2001).** *2020 Global Food Outlook Trends, Alternatives, and Choices.* International Food Policy Research Institute
- Rosenzweig C, Parry ML. (1994).** Potential impact of climate change on world food supply. *Nature* **367**: 133–138
- Ross J. (1981).** *The radiation regime and architecture of plant stands.* Springer Science & Business Media. The Hague, Netherlands
- Rötter RP, Tao F, Höhn JG, Palosuo T. (2015).** Use of crop simulation modelling to aid ideotype design of future cereal cultivars. *Journal Experimental Botany* **66**: 3463–3476
- Royer D. (2012).** Climate reconstruction from leaf size and shape: new developments and challenges. In L Ivany, B Huber eds., *Reconstructing Earth's deep-time climate- the state of the art in 2012, Paleontological Society short course.* The Paleontological Society Paper, Volume 18. pp. 195–212
- Ruban AV, Johnson MP, Duffy CDP. (2012).** The photoprotective molecular switch in the photosystem II antenna. *Biochimica et Biophysica Acta* **1817**: 167-181
- Russell G, Jarvis PG, Monteith J. (1989).** Absorption of radiation by canopies and stand growth. In G Russell, B Marshall, P Jarvis, eds, *Plant*

Canopies: Their Growth, Form and Function. Cambridge University Press, Cambridge, United Kingdom, pp 21–41

- Russell G, Jarvis PG, Monteith JL. (1989).** Absorption of Radiation by Canopies and Stand Growth. In *Plant Canopies : Their Growth, Form and Function*. pp. 21–39
- Ryel RJ, Beyschlag W, Caldwell M. (1993).** Foliage orientation and carbon gain in two tussock grasses as assessed with a new whole- plant gas-exchange model. *Functional Ecology* **7**: 115–124
- Sage RF, Monson R. (1999).** *C4 Plant Biology*. San Diego: Academic Press.
- Sage RF, Zhu X-G (2011).** Exploiting the engine of C₄ photosynthesis. *Journal of Experimental Botany* **62**: 2989–3000
- Sakamoto T, Matsuoka M. (2004).** Generating high-yielding varieties by genetic manipulation of plant architecture. *Current Opinion in Biotechnology* **15**: 144–147
- Santos T, Oliviera A. (2012).** Image-based 3D digitizing for plant architecture analysis and phenotyping. In *Workshop on Industry Applications (WGARI) in SIBGRAPI 2012 (XXV Conference on Graphics, Patterns and Images)*. Ouro Preto, MG, Brazil
- Sarlikioti V, de Visser PHB, Marcelis LFM. (2011).** Exploring the spatial distribution of light interception and photosynthesis of canopies by means of a functional-structural plant model. *Annals of Botany* **107**: 875–883
- Scheibe R, Backhausen JE, Emmerlich V, Holtgreffe S. (2005).** Strategies to maintain redox homeostasis during photosynthesis under changing conditions. *Journal of Experimental Botany* **56**: 1481–1489
- Schindler K, Grabner M, Leberl F. (2003).** Fast on-site reconstruction and visualization of archaeological finds. *Proceedings of the XIXth International Symposium, CIPA 2003: New Perspectives to Save Cultural Heritage*, Antalya (Turkey). pp. 463–468
- Sellier D, Fourcaud T. (2005).** A mechanical analysis of the relationship between free oscillations of *Pinus pinaster* Ait. saplings and their aerial architecture. *Journal of Experimental Botany* **56**: 1563–1573
- Setter T, Conocono E, Egdane J, Kropff M. (1995).** Possibility of increasing yield potential of rice by reducing panicle height in the canopy. I. Effects

of panicles on light interception and canopy photosynthesis. *Australian Journal Plant Physiology* **22**: 441–451

- Sharkey TD, Bernacchi CJ, Farquhar GD, Singsaas EL. (2007).** Fitting photosynthetic carbon dioxide response curves for C₃ leaves. *Plant, Cell and Environment* **30**: 1035-1040
- Shaw RH. (2012).** Wind movement within canopies. In J Hatfield eds. *Biometeorology in Integrated Pest Management*, Elsevier
- Shearman VJ, Sylvester-Bradley R, Scott RK, Foulkes MJ. (2005).** Physiological processes associated with wheat yield progress in the UK. *Crop Science* **45**: 175–185
- Sheehy JE, Hardy B, Mitchell P. (2000).** *Redesigning Rice Photosynthesis to Increase Yield*. International Rice Research Institute.
- Sheehy JE, Mitchell PL. (2011).** *Rice and global food security: the race between scientific discovery and catastrophe. Access not Excess—the search for better nutrition*. Smith-Gordon, Cambridgeshire, pp. 81-90
- Sheehy JE, Mitchell PL. (2013).** *Designing rice for the 21st century: The three laws of maximum yield*. Discussion Paper Series 48, International Rice Research Institute, Los Baños, Philippines.
- Sheehy JE, Mitchell PL. (2015).** Calculating maximum theoretical yield in rice. *Field Crops Research* **182**: 68-75
- Sheue C-R, Liu J-W, Ho J-F, Yao A-W, Wu Y-H, Das S, et al. (2015).** A variation on chloroplast development: The bizonoplast and photosynthetic efficiency in the deep-shade plant *Selaginella erythropus*. *American Journal of Botany* **102**: 500–511
- Simkin AJ, McAusland L, Headland LR, Lawson T, Raines CA. (2015).** Multigene manipulation of photosynthetic carbon assimilation increases CO₂ fixation and biomass yield in tobacco. *Journal of Experimental Botany* **66**: 4075–4090
- Sims DA, Pearcy RW. (1992).** Response of leaf anatomy and photosynthetic capacity in *Alocasia macrorrhiza* (Araceae) to a transfer from low to high light. *American Journal of Botany* **79**: 449-455
- Sims DA, Pearcy RW. (1994).** Scaling sun and shade photosynthetic acclimation of *Alocasia-Macrorrhiza* to whole-plant performance. 1.

carbon balance and allocation at different daily photon flux densities.
Plant Cell and Environment **17**: 881–887

Sinclair TR, Sheehy JE. (1999). Erect leaves and photosynthesis in rice.
Science **283**: 1456–1457

Singh B, Bronson KF, Singh YS, Khera TS, Pasuquin E. (2001). Nitrogen-15 balance as affected by rice straw management in rice-wheat rotation in northwest India. *Nutrient Cycle Agroecosystems* **59**: 227–237

Sinoquet H. (1993). Modelling radiative transfer in heterogeneous canopies and intercropping systems. In: Varlet-Grancher C, Bonhomme R, Sinoquet H, Eds, *Crop structure and light microclimate*. Paris: INRA editions, pp. 229-252

Sinoquet H, Le Roux X, Adam B, Ameglio T, Daudet FA. (2001). RATP: A model for simulating the spatial distribution of radiation absorption, transpiration and photosynthesis within canopies: Application to an isolated tree crown. *Plant Cell and Environment* **24**: 395–406

Sinoquet H, Rivet P, Godin C. (1997). Assessment of the three-dimensional architecture of walnut trees using digitising. *Silva Fennica* **3**: 265–273

Sinoquet H, Stephan J, Sonohat G, Lauri PÉ, Monney P. (2007). Simple equations to estimate light interception by isolated trees from canopy structure features: Assessment with three-dimensional digitized apple trees. *New Phytologist* **175**: 94–106

Sinoquet H, Thanisawanyangkura S, Mabrouk H, Kasemsap P. (1998). Characterization of the light environment in canopies using 3D digitizing and image processing. *Annals of Botany* **82**: 203–212

Smillie IRA, Pyke KA, Murchie EH. (2012). Variation in vein density and mesophyll cell architecture in a rice deletion mutant population. *Journal of Experimental Botany* **63**: 4563-4570

Smith VC, Ennos AR. (2003). The effects of air flow and stem flexure on the mechanical and hydraulic properties of the stems of sunflowers *Helianthus annuus* L. *Journal of Experimental Botany* **54**(383): 845–849

Snavely N, Seitz SM, Szeliski R. (2008). Modeling the world from Internet photo collections. *International Journal of Computer Vision* **80**: 189–210

Song Q, Xiao H, Xiao X, Zhu X-G. (2016). A new canopy photosynthesis and transpiration measurement system (CAPTS) for canopy gas exchange

research. *Agricultural and Forest Meteorology* **217**: 101–107

- Song Q, Zhang G, Zhu X-G. (2013).** Optimal crop canopy architecture to maximise canopy photosynthetic CO₂ uptake under elevated CO₂ – a theoretical study using a mechanistic model of canopy photosynthesis. *Functional Plant Biology* **40**: 109–124
- Sonohat G, Sinoquet H, Varlet - Grancher C, Rakocevic M, Jacquet A, Simon JC, Adam B. (2002).** Leaf dispersion and light partitioning in three - dimensionally digitized tall fescue-white clover mixtures. *Plant, Cell & Environment* **25**(4): 529-38
- Stadt KJ, Gendron F, Lieffers VJ, Messier C, Comeau PG. (1999).** Predicting and managing light in the understory of boreal forests. *Canadian Journal of Forest Research* **29**: 796–811
- Stegemann J, Timm HC, Kupperts M. (1999).** Simulation of photosynthetic plasticity in response to highly fluctuating light: an empirical model integrating dynamic photosynthetic induction and capacity. *Trees-Structure And Function* **14**: 145-160
- Stenberg P, Palmroth S, Bond BJ, Sprugel DG, Smolander H. (2001).** Shoot structure and photosynthetic efficiency along the light gradient in a Scots pine canopy. *Tree Physiology* **21**: 805–814
- Sterling M, Baker CJ, Berry PM, Wade A. (2003).** An experimental investigation of the lodging of wheat. *Agricultural and Forest Meteorology* **119**: 149-165
- Stewart D, Costa C, Dwyer L, Smith D, Hamilton R, Ma B. (2003).** Canopy structure, light interception, and photosynthesis in maize. *Agronomy Journal* **95**: 1465-1474
- Stiles KA, Van Volkenburgh E. (2002).** Light-regulated leaf expansion in two *Populus* species: dependence on developmentally controlled ion transport. *Journal of Experimental Botany* **53**: 1651–1657
- Still CJ, Berry JA, Collatz GJ, DeFries RS. (2003).** Global distribution of C3 and C4 vegetation: Carbon cycle implications. *Global Biogeochemical Cycles* **17**(1)

- Stitt M, Schulze D. (1994).** Does Rubisco control the rate of photosynthesis and plant growth? An exercise in molecular ecophysiology. *Plant Cell and Environment* **17**: 465–487
- Struik P. (2001).** *Crop Science: Progress and Prospects*. CABI.
- Suorsa M, Järvi S, Grieco M, et al. (2012).** PROTON GRADIENT REGULATIONS is essential for proper acclimation of Arabidopsis photosystem I to naturally and artificially fluctuating light conditions. *The Plant Cell* **24**: 2934–48
- Sussex IM, Kerk NM. (2001).** The evolution of plant architecture. *Current Opinion in Plant Biology* **4**: 33–37
- Takahashi S, Badger MR. (2011).** Photoprotection in plants: a new light on photosystem II damage. *Trends Plant Science* **16**: 53–60
- Takenaka A. (1989).** Optimal leaf photosynthetic capacity in terms of utilizing a natural light environment. *Journal of Theoretical Biology* **139**: 517-529
- Terashima I, Araya T, Miyazawa S, Sone K, Yano S. (2005).** Construction and maintenance of the optimal photosynthetic systems of the leaf, herbaceous plant and tree: an eco-developmental treatise. *Annals of Botany* **95**: 507-519
- Terashima I, Evans JR. (1988).** Effects of light and nitrogen nutrition on the organization of the photosynthetic apparatus in spinach. *Plant Cell Physiology* **29**: 143–155
- Terashima I, Saeki T. (1985).** A new model for leaf photosynthesis incorporating the gradients of light environment and of photosynthetic properties of chloroplasts within a leaf. *Annals of Botany* **56**: 489–499
- Theobald JC, Mitchell RAC, Parry MAJ, Lawlor DW. (1998).** Estimating the excess investment in Ribulose-1,5-Bisphosphate Carboxylase/Oxygenase in leaves of spring wheat grown under elevated CO₂. *Plant Physiology* **118**: 945–955
- Thomas SC, Winner WE. (2000).** A rotated ellipsoidal angle density function improves estimation of foliage inclination distributions in forest canopies. *Agricultural and Forest Meteorology* **100**: 19–24
- Thornley JHM. (2004).** Acclimation of photosynthesis to light and canopy nitrogen distribution: an interpretation. *Annals of Botany* **93**: 473–475

- Thresh JM. (1982).** Cropping practices and virus spread. *Annual Review of Phytopathology* **20**: 193–218
- Tikhonovich IA, Provorov NA. (2011).** Microbiology is the basis of sustainable agriculture: An opinion. *Annals of Applied Biology* **159**: 155-168
- Tikkanen M, Grieco M, Kangasjarvi S, Aro EM. (2010).** Thylakoid Protein Phosphorylation in Higher Plant Chloroplasts Optimizes Electron Transfer under Fluctuating Light. *Plant Physiology* **152**: 723-735
- Tikkanen M, Grieco M, Nurmi M, Rantala M, Suorsa M, Aro EM. (2012).** Regulation of the photosynthetic apparatus under fluctuating growth light. *Philosophical Transactions Royal Society London B Biology* **367**: 3486-3493
- Tilman D, Balzer C, Hill J, Befort B. (2011).** Global food demand and the sustainable intensification of agriculture. *Proceedings National Academy Science USA* **108**: 20260–20264
- Tilman D, Cassman KG, Matson PA, Naylor R, Polasky, S. (2002).** Agricultural sustainability and intensive production practices. *Nature* **418**: 671–677
- Tognetti R, Minotta G, Pinzauti S, Michelozzi M, Borghetti M. (1998).** Acclimation to changing light conditions of long-term shade-grown beech (*Fagus sylvatica* L.) seedlings of different geographic origins. *Trees* **12**: 326-333
- Topogun. (2012).** SC Pixelmachine SRL, version 2.0; www.topogun.com and Blender version 2.69; Blender Foundation; www.blender.org
- Tottman DR. (1987).** The decimal code for the growth stages of cereals, with illustrations. *Annals of Applied Biology* **110**: 441–454
- Trenbath BR, Angus JF. (1975).** Leaf inclination and crop production. *Field Crop Abstracts* **28**: 231–244
- Trnka M, Dubrovský M, Semerádová D, Žalud Z. (2004).** Projections of uncertainties in climate change scenarios into expected winter wheat yields. *Theoretical and Applied Climatology* **77**: 229–249
- Tsubo M, Walker S, Mukhala E. (2001).** Comparisons of radiation use efficiency of mono-/inter-cropping systems with different row orientations. *Field Crops Research* **71**: 17–29

- Turitzin SN, Drake BG. (1981).** The effect of a seasonal change in canopy structure on the photosynthetic efficiency of a salt marsh. *Oecologia* **48**: 79–84
- Turnball M, Doley D, Yates D. (1993).** The dynamics of photosynthetic acclimation to changes in light quantity and quality in three Australian rainforest tree species. *Oecologia* **94**: 218–228
- UNDP. (2012).** *Promoting ICT based agricultural knowledge management to increase production and productivity of smallholder farmers in Ethiopia.*
- Vainonen JP, Hansson M, Vener AV. (2005).** STN8 protein kinase in *Arabidopsis thaliana* is specific in phosphorylation of photosystem II core proteins. *Journal of Biological Chemistry* **280**: 33679–33686
- Valladares F, Dobarro I, Sánchez-Gómez D, Pearcy RW. (2005).** Photoinhibition and drought in Mediterranean woody saplings: scaling effects and interactions in sun and shade phenotypes. *Journal Experimental Botany* **56**: 483–494
- Valladares F, Niinemets U. (2007).** The architecture of plant crowns: from design rules to light capture and performance. In *Functional plant Ecology*. pp. 101–150
- Valladares F, Pearcy RW. (1999).** The geometry of light interception by shoots of *Heteromeles arbutifolia*: Morphological and physiological consequences for individual leaves. *Oecologia* **121**: 171–182
- Valladares F, Pugnaire F. (1999).** Tradeoffs between irradiance capture and avoidance in semi-arid environments assessed with a crown architecture model. *Annals Botany* **83**: 459–469
- Van Ittersum MK, Cassman KG, Grassini P, Wolf J, Tittonell P, Hochman Z. (2013).** Yield gap analysis with local to global relevance-A review. *Field Crops Research* **143**: 4–17
- Van Pelt R, Franklin J. (2000).** Influence of canopy structure on the understory environment in tall, old-growth, conifer forests. *Canadian Journal of Forest Research* **30**: 1231–1245
- van Tran D. (2001).** Closing the rice yield gap for food security. In J. Chataigner eds., *The New Development in Rice Agronomy and Its Effects on Yield and Quality in Mediterranean Areas*. pp. 2–12

- Van Volkenburgh E. (1999).** Leaf expansion – an integrating plant behaviour. *Plant Cell and Environment* **22**: 1463–1473
- Vandermeer J. (1989).** *The ecology of intercropping*. Cambridge, UK: Cambridge University Press
- Vergara B, Chang T. (1985).** *The flowering response of the rice plant to photoperiod: A review of the literature*. International Rice Research Institute (IRRI).
- Verhoeven AS, DemmigAdams B, Adams WW. (1997).** Enhanced employment of the xanthophyll cycle and thermal energy dissipation in spinach exposed to high light and N stress. *Plant Physiology* **113**: 817–824
- Vince Ö, Zoltán M. (2011).** *Plant Physiology*. Debreceni Egyetem, Nyugat-Magyarországi Egyetem, Pannon Egyetem.
- Virk P, Khush G, Peng S. (2004).** Breeding to enhance yield potential of rice at IRRI: the ideotype approach. *International Rice Research Notes* **29**: 5–9
- Visnovcova J, Gruen A, Zhang L. (2001).** Image-Based Object Reconstruction and Visualization for inventory of cultural heritage. In *Anwendungsbezogener Workshop zur Erfassung, Anwendungsbezogener Workshop zur Erfassung, Verarbeitung, Modellierung und Auswertung von 3D-Daten*. Berlin.
- von Braun J. (2007).** The World Food Situation: New Driving Forces and Required Actions. In *IFPRI's Bi-Annual Overview of the World Food Situation*.
- von Caemmerer S, Evans JR. (2010).** Enhancing C3 photosynthesis. *Plant Physiology* **154**: 589–592
- Vos J, Biemond H. (1992).** Effects of nitrogen on the development and growth of the potato plant. 1. Leaf appearance, expansion growth, life span of leaves and stem branching. *Annals of Botany* **70**: 27–35
- Vos J, Evers JB, Buck-Sorlin GH, Andrieu B, Chelle M, de Visser PHB. (2010).** Functional-structural plant modelling: a new versatile tool in crop science. *Journal of Experimental Botany* **61**: 2101–2115
- Vos J, Marcelis LFM, Evers JB. (2007).** Functional-Structural plant modelling in crop production: adding a dimension. *Frontis* **22**: 1–12

- Vos J, Van der Putten PEL. (1998).** Effect of nitrogen supply on leaf growth, leaf nitrogen economy and photosynthetic capacity in potato. *Field Crops Research* **59**: 63–72
- Vos J, Van der Putten PEL, Birch CJ. (2005).** Effect of nitrogen supply on leaf appearance, leaf growth, leaf nitrogen economy and photosynthetic capacity in maize (*Zea mays L.*). *Field Crops Research* **93**: 64–73
- Walters RG. (2004).** A mutant of *Arabidopsis* lacking the triose-phosphate/phosphate translocator reveals metabolic regulation of starch breakdown in the light. *Plant Physiology* **135**: 891–906
- Walters RG. (2005).** Towards an understanding of photosynthetic acclimation. *Journal of Experimental Botany* **56**: 435–447
- Walters RG, Horton P. (1994).** Acclimation of *Arabidopsis thaliana* to the light environment: Changes in composition of the photosynthetic apparatus. *Planta* **195**: 248–256
- Walters RG, Rogers JJM, Shephard F, Horton P. (1999).** Acclimation of *Arabidopsis thaliana* to the light environment: The role of photoreceptors. *Planta* **209**: 517–527
- Wang G, Dobermann A, Witt C, Sun Q, Fu R. (2001).** Performance of site-specific nutrient management for irrigated rice in southeast China. *Agronomy Journal* **93**: 869-878
- Wang G, Ji M, Deng J, Wang Z, Fan Z, Liu J, et al.. (2012).** Models and tests of optimal density and maximal yield for crop plants. *Proceedings of the National Academy of Sciences* **109**: 15823–15828
- Wang H, Zhao K, Song F. (2008).** Approach to modeling and virtual-reality-based simulation for plant canopy lighting. *Chinese Geographical Science* **18**: 374–381
- Wang QC, Niu YZ, Xu QZ, Wang ZX, Zhang XQ. (1995).** Relationship between plant type and canopy apparent photosynthesis in maize (*Zea mays L.*). *Biologia Plantarum* **37**: 85–91
- Wang Y, Li J. (2006).** Genes controlling plant architecture. *Current Opinion Biotechnology* **17**: 123–129
- Ware M, Belgio E, Ruban A. (2014).** Comparison of the protective effectiveness of NPQ in *Arabidopsis* plants deficient in PsbS protein and zeaxanthin. *Journal of Experimental Botany*: eru477

- Ware M, Belgio E, Ruban A. (2015).** Photoprotective capacity of non-photochemical quenching in plants acclimated to different light intensities. *Photosynthesis Research* **126**: 261–274
- Ware M, Dall’Osto L, Ruban, A. (2016).** An in vivo quantitative comparison of photoprotection in *Arabidopsis* xanthophyll mutants. *Frontiers in Plant Science* **7**: 841
- Watanabe T, Hanan JS, Room PM, Hasegawa T, Nakagawa H, Takahashi W. (2005).** Rice morphogenesis and plant architecture: Measurement, specification and the reconstruction of structural development by 3D architectural modelling. *Annals of Botany* **95**: 1131–1143
- Watling JR, Ball MC, Woodrow IE. (1997)** The utilization of light flecks for growth in four Australian rainforest species. *Functional Biology* **11**: 231-239
- Wayne PM, Bazzaz FA. (1993).** Birch seedling responses to daily time courses of light in experimental forest gaps and shadehouses. *Ecology* **74**: 1500-1515
- Weiss M, Baret F, Smith GJ, Jonckheere I, Coppin P. (2004).** Review of methods for in situ leaf area index (LAI) determination: Part II. Estimation of LAI, errors and sampling. *Agricultural and Forest Meteorology* **121**: 37–53
- Werner C, Ryel RJ, Correia O, Beyschlag W. (2001).** Effects of photoinhibition on whole-plant carbon gain assessed with a photosynthesis model. *Plant Cell Environment* **24**: 27–40
- Weston E, Thorogood K, Vinti G, Lopez-Juez E. (2000).** Light quantity controls leaf-cell and chloroplast development in *Arabidopsis thaliana* wild type and blue-light-perception mutants. *Planta* **211**: 807-815
- Wheeler T, von Braun J. (2013).** Climate change impacts on global food security. *Science* **341**: 508–513
- White JW, Andrade-Sanchez P, Gore MA, Bronson KF, Coffelt TA, Conley MM, et al. (2012).** Field-based phenomics for plant genetics research. *Field Crops Research* **133**: 101–112
- Willenbockel D. (2012).** Extreme weather events and crop price spikes in a changing climate: illustrative global simulation scenarios. *Oxfam Research Reports*, September 2012

- Willey RW. (1979).** Intercropping - Its importance and research need. Part 1. Competition and yield advantages. *Field Crop Abstracts* **32**: 1–10
- Willey RW. (1990).** Resource use in intercropping systems. *Agricultural Water Management* **17**: 215–231
- Williams J, Haq N. (2002).** *Global research on underutilized crops. An assessment of current activities and proposals for enhanced cooperation.* Southampton, UK.
- Wilson J. (1963).** Estimation of foliage denseness and foliage angle by inclined point quadrats. *Australian Journal of Botany* **11**: 95-105
- Wolfe M. (1985).** The current status and prospects of multiline cultivars and variety mixes for disease resistance. *Annual Review of Phytopathology* **23**: 251–273
- Wolfe MS. (2000).** Crop strength through diversity. *Nature* **406**: 681–682
- Woodward F. (1993).** Leaf responses to the environment and extrapolation to the larger scale. In A Solomon, H Shugart eds., *Vegetation Dynamics and Global Change.* Chapman and Hall. pp. 71–100
- World Bank. (2016).** <http://data.worldbank.org/indicator/AG.LND.AGRI.ZS>
- Wu C. (2011).** *Visual SFM: A visual structure from motion system.* <http://ccwu.me/vsfm>
- Yamori W, Masumoto C, Fukayama H, Makino A. (2012).** Rubisco activase is a key regulator of non-steady-state photosynthesis at any leaf temperature and, to a lesser extent, of steady-state photosynthesis at high temperature. *Plant Journal* **71**: 871–880
- Yang H, Shao L, Zheng F, Wang L, Song Z. (2011).** Recent advances and trends in visual tracking: A review. *Neurocomputer* **74**: 3823-3831
- Yano STI, Terashima I. (2001).** Separate localization of light signal perception for sun or shade type chloroplast and palisade tissue differentiation in *Chenopodium album*. *Plant and Cell Physiology* **42**: 1303–1310
- Yin ZH, Johnson GN. (2000).** Photosynthetic acclimation of higher plants to growth in fluctuating light environments. *Photosynthesis Research* **63**: 97-107
- Yuan L. (1997).** New trends in super rice breeding. *Hybrid Rice* **12**: 4–6

- Zadoks JC, Chang TT, Konzak CF. (1974).** A decimal code for the growth stages of cereals. *Weed Research* **14**: 415–421
- Zaks J, Amarnath K, Kramer DM, Niyogi KK, Fleming GR. (2012).** A kinetic model of rapidly reversible nonphotochemical quenching. *Proceedings of the National Academy of Sciences* **109**: 15757-15762
- Zamir D. (2001).** Improving plant breeding with exotic genetic libraries. *Nature Reviews. Genetics* **2**: 983–989
- Zhang D, Zhang L, Liu J, Han S, Wang Q, Evers J, Liu J, van der Werf W, Li L. (2014).** Plant density affects light interception and yield in cotton grown as companion crop in young jujube plantations. *Field Crops Research* **169**: 132-139
- Zhang N, Zhao Y. (2007).** Effects of plant crown shape on reflectance of grassland. *Journal of Remote Sensing* **11**: 9–19
- Zhang YL, Jian-Bo FA, Dong-Sheng WA, Qi-Rong SH. (2009).** Genotypic differences in grain yield and physiological nitrogen use efficiency among rice cultivars. *Pedosphere* **19**: 681-91
- Zhao F, Strahler AH, Schaaf CL, Yao T, Yang X, Wang Z, et al.. (2012).** Measuring gap fraction, element clumping index and LAI in Sierra Forest stands using a full-waveform ground-based lidar. *Remote Sensing of Environment* **125**: 73–79
- Zheng B, Guo Y, Ma Y, Shi L, Deng Q, Li B. (2008).** Comparison of architecture among different cultivars of hybrid rice using a spatial light model based on 3-D digitising. *Functional Plant Biology* **35**: 900–910
- Zheng B, Guo Y, Ma Y, Shi L, Deng Q, Li B. (2008).** Comparison of architecture among different cultivars of hybrid rice using a spatial light model based on 3-D digitising. *Functional Plant Biology* **35**: 900–910
- Zheng B, Guo Y, Ma Y, Shi L, Deng Q, Li B. (2008).** Comparison of architecture among different cultivars of hybrid rice using a spatial light model based on 3-D digitising. *Functional Plant Biology* **35**: 900-910
- Zhou K, Ma Y, Liu T, Shen M. (1995).** The breeding of subspecific heavy ear hybrid rice: Exploration about super-high yield breeding of hybrid rice. *Journal of Sichuan Agricultural University* **13**: 403–407

- Zhu J, van der Werf W, Anten N, Vos J, Evers J. (2015).** The contribution of phenotypic plasticity to complementary light capture in plant mixtures. *New Phytologist* **207**: 1213–1222
- Zhu J, van der Werf W, Vos J, Anten N, van der Putten P, Evers J. (2016).** High productivity of wheat intercropped with maize is associated with plant architectural responses. *Annals of Applied Biology* **168**: 357–372
- Zhu X-G, Long SP, Ort DR. (2008).** What is the maximum efficiency with which photosynthesis can convert solar energy into biomass? *Current Opinion in Biotechnology* **19**: 153-159
- Zhu X-G, Long SP, Ort DR. (2010).** Improving photosynthetic efficiency for greater yield. *Annual Review of Plant Biology* **61**: 235–261
- Zhu X-G, Ort DR, Whitmarsh J, Long SP. (2004).** The slow reversibility of photosystem II thermal energy dissipation on transfer from high to low light may cause large losses in carbon gain by crop canopies: a theoretical analysis. *Journal of Experimental Botany* **55**: 1167–1175
- Zhu X-G, Shan L, Wang Y, Quick WP. (2010).** C₄ Rice - an ideal arena for systems biology research. *Journal of Integrative Plant Biology* **52**: 762-770
- Zhu X-G, Wang Y, Ort DR, Long SP. (2013).** e-photosynthesis: a comprehensive dynamic mechanistic model of C₃ photosynthesis: from light capture to sucrose synthesis. *Plant, Cell and Environment* **36**: 1711-1727
- Zhu Z. (1997).** Fate and management of fertilizer nitrogen in agro-ecosystems. In: Zhu Z, Wen Q, Freney JR. Eds. *Nitrogen in Soils of China*. Kluwer Academic Publishers, Dordrecht, The Netherlands, pp. 239–279
- Zhu ZL, Chen DL. (2002).** Nitrogen fertilizer use in China - Contributions to food production, impacts on the environment and best management strategies. *Nutrient Cycling in Agroecosystems* **63**: 117–127
- Zivcak M, Brestic M, Kalaji HM. (2014).** Photosynthetic responses of sun- and shade-grown barley leaves to high light: Is the lower PSII connectivity in shade leaves associated with protection against excess of light? *Photosynthesis Research* **119**: 339–354

Appendices

Appendix I

Ray Tracing Details and Command Line

- *Ray Tracing Details*

The following section will show the command line for running *fastTracer3* before describing each of the input parameters.

- *Command line*

```
./fastTracer3 latitude solarTimeNoon atmosphericTransmittance day hour  
min_x max_x min_y max_y min_z max_z closestRayDistance canopyModel  
output_PPFD_file transmittance reflectance modelType isWholeDay startHour  
endHour hourInterval
```

The command line consists of 16 parameters plus the input and output file, both of which will be in the same directory. Each of the parameters will now be explained:

1. Latitude: the latitude of location, which will be used to calculate the light environment. This will determine the intensity and direction of light and takes into account solar movement.
2. Solar time noon: the time of solar noon, this is used to calculate the solar elevation angle. In general this will be 12.
3. Atmospheric transmittance: a weather parameter, used to calculate the diffuse light intensity and direct light intensity. 0.7-0.8 is an expected value for a sunny day.
4. Day: day of a year, January 1st is 1, December 31st is 365
5. Hour: hour of a day, (0-24), usually set at 1.
- 6.-11. Min and max_x, y, z are coordinate values used to set the ray tracing boundary, a cuboid. The cuboid is that:
 - X axis: (min_x ~ max_x);
 - Y axis: (min_y ~ max_y);
 - Z axis: (min_z ~ max_z).

12. Closest ray distance: a parameter used to define the density of rays of light source. The value represents the closest distance between two rays.

13. Canopy model: the canopy model file to input in the form of a .txt file.

14. Output file: the output file that fastTracer will write into in the form of a .txt file.

15. Transmittance: the proportion of light that will transmit to a leaf, usually set at 0.075

16. Reflectance: the proportion of light that will reflect from a leaf, usually set at 0.075.

17. Model type: the type of input model format. Either:

1: the first 9 columns are canopy structure, uniformed leaf transmittance and reflectance, which are input from command line (with 'Transmittance', and 'Reflectance' parameters).

2: the first 9 columns are canopy structure, 10th -13th columns are Leaf ID, Leaf length, position of facet on the leaf (distance from leaf base to current facet), and SPAD value of chlorophyll, the 14th and 15th columns are leaf transmittance and reflectance for current facet, and the 16th column is leaf nitrogen concentration.

3: the first 9 columns are canopy structure, 10th -13th columns are Leaf ID, Leaf length, position of facet on the leaf (distance from leaf base to current facet), and SPAD value of chlorophyll, 16th column is leaf nitrogen concentration, leaf transmittance and reflectance are set with parameters 'Transmittance', and 'Reflectance'.

N.B. Only model type 1 will be used during this project as this is the data output from the reconstructions.

18. isWholeDay: this value will be either 0 or 1. If a value of 0 is chosen, the simulation will be for one single time point designated by the input parameter 'hour' (number 5). If a value of 1 is chosen, the simulation will be for a whole day from 'startHour' to 'endHour' with interval of 'hourInterval'. For this option, start and end hour will usually refer to sunrise and sunset. This second option will be used in this project unless otherwise stated.